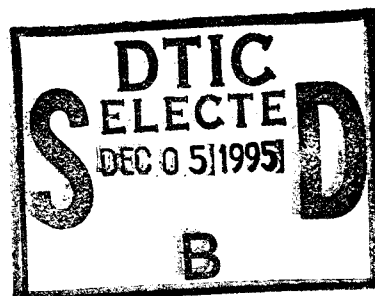


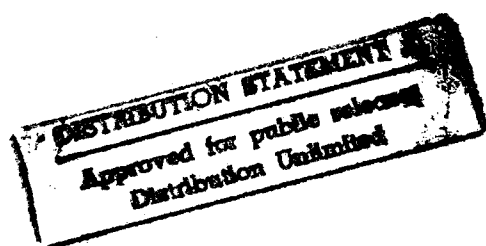
NASA CP-001

PROCEEDINGS OF THE SCAR CONFERENCE

PART 2



Held at
LANGLEY RESEARCH CENTER
Hampton, Virginia,
November 9-12, 1976

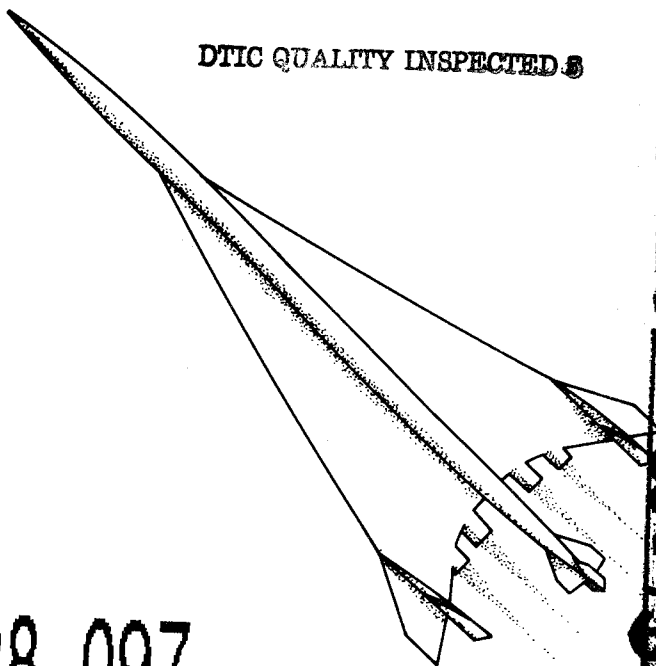


DTIC QUALITY INSPECTED 8



19951128 097

PLASTIC 30570-30570-3



NASA Conference Publications (CP Series) contain compilations of scientific and technical papers or transcripts arising from conferences, workshops, symposia, seminars and other professional meetings that NASA elects to publish.

The text of these proceedings was reproduced from author-supplied manuscripts. NASA reviewed each paper for adherence to format, use of the International System of Units, and basic grammatical accuracy.

*MSG D14 DROLS PROCESSING-LAST INPUT IGNORED

-- 1 OF 4 ***DTIC DOES NOT HAVE THIS ITEM***
-- 1 - AD NUMBER: D426326
-- 5 - CORPORATE AUTHOR: NATIONAL AERONAUTICS AND SPACE ADMINISTRATION
-- HAMPTON VA LANGLEY RESEARCH CENTER
-- 6 - UNCLASSIFIED TITLE: PROCEEDINGS OF THE SCAR CONFERENCE PART I.
--11 - REPORT DATE: NOV 09, 1976
--12 - PAGINATION: 477P
--14 - REPORT NUMBER: NASA CP-001
--20 - REPORT CLASSIFICATION: UNCLASSIFIED
--21 - SUPPLEMENTARY NOTE: 'PROCEEDINGS OF THE SCAR CONFERENCE PART I',
9-12 NOV 76, HAMPTON, VA. SPONSORED BY NATIONAL AERONAUTICS AND
SPACE ADMINISTRATION, LANGLEY RESEARCH CENTER.
--22 - LIMITATIONS (ALPHA): APPROVED FOR PUBLIC RELEASE; DISTRIBUTION
UNLIMITED. ~~AVAILABILITY: NATIONAL TECHNICAL INFORMATION SERVICE~~
~~SPRINGFIELD, VA. 22161. NASA CP-001.~~
--33 - LIMITATION CODES: 1 ~~2~~

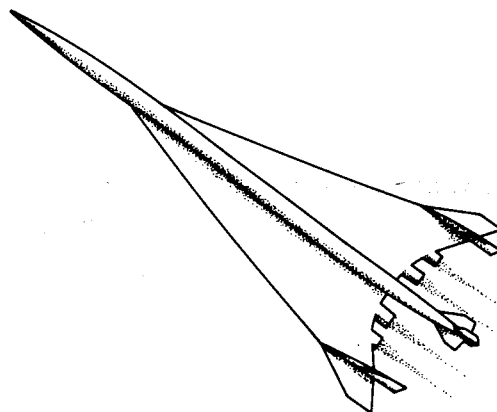
-- END Y FOR NEXT ACCESSION END

NASA CP-001

PROCEEDINGS OF THE SCAR CONFERENCE

PART 2

Held at
Langley Research Center
Hampton, Virginia
November 9-12, 1976



For sale by the National Technical Information Service
Springfield, Virginia 22161
Price: \$12.50

PREFACE

Since 1972 the Supersonic Cruise Aircraft Research (SCAR) Program has provided an accelerated and focused technology effort which has resulted in development of improved analytical techniques, design procedures, and an expanded experimental data base. Major advances have been achieved and were reported to the technical community at the SCAR Conference held at Langley Research Center, November 9-12, 1976.

This document is a compilation of papers presented by 49 speakers representing airframe and engine manufacturers, the Federal Aviation Administration, and four NASA research centers.

The Conference was organized in six sessions as follows:

- I. Aerodynamics
- II. Stability and Control
- III. Propulsion
- IV. Environmental Factors
- V. Airframe Structures and Materials
- VI. Design Integration

Papers and the authors thereof are grouped by session and identified in the CONTENTS. The order of papers is the actual order of speaker appearance at the Conference. The Lockheed-California Company four-part oral presentation in the Design Integration session has been consolidated into one paper by the three speakers.

The size of the compilation necessitated publication in two parts (Parts I and II). A list of attendees, by organizational affiliation, is included at the back of Part II.

We would like to express appreciation to session chairmen and speakers whose efforts contributed to the technical excellence of the Conference.

C. Driver
Conference Chairman

Hal T. Baber, Jr.
Conference Coordinator

Accession For	
NTIS GRA&I	<input checked="" type="checkbox"/>
DTIC TAB	<input type="checkbox"/>
Unannounced	<input type="checkbox"/>
Justification	
<i>Printed enclosed</i>	
<i>DNCAI (memo)</i>	
By <i>2 Nov 95</i>	
Distribution/	
Availability Codes	
Dist	Avail and/or Special
<i>A-1</i>	

CONTENTS

Part I*

PREFACE	iii
SCAR PROGRAM OVERVIEW	1
F. Edward McLean	

SESSION I - AERODYNAMICS Chairman: Robert E. Bower

INTRODUCTION	7
Robert E. Bower	
1. A LINEARIZED THEORY METHOD OF CONSTRAINED OPTIMIZATION FOR SUPERSONIC CRUISE WING DESIGN	9
David S. Miller, Harry W. Carlson, and Wilbur D. Middleton	
2. ADVANCED SURFACE PANELING METHOD FOR SUBSONIC AND SUPERSONIC FLOW . . .	25
Larry L. Erickson, Forrester T. Johnson, and F. Edward Ehlers	
3. DEVELOPMENT OF AN AERODYNAMIC THEORY CAPABLE OF PREDICTING SURFACE LOADS ON SLENDER WINGS WITH VORTEX FLOW	55
Blair B. Gloss and Forrester T. Johnson	
4. THE ROLE OF FINITE-DIFFERENCE METHODS IN DESIGN AND ANALYSIS FOR SUPERSONIC CRUISE	69
James C. Townsend	
5. THEORETICAL AND EXPERIMENTAL PRESSURE DISTRIBUTIONS FOR A 71.2° SWEPT ARROW-WING CONFIGURATION AT SUBSONIC, TRANSONIC, AND SUPERSONIC SPEEDS	85
Percy J. Bobbitt and Marjorie E. Manro	
6. RESULTS OF RECENT NASA RESEARCH ON LOW-SPEED AERODYNAMIC CHARACTERISTICS OF SUPERSONIC CRUISE AIRCRAFT	123
Paul L. Coe, Jr., and A. B. Graham	
7. UPPER SURFACE NACELLE INFLUENCE ON SCAR AERODYNAMIC CHARACTERISTICS AT TRANSONIC SPEEDS	137
Charles E. Mercer and George T. Carson, Jr.	
8. AERODYNAMIC VALIDATION OF A SCAR DESIGN	155
Robert L. Roensch	

*Papers 1 to 21 are presented under separate cover.

SESSION II - STABILITY AND CONTROL

Chairman: Berwin M. Koch

9. DEVELOPMENT OF LONGITUDINAL HANDLING QUALITIES CRITERIA FOR LARGE
ADVANCED SUPERSONIC AIRCRAFT 171
Robert W. Sudderth and Walter E. McNeill
10. HANDLING QUALITIES ASPECTS OF NASA YF-12 FLIGHT EXPERIENCE 193
Donald T. Berry, Donald L. Mallick, and Glenn B. Gilyard
11. SIMULATOR STUDY OF THE LOW-SPEED HANDLING QUALITIES OF A SUPERSONIC
CRUISE ARROW-WING TRANSPORT CONFIGURATION DURING APPROACH AND
LANDING 215
William D. Grantham, Luat T. Nguyen, M. J. Neubauer, Jr.,
and Paul M. Smith
12. FLEXSTAB - A COMPUTER PROGRAM FOR THE PREDICTION OF LOADS AND
STABILITY AND CONTROL OF FLEXIBLE AIRCRAFT 249
Brian R. Perkin and Larry L. Erickson
13. PROPULSION SYSTEM/FLIGHT CONTROL INTEGRATION FOR SUPERSONIC
AIRCRAFT 281
Paul J. Reukauf and Frank W. Burcham, Jr.
14. FLUTTER SUPPRESSION BY ACTIVE CONTROL AND ITS BENEFITS 303
Robert V. Doggett, Jr., and James L. Townsend

SESSION III - PROPULSION

Chairman: Warner L. Stewart

- INTRODUCTION 337
Warner L. Stewart
15. VARIABLE STREAM CONTROL ENGINE CONCEPT FOR ADVANCED SUPERSONIC
AIRCRAFT - FEATURES AND BENEFITS 341
Robert A. Howlett
 16. ADVANCED SUPERSONIC TECHNOLOGY STUDY - ENGINE PROGRAM
SUMMARY: SUPERSONIC PROPULSION - 1971 to 1976 353
J. N. Krebs
 17. VARIABLE CYCLE COMPONENT TEST PROGRAM FOR VARIABLE-CYCLE ENGINES . . . 371
Albert G. Powers, John B. Whitlow, and Leonard E. Stitt
 18. SUPERSONIC CRUISE INLETS FOR VARIABLE-CYCLE ENGINES 387
David N. Bowditch
 19. CONTROL OF PROPULSION SYSTEMS FOR SUPERSONIC CRUISE AIRCRAFT 399
Kirby W. Hiller and Daniel I. Drain

20. YF-12 PROPULSION RESEARCH PROGRAM AND RESULTS	417
James A. Albers and Frank V. Olinger	
21. COMPOSITE MATERIALS RESEARCH IN SUPPORT OF SUPERSONIC PROPULSION SYSTEMS	457
Robert A. Signorelli	

Part II

SESSION IV - ENVIRONMENTAL FACTORS

Chairman: Harry W. Johnson

22. AEROACOUSTIC STUDIES OF COANNULAR NOZZLES SUITABLE FOR SUPERSONIC CRUISE AIRCRAFT APPLICATIONS	471
Orlando A. Gutierrez	
23. COANNULAR NOZZLE NOISE CHARACTERISTICS AND APPLICATION TO ADVANCED SUPERSONIC TRANSPORT ENGINES	491
Hilary Kozlowski	
24. COANNULAR PLUG NOZZLE NOISE REDUCTION AND IMPACT ON EXHAUST SYSTEM DESIGNS	505
Robert Lee	
25. CURRENT RESEARCH IN SONIC-BOOM MINIMIZATION	525
Christine M. Darden and Robert J. Mack	
26. TECHNOLOGY FOR CONTROLLING EMISSIONS OF OXIDES OF NITROGEN FROM SUPERSONIC CRUISE AIRCRAFT	543
Gregory M. Reck and Richard A. Rudey	
27. CONSIDERATIONS OF HIGH ALTITUDE EMISSIONS	565
Anthony J. Broderick and Nicholas P. Krull	

SESSION V - AIRFRAME STRUCTURES AND MATERIALS

Chairman: Richard R. Heldenfels

INTRODUCTION	577
Richard R. Heldenfels	
28. TITANIUM AND ADVANCED COMPOSITE STRUCTURES FOR A SUPERSONIC CRUISE ARROW WING CONFIGURATION	579
M. J. Turner and J. M. Hoy	
29. ADVANCED STRUCTURES TECHNOLOGY APPLIED TO A SUPERSONIC CRUISE ARROW-WING CONFIGURATION	603
I. F. Sakata and G. W. Davis	

30. COMPUTER-AIDED METHODS FOR ANALYSIS AND SYNTHESIS OF SUPERSONIC CRUISE AIRCRAFT STRUCTURES	637
Gary L. Giles	
31. STRUCTURAL DESIGN STUDIES OF A SUPERSONIC CRUISE ARROW WING CONFIGURATION	659
Jaroslaw Sobieszczanski, L. Arnold McCullers, Rodney H. Ricketts, Nick J. Santoro, Sharon D. Beskenis, and William L. Kurtze	
32. LOADS TECHNOLOGY FOR SUPERSONIC CRUISE AIRCRAFT	685
Robert C. Goetz	
33. DEVELOPMENTS IN STEADY AND UNSTEADY AERODYNAMICS FOR USE IN AEROELASTIC ANALYSIS AND DESIGN	707
E. Carson Yates, Jr., and Samuel R. Bland	
34. FATIGUE OF TITANIUM ALLOYS IN A SUPERSONIC-CRUISE AIRCRAFT ENVIRONMENT	739
L. A. Imig	
35. NEW ADVANCEMENTS IN TITANIUM TECHNOLOGY AND THEIR COST AND WEIGHT BENEFITS	757
Leonard A. Ascani and John K. Pulley	
36. FABRICATION AND EVALUATION OF ADVANCED TITANIUM AND COMPOSITE STRUCTURAL PANELS	783
Thomas T. Bales, Edward L. Hoffman, Lee Payne, and Alan L. Carter	
37. TIME-TEMPERATURE-STRESS CAPABILITIES OF COMPOSITES FOR SUPERSONIC CRUISE AIRCRAFT APPLICATIONS	799
J. F. Haskins, J. R. Kerr, and B. A. Stein	
38. ADVANCED SUPERSONIC TECHNOLOGY FUEL TANK SEALANTS	829
Robert W. Rosser and John A. Parker	

SESSION VI - DESIGN INTEGRATION
Chairman: William S. Aiken, Jr.

INTRODUCTORY REMARKS	847
William S. Aiken, Jr.	

TOWARD A SECOND GENERATION FUEL EFFICIENT

SUPERSONIC CRUISE AIRCRAFT

39. DESIGN CHARACTERISTICS AND FEASIBILITY	849
Frank D. Neumann	

40. STRUCTURAL DESIGN FOR EFFICIENCY	867
James M. Hoy	

41. PERFORMANCE CHARACTERISTICS AND BENEFITS	881
John D. Vachal	

TECHNOLOGY DEVELOPMENT OF A SCAR DESIGN

42. DESIGN FEASIBILITY OF AN ADVANCED TECHNOLOGY SUPERSONIC CRUISE AIRCRAFT	895
William T. Rowe	

43. STRUCTURAL DESIGN OF SUPERSONIC CRUISE AIRCRAFT	911
J. E. Fischler	

44. PERFORMANCE AND BENEFITS OF AN ADVANCED TECHNOLOGY SUPERSONIC CRUISE AIRCRAFT	927
Richard D. FitzSimmons	

45. AN ADVANCED CONCEPT THAT PROMISES ECOLOGICAL AND ECONOMIC VIABILITY . .	939
Bruce R. Wright, Thomas A. Sedgwick, and David M. Urie	

46. AIRLINE SCHEDULING FOR A SCAR DESIGN (Paper not available for publication)	
R. L. Foss	

47. MARKET TRENDS	985
Richard D. FitzSimmons	

ATTENDEES	1001
---------------------	------

SESSION IV - ENVIRONMENTAL FACTORS

AEROACOUSTIC STUDIES OF COANNULAR NOZZLES SUITABLE
FOR SUPERSONIC CRUISE AIRCRAFT APPLICATIONS

Orlando A. Gutierrez
NASA Lewis Research Center

SUMMARY

Research programs have been conducted to investigate experimentally the aeroacoustic characteristics of scale-model, inverted-velocity-profile coannular nozzles. These programs include studies of unsuppressed configurations with and without center plugs over a variety of radius ratios and area ratios. Also included in these studies have been suppressed configurations, the effect of ejectors, and some simulated flight effects. Unsuppressed inverted-velocity-profile coannular nozzles seem to allow jet mixing noise compliance with present FAR-36 regulations when applied to supersonic cruise aircraft engine cycles. Simulated flight tests suggest that the aeroacoustic benefits of the inverted-velocity-profile coannular nozzles would be maintained in flight.

INTRODUCTION

The results of aeroacoustic studies of inverted-velocity-profile coannular nozzles suitable for supersonic cruise aircraft applications are briefly reviewed. These studies have been conducted over the past 3 years by the General Electric Company and the Pratt & Whitney Aircraft Division of United Technologies Corp. under contract to the NASA Lewis Research Center.

Mission analysis studies under the supersonic cruise aircraft research (SCAR) program (refs. 1 and 2) have identified low-bypass-ratio turbofan engines as likely candidates for use in future supersonic cruise aircraft. Two engine concepts of this type are shown in figures 1 and 2. Both concepts feature exhaust systems consisting of two unmixed coaxial streams at takeoff conditions, with the outer stream operating at a higher velocity than the inner stream. The concept shown in figure 1 yields a higher outer-stream velocity by over-extracting the core stream and augmenting the fan stream through burning in the fan duct (duct-burning turbofan (DBTF)). In the concept shown in figure 2, the inverted profile is obtained by ducting the higher velocity core flow outward and ducting the lower velocity, cooler fan air inward. The fan air then surrounds the center plug (double-bypass, variable-cycle engine).

The inverted-velocity-profile exhaust concept should introduce acoustic benefits during the takeoff and landing portions of the mission. These expected benefits, associated with the small radial height of the high-velocity stream, are as follows: (1) peak noise generation at higher frequency, which

is more amenable to dissipation through atmospheric absorption or, in the case of an ejector, to application of acoustic liners to the ejector walls; and (2) the easier application of mechanical suppressors because the narrow height of the outer stream would allow easier stowing of the hardware for those portions of the mission where noise generation is unimportant. However, insufficient information was available in the literature to allow evaluation of the actual noise characteristics of the inverted-velocity-profile coannular nozzles, with or without the use of mechanical suppressors.

The work described herein is the result of NASA-sponsored programs dedicated to filling that void. Under these experimental research programs, static aeroacoustic data have been obtained for a variety of inverted-velocity-profile coannular nozzles covering a wide range of geometric configurations, temperature and pressure ratios, and velocity conditions. The scale-model test nozzles were 13 to 15 centimeters in equivalent diameter. The scale-model nozzles included unsuppressed coannular nozzles, with and without center plugs; suppressed fan stream configurations (including multitube, convoluted, and multichute suppressors); and the application of lined and unlined ejectors. The effect of varying area and radius ratios on the unsuppressed coannular nozzles was also investigated. Data were obtained at stream temperatures from ambient to 1090 K, pressure ratios from 1.3 to 4.0, and velocities from 170 to 870 meters per second. In addition, simulated flight studies were made with smaller, 5.5-centimeter-equivalent-diameter, unsuppressed coannular nozzles over a reduced range of operating conditions.

The principal results obtained to date in these programs are summarized herein. These results and the continuing studies are characterized by very favorable acoustic and aerodynamic (high thrust coefficient) performance obtained with the unsuppressed coannular nozzles. These results could lead to the design of a practical supersonic cruise commercial aircraft.

COANNULAR NOZZLES

A simplified sketch of a coannular nozzle showing the inner, or core, nozzle surrounded by the outer, or fan, nozzle is shown in figure 3. The two exhaust streams form three regions of turbulence that are important to the generation of jet noise: region I, where the inner flow and outer flow mix; region II, where the outer flow mixes with the ambient air; and region III, where the merged jets mix with the ambient air. Each region generates noise. Their relative importance to the overall jet noise signature of a particular coannular nozzle depends on the relative sizes and velocities of the two streams.

The velocity profile characteristics of conventional subsonic coannular nozzles are shown in figure 4. These nozzles have large outer-stream to inner-stream area ratios A_o/A_i with outer-stream to inner-stream velocity ratios V_o/V_i of the order of 0.7 to 0.8. In this type of coannular nozzle, the inner-stream/outer-stream and merged-jet/ambient-air mixing regions (regions I and III, respectively, in fig. 2) are the significant noise-producing parts of the jet. These nozzles are applicable to high-bypass-ratio turbofan engines suit-

able for conventional and short-takeoff-and-landing (STOL) aircraft applications. Sufficient experimental work (e.g., refs. 3 and 4) has been conducted on nozzles of this type covering a wide enough variation in area ratio, velocity ratio, and exit plane offset to permit the generation of prediction curves. These prediction curves have already been incorporated into design procedures such as the NASA aircraft noise prediction program (ref. 5) and the currently proposed SAE prediction procedure.

Coannular nozzles that operate with inverted velocity profiles (outer-stream velocity greater than inner-stream velocity) have become primary candidates for application to low-bypass-ratio turbofan engines being considered for use in future supersonic cruise aircraft. This type of nozzle, shown schematically in figure 5, is characterized by a small A_o/A_i ratio (of the order of 1) and a V_o/V_i ratio in the range of 1.5 to 2.0. With this type of nozzle, the outer-stream/ambient-air and merged-jet/ambient-air mixing regions (regions II and III, respectively, in fig. 2) are the dominant sources of jet noise. The prediction methods based on conventional coannular jet data, where the inner-stream/outer-stream and merged-jet/ambient-air mixing regions are dominant and V_o/V_i ratios are less than 1, do not apply. To fill this gap in jet mixing noise technology, the Lewis Research Center sponsored experimental studies over the last 3 years with Pratt & Whitney Aircraft and General Electric to determine the noise characteristics of inverted-velocity-profile coannular nozzles.

The jet noise prediction method for coannular jets published by the SAE in 1965 (ref. 6) was used to establish a noise-level reference for the inverted-velocity-profile nozzles. This method, herein referred to as "synthesis," recommends that the coannular noise be synthesized by adding antilogarithmically the noise levels produced by two convergent nozzles with areas and jet velocities corresponding to each stream as if it were acting alone. This SAE procedure for synthesizing coannular noise is shown schematically in figure 6 and is used in this paper as an arbitrary reference against which to compare experimental results. The synthesis method does not account for the effect of stream interaction on jet noise generation.

INVERTED-VELOCITY-PROFILE COANNULAR NOZZLE INVESTIGATIONS

The experimental work conducted to date under this program has covered the following:

- (1) Static performance of basic unsuppressed coannular nozzles
- (2) Static performance of suppressed coannular nozzles
- (3) Effect of geometric variables on unsuppressed coannular nozzles
- (4) Simulated flight effects on unsuppressed coannular nozzles

Basic Unsuppressed Configurations

The two basic unsuppressed nozzle configurations tested in the contractor scale-model studies are shown in figure 7. A coannular nozzle without a plug,

with an area ratio of 0.75, and with an outer-stream radius ratio $R_{1,o}/R_{2,o}$ of 0.76 is shown in figure 7(a). (This radius ratio is defined as the ratio of the outer-stream inner radius to the outer-stream outer radius.) The nozzle shown in figure 7(b) is a coannular nozzle with a central plug, an area ratio of 0.67, and an outer-stream radius ratio of 0.90. These test nozzle configurations had equivalent total diameters of 13 and 15 centimeters, respectively.

Results from the experimental research programs are plotted in figure 8 as peak perceived noise level (normalized for jet density effects)¹ as a function of outer-stream velocity for cases where the outer-stream velocity was at least 1.5 times the inner-stream velocity. The jet noise levels for the coannular nozzles are 6 to 10 PNdB lower than the synthesized value calculated by the method shown in figure 6 (both jets exhausting through separate conical nozzles). The configuration with a central plug, which had a higher outer-stream radius ratio, showed a 2-PNdB-greater noise reduction than the nozzle without a plug, which had a lower outer-stream radius ratio. The measured thrust losses are about 1.5 to 2.0 percent (referred to an ideal nozzle).

In figure 9 the unsuppressed coannular acoustic power level (PWL) spectrum has been scaled up to engine size and compared with the spectrum for a mixed turbofan (single convergent exhaust nozzle) with the same total flow rate and thrust. As shown in figure 9 the unsuppressed coannular nozzle at these operating conditions is about 5 to 6 decibels lower in overall PWL than the mixed-turbofan exhaust nozzle at equal flow and thrust conditions.

Suppressed Annular Configurations

In addition to these basic unsuppressed coannular configurations, configurations with mechanical suppressors were also tested by adding chutes, convolutions, or tubes to the outer stream and, in some cases, including ejectors. These suppressed configurations are shown in figure 10. The coannular configuration without a plug was tested with multitube and convoluted suppressors; the nozzle with a center plug incorporated multitube and multichute suppressors. In both cases, tests were made with and without ejectors, and the ejectors were tested with and without acoustic liners. In all cases the total flow area and the A_o/A_i were the same as for the corresponding basic unsuppressed coannular nozzle.

Noise data. - In figure 11 the acoustic results obtained for the suppressed configurations are presented in terms of normalized peak perceived noise level as a function of outer-stream velocity. The crosshatched areas represent the suppressed coannular results. The dashed lines are a reproduction of the synthesized and unsuppressed coannular nozzle results already presented in figure 8. At the higher velocities the suppressed configurations yield an additional 3 to 7 PNdB reduction in noise but at the expense of rela-

¹The exponent on the fan jet density is based on conical nozzle results, and for the range of velocity shown here varies from 1.0 at 373 m/sec to 2.0 at velocities above 540 m/sec.

tively large thrust losses (as much as 8 percent greater than with the unsuppressed coannular nozzles).

Comparisons of suppressed and unsuppressed configurations. - The axial velocity decays for suppressed and unsuppressed coannular plug configurations are compared in figure 12. These data were taken with a laser velocimeter at supersonic outer-stream conditions in order to help establish the relation between velocity decay and total noise generation for future analytical coannular jet noise models. In addition to the coannular plug nozzle data, a typical conical nozzle decay curve is shown. The velocity of the unsuppressed coannular nozzle decays much more rapidly than that for the conical nozzle, which is consistent with the lower noise generation shown in figure 8. Both suppressed coannular nozzles shown in figure 12 have about the same velocity decay characteristics, but both have a more rapid decay rate than the unsuppressed coannular nozzle. This trend agrees with the larger noise reductions shown in figure 11 for the suppressed configurations.

The jet noise reductions obtained from suppressed and basic unsuppressed inverted-velocity-profile coannular nozzles are compared in figures 13 and 14 by means of bar graphs. In these figures, the PNL reductions with relation to the synthesized value for the basic unsuppressed configurations without ejectors are given for one outer-stream and one inner-stream velocity in the range of application to supersonic cruise engines. In figure 13 the results of the configurations without plugs are covered, with the reductions ranging from 7 decibels for the unsuppressed coannular nozzle to 15.5 decibels for the multitube coannular nozzle with treated ejector. Similar results are shown in figure 14 for the configurations with center plugs for approximately the same fan velocity as in figure 13. For these configurations the reductions ranged from 10 decibels for the unsuppressed nozzle to 17.7 decibels for the multitube coannular nozzle with treated ejector.

Geometric Variations of Unsuppressed Coannular Nozzles

A study was also conducted of the effect of several geometric variations on the static aeroacoustic performance of the unsuppressed coannular nozzle with center plug. The geometric effects investigated were primarily the radius ratio and area ratio effects. At the same time the velocity ratio effect was expanded over a wider range, reaching the extreme low point where the inner stream was completely shut off. This study used variations of the basic unsuppressed coannular nozzle with center plug shown in figure 7(b). The geometric characteristics of the variations investigated are described in table I.

The effects of velocity ratio on the noise reduction for two different-area-ratio coannular plug nozzles with constant outer-stream radius ratio are shown in figure 15. The noise level relative to the synthesized level predicted for noninteracting jets is plotted as a function of V_i/V_o ratio for constant outer-stream operating conditions. (The inner-stream velocity was changed by varying both temperature and pressure.) Over this range, the A_o/A_i ratio has very little effect on the noise. Maximum noise reduction occurs between V_i/V_o ratios of 0.3 and 0.5. As the inner flow is reduced to very low values, less

noise reduction is obtained, which could be attributed to the lack of sufficient inner flow to promote rapid velocity decay in the energetic outer stream. When the inner flow is increased above a velocity ratio of 0.5, less noise reduction is again obtained, in this case because the inner stream affects the jet noise generated in the merged-jet/ambient-air mixing region (fig. 3).

The effects of outer-stream radius ratio on aeroacoustic performance are shown in figure 16. As the radius ratio is increased (fig. 16(a)), the noise reduction is also increased, indicating the desirability, from an acoustic viewpoint, of designing engine nozzles with a high outer-stream radius ratio. The effect of outer-stream radius ratio on the aerodynamic characteristics is shown in figure 16(b). For a V_i/V_o ratio of 0.5, static thrust losses were between 1 and 2 percent relative to a convergent nozzle. Increasing the outer-stream radius ratio increased thrust losses, indicating the need, from a designer's point of view, to trade off the thrust losses with the noise reduction in order to select the optimum nozzle radius ratio for an engine exhaust system.

Simulated Flight Effects

The acoustic information presented so far on the inverted-velocity-profile coannular nozzles has been static data. However, a most important consideration is whether these noise reductions relative to a convergent nozzle are maintained under flight conditions. Consequently, the acoustic program has also included experimental investigations of some models under simulated flight conditions in an acoustic wind tunnel by Pratt & Whitney Aircraft under NASA Lewis contract. The nozzles used for this part of the program were similar to the unsuppressed coannular nozzle without a plug described in figure 7(a), except that the models were 5.5 centimeters in equivalent diameter due to size limitations imposed by the wind tunnel. Typical results obtained with subsonic velocities in both streams ($V_o/V_i \sim 1.5$) are shown in figure 17. The data are presented in terms of overall sound pressure level (OASPL) as a function of the radiation angle from the nozzle inlet. The wind tunnel results have been corrected for the shear layer and sound convection effects of the tunnel stream and converted to a flight frame of reference by the methods of reference 7. The dashed curve represents the static conditions, and the dash-dot and solid curves show directivities at free-stream Mach numbers of 0.18 and 0.30, respectively. Reductions in jet noise were obtained throughout the measured arc from 70° to 150° from the inlet axis. The peak noise reduction was 5 to 7 decibels below the static case. The most significant result was that the noise reduction due to forward velocity was the same as for a convergent nozzle, indicating that the noise reduction benefit evident for static conditions would be maintained in flight.

Similar results are shown in figure 18 for a case where the outer stream was supersonic (pressure ratio, 2.5). The subsonic inner-stream conditions are the same as for figure 17, producing a V_o/V_i ratio of 1.9 here. The results are very similar except that the peak noise reductions are somewhat smaller in magnitude (by about 1.5 dB) and that in the forward quadrant there is an actual increase in noise level. These changes from the subsonic case are caused by shock-generated noise. However, this forward-quadrant effect does not change

the noise reduction during flight relative to a convergent nozzle because the convergent nozzle is similarly affected. For the 0.30 Mach number data shown, the thrust coefficient losses were increased by an additional 1 percent over those measured for static conditions. As in the subsonic case, the most significant result is that the noise reduction benefit evident for static conditions would be maintained in flight.

CONCLUDING REMARKS

Aeroacoustic experimental investigations on inverted-velocity-profile coannular nozzles have been carried out by the General Electric Company and Pratt & Whitney Aircraft under contract to the NASA Lewis Research Center. The results available to date indicate that this type of coannular nozzle, without the use of mechanical suppressors, generates less noise than two independent convergent jets of equal velocities and areas in the absence of interaction effects. The results also show that at high velocity levels the noise generated is lower than that from an equal-flow and equal-thrust internally mixed turbofan nozzle. Mission analysis studies suggest that the jet mixing and shock noise levels attainable with the unsuppressed coannular nozzles, coupled with the low thrust losses involved (~ 1.5 to 2 percent), are sufficiently low to permit the design of practical supersonic cruise commercial aircraft that will meet present FAR-36 noise requirements.

Mechanically suppressed inverted-velocity-profile coannular nozzles produce larger reductions in noise but are accompanied by significant thrust losses.

The unsuppressed inverted-velocity-profile coannular nozzles generate less noise under simulated flight conditions than under static conditions. This reduction in noise appears to be of the same magnitude as that experienced by convergent nozzles. Therefore, the coannular noise benefits experienced statically should be maintained, for the most part, in flight.

These programs have generated an extensive data base for inverted-velocity-profile coannular nozzles with and without center plugs, over a variety of area ratios and radius ratios, at an extensive combination of velocities, pressures, and temperatures. This data base also covers mechanically suppressed coannular nozzles as well as the effects of lined and unlined ejectors.

APPENDIX

SYMBOLS AND ABBREVIATIONS

The following symbols and abbreviations are used in the table and figures.

A_i	inner-stream area, cm^2
A_o	outer-stream area, cm^2
C_V	thrust coefficient, dimensionless
D	ejector diameter, m
D_{ref}	reference diameter, 1.523 m
h_i	inner-stream height, m
L	ejector length, cm
PNL	perceived noise level, PNdB
PNL_{pk}	peak perceived noise level, PNdB
PNL_{syn}	PNL for synthesized coannular nozzle, PNdB
PWL	acoustic power level, dB re 10^{-12} W
OASPL	overall sound pressure level, dB re $20 \mu\text{N/m}^2$
$R_{1,i}$	inner radius of inner stream, m
$R_{1,o}$	inner radius of outer stream, m
$R_{2,i}$	outer radius of inner stream, m
$R_{2,o}$	outer radius of outer stream, m
SPL_i	sound pressure level for convergent nozzle with area and velocity equal to those of inner stream, dB re $20 \mu\text{N/m}^2$
SPL_o	SPL for convergent nozzle with area and velocity equal to those of outer stream, dB re $20 \mu\text{N/m}^2$
SPL_{syn}	SPL for synthesized coannular nozzle (antilogarithmic sum of SPL_i and SPL_o), dB re $20 \mu\text{N/m}^2$
T_i	inner-stream total temperature, K
T_{mix}	internally mixed turbofan jet total temperature, K
T_o	outer-stream total temperature, K
V	local peak axial velocity, m/sec
V_i	inner-stream velocity, m/sec
V_{mix}	jet velocity of internally mixed turbofan nozzle, m/sec
V_o	outer-stream velocity, m/sec
V_{ref}	reference velocity, 304.8 m/sec
X	axial distance from nozzle exit, cm

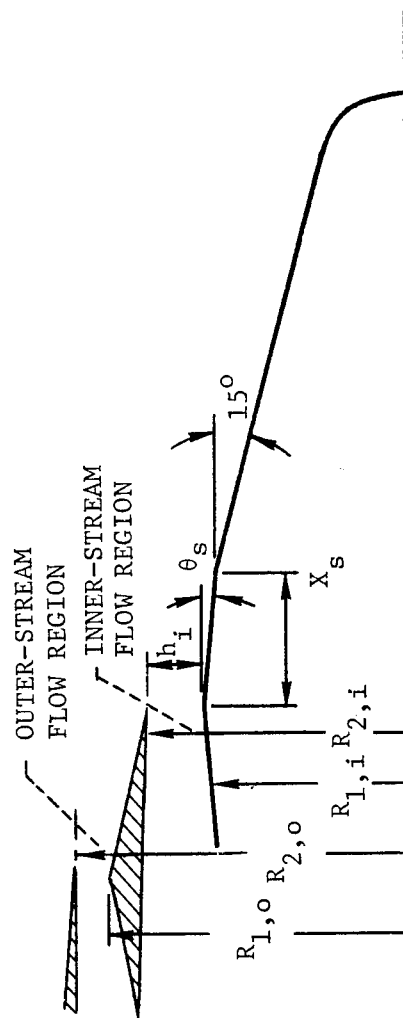
X_s distance from inner-stream exit to plug inflection point, cm
 θ angle from nozzle inlet axis, deg
 θ_s ramp angle of inner plug, deg
 ρ_{isa} ambient density at standard conditions, kg/m^3
 ρ_o outer-stream density, kg/m^3
 ω density correction exponent

REFERENCES

1. Howlett, R. A.; et al.: Advanced Supersonic Propulsion Study, Phase 2. (PWA-5312, Pratt and Whitney Aircraft; NAS3-16948) NASA CR-134904, 1975.
2. Szeliga, R.; and Allan, R. D.: Advanced Supersonic Technology Propulsion System Study. (R74AEG330, General Electric Co.; NAS3-16950) NASA CR-143634, 1974.
3. Williams, T. J.; Ali, M. R. M. H.; and Anderson, J. S.: Noise and Flow Characteristics of Coaxial Jets. J. Mech. Eng. Sci., vol. 11, no. 2, April 1969, pp. 133-142.
4. Olsen, W.; and Friedman, R.: Jet Noise from Co-Axial Nozzles Over a Wide Range of Geometric and Flow Parameters. AIAA Paper 74-43, Jan. 1974.
5. Stone, James R.: Interim Prediction Method for Jet Noise. NASA TM X-71618, 1974.
6. Jet Noise Prediction. Aerospace Information Report 876, SAE, July 1965.
7. Amiet, R. K.: Correction of Open Jet Wind Tunnel Measurements for Shear Layer Refraction. AIAA Paper 75-532, Mar. 1975.

TABLE I. - SUMMARY OF GEOMETRIC CHARACTERISTICS OF VARIATIONS TESTED FOR UNSUPPRESSED

COANNULAR NOZZLE WITH CENTER PLUG



Configuration	Step height, h_i , cm	Outer-stream radius ratio, $R_{1,o}/R_{2,o}$	Inner-stream radius ratio, $R_{1,i}/R_{2,i}$	Outer-stream area, A_o , cm^2	Inner-stream area, A_i , cm^2	Area ratio, A_o/A_i	Ratio of distance from inner-stream exit to plug inflection point to step height, X_s/h_i	Ramp angle of inner plug, θ_s , deg
1	2.63	0.902	0.673	71.3	111.3	0.65	18.75	2.9
2	1.61	↓	.800	↓	73.2	.97	0	15.0
3	.79	↓	.902	↓	37.9	1.88	0	15.0
4	1.61	.853	.800	116.4	73.2	.97	9.194	2.9
5	1.61	.926	.800	51.7	73.2	1.59	0	15.0
6	1.61	.926	.800	116.4	73.2	.71	0	15.0
7	.79	.853	.902	116.4	37.9	3.07	0	15.0

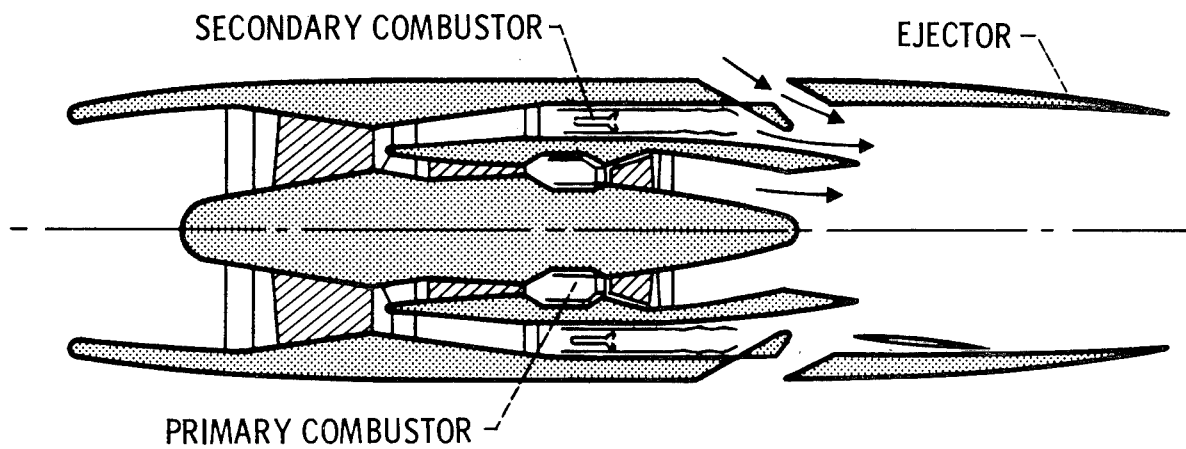


Figure 1.- Low-bypass turbofan concept - duct-burning turbofan (DBTF).

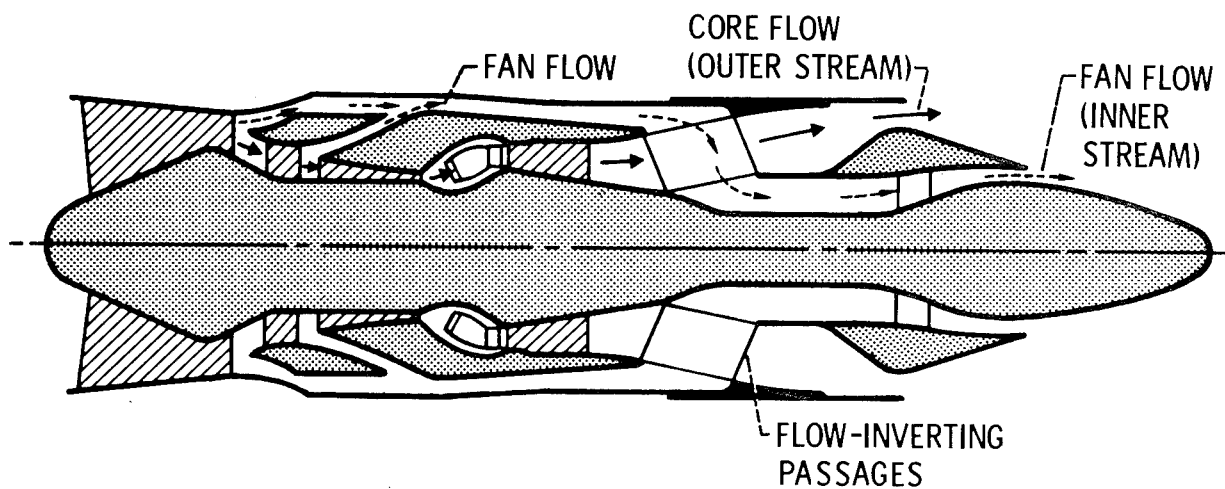
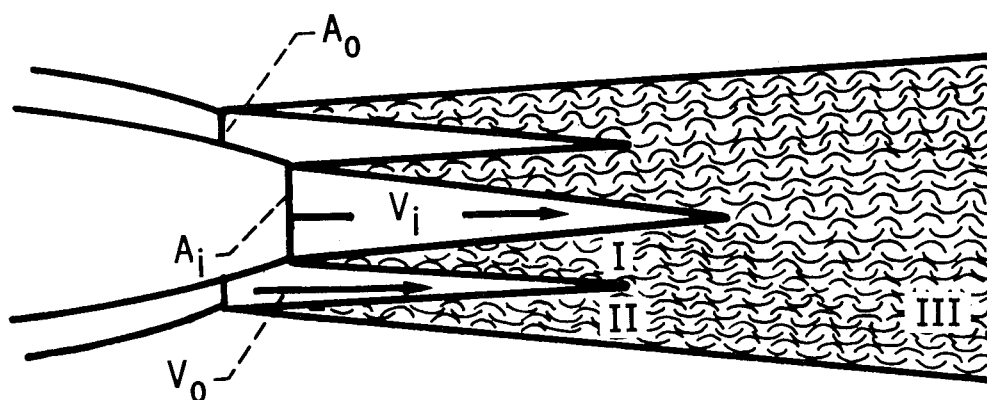


Figure 2.- Low-bypass turbofan concept - double-bypass, variable-cycle engine (VCE).



THREE NOISE-PRODUCING REGIONS:

I. INNER-STREAM/OUTER-STREAM MIXING

II. OUTER-STREAM/AMBIENT-AIR MIXING

III. MERGED-JETS/AMBIENT-AIR MIXING

Figure 3.- Noise-producing regions in coannular jets.

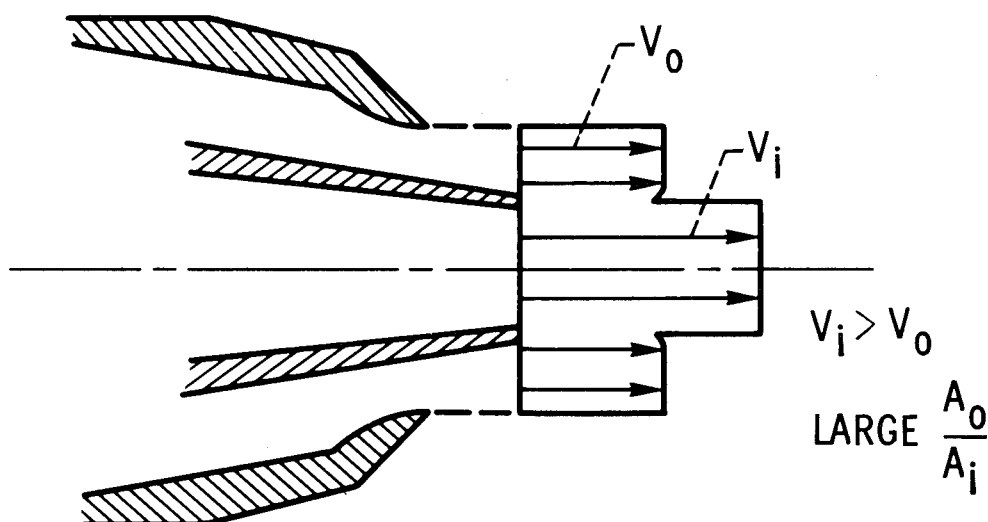


Figure 4.- Conventional coannular nozzles typical of high-bypass-ratio turbofans applicable to CTOL and STOL aircraft.

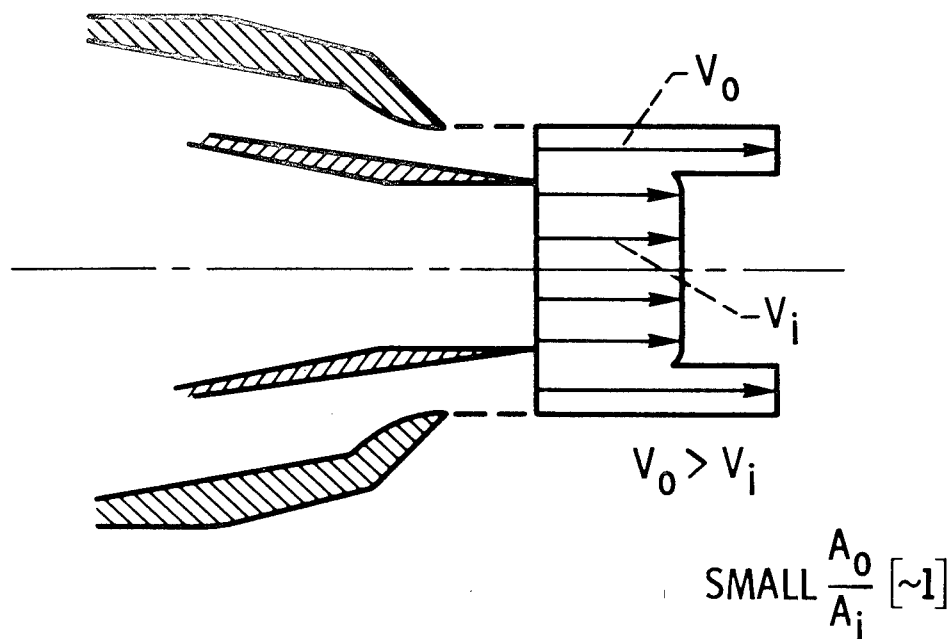


Figure 5.- Inverted-velocity-profile coannular nozzles typical of low-bypass-ratio turbofans applicable to supersonic cruise aircraft.

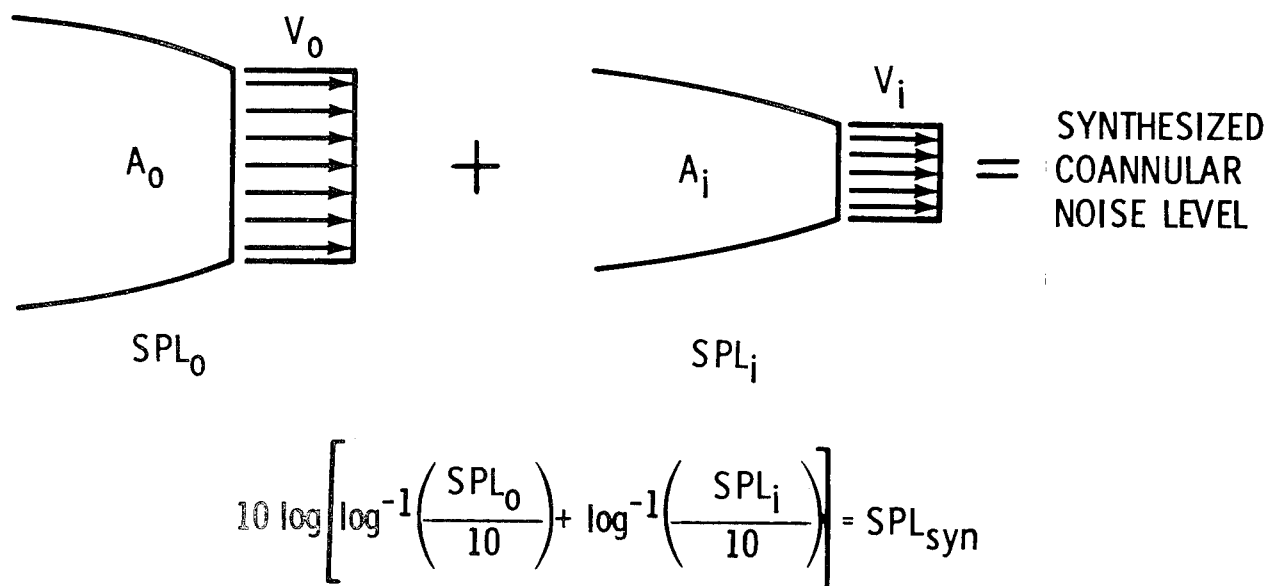


Figure 6.- Synthesis of coannular noise level (identical to recommended prediction procedure SAE AIR876, July 10, 1965).

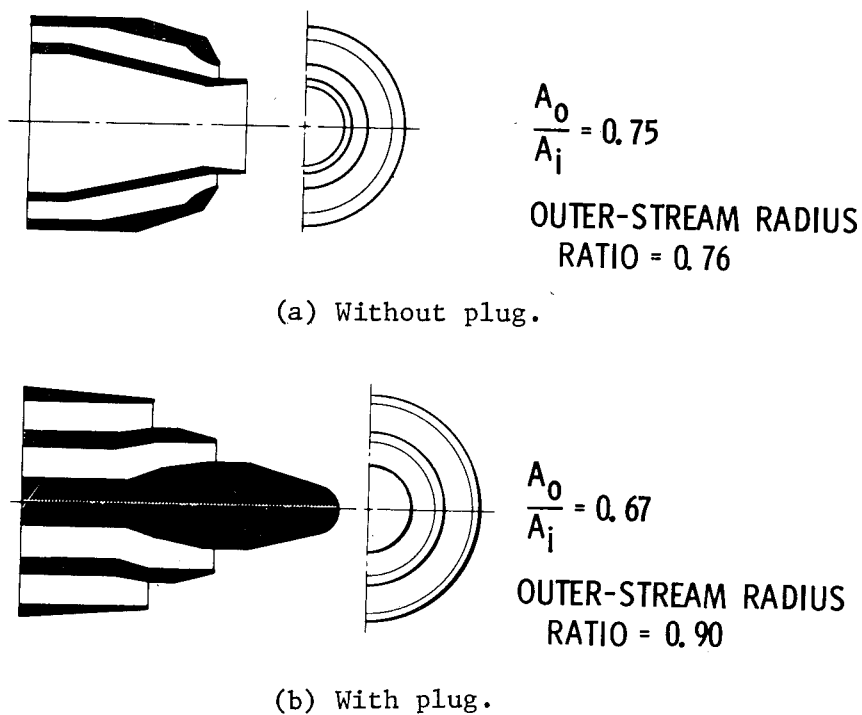


Figure 7.- Representative test configurations of inverted-velocity-profile unsuppressed coannular nozzles.

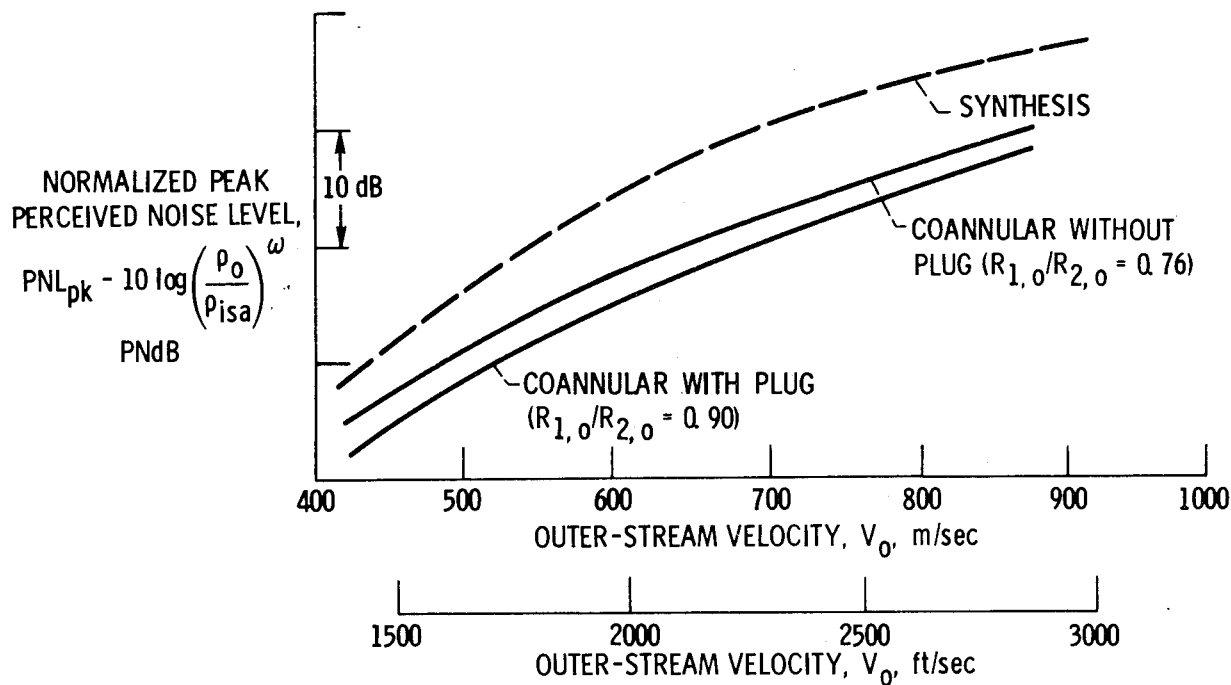


Figure 8.- Peak noise level as function of outer-stream velocity for typical inverted-velocity-profile unsuppressed coannular nozzles. Sideline distance, 649 m (2128 ft); altitude, 366 m (1200 ft); $V_o \geq 1.5 V_i$.

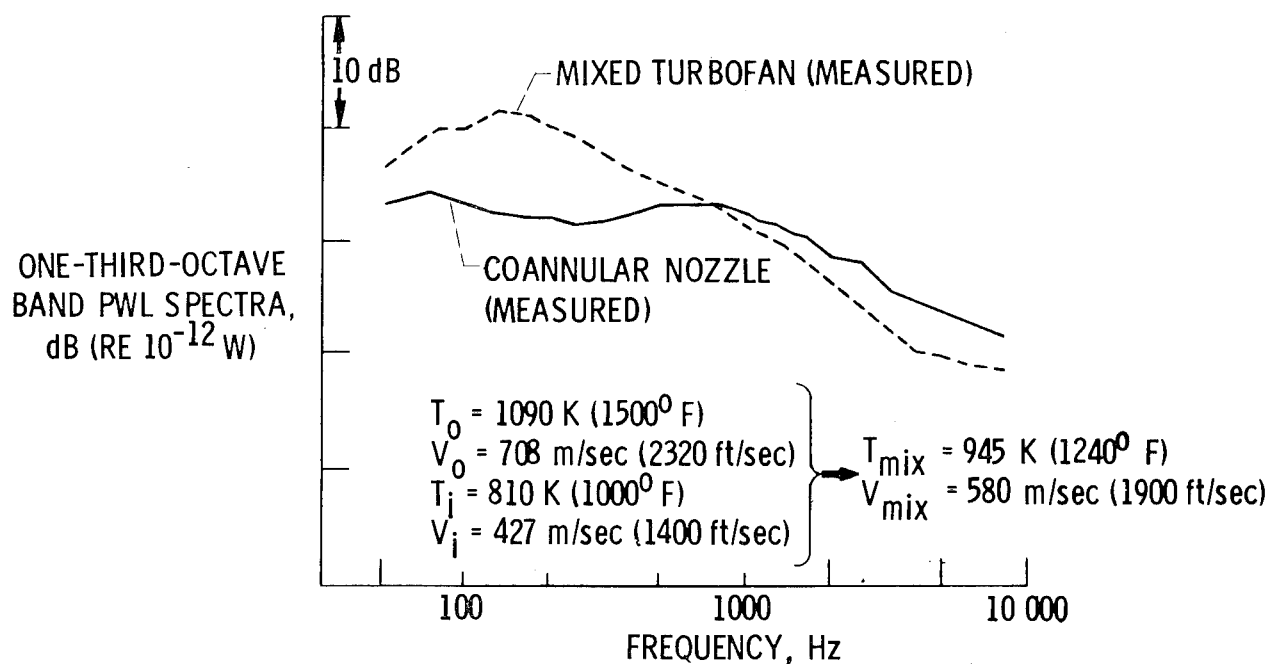


Figure 9.- Acoustic power spectra of unsuppressed inverted-velocity-profile coannular nozzle compared with equivalent mixed-turbofan single nozzle at equal flow and thrust conditions.

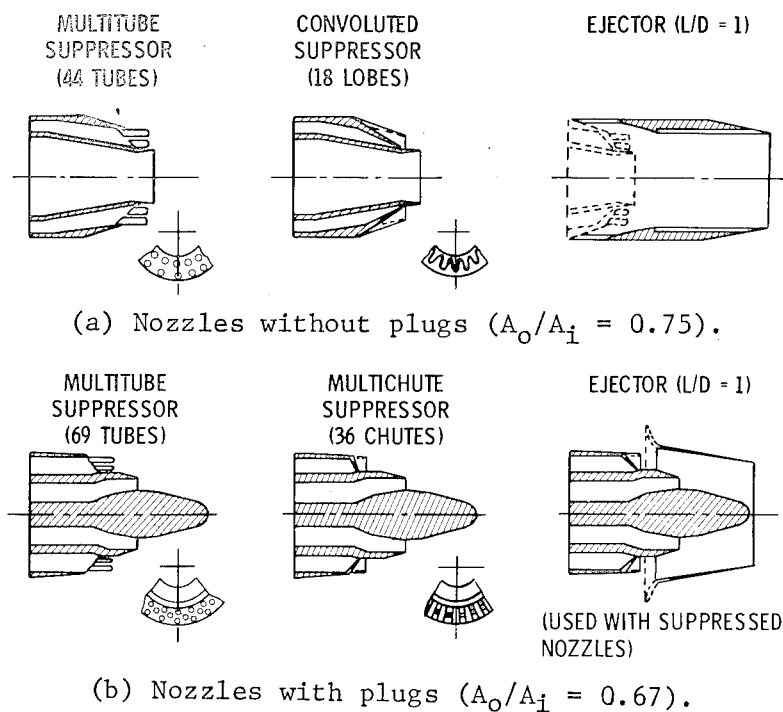


Figure 10.- Test configurations of inverted-velocity-profile coannular nozzles with outer-stream suppressors.

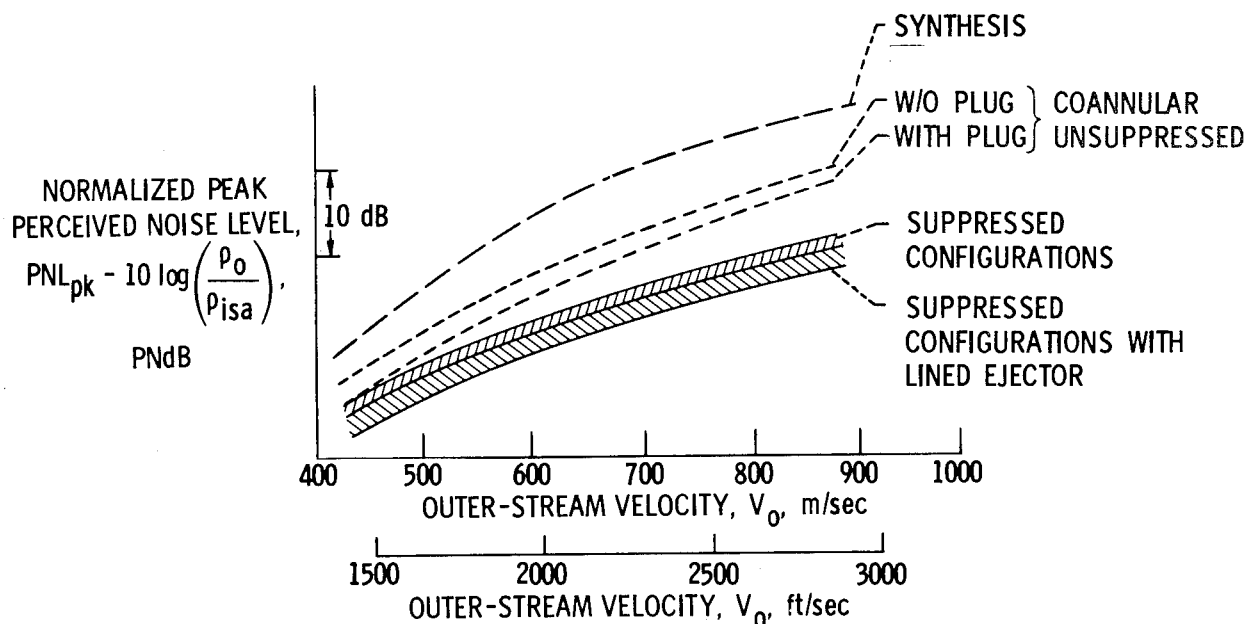


Figure 11.- Peak noise level as function of outer-stream velocity for typical inverted-velocity-profile coannular nozzles. Sideline distance, 649 m (2128 ft); altitude, 366 m (1200 ft); $V_o \geq 1.5 V_i$.

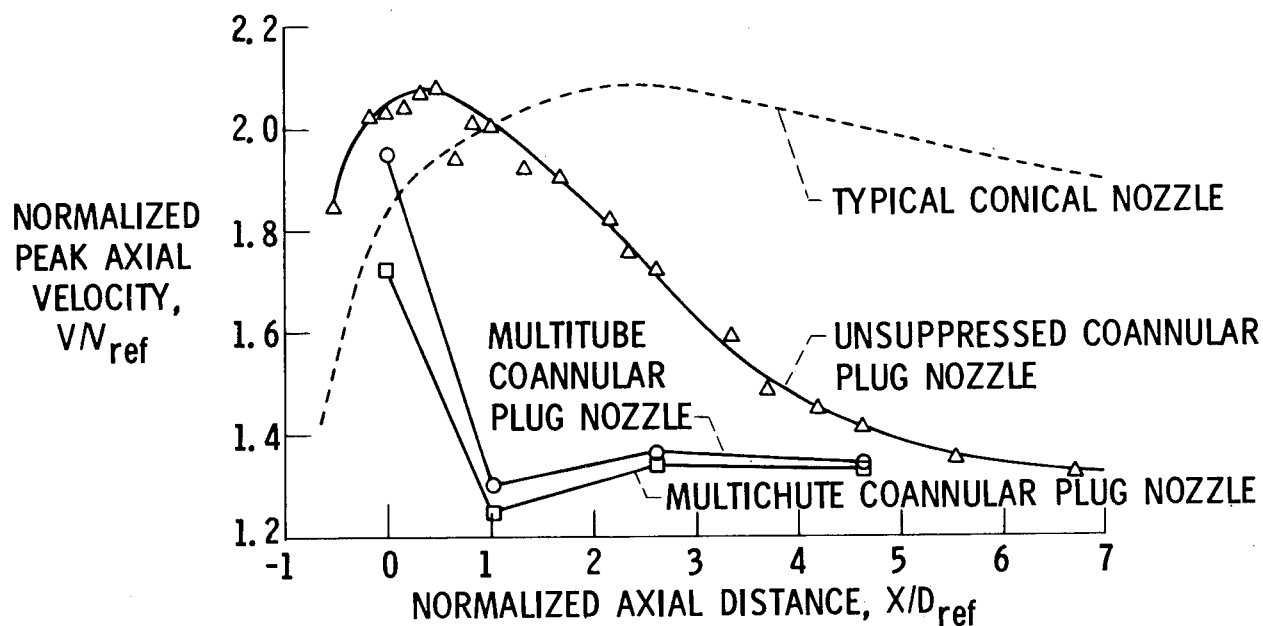


Figure 12.- Variation of peak axial velocity for suppressed and unsuppressed coannular plug nozzles. Total pressure ratio: inner stream, 1.5; outer stream, 2.86. Total temperature: inner stream, 812 K; outer stream, 784 K. Reference velocity, 304.8 m/sec (1000 ft/sec); reference diameter, 15.23 cm (6 in.).

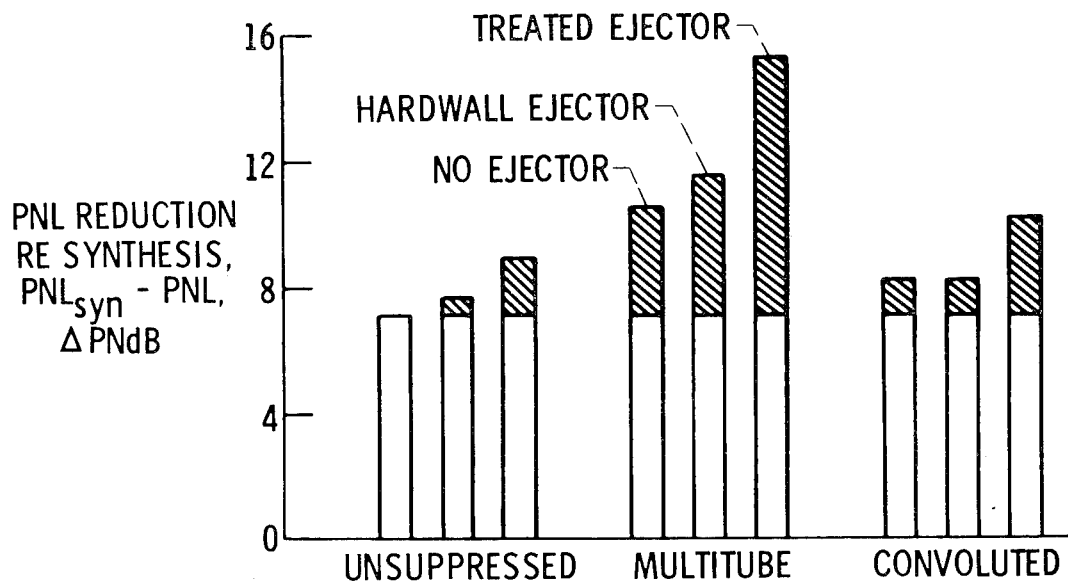


Figure 13.- Jet noise reductions relative to synthesized values for suppressed and unsuppressed coannular nozzles without plugs. Outer-stream velocity V_o , 714 m/sec (2340 ft/sec); inner-stream velocity V_i , 503 m/sec (1650 ft/sec).

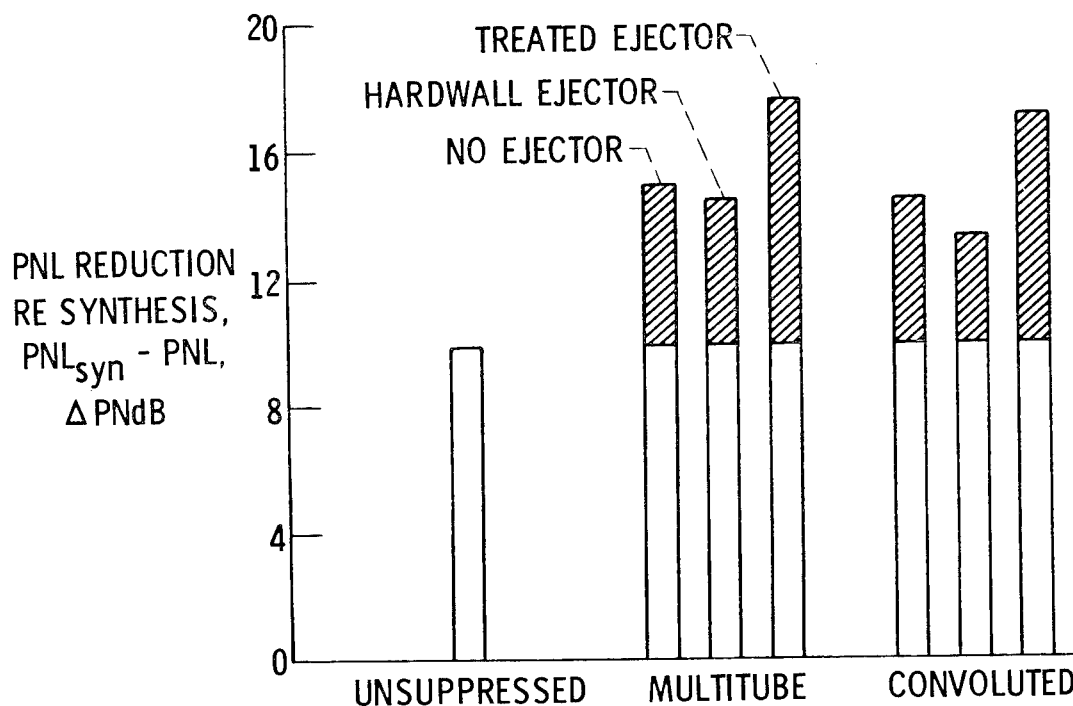


Figure 14.- Jet noise reductions relative to synthesized values for suppressed and unsuppressed coannular nozzles with plugs. Outer-stream velocity V_o , 732 m/sec (2400 ft/sec); inner-stream velocity V_i , 366 m/sec (1200 ft/sec).

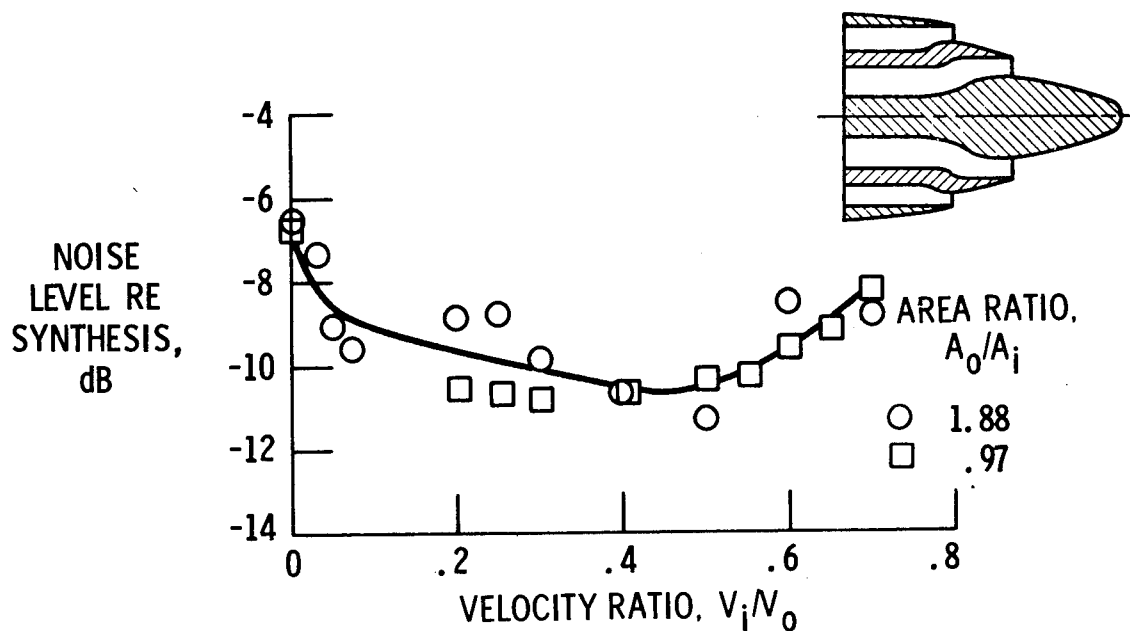


Figure 15.- Noise reduction of inverted-velocity-profile coannular nozzles as function of velocity ratio. Outer-stream radius ratio $R_{1,o}/R_{2,o}$, 0.90; outer-stream velocity V_o , 700 m/sec (2300 ft/sec); outer-stream temperature T_o , 958 K (1725° R); angle from nozzle inlet axis θ , 130°.

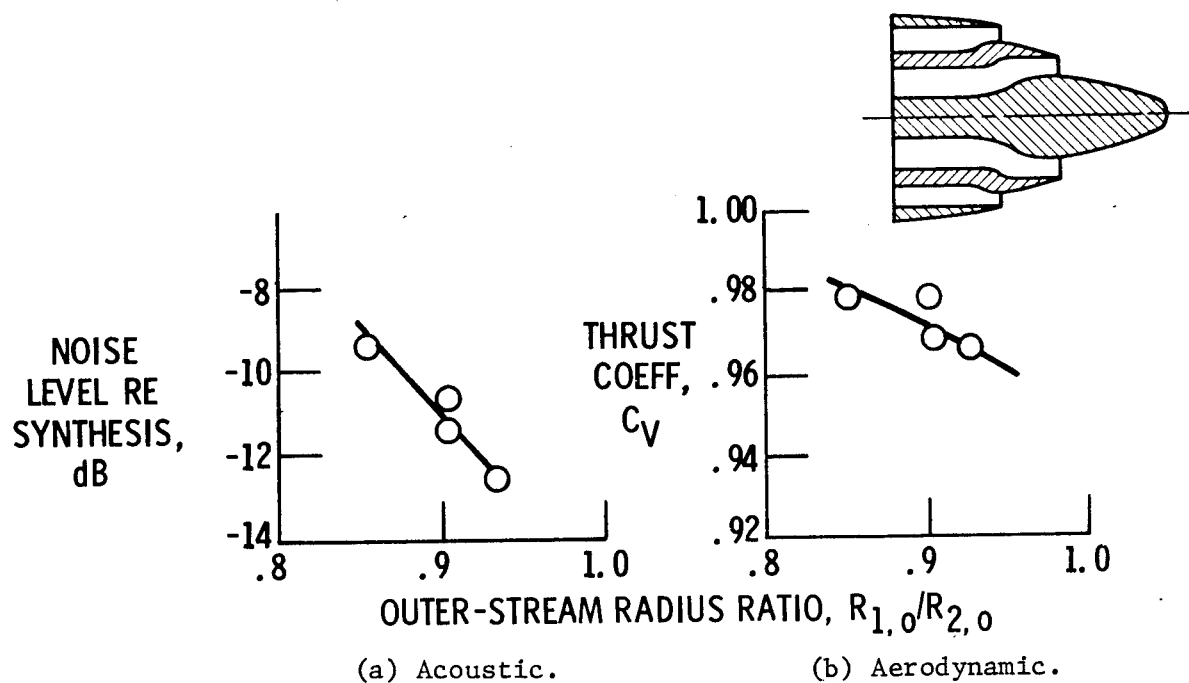


Figure 16.- Aeroacoustic performance of inverted-velocity-profile coannular nozzles as function of outer-stream radius ratio. $V_i/V_o = 0.5$.

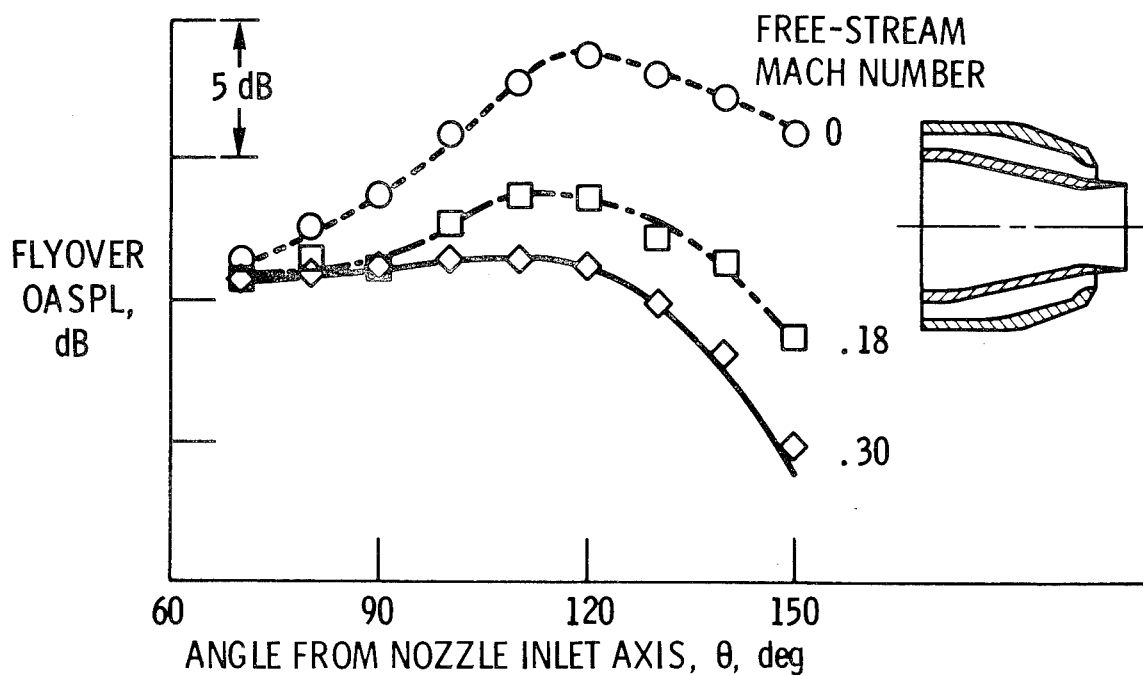


Figure 17.- Static and simulated flight directivities for inverted-velocity-profile coannular nozzles with subsonic outer streams (outer-stream pressure ratio, 1.8). $V_o/V_i \sim 1.5$.

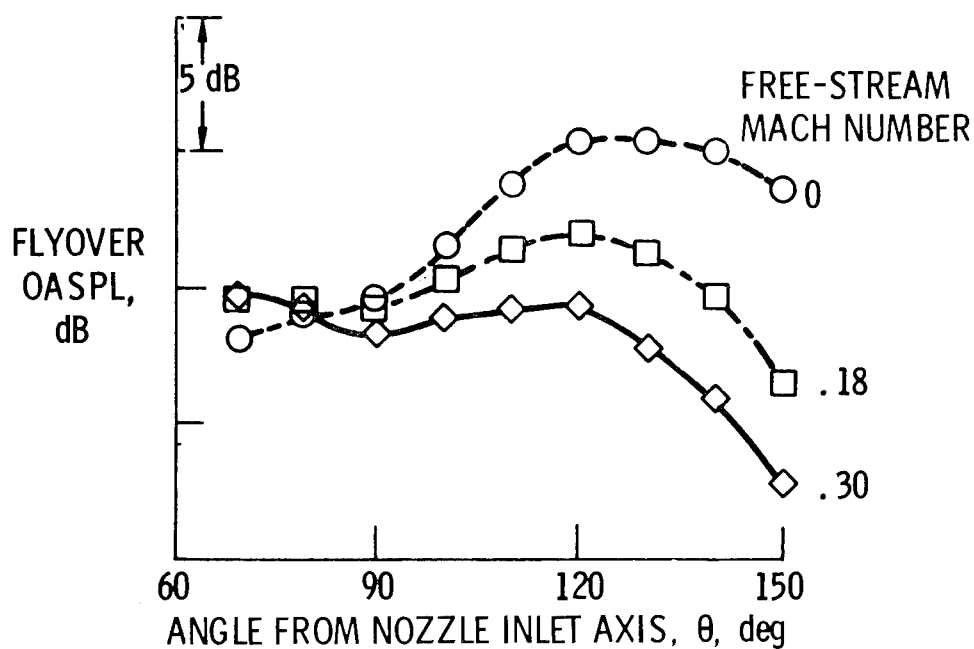


Figure 18.- Static and simulated flight directivities for inverted-velocity-profile coannular nozzles with supersonic outer streams (outer-stream pressure ratio, 2.5). $V_o/V_i = 1.9$.

COANNULAR NOZZLE NOISE CHARACTERISTICS AND APPLICATION TO ADVANCED SUPERSONIC TRANSPORT ENGINES

Hilary Kozlowski
Pratt & Whitney Aircraft Group

SUMMARY

Recent programs in the field of jet noise, sponsored by the NASA Lewis Research Center, have indicated that the variable stream control engines (VSCE) which are being considered for advanced supersonic cruise aircraft have inherent jet noise advantages over earlier engines. This characteristic is associated with the exit velocity profile produced by such an engine. The high velocity fan stream, on the outer periphery, is acoustically dominant while the primary stream is held to a low velocity and therefore contributes little to the overall noise.

Scale model tests have indicated low noise levels. Operation under static conditions, as well as in a relative velocity field (simulating take-off speeds) has indicated large reductions are available from the coannular nozzle and the VSCE. The inherently low levels of jet noise prompted changes in the cycle, which allowed an increase in the amount of augmentation incorporated in the fan stream, without exceeding the suggested noise guidelines, thereby allowing the use of a considerably smaller engine, with obvious vehicle advantages.

INTRODUCTION

The aero/acoustic evaluation of coannular nozzles associated with the VSCE filled a technology void which previously existed in the area of jet noise from such a configuration. Earlier work on coannular nozzles had generally been done with a cold stream surrounding a hot center stream. The VSCE as illustrated in figure 1 produces a hot, high velocity stream surrounding a low temperature, low velocity primary stream. Extensive scale model tests and analyses have indicated the coannular nozzle operating under such conditions produces a low level of jet noise. It is much quieter than predictions used in the early system studies. Under many conditions it is also quieter than comparable convergent nozzles. The results of these evaluations are presented in reference 1.

SYMBOLS

Values are given in SI units only. The measurements and calculations were made in U.S. Customary Units.

A	area $\sim \text{m}^2$
A*	throat area $\sim \text{m}^2$
C-D	convergent-divergent
Cv	actual thrust/ideal thrust
EPNdB	effective perceived noise level in dB
FAR36	Federal Aviation Regulations - Part 36
LBE	low bypass engine
OASPL	overall sound pressure level $\sim \text{dB}$
P	pressure
PNL	perceived noise level
r	radius
SPL	sound pressure level $\sim \text{dB}$
T	temperature $\sim ^\circ\text{K}$
V	velocity $\sim \text{mps}$
VSCE	variable stream control engine
W	mass flow
ρ	density
θ	angle from inlet centerline
ω	correlating exponent

Subscripts:

a	ambient
ex	exit
f	fan stream
i	inner
o	outer
p	primary stream
t	total
∞	free stream

BASIC COANNULAR NOZZLE CHARACTERISTICS

The scale model tests simulating the VSCE in the take-off mode employed basic coannular nozzle configurations as illustrated typically in figure 2. The models used in the static phase of the study were approximately 1/10 of full scale size. In addition, an equivalent convergent nozzle was included to serve as a reference configuration.

The basic advantage of the coannular nozzle is illustrated in figure 3. The noise spectra of a coannular nozzle is compared to a convergent nozzle having the same area as the fan stream of the coannular nozzle, and operating at the same conditions. The primary stream in the coannular arrangement has a low velocity, and is therefore not acoustically significant itself. As illustrated, there is a very large, broadband reduction in sound pressure level associated with the coannular nozzle. A portion of this reduction is due to the presence of the primary stream, as evidenced by the increase in the sound pressure level when the primary stream was turned off (resulting in the annular configuration). The remainder of the original reduction is associated with the interaction of the fan stream with the ambient air. This therefore illustrates the inherent benefit of the coannular nozzle, in which the dominant noise stream is located near the outer periphery of the nozzle. The physical phenomenon causing the noise reduction is the rapid velocity decay produced in the coannular nozzle. This is illustrated in figure 4. The convergent nozzle velocity decays at a relatively slow rate and the region generating the peak noise (at the end of the potential core) is at a relatively high velocity. The coannular nozzle velocity however, decays at a very rapid rate, since the fan stream is being acted upon by both the outer ambient air and the primary flow in the core. The region of the plume from the coannular nozzle which is generating the peak noise is therefore at a low velocity and therefore produces a low noise level.

The use of a coannular nozzle does not introduce any significant thrust losses relative to a convergent nozzle. The aerodynamic performance of the coannular nozzle at static conditions is compared to that of the convergent nozzle in figure 5, where the average measured performance levels of the configurations are illustrated over a range of pressure ratios. The performance is presented in terms of mass averaged total pressure ratio so that both nozzles can be compared. The difference between the convergent nozzle and the coannular nozzle is due to the presence of a convergent-divergent nozzle in the primary stream of the coannular configuration, as well as the increased friction associated with the coannular nozzle. The primary nozzle incorporated a C-D section to reflect the design requirements of high flight speeds associated with a supersonic cruise vehicle while assuming a fixed geometry nozzle. The C-D nozzle ($A_{ex}/A^* = 1.1$) is overexpanded at the low primary pressure ratio (1.53) simulated in this series of tests. P&WA SCAR study engine designs employ variable geometry in the primary nozzle which will eliminate these overexpansion losses. The frictional losses are due to additional wetted area with the coannular nozzle. Therefore, the only inherent difference between the two nozzles is a small amount of friction, amounting to approximately 0.5% at take-off conditions.

The influence of fan stream velocity on the reduced noise levels of a coannular nozzle is illustrated in figure 6. Actual coannular nozzle test data, scaled 10X, and adjusted to a sideline distance of 648.6m, are compared to the original prediction (i.e., coannular synthesis) and to data for a "mixed flow" configuration. The synthesis represents the early method of predicting coannular jet noise. In this method, the noise level of the coannular nozzle is said to be equal to the sum of the two streams analyzed independently of each other, as if each was a convergent nozzle operating at the appropriate conditions. The synthesized perceived noise level of the coannular nozzle is defined as:

$$\text{Perceived noise level (PNL)} = 10 \text{ Log } \left[\text{Log}^{-1} \left(\frac{\text{PNL}}{10} \right)_p + \text{Log}^{-1} \left(\frac{\text{PNL}}{10} \right)_f \right]$$

As illustrated in figure 6, the actual data are well below the synthesized level. The difference occurs because the synthesis approach ignores the shape of the jet and any interactions between the streams. It should be noted that this synthesis method was commonly used in early cycle and system studies.

The noise of the "mixed flow" nozzle was obtained from convergent nozzle test data at conditions which would exist if the two streams of the coannular nozzle were ideally totally mixed. It is presented to serve as another reference configuration in order to enhance the understanding of the coannular nozzle phenomena. In many cases, especially at high velocities, the coannular nozzle is quieter than the "mixed flow" convergent nozzle. However, the advantages of the coannular nozzle are dependent on both the fan and primary conditions. The difference between a coannular nozzle arrangement and the equivalent "mixed flow" convergent nozzle is illustrated typically in figure 7 over a range of conditions. The advantage of the coannular arrangement diminishes (for the same variation in fan velocities) as the primary velocity is decreased. When either stream has a very low velocity it would be beneficial from an acoustic viewpoint to mix the two streams producing one larger, but much lower velocity stream. However, for the engines projected for supersonic flight application, high velocities are desired in both streams, and under these conditions the coannular arrangement offers a distinct advantage.

The effect of an ejector on the peak PNL of the coannular nozzle is shown in figure 8. A slight (< 1 dB) reduction was obtained by adding a hardwall ejector. The presence of acoustical treatment in the ejector produced a small amount of additional suppression. Across the test range, 2 PNdB or less total suppression was obtained. Since the coannular nozzle results indicated that the high frequency noise was generated in the fan annular exhaust near the nozzle exit and the low frequencies in the mixed jet downstream, some shielding suppression of the high frequency noise was expected by addition of the ejector, and further reduction is consistent with the addition of acoustic treatment.

The peak PNL of the basic coannular nozzle has been correlated in terms of fan stream velocity and the fan-to-primary velocity ratio, as illustrated in figure 9. The noise level has been normalized for the effects of density by application of the factor $10 \log (\rho_f / \rho_a)^\omega$, where ω is based on the information presented in reference 2. The perceived noise level generally decreases as the velocity ratio is increased from 1.0 to 2.0. An increase in the velocity ratio beyond 2.0 is not beneficial.

Very recent model tests in a relative velocity environment have indicated that the advantages of the coannular nozzle, as identified in the earlier static evaluations, are maintained at take-off airspeeds. The impact of take-off speeds on the overall sound pressure level (OASPL) is illustrated in figure 10. The actual coannular nozzle data at both static and take-off conditions ($V_\infty = 104$ mps) are presented along with the synthesized levels at each condition. The synthesized OASPL values are based on convergent nozzle test data, using the procedure described earlier (for PNL). The difference between the actual data and the synthesized levels, observed at static conditions, is essentially unchanged at take-off speeds. In other words, the coannular nozzle advantages are not attenuated by the introduction of take-off flight speed. At take-off speeds, both the synthesized values (based on convergent nozzle data) and the actual coannular data are considerably lower than the static levels since in general, the free stream velocity (V_∞) weakens the noise generating properties in the jet exhaust.

APPLICATION TO CYCLE STUDIES

The data generated under these NASA sponsored programs have allowed predictions of jet noise to be made, with improved accuracy, for the advanced engines being considered for application to supersonic cruise vehicles. The noise levels for an advanced VSCE are presented in figure 11 over a range of thrust at both static and take-off conditions. The reduction in peak perceived noise level, going from static to take-off conditions, is essentially constant as engine thrust is varied. The relative velocity effect seen with conventional subsonic jets would be expected to produce a decreasing reduction as thrust is increased (i.e., as exit velocity is increased). However since the shape of the jet noise spectra of a VSCE changes considerably with thrust, there are counteracting effects. At high thrust levels the jet noise is dominated by the low frequency contribution generated in the downstream plume. At the low thrust levels, the significance of shock noise (which is not reduced in-flight) increases. The net effect of these changing spectra, of this VSCE, is a nearly constant reduction in static noise levels, at all thrust settings. The anticipated noise level for a comparable low bypass ratio engine (LBE) is also illustrated. This engine has acoustic characteristics which are essentially the same as a turbojet. The impact of take-off speed is approximately the same as the VSCE, but the overall level is considerably higher. In this comparison, it should be noted that in both cases the engines are analyzed using only the basic nozzle arrangement and do not include secondary nozzle (e.g., ejector) influences. It is however expected that an acoustically treated ejector would be more beneficial to the VSCE since high frequency noise, which is amenable to treatment, tends to be dominant in the spectra of the VSCE coannular nozzle.

The overall improvements that the new advanced VSCE offers over the first generation unsuppressed turbojet engines are illustrated in figure 12. The same aircraft size and technology level was assumed for both cycles, with the basic variation in noise level with range due to engine sizing. The acoustic advantages of the coannular nozzle in the VSCE provide an 8 EPNdB reduction in sideline jet noise, while the cycle differences and component technology levels produce a 25% improvement in range capability. The variation in the range with the VSCE, at a given noise level, is associated with programmed throttle scheduling in combination with the detailed noise analysis of the system, involving ground attenuation and engine shielding assumptions. The band associated with the first generation turbojet engines reflects engine scaling uncertainties and cycle options. The noise prediction for the turbojet engines is based on the SAE procedure presented in reference 2. The VSCE noise levels are based on the parametric scaling relationships for coannular jet noise developed from the model test program conducted by P&WA. The flight effects for both sets of engines are based on procedures proposed to the SAE in reference 3. The latter procedure was employed, since the very recent relative velocity data generated by P&WA has not yet been incorporated into the computerized prediction system.

TECHNOLOGY REQUIREMENTS

In order to explore the full potential of the coannular nozzle, a program sponsored by the NASA Lewis Research Center is currently underway to systematically identify the interactions between basic nozzle geometry and aero/acoustic characteristics. As illustrated in figure 13 the radial placement of the fan stream (i.e., r_{ff}/r_{of}) will be explored since it is felt this is an important variable in the noise reduction process. In addition, a centerbody will be introduced in the primary streams of several configurations, thereby altering in another manner the interaction between the two streams.

This will be combined with the earlier information, which centered on a few selected nozzle configurations, to formulate an aero/acoustic design system. This design system will then allow take-off noise considerations to be incorporated, in a consistent, quantitative manner, into the overall design process of an exhaust system suitable for powering a supersonic aircraft.

The next logical step in the study of coannular nozzles for the VSCE is a large scale exhaust system evaluation to confirm the aero/acoustic characteristics observed with laboratory models. As illustrated in figure 14, a technology test bed could be obtained by modifying an existing engine to resemble a VSCE. A comparison of the exhaust properties from the VSCE and those obtainable with the test bed engine is presented in table 1. As indicated, the temperatures and velocities of interest can be well covered, allowing the demonstration of not only the nozzle characteristics but also the duct burner emission characteristics.

Such a program would pave the way for a more complete exhaust system development program required for a successful aircraft.

CONCLUSION

The NASA sponsored programs to date, on the aero/acoustic characteristics of the coannular nozzle as incorporated in the VSCE, have greatly improved the acoustic outlook for future supersonic aircraft. The results of these technology programs have had a major impact on the design of the powerplant and have allowed substantial improvements in overall supersonic vehicle characteristics. It is important to the supersonic technology program to continue this activity and demonstrate these acoustic benefits in full scale, thus paving the way for a successful development program.

REFERENCES

- (1) Kozlowski, H. and Packman, A.B.: Aero-Acoustic Tests of Duct-Burning Turbofan Exhaust Nozzles, Final Report, NASA CR-2628, 1977.
- (2) Society of Automotive Engineers Inc., "Proposed ARP 876 Gas Turbine Jet Exhaust Noise Prediction:", SAE Committee Correspondence, April 1, 1975.
- (3) Bushell, K.W., "Static to Flight Jet Noise Data for Presentation to the SAE A21 Jet Noise Subcommittee Meeting, October 2, 1974," SAE Committee Correspondence, 25 September 1974.

TABLE 1

COMPARISON OF VSCE AND TEST BED ENGINE PARAMETERS

	VSCE	Test Bed
T_{tf}	444 – 1700°K	444 – 1700°K
T_{tp}	811 – 978°K	756 – 922°K
V_f	457 – 945 mps	457 – 884 mps
V_p	366 – 610 mps	457 – 610 mps

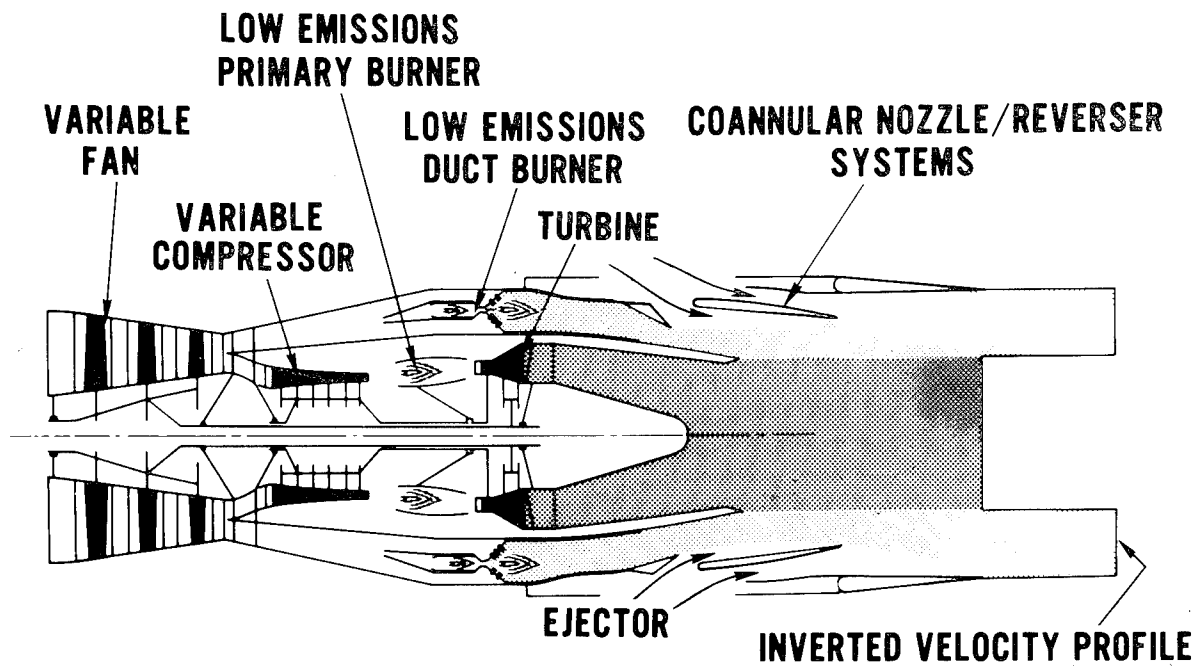


Figure 1.- Variable stream control engine.

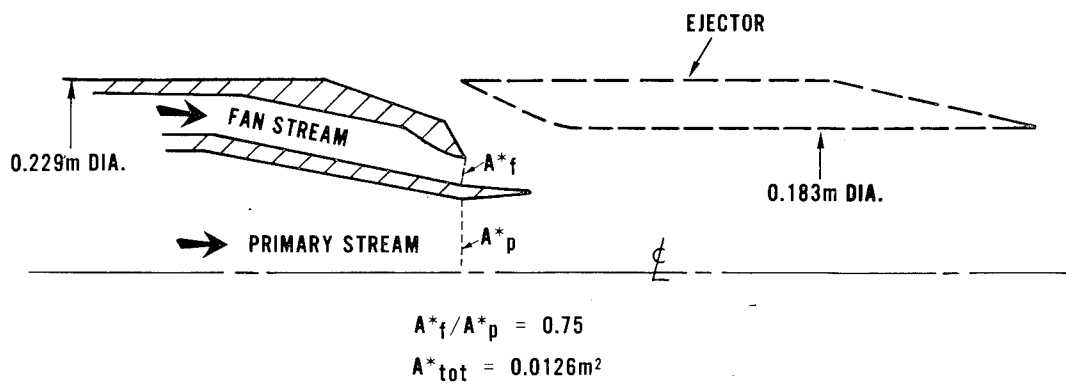


Figure 2.- Coannular nozzle model.

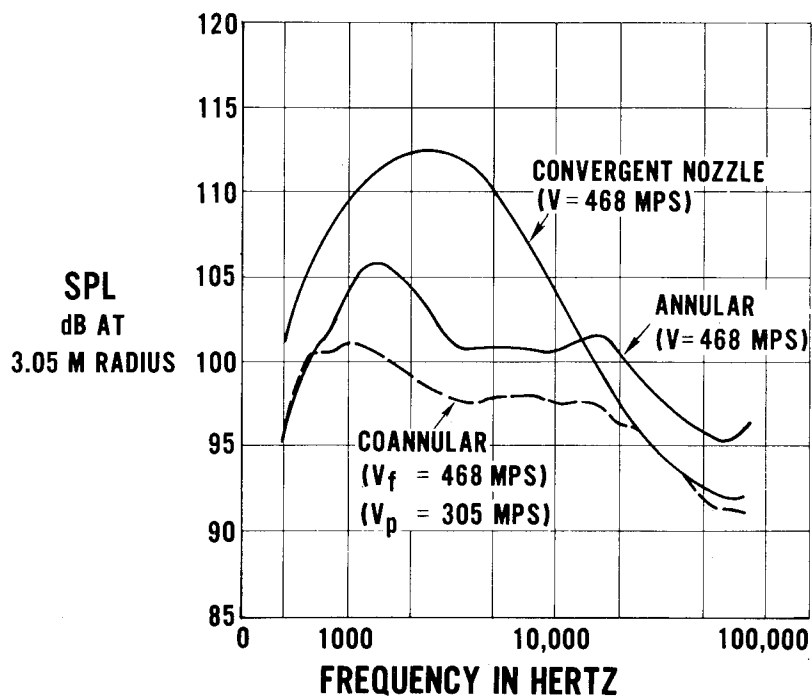


Figure 3.- Coannular benefit.

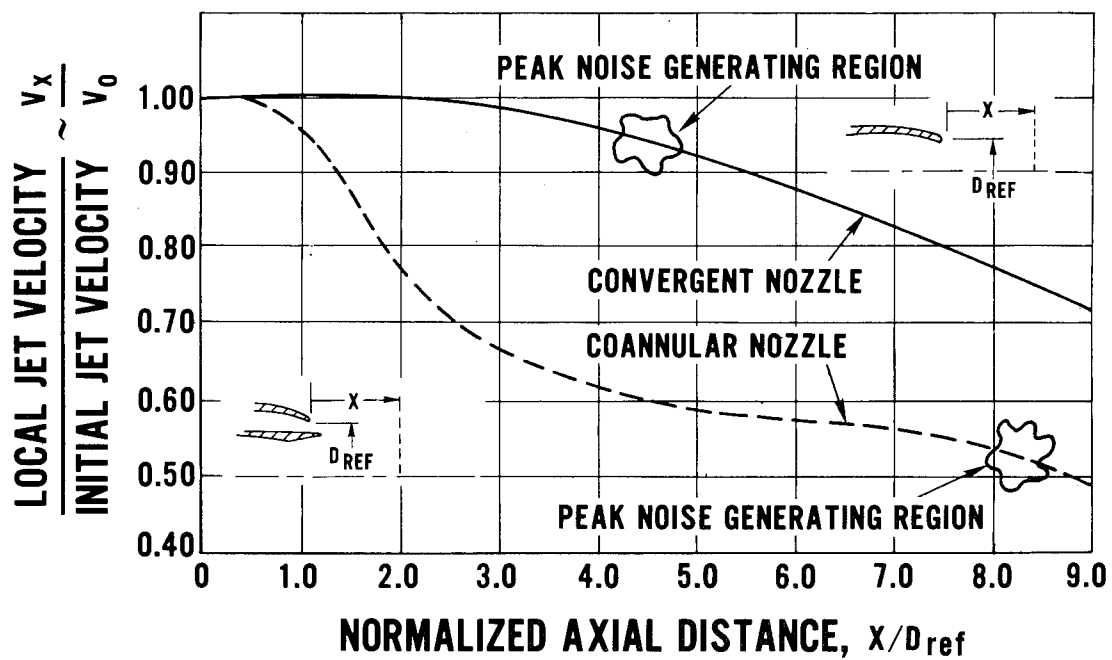


Figure 4.- Nozzle mixing characteristics.

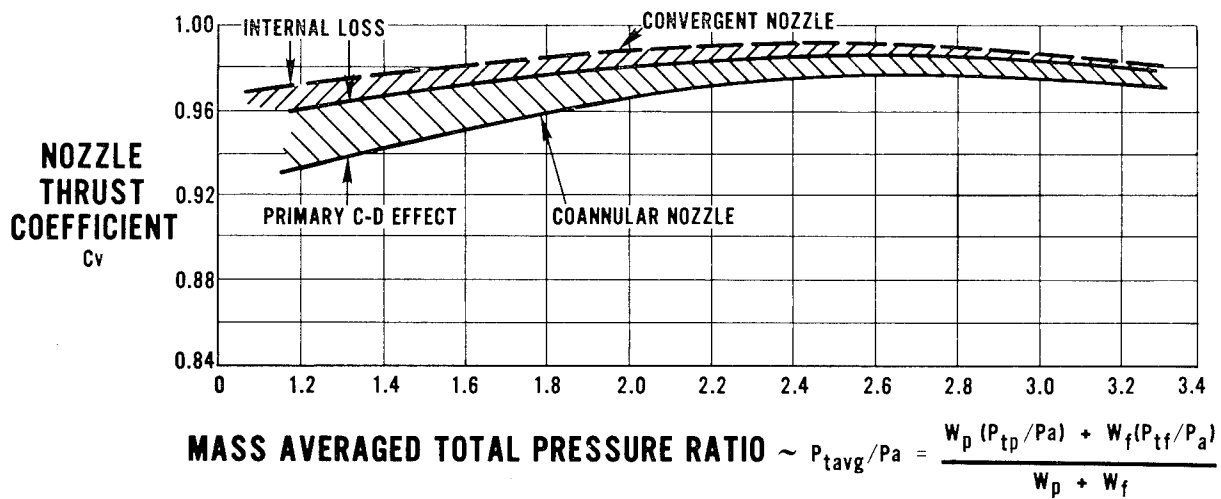


Figure 5.- Aerodynamic performance comparison.

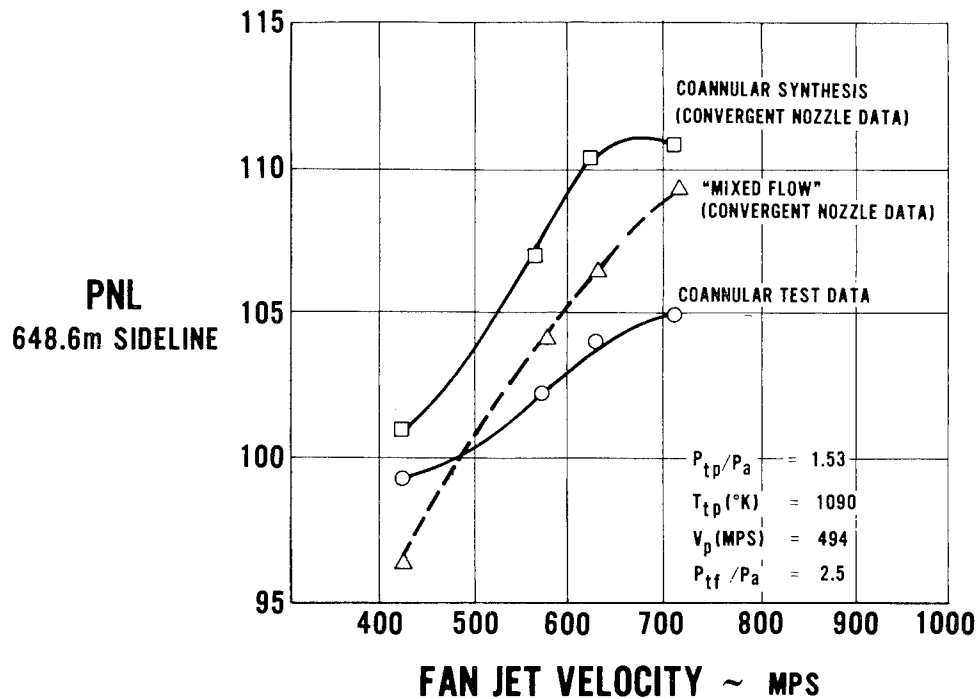


Figure 6.- Coannular nozzle characteristics.

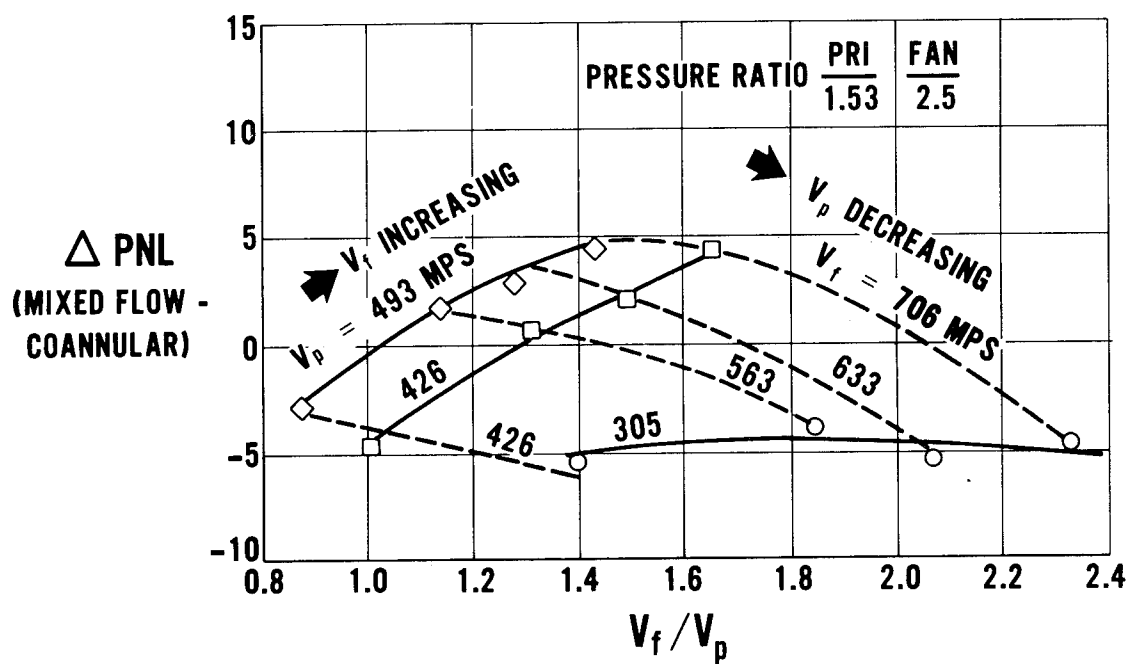


Figure 7.- Impact of operating conditions on jet noise comparison.

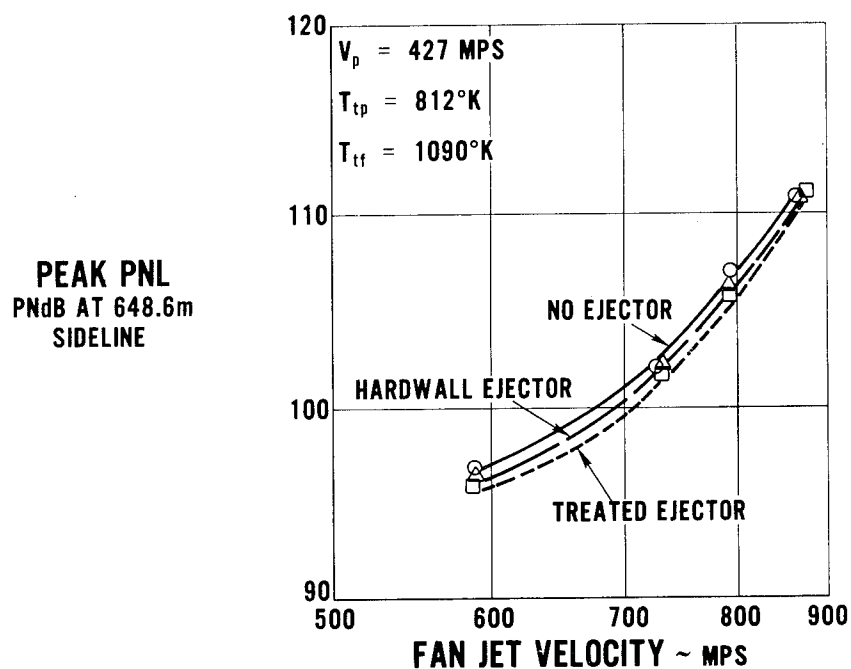


Figure 8.- Effect of ejector on peak PNL.

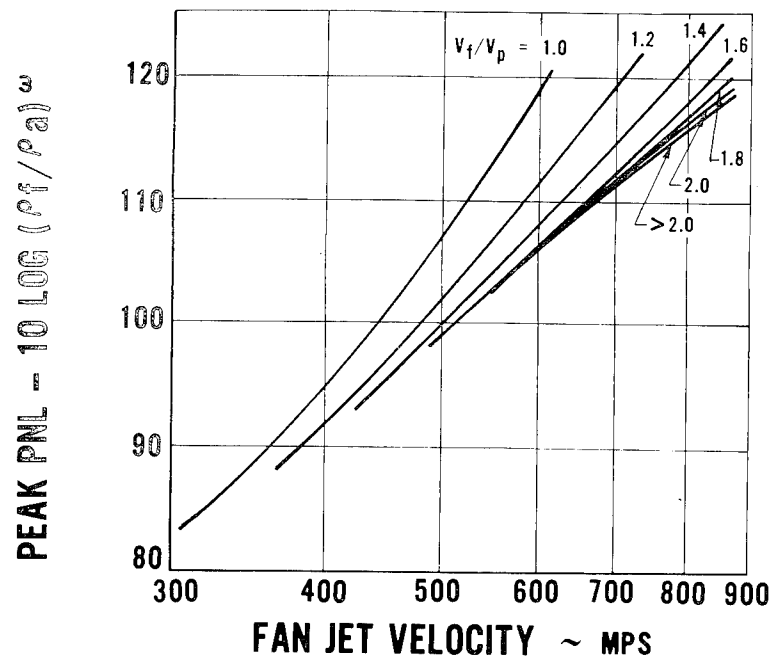


Figure 9.- Correlation of peak PNL.

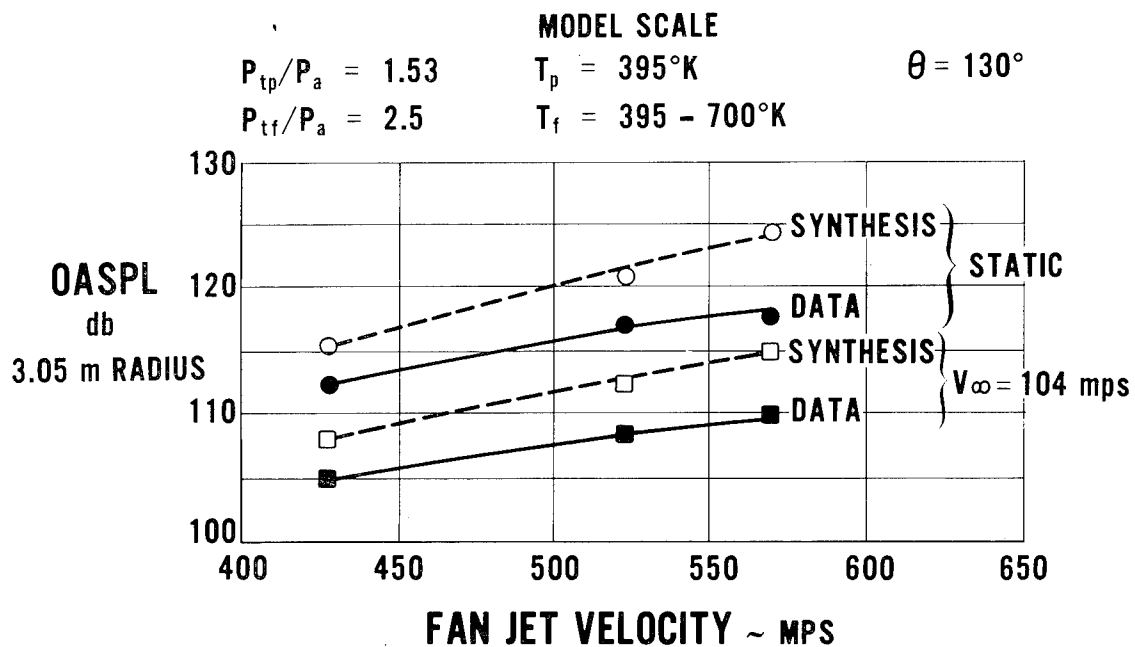


Figure 10.- Effect of take-off speed on OASPL of coannular nozzle.

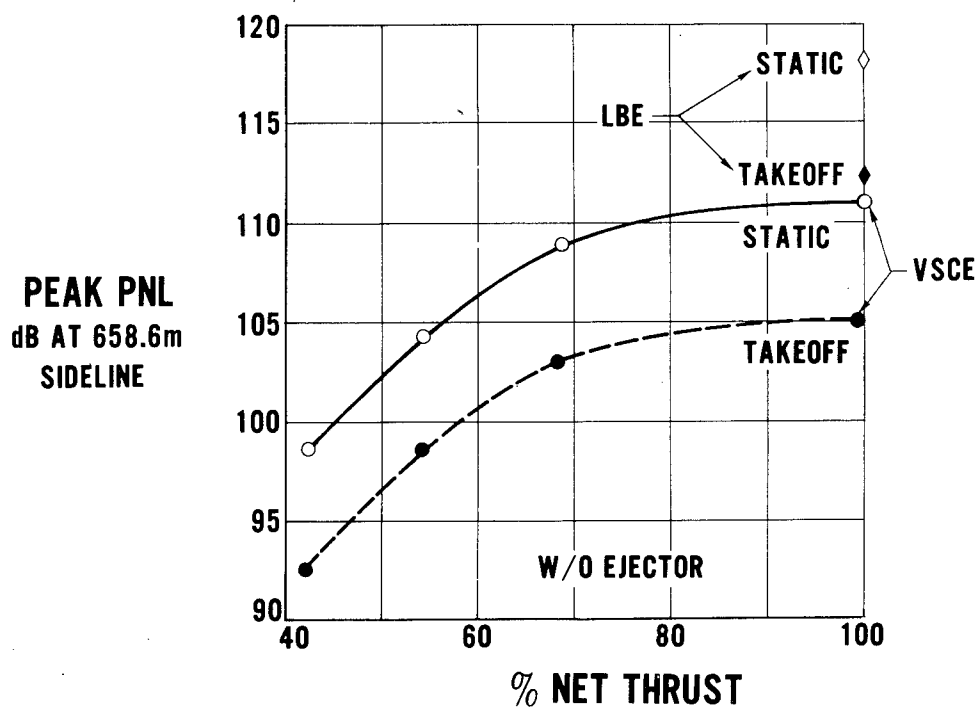


Figure 11.- Predicted peak PNL.

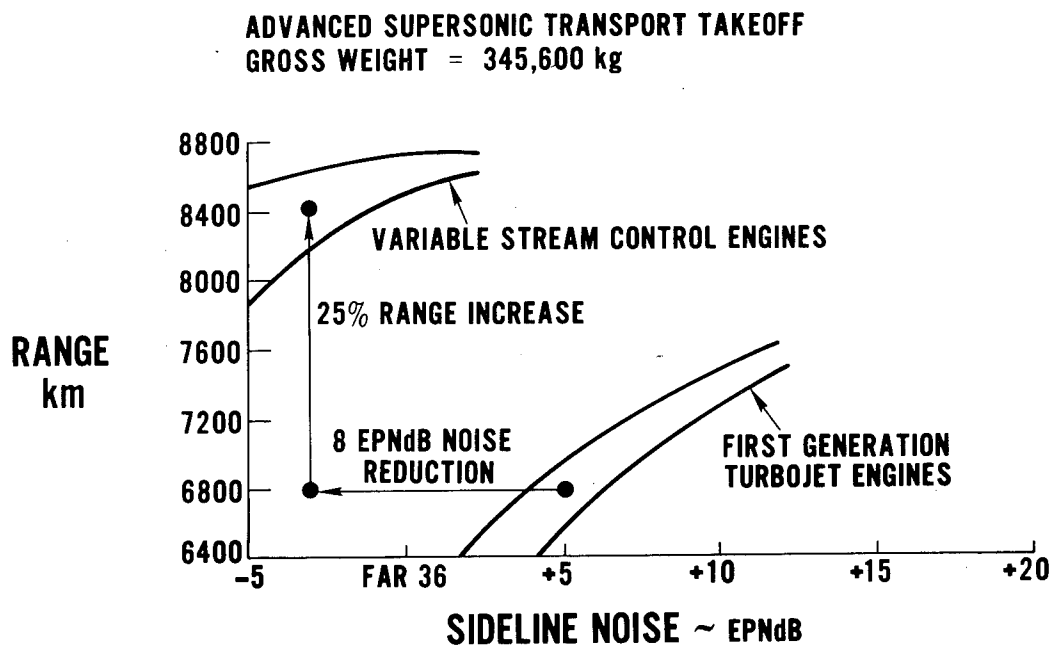


Figure 12.- Potential impact of advanced supersonic technology on aircraft range and noise.

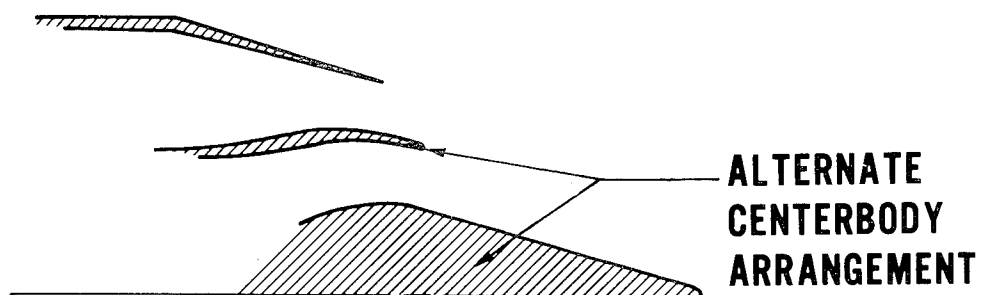
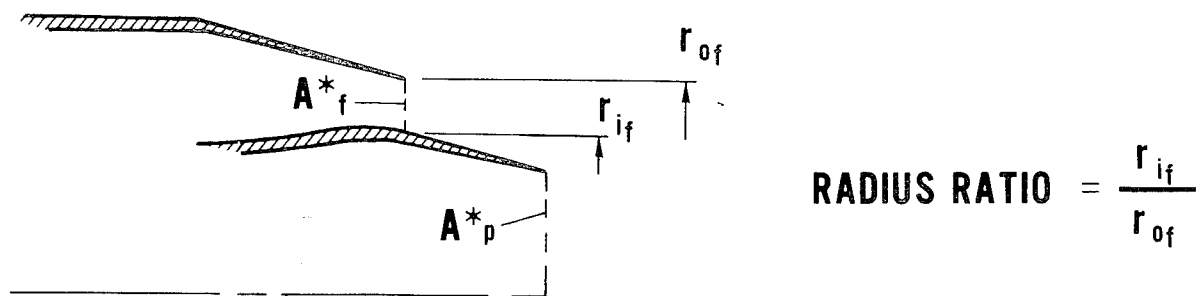


Figure 13.- Variations planned to extend technology base.

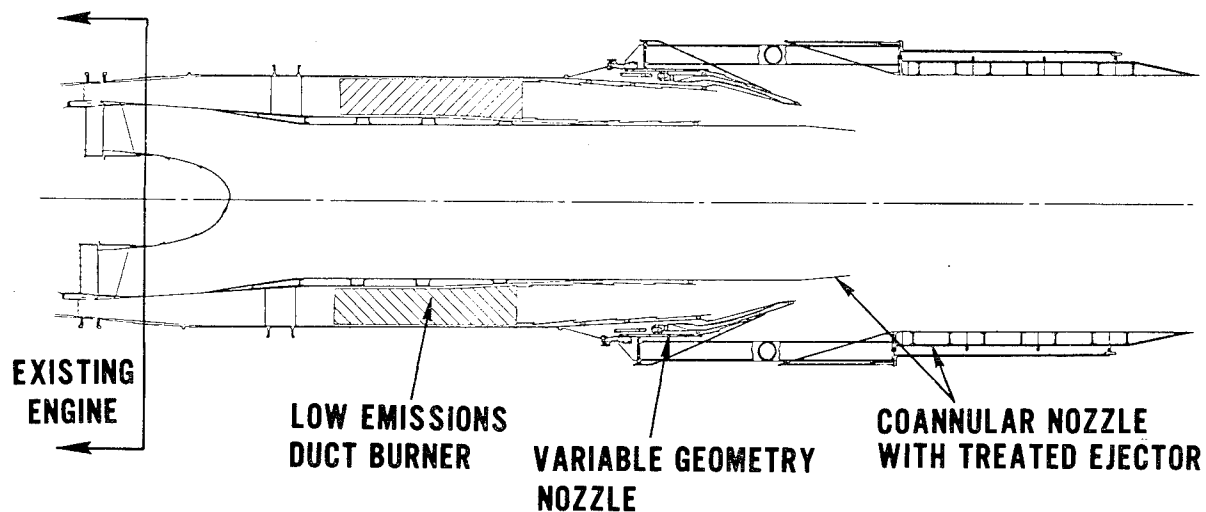


Figure 14.- Critical technology test bed program.

COANNULAR PLUG NOZZLE NOISE REDUCTION AND IMPACT

ON EXHAUST SYSTEM DESIGNS

Robert Lee
Aircraft Engine Group
General Electric Company

INTRODUCTION

Finding a satisfactory and practical method for reducing the noise generated by high velocity jets has confronted engine designers and acoustics workers alike for the past fifteen years. Figure 1 shows some of the jet noise suppressor configurations that have been investigated by General Electric in the past. With the exception of the early CJ-805 daisy suppressor nozzle which found successful application on the Convair 990 airplane, the others were developmental hardware at different stages of the effort in the past eight years - all aiming at potential supersonic cruise aircraft applications. We are happy to report here that some further significant progress has been made as the result of work supported by NASA and FAA in the past two to three years. This work pertains to the concept demonstration and scale model testing of coannular plug nozzles with inverted velocity profile, and to the preliminary study of its application to advanced variable cycle engines (VCE) appropriate for supersonic cruise aircraft.

COANNULAR PLUG NOZZLE NOISE INVESTIGATIONS AT GENERAL ELECTRIC

Two programs were carried out under the sponsorship of NASA (Lewis) from 1973 to 1976. The first program* aimed mainly at the investigation of multi-element suppressors added to the outer stream of the coannular plug nozzle for possible application to duct burning turbofan cycle. It included the study of two baseline (unsuppressed) coannular nozzles. Two configurations tested in this program are shown in figure 2. The second program** was confined to the unsuppressed coannular plug nozzle, but with extended range of configurations and test parameters such that possible applications of the unsuppressed coannular nozzle concept to variable cycle engine exhaust systems, with or without outer stream burning, can be fully evaluated. Performance tests as well as scale model acoustics tests were carried out in this program. Figure 3 shows a coannular plug nozzle installed in the NASA 8' x 6' wind tunnel for aero performance testing. All the acoustics testing was carried out in the new General Electric anechoic jet noise facility.

* Supported under NASA-Lewis Contract NAS-3-18-008

**Supported under NASA-Lewis Contract NAS-3-19-777

Eight configurations were investigated. Their general design outlines are shown in figure 4. The selection of these configurational designs were made with the view toward investigating the influence of the following geometric parameters on noise and takeoff performance: ratio of inner to outer areas, outer stream radius ratio, inner stream radius ratio, and plug shape. Test variables included velocity and temperature conditions of the two streams.

COANNULAR PLUG NOZZLE NOISE CHARACTERISTICS

The acoustical benefit associated with the interaction between the two streams issuing from an inverted coannular nozzle (high outer velocity and low inner velocity) can best be shown by comparing the measured noise characteristics of the coannular nozzle against that obtained by simply log summing the measured or known noise levels of two conical nozzles having the exit nozzle areas and flow conditions equal to those of the two exhaust streams of the coannular nozzle. The calculated noise level so obtained on the tacit assumption of no interaction between the two streams is hereinafter referred to as the synthesized conical or synthesized baseline noise level.

Figures 5 and 6 show such typical comparisons in terms of sound pressure spectrum at the 130° maximum sideline angle of several coannular configurations. Examination of these spectral comparisons and others not shown here indicate that the benefits due to interaction of the two annular streams in a coannular nozzle are: (a) concentrated mainly in the mid-frequency region, (b) increased sharply with increase in the ratio of inner area over outer area, and (c) dependent to some extent also on the outer nozzle radius ratio and the velocity ratio. The exact trend here, however, has not been fully pinned down at this time.

It was also observed that with the inner flow shut off ($v_i = 0$) the noise level of the outer annular nozzle alone is still considerably lower than that of the equivalent conical baseline (same exit area and velocity). The extent of this inherent noise advantage of the annular nozzle (with a large base area) increases with increase in radius ratio.

The noise benefit of the coannular nozzle relative to the synthesized baseline is also quite evident, as would be expected, at other radiation angles and over a rather wide velocity range. This is illustrated by typical comparison plots of noise vs. angle and noise vs. outer velocity in figures 7 and 8. As will be discussed later, the noise advantage of the coannular nozzle shown at forward quadrants is partly due to shock noise reductions. Noise due to turbulent jet mixing alone associated with the inverted coannular nozzle is only slightly lower than that of the referenced synthesized baseline at forward quadrants.

COANNULAR PLUG NOZZLE NOISE CORRELATIONS

Based on noise data so far analyzed, exact generalization of how various geometric and flow variables govern the noise generation is not possible. It is nevertheless desirable to obtain an approximate engineering correlation that can put into perspective how the salient parameters would affect the overall noise levels of the coannular nozzle. Analogous to the well established fact that the noise of a simple conical nozzle is primarily the function of exhaust velocity, it is believed that the noise of a more complex coannular plug nozzle, at least to the first order of approximation, may also be primarily the function of some "characteristic" velocity. The selected "characteristic" velocity is the mass flow averaged velocity for the two coannular streams; thus,

$$V_{ave} = \frac{w^i v^i + w^o v^o}{w^i + w^o}$$

where w and v are mass flow and velocity, and superscripts i and o refer to inner and outer streams respectively. The correlations of normalized total sound power and normalized maximum sideline PNdB against this flow averaged velocity for all test data from the eight configurations and for all test conditions are shown in figures 9 and 10. Plotting of the relative maximum sideline PNdB and relative sound power were normalized for density and ideal thrust in the following manner:

$$\left\{ \begin{array}{l} \text{Relative PNdB} \\ \text{Relative PWL} \end{array} \right\} \propto \left\{ \begin{array}{l} \text{PNdB} \\ \text{PWL} \end{array} \right\} - 10 \log(w^o v^o + w^i v^i) - 10 \log_{10} \left(\frac{\rho_m}{\rho_{isa}} \right)^{\omega-1}$$

$$\text{where } \rho_m \text{ (mixed density)} = \frac{2.7 \times \rho_{isa}}{T_{sm}}$$

$$T_{sm} \text{ (mixed static temperature)} = T_{tm} - \frac{V_{ave}^2}{2gJc_p}$$

$$T_{tm} \text{ (mixed total temperature)} = \frac{(T_t^o w^o + T_t^i w^i)}{w^o + w^i}$$

T_t is total temperature

ω is SAE density exponent (ARP 876, July 75 revision)

The collapsing of all the test data within a band of about ± 2 dB to show a single trend band supports the reasonableness of the notion of a "characteristic velocity." This then provides a relatively simple basis for predicting the overall PWL and max sideline PNdB levels of the inverted coannular plug nozzle. Further work is needed to provide detailed spectral and directivity correlations.

It is recognized that the mass flow average velocity for a coannular nozzle is really the specific thrust of the engine exhaust system; namely, $\frac{F_{\text{ideal}}}{w_t} \times g$ (F is ideal total gross thrust, and w_t is total weight flow).

The fact that the correlation curve (band) lies about 3 dB in sound power and about 5 dB in maximum perceived noise level lower than that of the conical nozzle for equal specific thrust is another way of showing the inherent jet noise advantage of inverted coannular nozzle. This, of course, suggests the very important conclusion; namely, for a bypass (e.g. VCE) engine, use of an inverted coannular plug nozzle system will produce significantly lower jet noise than that associated with the use of a fully mixed flow exhaust system, when compared under equal thrust and equal total flow conditions.

DETAILED AERO-ACOUSTIC MODELING AND THEORETICAL PREDICTION

A comprehensive aero-acoustic prediction method for complex jet flows is currently under development at General Electric. This effort is part of the High Velocity Jet Noise program sponsored by the FAA*. The primary objective of this effort is to gain fundamental understanding of the mechanisms of jet noise generation and reduction.

The aero-acoustic prediction procedure utilizes an extension of Reichardt's theory to predict the jet plume development, including mean axial velocity, temperature, and turbulence intensity distributions. It can accommodate arbitrary nozzle planform shapes. The acoustic characteristics are predicted based on the classical concepts of turbulent mixing noise, combined with recently developed analytic methods for modeling the acoustic/mean flow interactions, commonly termed fluid shielding. The prediction procedure is designed to predict absolute levels, as well as spectrum shapes and directivities.

Although the prediction method is still in a development stage, some useful preliminary information on predicted jet noise characteristics has been obtained. Predictions of the noise characteristics of several inverted flow coannular nozzles were performed and compared with available scaled model test data. A typical example is shown in figure 11. There is excellent agreement between predicted and measured noise spectra for the inverted coannular nozzle.

*DOT Contract OS-30034

To demonstrate the advantage of an inverted dual flow nozzle system over the non-inverted or conventional bypass type (high velocity jet surrounded by a low velocity bypass stream), a prediction of the characteristics of the two types is shown in figure 12. It can be seen that the inverted flow nozzle noise is somewhat higher at high frequencies but considerably lower at mid and low frequencies, with significant net reductions in peak noise level for observer angles greater than 80° . To be noted also is the smaller slope to the directivity pattern relative to the conventional bypass nozzle as shown in figure 13. This is attributed to the more rapid plume decay (also predicted by the model but not shown here), resulting in smaller eddy convection speeds, and hence lower convective amplification. Further exercise of the theoretical prediction method will shed additional insight and physical understanding of the coannular nozzle noise characteristics.

COANNULAR NOZZLE SHOCK NOISE CHARACTERISTICS

Mixing jet noise advantage is but one important attribute of the coannular nozzle. Preliminary analysis of the data obtained indicate that shock noise (arising from the interaction of turbulence with shock; both tones and broadband) of coannular plug nozzles appear to be consistently lower than that of conical nozzles under comparable nozzle pressure ratios which has been generally established as the key variable affecting shock noise. Figure 14 shows typically significant reduction in shock noise - varying from 6 to 12 dB in the frequency range between 600 to 12,500 Hz - for a coannular nozzle. Both outer and inner stream pressure ratios are 2.79, and the outer and inner velocities are 2000 and 1340 feet per second respectively. The baseline conical nozzle was operated at the same pressure ratio and velocity as those for the coannular outer nozzle. This comparison was made at the 50° sideline angle. Figure 15 shows a comparison of the overall noise levels of a coannular nozzle operating at constant velocity, but at different pressure ratios. It is believed that, in the forward quadrant, the rising noise with increase in nozzle pressure ratio is associated with the increasing presence of shock noise. Even then, the projected shock noise at a nozzle pressure ratio of 3.96 is still about 5 dB less than that of the conical nozzle at the same pressure ratio.

The importance of shock noise and the even greater role it may play under flight conditions cannot be overestimated. More effort should be given to this subject in future jet noise technology work for supersonic cruise aircraft.

IMPACT OF COANNULAR NOZZLES ON EXHAUST SYSTEMS DESIGNS

The coannular plug nozzle can be fairly easily adapted to the exhaust system of a variable cycle engine. The desired inverted velocity profile can be

accomplished by ducting the bypass flow to the inner core nozzle, and permitting the main thrust producing, high velocity, and high temperature stream to issue as the annulus.

A preliminary design study comparing the uses of coannular nozzle and conventional retractable multi-element suppressor was carried out, and the key results are shown in Table I. It is seen that the coannular nozzle system enjoys significantly improved performance, reduced weight, and reduced complexity. Reduced complexity implies improved reliability and maintenance. Performance estimates shown were based on data obtained in the NASA (Lewis) 8' x 6' wind tunnel, showing $C_{fg} \approx .965$ and $.92$ for coannular nozzle and chute suppression, respectively, at about 3.5 Mach. The final estimated noise level of the coannular nozzle, though still above 3 EPNdB higher than that obtainable with a full suppressor, approaches the FAR36(1969) sideline limit for subsonic aircraft. The exact EPNdB noise level will depend on the engine size selection.

CONCLUDING REMARKS

An inherent noise advantage of coannular plug nozzle with inverted velocity profile has been demonstrated statically as the result of scale model acoustical testing. Application of this concept to variable cycle engine exhaust systems appears feasible. Relative to the use of conventional turbojet type mechanical suppressors, coannular plug nozzles have significantly lower weight for the total exhaust system, reduced complexity, and far less takeoff performance loss. Their impact on aircraft mission range and direct operating cost is expected to be favorable.

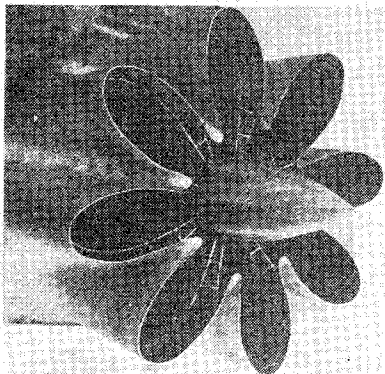
Although the research results described in this paper are believed to be significant from the viewpoints of both potential applications and basic knowledge on jet noise reduction, it is not my view that the acoustic technology needed to achieve airport acceptable noise levels for an economically viable supersonic cruise aircraft is already on hand. A great deal of additional technology development work is necessary in order to fully exploit the inverted coannular plug nozzle concept and to more realistically demonstrate its application to future advanced technology engines. Such additional technology work should include, as a minimum, (a) investigation of jet related shock noise and means for its control, (b) investigation of the effect of flight on both jet mixing and shock noise, (c) continued investigation of the possible use of advanced and mechanically simple suppressors, evolved around the basic inverted coannular plug concept (in order to test the feasibility of even lower noise limits, as required, and (d) full scale component demonstration and optimization of the nozzle design.

Work done so far on inverted coannular nozzles by General Electric and others is a significant step forward. Much work lies ahead.

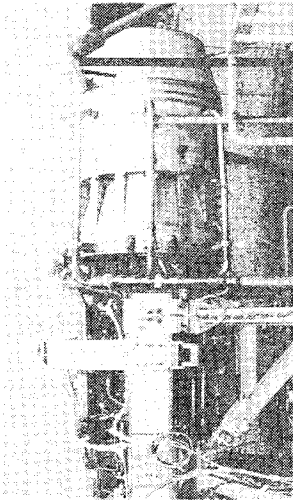
TABLE I
IMPACT OF COANNULAR NOZZLE ON EXHAUST SYSTEM

Four 266 880 N (60 000 lb) Thrust Engines

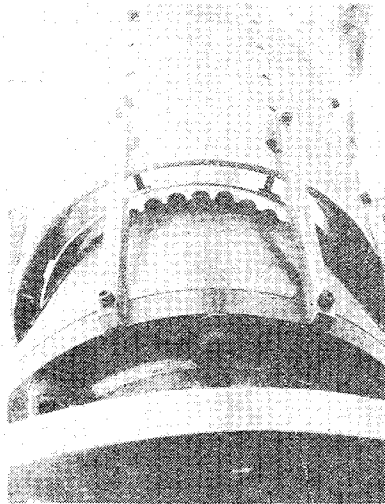
	<u>MIXED FLOW BASELINE</u>	<u>MIXED FLOW PLUS CHUTE SUPPRESSOR</u>	<u>INVERTED COANNULAR</u>
PERFORMANCE LOSS; T. O.	BASE	5 TO 6%	1.5%
NOZZLE WEIGHT	BASE	+ 31%	- 11%
COMPLEXITY	MODERATE	HIGH	MODERATE
NOISE; Δ EPNdB			
RELATIVE FAR36 (1969)	6 TO 9	-3 TO 0	0 TO 3
649 m (2128 ft) SIDELINE			



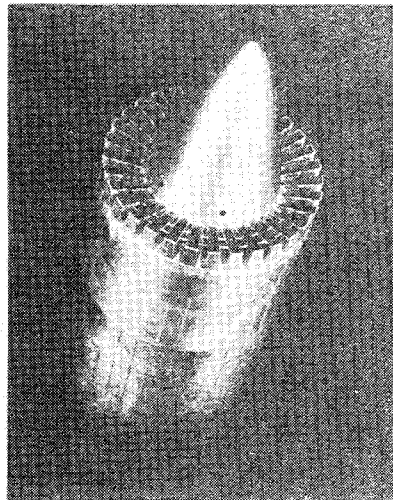
A. CJ805 DAISY (1960)



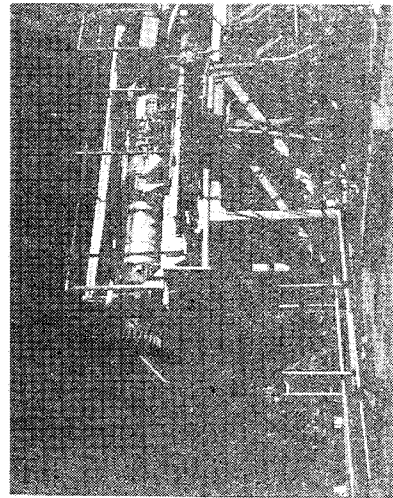
**B. SST/GE4 ENGINE WITH
TWO-STAGE EJECTOR
NOZZLE (1968)**



**C. MULTI-TUBE WITH
EJECTOR (1970)**



**D. MULTI-CHUTE PLUG
(1971)**



**E. ADVANCED 32-CHUTE
PLUG (1975)**

Figure 1.- Typical turbojet jet noise suppressor configurations 1960 - 1975 technology.

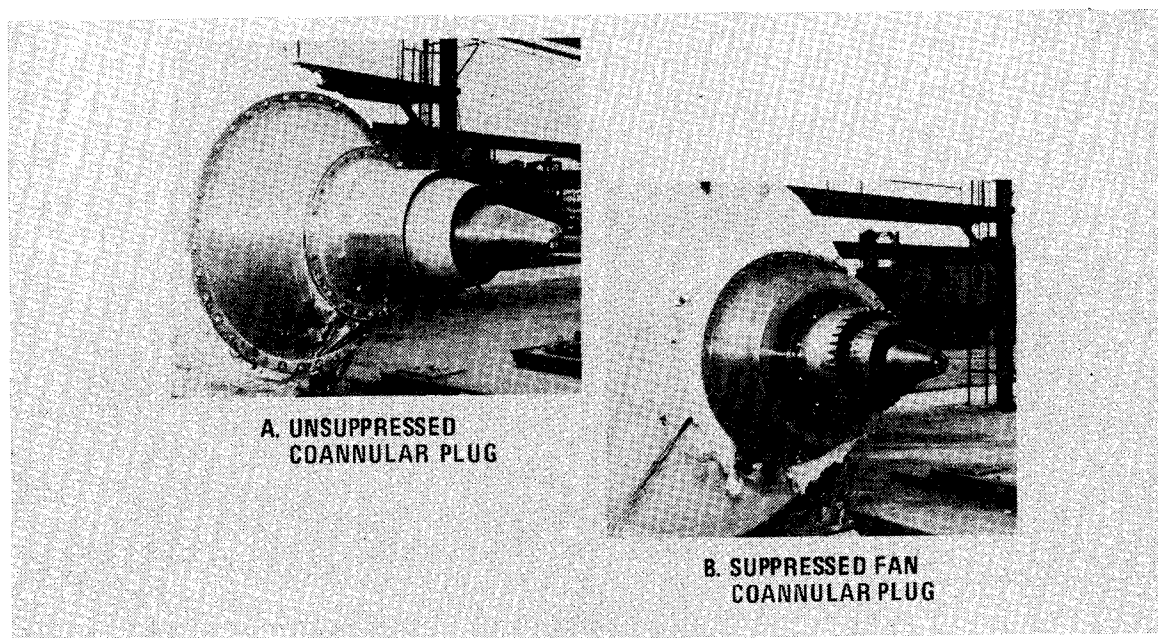


Figure 2.- Advanced engine cycle coannular plug nozzle/suppressor configurations - 1976 technology.

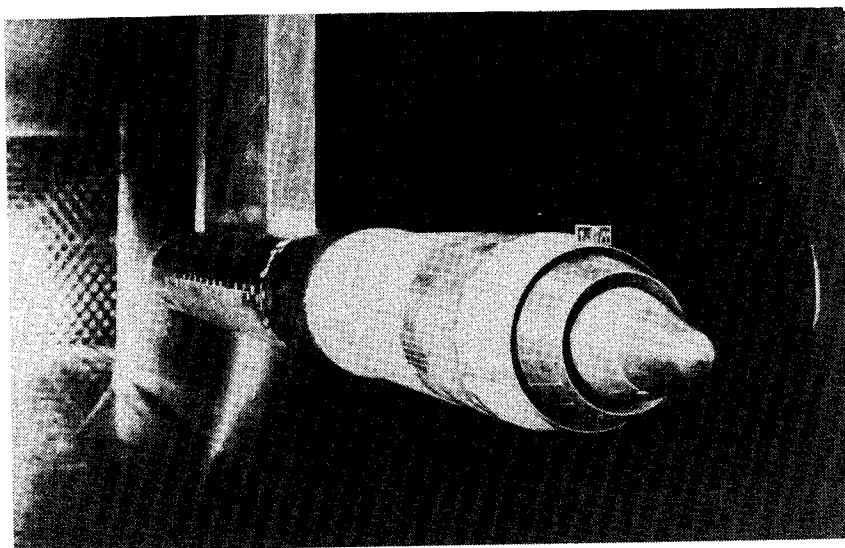


Figure 3.- High radius ratio coannular plug nozzle installed in NASA Lewis 8' x 6' wind tunnel.

CONFIGURATION		1	2	3	4	5	6	7	8
PARAMETER									
TYPE TEST	R_r^o	.902	.902	.902	.902	.853	.926	.853	.853
	R_r^i	.673	.800	.902	.800	.800	.800	.902	.800
A^i/A^o		1.530	1.030	.530	1.030	.630	1.420	.330	.630
TYPE TEST	ACOUSTIC	X	X	X	X	X	X	X	
	AERODYNAMIC	X	X	X	X	X	X	X	X

CONFIGURATION #1 CONFIGURATION #2 CONFIGURATION #3 CONFIGURATION #4



CONFIGURATION #5 CONFIGURATION #6 CONFIGURATION #7 CONFIGURATION #8



Figure 4.- Summary of configuration and key geometric parameters.

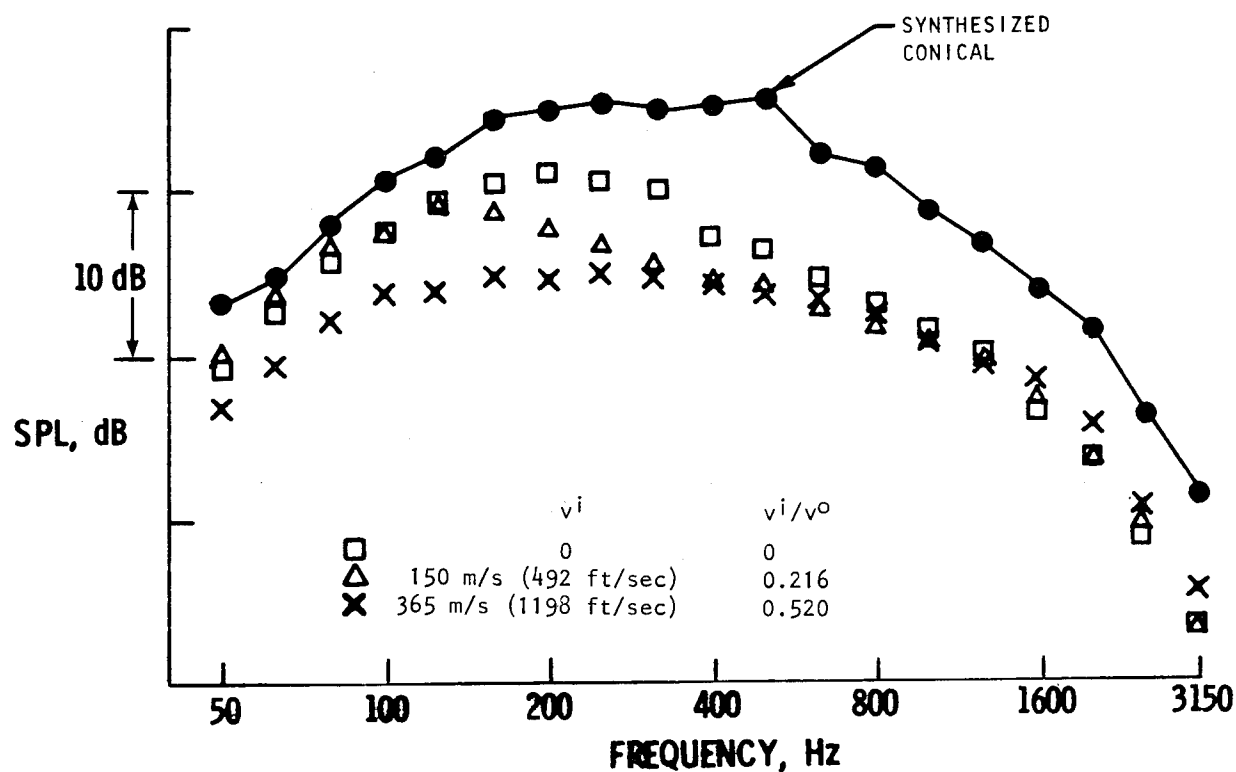


Figure 5.- Typical inverted coannular plug nozzle spectral characteristics. 732 m (2400 ft) sideline; data scaled to $.33 \text{ m}^2$ (513 in^2); $V^o = 701 \text{ m/s}$ (2300 ft/sec); $T_T = 967 \text{ K}$ (1740° R); $\theta_I = 130^\circ$; configuration No. 3; $A_R = .53$.

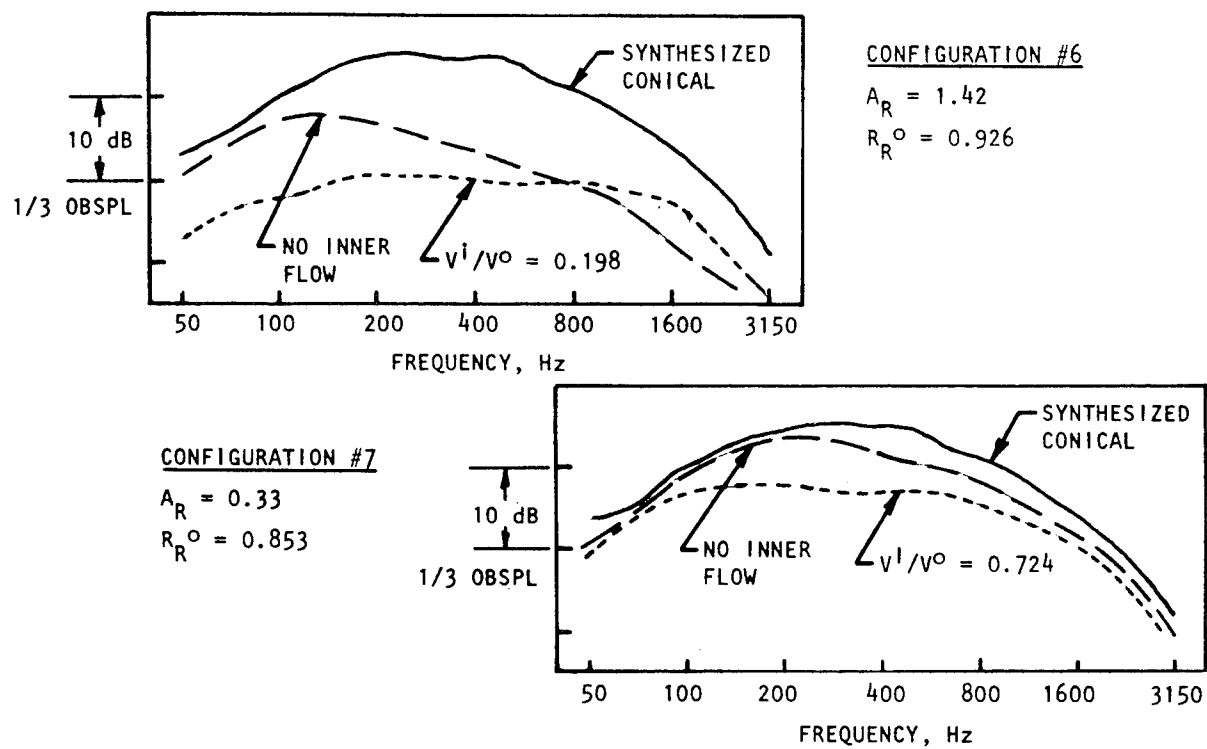


Figure 6.- Additional typical inverted coannular plug nozzle spectra.
 732 m (2400 ft) sideline; data scaled to $.33 \text{ m}^2$ (513 in^2);
 $\theta_I = 130^\circ$; $V^O = 701 \text{ m/s}$ (2300 ft/sec).

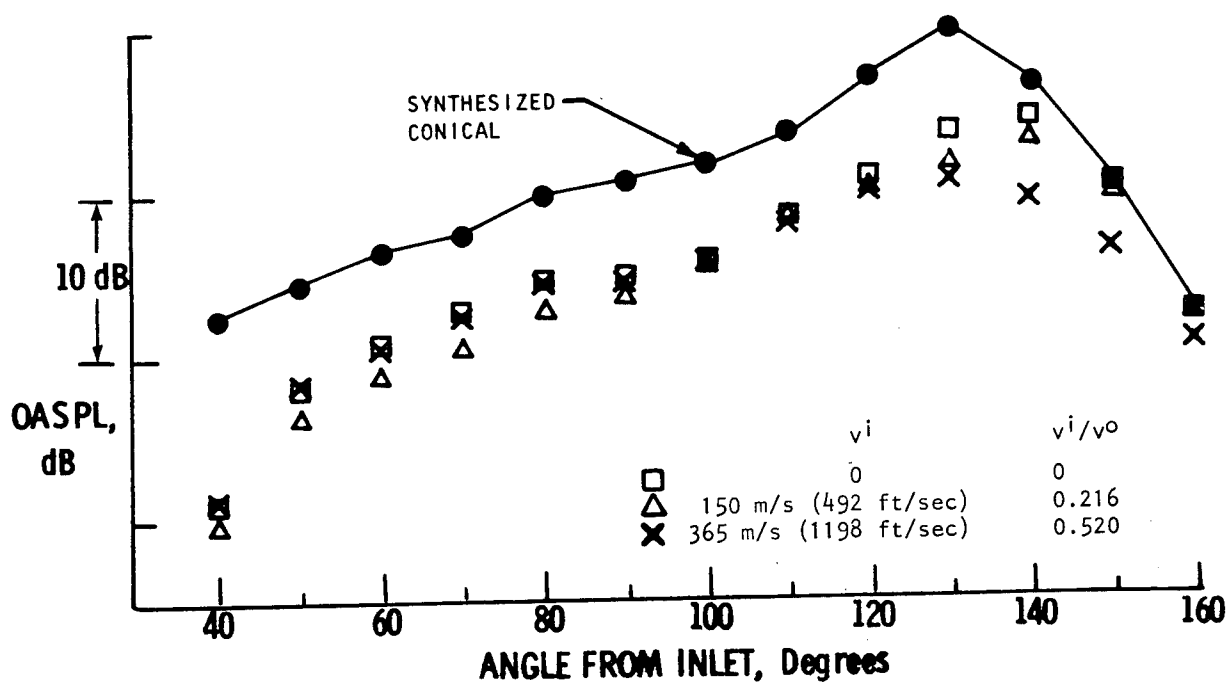


Figure 7.- Typical inverted coannular nozzle directivity characteristics.
 732 m (2400 ft) distance; data scaled to $.33 \text{ m}^2$ (513 in^2); $V_o = 701 \text{ m/s}$ (2300 ft/sec); $T_T = 967 \text{ K}$ (1740° R); configuration No. 3; $A_R = 0.53$.

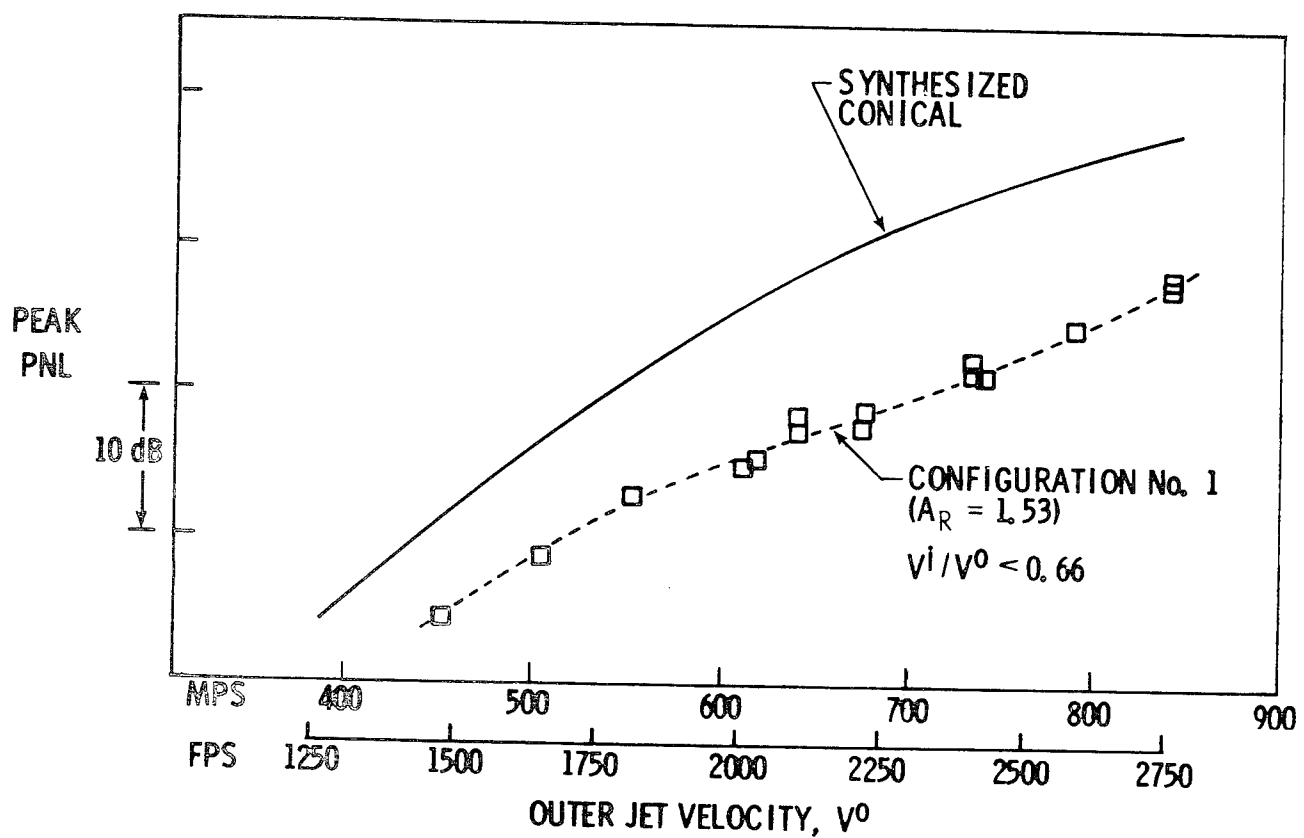


Figure 8.- Typical inverted coannular nozzle noise reduction relative to a synthesized conical nozzle as a function of outer velocity. 732 m (2400 ft) distance; scaled to $.33 \text{ m}^2$ (513 in^2); static.

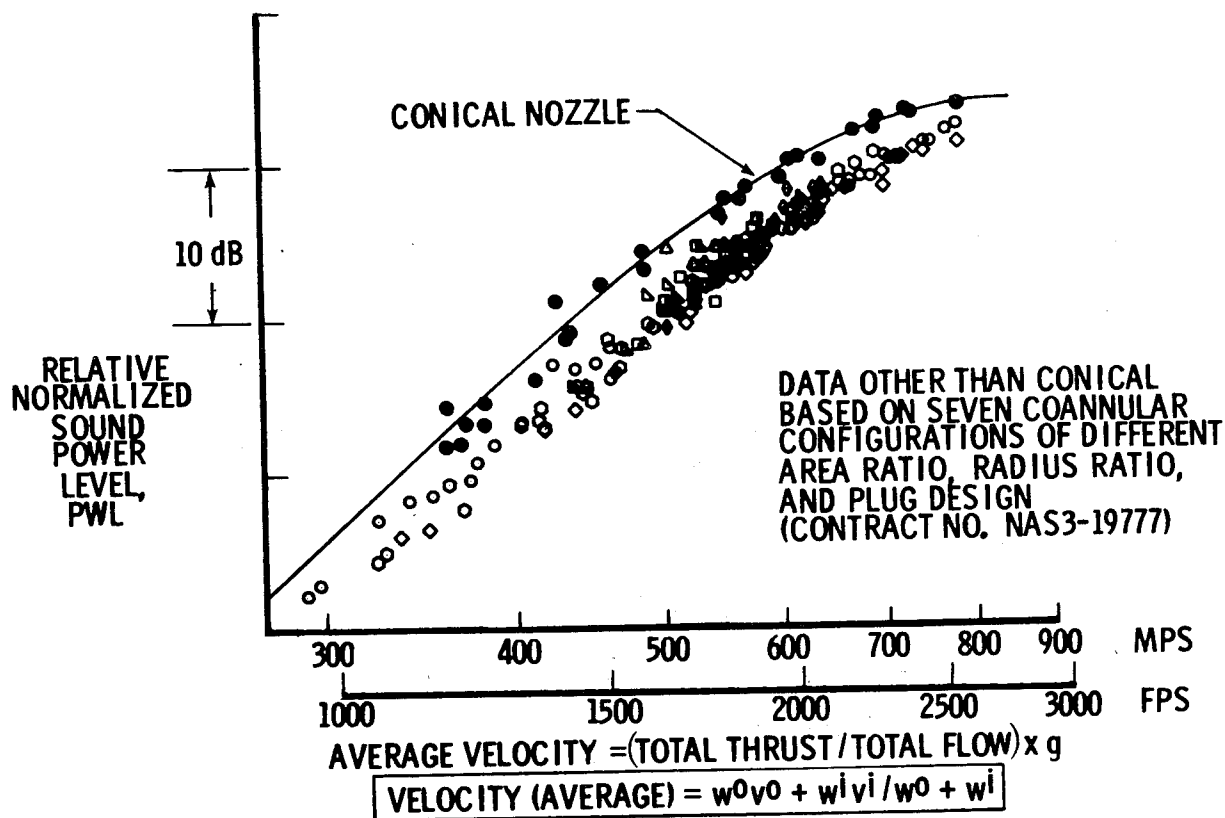


Figure 9.- Coannular nozzle sound power level (PWL) correlation.
 PWL normalized for density and thrust (ideal); .33 m² (513 in²)
 nozzle area.

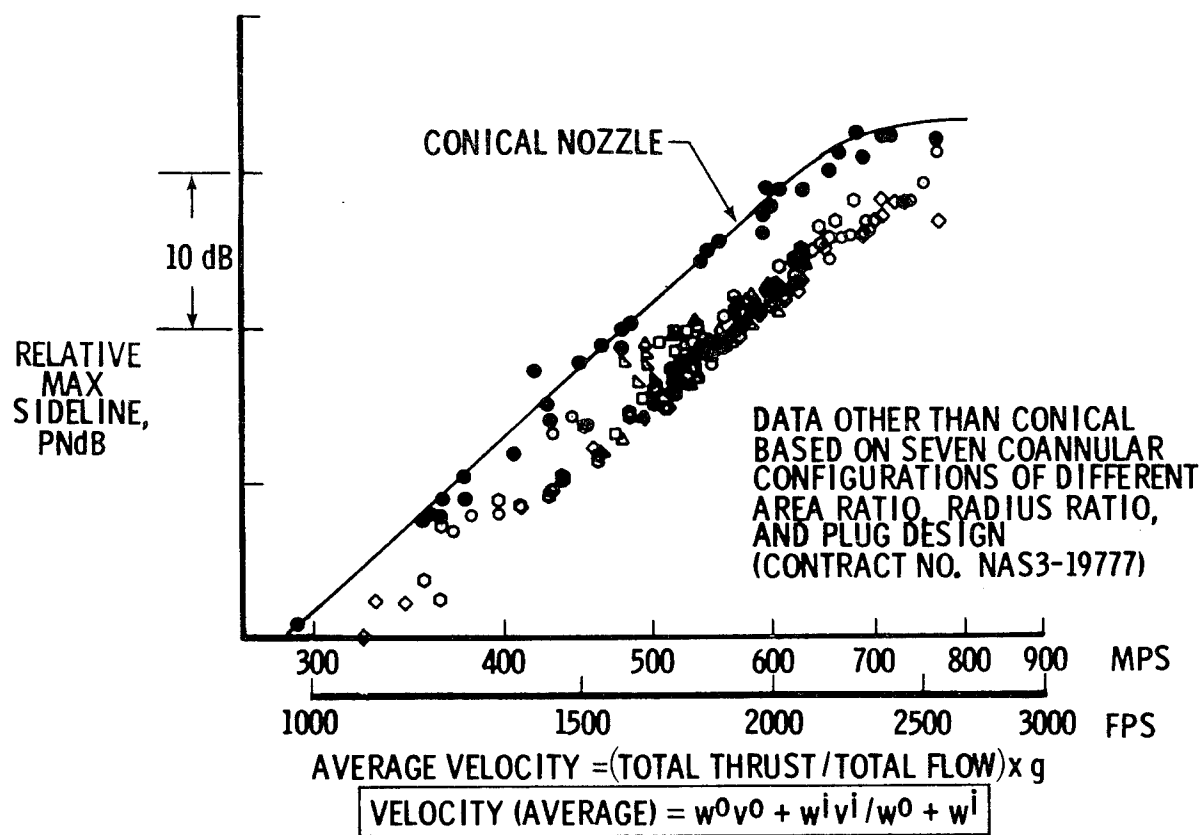


Figure 10.- Coannular nozzle maximum perceived noise level (PNdB) correlation. PNdB normalized for jet density and thrust (ideal); 732 m (2400 ft) distance; .33 m² (513 in²) nozzle area.

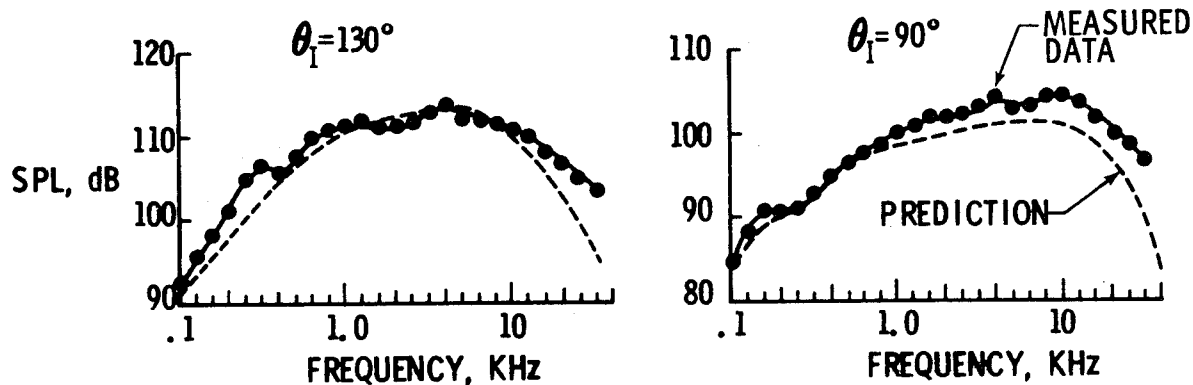


Figure 11.- Comparison between measured and predicted spectra for inverted coannular nozzle. See figure 12 for area and flow conditions.

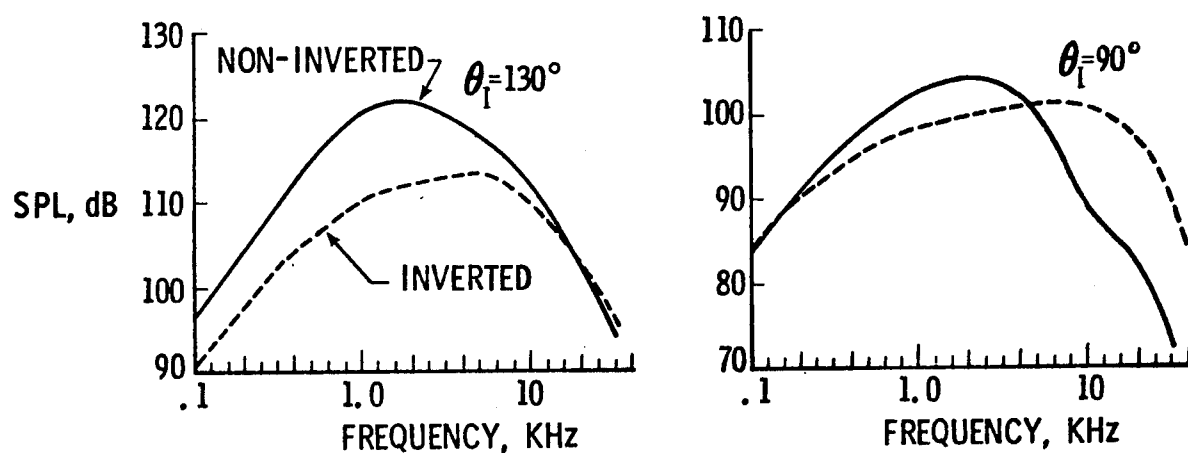


Figure 12.- Theoretical predictions of spectral characteristics of inverted versus non-inverted (conventional bypass) coannular nozzles. (Predictions based on preliminary results from work supported by FAA contract DOT OS 30034.) Scale model size; high velocity stream: $V = 721$ m/s (2366 ft/sec); low velocity stream: $V = 372$ m/s (1219 ft/sec); 12.2 m (40 ft) arc.

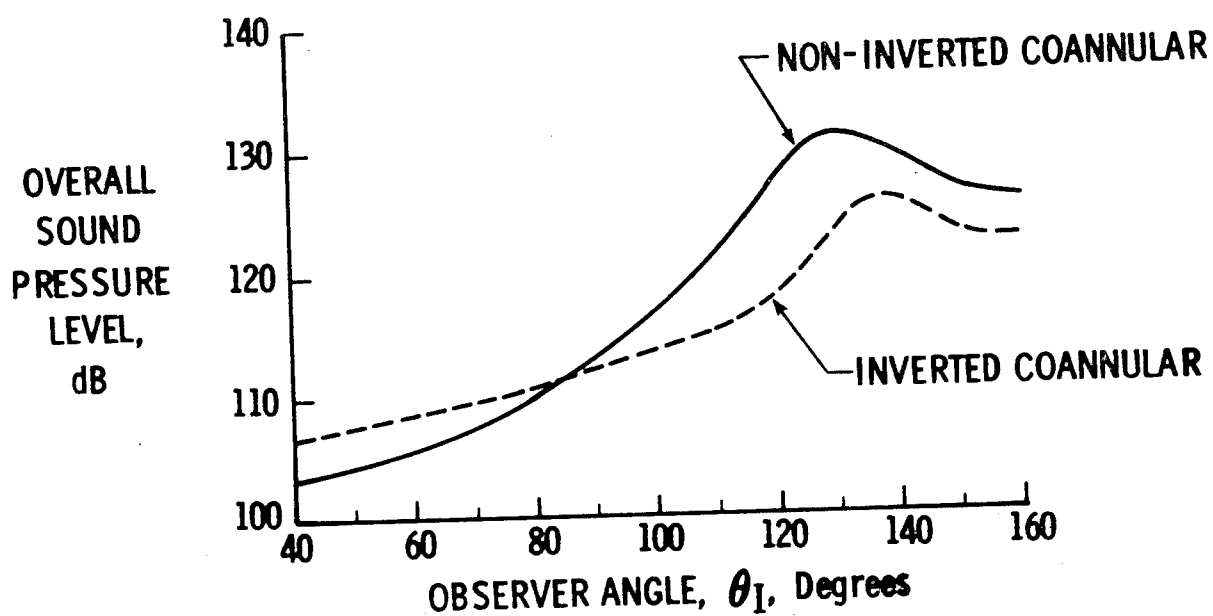


Figure 13.- Theoretical prediction of directional characteristics of inverted and non-inverted (conventional bypass) coannular nozzles. (Prediction based on preliminary results from work supported by FAA contract DOT OS 30034.) See figure 12 for area and flow conditions; scale model size; 12.2 m (40 ft) arc.

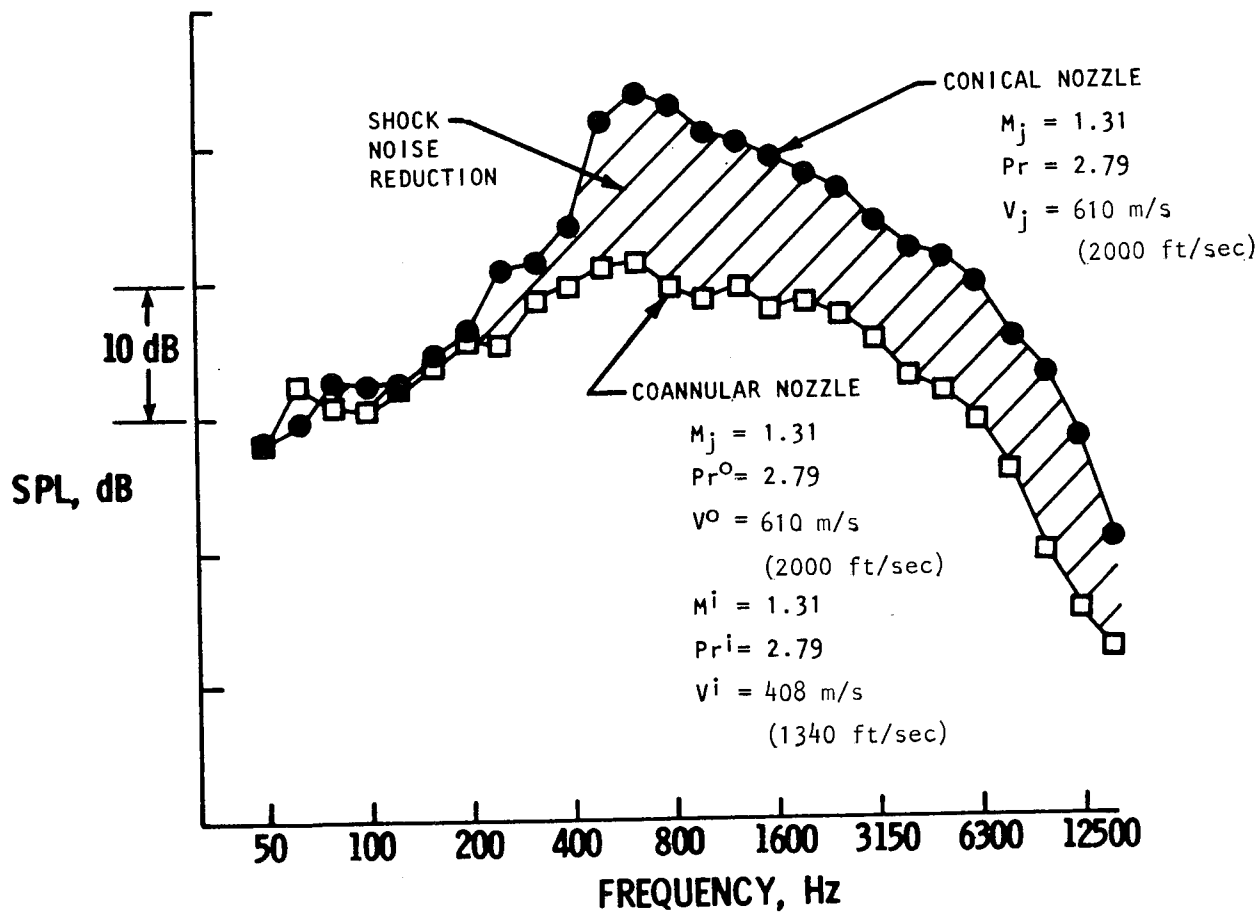


Figure 14.- Inverted coannular nozzle shock noise spectral characteristics relative to a conical nozzle, configuration 7. 91 m (300 ft) sideline; data scale to $.33 \text{ m}^2$ (513 in^2); $\theta_I = 50^\circ$.

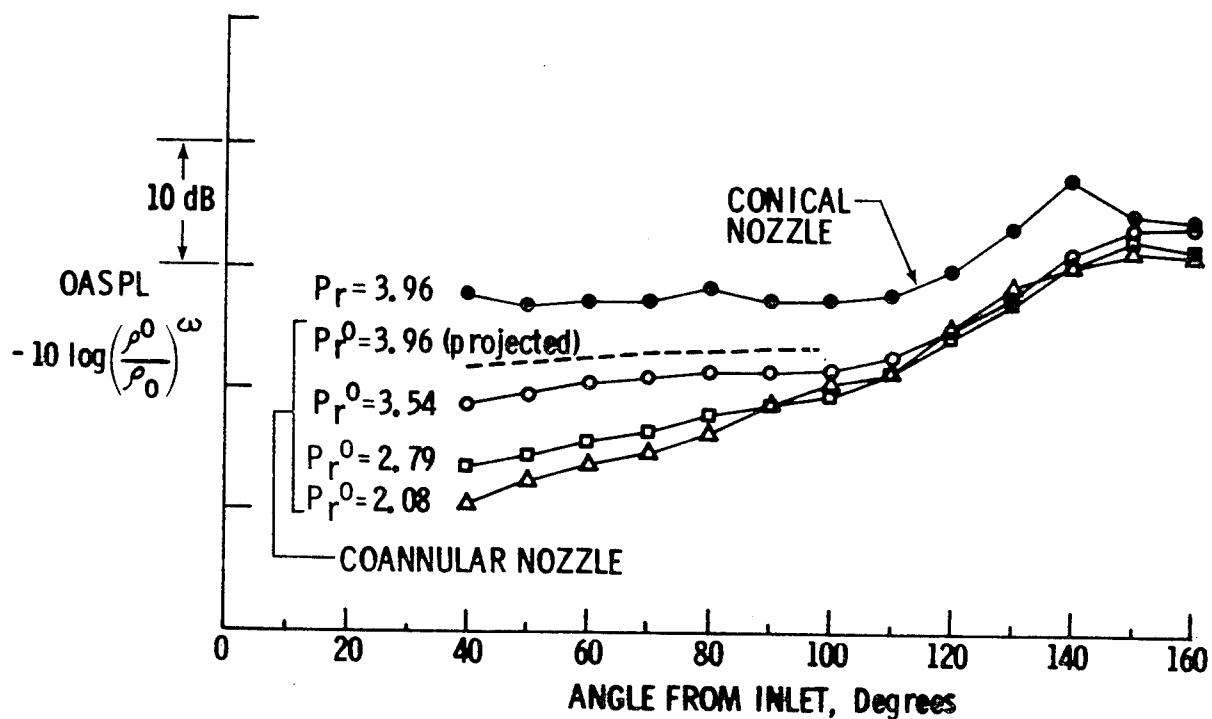


Figure 15.- Inverted coannular nozzle shock noise directivity characteristics relative to a conical nozzle. 45.7 m (150 ft) arc; data scaled to $.33 \text{ m}^2$ (513 in^2); $V_j = V^0 = 610 \text{ m/s}$ (2000 ft/sec) for all cases; $V^i = 414 \text{ m/s}$ (1360 ft/sec); $P_{r,i} = 2.8$ for all cases; configuration No. 7.

CURRENT RESEARCH IN SONIC-BOOM MINIMIZATION

Christine M. Darden and Robert J. Mack
NASA Langley Research Center

SUMMARY

A review is given of several questions as yet unanswered in the area of sonic-boom research. Efforts, both here at Langley and elsewhere, in the area of minimization, human response, design techniques and in developing higher order propagation methods are discussed. In addition, a wind-tunnel test program being conducted to assess the validity of minimization methods based on a forward spike in the F-function is described.

INTRODUCTION

Much progress has been made in the understanding of sonic-boom phenomena in the past two decades — especially in the areas of generation and propagation. Many advances have also been made in the area of sonic-boom minimization. With scheduled flights of the Concorde and the TU144 having begun in recent months, the era of commercial supersonic flight is here. Even so, restrictions on such flights because of noise and especially because of the sonic boom reduce their economic viability. Route structures must be planned to limit supersonic operation to water or desert areas. Designers of second-generation transports which cruise supersonically must be concerned with the sonic-boom problem if the economic outlook is to improve.

There are still many unanswered questions in sonic-boom research. The most important question (since the ultimate aim is overland supersonic flight) concerns the level of sonic boom which would prove acceptable for regularly scheduled flights conducted over a long period of time. Consideration here must be given to the response of humans and animals, both indoors and out, and to the response of building structures. Studies of such responses in both simulation tests and actual flight tests have been made and published in recent years but as of yet no acceptable levels have been established. These studies have shown, however, that the shock level of the pressure signature seems to be

the most disturbing feature of the signature for outside exposure and the impulse most disturbing for indoor exposure. Since indoor and outdoor disturbances are seemingly controlled by two different parameters of the signature, the question then is, what parameter of the pressure signature should be minimized? Knowledge of how to minimize certain familiar parameters of the pressure signature already exists. The capabilities of the sonic-boom minimization program developed here at Langley and some results of this program are discussed.

Because economics of supersonic flight are of fundamental concern, avoidance of excessive penalties to the efficiency of airplane designs which attempt to minimize the sonic boom must also be a primary concern. Contrary to earlier beliefs, it has been found that improved efficiency and lower boom characteristics do not always go hand in hand. Extensive trade-off studies are needed to determine just how much efficiency must suffer to meet acceptable boom levels. Application of the previously mentioned minimization program in the conduct of one phase of these trade-off studies is illustrated.

Atmospheric turbulence and the necessary accelerations and maneuvers of supersonic aircraft cause an intersection of rays forming a phenomena known as a caustic. Linearized theory fails to make predictions of the "superboom" that occurs at a caustic, and questions still remain about the validity of other methods advanced to make these predictions. Caustics do at times reach the ground and thus make this condition a critical point in sonic-boom research.

Restrictions on the sizes of wind-tunnel models because of limitations of current propagation and extrapolation methods point out the need for propagation methods which include asymmetric effects. Such methods would allow larger, better defined models, more accurate measurements, and improved overall results. Consideration of flights at higher Mach numbers and altitudes have also led to a need for propagation methods which include second-order effects. Efforts at New York University to develop methods such as these will be discussed.

With the addition of sonic boom as a design constraint, current methods of design have been found to be inadequate. More direct analytical methods are needed to replace the iterative procedures of design which will be described in this paper.

Previous wind-tunnel experiments have verified in principal the validity of earlier less sophisticated design methods applicable to boom reduction at transonic acceleration conditions. A new experimental investigation to assess the applicability of the newer methods to cruise conditions at Mach numbers up to 2.7 is now underway. The design concepts employed, the scope of the test program, and the goals of the research are discussed.

SYMBOLS

Although results have been shown in both the International System of Units and U.S. Customary Units, primary calculations were made in U.S. Customary Units;

hence, the peculiar values presented for parameters.

A	equivalent area
C_D	drag coefficient
F	Whitham F-function
h	altitude
I	impulse
l	length
M	Mach number
t	time
W	weight
x	axial distance
y_f	nose length or balance point of front shock in F-function
Δp	overpressure or shock level
α	cone half-angle
μ	Mach angle
τ	rise time
Subscript:	
r	reference conditions
max	maximum

REVIEW OF PREDICTION AND MINIMIZATION METHODS

The sonic-boom pressure field as generated by an aircraft in supersonic flight is briefly reviewed in figure 1. The complete field of disturbance of the aircraft is confined to a generally conical region extending back from the nose of the aircraft. The entire region of ground disturbance is defined by the intersection of the "Mach cone" and the ground. Supersonic aircraft of today produce far-field N-wave signatures in this region. For a more detailed review of sonic-boom generation, see reference 1.

Prediction methods in sonic-boom theory have been to a large extent based on methods developed by Whitham, Walkden, and Hayes (refs. 2 to 4), and on geometric acoustics. An outline of the basic procedure is illustrated in figure 2. From the complex airplane an equivalent area distribution is defined by passing Mach cuts through its volume and lift distribution. A mathematical expression is then used to define the "Whitham F-function" from the second derivative of the area distribution. This F-function represents the source distribution which causes the same disturbances as the aircraft at large distances from the aircraft. Because the linear pressure signal propagates at the local speed of sound and each point of the signal advances according to its amplitude, the signal is distorted at the ground and could theoretically be multivalued. The physically unrealistic multiple values of pressure in the ground signal are, however, eliminated by the introduction of shocks. Shock location, based on the observation that for weak disturbances the shock bisects the angle between two merging characteristics lines, is determined by a balancing of the signature area within loops on either side of the shocks.

Historically, sonic-boom minimization has been based on finding the minimizing form of the F-function and then inversely defining the equivalent area distribution. The first minimization efforts were aimed at the far-field N-wave (refs. 5 and 6). With the observation that it might indeed be the mid-field wave which intersected the ground (refs. 7 and 8) advances were made in minimizing first the bow shock (refs. 9 and 10) and then both shocks of the pressure signature (refs. 11 and 12). All the minimums were found to require an F-function characterized by a delta function at $x = 0$.

A sonic-boom minimization program employed here at Langley and illustrated in figure 3 is based on theories developed by Seebass and George at Cornell University. With their method, it is possible to minimize either the initial shock of the signature or the overpressure (ref. 13). Their analysis was applied to propagation through an isothermal atmosphere and the minimizing F-function utilized the characteristic delta function at $x = 0$. The version of this program developed at Langley was modified to provide for propagation in the real atmosphere (refs. 14 and 15) and to allow for relaxation of the delta function to a spike of finite width (ref. 16). It has been found that by adding a finite width to the spike of the F-function, the extreme bluntness called for by the delta function can be relaxed to a conical nose shape. Defining parameters for this signature are Δp , the initial shock; Δp_{\max} , the maximum level of overpressure; τ , the rise time between Δp and Δp_{\max} ; and I , the impulse or the area of the positive portion of the signature. For this example, the initial

shock has been minimized. If the overpressure had been minimized for the same set of conditions, the resulting signature would be a "flat top" signature with no rise time.

The input to this computer program consists of the flight conditions of Mach number, altitude, length, and weight. In addition, the parameter to be minimized in the pressure signature must be specified as well as the base width of the F-function spike. The algorithm then specifies the minimizing F-function for these conditions, the accompanying ground pressure signature, and the equivalent area distribution of the aircraft.

Although the question of what should be minimized in a pressure signature is unanswered, it is felt that experience gained in minimizing the familiar parameters will be valuable if a new parameter or combination of parameters is found which better describes the total disturbance of the pressure signature.

APPLICATION TO LOW-BOOM AIRCRAFT DESIGN

To obtain maximum benefit from the results of a program such as this, one needs methods for producing airplane designs which match the resulting equivalent area. Let us briefly review the methods used for designing aircraft for boom minimization as outlined in figure 4. After deciding upon the design cruise condition, the type of signature desired, and an intermediate spike width or in other terms the extent of nose blunting, these values are used in the program to generate the equivalent area distribution. Initial designs of planform, fuselage, horizontal and vertical tails, nacelles, etc. are made and the area distribution (or volume contribution) is calculated by using the wave drag program (ref. 17) and the lift distribution is calculated by using the linearized wing theory program (ref. 18). From these two distributions a total equivalent area is generated and compared with the ideal area. Through an iterative process configurations are found which match reasonably well the ideal area. It should be noted here that there is a need for better analytical methods in this design process. Even neglecting the fact that this manual iteration is a very cumbersome process, it is nearly impossible to match areas exactly in this way and slight differences are quite significant since the relationship between the area and the resulting pressure signature is through the second derivative.

APPLICATION TO STUDY OF MINIMIZATION PARAMETERS

Application of sonic-boom minimization concepts to the design of models for a wind-tunnel test program to assess their validity is discussed later. Now it might be more appropriate to consider program results which serve to establish design goal levels of sonic-boom parameters and to show their variation with the significant airplane and operational parameters. Shown in figure 5 is the variation of the overpressure and impulse of the pressure signature with the airplane parameters of length and weight. These results are for minimum

overpressure- "flat-top" signatures for which the F-function is characterized by a delta function at $x = 0$. For convenience, all variables have been non-dimensionalized with respect to the cruise conditions shown. The reference overpressure and impulse are the values obtained for these parameters at the reference flight conditions. Note that, as expected, an increase in both overpressure and impulse with the weight of the aircraft and a decrease in both of these parameters with the length occur.

The variation of the parameters with the operating conditions of Mach number and altitude is shown in figure 6. Here it is seen that there is an increase in the overpressure level with Mach number but a decrease in the impulse. Recalling that each of these parameters is a measure of a different type of disturbance from the pressure signature, this opposite variation highlights clearly the problem of selecting the parameter of the signature to be minimized. With altitude, an increase in impulse for the range shown as well as an increase in overpressure for most of the range occurs. The minimum value shown on the overpressure plot occurs approximately at the beginning of the stratosphere. Although flights at this altitude would seem to be attractive for boom considerations, drag and range penalties would be quite severe.

BOOM — DRAG TRADE-OFF

Researchers earlier thought that those factors which improved the efficiency of an aircraft would also tend to lower the sonic boom; however, it has now been found that this is not necessarily so. To explain this somewhat paradoxical situation, figure 7 shows a comparison of the wave pattern propagating to the ground. The low boom aircraft is seen to have an extremely blunt nose and special shaping so that even though there is a high shock level at the aircraft, and thus a high drag level, the pattern of propagation is such that no further coalescence of shocks occurs. There, in fact, are no other shocks behind the bow shock; there is only an expansion field. Because of this, the shock at ground level is greatly attenuated. The drag configured, sharp-nosed aircraft, on the other hand, had a comparatively lower shock at the aircraft, but because of shock coalescence the ground signature has a relatively higher level shock.

To answer the question of how much aircraft efficiency must suffer in order to meet boom requirements, extensive trade-off studies must be conducted by design teams. The ability to vary the width of the spike in the F-function which, in turn, adds a cusp-like nose region of the equivalent area distribution makes the previously described minimization program valuable as an important part of such studies. As a rough idea of such a trade-off study, drag levels, overpressure, and impulse are shown as a function of nose length, y_f/l in figure 8. As the nose length is increased, levels of drag decrease as expected, but there is a corresponding increase in the levels of overpressure and impulse. This study was made with bodies of revolution being used to get approximate drag increments. The important point, however, is not the result of this example, but the new capabilities for meaningful design studies now provided.

RELATED WORK

There is no work going on at Langley concerning the acceptable level of sonic boom or concerning the parameter which should be minimized. However, some work in this area, which in fact stems from our minimization studies, is being conducted at the University of Toronto Institute for Aerospace Studies (ref. 19). A series of pressure signatures such as that shown in figure 9 are being prepared for reproduction in acoustically sealed chambers so that studies may be made of their effects on humans. Although each of these signatures is distinctly different, they all represent the same flight conditions. For reference, the equivalent area distribution corresponding to each signature is shown, with the area distribution for the N-wave repeated on the others as a dashed line for comparison. Note that for the large shock difference occurring between the N-wave and the flat-top signature, there is only a small redistribution of equivalent area needed.

Testing methods in sonic-boom research have progressed from the use of 1-inch models when only far-field theories were available to roughly 6-inch models with the currently used mid-field theory. Model sizes are limited today because currently used propagation methods require nearly axisymmetric input, and thus readings must be taken far enough away to reduce significantly the error produced by the nonsymmetry of volume and lift. This restriction in size makes it difficult to incorporate with sufficient accuracy such features as camber and twist to define more realistic models.

Propagation methods being developed at New York University under a NASA Grant promise to improve this experimental situation. A computer program which accounts for the nonsymmetry in the linear lift distribution (ref. 20) is now operable and work is currently being done, Lu Ting being the primary investigator, to include the effects of nonsymmetry in spanwise volume and lift. Such programs allow larger models to be used — roughly 30 to 45 cm (12 to 18 in.) in length. In addition to allowing more accuracy, larger models will also allow some wind-tunnel tailoring of models as a means of compensation for inaccuracies in some of the presently used minimization theories.

A comparison of currently used propagation methods (refs. 21 and 22) with recent methods developed at New York University is shown in figure 10. Note that at this fairly high Mach number, significant differences occur in the results when second-order effects and entropy variation are included. A smaller difference occurs when asymmetric effects of the linear lift distribution are included.

There is no active research here at Langley concerning the predictions of overpressure levels occurring at a caustic. Descriptions of recent efforts in this area may be found in references 23 to 25.

EXPERIMENTAL PROGRAM

To test the validity of minimization methods described, an experimental program incorporating five models and tests at two different Mach numbers is being conducted. Two of the models, one with a conventional delta-wing planform and the other with a familiar arrow wing planform, are to be tested to provide a basis for comparison with the overpressure levels and signature shapes obtained with sonic-boom optimized models. The low-boom models were designed along conceptual lines put forth in references 26 and 27, although in this case some of the aircraft features such as vertical- and horizontal-tail surfaces, nacelles, etc, were omitted for the sake of simplicity and because of limitations of tunnel testing methods.

The low-boom wind-tunnel models were 1/600-scale versions of a wing-body configuration which met the following specifications:

- 1) Cruise Mach number of 1.5 and 2.7
- 2) Beginning cruise weight of 272 155 kg (600 000 lb)
- 3) Cruise altitude of 15 240 m (60 000 ft)
- 4) Seating room for at least 200 passengers
- 5) Aircraft length of 91.44 m (300 ft)
- 6) Maximum overpressure of 41.03 Pa (0.857/lb/ft²) and 50 Pa (1.044 lb/ft²)

Special features included in the design and shown in figure 11 are:

- 1) A boom-contoured nose section
- 2) A highly swept wing leading edge
- 3) Varying thickness ratio from wing root to wing top
- 4) Positive wing dihedral for an effective length of 91.44 m (300 ft)
- 5) An area-ruled fuselage
- 6) A long lift-tailored wing planform

The five models for the test program are shown in their proper relative sizes in figure 12. For the three low boom models, a modified arrow planform was chosen for a configuration designed to cruise at Mach 2.7, a low notch ratio arrow wing was employed in a configuration optimized for a cruise Mach number of 1.5, and a special blunt apex and low notch ratio arrow-wing planform was used to represent an advanced blended wing fuselage configuration designed for $M = 2.7$. These models and tests will be used to explore the applicability of the Seebass and George method at a low supersonic Mach number where small disturbance linearized theory methods are generally valid and at a relatively high Mach number where the applicability of linearized theory is questionable.

In figure 13 the theoretical predictions for the two base line model configurations and for the modified arrow designed for Mach 2.7 cruise are shown. For the low-boom configuration the difference between the signatures produced by the ideal area and the designed area again emphasize the sensitivity of the design process.

CONCLUDING REMARKS

A review has been made of some of the questions as yet unanswered in sonic-boom research. Current efforts here at Langley and elsewhere in minimization, human response, higher order asymmetric propagation methods and current techniques of design with sonic-boom constraints have been discussed. In addition, a wind-tunnel test program now being conducted to assess the applicability of minimization methods based on a forward spike in the F-function has been described.

REFERENCES

1. Carlson, H. W.; and Maglieri, D. J.: Review of Sonic Boom Generation Theory and Prediction Methods; J. Acoust. Soc. America, vol. 51, 1972, pp 675-682.
2. Whitham, C. B.: The Flow Pattern of a Supersonic Projectile. Commun. Pure and Applied Math., vol. 5, no. 3, Aug. 1952, pp. 301-348.
3. Walkden, F.: The Shock Pattern of a Wing-Body Combination Far From the Flight Path. Aeronautical Quarterly, vol. 9, May 1958, pp. 164-194.
4. Hayes, Wallace D.: Linearized Supersonic Flow, Ph.D. Thesis, California Inst. Tech., 1947. Reprinted as North American Aviation Rept. A1-222.
5. Jones, L. B.: Lower Bounds for Sonic Bangs. J. Roy Aeronaut. Soc., vol 65, no. 606, June 1961, pp. 433-436.
6. Jones, L. B.: Lower Bounds for Sonic Bangs in the Far Field. Aeronaut. Quart., vol. XVIII, pt. 1, Feb. 1967, pp. 1-21.
7. McLean, F. Edward: Some Nonsymptotic Effects on Sonic Boom of Large Airplanes. NASA TN D-2877, 1965.
8. Hayes, Wallace D.: Brief Review of Basic Theory. Sonic Boom Research. A. R. Seebass, ed., NASA SP-147, 1967, pp. 3-7.
9. Seebass, R.: Minimum Sonic Boom Shock Strengths and Overpressures. Nature, vol. 221, Feb. 1969, pp. 651-653.
10. George, A. R.: Lower Bounds for Sonic Booms in the Midfield. AIAA J., vol. 7, no. 8, August 1969, pp. 1542-1545.
11. George, A. R.; and Seebass, R.: Sonic Boom Minimization Including Both Front and Rear Shocks. AIAA J., vol. 9, no. 10, October 1971, pp. 2091-2093.
12. Seebass, R.; and George, A. R.: Sonic Boom Minimization. J. Acoust. Soc. America, vol. 51, no. 2, pt. 3, Feb. 1972, pp. 686-694.

13. Lung, J. L.: A Computer Program for the Design of Supersonic Aircraft to Minimize Their Sonic Boom. M.S. Thesis, Cornell University, 1975, 75 pp.
14. George, A. R.; and Plotkin, Kenneth J.: Sonic Boom Waveforms and Amplitudes in a Real Atmosphere. AIAA J., vol. 7, no. 10, Oct. 1969, pp. 1978-1981.
15. Darden, Christine M.: Minimization of Sonic Boom Parameters in Real and Isothermal Atmosphere. NASA TN D-7842, March 1975.
16. Darden, Christine M.: Sonic Boom Theory: Its Status in Prediction and Minimization. Paper presented at 14th Aerospace Sciences Meeting, Washington, D.C., Jan. 26-28, 1976.
17. Harris, R. V., Jr.: An Analysis and Correlation of Aircraft Wave Drag. NASA TM X-947, 1964.
18. Middleton, Wilbur D.; and Carlson, Harry W.: A Numerical Method for Calculating the Flat-Plate Pressure Distributions on Supersonic Wings of Arbitrary Planforms. NASA TN D-2570, January 1965.
19. Gottlieb, J. J.: Sonic Boom Research at UTIAS. Canadian Aeronautics and Space Journal, vol. 20, May 1974, pp. 199-222.
20. Ferri, A.; Ting, L.; and Lo, R. W.: Nonlinear Sonic Boom Analysis Including the Asymmetric Effects. AIAA Paper No. 76-587. 3rd AIAA Aero-Acoustics Conference, Palo Alto, Calif., July 20-29, 1976.
21. Hayes, Wallace D.; Haefeli, Rudolph C.; and Kulsrud, H. E.: Sonic Boom Propagation in a Stratified Atmosphere With Computer Program. NASA CR-1299, April 1969.
22. Middleton, Wilbur D.; and Carlson, Harry W.: A Numerical Method for Calculating Near-Field Sonic-Boom Pressure Signatures. NASA TN D-3082, 1965.
23. Onyeonwu, Ronald O.: On the Forward Throw of the Caustic Associated With Transonic Acceleration of a Supersonic Transport. The Aeronautical Journal of the Royal Aeronautical Soc., May 1976.
24. Onyeonwu, R. O.: Sonic Boom Signatures and Ray Focussing in General Maneuvers. I. Analytical Foundations and Computer Formulation. Journal of Sound and Vibration, vol. 42, pt. 1, 1975, pp. 85-102.
25. Lung, J. L.; Tiegerman, B.; Yu, N. J.; and Seebass, A. R.: Advances in Sonic Boom Theory. Part II, NASA SP-347, 1975, pp. 1033-1048.
26. Carlson, Harry W.; Barger, Raymond L.; and Mack, Robert J.: Application of Sonic-Boom Minimization Concepts in Supersonic Transport Design. NASA TN D-7218, June 1973.
27. Kane, Edward J.: A Study to Determine the Feasibility of a Low Sonic Boom Supersonic Transport. NASA CR-2332, December 1973.

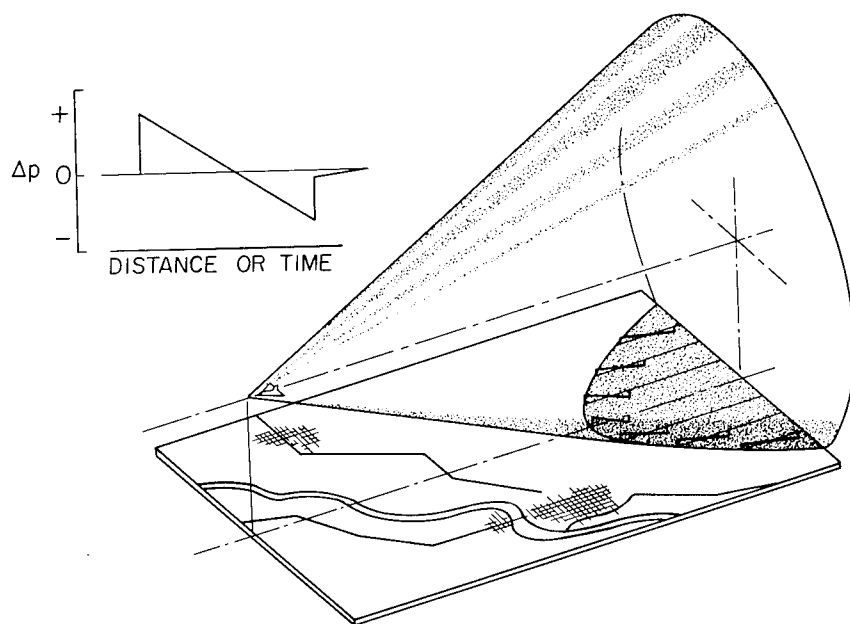


Figure 1.- The sonic boom pressure field.

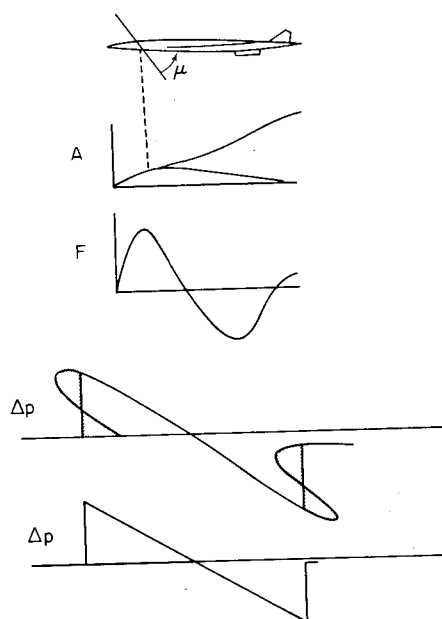


Figure 2.- Prediction methods.

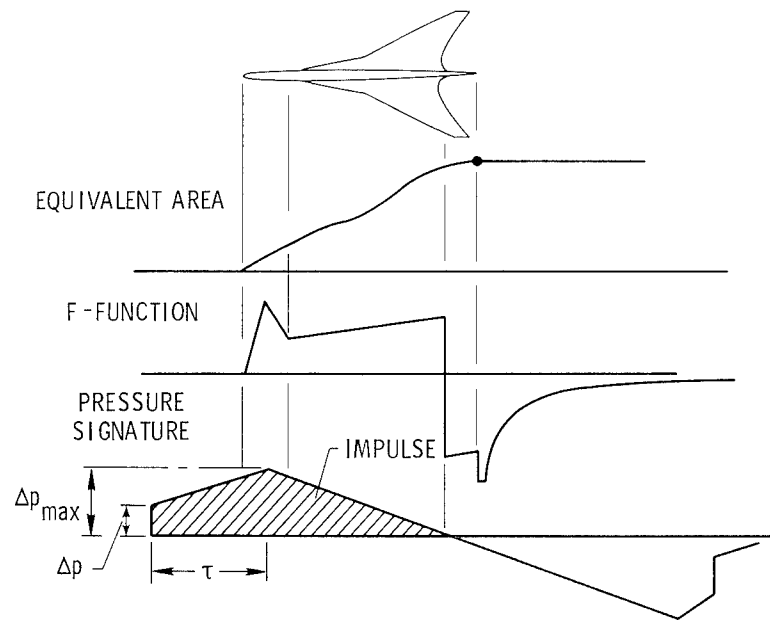


Figure 3.- Sonic-boom minimization concepts.

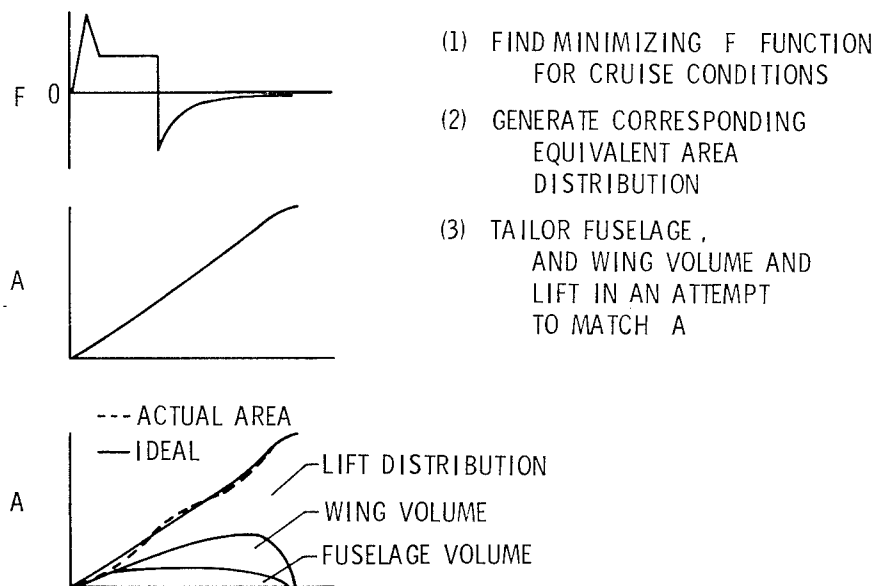


Figure 4.- Minimizing techniques and design methods.

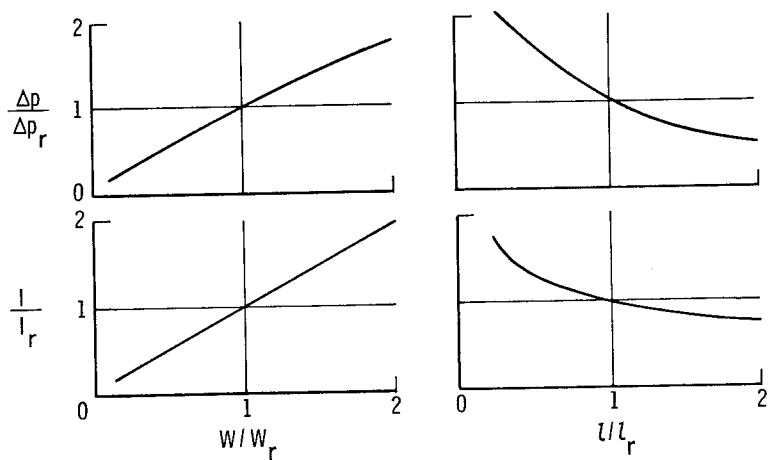


Figure 5.- Sonic-boom variation with airplane parameters. Optimized configuration: $M = 2.7$; $h = 18\,288\text{ m}$ (60 000 ft); $W_r = 272\,155\text{ kg}$ (600 000 lb); $l_r = 91.44\text{ m}$ (300 ft); $\Delta p_r = 45.51\text{ Pa}$ (0.951 lb/ft²); $I_r = 6.48\text{ Pa-sec}$ (0.135 lb-sec/ft²).

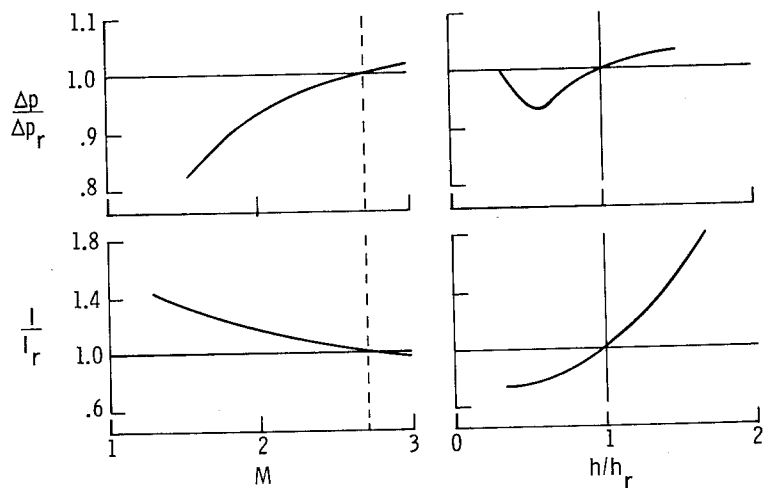


Figure 6.- Sonic-boom variation with operational parameters. Optimized configuration: $W = 272\,155\text{ kg}$ (600 000 lb); $l = 91.44\text{ m}$ (300 ft); $h_r = 18\,288\text{ m}$ (60 000 ft); $M = 2.7$; $\Delta p_r = 45.51\text{ Pa}$ (0.951 lb/ft²); $I_r = 6.48\text{ Pa-sec}$ (0.135 lb-sec/ft²).

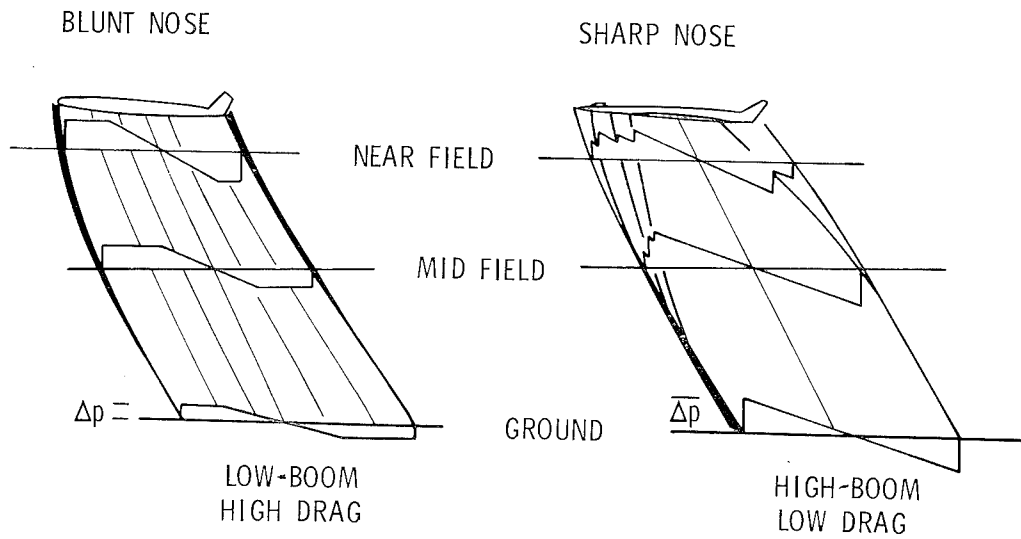


Figure 7.- Drag-boom paradox.

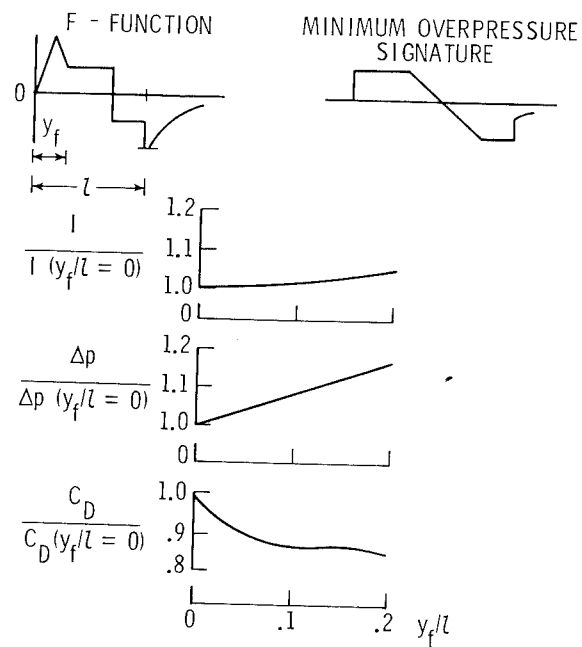


Figure 8.- Estimated drag increments in minimization.

$M = 2.7$ $h = 18288 \text{ m}$ $l = 91.44 \text{ m}$ $W = 272155 \text{ kg}$

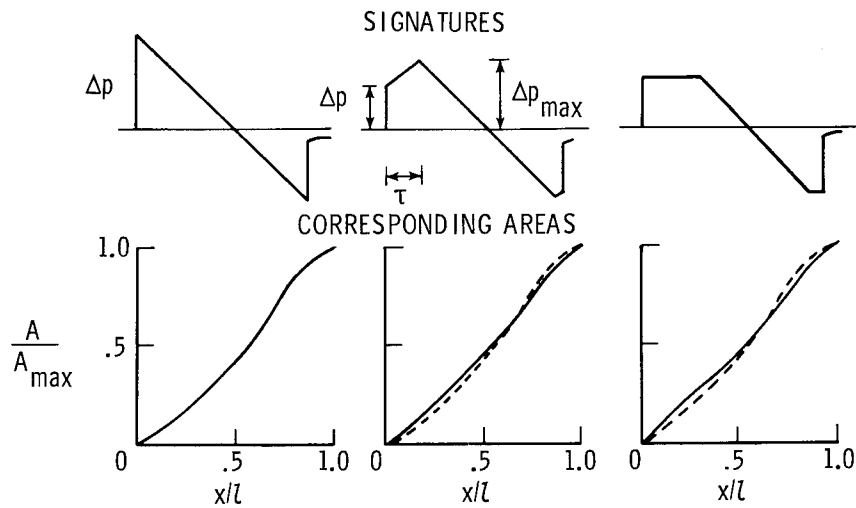


Figure 9.- Human response studies at the University of Toronto Institute for Aerospace Studies.

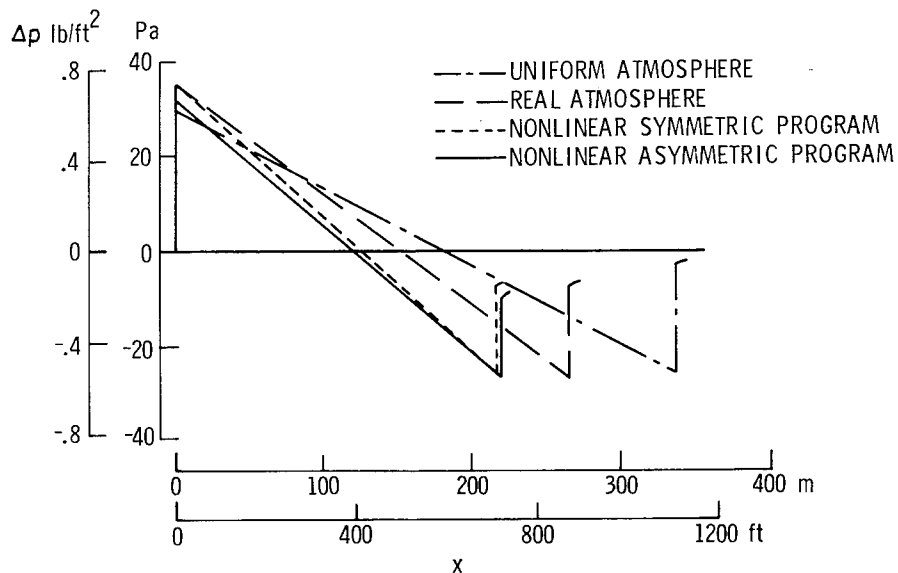


Figure 10.- Higher order propagation methods. $M = 4.0$; $h = 24\,384 \text{ m}$ (80 000 ft); $\alpha = 5$.

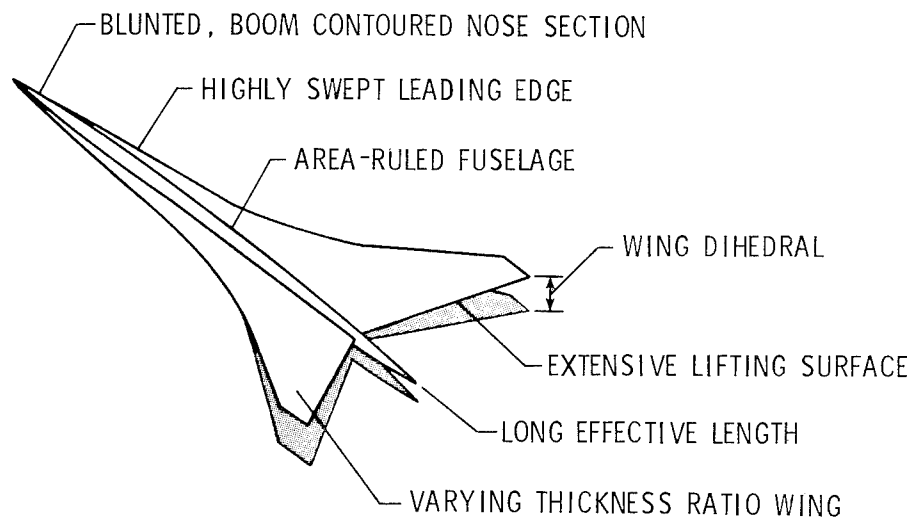


Figure 11.- Features of low-boom study models.

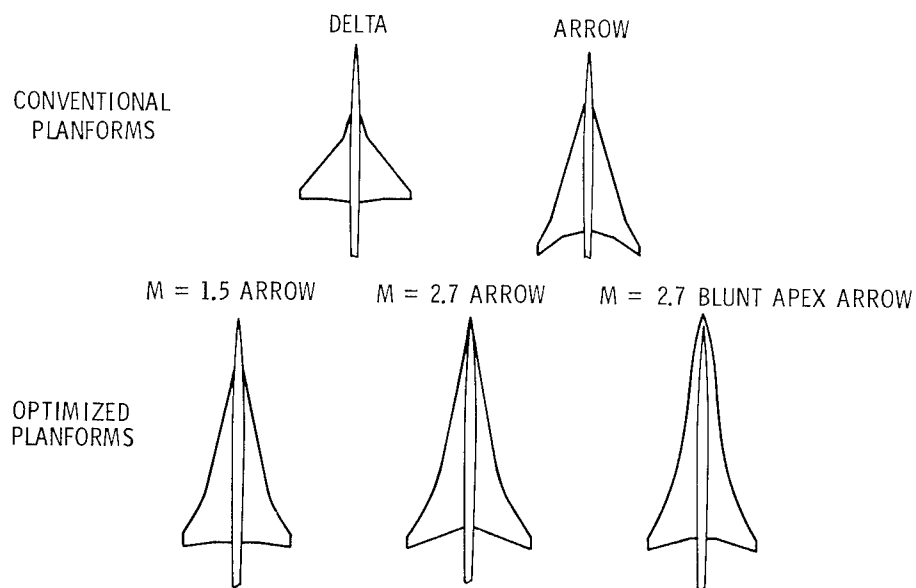


Figure 12.- Planforms for an experimental study of optimization.

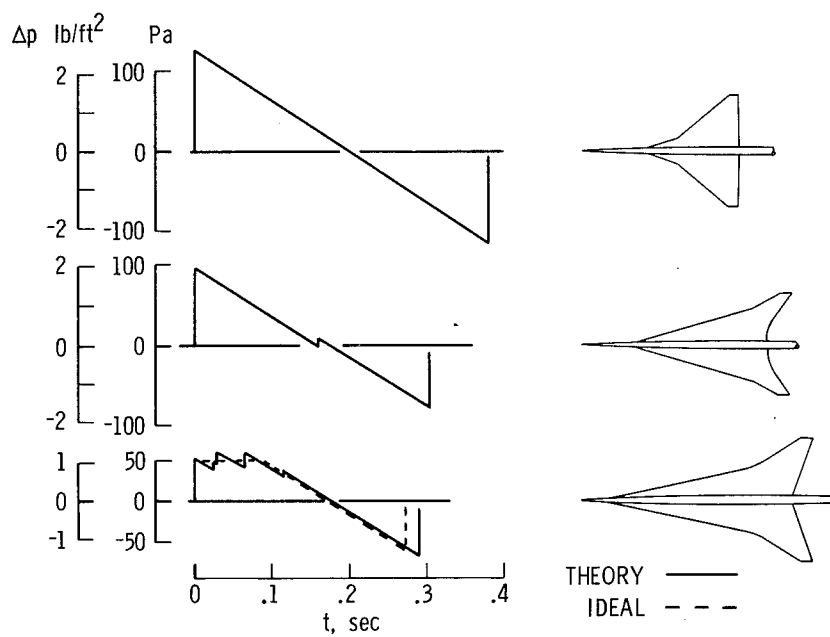


Figure 13.- Ground pressure signatures of models.

TECHNOLOGY FOR CONTROLLING EMISSIONS OF OXIDES OF NITROGEN FROM SUPERSONIC CRUISE AIRCRAFT

Gregory M. Reck and Richard A. Rudey
NASA Lewis Research Center

SUMMARY

Various experiments have been and continue to be sponsored by and conducted by NASA to explore the potential of advanced combustion techniques for controlling aircraft engine emissions into the upper atmosphere. Of particular concern are the oxides of nitrogen (NO_x) emissions into the stratosphere. The experiments utilize a wide variety of approaches varying from advanced combustor concepts to fundamental flame-tube experiments. Results are presented which indicate that substantial reductions in cruise NO_x emissions should be achievable in future aircraft engines. A major NASA program is described which focuses the many fundamental experiments into a planned evolution and demonstration of the prevaporized-premixed combustion technique in a full-scale engine.

INTRODUCTION

This paper describes those activities currently under way at NASA that are specifically directed toward reducing the cruise oxides of nitrogen (NO_x) emissions of high-altitude aircraft.

Two recent studies regarding the potential adverse impact of aircraft exhaust emissions on the upper atmosphere (stratosphere) concluded that the NO_x and oxides of sulfur (SO_x) emitted by future fleets of high-altitude cruise aircraft could influence the stratospheric ozone concentration and the albedo of the Earth (refs. 1 and 2). Both studies recommended that major reductions in both NO_x and SO_x be sought in future gas turbine engines for high-altitude cruise aircraft. The recommended SO_x levels can be achieved by removing the sulfur contained in the fuel for the aircraft. However, the recommended NO_x emission reductions to levels from 1/6 to 1/20 of current levels will require major modifications to conventional engine combustion systems. NASA is promoting, conducting, and sponsoring projects that are directed toward evaluating the combustion techniques needed to achieve these reductions, and if possible, to incorporate attractive NO_x emission reduction techniques into the design of practical engine combustors. These projects encompass levels of technology ranging from minor

modifications to existing conventional engine combustors to fundamental flame-tube studies. The final goal of these efforts is to reduce cruise NO_x emissions to the lowest possible level while still maintaining acceptable performance in terms of fuel consumption, durability, maintainability, and safety. In addition to these constraints, any viable combustion system must be also capable of meeting local environmental standards, such as the proposed Environmental Protection Agency (EPA) supersonic aircraft standards. Therefore, emissions at idle, climbout, and takeoff must also be controlled.

This paper presents and discusses some of the results obtained from research and development programs being sponsored, directed, and/or conducted by NASA. Although we recognize that much important work is being conducted at or sponsored by universities, private industry, and other government agencies (DOD, FAA, EPA, etc.), this paper concentrates on NASA programs only. Activities ranging from investigating variations of conventional combustion systems to evaluating advanced catalytic techniques are being pursued. Application of these techniques to future aircraft engines are being considered. The results pertinent to the NO_x emission reduction efforts are presented and discussed along with an assessment of the projected development difficulties and a forecast of potential emission level reductions. A recently implemented NASA effort called the Stratospheric Cruise Emission Reduction Program (SCERP) is also described and discussed.

OXIDES OF NITROGEN EMISSION CONTROL TECHNIQUES

The largest single factor which controls the formation of NO_x in a combustion process is the flame temperature in the reaction zone. An example of this effect is illustrated in figure 1, where NO_x concentration is plotted as a function of flame temperature. The values shown were calculated by using a well-stirred-reactor model and are representative of the levels generated in a completely homogeneous prevaporized-premixed combustion process with a 2-msec residence time (typical of contemporary engine combustors).

Because of the exponential variation of NO_x formation as a function of flame temperature, controlling flame temperature in a combustion process should provide a very powerful tool for controlling NO_x emissions. Combustion scientists and engineers are pursuing and evaluating techniques to achieve flame temperature reductions by using the so-called lean-combustion approach. Lean combustion is presently taken to be associated with an equivalence ratio (ratio of local to stoichiometric fuel-air ratio) ϕ between 0.4 and 1. The NASA aircraft gas turbine engine NO_x emission reduction efforts are primarily directed toward exploring the potential of this lean-combustion approach for eventual application to practical engine combustors.

Lean-Combustion Experiments

Conventional combustion. - Advanced technology approaches using conventional techniques for emission reduction are being evaluated in the NASA Experimental Clean Combustor Program (contract effort with General Electric and Pratt & Whitney) (refs. 3 and 4), and a variety of modifications have been evaluated. Examples of several of these modifications are described in the section APPLICATION OF EMISSION CONTROL TECHNIQUES. Work done up to this time indicates that NO_x reductions of up to 50 percent may be achievable in conventional type combustors by employing lean combustion in the primary zone and by controlling residence time. It also appears that these reductions can be achieved along with acceptable combustor performance, as indicated in references 3 and 4.

Forced-circulation technique. - The term "forced circulation" is used to describe the use of strong swirling flow or impinging jets to form one or more powerful recirculation cells in a combustor primary zone. The powerful recirculation cell provides a mechanism for entraining hot combustion gases into the flame region and thereby establishing a stable zone for lean combustion to occur. When these recirculation cells are coupled with a partially prevaporized-premixed fuel-air mixture, as is illustrated in figure 2, the combustion process can begin to approach the homogeneous process more closely than any modification using conventional combustion techniques. The two concepts shown in figure 2, jet induced circulation (JIC) and vortex airblast (VAB), are being evaluated under NASA contract to the SOLAR Division of International Harvester Company. To date these concepts have been and continue to be evaluated in a tubular configuration, but use of a full annular model is planned for the future. References 5 and 6 give details of these experiments, and a representative plot of the best emission results obtained is shown in figure 3. The VAB concept achieved a NO_x emission index of approximately 1 g NO_2 /kg fuel at the designated simulated supersonic cruise operating design point (although inlet pressure was not a true simulation). The JIC concept was capable of producing a NO_x emission index of 2 g NO_2 /kg fuel. Both of these values represent substantial reductions (to a level of approximately 1/10 of conventional combustor emissions) at similar operating conditions. Both concepts were optimized for lean combustion at the design point (designated cruise conditions); hence, low temperature rise performance was characterized by instability and low efficiency. Design point efficiency was in excess of 99.5 percent. Currently, the ability of these concepts to satisfy off-design (idle through takeoff) operating requirements is being evaluated.

Prevaporized-premixed technique. - Perhaps the most successful method of reducing NO_x emissions to extremely low levels has been the completely prevaporized-premixed combustion technique. Studies of this technique have been conducted by a large cross section of the combustion technical community. In most instances, the

studies are conducted in experimental flame tubes such as the two illustrated in figure 4. Both flame tubes employ a vaporizer-mixer section, a flameholder (a cone in the General Applied Science Laboratory (GASL) apparatus and a perforated plate in the NASA apparatus), a flame zone, and a gas sample extraction probe. The NASA apparatus has both liquid and vapor fuel capability. Application of the completely prevaporized-premixed technique to actual combustors has been suggested, but no combustorlike hardware has been investigated by NASA.

The results of some of the NASA and GASL experiments (sponsored by NASA) are summarized in figures 5 and 6. Details regarding these experiments are given in references 7 and 8. Values of NO_x emission index below $0.5 \text{ g NO}_2/\text{kg fuel}$ were achieved in both of the experiments, and close agreement between the results of the two experiments was realized. From figure 5 one can see that, if combustion efficiency is to be maintained above 99.5 percent (a likely requirement for cruise performance), the NO_x emission index would have to be $0.4 \text{ g NO}_2/\text{kg fuel}$ or higher. A principal factor which controls efficiency of the prevaporized-premixed combustion process is residence time, as shown in figure 6. If one allows residence time to increase (either by reducing flow velocity or making the combustor larger), high values of efficiency can be obtained at the very low equivalence ratios needed for obtaining extremely low NO_x emissions. Therefore, values below $0.5 \text{ g NO}_2/\text{kg fuel}$ would be obtainable if residence time could be independently controlled. In evaluating the values of emission index obtained in these experiments and displayed in figures 5 and 6, one should use considerable caution. These were carefully controlled experiments, wherein all parameters such as airflow, fuel flow, pressure, and temperature were maintained very stable; this environment does not necessarily represent that which would be present within a normal gas turbine engine. Also, the experiments represent near design point operation (particularly inlet temperature), where conditions are favorable for effective fuel vaporization and lean-combustion stability. Nevertheless, the results do indicate that the prevaporized-premixed combustion technique is a strong candidate for reducing aircraft NO_x emissions to extremely low values and certainly warrants continued investigation.

Catalytic Combustion Experiments

Perhaps one of the most unique concepts for reducing aircraft gas turbine emissions is the potential application of catalyst elements to enhance the reaction process of extremely lean fuel-air mixtures. For exploring the potential of this concept, NASA is employing the apparatus shown schematically in figure 7 and described in detail in reference 9. The apparatus consists of a vaporizer-mixer section, a catalyst element section, and a probe for extracting a gas sample for analysis. The schematic illustra-

tion shows that up to four catalyst elements can be used in a typical test. All four elements can be varied in terms of the catalyst type and the substrate structure. This allows for an optimization of pressure drop and temperature rise across the entire catalyst bed. Extremely low NO_x emissions (below measurable quantities) have been obtained in experiments in which propane fuel premixed with air was used. Propane was used to ensure complete vaporization prior to contact with the catalyst elements. Several of the problems of using this concept are the inherently narrow efficient operating range (dramatic efficiency losses occur at very low off-design equivalence ratios), the temperature limitation due to catalyst and substrate melting, potential catalyst poisoning by fuel impurities, and the need to preheat the bed or fuel-air mixture to initiate reactions (cold starting is not possible). Nevertheless, the catalyst concept will continue to be explored both as a total combustion system and as a possible lean stability augmentation device for application to a hybrid catalyst - prevaporized-premixed combustion system.

Off-Design Considerations

Up to this point all the discussion has centered about results obtained at selected design points simulating supersonic cruise conditions. Optimization for low NO_x emissions at this condition requires the use of lean burning, which for a primary-zone ϕ of less than 0.5 uses much of the available air in the combustion process. This type of airflow distribution presents a problem when the combustor must be operated at the low overall equivalence ratios that are required for engine idle. Poor stability and poor efficiency generally are the result. The SOLAR VAB concept was reconfigured to optimize the primary-zone ϕ for the idle condition in order to improve stability and to minimize the formation of idle pollutants such as carbon monoxide (CO). The effect of this change on both the idle and cruise point emissions is shown in figure 8. As the fuel flow was increased to obtain the required cruise temperature rise, the primary-zone ϕ went through stoichiometric and into a rich burning condition. The result was unacceptably high levels of NO_x and CO emissions.

Results such as these clearly indicate the need for either some form of staged combustion or variable control that can maintain primary-zone ϕ at the optimum level needed to satisfy both engine demands and emission level requirements. A significant effort to evaluate the potential of the staged combustion approach, using conventional combustion techniques, has been and continues to be put forth in the NASA Experimental Clean Combustor Program (refs. 3 and 4). NASA plans to explore the potential of the variable-geometry approach in SCERP, which is described in the section STRATOSPHERIC CRUISE EMISSION REDUCTION PROGRAM. Regardless of which technique proves to be the most desirable and practical, the impact of off-design

performance and emission requirements must be considered in evaluating the level of potential gains that may be achieved by employing the advanced combustion techniques currently being investigated. Many compromises are certainly going to be required in order to evolve practical, operational combustors for future aircraft engines.

APPLICATION OF EMISSION CONTROL TECHNIQUES

Since future supersonic cruise aircraft may employ variable-cycle engines with possible thrust augmentation, the potential application of the NO_x emission control techniques must be evaluated in terms of both primary combustors and thrust augmentors (especially duct burners). In response to the need for evaluating the problems involved in these applications, NASA is currently conducting studies to apply conventional (staged) low NO_x combustion techniques to contemporary engine primary burners and to experimental duct burners. Two of these efforts are described in this section. No comparable effort has been undertaken to evaluate the application difficulties expected for the forced-circulation, prevaporized-premixed, or catalytic techniques up to the present time, although plans to do so in the future are being formulated and are described in the section STRATOSPHERIC CRUISE EMISSION REDUCTION PROGRAM.

Main Burners

The principal effort to apply conventional lean-burning techniques to primary burners of current subsonic and possible future supersonic cruise aircraft engines has been conducted in the Experimental Clean Combustor Program. In all cases, the desired application required the use of the staged combustion approach, wherein one stage (pilot) was optimized for acceptable idle and taxi emissions and performance, and one stage (main) was optimized for high power takeoff emissions and performance. Several examples of staged concepts are illustrated in figure 9. Figures 9(a) and (b) represent cross sections of full annular adaptations of a two-row swirl-can-modular concept and a double-annular concept for a General Electric CF6-50 engine, and figure 9(c) represents a concept for a Pratt & Whitney JT9D-7 engine called a vorbix. Although these concepts were designed for specific subsonic engines, they were also modified in an attempt to optimize their NO_x emission performance at simulated supersonic cruise conditions (refs. 3 and 4). Proper scheduling of both fuel flow and airflow between the two stages reduced NO_x emissions approximately 50 percent at selected subsonic and supersonic cruise conditions, as compared with those of present in-service engines at comparable operating conditions. The principal development activities still needed to make these two-stage combustors acceptable for operational engine adaptation include (1) defining and optimizing the staging characteristics during

acceleration, deceleration, and part power operation and (2) defining accurate control parameters and control functions to permit smooth staging to occur. A considerable amount of information regarding these staging characteristics as well as emission performance will be generated during the full-scale engine tests of the double annulus in the CF6-50 and the vorbix in the JT9D-7 that are scheduled during the latter part of 1976.

Duct Burners

NASA currently is sponsoring two activities with the objective of defining the expected emission levels that can be obtained by applying NO_x emission control techniques to candidate duct burners for possible supersonic cruise aircraft engines. Both efforts, an experimental study by General Electric and an analytical study by Pratt & Whitney, are being conducted under contract with NASA. The NO_x emission level goal for the duct burner application is 1 g NO_2 /kg fuel at the designated supersonic cruise condition with a 99 percent or higher combustion efficiency. Further considerations include the necessity to meet proposed local emission standards currently under study by the EPA and performance requirements during transonic acceleration (most severe temperature rise condition). These multiple requirements when coupled with operational considerations, such as "soft" lightoff, led to the need for a staged combustion concept.

A schematic illustration of one configuration of a staged combustion concept currently under evaluation at General Electric is shown in figure 10. As with the main burners, one stage (pilot) is optimized to provide low CO and unburned hydrocarbon emissions at low power, and the other stage (main) low NO_x at high power. The configuration shown is a variation of a radially and axially staged primary combustor that was evaluated in the work of reference 3. Experimental testing has just recently begun.

The Pratt & Whitney analytical study is examining a number of concepts for both pilot and main stages of a staged duct burner combustion system. These concepts include premixers, prevaporizers, swirl stabilizers, flash vaporizers, variable-geometry features, and other advanced techniques. The analytical study is being expanded into an experimental study of several of the most attractive concepts.

ASSESSMENT OF RESULTS

The NO_x emission reduction potential of the various control techniques for future engines was estimated by utilizing projected engine cycle conditions and accepted extrapolation and correlation methods. Although extrapolation and correlation methods are constantly being updated as experimental results are obtained, the results of the previously described activities were extrapolated to the projected cycle conditions by using the following equation:

$$(EI)_2 = (EI)_1 \left[\frac{(P_3)_2}{(P_3)_1} \right]^{0.5} \exp \left[\frac{(T_3)_2 - (T_3)_1}{288} \right] \left[\frac{(T_4)_2}{(T_4)_1} \right] \quad (1)$$

where

- EI emission index
- P_3 combustor inlet pressure
- T_3 combustor inlet temperature
- T_4 combustor outlet temperature
- 1 experimental test conditions
- 2 designated operating conditions

Projected Engine Cycles

The projected supersonic cruise engine cycle parameters that are needed as inputs to equation (1) are presented in table I. The operating conditions of the SNECMA/Rolls-Royce Olympus 593 (as reported in ref. 10) and two advanced study engines were used. The Olympus 593 engine represents current turbojet technology with an engine cycle pressure ratio of approximately 15:1. The cycle cruise parameters for the Olympus 593 were computed at a Mach 2.0 cruise speed and a 17.7-km altitude. The afterburner is not used for steady-state cruise. The two study engine cycles, one by Pratt & Whitney and one by General Electric, represent current values from a NASA sponsored study to evaluate potentially attractive propulsion systems for possible future supersonic cruise aircraft. These study engines encompass an engine cycle pressure ratio range of approximately 20:1 to 25:1, and a Mach 2.32 cruise speed at an average altitude of 16 km was used to compute the engine cycle parameters. Since the NASA sponsored study is not yet complete, the final values for the cycle parameters of the two study engines could vary somewhat from those shown in table I. However, for the purpose of estimating the NO_x emissions for future supersonic cruise aircraft engines, the values shown should be reasonably representative.

Emission Level Forecast

From the engine cycle cruise parameters shown in table I, emission level forecasts were made for the various NO_x control techniques previously described. In figures 11 and 12 the emission level forecasts are presented and compared with levels

that could be expected from current technology combustors operating at the same cycle parameter conditions. All the values shown in these figures represent extrapolations from either rig or engine test conditions to the designated cruise conditions made by using equation (1). They also represent NO_x emission levels at combustion efficiencies in excess of 99.5 percent.

The application of the clean combustor technology to the contemporary turbojet (Olympus 593) cycle parameters shown in figure 11 would provide a potential reduction in projected cruise NO_x emissions to a level of about 1/2 of current levels. If reductions to a level of 1/6 of current levels (recommendation of ref. 1) are to be achieved, the implementation of either the forced-circulation, prevaporized-premixed, or catalytic combustion techniques will be required. Of these three techniques, the forced-circulation technology is farthest along in the process of converting fundamentals to combustor hardware but also offers the least gains. Based on the extrapolations, only the prevaporized-premixed and catalytic techniques offer the potential for reducing emissions below 1 g NO_2 /kg fuel at the designated cruise conditions.

The projected emission levels of the various techniques for the advanced study engine cycles are shown in figure 12. As in the contemporary turbojet projections, the level of potential reduction is greater with the lesser developed techniques. In addition, the projected values for the advanced engines are approximately a factor of 2 higher than the projected values for the contemporary turbojet engine because the combustor inlet and outlet conditions are more severe from a NO_x formation standpoint (higher cycle pressure ratios). Because of the more severe conditions in the advanced engine cycles, employing clean combustor technology would result in reducing the NO_x emissions to levels nearly equal to those of the current supersonic aircraft turbojet engines (≈ 20 g NO_2 /kg fuel). Achieving reductions to a level of 1/6 or less of the current 20 g NO_2 /kg fuel level will definitely require the application of prevaporized-premixed or catalytic techniques.

The actual achievable levels may be somewhat different from those shown in figures 11 and 12 when the described emission control techniques are developed into operational engine hardware. Tradeoffs among emissions, performance, altitude relight, durability, maintainability, and complexity as well as the influence of the actual engine environment as opposed to the carefully controlled rig experimental conditions will have to be considered. The end result will likely be some upward adjustment to the levels shown in figures 11 and 12. Actual engine demonstration and technology development must be conducted before the levels can be quantified and considered to represent achievable levels accurately. However, the general trends displayed by employing the various techniques should be correct.

In evaluating these results, please bear in mind that the levels were extrapolated to the designated conditions by using equation (1). In some of the fundamental investi-

gations (e. g. , prevaporized-premixed concept), the effect of combustor inlet pressure and temperature resulted in some anomalies from the relations described by equation (1). These anomalies could have an impact on the final extrapolated levels and are discussed in the next section. The trends, however, are clear. The low levels of cruise NO_x emissions recommended by references 1 and 2 will most likely require the development and implementation of the less developed, higher risk technology associated with the prevaporized-premixed and catalytic techniques.

STRATOSPHERIC CRUISE EMISSION REDUCTION PROGRAM

In response to the need for substantial cruise NO_x emission reductions, highlighted by the studies mentioned previously (refs. 1 and 2), NASA has initiated SCERP. The SCERP objectives are to develop and demonstrate the technology necessary to reduce cruise NO_x emissions to a level of 1/6 or less of current levels and to meet the current EPA 1979 emission standards (ref. 11) for the airport vicinity. The technology will be designed for the high-bypass-ratio, high-pressure-ratio engines currently powering the wide-body subsonic transports. Technology evolved by SCERP, although not directly applicable, should also aid in the development of low NO_x combustors for future supersonic cruise aircraft engines.

The prevaporized-premixed technique for emission reduction will be explored in the SCERP activity. The results shown in figure 5 indicate that this technique has the potential to meet or exceed the program goal. While this technique does not offer the emission reduction potential of the catalytic approach, the practical problems associated with its application are viewed as less severe. However, from the earlier discussion of off-design considerations it is apparent that a form of variable geometry will likely be necessary to maintain acceptable combustor performance as well as low emissions over the entire flight envelope. In addition, it is expected that an advanced digital control system will likely be required for the eventual engine application.

The program plan for SCERP is broken into an initial phase consisting of a number of fundamental studies to establish design criteria for prevaporizing-premixing combustors and a final phase wherein promising combustor designs will be experimentally evaluated, developed, and eventually demonstrated in an engine. The fundamental studies in the initial phase are grouped in the following four areas: lean combustion, fuel-air mixture preparation, autoignition and flashback, and engine constraints. Specific studies in each of these areas are being initiated by NASA through a combination of both in-house and contracted research as well as university grant activities.

In the first area, lean combustion, a study will be conducted to examine the effect on emissions of various fuel spray characteristics including the degree of vaporization, the mean drop size, the fuel-air distribution, and other factors. Another lean

combustion study will parametrically examine the effects of engine cycle parameters on emissions in order to develop correlations. Emission measurements of a premixed-propane combustor will be made over a wide range of conditions up to 40 atm and 1000 K. The problem of extrapolating emission data over a wide range of conditions is illustrated in figure 13, which shows emission data taken from the GASL experiment described in reference 8. The expected dependency of NO_x emission index on the square root of pressure is not evident, and emission minimums occur near 8 atm. This effect is likely associated with the prevaporizing-premixing process and may result from an improvement in degree of vaporization or fuel distribution at the higher pressure conditions. Other lean-combustion studies include an investigation of the effect of flameholder geometry on emissions and performance and an examination of several schemes for improving lean stability limits.

In the second area, fuel-air mixture preparation, engine measurements are being made to characterize the compressor discharge turbulence. The nature of the turbulence in the diffuser inlet may promote fuel mixing and vaporization if fuel is introduced in this region. In addition, techniques for vaporizing fuel external to the combustor will be studied, and schemes for controlling radial fuel-air distribution will be examined.

The third area, autoignition and flashback, presents serious hazards to potential prevaporizing-premixing combustors. In many of the flame-tube studies, including those at GASL and NASA, autoignition or flashback have occurred at some conditions. Figure 14 illustrates the autoignition problem. The vaporization times shown in the figure were derived from a simplified model developed at NASA, and the ignition delay values were obtained from reference 12. It is apparent that, if the fuel is given sufficient time to vaporize completely at the higher cycle pressure ratios, it may autoignite. The SCERP studies in this area include a parametric study of the factors influencing autoignition delay up to pressures in excess of 30 atm, a study of the effect of hot surfaces on autoignition, and an examination of the effects of boundary layers and engine transients on flashback.

The fourth area, identified as engine constraints, refers to problems arising from the interfaces between the combustor and the engine. The characteristics of the compressor discharge airflow are of particular concern in a premixing combustor to assure control of the homogeneity of the fuel-air mixture. In addition to the turbulence measurements mentioned previously, an investigation of the circumferential airflow uniformity at the compressor exit will be conducted. Another study will examine the effects of nonideal turbine inlet temperature profiles on turbine life and performance. With an extremely lean primary zone, considerably less dilution air may be available for tailoring the combustor exit temperature profile. And finally, a simplified combustor model will be incorporated into an engine transient performance computer

routine to investigate the interaction of the combustor with the remainder of the engine during acceleration and deceleration. With variable geometry, transient performance may be a serious concern.

As the results of the initial studies become available, the design data will be applied to combustor concepts. Variable-geometry techniques and controls will be incorporated into the designs as required. As the designs evolve, an assessment of their potential with regard to both emissions reduction and practical application will be made. The most promising concepts will then be selected for experimental screening.

CONCLUDING REMARKS

Results obtained from a variety of projects, varying in degree of technological advancement, currently being conducted and sponsored by NASA indicate that substantial reductions in cruise NO_x emissions should be achievable in future supersonic aircraft gas turbine engines. The degree of reduction achievable is, of course, dependent upon the level of advanced combustion technology that is judged to be developable into operational combustors. At designated cruise design points for current intermediate-pressure-ratio engines, advanced combustor technology of the type being evaluated in the NASA Experimental Clean Combustor Program offers the promise of reducing NO_x emissions to a level of 1/2 of current engine levels. Reductions beyond these levels will require the application of higher risk technology such as prevaporized-premixed combustion concepts. Results from controlled experiments indicate that this more advanced technology may provide reductions to levels of 1/6 of current levels. It is important to note that these reductions have only been achieved in controlled rig experiments and they must certainly be quantified in full-scale engines. Since control of emissions at all operating conditions, from idle and taxi up to cruise, will be required in future engines, some form of combustion staging or variable geometry will be needed regardless of the level of advanced technology employed. This added complexity will likely affect the final achievable levels of cruise NO_x and will also increase the development risk involved. Much additional information is still needed before the impact of off-design conditions can be quantified.

Continuing studies directed toward defining the probable engine cycle conditions for future supersonic cruise vehicles indicate that cycle pressure ratios are likely to be higher than those previously used for estimating future engine emissions. These higher cycle pressure ratios have a direct impact on the NO_x emission levels that can be forecast on the basis of the present experimental results. Values considerably higher than previous estimates are projected when conventional correlating parameters are applied. Recent parametric tests of the full and partial prevaporized-premixed techniques, however, revealed some anomalies with regard to the pressure and tem-

perature effects on NO_x formation. Much more information on these effects must be obtained before reasonably accurate extrapolations can be made.

The message then would seem to be clear. A careful, systematic approach is needed to answer the anomalies; to fill in the gaps in fundamental knowledge, such as autoignition and flashback; to determine the tradeoffs between complexity and emission reduction potential; and finally to demonstrate the performance of the high risk, low NO_x emission technology in an actual engine environment. The goals and approach of the NASA Stratospheric Cruise Emission Reduction Program (SCERP) have been structured to satisfy most of these needs. Because of the NO_x emission reduction promise that the high risk technology has indicated in controlled experiments, programs such as SCERP are needed to provide the data bank required to assess properly the ability to convert this technology into practical engine combustors. This then will help determine the ability of future high-altitude cruise aircraft engines to meet the levels recommended by environmental studies.

REFERENCES

1. Grobecker, A. J.; Coroniti, S. C.; and Cannon, R. H., Jr.: The Effects of Stratospheric Pollution by Aircraft. DOT-TST-75-50, Dept. of Transportation, 1974.
2. Environmental Impact of Stratospheric Flight. Nat. Acad. Sci., 1975.
3. Bahr, D. W.; and Gleason, C. C.: Experimental Clean Combustor Program, Phase I. (GE-74AEG380, General Electric Co.; NAS3-16830), NASA CR-134737, 1975.
4. Roberts, R.; Peduzzi, A.; and Vitti, G. E.: Experimental Clean Combustor Program, Phase I. (PWA-5153, Pratt & Whitney Aircraft; NAS3-16829), NASA CR-134736, 1975.
5. Roberts, P. B.; White, D. J.; and Shekleton, J. R.: Advanced Low NO_x Combustors for Supersonic High-Altitude Aircraft Gas Turbines. (RDR-1814, Solar; NAS3-18028), NASA CR-134889, 1975.
6. Roberts, P. B.; et al.: Advanced Low NO_x Combustors for Supersonic High-Altitude Aircraft Gas Turbines. ASME Paper 76-GT-12, Mar. 1976.
7. Anderson, D.: Effects of Equivalence Ratio and Dwell Time on Exhaust Emissions from an Experimental Premixing Prevaporizing Burner. ASME Paper 75-GT-69, Mar. 1975.
8. Roffe, Gerald; and Ferri, Antonio: Prevaporization and Premixing to Obtain Low Oxides of Nitrogen in Gas Turbine Combustors. NASA CR-2495, 1975.
9. Anderson, David N.: Preliminary Results from Screening Tests of Commercial Catalysts with Potential Use in Gas Turbine Combustors. Part II. Combustion Test Rig Evaluation. NASA TM X-73412, 1976.
10. Propulsion Effluents in the Stratosphere. CIAP Monograph 2. DOT-TST-75-52, Dept. of Transportation (PB-24631918), 1975.
11. Control of Air Pollution for Aircraft Engines - Emission Standards and Test Procedures for Aircraft. Federal Register, vol. 38, no. 136, July 17, 1973, pp. 19087-19103.
12. Spadaccini, L. J.: Autoignition Characteristics of Hydrocarbon Fuels at Elevated Temperatures and Pressures. ASME Paper 76-GT-3, March 1976.

TABLE I. - ENGINE CYCLE CRUISE PARAMETERS

ENGINE	COMBUSTOR INLET PRESSURE, atm	COMBUSTOR INLET TEMPERATURE, K	COMBUSTOR EXIT TEMPERATURE, K
OLYMPUS 593 ^a	6.5	824	1320
GENERAL ELECTRIC DOUBLE BYPASS ^b	9.4	887	1809
PRATT & WHITNEY VARIABLE STREAM CONTROL ^b	14.1	985	1755

^aMACH 2.0; 17.7-km ALTITUDE (NONAFTERBURNING).

^bMACH 2.32; 16-km ALTITUDE.

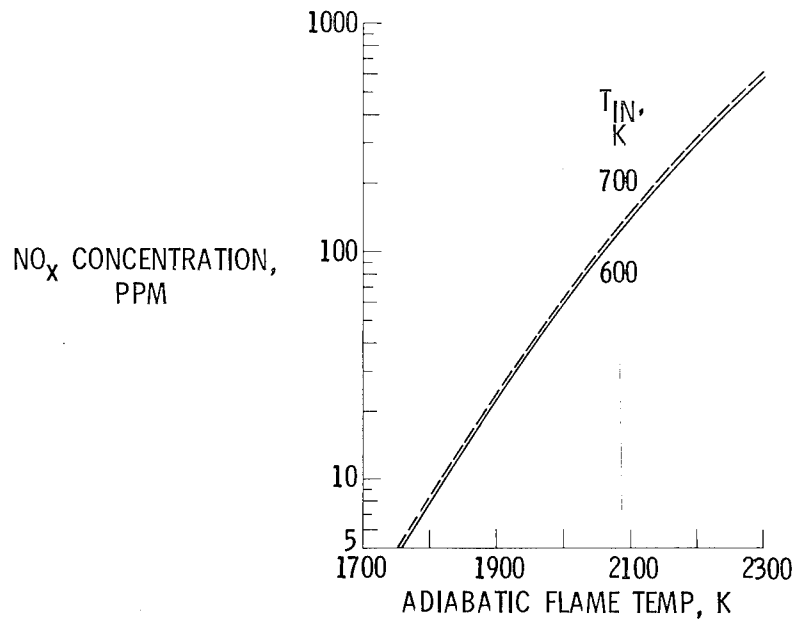
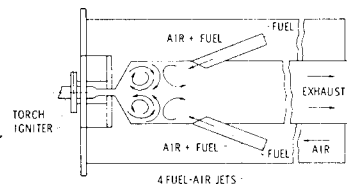
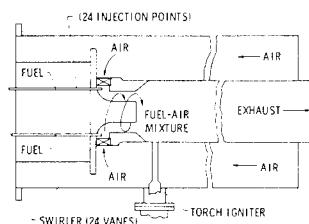


Figure 1.- Effect of flame temperature on theoretical oxides of nitrogen concentration formed in homogeneous prevaporized-premixed combustion process (from well-stirred-reactor prediction). Inlet pressure, 56 N/cm²; residence time, 2 msec.

FORCED CIRCULATION TECHNOLOGY



JET-INDUCED CONCEPT



VORTEX AIRBLAST CONCEPT

Figure 2.- Schematic illustrations of advanced combustor concepts used in fundamental experiments at SOLAR.

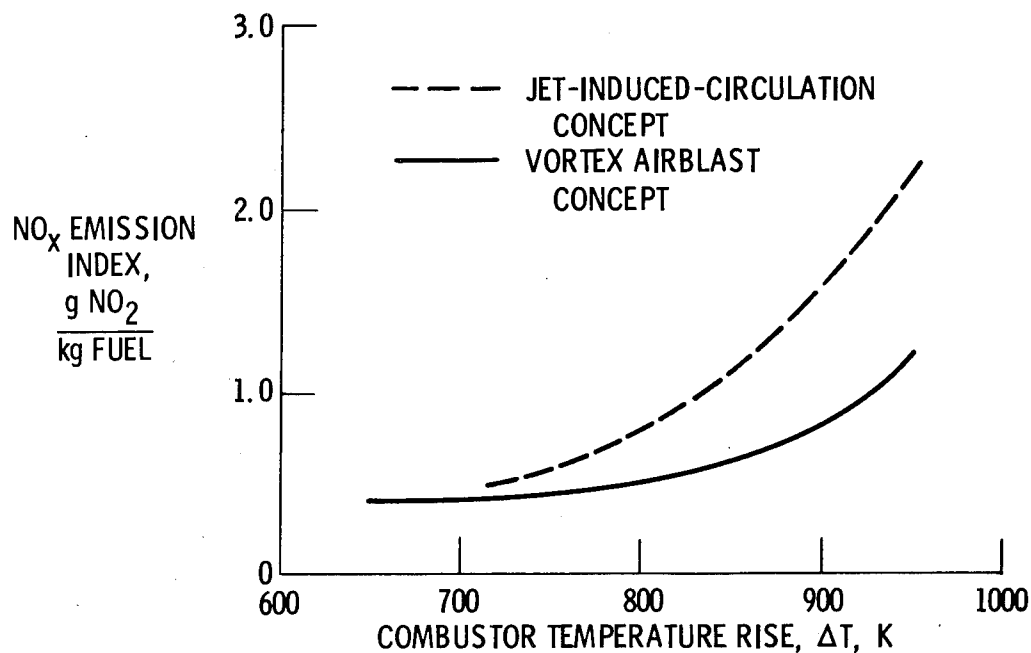
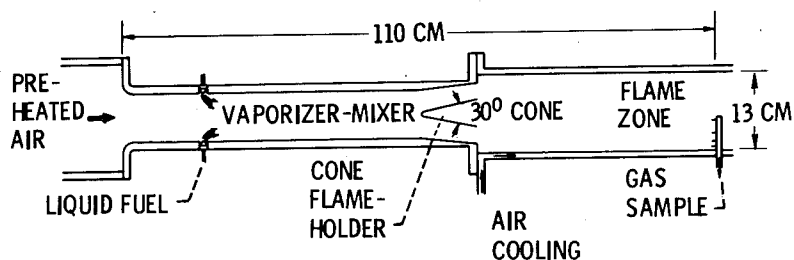
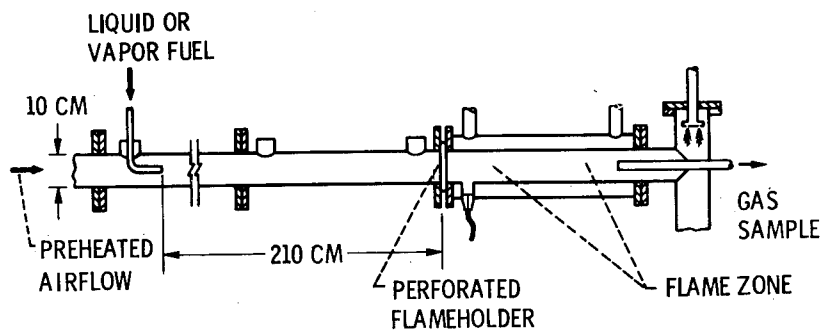


Figure 3.- Effect of combustor temperature rise on NO_x emissions of two SOLAR low NO_x combustor concepts. Jet A-1 fuel; inlet temperature, 830 K; inlet pressure, $\sim 20 \text{ N/cm}^2$.



(a) GASL premixed primary zone test section.



(b) NASA premixed primary zone test section.

Figure 4.- Schematic illustrations of experimental flame-tube apparatus used in GASL and NASA prevaporized-premixed combustion studies.

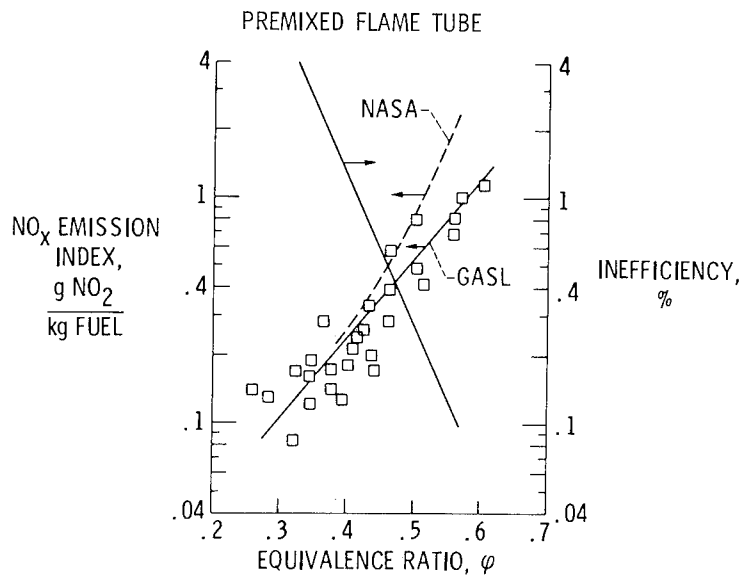


Figure 5.- Impact of combustion equivalence ratio on formation rate of oxides of nitrogen and on combustion inefficiency for GASL and NASA fundamental experiments. Inlet pressure, 40 N/cm²; inlet temperature, 830 K; Jet-A fuel.

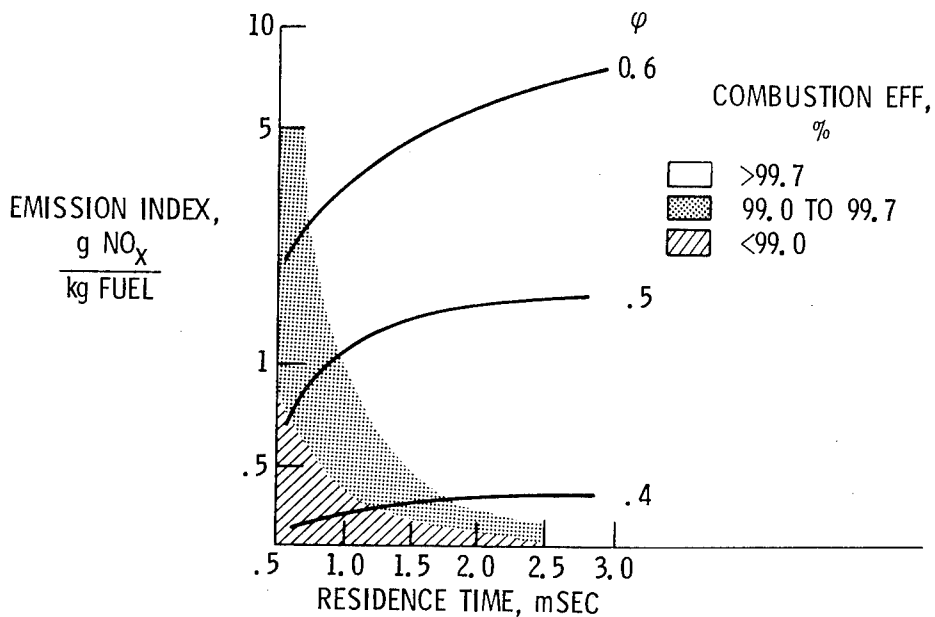
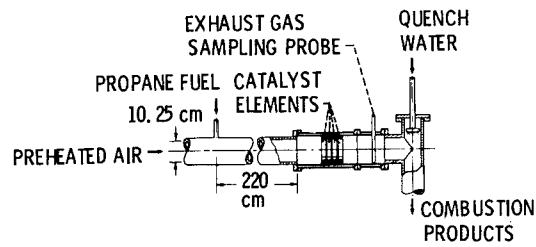
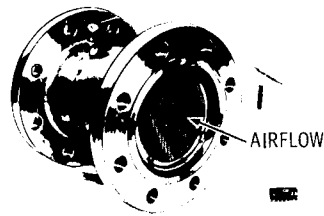


Figure 6.- Impact of combustion residence time and equivalence ratio on formation of oxides of nitrogen and combustion efficiency in prevaporized-premixed flame zone. Inlet pressure, 60 N/cm²; inlet temperature, 700 K; gaseous propane fuel.



OVERALL SCHEMATIC OF TEST APPARATUS



CATALYTIC REACTOR

Figure 7.- NASA catalyst element experimental test apparatus.

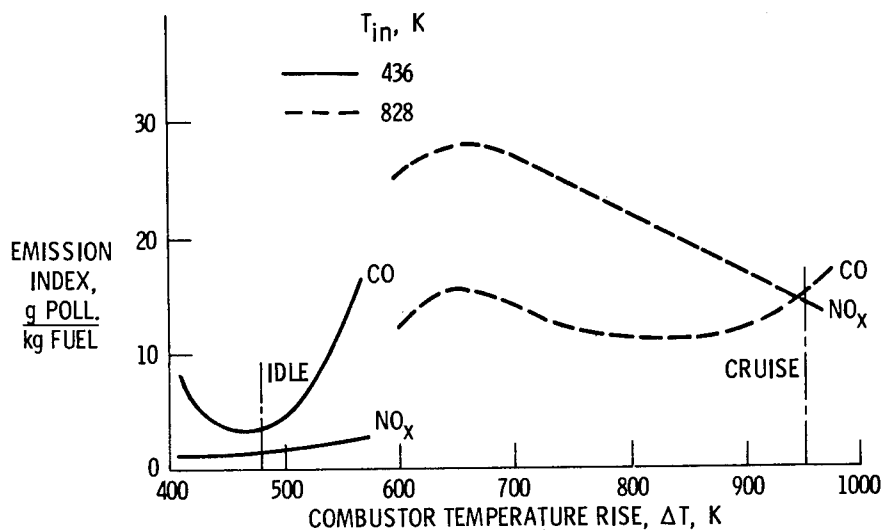


Figure 8.- Effect of optimized idle equivalence ratio on cruise emissions of fixed geometry configuration of SOLAR VAB concept. Inlet pressure, 14 N/cm²; Jet A-1 fuel.

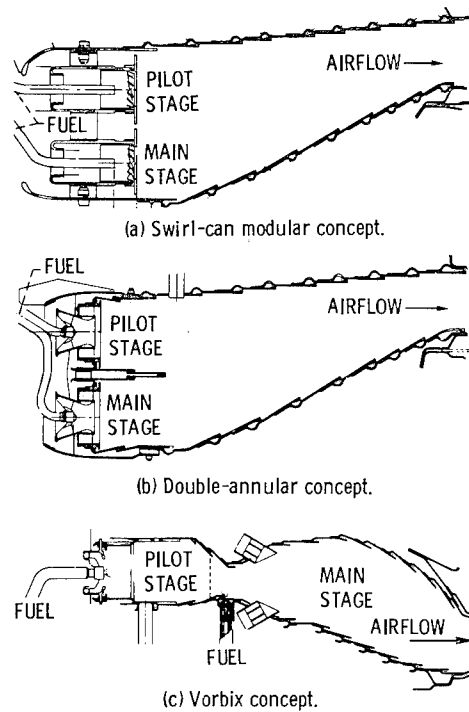


Figure 9.- Schematic illustrations of three types of advanced combustor concepts evaluated at simulated supersonic cruise conditions.

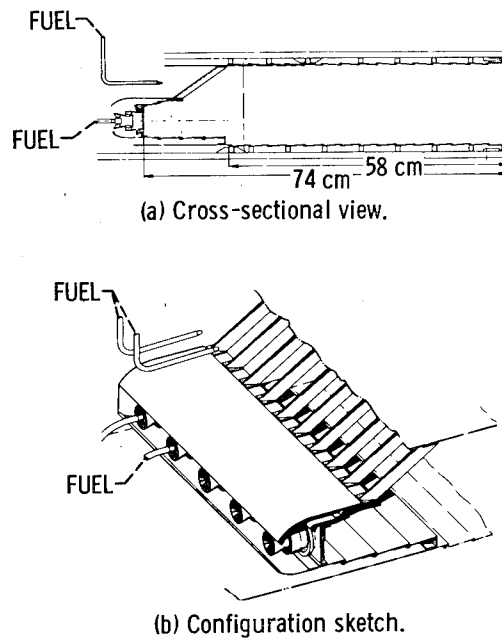


Figure 10.- Schematic illustrations of staged-combustion advanced duct-burner concept for supersonic cruise engine.

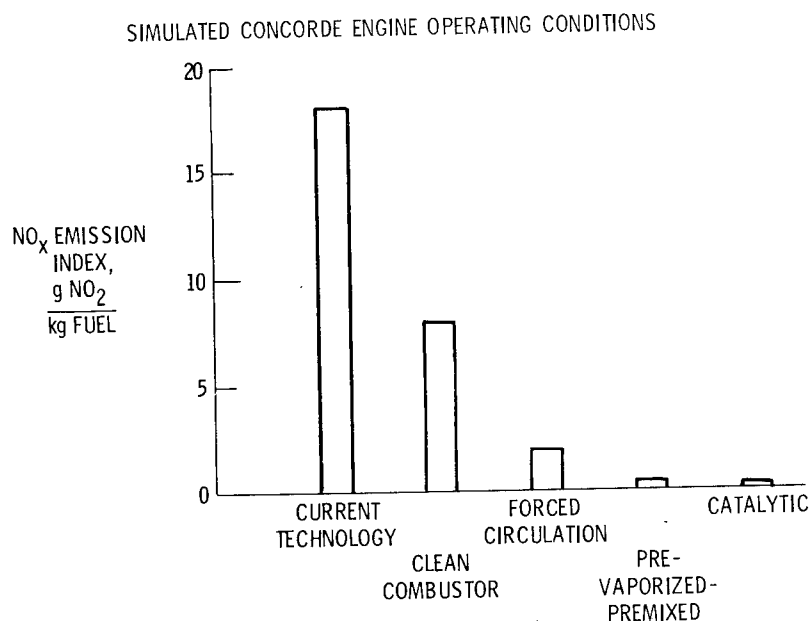


Figure 11.- NO_x emission index forecast for contemporary turbojet engine cycle (Olympus 593) for nonafterburning supersonic cruise. Mach number, 2.0; altitude, 17.7 km.

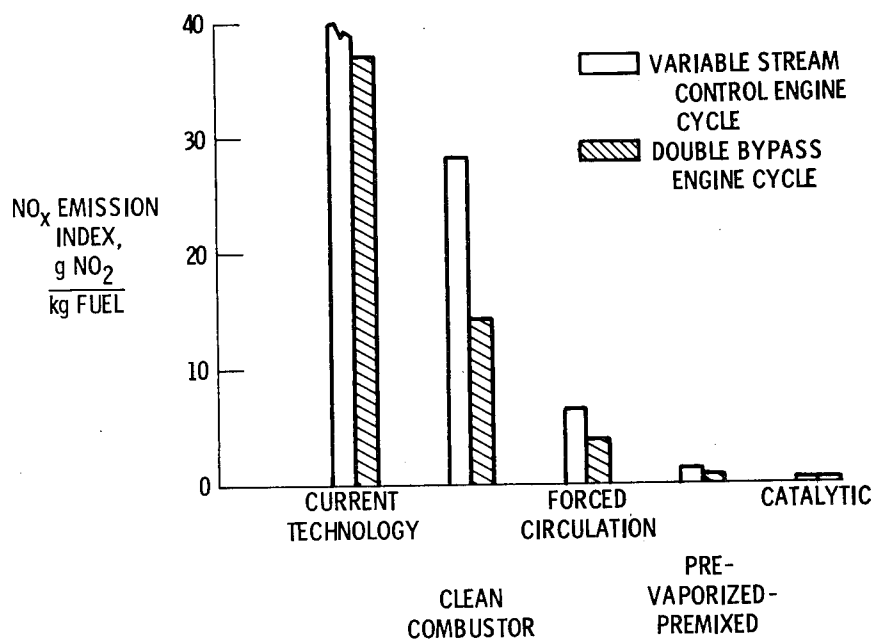


Figure 12.- NO_x emission index forecast for advanced engine cycles for supersonic cruise. Mach number, 2.32; altitude, 16 km.

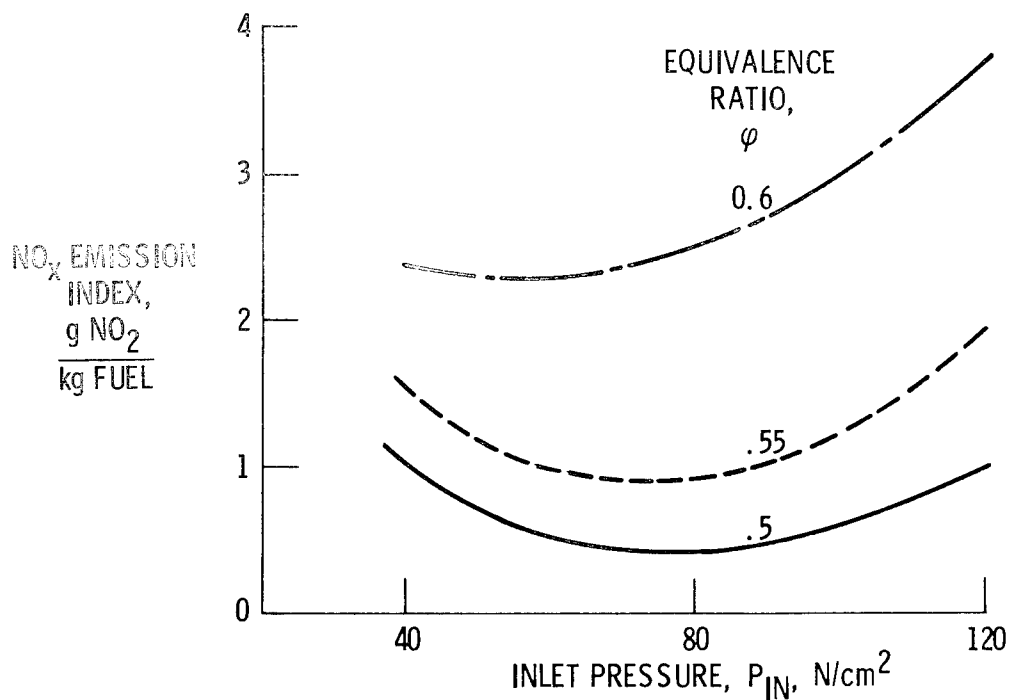


Figure 13.- Effect of inlet pressure and equivalence ratio on NO_x emissions from GASL experiment. Inlet temperature, 900 K; Jet-A fuel.

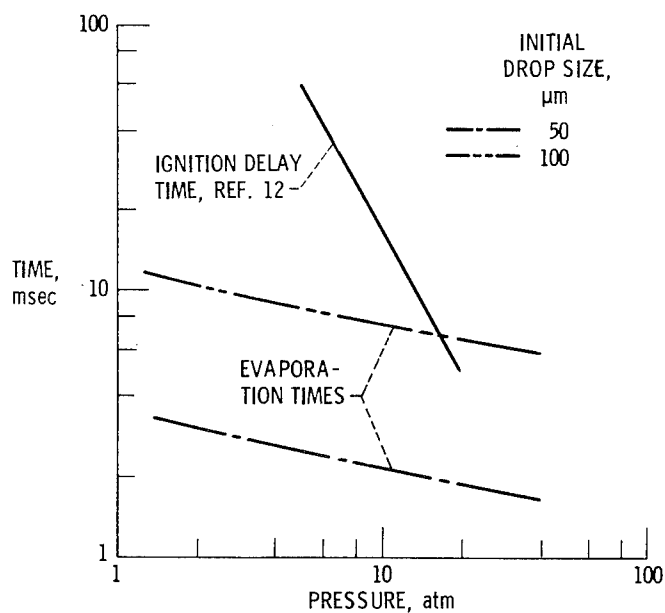


Figure 14.- Effect of pressure on ignition delay and vaporization times for JP-4. Inlet air temperature, 833 K.

CONSIDERATIONS OF HIGH ALTITUDE EMISSIONS

Anthony J. Broderick and Nicholas P. Krull

Office of Environmental Quality
Federal Aviation Administration

SUMMARY

Since the early 1970s, various concerns (sometimes conflicting) have been expressed about the possibility of adverse environmental effects of stratospheric exhaust emissions from aircraft. This paper describes the status of the Federal Aviation Administration's High Altitude Pollution Program, which was instituted in 1976 to develop the detailed quantitative information needed to judge whether or not regulatory action to limit such emissions would be necessary. The complexities of this question and the nature and magnitude of uncertainties still present in our scientific understanding of the potential interactions between aircraft exhaust emissions and stratospheric ozone and climate are reviewed. The direction and scope of future Federal and international activities are described.

INTRODUCTION

About 1970, questions concerning the environmental consequences of high altitude aircraft emissions from a fleet of civil supersonic transport aircraft (SSTs) were first raised. Since that time, we have seen two major studies completed (refs. 1 and 2), both of which included the conclusion that a large fleet of SSTs carried with it the likelihood of significant ozone reduction from a stratospheric accumulation of aircraft engine exhaust-oxides of nitrogen. In addition, both reports claimed that qualitatively similar effects could be expected to result from stratospheric flight of subsonic aircraft, though the lower altitudes associated with subsonic flight made the effects correspondingly less severe on a "per aircraft" basis.

Specifically, Figure 1 depicts the estimates of the Department of Transportation's Climatic Impact Assessment Program (CIAP) (ref. 1). It can be seen that, according to this now-outdated estimate, it would have been reasonable to assume that an economically viable fleet of SSTs — say a production run of several hundred aircraft — would be required to have lower oxides of nitrogen emission in order to be environmentally acceptable. Upon reflection, it is also seen that Figure 1 implied a potential problem for large fleet subsonic aircraft which cruise in the 40 to 45,000 ft. region (about 13.5 km). The contemporary report of the National Academy of Sciences estimated somewhat more serious effects from similar aircraft, by about a factor of two.

Both of these reports carried with them the caveat that our understanding of this complex atmospheric science problem was not perfect, and gave estimates of uncertainty associated with their predictions of ozone destruction. These uncertainty estimates are reproduced in Table 1 (ref. 2, p. 17; ref. 1, p. xvi, p. 29), where "subsonic aircraft" are taken to be similar to today's modern 4-engine wide-bodied transport.

Both reports called for additional study and suggested an immediate start on a plan for developing appropriate international regulation to avoid undesirable environmental effects. In the United States, the Federal Aviation Administration is the agency responsible for civil aircraft regulation, and it has established the High Altitude Pollution Program (HAPP) (ref. 3). The purpose of this program is to quantitatively determine the requirements for reduced cruise-altitude exhaust emissions and, in conjunction with appropriate Federal and international agencies, to ensure that, if necessary, appropriate regulatory action is taken to avoid environmental degradation.

HIGH ALTITUDE POLLUTION PROGRAM

HAPP was organized in the recognition that the uncertainties described by the previous studies could not be ignored if the Federal government was to develop an appropriate regulatory policy with regard to high altitude flight by either supersonic- or subsonic-cruising aircraft. Simply stated, we are not now in a position to predict with reasonable certainty the environmental effects of high altitude flight. To reduce these uncertainties to a tolerable level, the HAPP effort has been planned to carry out studies and analyses in a variety of disciplines:

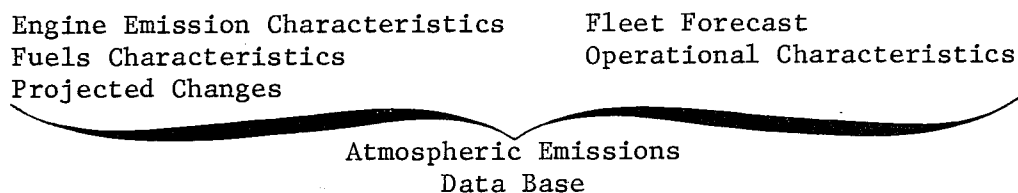
Engines and Fuels	Assessment
Laboratory Measurements	Regulation
Field Measurements	Monitoring
Models	

We recognize, and believe it important for others to do so, that this program cannot be carried out in isolation. HAPP depends on a number of other Federal agencies to carry out their own presently-planned mission-oriented programs which are expected to provide important information for our analysis. Specifically, though not a complete list, there are important related efforts in the National Aeronautics and Space Administration, National Oceanic and Atmospheric Administration, Department of Defense, Energy Research and Development Administration, National Science Foundation and Environmental Protection Agency. In addition, contributing activities are ongoing or planned in a number of foreign countries, including the United Kingdom, France, Canada, Belgium, Japan, Germany, Australia, and the Soviet Union. Finally, international bodies including the International Civil Aviation Organization, World Meteorological Organization, World Health Organization, United Nations Environment Programme, and others are also contributing valuable information. Activity on such a broad front must be continued if we are to be able to reach timely conclusions on the need for, type of, and timing of any regulations which might

be necessary to ensure protection from adverse environmental consequences of high altitude flight. The following paragraphs are devoted to a brief description of the four major technical elements of HAPP.

Engines and Fuels

The major objective of our activity in the field of engines and fuels is to provide an accurate technical data base of aircraft exhaust emissions for the worldwide fleet of aircraft expected to be operating at high altitudes over the next few decades. As shown in the following list, this is not the simplest of tasks:



First, we must accumulate an accurate data base on the characteristic emissions of all types of aircraft engines, the characteristics of fuels that are expected to be burned, and the associated changes in these parameters that are expected to result from new engine technology and possible new sources of hydrocarbon fuels. Next, we must develop — as part of the FAA's continuing work on aviation forecasting — a reasonably accurate forecast of global aviation use over the next few decades: How many hours will be spent, at what cruise altitudes, by what types of aircraft? Third, we must develop an accurate picture of real-world operational influences on aircraft emission rates, since oxides of nitrogen emissions especially are affected by variations in cruise altitude, power setting, flight speed, and aircraft gross weight. Finally, all these factors are combined to result in the desired end product: an accurate forecast of the emissions of the world's aircraft fleet, resolved into about 1 km high by 10° wide latitude shells, from about 6 km altitude upward to about 20 km.

We would be remiss if we did not acknowledge the importance to our effort of the fine work presently carried out at NASA's Lewis Research Center. We strongly support and encourage continuation of those efforts.

Laboratory Measurements

The major objective of work carried out in our laboratory measurements program area is to provide an accurate data base on important stratospheric chemical reaction rates for use in atmospheric models. This work includes considerations of heterogeneous chemical reactions (i.e., those between species in different physical phases, like gas-particle interactions) and phase equilibria of demonstrated importance to better understanding the impact of aviation. In addition, we envision the probable need for a limited amount of work directed at obtaining better spectroscopic data, both for use in the

photochemistry part of atmospheric models and for the identification of trace constituents in the atmosphere through field measurements. The following list explicitly shows our planned activities in this program area:

- Chemical Data Evaluation
- Photolytic Quantum Yields
- Gas-Phase Reactions
- Molecular Spectroscopy
- Heterogeneous Processes
- Experimental Simulations
- New Technique Development

We intend to continue support of the Chemical Kinetics Data Evaluation Project at the National Bureau of Standards. This effort, jointly funded by us and NASA's Upper Atmospheric Research Office, has proven particularly useful in providing an unbiased assessment of the best estimate of the accuracy with which important chemical reaction rate data are known. In FY 1976, for the first time, our support of this activity was broadened to permit NBS to include consideration of reaction rates of importance in the formation of oxides of nitrogen in high temperature combustion systems.

One other project in the planning stage deserves mention, and that is our recognition of the need to contribute at least partial support to development of new measurement techniques which show promise of enabling actual measurement of previously estimated chemical reaction rates on atmospheric species of importance to aviation. Noteworthy in this area is our expressed desire to join forces with the staff of the Atmospheric Science Division at Langley Research Center to support development of tunable diode lasers by a new diode-fabrication process. Availability of such devices, we are convinced, would be invaluable in certain key areas where measurements have been previously beyond reach.

Field Measurements

Perhaps it goes without saying that actual measurement of atmospheric species concentrations forms a necessary part of HAPP. Unfortunately, the nature of these projects renders them expensive. Our major objective in this program area is to build upon the existing stratospheric composition data base to make it more accurate and meaningful, concentrating, of course, on species important to developing a better understanding of aircraft impact. More specifically, better knowledge is needed of the concentration of gaseous compounds in the oxides of nitrogen and water "families" in their spatial distribution, diurnal and seasonal variation, and sources and sinks. Major planned projects are as follows:

- NO-NO₂-N₂O₅-O₃ Measurements
- NO-NO₂-N₂O₅-HNO₃-O₃ Measurements
- "Tracers" of Atmospheric Motions
- Rainout/Washout Measurements
- Critical Data Analysis
- Instrument Development

As can be seen, our emphasis is heavily on simultaneous, in-situ measurements of photochemically-related species. We are long past the point where a single stratospheric measurement of a species like nitric oxide is of value. It is now generally recognized that significant improvement in our understanding will only come from a series of coordinated measurements of the complete oxides of nitrogen family, for example. The same is largely true for similar atmospheric science questions, like that surrounding the continued use of fluorocarbons.

It is perhaps worth noting that one of our currently-funded projects involves critical analyses of measurement data. This represents an initial modest effort modeled after the chemical kinetics data evaluation work of NBS mentioned earlier. Here, our main objective is to attempt to eliminate some of the unexplained variability in reported atmospheric measurements by a detailed review including consideration of such normally-ignored factors as prevailing local meteorology, corrections for method of sensor-altitude reporting, possible bias arising from choice of measurement technique, etc. We expect this initial step will pave the way for development of a methodology which will permit substantially more meaningful incorporation of such data into atmospheric models by those less skilled in interpretation than in their use.

Atmospheric Models

It would be desirable to actually observe and quantitatively measure any atmospheric effects which might arise from high altitude aircraft exhaust, but it is not practical to do so, since the effects at present are far too small to be directly detected. Thus, to provide the information upon which future designs should be based, it is necessary to use predictive atmospheric models. The objective of our work in this program area is to maintain and continually update our capability to synthesize the information available from the best atmospheric models to analyze and predict the environmental effects from high altitude aircraft emissions. The project areas included are as follows:

1-Dimensional	Thermal-Radiation
2-Dimensional	Chemical Kinetics
3-Dimensional	Sensitivity Studies
Theoretical Considerations	Meteorological Analysis

This program area includes, in addition to the expected use of one-, two- and three-dimensional atmospheric transport models (with and without coupled chemical kinetics and thermal-radiation calculations), three investigations which deserve further examination.

FAA values sensitivity studies highly. By carefully combing through a model to ascertain which input parameters or assumed relationships (like chemical reaction rates, etc.) have the greatest impact on the model results, we can develop a good idea of the relative importance of the uncertainties in these factors. Thus, this approach provides a unique management tool in our problem-oriented study: we are able to rank order the priorities in our

research support, and are better able to plan a program where the expenditure of research funds is closely tied to optimum return — a corresponding improvement in the reduction of uncertainty in the model's output.

A second point we should explain more fully is the part called "meteorological analyses." It is clear to us that, since the debate on the effects of high altitude flight began, there has been generally insufficient attention paid to fundamental meteorology. Atmospheric contaminants like nitric oxide are moved about by air motions and, for the high altitude flight problem, these motions are quite critical. The tropopause region, which separates the stratosphere from the troposphere, is exceedingly complex from the meteorological viewpoint. Transport in and from this region—either upward to the stratosphere, which produces enhanced effects on ozone, or downward to the troposphere, where the substances are rapidly removed from the atmosphere—is poorly understood. We intend to focus attention on developing a much better understanding of this so-called stratosphere-troposphere exchange. Meteorology of the tropopause region is an area of much greater significance to understanding aircraft effects than to questions about the stratospheric effects of fertilizers or fluorocarbons, substances which are not directly injected into this region. The region of interest, between about 10 and 25 km, is dominated by transport effects rather than chemical/photochemical processes.

Finally, we will conduct several studies of a theoretical nature to better understand the limits within which predictive models can be reasonably relied upon. To cite one example of this type of problem, most are aware that the so-called "eddy diffusion coefficient" employed as the transport mechanism in a one-dimensional model is generally derived by inversion of the global-average vertical distribution of mixing ratio obtained for a reliable "tracer" of atmospheric motion, such as methane (see ref. 4). In performing this inversion, care must be taken to include proper considerations of all significant atmospheric sources and sinks of the tracer to avoid misinterpreting, for example, a chemical loss process as more rapid than atmospheric transport. What is not generally recognized is the implication of the acknowledged fact that this approach does not explicitly decouple the chemistry from the transport (ref. 5). Rather, in using the model, one assumes that the calculated chemical changes — for example, in ozone — do not significantly affect the previously-assumed formulation of atmospheric transport. But what happens when new data indicate the need for a modification of one of the parameters that went into the original derivation of the eddy diffusion coefficient? Clearly, the old calculation is now invalid, but what implication does this have for its continued use? Such is typical of the as-yet-unresolved questions we will attempt to answer.

PROGRAM STATUS

The preceding paragraphs have briefly reviewed four of the major areas of study in the FAA High Altitude Pollution Program. The program has been underway for about a year now, and is planned to continue for another seven, unless we can develop reliable answers in a shorter time. In the next few months, we will complete and release a major report on this program. The

report will summarize the status of our current understanding of the environmental effects, discuss the immediacy of the need for regulatory action directed at ensuring reduced levels of cruise-altitude exhaust emissions, and detail plans for further work in the program. Two other reports will also be shortly available as a result of our contracted studies. The first, developed under contract with the Institute for Defense Analyses, Arlington, VA., will provide a relatively comprehensive state-of-the-art summary and comparison of reports which have treated these subjects over the last several years. Major points of agreement and difference will be noted and expanded upon. The second, developed for HAPP by Lawrence Livermore Laboratory of the Energy Research and Development Administration, will summarize the first year of their participation in the program — the major activity in our atmospheric modeling program area. Of particular interest is their work in developing a better understanding of the uncertainties in our present knowledge.

Obviously, the contents of these not-yet-completed reports cannot be summarized here. We can point to some of the areas which will be discussed in them, however.

Uncertainty Studies

We have developed information which indicates that the uncertainties in the aircraft/ozone-reduction relationship estimated by both the CIAP and National Academy of Sciences studies, and summarized above in Table I, reflected a significant overestimate of the accuracy of their predictions. Specifically, it is likely that the estimates of SST effects on ozone were overestimated by perhaps an order of magnitude or more. This should not be confused with the uncertainty previously placed on those estimates — a factor of two to three. These differences arise principally from three new factors: improved understanding of the rates at which important chemical reactions proceed in the stratosphere, especially those involving the oxides of nitrogen; similarly improved data on reactions involving water-derived species; consideration of the interactions between aircraft-produced oxides of nitrogen and fluorocarbon-produced oxides of chlorine.

Subsonic Aircraft Effects

Both the previously-cited studies extrapolated results obtained from models developed primarily for evaluation of 20 km cruise-altitude effects to regions well below that altitude, to include consideration of subsonic aircraft as well. Both correctly pointed to difficulties inherent in estimating transport characteristics in this difficult region, which was implicitly the reason for assigning much higher uncertainty—a factor of ten—to projections of ozone reduction from subsonic aircraft flight in the upper troposphere and lower stratosphere. Neither study, however, contemplated that secondary effects in the models' treatment of ozone-producing chemistry—effects which were known at the time (ref. 6) — would have a significant impact on their findings.

Our study to date indicates the likelihood, in part owing to our including ozone-producing reactions in model calculations, that previous estimates of the effects of subsonic aircraft on ozone are seriously in error, to the point where it is now reasonable to project an increase in ozone for many—if not all—of these flights.

Effect of Including Fluorocarbons

The recently-completed National Academy of Sciences Study (1976) on the effects of fluorocarbons (Freons) on stratospheric ozone documented the direct and indirect (through reactions with water vapor-derived species) coupling of the reactions of oxides of nitrogen and fluorocarbon-derived chlorine-containing species. Implicit in their analysis is the fact that these later results have a major impact on the earlier calculations of aircraft effects. Unfortunately, this was not explicitly treated by the academy, and the task of such a synthesis is left to others. What can be said now is that the effect of fluorocarbons already released into the atmosphere is to reduce the ozone-destruction potential of a unit injection of oxides of nitrogen by aircraft. (Indeed, this is one of the reasons that earlier estimates of aircraft effects were too high, as mentioned above.) At the same time, this factor adds a major complication to analyses of future fleet effects, since the amount of stratospheric chlorine must now be forecast, in addition to the size of the aircraft fleet.

CONCLUDING REMARKS

Considerations of high altitude emissions effects must form an important part of designing environmentally-compatible advanced generations of aircraft. The Federal Aviation Administration has acknowledged its responsibility to provide the guidance required by government-industry teams working toward the goal of improving the quality of service rendered by the nation's air transportation system. FAA has made a major, long-term commitment to this end by establishing and conducting the High Altitude Pollution Program, fully supported by the Secretary of Transportation. Results of this effort to date substantiate the need for this activity, by demonstrating the inaccurate and qualitative nature of previous efforts. It is important to recognize, however, that the preliminary findings described earlier are necessarily tentative in nature, and require further refinement and documentation before they can form a sufficiently reliable basis for policy formulation. We appreciate and will continue to rely heavily upon cooperation with other government- and industry-sponsored efforts to achieve our goal.

REFERENCES

1. Grobecker, A. J., S. C. Coroniti and R. H. Cannon, Jr. (1974). CIAP Report of Findings — The Effects of Stratospheric Pollution by Aircraft. Report No. DOT-TST-75-50, U.S. Department of Transportation, Washington, D.C. (Available from NTIS as AD-A005458.)
2. National Academy of Sciences, Climatic Impact Committee (1975) Environmental Impact of Stratospheric Flight, National Academy of Sciences, Washington, D.C.
3. Meister, Frederick A. (1975). Transcript of Panel Discussion in Proceedings of the Fourth Conference on CIAP, T. M. Hard and A. J. Broderick (eds), Report No. DOT-TSC-OST-75-38, U.S. Department of Transportation, Transportation Systems Center, Cambridge, Massachusetts.
4. Hunten, Donald M. (1975). "The Philosophy of One-Dimensional Modeling," in Proceedings of the Fourth Conference on CIAP, T. M. Hard and A. J. Broderick (eds), Report No. DOT-TSC-OST-75-38, U.S. Department of Transportation, Transportation Systems Center, Cambridge, Massachusetts.
5. Chang, Julius S. (1975). "Uncertainties in the Validation of Parameterized Transport in 1-D Models of the Stratosphere," in Proceedings of the Fourth Conference on CIAP, T. M. Hard and A. J. Broderick (eds), Report No. DOT-TSC-OST-75-38, U.S. Department of Transportation, Transportation Systems Center, Cambridge, Massachusetts.
6. Johnston, Harold S. and E. Quiteis (1974). "The Oxides of Nitrogen with Respect to Urban Smog, Supersonic Transports and Global Methane," presented at the International Conference on Radiation Research, Seattle, Washington, July, 1974.

TABLE I.- CIAP AND NAS UNCERTAINTY ESTIMATES

Ozone Reduction In Northern Hemisphere

Percent Per 100 Aircraft
(1974 Engine Emissions Assumed)

	NAS Estimate	Uncertainty Factor	CIAP Estimate	Uncertainty Factor
Subsonic (~ 11 km)	0.02	± 10	0.014	-10;+2
Subsonic (13.5 km)	0.2	± 10	0.079	-10;+2
Supersonic (16.5 km)	0.7	± 3	0.39	-3.3;+1.5
Supersonic (~ 19 km)	3	± 2	1.74	-3.3;+1.5

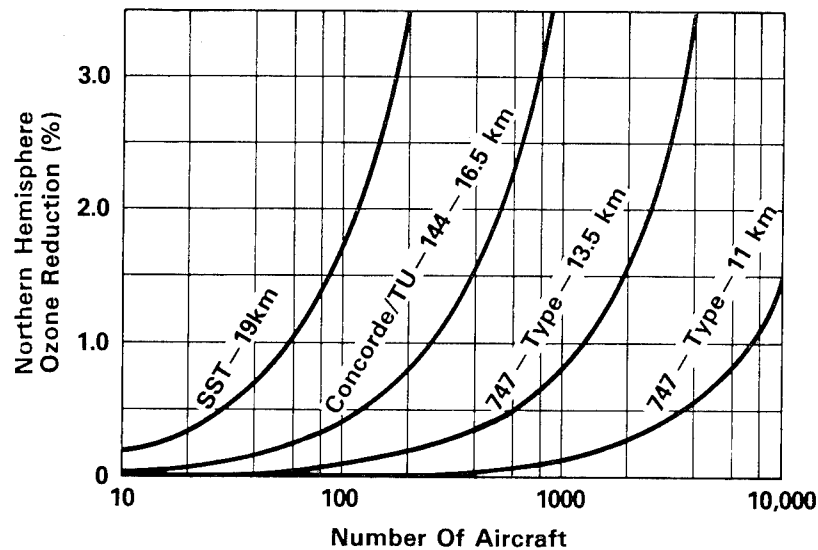


Figure 1.- CIAP - estimated ozone reduction.

SESSION V - AIRFRAME STRUCTURES AND MATERIALS

INTRODUCTION

Richard R. Heldenfels
NASA Langley Research Center

This session consists of 11 papers which summarize recent advances in airframe structures and materials technology for supersonic cruise aircraft. They are the result, primarily, of 4 years of effort in the SCAR program with the objective of reducing the cost and weight of structures for large, flexible airframes. These structures must be safe and durable during a long service life at supersonic speeds. The SCAR airframe structures and materials program is summarized in reference 1, an abridged version of reference 2. A bibliography of SCAR publications is given in reference 3.

Airplanes usually have a higher structural weight than desired; this becomes a greater problem as cruise speed increases. High-speed aircraft also tend to have optimum aerodynamic configurations that are not structurally efficient. The structure of the National SST was too heavy and the configuration had an unresolved flutter problem when the program was stopped. Today much better design methods are available to cope with such problems early in the design process and thus achieve a more nearly optimum overall configuration.

The first four papers report on structural design studies of the arrow-wing configuration. These studies make extensive use of computerized analysis and design methods. The results show that the early use of these new multidisciplinary computer-aided design techniques can save much time and effort in defining the required structural mass distribution in a large, flexible airframe.

The next two papers describe work underway to define more accurately both static and dynamic loads.

Four papers discuss manufacturing techniques for and environmental resistance of titanium alloys and composite materials. New manufacturing techniques for titanium promise substantial cost and weight reductions in future structures. The graphite-polyimide composites appear to have the most potential of those being tested for high-temperature service.

The final paper reports progress on development and evaluation of fuel tank sealants for high-temperature service.

These papers show that much progress has been made to provide new data and methodology for structural design of supersonic cruise aircraft. Continued research and development is expected to produce additional advances.

REFERENCES

1. Cooper, Paul A.; and Heldenfels, Richard R.: The NASA Structures and Materials Research Program for Supersonic Cruise Aircraft. Astronaut. & Aeronaut., vol. 14, no. 5, May 1976, pp. 26-37.
2. Cooper, Paul A.; and Heldenfels, Richard R.: NASA Research on Structures and Materials for Supersonic Cruise Aircraft. NASA TM X-72790, 1976.
3. Hoffman, Sherwood: Supersonic Cruise Aircraft Research (SCAR) Program — Bibliography July 1972 Through June 1976. NASA TM X-73950, 1976.

TITANIUM AND ADVANCED COMPOSITE STRUCTURES

FOR A SUPERSONIC CRUISE ARROW WING

CONFIGURATION

M. J. Turner and J. M. Hoy
Boeing Commercial Airplane Company

SUMMARY

Two structural design studies were made, based on current technology and on an estimate of technology to be available in the mid 1980's, to assess the relative merits of structural concepts and materials for an advanced arrow wing configuration cruising at Mach 2.7. Preliminary studies were made to insure compliance of the configuration with general design criteria, integrate the propulsion system with the airframe, and define an efficient structural arrangement. Material and concept selection, detailed structural analysis, structural design and airplane mass analysis were completed for the first study based on current technology. In the second study, based on estimated future technology, structural sizing for strength and a preliminary assessment of the flutter of a strength designed composite structure were completed. In both studies, an advanced computerized structural design system was used, in conjunction with a relatively complex finite element model, for detailed analysis and sizing of structural members.

INTRODUCTION

This paper presents a general description of a study and a summary of results obtained to date by the Boeing Commercial Airplane Company under a contract with the NASA Langley Research Center as a part of the NASA Supersonic Cruise Aircraft Research Program. Detailed structural studies were conducted to establish a realistic metallic aircraft design and an accurate mass estimate for a specific aerodynamic configuration. Further studies are in progress to evaluate potential mass reductions that may be achieved by application of advanced structural concepts and advanced composite materials to the same configuration. A Mach 2.7 arrow wing supersonic cruise configuration was selected for these baseline studies because previous investigations have shown this configuration to be one of the most promising aerodynamic configurations for supersonic cruise applications.

Since supersonic cruise aircraft tend to be large and flexible, aeroelasticity is a major design consideration, and realistic aeroelastic considerations based on analysis of finite-element structural models and sophisticated aerodynamic loading analysis, both steady and unsteady, are required even in a preliminary design study of such a vehicle. The strong interaction of the various disciplines in aeroelastic problems required the use of computer-aided design methods to improve and expedite the aeroelastic and structural resizing cycle (see for example, refs. 1 through 8).

In addition to the usefulness of the results obtained for a specific configuration, these studies provided a unique opportunity to appraise the computer aided design methods, and to identify problems and technology areas requiring further study and development.

CONFIGURATION AND FLIGHT ENVELOPE

During the initial phase of the study, an arrow wing configuration supplied by NASA was analyzed in considerable detail, using criteria and data from the National SST Program, from NASA wind tunnel tests and from an earlier Boeing study of an arrow wing configuration performed under Department of Transportation Contract No. FA-SS-67-3. Refinements were introduced to meet criteria for controllability, stability and performance. To meet minimum safe operational criteria throughout the flight envelope longitudinal and lateral-directional flight critical augmentation systems were incorporated in the design.

An advanced technology afterburning turbojet engine, developed in a study conducted for Langley by the Boeing Commercial Airplane Company (Contract NAS1-11938), was selected for integration with the aircraft. Although this engine definition was considered satisfactory for the structural study, its performance parameters are not representative of current concepts, such as variable cycle engines, both in terms of specific fuel consumption and sideline noise. Thus, no attempt was made to determine the absolute range of the aircraft.

The final configuration used in the structural design study, designated as 969-512B, and the flight envelope are shown in figures 1 and 2, respectively.

STRUCTURAL SELECTION

On completion of the configuration definition, a study of internal structural arrangement was made, utilizing the arrangement developed in the earlier arrow wing study as baseline. Mass differences were evaluated for structural variations, and a multispar arrangement with a small number of ribs, very similar to the baseline arrangement and to that employed on the National SST, was selected for subsequent detail design studies.

Selection of materials based upon current technology for cruising at Mach 2.7 was restricted to those that were proven for primary airframe applications, and Ti-6Al-4V alloy was selected as the primary structural material.

Structural components making the largest contributions to aircraft mass were selected for intensive study. These included wing cover panels, wing internal structure, and the body shell. Many structural concepts were analyzed for mass, manufacturing complexity, stiffness, fatigue, thermal conductance and material cost and assessed qualitatively for maintainability and fail safety requirements. Design loads and environmental conditions were established from the earlier arrow wing study to provide a consistent basis for comparison of concepts. Three locations on the wing and four on the body were chosen for concept evaluation. Wing panel control points and the concepts considered in the concept evaluation process are presented in figure 3.

As shown in figure 4, sandwich panels with titanium face sheets aluminum brazed to a titanium honeycomb core were selected for the entire upper wing surface. The same concept was also selected for the forward, lightly loaded portion of the wing lower surface and both surfaces of the wing tips, outboard of the wing mounted fins. For the heavily loaded portion of the wing lower surface, an integrally machined and welded concept was selected for the portion outboard of the fuselage which carries large tensile loads, while integrally machined waffle construction was selected for the region under the fuselage where large biaxial loads occur. For wing internal structure (spars and ribs), stiffened flat sheet webs were selected for the heavily loaded aft portion and sinusoidally corrugated webs were chosen for the forward portion. Conventional sheet-stringer construction was selected for the fuselage. Initial screening of concepts was governed primarily by mass comparisons; manufacturing complexity, stiffness, maintainability and fatigue contributed significantly to the final selections. In retrospect, after a more thorough evaluation of insulation requirements, it is believed that brazed titanium sandwich would have been a better choice for the entire lower surface of the wing.

ANALYSIS AND DESIGN PROCESS

The computerized system that was used for structural analysis and design was organized around an interim version of the ATLAS Structural Analysis and Design System, interfaced with external programs for flutter analysis and with the FLEXSTAB System for loads analysis. ATLAS is a modular system of computer codes, integrated within a common executive and data base framework, that is operational on the Control Data Corporation (CDC) 6600/CYBER Computers. It was initially developed by the Boeing Commercial Airplane Company and it is currently being extended under a cooperative effort with the NASA Langley Research Center. FLEXSTAB, employed for loads analysis, is a system of programs originally developed under contract to NASA Ames Research Center for stability analysis of elastic airplanes. Modifications to FLEXSTAB to provide loads analysis capability were developed by the contractor in preparation for the arrow wing study.

The major subtasks that make up the structural analysis and design process are identified in figure 5. This may be visualized as three interconnected discipline-oriented segments with the interconnection being provided by the ATLAS system. On the left of the figure is FLEXSTAB used for prediction of steady aeroelastic loads which provides input to the strength design segment shown in the center of the figure. On the right is a group of operations associated with the flutter analysis and design to satisfy flutter criteria. The computer programs performing the various functions are shown in the upper portions of the boxes.

MATHEMATICAL REPRESENTATION OF THE AIRPLANE

Basic data describing the aircraft were developed during the initial stages of the contract, and this information, comprising aircraft geometry, structural arrangement, structural concept, and structural materials, was then used to develop structural, aerodynamic, and mass models of the aircraft to initiate the analysis and design cycle.

Two similar mass models were generated, one for use with FLEXSTAB for loads analysis and the other for use in the flutter analysis. The models differed primarily in the retained node set used. Each model was defined for several total aircraft mass levels. Theoretical masses of structural elements were calculated directly from sizing data. Design studies of local structural details and experience from the National SST Program were then used in converting the theoretical values to actual structural masses.

The structural model of one-half of the aircraft contains approximately 2000 nodes, 4200 elements, and 8500 active degrees of freedom. The sketch in the upper part of figure 6 depicts the complete model. The wing and adjacent fuselage structure are modeled with two-dimensional elements and the remainder of the aircraft simulated with beam elements. Modeling of wing and fin components are shown in other views in the figure. For dynamic analyses a much smaller number of degrees of freedom are retained, 225 for symmetric conditions and 260 for antisymmetric conditions. The complexity of the structural model results from (1) the use of one basic model for both stress and flutter analyses and (2) the detail requirements for meaningful flutter analysis. For the wing, these requirements include structural modeling of the engine support structure (allowing complete motions of the engines), leading and trailing edge controls, wing secondary structure, landing gear and wheel well cutouts, and wing mounted fins as well as primary wing structure. In modeling the remainder of the aircraft, a detailed body idealization is required for wing attachment, while a less sophisticated model is considered adequate for the remainder of the fuselage and the empennage.

INITIAL SIZING AND PRELIMINARY FLUTTER ANALYSIS

Initial structural sizing to start the iterative design cycle was derived from the earlier design study of the arrow wing configuration, with appropriate adjustments to reflect the increase in maximum taxi mass to 340000 kg. This was followed by a preliminary flutter analysis which showed a large deficiency in flutter speed. To insure that airloads and stresses would not be determined for a structure having large flutter deficiencies, the wing tip structure and engine support beams were stiffened to impose realistic stiffness constraints on the strength design process.

LOADS

Load conditions for structural design were based on Federal Aviation Regulations, Part 25, and the Tentative Airworthiness Standards for Supersonic Transports. Loads analysis experience on the National SST Program and the previous study of the arrow wing configuration were used in selecting design conditions. Structural loads were examined for 154 operating conditions, including maneuvers with normal load factors between +2.5g and -1.0g, gust and ground conditions. From these, 25 of the most critical conditions were selected for design. Elastic properties of the structural model with stiffness increases resulting from

the preliminary flutter analysis were used in the FLEXSTAB analysis for determination of static aeroelastic loads.

In addition to airloads, inertia loads and ground loads, several additional factors influencing structural sizing were considered. These included pressurization, fuel containment, acoustic loads, hailstone impingement, lightning strike and thermal effects.

STRENGTH DESIGN OF TITANIUM STRUCTURE

An iterative technique was used in sizing the structure to satisfy strength criteria for the critical load conditions. This required for each resize cycle (1) evaluation of stresses due to the various load conditions, (2) calculation of margins of safety, and (3) determination of changes in member sizing to obtain the desired value of margins of safety. A stability interaction equation was used for evaluation of margins of safety in biaxial compression and shear in the honeycomb sandwich wing covers, and for strength-critical loading conditions a modified Hill's yield criterion was used. A fully stressed design algorithm was used to obtain new member sizes.

Elements in the fuselage were resized by hand, and the resizing process for these elements converged in two design cycles. Lumped areas used in model beam elements in the fuselage are composed in part of effective skin areas, and these are influenced by buckling, body pressurization and thermal stresses. Automated resizing of the fuselage elements was not attempted because of the problem posed by buckled skins and the smaller structural weight savings expected in the fuselage.

Elements in the wing covers were resized using an automated resizing module with convergence, as measured by total mass change, occurring in three cycles. Successive change in total face sheet thickness and theoretical wing weight are displayed in figures 7 and 8, respectively. In figure 7, three sets of gages are shown for selected panels. Reading from top to bottom, the first set of values are the initial values of upper/lower surface panel gages. The second and third sets of gages were obtained from successive cycles of automated resizing. For lower surface panels of integrally stiffened skin construction, the initial value is the area per cm of skin plus stiffener while the second value, in parentheses, is the skin gage. For upper and lower surface panels of honeycomb sandwich construction, the single value shown is the sum of inner and outer face sheet gages. Margins of safety were calculated considering stability, material strength (or allowable stress level), and fail safety for multiple load cases. The loading components included membrane stress resultants due to overall load condition, bending due to

local pressure loading, and thermally induced loads. Minimum gage constraints were based on foreign-object damage and acoustic effects. Constraints relating the sizing of adjacent elements, such as maintaining cap areas of at least one-quarter of the area of the largest adjacent panel for fail safety, were manually imposed between resize cycles. Conditions governing wing cover thicknesses in the strength design are shown in figure 9.

FLUTTER ANALYSIS AND SIZING OF TITANIUM STRUCTURE FOR STIFFNESS

Engineering judgment, based on experience on the National SST Program, was used in defining structural design changes to meet flutter criteria. The starting point for stiffness redesign was the strength-designed structure; no reductions in gages or member sizes, below the values specified for strength, were allowed.

A condition of symmetric flutter at $M = .9$ and heavy gross mass was selected for analysis to evaluate effects of design changes on the flutter margin. This was confirmed later, as a satisfactory approximation to the critical design condition, by conducting symmetric and antisymmetric flutter analyses of the final design at high and low masses for a range of subsonic and supersonic Mach numbers. Flutter speeds calculated for the critical condition at several stages in the structural design process are shown in figure 10.

The stiffness modifications of the initial structure, prior to strength sizing, consisted of increases in stiffnesses of nacelle support beams to 4.5 times the initial value, an increase in low-speed (outboard) aileron cover thickness by a factor of 4.0, a two fold increase in spar and wing-cover thicknesses outboard of the wing-mounted fin, and addition of high-speed control locks to the low-speed aileron and outboard flap. After strength resizing, with a slight decrease in flutter speed, the effect of wing-tip stiffening and control locks were evaluated individually, and they were then retained in subsequent analyses.

A total of nine flutter analyses were made in establishing the final stiffness design. In addition to increasing the stiffness of individual structural members the maximum wing thickness ratio was increased from 2.8% to 3.5% at the fin station with the increment decreasing linearly to zero at the wing tip and at the outboard nacelle station. Then a complete analysis of the final configuration was made for symmetric and antisymmetric flutter at high and low gross masses for subsonic and supersonic conditions.

The mass increase associated with structural changes and the mass equivalent of the drag increase due to the wing-tip thickening is 4640 kg. It was concluded that further effort to increase the flutter speed by structural changes based on engineering judgment would produce an unrealistically high weight penalty. Hence, the subsonic dive placard, V_D , was reduced by 93.6 km/hr, imposing a range decrease of 40 km with fixed fuel loading, or an increase of 600 kg in fuel load required for constant range. Undoubtedly a significant mass reduction and/or a higher placard could be achieved by using formal optimization techniques. However, that approach could not be implemented within the scope of the study.

STRUCTURAL CONCEPTS FOR ADVANCED COMPOSITES

The candidate advanced composite structural concepts (honeycomb sandwich, sheet stiffener and stiffened thin honeycomb sandwich) are shown in figure 11. Comparisons of mass per unit area for each of the concepts, in borsic-aluminum, shows that the conventional honeycomb sandwich panel has the lowest mass. (It should be noted that three of the panels have been evaluated with two different allowable shear stresses. The lower values were based on preliminary published data. Unpublished test data were obtained through consultation with NASA personnel, which provided justification for higher allowable shear stresses.) A further mass comparison between borsic-aluminum sandwich and graphite-polyimide indicated the latter was the lighter of the two.

Thermal insulation of the fuel is a critical design consideration since the fuel is used as a heat sink. The conventional sandwich panel requires the least additional thermal insulation of the three concepts considered. The honeycomb sandwich panel also offers the least fuel vapor ignition hazard from lightning strike. Based on this evaluation, the honeycomb sandwich panel concept was selected.

MATERIAL SELECTION

Projected properties of candidate material systems for the year 1986 are shown in table 1. It was assumed in this study that matrix development will resolve the microcracking problem of transversely loaded lamina so that cross-ply laminates will be fiber critical. During the material selection process, only balanced symmetrical laminates were considered. Based on a comparison of specific strengths and stiffnesses, high strength graphite polyimide and boron polyimide were selected for further study. As a result of comparative mass analyses of panels designed for representative loading conditions high strength

graphite polyimide was finally selected for use in honeycomb sandwich panel face sheets.

Approximately 50% of the wing surface was minimum gage in the titanium design. This percentage will increase for the composites with polymer matrix materials. Estimated minimum gages of tapes to be available by 1986 and a mass per unit area comparison are shown in table 2.

WING SKIN PANELS RESIZED FOR ADVANCED COMPOSITE

To evaluate mass reductions that may be achieved by application of advanced composite materials, cover panels of the primary wing box were replaced with sandwich panels of graphite/polyimide for detailed analysis. The internal titanium rib and spar structure was not revised. Balanced, symmetric laminates were utilized in panel face sheets to avoid post-cure warping and to simplify analysis.

The wing surface panels of the main wing box were divided into 16 zones for generation of preliminary sizing input (see figure 12). Each zone generally contained panels having the same layup and subjected to similar spanwise, chordwise and shear load components or similar constraint conditions, such as minimum gage. For the initial input layups were estimated for the load intensities determined in the earlier analysis of the titanium structure.

The ATLAS design module resized the panels based only on allowable material properties, since buckling is not presently included in automated analysis and design capability. For this reason, the materials designated for the upper surface are distinct from those designated for the lower surface to permit the use of reduced allowable strains to satisfy the buckling requirement. Stability analyses were performed separately with the Boeing-developed COOPB program.

Figure 13 illustrates the normalized theoretical weight changes in the wing box primary structure for successive changes in the wing box primary structure for successive resize cycles. The first two resizes were performed with only the lower bound restriction that the laminae in any one of the orientation angles (0 , $\pm\pi/4$ and $\pi/2$) could not disappear. In the limit this would require four laminae per face sheet. In the third resize cycle the minimum gage constraint previously specified for graphite polyimide face sheets was imposed. The weight increment from the second to the third resize indicates that a significant penalty is involved in satisfying the minimum gage constraint.

Figure 14 shows some panel sizing results from the ATLAS automated resizing. The upper values for a given panel represent the initial sizing, with the upper surface sizing listed on the left and lower surface sizing on the right. The sizing notation corresponds to the Standard Laminate Code (e.g. 16/8/8 describes the laminate $[0_{16}/\pm\pi/48/\pi/28]$). The 0 direction is parallel to the spar at the aft edge of the element. When the inner and outer face sheets for either the upper or lower panel have different sizing, the two values are shown within a brace. These are easily distinguished since the inner face sheet is always equal to or less than the outer face sheet for a given panel. Reading from top to bottom for a given panel, the consecutive values are the initial sizing, the sizing after the first resize, the sizing after the second resize and the final sizing which satisfies strength and minimum gage constraints. If a fourth value is not listed, the third value satisfies strength and minimum gage constraints.

With the exception of the lower surface just inboard of the outboard engine beam, the panels adjacent to the rear spar are predominantly unidirectional laminates oriented parallel to the rear spar.

Along the side-of-body on the lower surface, body bending induces chordwise loads that peak inboard of the wheel well where up to six $\pi/2$ plies are required.

The largest requirement for $\pm\pi/4$ laminae occurs 6 spars forward of the rear spar midway between the engine beams on the upper surface. Note that the lower panel does not require the $\pm\pi/4$ plies.

Flutter Appraisal of Advanced Composites Strength Design

The thickened wing tip, locked low speed controls, stiffened engine beams with diffusion ribs and stiffened wing rear spar which were developed during stiffness redesign of the metallic aircraft design were imposed as constraints during strength resizing of the advanced composite cover panels.

The flutter appraisal technique, based on energy balance at neutral stability and engineering judgment, that was utilized for the metallic aircraft study is also being used for the advanced composite study. The predominantly spanwise laminates, which characterize the strength design in advanced composites, result in a relatively low flutter speed and frequency compared with the equivalent metallic strength design as shown in figure 15. A comparison of modal frequencies and dominant contributions to the energy balance at neutral stability is shown in table 3. The first significant mode shape change appears for mode 6 where increased wing tip torsion with the advanced composite cover

panels is responsible for considerably greater energy extraction from the airstream.

Stiffness Redesign of Composite Cover Skins

Two approaches have been explored to satisfy flutter criteria in the advanced composite study. In the first approach, the balanced, symmetric (orthotropic) composite layup philosophy used in the strength design was preserved but sufficient $\pm\pi/4$ plies were added to increase wing torsional stiffness in the heavily loaded aft wing box, such that the effective shear modulus of a representative composite panel layup is equal to one-half the shear modulus of the corresponding titanium panel. This resulted in a 13/9/1 layup. Finally, both bending and torsional stiffness were increased in the wing tip by adopting a 12/8/8 layup, which provides the equivalent of one-half the titanium panel stiffness design in the earlier study.

The second stiffness redesign strategy is intended to exploit the potential advantages of an anisotropic layup in the wing tip region as discussed by Austin et al. in reference 9.

The general character of this study is illustrated in figure 16, in which the twist coupling coefficient, η , is plotted versus effective shear modulus for various orthotropic and anisotropic cover layups. The twist coupling coefficient is considered positive when nosedown rotation of a streamwise wing section is induced by upward loading (positive washout). Effects of two types of anisotropy are illustrated -- (1) inequality of $+\pi/4$ and $-\pi/4$ lamina; (2) orientation other than 0 of the initially listed lamina, as indicated by subscripts. Favorable effects on flutter speed are generally associated with decreasing η and increasing shear modulus. Compared with the 12/8/8 wing tip layup, an increase of about 22% in effective shear modulus and a decrease of 15% in η is achieved with a $15_{+\pi/2}/10/1$ layup (spanwise fibers oriented $\pi/12$ rad. aft).

Calculated flutter speeds for the stiffened orthotropic and the anisotropic layup are 173 and 175 m/sec, respectively, at $M = .9$. The flutter frequency is 1.62 Hz for both cases. In order to obtain the required flutter speed (see figure 15), it probably will be necessary to further stiffen the structure as described above to the level of the metallic aircraft. Also, it may be advantageous to employ fibers with properties that are intermediate between the values for high strength and high modulus fibers.

CONCLUDING REMARKS

An in-depth structural design study of an arrow wing supersonic cruise aircraft has been completed utilizing structural materials and concepts that are representative of the current level of technology. This part of the study has provided a baseline aircraft design for application and evaluation of advanced technology, such as composite structural materials and active controls.

The analysis and design of the composite wing shell has provided a successful demonstration of automated design capability for application of an advanced composite material to a complex structure. It is expected that an all composite structure will permit a greater reduction in structural mass than the combination of metal and composite materials that was used in the current study. Because of the importance of aeroelastic requirements, particularly flutter prevention, further consideration should also be given to the development of optimum fiber properties, intermediate between the high strength and high modulus fibers that were considered here. Unbalanced and unsymmetrical laminates should also be explored further for potential benefits in the solution of aeroelastic problems and for manufacturing feasibility.

The following conclusions are considered generally applicable to the structural design of large supersonic cruise aircraft, irrespective of the choice of material:

- (1) An integrated design system should be used in the preliminary design phase.
- (2) Static aeroelastic effects and flutter should be considered as early as possible in the design process.
- (3) Automated modeling methods and sophisticated graphics capability are desirable to decrease manpower and flow time for generation and validation of the structural model.
- (4) Automated resizing for strength, using unrefined initial estimates of member sizes, is an important factor in reducing design cycle time.

These points are discussed at some length in reference 8.

Experience gained from this study has identified the following problem areas in basic technology where further work is needed:

(1) Use of Mechanical Fasteners in Composite Materials

Design and development effort is needed to investigate new and innovative methods for efficient transfer of high concentrated loads.

(2) Standard Test Specimens and Test Procedures for Composites

Work is needed to develop standard test specimens and test procedures and to define the relationship between basic material properties and the strength of structural elements.

REFERENCES

1. Thomas, R. M., et al.: "Aircraft Strength and Stiffness Design Automation," U.S.-Japan Design Automation Symposium, Tokyo, Japan, August 21-22, 1975.
2. Giles, G. L.: "Procedure for Automating Aircraft Wing Structural Design," Transactions of the ASCE, Journal of the Structural Division, January 1971, pp. 99-113.
3. Giles, G. L.; Blackburn, C. L.; and Dixon, S. C.: "Automated Procedures for Sizing Aerospace Vehicle Structures (SAVES)," Journal of Aircraft, Vol. 9, No. 12, Dec. 1972, pp. 812-819.
4. Heldenfels, R. R.: "Automating the Design Process: Progress, Problems, Prospects, Potential," AIAA Paper 73-410, Williamsburg, Virginia, 1973.
5. Miller, R. E., Jr.; and Hansen, S. D.: "Large-Scale Structural Analysis of Current Aircraft," Symposium on Large Computations, ASME, New York, 1970.
6. Swan, W. C.; and Kehrner, W. T.: "Design Evolution of the Boeing 2707-300 Supersonic Transport; Part I, Configuration Development, Aerodynamics, Propulsion, and Structures; Part II, Aircraft Design Integration and Optimization," Presented at the 43rd Meeting of the Flight Mechanics Panel of AGARD, Florence, Italy, October 1-4, 1974. AGARD Conference Proceedings No. 147.
7. Turner, M. J.; and Bartley, J. B.: "Flutter Prevention in Design of the SST," Symposium on Dynamics of Structures, Stanford University, 1971.
8. Robinson, J. C.; Yates, E. C., Jr.; Turner, M. J.; and Grande, D. L.: "Application of an Advanced Computerized Structural Design System to an Arrow-Wing Supersonic Cruise Aircraft," AIAA Paper 75-1038, Los Angeles, California, 1975.
9. Austin, F.; Hadcock, R.; Hutchings, D.; Sharp, D.; Tang, S.; and Walters, C.: "Aeroelastic Tailoring of Advanced Composite Lifting Surfaces in Preliminary Design," Proceedings of AIAA/ASME/SAE 17th Structures, Structural Dynamics and Material Conference, King of Prussia, Pennsylvania, 1976.

TABLE 1.- 1986 ADVANCED-COMPOSITE DESIGN ALLOWABLES, "B" VALUES

		HIGH STRENGTH GRAPHITE/POLY	HIGH MODULUS GRAPHITE/POLY	BORON/ POLYIMIDE	BORSIC/ ALUMINUM
TENSILE STRENGTH	GPa	2.03	1.020	1.344	1.344
COMPRESSIVE STRENGTH	GPa	2.00	.869	2.41	2.43
TENSILE MODULUS	TPa	0.1379	.276	.221	.221
COMPRESSIVE MODULUS	TPa	0.1379	.276	.221	.221
TENSILE STRAIN	$\mu\text{m/m}$	14,750	3,700	6,100	6,100
COMPRESSIVE STRAIN	$\mu\text{m/m}$	14,500	3,150	11,000	11,000
DENSITY	kg/m^3	.1550	.1605	.2010	.2710
FIBER VOLUME FRACTION		.60	.60	.50	.50

TABLE 2.- MINIMUM GAGE CONSIDERATIONS

MATERIAL	UPPER SURFACE			LOWER SURFACE		
	SKIN GAGE (mm)		MASS kg/m^2	SKIN GAGE (mm)		MASS kg/m^2
	INNER	OUTER		INNER	OUTER	
TITANIUM	.254	.381	2.81	.254	.508	3.37
H/S GRAPHITE POLYIMIDE (0/±45/90) _s	.406	.610	1.577	.406	.813	1.889
BORON POLYIMIDE (0/±45/90) _s	.925	.925	3.71	.925	.925	3.71

BASED ON:

MINIMUM GAGE OF TAPES AVAILABLE BY 1986

GRAPHITE POLYIMIDE .051 mm/PLY

BORON POLYIMIDE .132 mm/PLY

MINIMUM GAGE FOR PRACTICAL CONSIDERATIONS

GRAPHITE POLYIMIDE

.076 mm/PLY UPPER SURFACE OUTER SKINS

.102 mm/PLY LOWER SURFACE OUTER SKINS

TABLE 3.- STRENGTH DESIGN COMPARISON FOR FLUTTER

MODE	FREQUENCY (Hz)		ENERGY CONTRIBUTION AT NEUTRAL STABILITY (SOURCE POSITIVE)	
	METALLIC	COMPOSITE	METALLIC	COMPOSITE
PLUNGE	0.	0.	-.082	-.075
PITCH	0.	0.	-.104	-.138
1	0.98	0.80	-.620	-1.0
2	1.19	0.97	-1.0	-.415
3	2.16	1.82	.854	.637
4	2.40	2.00	-.167	-.551
5	2.77	2.69	.039	-.152
6	3.12	2.89	.138	.606
7	3.39	2.99	.613	.438
8	3.80	3.30	-.004	.016
9	4.11	3.55	.002	.142
10	4.85	3.86	-.023	.061
11	4.94	4.63	-.024	-.041
12	5.77	5.04	.267	.267
13	6.23	5.43	-.003	-.006
14	6.62	5.66	.165	.066
15	6.87	5.78	-.013	.170
16	7.64	6.51	-.004	-.008
17	7.84	7.36	-.013	-.009
18	8.39	7.40	-.013	-.010

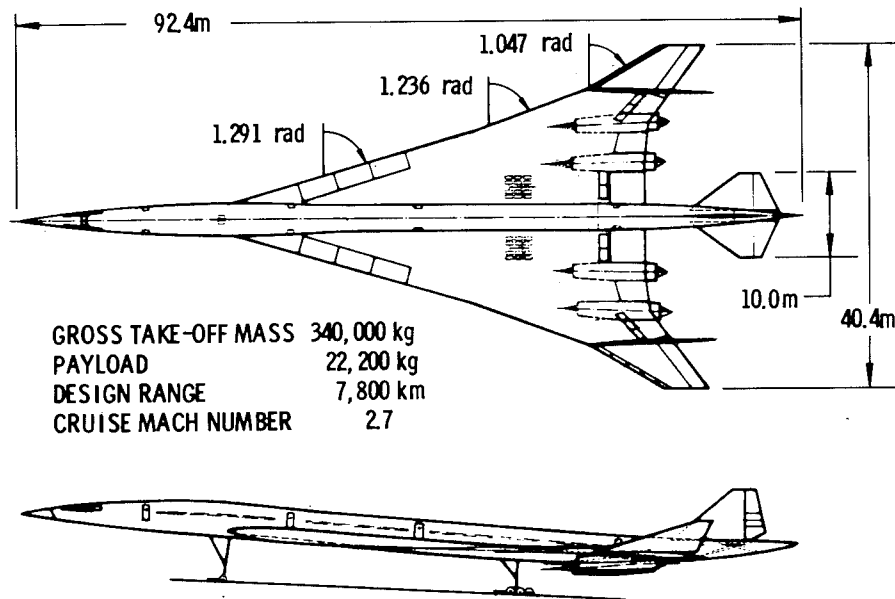


Figure 1.- Configuration - model 969-512B.

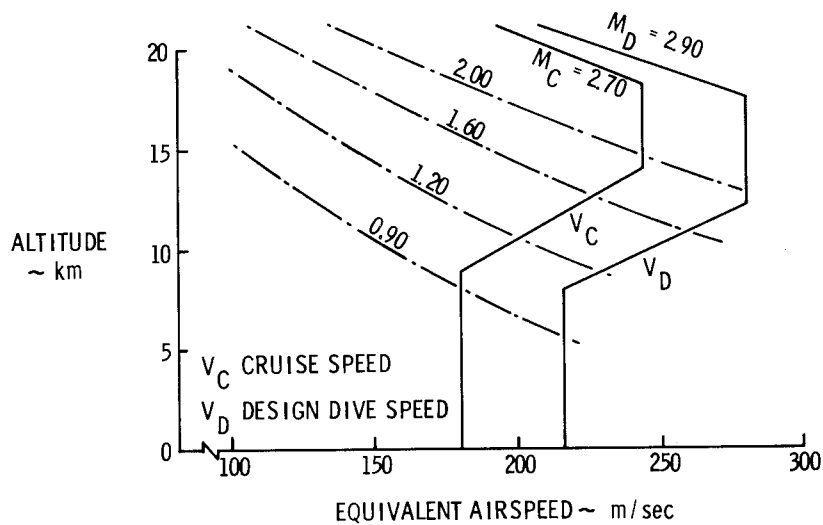


Figure 2.- Flight envelope.

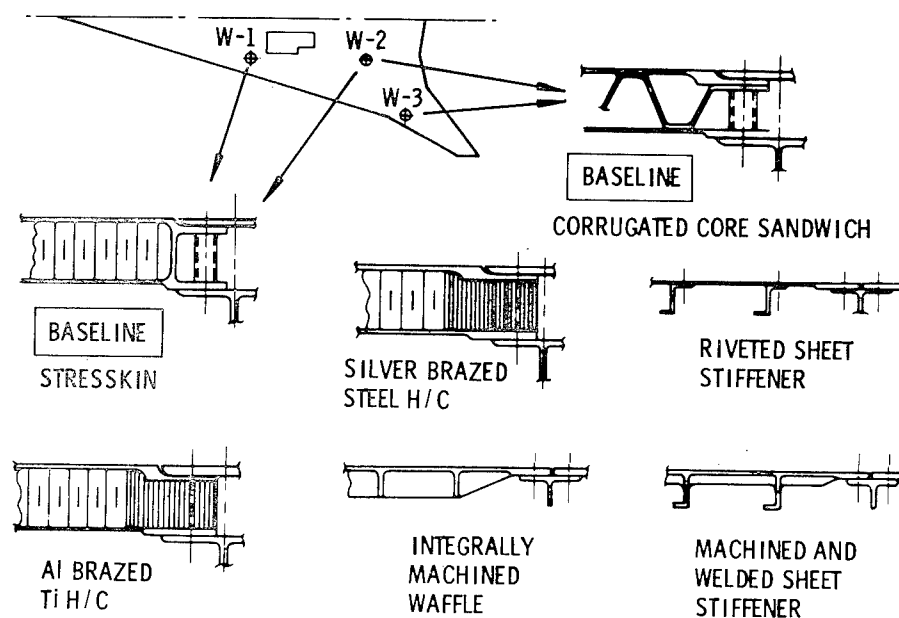


Figure 3.- Wing panel structural concepts.

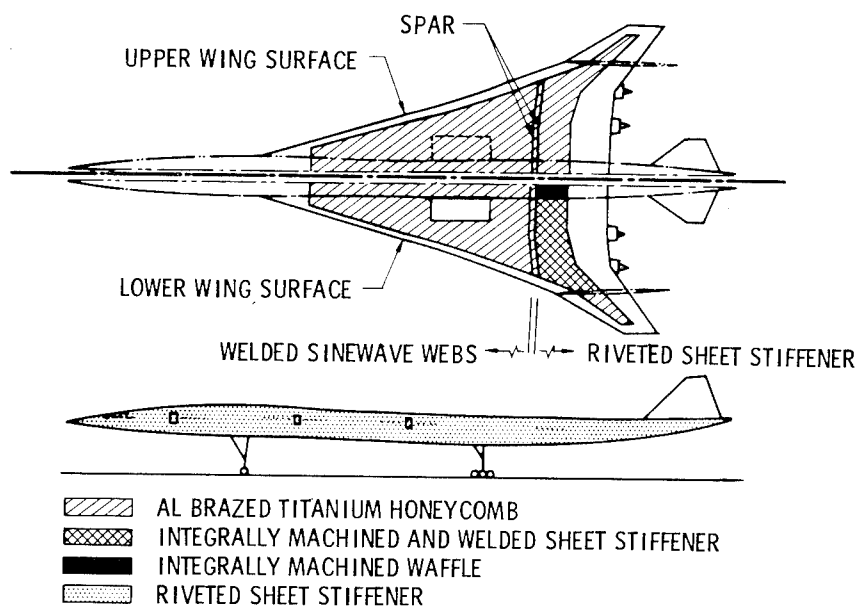


Figure 4.- Wing and body structural selection.

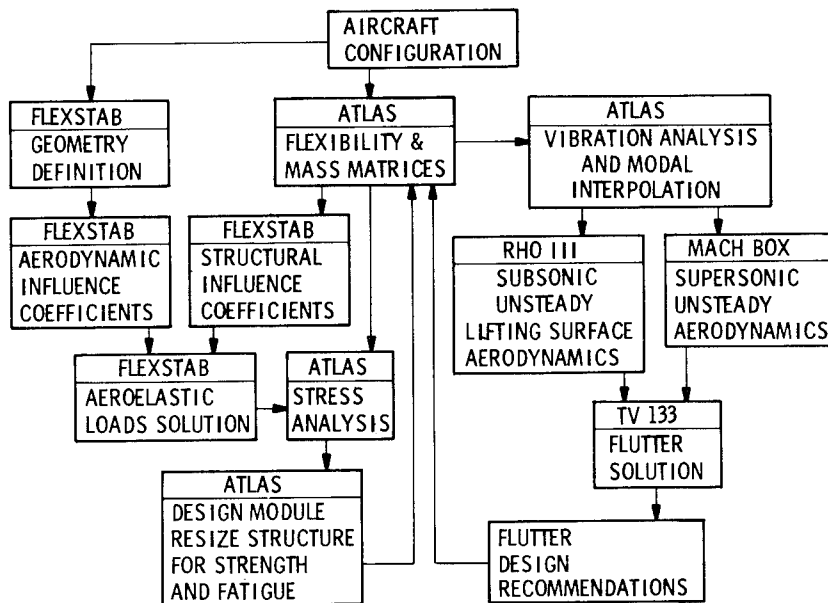


Figure 5.- Analysis and design process.

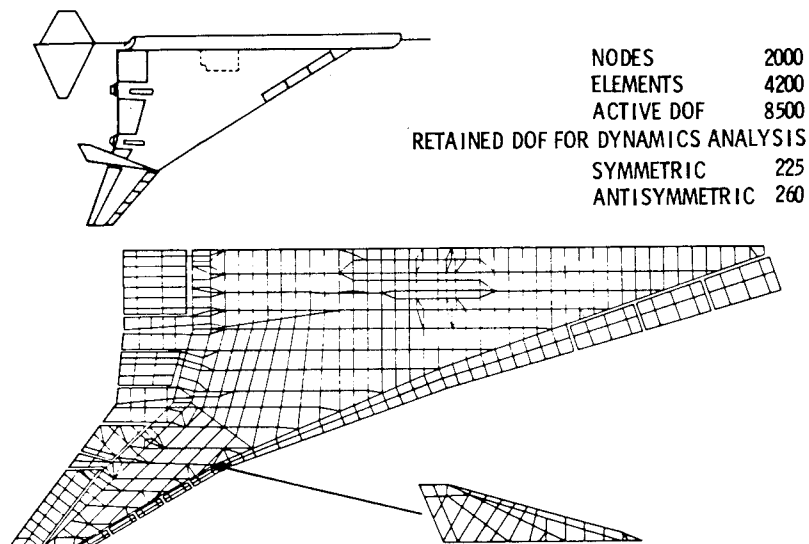


Figure 6.- Finite-element model.

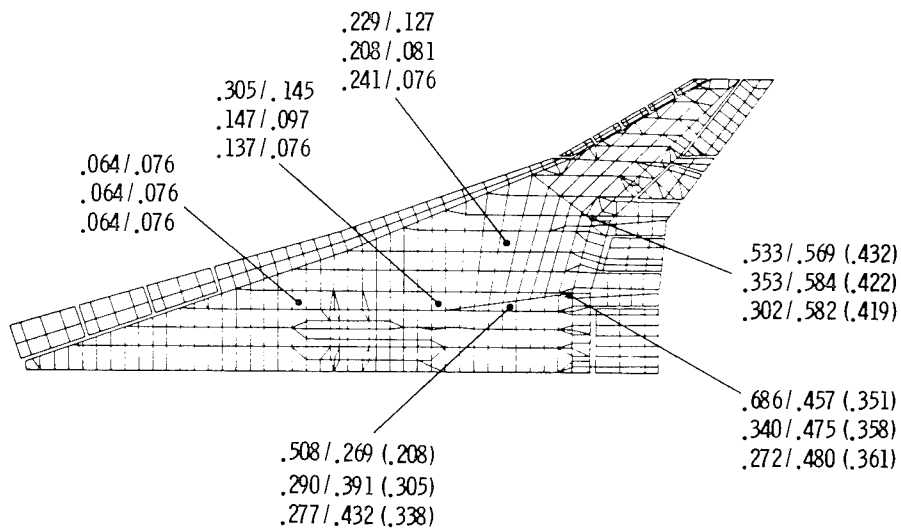


Figure 7.- Structural changes due to strength resizing.

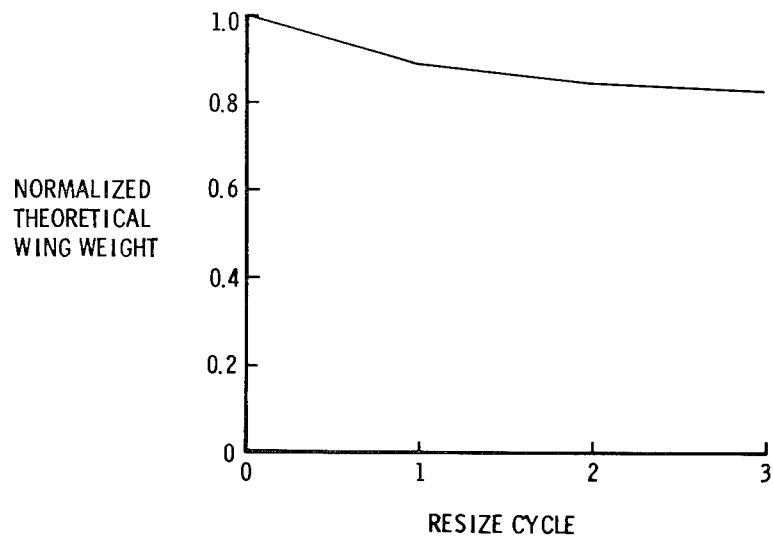


Figure 8.- Theoretical wing weight from ATLAS resizing.

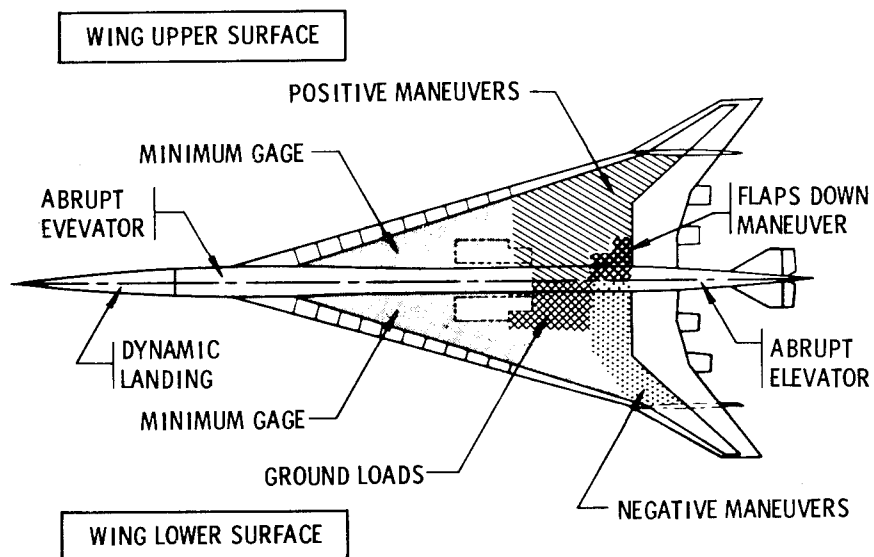


Figure 9.- Critical design conditions.

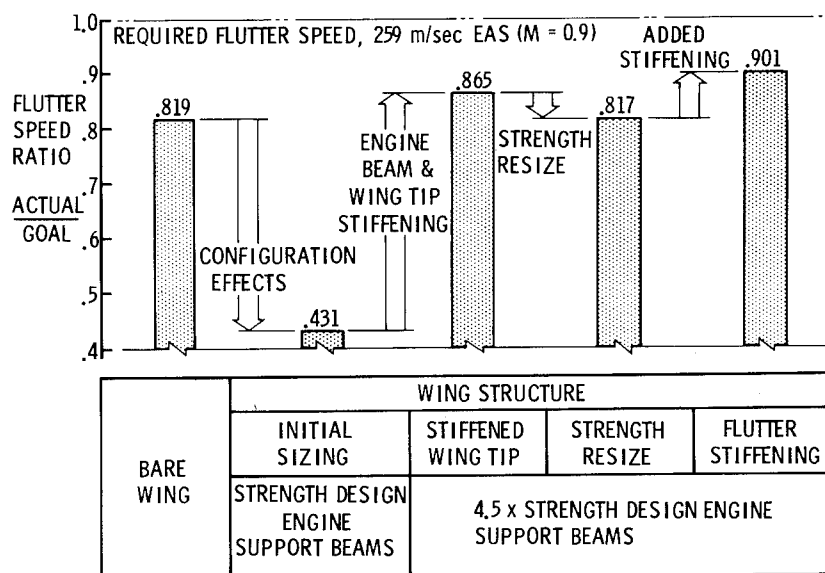
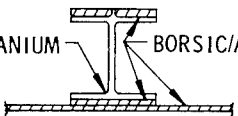
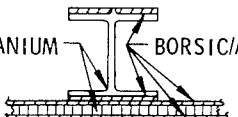
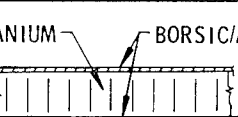


Figure 10.- Effect of structural changes on critical flutter speed.

STRUCTURAL CONCEPT	UNIT MASS, KILOGRAMS PER SQUARE METER		
	BODY	WING UPPER SURFACE	WING LOWER SURFACE
	21,1	** 20,9	20,7 16,89*
	20,9	19,29 16,45*	** 21,5
	17,63	** 17,63	19,58 16,7*

INDICATED MASSES DO NOT INCLUDE THERMAL INSULATION

* HIGH SHEAR ALLOWABLE DERIVED FROM NASA LRC TESTS

** NOT ANALYZED WITH HIGH SHEAR ALLOWABLE -- SIMILAR COMPARISONS EXPECTED

Figure 11.- Structural concept selection - mass comparison.

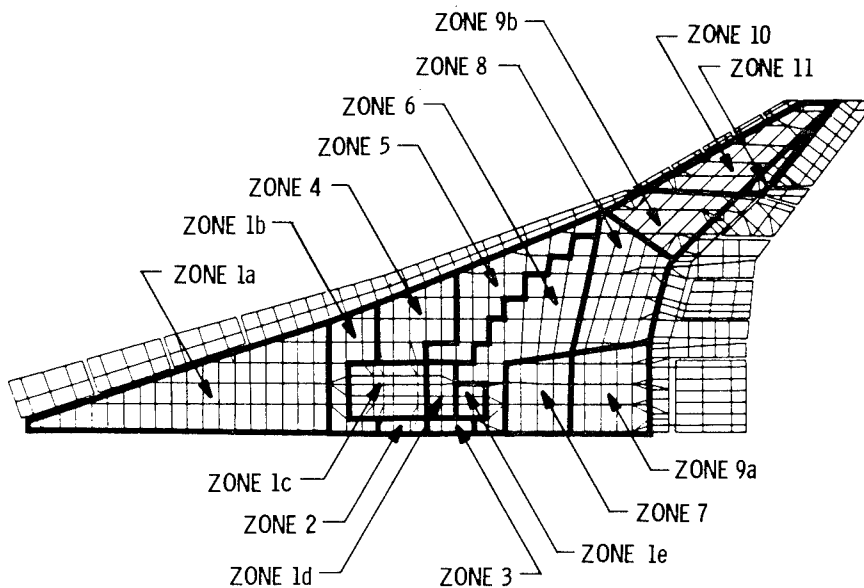


Figure 12.- Zones used for resize.

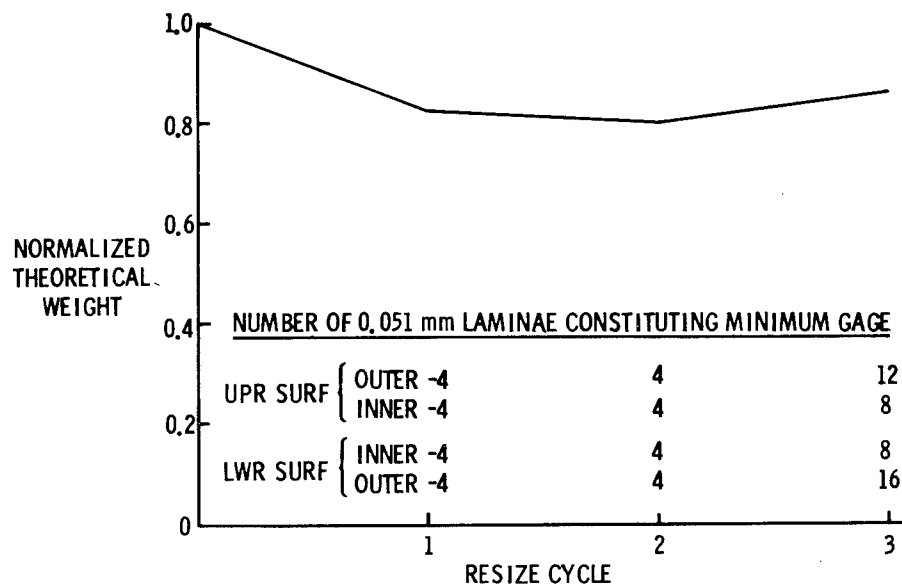


Figure 13.- Theoretical weight changes for wing-box primary structure from ATLAS resizing.

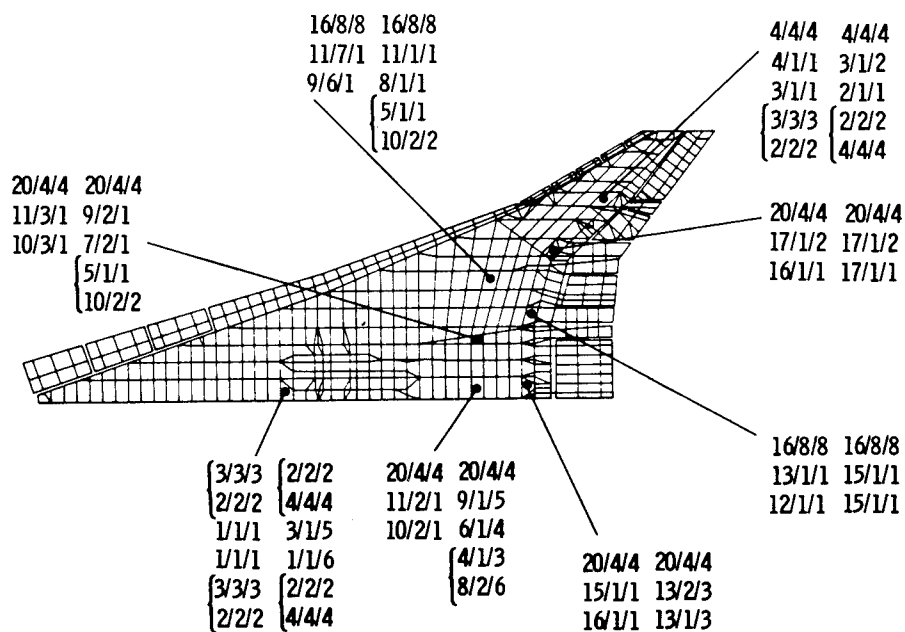


Figure 14.- Typical wing panel resizing.

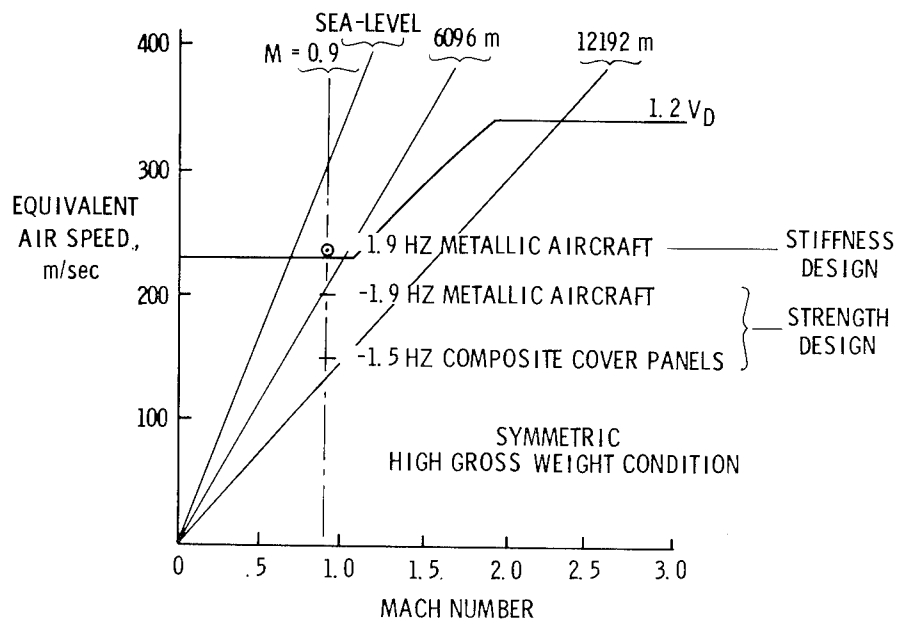


Figure 15.- Comparison of flutter speeds.

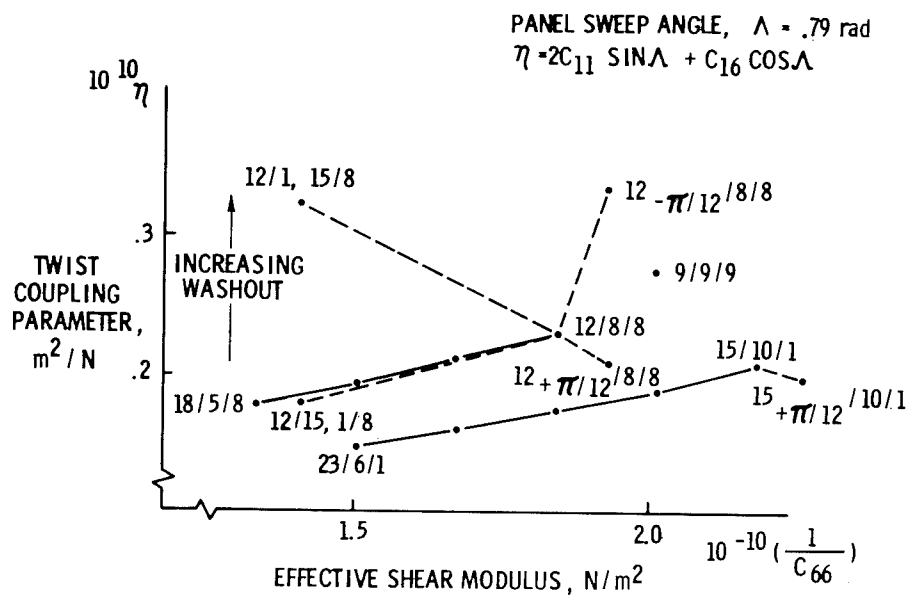


Figure 16.- Anisotropic coupling trends with high-strength graphite polyimide.

ADVANCED STRUCTURES TECHNOLOGY APPLIED TO A
SUPERSONIC CRUISE ARROW-WING CONFIGURATION

I. F. Sakata and G. W. Davis
Lockheed-California Company

ABSTRACT

The application of advanced technology to a promising aerodynamic configuration was explored to investigate the improved payload-range characteristics over the configuration postulated during the National SST Program. Highlighted are the results of an analytical study performed by the Lockheed-California Company to determine the best structural approach for design of a Mach number 2.7 arrow-wing supersonic cruise aircraft. The data from this study, conducted under the auspices of the Structures Directorate of the National Aeronautics and Space Administration, Langley Research Center, established firm technical bases from which further trend studies were conducted to quantitatively assess the benefits and feasibility of using advanced structures technology to arrive at a viable advanced supersonic cruise aircraft.

INTRODUCTION

For the past several years, the National Aeronautics and Space Administration (NASA) Langley Research Center has been pursuing a supersonic cruise aircraft research program (SCAR) to provide sound technical bases for future civil and military supersonic vehicles, including possible development of an environmentally acceptable and economically viable commercial supersonic transport.

The design of a satisfactory advanced supersonic cruise aircraft requires reduced structural mass fractions attainable through application of new materials and concepts, and advanced analytical methods. Configurations, such as the arrow-wing (fig. 1), show promise from the aerodynamic standpoint; however, detailed structural design studies are needed to determine the feasibility of constructing this type of aircraft with sufficiently low structural mass. Past design studies have shown that excessive structural mass was required to satisfy the strength and stiffness requirements of the arrow-wing configuration. In addition, aerodynamic complications were accentuated at low-speed by the low aspect ratio, highly swept configuration.

This paper presents the highlights of the study conducted by the Lockheed-California Company to subject promising structural concepts to in-depth analyses, including the more important environmental considerations that could affect the selection of the best structural approach for design of wing and fuselage primary structure of a given Mach 2.7 arrow-wing supersonic cruise aircraft assuming a near-term start-of-design technology(ref. 1).

(Results of a similar study conducted by the Boeing Commercial Airplane Company are presented in ref. 2.)

This aforementioned structural evaluation (ref. 1) was conducted in three phases: 1) a design concept evaluation study wherein a large number of candidate structural concepts were investigated and evaluated to determine the most promising concepts; 2) a detailed engineering design-analysis study of the selected structural approach to define the critical design parameters and conditions, and the estimated structural mass of the near-term technology airplane; and 3) supplementary studies to identify opportunities for structural mass reduction resulting from the application of advanced technology to define a far-term technology airplane.

The structural evaluation of the near-term airplane involved detail analytical studies that encompassed airplane configuration refinement, design/manufacturing cost studies, and a structural evaluation involving the complex interactions between airframe strength and stiffness, static and dynamic loads, flutter, fatigue and fail-safe design, thermal loads, and the effects of variations in structural arrangements, concepts and materials on these interactions. Extensive use of computer programs and their associated math models were essential to perform the large-order analytical calculations required for this study. Math models were used in association with the aerodynamic heating, basic aerodynamics, external loads, internal loads and vibration and flutter analyses. In addition, interactive computer graphic programs were used in the flutter optimization and stability and control assessments.

The impact of the application of the various advanced structures technology to the near-term design airplane displayed performance gains realized by investing the mass savings into fuel/payload or in a resized (smaller) aircraft that would have the same performance at potentially lower cost. These trends, shown in figure 2, provided insight into future research requirements in the areas of advanced lightweight structural design concepts, advanced composite materials, advanced manufacturing approaches and active controls technology to provide a viable supersonic cruise aircraft.

More detailed results of the design concepts study including substantiating data and supersonic airframe technology recommendations are presented in references 1 and 3. A summary of the producibility technology studies is presented in reference 4.

CONFIGURATION

Reference Configuration

The reference configuration shown in figure 1 is a discrete wing-body airplane with a low wing which, in general, is continuous under the fuselage. The external shape of the airplane was defined at the design lift coefficient by a computer card deck supplied by NASA. This referenced configuration had neither a canard nor inboard leading-edge devices, but relied on the horizontal tail for pitch control and trim.

Configuration Refinement

Several areas of concern were identified with regard to the reference configuration, and refinements to these areas were examined and appropriate changes incorporated into the design. To provide suitable passenger accommodations in terms of comfort, baggage storage, cargo and passenger services, the fuselage depth was increased. A decrement in airplane lift-to-drag ratio equal to 0.10 resulted from this modification. A main landing gear concept was adopted which avoided the necessity for deviations from the NASA-supplied external contour, thus avoiding a drag penalty and minimizing the complexity and mass of the wing structure.

The low-speed pitch-up characteristics were examined using an interactive computer graphics technique that simulates, in real-time, the longitudinal behavior of the airplane response to control disturbances. Findings showed that if adequate control authority was provided, it was feasible to use the horizontal tail to provide automatic pitch limiting capability and good handling qualities. However, two requirements must be met: (1) a definite tail size to center-of-gravity relationship must be maintained, and (2) the pitch limiter system must be fail-operative. On the basis of these considerations, a minimum tail volume coefficient of 0.07 would yield an acceptable center-of-gravity range; with the further constraint that the airplane center of gravity be at 55 percent mean aerodynamic chord for the maximum landing mass.

Configuration development studies explored application of leading and trailing edge devices with auxiliary trimming surfaces (canards and horizontal tail) to provide schemes for supplementing the low-speed lift capabilities. The objective was to maximize the usable lift at takeoff attitudes considering in-ground effects. Methods of low-speed pitch stability improvement were also studied. This involved airplane balance, including the fuel system and its related tankage arrangement. On the final configuration a change in wing tip sweep from 1.13 rad (64.6 deg) as defined by the NASA-supplied data to a 1.05 rad (60 deg) sweep was made. This change reduced the demands on the longitudinal stability augmentation system and permitted a more aft center-of-gravity location with the existing horizontal tail power.

Final Configuration

The final airplane arrangement is shown on figure 3. The fuselage accommodates 234 passengers in five-abreast seating with an overall length of 90.5 m (296.9 ft) and a wing span of 40.4 m (132.6 ft). The leading edge sweep of the wing tip has been decreased to 1.05 rad (60 deg). The wing-mounted main landing gear employs a three-wheel axle design and retracts into a well just outboard of the fuselage.

The aircraft is equipped with a three-axis stability augmentation system (SAS) with adequate redundancy to be fail-operative. The primary

control surfaces are indicated on figure 3 and includes an all-moving horizontal stabilizer with a geared elevator for pitch control. For yaw control, a fuselage mounted all-moving vertical tail with a geared rudder is provided. The tail volume coefficients for the horizontal stabilizer (\bar{V}_H) and the vertical tail (\bar{V}_V) are 0.07 and 0.024, respectively. The inboard wing flaps are used as lift devices at low speed. Leading edge flaps are provided on the outer wing for subsonic and transonic speeds, and ailerons on the trailing edge for low speed. At supersonic speeds, the inverted spoiler-slot deflector and spoiler-slot deflectors provide the primary roll control.

Four duct-burning turbofan engines, each with 398,560 N (89,600 lbf) of uninstalled thrust, are mounted in under wing pods having axisymmetric mixed compression inlets and have thrust reversers located aft of the wing trailing edge. The engine characteristics selected were based on the results of a NASA funded systems study (ref. 5). The engines are sized to provide a total thrust-to-airplane mass ratio of 0.36 at takeoff. The engine mounts are located aft of the wing rear beam and are attached to box beams which are cantilevered off the wing structural box.

The tank arrangement shown in figure 3 provides for a fuel storage capacity of 178,500 kg (393,600 lbm) with a significant portion of the total fuel for the 16 tanks stowed within the protected wing center section. Approximately 43 percent of the total storage capacity is contained in these "protected-volume" locations where the upper surface is exposed to the cooled and controlled environment of the fuselage cabin while the wing lower surface is shielded from the outside airstream by a fairing.

DESIGN CRITERIA

Evaluation of structural concepts for the Mach 2.7 supersonic cruise aircraft was based on an aircraft with an economic life of 15 years and a service life of 50,000 flight hours. The environment was determined from a design flight profile for an international mission which is approximately 3.4 hours in duration; three-quarters of that time, or 2.5 hours, is at Mach 2.62 (Hot Day) cruise.

For design purposes, a maximum taxi mass of 340,000 kg (750,000 lbm), a maximum landing mass of 191,000 kg (420,000 lbm), a payload of 22,000 kg (49,000 lbm), and a design range of 7800 km (4200 nmi) were specified for the airplane.

Maneuver loads analyses were based on solution of the airplane equations of motion for pilot-induced maneuvers. Except where limited by a maximum usable normal force coefficient or by available longitudinal controls deflections, the limit load factors (n_z) were as follows: (1) Positive maneuvers: $n_z = +2.5$ at all design speeds;² (2) Negative maneuvers: $n_z = -1.0$ up to V_C ¹ and varies linearly to zero at V_D ; (3) Rolling maneuver entry load factors: an upper limit $n_z = +1.67$ at all design speeds, with a lower limit $n_z = 0$ up to V_C and varies linearly up to $+1.0$ at V_D .

¹Symbols and abbreviations not defined in the text and figures may be found in the appendix.

Fatigue analyses were based on a representative loading spectrum developed for the National SST Program which provides a moderately conservative representation of a loading history for supersonic cruise aircraft. The reference load levels and oscillatory flight loads included representative tensile thermal stress increments and ground loadings. The basic fatigue criterion was to provide a structure with a service life of 50,000 flight hours. Appropriate multiplying factors were applied to the design life for use in establishing allowable design tension stresses. For structure designed by the spectrum loadings, the allowable stresses were defined using a factor of 2 times the design service life of 50,000 hours. For areas of the fuselage designed by constant amplitude cabin pressure loading, the allowable stresses were based on 200,000 flight hours of service ($50,000 \times 4$).

A fail-safe design load of 100-percent limit load was used for the analysis of the assumed damage conditions. The residual strength of the damaged structure must be capable of withstanding these limit loads without failure.

The selection of minimum gages for regions not designed to specific strength or fatigue requirements was based on consideration of the structural concept employed, fabrication constraints, and foreign object damage (FOD) effects.

STRUCTURAL DESIGN CONCEPTS

A spectrum of structural approaches for primary structure design that have found application or had been proposed for supersonic aircraft, such as the Anglo-French Concorde supersonic transport, the Mach 3.0 plus Lockheed YF-12, and the proposed Lockheed L-2000 and Boeing B-2707 supersonic transports, were systematically evaluated for the given configuration and design criteria.

Design and manufacturing concepts studies (ref. 4) established feasibility of the application of advanced manufacturing techniques to large-scale production. Basic design parameters and design guidelines were established for each structural arrangement and each concept to provide consistency between manufacturing design studies and analyses.

Candidate materials included both metallic and composite material systems. Alpha-Beta (Ti-6Al-4V) and Beta (Beta C) titanium alloys, both annealed and solution treated and aged, were evaluated to identify the important characteristics for minimum mass designs as constrained by the specified structural approach and life requirements.

Among the composite materials considered were both organic matrix (graphite-polyimide, boron-polyimide) and metallic matrix (boron-aluminum) systems. Selective reinforcement of the basic metallic structure was considered as the appropriate level of composite application for the near-term design. Furthermore, based on the principle of maximum return for minimum cost and risk, the application was primarily unidirectional reinforcing

of members carrying axial loads, such as: spar caps, rib caps and stiffeners of wing and fuselage panel designs.

Wing Structure Concepts

The structural design concepts for the wing primary load-carrying structure are shown in figure 4 and consists of two basic types: monocoque and semimonocoque constructions.

Monocoque construction (fig. 4a) consists of biaxially-stiffened panels which support the principal loads in both the span and chord directions. The substructure arrangement consists of both multirib and multispar designs.

The biaxially-stiffened panels considered were the honeycomb core and the truss-core sandwich concepts. The honeycomb core panels were assumed to be aluminum brazed (Aeronca process); whereas, both diffusion-bonded and welded (spot and EB) joining process were assumed for the truss-core sandwich panel configuration.

In the monocoque concepts, as well as in all the other primary structure concepts, circular-arc (sine-wave) corrugated webs were used at the tank closures. Truss-type webs were used for all other areas. The caps of the spars and ribs are inplane with the surface panels for the monocoque concepts to minimize the effect of eccentricities.

The two types of semimonocoque concepts are: (1) panels supporting loads in the spanwise direction (fig. 4b), and (2) panels supporting loads in the chordwise direction (fig. 4c). Both contain the same type of rib and spar webs as the monocoque structure. Discrete spar and rib caps are provided for the semimonocoque concepts since the spar cap or rib cap must support the inplane loads acting normal to the panel stiffeners.

The spanwise-stiffened wing concept is essentially a multirib design with closely spaced ribs and widely spaced spars. The surface panel configurations shown in the figure have effective load-carrying capability in their stiffened direction with smooth skins required for aerodynamic performance. Zee-and hat-stiffened designs are examples of these wing concepts.

The chordwise-stiffened arrangement is essentially a multispar structure with widely spaced ribs. The surface panel concepts for this arrangement have stiffening elements oriented in the chordwise direction. Structurally efficient beaded-skin designs were explored, e.g., circular-arc convex beaded skin concept. These efficient circular-arc sections of sheet metal construction provide effective designs when properly oriented in the airstream to provide acceptable performance, as demonstrated on the Lockheed YF-12 aircraft. The shallow depressions or protrusions provide smooth displacements under thermally induced strains and operational loads and offer significant improvement in fatigue life. Panel spanwise thermal stresses are minimized by allowing thermal deformation of the curved elements. Submerged spar caps are provided except at panel closeouts and at fuel tank bulkheads.

Selective reinforcement of the basic metallic structure (figure 4d) was

considered as the appropriate level of composite application for the near-term design. The chordwise-stiffened arrangement described above provides the basic approach offering the maximum mass saving potential and was used for the exploration of composite reinforcing. In addition to the surface panels, multi-element (fail-safe) composite reinforced spar cap designs were investigated.

Fuselage Structure Concepts

The structural design concepts initially considered for fuselage design included both sandwich shell construction and skin-stringer and frame shell construction.

The sandwich shell design was thought to have a potential mass savings over the more conventional skin-stringer and frame design, with specific advantages with regard to sonic-fatigue resistance and reduced sound and heat transmission. Preliminary structural design and analyses were conducted to assess the potential mass savings benefit and manufacturing/design feasibility of a sandwich shell. The manufacturing complexity and the parasitic mass which the sandwich must carry, in terms of core and bonding agents, proved to be a disadvantage, and thus this concept was not included as part of the study.

Hence, the basic structural arrangement considered for the design fuselage was that of a uniaxially stiffened shell with closely spaced supporting frames. The panel configurations with the most potential were the zee-stiffened and the hat-stiffened configurations. In addition, these stiffener concepts all contain flat elements which are amenable to composite reinforcing. Supporting frames that merited consideration were both the fixed and floating type. The joining methods evaluated for fabricating these concepts include mechanical fastening, welding and bonding.

DESIGN METHODOLOGY AND ANALYSES

A systematic multidisciplinary design-analysis process was used for the structural evaluation. The corresponding analytical design cycle is illustrated in figure 5. The evaluation encompassed in-depth studies involving the interactions between airframe strength and stiffness, static and dynamic loads, flutter, fatigue and fail-safe design, thermal loads, and the effects of variations in structural arrangement, concepts and materials on these interactions. Due to the complex nature of these studies, extensive use was made of computerized analysis programs, with the predominant use of Lockheed-California Company's integrated NASTRAN-FAMAS structural analysis system. The system incorporates the Lockheed-California Company-modified version of the NASTRAN finite element analysis program and the Company's FAMAS program system for aeroelastic loads and flutter analysis.

Design Concepts Evaluation

To initiate the structural evaluation, an investigation was conducted using a single finite-element model to obtain a representative set of wing

and fuselage load intensities for selective maneuver conditions. These load intensities were used in conjunction with computer sizing programs to obtain representative values of structural stiffness for each general type of wing load-carrying structure, i.e., chordwise-stiffened, spanwise-stiffened, and biaxially-stiffened wing surface panels, and for a representative skin-stringer-frame fuselage shell. Using these stiffnesses, NASTRAN finite-element structural models were established for each general type of structure. To conserve resources during this investigation these models were "two-dimensional", that is, they are generated to be symmetrical about an assumed flat mean camber surface. One half the airplane was represented with 1300 elements and approximately 1050 degrees of freedom.

Internal forces/stresses and deflections were obtained for each general type of structure using the appropriate structural model and the corresponding aeroelastic loads caused by maneuver conditions (based on subsonic and supersonic potential-flow theories), and ground operations (based on company experience and the requirements of FAR 25). These internal forces were supplemented with pressure and temperature data to define the load-temperature environment used for conducting the point design analysis.

Three areas on the wing and four areas on the fuselage were selected for conducting point design analyses of the candidate structural concepts. Each area represented a different general structural requirement and was sized using the aforementioned load-temperature environment derived from the appropriate finite-element model; e.g., the internal loads for the chordwise finite-element model were used to analyze the candidate chordwise wing panel concepts.

The point design analyses were conducted using structural optimization computer programs and resulted in a ranking by mass of each of the structural concepts. The least-mass concept (most promising) of each general arrangement (i.e., chordwise-stiffened, spanwise-stiffened and monocoque) was selected and subjected to further point design analysis for three additional wing regions. Total mass data of these strength-sized concepts were obtained by extrapolation of the unit mass of the point design regions over the remainder of the structure. These strength-sized arrangements were evaluated for damage tolerance, flutter, and the effects of aeroelasticity on stability and control.

Vibration and flutter analyses were performed on each general arrangement using the stiffness matrix derived from the finite-element model condensed by Guyan reduction (ref. 6) to 188 and 178 degrees of freedom, symmetric and antisymmetric, respectively. The inertia matrices were formed for two airplane masses: the operating mass empty and the full fuel and full payload condition. These conditions represent the extremes of minimum and maximum airplane mass. No intermediate mass conditions were examined. Flutter analyses encompassed both symmetric and antisymmetric boundary conditions for selected Mach numbers. Flutter deficiencies were corrected by use of an interactive computer system (ref. 7) where sensitivities to operator selected variables were determined and structural parameters incremented by the operator. New modes and frequencies were

calculated for each structural change because of the nonlinear stiffness effect introduced by the Guyan reduction process. This method provided a good estimate, in short time, of the amount and location of required additional structural material. This mass penalty was added to the strength-sized structure mass to obtain a total mass estimate for the airframe.

All of the primary structures, analyzed for consistent load-temperature criteria, are satisfactory from the standpoint of static aeroelasticity, lifting surface flutter, static and dynamic loads, fatigue and fail-safe design, acoustics, thermal stress, and stability and control.

For each of the design concepts, advanced producibility techniques considering the use of welding, brazing or bonding technology were applied. Extensive use of welding and bonding resulted in improved fatigue quality through minimizing fasteners and the number of manufactured joints, and elimination of tank sealing.

Detailed mass breakdowns and comparisons are given in reference 1.

Concept Selection

The wing primary-structure design concepts were ranked (table 1) on the basis of relative mass (constant gross mass airplane). When these primary-structure concepts were applied to constant payload-range aircraft (by interaction evaluation of structural mass, cost, and performance), the ranking of the primary-structure concepts was unchanged, and the relative direct operating cost shown on the table were obtained.

The relative cost increases show the effect that structural efficiency has on overall cost. Small mass inefficiencies evaluated under range-payload constraints can and do raise costs appreciably.

The results of this phase of the design study indicated that a hybrid design using a combination of a chordwise-stiffened and monocoque wing structural arrangement (fig. 6) has least mass and cost and thus provides the most promising arrangement for further detailed evaluation. The stiffness critical wing tip is monocoque construction to make use of the high biaxial stiffness of the aluminum brazed titanium honeycomb sandwich to satisfy the flutter requirements. In the remainder of the wing, low-profile convex beaded surface panels of weld bonded titanium alloy (6Al-4V) are used. The cover panel stiffening is oriented in the chordwise direction with discrete spanwise submerged titanium spar caps reinforced with unidirectional multielement boron-polyimide composites. The fuselage has a hat-stiffener shell design with supporting frames.

Although the Beta alloy showed desirable strength properties and fabrication benefits, it did not exhibit the density compensated elastic properties for minimum mass for the surface panel design.

Engineering Design Analysis

Detailed engineering design analyses of the hybrid design concept were made to define the critical design conditions and requirements, and estimate the structural mass of the near-term technology airplane.

A more detailed 3-dimensional finite-element model was developed and used as the basis for the final structural analyses. The finite-element model (fig. 7) contains approximately 2200 degrees of freedom and 2450 elements. The external loads, internal forces, and displacements for the hybrid design were determined. Strength sizing and one resizing were conducted at six wing regions and four fuselage regions.

The allowable stresses and distribution of the structural material reflected strength requirements, fatigue effects (both load and sonic) and damage tolerance consideration for a commercial airplane. In addition, material distribution was constrained by fabrication and minimum gage design considerations.

The results of these analyses defined a strength-level design. Flutter characteristics for this airplane were then determined at the Mach numbers of 0.60, 0.90, and 1.85 to assess the additional stiffness requirements to correct flutter deficiencies.

The math model for the near-term airplane incorporated the additional stiffness dictated by aeroelastic requirements as well as design/manufacturing considerations to provide a realistic structural design. Structural influence coefficients, internal loads, and aeroelastic displacements were calculated for this airplane.

Relative to the flutter-speed requirements defined from the operating envelope all Mach numbers investigated have adequate flutter margins of safety. Roll-control reversal speeds and FAR requirements were compared for both the normal scheduled surface combinations and for selected fail-safe conditions which involve loss of a surface which has the most adverse effect on roll-control reversal speed. In all cases, the airplane met or exceeded the specified requirements.

NEAR-TERM TECHNOLOGY AIRPLANE

The near-term technology aircraft has a takeoff gross mass of 340,000 kg (750,000 lbm), and a wing loading of 334 kg/m^2 (68.7 lbm/ft^2). A fail-operative ("hardened") three-axis stability augmentation system (SAS), integral to the primary control system concept, is provided. Active controls such as flutter mode control and load alleviation were not included. The zero-fuel mass for the aircraft is 164,600 kg (362,800 lbm). The near-term aircraft reflects a 1980 start-of-design technology employing titanium alloy 6Al-4V as the primary construction material with composite materials accounting for approximately 7 percent of the airframe mass.

Wing Structure

The hybrid wing design shown in figure 6 employs a combination of chordwise-stiffened and monocoque structural arrangements. Structurally efficient convex-beaded surface panels are used in both the forward and aft box. Submerged titanium alloy spar caps, reinforced with multi-element unidirectional boron-polyimide composites, are found in the strength-critical aft box structure. Design details of the chordwise-stiffened beaded surface panel and structure are shown in figure 8. With the beaded skin design, wing bending material is concentrated in the spar caps and the surface panels primarily transmit the chordwise and shear inplane loads and out-of-plane pressure loads.

Weldbonding is the basic method proposed for joining the inner and outer skins of the surface assembly. Surface panel size was held to 4.6 x 10.7 m (15 x 35 ft). The length limit was based on tooling considerations for hot vacuum forming of the skin while the width limit was based on postulated size of spot-welding equipment.

In locating wing spars in the chordwise-stiffened wing area, a minimum spacing of 0.53 m (21 in) was maintained between constraints such as fuel tank boundaries. Wing rib spacing was a nominal 1.52 m (60 in) but was modified as required to suit geometrical design constraints. These dimensions define minimum mass conditions which were determined through studies involving various spar and rib spacing. In the chordwise-stiffened and transition areas, welded truss spars were used except where a spar serves as a fuel tank well. At such locations, spars have welded circular arc webs with stiffened "I" caps. To facilitate fuel sealing, surface beads do not extend across tank boundaries. Wing spars in the aft wing box were fabricated as continuous subassemblies between BL 470 L and R. Boron-polyimide was selected for the spar cap reinforcement for its structural efficiency. The multielement approach results in damage tolerance capability.

Aluminum brazed titanium alloy honeycomb-core sandwich panels are used in the stiffness critical wing tip region.

The sandwich surfaces were brazed together using 3003 aluminum alloy as the brazing material (the "Aeronca" process). Welded circular-arc spars and ribs were used since the minimum need for web penetrations allows the realization of their inherent minimum mass and design simplicity feature. Composite reinforcement was not used in the brazed surfaces or the welded circular arc spars and ribs. A size limit of 1.73 x 12.19 m (5.66 x 40 ft) for brazed surfaces was postulated as a guide after consultation with Aeronca. The panel configurations were based on the design philosophy that all or some panels of the upper surfaces are attached with screws and are removable for inspection and maintenance purposes.

The flexibility of the aluminum braze process was exploited by incorporating crack stoppers and panel edge doublers in the surface panel brace-ments. Also, the capability of tapering the panel thickness was utilized in the joint between the chordwise and monocoque surface areas. In this joint area, where transition in arrangement was made, the outboard sandwich

surfaces were extended inboard so that spanwise components of the outboard sandwich surfaces were extended inboard so that spanwise components of the outboard surface loads due to wing bending loads are transferred directly to the chordwise-stiffened structure at the interface rib.

Fuselage Structure

The fuselage shell incorporates machined extrusion stringers, crack-stoppers between frames, and floating zee frames with shear clips. Closed hat-section extruded stringers which provide structural efficiency were proposed to be machined to provide for crack stoppers and to vary stringer thickness. Extruded stringers also were found to be well suited to effective installation of composite reinforcement. The floating zee frames with shear clips were considered preferable, from a fatigue standpoint, to full depth frames having notches for stringers. Also, zee frames avoid the offset shear center associated with channel section frames.

Weldbonding was proposed to be used for attaching frames, stringers and crack-stoppers to the skin because of economy, minimum mass, good fatigue characteristics, and the avoidance of sealing problems. Satisfactory weldbonding of three thicknesses, as encountered at some locations, may require development. Weldbrazing was considered as a possible backup to weldbonding. Where fasteners were used at shear clips and frame/stringer attachments, fastener-bonding was utilized in lieu of fasteners alone to obtain enhanced properties. The size of fuselage skin panel assemblies has been limited to 4.57 x 15.25 m (15 x 50 ft); the former is based on the postulated size of spotwelding equipment, the latter on the postulated length of the adhesive curing ovens.

Longitudinal skin-panel splices were located only at the top centerline of the fuselage and at the floor/shell intersections fore and aft of the wing carry-through area. These longitudinal splices utilize external and internal splice plates in conjunction with fastener-bonding to achieve a double shear splice having damage tolerance capabilities and good fatigue properties. Suitable combinations of fastener size and external splice-plate thickness were utilized to avoid feather edges at countersinks for flush fasteners. At circumferential panel splices and other locations as required, feather edges were avoided by incorporating thickened pads in the external skin in a manner similar to that for wing skins. Chemical milling was used to vary fuselage skin thickness in accordance with load requirements.

Critical Design Conditions and Requirements

The design conditions and requirements that sized various portions of the near-term design are shown in figures 9 and 10. In figure 9, the upper and lower surface of the wing are divided into three distinct zones according to the design requirements that dictated structural sizes.

The tip structure was stiffness critical and sized to meet the flutter requirements. The highly loaded aft box and some portions of the forward box structures were strength-designed to transmit the wing spanwise and chordwise bending moments and shears. The forward box structural sizing resulted in surface panels and substructure components with active minimum gage constraints. Foreign object damage was the governing criterion for selection of minimum gage.

The conditions which displayed the maximum surface panel design loads are presented in figure 10. An exception was the tip structure which was stiffness critical for the Mach 1.85 condition. The supersonic cruise aircraft displayed critical loads at transonic and low supersonic Mach numbers wherein the structural temperatures did not influence the design appreciably. Although major areas of the wing lower surface were impacted by the thermal environment, analysis of surface panels and substructure using the applicable load-temperature environment resulted in the symmetric maneuver condition at Mach 1.25 as the critical design condition. The upper surface in the forward box was constrained by the minimum gage criterion. The forebody shell region was loaded principally by fuselage pressurization, and therefore critical for the operational environment at Mach 2.7. The constant amplitude loading imposed upon this structure requires reduced allowable stresses to achieve the life requirements.

The fuselage design was influenced by the high temperature environment for the major portion of the upper shell and the pressure critical forebody shell. As indicated on figure 10 a major part of the shell structure was bending critical; the lower shell being critical for the dynamic landing conditions. The forebody and aftbody conditions display critical downbending which occur at varying time from main landing gear impact.

Airplane Mass Estimates

Detailed mass descriptions of the wing and fuselage are presented in tables 2 and 3, respectively. The wing mass description includes fail-safe provisions, allowance for flutter prevention, and panel-thickness changes for manufacturing/design constraints. The fixed mass consists of those items invariant with box structural concept, such as engine-support beams, and leading and trailing edge structure. The fuselage mass was also divided into two major categories: shell mass and fixed mass. Here again the shell mass was dependent upon structural concept while the fixed mass such as doors, windows, flight station, and fairings were invariant.

The mass properties for the near-term technology airplane were determined as shown in table 4 as an Estimated Group Mass Statement. The data reflects a fixed size aircraft with a takeoff gross mass of 340,000 kg (750,000 lbm) and payload of 22,000 kg (49,000 lbm).

ADVANCED TECHNOLOGY ASSESSMENT

Starting with the near-term design, projections for airplane structural mass were determined for an aircraft employing technologies beyond the 1980 time period. It was postulated that by the 1990's advanced composites using polyimide resin systems for long-time application in the Mach 2.7 environment would be sufficiently matured to be aggressively used for both primary and secondary structural application. Similarly, advances in the titanium technology would be in-hand to apply to specific regions of the airframe for reduced mass and cost. Furthermore, advanced controls concepts would be employed in reducing structural mass as well as reduce normal accelerations to provide satisfactory ride quality and fatigue damage control.

Advanced Composite Technology

Projected composite development trends postulated the availability of improved stable high temperature resin systems such as thermoplastic polyimides or high temperature polyaromatics, large numerically controlled tape laying equipment, filament winding and pultrusion equipment, and larger autoclaves. Reference 1 studies indicated that, with aggressive application of composite materials and fabrication technology, the payload-range characteristics could be improved by 12 percent for a constant gross mass aircraft or the takeoff mass reduced 14 percent for a given design payload-range goal.

To obtain the mass for the wing and fuselage primary structure, the results of the design concepts evaluation study were employed to size specific point design regions in graphite-polyimide and boron-polyimide. The sizing data included the internal loads and stiffness requirements for the appropriate airframe arrangement (i.e. chordwise-stiffened and monocoque designs). A comparison was then made between the near-term design and similar designs in graphite and boron composites. For secondary structure and other structural components (i.e. landing gear, nacelle, etc.), reduction factors were used based on Lockheed experience.

Evaluation of the wing box mass data for the near-term design and the composite material system design (ref.1) indicated the mass advantage of the minimum gage titanium alloy beaded panels of the forward box, as compared to an equivalent stiffness composite design of either graphite-polyimide or boron-polyimide. For the strength critical aft box and stiffness critical wing tip structure, an all-composite design indicated a 5-percent savings in total wing box mass. Composite application to the fuselage shell reflected a decrease in shell unit mass at all point design regions; the magnitude varied from 4 percent to 21 percent. A mass saving for the total shell when employing composites was 13.7 percent. A mass reduction factor applied to the secondary and other structural components (i.e. tail, nacelle, etc.) resulted in 9,500 kg (21,000 lbm) savings. These items alone offered a significant mass payoff and potentially improves the aircraft performance by approximately 650 km (350 nmi).

These data, although preliminary in nature, show that advanced composites application to the far-term structural approach offers significant improvement in the fuel fraction for the constant gross mass airplane. The 12,200-kg (26,800 lbm) total mass saving relates to a range increase of 830-km (450-nmi) or a total range potential of 8,630 km (4,650 nmi).

Advanced Controls Technology

The near-term technology airplane postulated the use of a 3-axis stability augmentation system (SAS) that was fail-operative. The mass benefits of reduced tail size were incorporated into the design, as well as the additional mass required for automatic sensors which detect motions (yaw, pitch, roll) of the aircraft and results in the actuation of the normal flight control to provide artificial stability.

Two other potential sources of structural mass reduction related to the application of active controls were identified on the near-term design airplane. They include: load alleviation and flutter mode control. The design conditions and requirements of the near-term airplane showed that the aft box structure was strength-critical. The wing mass data also indicated that the spars which transmit the bending moments and shears had a mass of 3,890 kg (8,570 lbm). By the application of an active load alleviation concept, it was postulated that the span load distribution could be sufficiently altered by deflection of the trailing edge devices so as to appreciably reduce the bending moments during maneuver. An overall 25-percent reduction in bending requirements could potentially reduce the structural mass by 950 kg (2,100 lbm). To suppress the critical flutter modes envisioned the use of the trailing edge surfaces which were automatically actuated to increase aerodynamic damping. It was postulated that sufficient structural stiffness was required to meet the dive speed (V_D) boundary at all Mach numbers, and that the stiffness increment required to achieve 1.2 V_D could be potentially eliminated. Thus, using this premise, the results of flutter optimization studies (ref. 3) were reviewed and a possible mass savings of 720 kg (1,600 lbm) was forecasted for the wing tip structure. Collectively these two advanced control concepts have a potential for reducing 1,670 kg (3,700 lbm) from the structural mass affording an increase in range of 110 km (60 nmi).

Advanced Technology Trends

A major potential source for structural mass reduction identified on the near-term aircraft and through the advanced technology assessment was the increased use of advanced composite materials. This was particularly true when the cascading effects on the aircraft size and cost were considered. The application, however, must be consistent with the projected start-of-design date and the availability date of composite materials and manufacturing technology.

A sequential application of new technology to the near-term airplane is displayed in figure 11. These trends postulate the availability of the technology because of the requirement of minimum development and risk, and/or as a direct fallout of technology currently pursued by government and industry.

- (1) The near-term design (1980 technology) is shown as an aircraft with a takeoff gross mass of 340,000 kg (750,000 lbm) and a range of 7800 km (4200 nmi). The aircraft has a fail-operative three-axis stability augmentation system concept and approximately 7-percent composite material application.
- (2) Design changes were made to the near-term design by applying composite materials to the secondary structure of the wing and fuselage and to the empennage structure and wing verticals. These structures were related to the requirement for minimum development and risk, thus identified as 1985 technology. The secondary components are categorized as those that are noncritical to flight safety components, inspectable components where damage would be apparent in routine maintenance operations, and repairable or replaceable components. For this assessment, control surfaces and leading edge structures were included in this category, recognizing that proper allowance for temperature must be made in selecting materials and allowables. The composite empennage postulates technology transfer of current development of an advanced composite vertical fin for the L-1011 aircraft being pursued by Lockheed-California Company under the auspices of NASA Langley (ref. 8). The aforementioned level of application provides a mass savings of 5,670 kg (12,500 lbm) and a range increment of 390 km (210 nmi) for the 340,000 kg (750,000 lbm) aircraft. This composite material usage accounts for approximately 23 percent of the structural mass.
- (3) Further range improvement of 110 km (60 nmi) was realized by the application of load alleviation and flutter mode control. Mass saving in the flutter critical wing tip was realized by providing structure to meet the V_D requirement at the critical Mach number for the bending and torsion mode flutter. Appropriate reduction in the bending material requirement of the aft box structure was also made. The composite materials application and technology level remains as determined for the design change (2). Early introduction of active controls technology (ACT) is based on a current program which includes the demonstration of near-term feasibility of ACT for commercial application as part of NASA's Aircraft Energy Efficiency/Energy Efficient Transport Program. The program looks to the application of active controls to the Lockheed L-1011 for increased energy efficiency, with application to today's fleet as early as 1981.
- (4) The aggressive application of advanced composite materials, active controls concepts, and advanced production technologies were the basis for defining the far-term (1990 technology) airplane trends.

Composite application encompassed the previously identified secondary structure and empennage plus the wing aft box and tip, and the fuselage shell. The composite material mass represents 51 percent of the total structural mass of the aircraft. A range increment of 430 km (230 nmi) was realized for the 340,000 kg (750,000 lbm) aircraft.

These various "state-of-the-art" aircraft were constrained to a constant takeoff gross mass of 340,000 kg (750,000 lbm) and all equal or exceed the design range goal of 7800 km (4200 nmi). Resizing these aircraft for varying degrees of advanced technology are noted by the decreasing mass and range trends.

FAR-TERM TECHNOLOGY AIRPLANE

The far-term airplane employs those technologies available for application beyond the frame work of the near-term (1980 technology) approach. Potential areas include advanced composite materials, advanced controls concepts, and cost reducing production approaches. It is postulated that the various potential technologies will be pursued in a timely manner through appropriate research and development and be available for application by the year 1990.

The hybrid wing structural approach shown in figure 12 employs both advanced metallic and composite materials, and a combination of the chord-wise-stiffened and monocoque arrangements. The convex-beaded surface panel concept of titanium alloy 6Al-4V with the submerged spar caps resulted in minimum mass for the forward box structure. Advanced titanium manufacturing concepts, such as the Lockheed-California Company's low cost/no draft precision titanium forging technology and Rockwell-International's superplastic forming-diffusion bonding technology may find application for reduced mass and cost. Both concepts eliminate machining requirements and, in particular, the low cost/no draft precision titanium forging technology has been successfully applied to a rather complicated structural component used on the Lockheed L-1011 aircraft. A mass savings in raw material of 91 percent over the current method of machining from a plate stock was demonstrated with a total cost reduction (per part) of 77 percent realized.

A graphite-polyimide honeycomb sandwich panel concept is used in the strength and stiffness critical aft- and tip-box structure, respectively. For environmental protection of the composite material system, aluminum wire fabric is also employed. Composite materials account for approximately 58 percent of the wing structure mass.

The fuselage shell is a graphite-polyimide skin-stringer-frame design. In the pressure critical forebody a T-stiffened skin is employed; the closed-hat stiffened skin is used in the more highly loaded centerbody and aftbody structure. Fuselage frames are spaced at 50.8 cm (20 in) and the frame height constrained at 7.6 cm (3.0 in). The composite shell and secondary structure represents 77 percent of the total body mass.

Composite materials application to the other structural components (i.e. landing gear, tail, nacelle, air induction system) varies between 12 to 40 percent of the respective component mass.

The aircraft employs advanced controls concepts that are related to reducing structural mass (i.e. load alleviation, flutter mode control) as well as those concepts that are fundamental ingredients for viability of a slender, highly flexible arrow-wing configuration (i.e. ride quality control, elastic mode suppression, etc.).

The aircraft was resized (smaller) for a constant design payload-range and has a takeoff gross mass of 291,000 kg (642,000 lbm). The zero-fuel mass of the aircraft was reduced 15 percent from the near-term design with a commensurate reduction in flyaway cost. Composite materials account for approximately 51 percent of the total structural mass.

CONCLUDING REMARKS

The best structural approach for design of wing and fuselage primary structure of a Mach 2.7 arrow-wing configuration aircraft was determined considering near-term start-of-design technology. To accomplish this goal, a systematic multidisciplinary design-analysis process was used to assess the effects of the more important environmental considerations (e.g., thermal, airload, flutter) on the selection of the structural arrangement for a flexible arrow-wing configuration. Detail studies defined a near-term design airplane and its characteristics, and showed that the airplane was viable in terms of structural mass and flexibility. Supplemental studies provided airplane mass and performance trends as impacted by the application of structures technology postulated to be available beyond the near-term design time period. Significant improvement in fuel fraction for the constant mass airplane, with varying degree of advanced structures technology application, displayed performance improvements between 6 to 14 percent over the near-term design. Resizing the aircraft to the design payload-range goal resulted in a 15-percent reduction in empty mass and a commensurate reduction in flyaway cost.

A design methodology to cope with the various interactive parameters was established and provides guidance for future studies of this type. The study illustrated that the design analysis of large, flexible aircraft requires realistic aeroelastic evaluation based on finite-element analyses, and steady and unsteady aerodynamic loading determination. Static aeroelastic and flutter characteristics are important design considerations, and should be investigated early in the design cycle. Significant additional structure, over and above that required for strength, was required in the wing tip and the engine support rails to eliminate initial flutter deficiencies. Innovative application of computer graphics in the design process was demonstrated in the flutter optimization and low-speed handling quality time-history studies. These graphic systems

were conducted using a relatively detailed analytical model of a supersonic cruise aircraft and showed the feasibility and cost-effectiveness in terms of decreasing manpower expenditures and design calendar time.

The study developed a realistic flexible model of an advanced arrow-wing supersonic cruise aircraft and has shown that the application of advanced structural panel concepts and uniaxial reinforcement of the titanium spar caps with composite materials is a promising approach for a 1980 technology design. Although the proposed design concepts for the near-term design airplane satisfy the mission requirements, a considerable amount of research effort is required in (1) aerodynamics and configuration refinements, (2) experimental validation of the promising concepts, (3) advanced materials and fabrication development, including composites, and (4) continued development of advanced design-analysis methods to accelerate the design process. Included in the latter are automated data generation, integration of the design-analysis system and associated data management system, and interactive design analysis.

Also, as a part of the aircraft stability and control and performance investigations, the use of active controls was postulated. Further studies are needed concerning their use for stability augmentation and handling quality investigations particularly from the structural loads standpoint. Methodology for application of advanced control concepts to the airplane design must be pursued, addressing those concepts not only related to reducing structural mass (i.e. flutter mode control, load alleviation) and life enhancement (fatigue reduction) but also those concepts that are fundamental ingredients for viability of slender, highly flexible airframe configurations (i.e. ride quality, elastic mode suppression). In addressing these control concepts, focus must also be placed on improving the analytical representation of the transonic, nonlinear unsteady aerodynamic flow characteristics and the interaction of control surface and structural deformations under aerodynamic loading.

Of most concern and challenge for commercial application of advanced technology is the achievement of a systems reliability sufficiently high so that no failure would cause catastrophic loss of aircraft control or structural failure during the complete life of the aircraft. The results of the NASA development and flight evaluation program for both advanced composite primary structure and active controls application to the L-1011 will greatly enhance the advanced technology challenge and contribute immeasurably towards the development of a viable supersonic cruise aircraft.

APPENDIX

SYMBOLS AND ABBREVIATIONS

t	thickness
V_C	design cruise speed
V_D	design dive speed
Λ	sweep angle
B/AL	boron/aluminum
B/PI	boron/polyimide
EMS	elastic mode suppression
FMC	flutter mode control
GA	gust alleviation
MLC	maneuver load control
MLG	main landing gear
RQ	ride quality
RSS	relaxed static stability

REFERENCES

1. Sakata, I. F.; Davis, G. W.; Evaluation of Structural Design Concepts for an Arrow-Wing Supersonic-Cruise Aircraft. NASA CR 2667, 1977.
2. Robinson, J. C.; Yates, E. C. Jr.; Turner, M. J. and Grande, D. L.; Application of an Advanced Computerized Structural Design System to an Arrow-Wing Supersonic Cruise Aircraft. AIAA Paper 75-1038, Aug. 4-7, 1975.
3. Sakata, I.F.; and Davis, G. W.: Substantiating Data for Arrow-Wing Supersonic Cruise Aircraft Structural Design Concepts Evaluation. NASA CR-132575-1, -2, -3, -4, October 1975.
4. Van Hammersveld, John: Producibility Technology Studies - Supersonic Cruise Aircraft. 21st National SAMPE Symposium and Exhibition, Los Angeles, California, April 6-8, 1976.
5. Executive Summary. Studies of the Impact of Advanced Technologies Applied to Supersonic Transport Aircraft. NASA CR-145057, 1974.
6. Guyan, R. J., Reduction of Stiffness and Mass Matrices, AIAA Journal, Volume 3, No. 2, February 1965 (Page 380)
7. O'Connell, R.F., Hassig, H.J., and Radovcich, N.A.: Study of Flutter Related Computational Procedures for Minimum Weight Structural Sizing of Advanced Aircraft. NASA CR-2607, March 1976.
8. James, A. M.; et. al.: Flight Service Evaluation of an Advanced Composite Empennage Component on Commercial Transport Aircraft. NASA CR-144986, May 1976.

TABLE 1. CONCEPT EVALUATION SUMMARY

WING PRIMARY STRUCTURE CONCEPT ^(d)	MASS COMPARISON FOR BASELINE-SIZE AIRCRAFT ^(a)		COST ^(b) COM- PARISON FOR OPTIMUM-SIZE AIRCRAFT ^(c)	
	WING MASS		RELATIVE MASS	RELATIVE COST
	kg/m ²	lbm/ft ²		
(1) Chordwise stiffened - convex-beaded panels; B/PI reinforced spars; and aluminum brazed honeycomb core tip panels	39.99	8.19	1.00	1.00
(2) Chordwise stiffened - convex-beaded panels; B/PI reinforced spars	40.28	8.25	1.01	1.00
(3) Monocoque - aluminum brazed honeycomb core panels (mech. fastened)	41.70	8.54	1.04	1.07
(4) Monocoque - aluminum brazed honeycomb core panels (welded)	43.21	8.85	1.08	1.10
(5) Spanwise stiffened - hat-stiffened panels	47.26	9.68	1.18	1.09
(6) Chordwise stiffened - convex-beaded panels	47.85	9.80	1.20	1.11
<p>(a) Gross takeoff mass = 340,000 kg (750,000 lbm)</p> <p>(b) Direct operating cost for 25×10^9 ton-mile fleet mission</p> <p>(c) Gross takeoff mass varies</p> <p>(d) Each with a skin-stringer/frame fuselage structure</p> <p>(e) Wing mass per unit planform area</p>				

TABLE 2. MASS ESTIMATES FOR NEAR-TERM DESIGN WING

ITEM	PLANFORM AREA		MASS	
	ft ²	m ²	lbm	kg
<u>Variable Mass</u>			50,432 ^(A)	22,876 ^(A)
Forward Box	4136.6	384.3	(20,580)	(9,335)
• Surfaces - convex beaded, chordwise stiffened			9,452	4,287
• Spars - including 522 lb (227 kg) composites			8,558	3,882
• Ribs			2,570	1,166
Aft Box	2132.4	198.1	(17,384)	(7,885)
• Surfaces - convex beaded, chordwise stiffened			7,302	3,312
• Spars - including 3,762 lb (1706 kg) composites			8,568	3,886
• Ribs			1,514	687
Transition - Aft Box to Tip Box			(1,380)	(626)
Tip Box	947	88.0	(11,088)	(5,030)
• Surfaces - brazed honeycomb sand., mech. fast.			9,435	4,280
• Spars			1,336	606
• Ribs			317	144
(A) Includes fail-safe penalty of 373 kg (822 lbm)				

TABLE 2. MASS ESTIMATES FOR NEAR-TERM DESIGN WING (Continued)

ITEM	PLANFORM AREA		MASS	
	ft ²	m ²	lbm	kg
<u>Fixed Mass</u>			40,152	18,213
Leading Edge	1047	97.3	5,235	2,375
Trailing Edge	1941	180.3	4,888	2,217
Wing/Body Fairing	800	74.3	1,600	726
Leading Edge Flaps/Slats	133	12.4	1,130	512
Trailing Edge Flaps/ Flaperons	553	51.4	5,890	2,672
Ailerons	250	23.2	1,250	567
Spoilers	225	20.9	1,380	617
Main Landing Gear - Doors	484	45.0	2,904	1,317
Sup't Structure			3,750	1,701
B.L. 62 Ribs			1,430	649
B.L. 470 Ribs			700	318
Fin Attach Ribs (B.L. 602)			435	197
Rear Spar			3,400	1,542
Engine Support Structure			2,380	1,080
Fuel Bulkheads			3,800	1,724
Total Wing Mass			90,584	41,088

TABLE 3. MASS ESTIMATES FOR NEAR-TERM DESIGN FUSELAGE

ITEM	MASS	
	lbm	kg
<u>Shell Structure</u>	22,582 ^(A)	10,243 ^(A)
Skin	11,144	5,055
Stiffeners	7,921	3,593
Frames	3,517	1,595
<u>Fixed Mass (B)</u>	19,540 ^(B)	8,863 ^(B)
Nose and Flight Station	2,500	1,134
Nose Landing Gear Well	900	408
Windshield and Windows	1,680	762
Flooring and Supports	3,820	1,733
Doors and Mechanism	4,170	1,891
Underwing Fairing	1,870	848
Cargo Compartment Prov.	1,060	481
Wing to Body Frames and Fittings	1,500	680
Tail to Body Frames and Fittings	600	272
Prov. for Systems	740	336
Finish and Sealant	700	318
Total Fuselage Mass	42,122	19,106
(A) Includes fail-safe penalty of 650 kg (1,432 lbm)		
(B) Includes composite material mass of 508 kg (1,120 lbm)		

TABLE 4. ESTIMATED GROUP MASS STATEMENT
NEAR-TERM DESIGN AIRPLANE

ITEM	MASS	
	lbm	kg
Wing	90,584	41,088
Tail - Fin on Wing	2,800	1,270
Tail - Fin on Body	2,600	1,179
Tail - Horizontal	7,950	3,606
Body	42,122	19,106
Landing Gear - Nose	3,000	1,361
Landing Gear - Main	27,400	12,428
Air Induction	19,760	8,963
Nacelles	5,137	2,330
Propulsion - Turbofan Engine Inbd.	25,562	11,595
Propulsion - Turbofan Engine Outbd.	25,562	11,595
Propulsion - Systems	7,007	3,178
Surface Controls	8,500	3,856
Instruments	1,230	558
Hydraulics	5,700	2,585
Electrical	4,550	2,064
Avionics	1,900	862
Furnishing & Equipment	11,500	5,216
Environmental Control System	8,300	3,765
Tolerance & Equipment	1,980	898
Manufacturer Empty Mass	303,144	137,504
Std & Oper. Eq.	10,700	4,853
Operating Empty Mass (OEM)	313,844	142,357
Payload	49,000	22,226
Zero-Fuel Mass	362,844	164,583
Fuel	387,156	175,611
Taxi Mass	750,000	340,194
<p>LEMAC = FS 1548.2 in. (39.32 m) MAC = 1351.06 in. (34.32 m)</p> <p>X ARM = Distance from F.S. 0.</p> <p>Fus. Nose at F.S. 279 in. (7.09 m)</p>		

SCAT 15F
 $\Delta \text{Tip} = 1.13 \text{ rad } (64.6^\circ)$
 $\bar{V}_H = .055$
 Turbojet

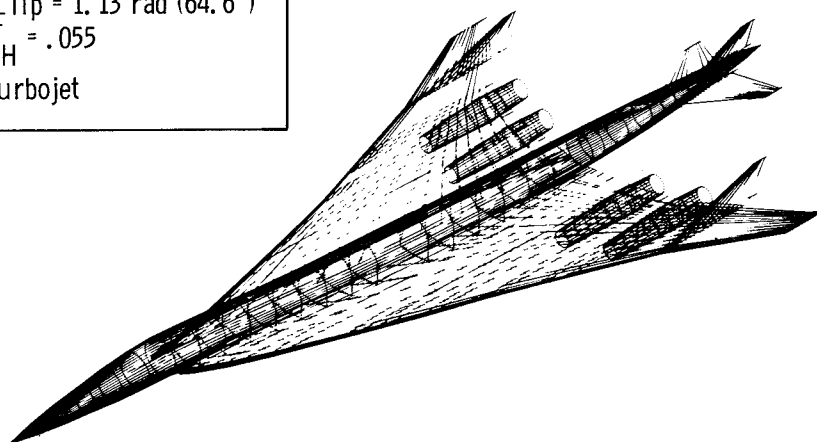


Figure 1.- Reference configuration.

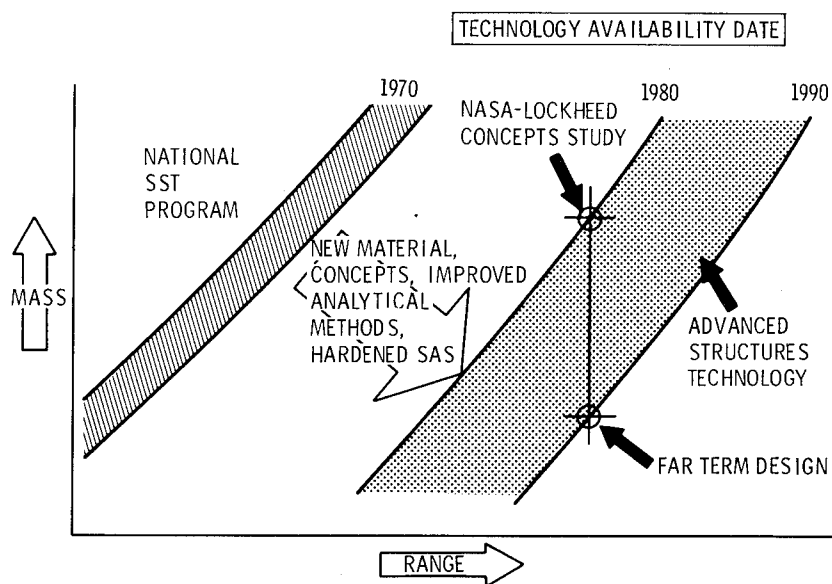


Figure 2.- Advanced technology trends.

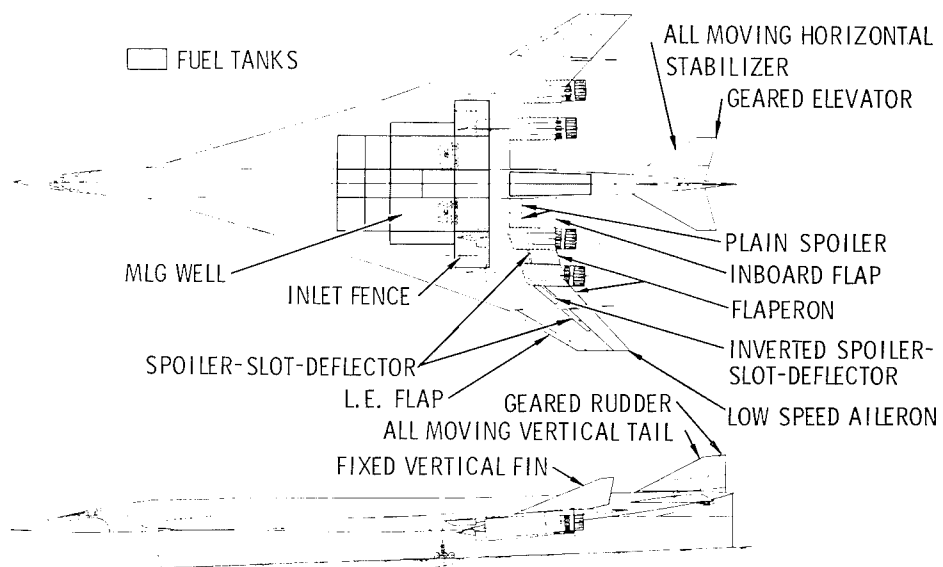
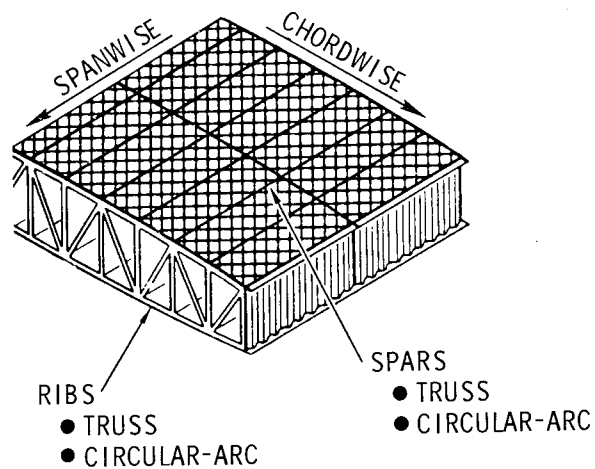


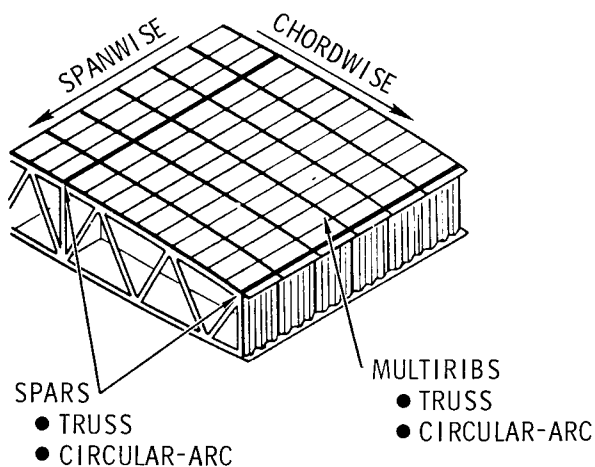
Figure 3.- Final arrangement.



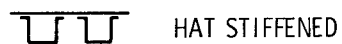
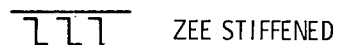
PANEL STRUCTURAL CONCEPTS



(a) Monocoque (biaxially stiffened).

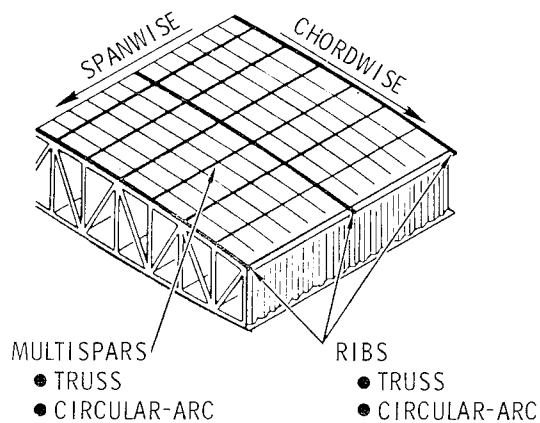


PANEL STRUCTURAL CONCEPTS



(b) Spanwise stiffened.

Figure 4.- Wing structural arrangement.



PANEL STRUCTURAL CONCEPTS



CIRCULAR-ARC
CONCAVE BEADED SKIN



CIRCULAR-ARC
CONVEX BEADED SKIN

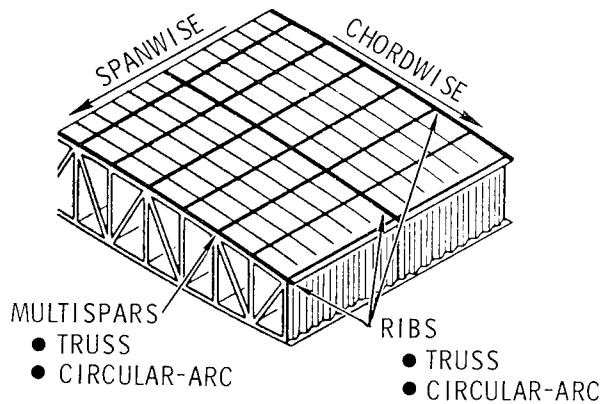


TRAPEZOIDAL CORRUGATION
CONCAVE BEADED SKIN



BEADED CORRUGATION
CONCAVE BEADED SKIN

(c) Chordwise stiffened.



STRUCTURAL CONCEPTS



REINFORCED PANEL



REINFORCED CAPS

(d) Chordwise stiffened composite reinforced concepts.

Figure 4.- Concluded.

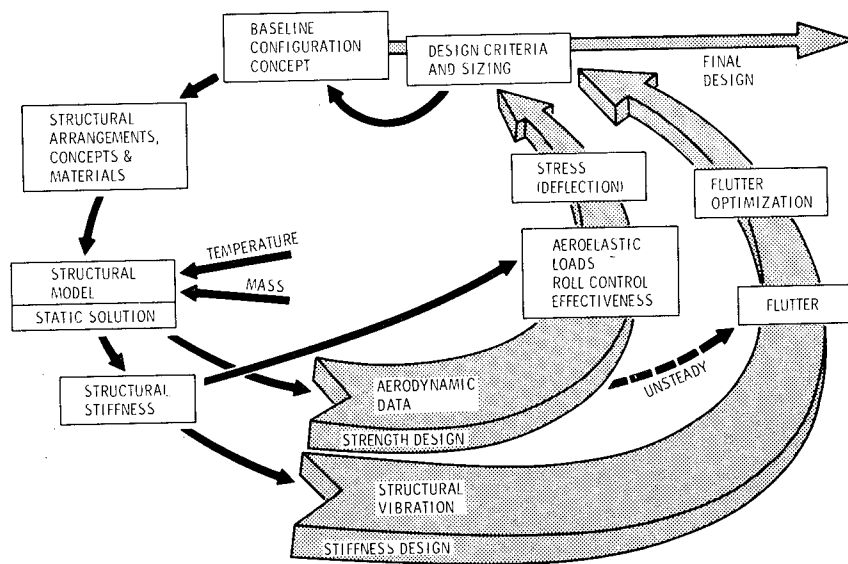


Figure 5.- Analytical design cycle.

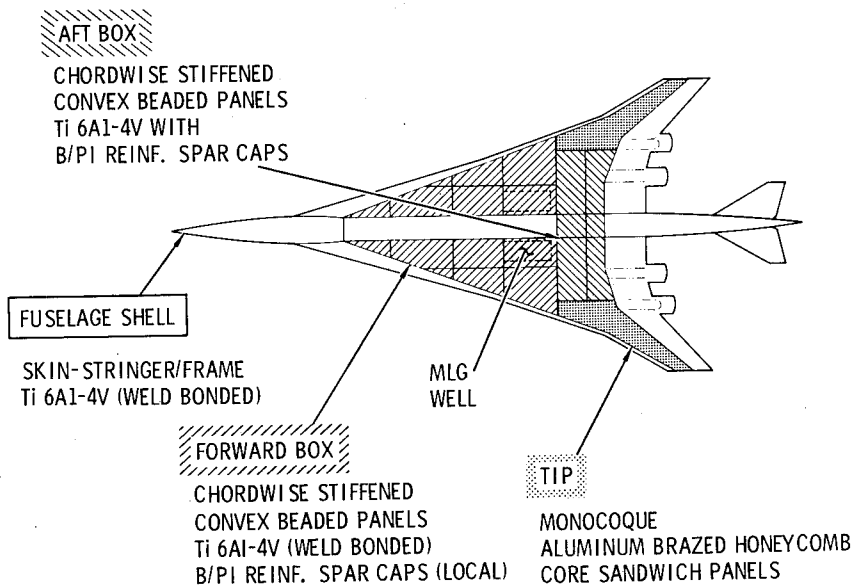


Figure 6.- Hybrid structural concept for near-term design.

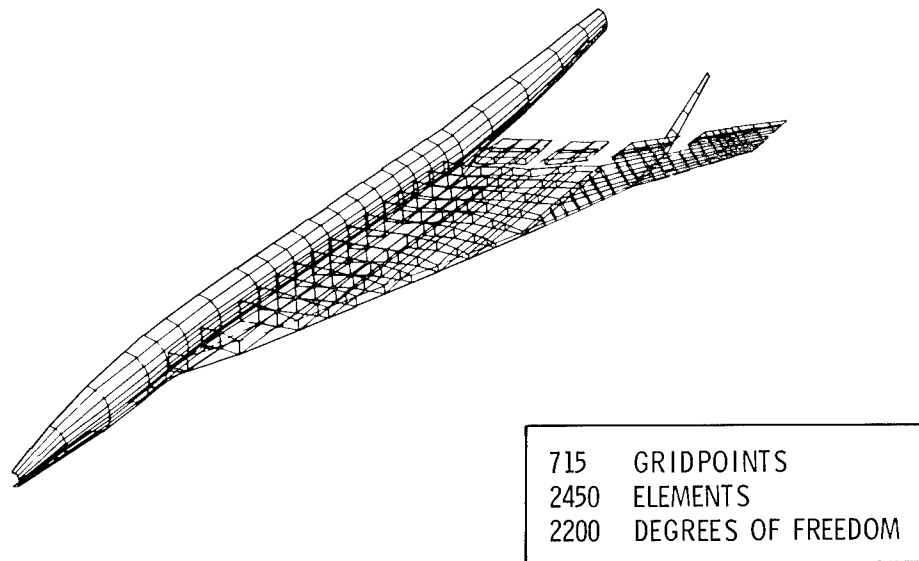


Figure 7.- Finite-element structural model.

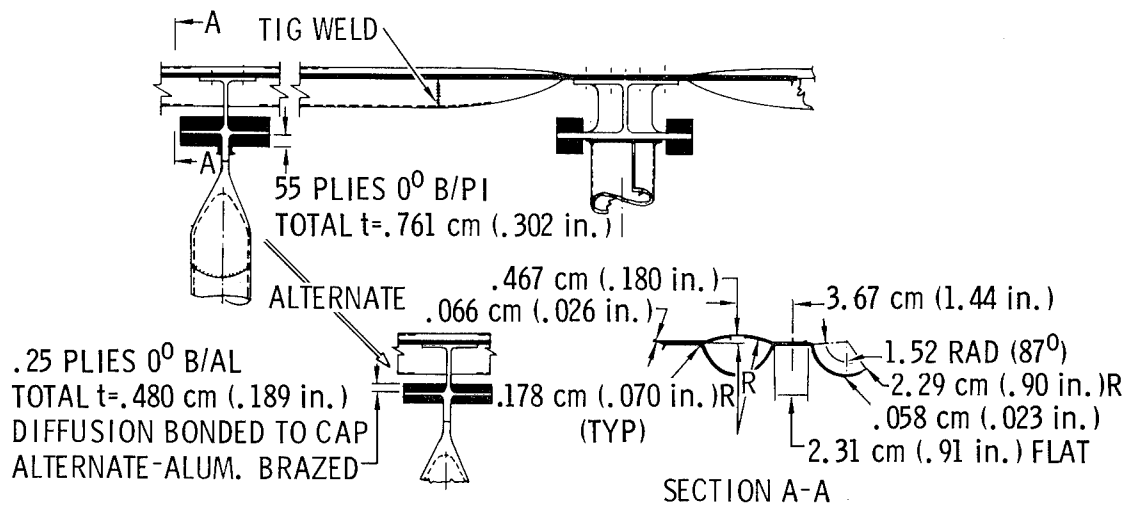


Figure 8.- Structural details for hybrid structural concepts.

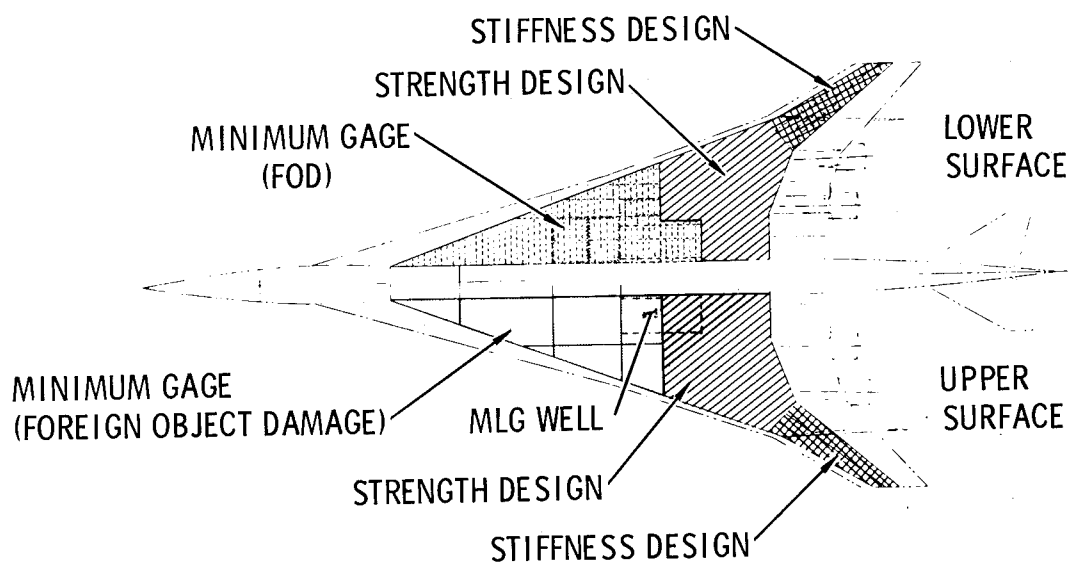


Figure 9.- Critical design requirements for wing.

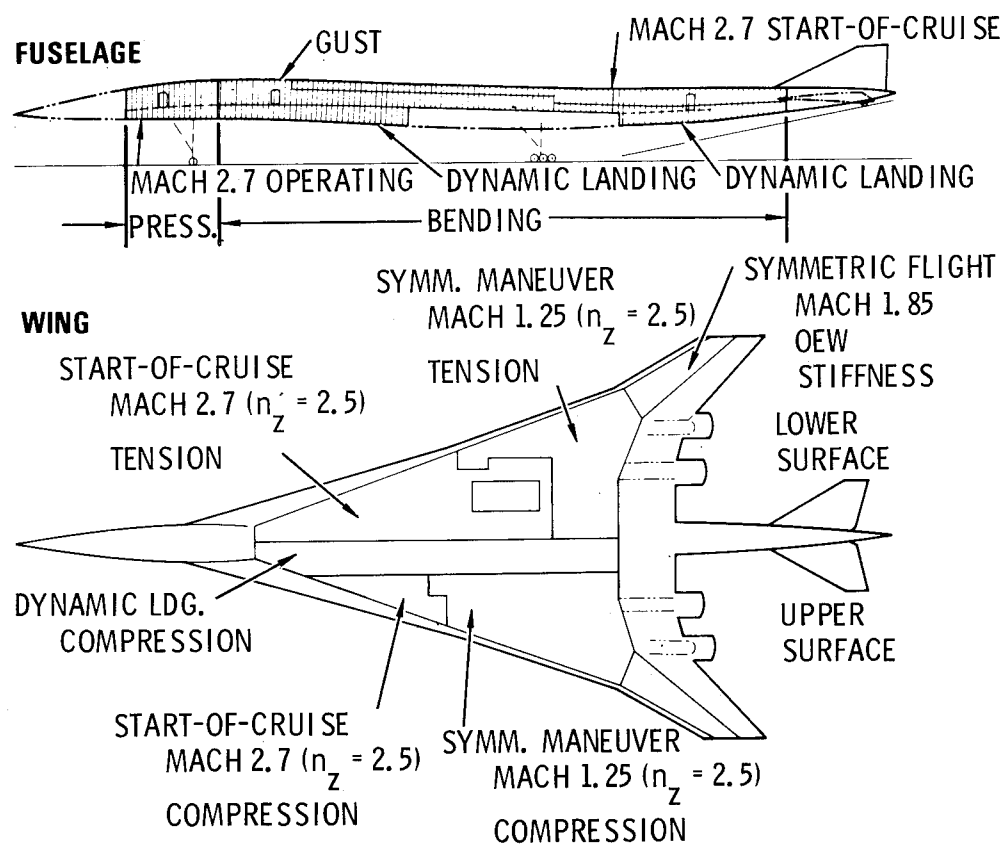


Figure 10.- Critical design conditions.

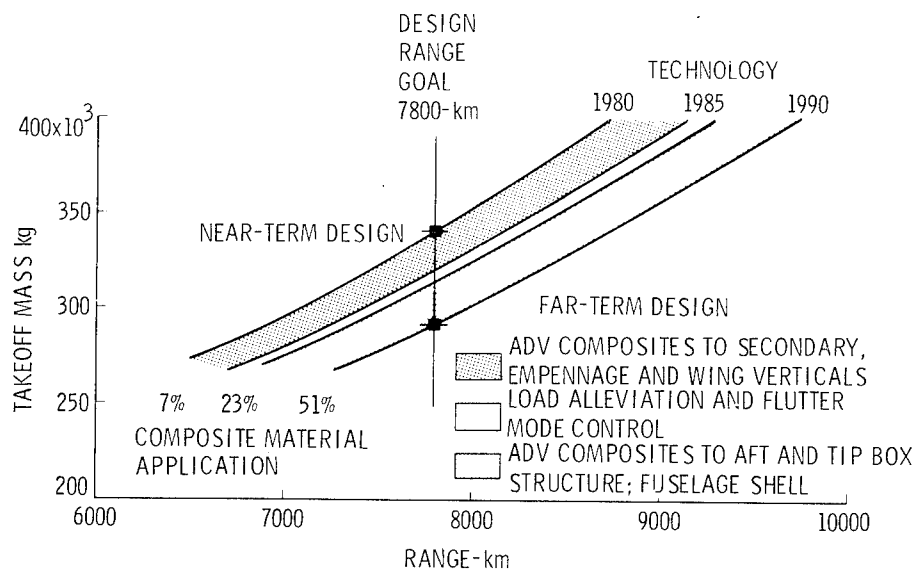


Figure 11.- Advanced structures technology trends.

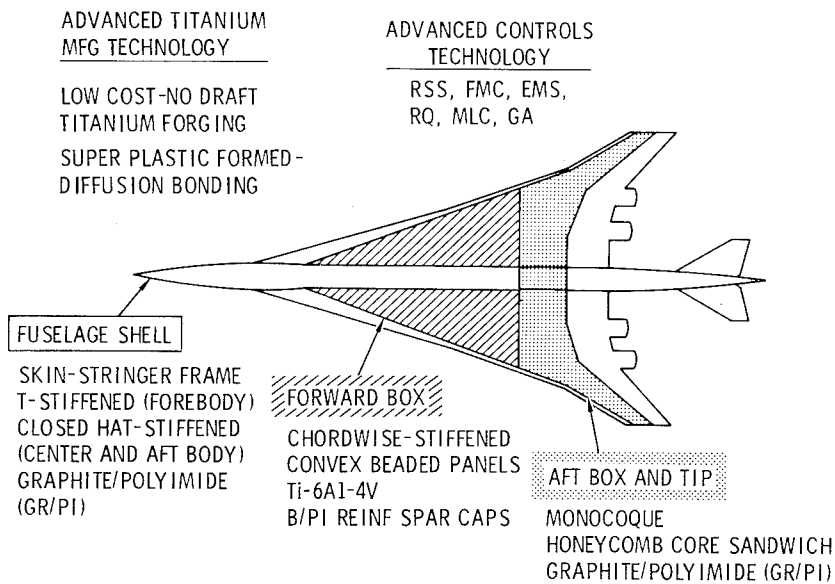


Figure 12.- Advanced hybrid structural approach - far term (1990 start of design).

COMPUTER-AIDED METHODS FOR ANALYSIS AND SYNTHESIS OF SUPERSONIC CRUISE AIRCRAFT STRUCTURES

Gary L. Giles

NASA Langley Research Center

SUMMARY

The design and analysis of proposed supersonic cruise aircraft structures has required extensive use and new development of computer-aided methods. This paper reviews such computer-aided methods which have been and are being developed by Langley Research Center in-house work and by related grants and contracts. Synthesis methods to size structural members to meet strength and stiffness (flutter) requirements have been emphasized in this work and are described. Because of the strong interaction among the aerodynamic loads, structural stiffness, and member sizes of supersonic cruise aircraft structures, these methods have been combined into systems of computer programs to perform design studies. The approaches used in organizing these systems to provide efficiency, flexibility of use in an iterative process, and ease of system modification are discussed.

INTRODUCTION

Supersonic cruise aircraft tend to be large and flexible, and realistic determination of their aeroelastic behavior requires finite-element structural analysis and sophisticated steady and unsteady aerodynamic loading analysis. Such analysis methods have been developed and are available in the form of computer programs and systems for use in supersonic cruise aircraft research; see, for example, references 1 - 4. The capability to size structural members to have low structural mass and retain adequate strength and stiffness to meet all the design requirements is also important. Computer-aided methods for structural synthesis are receiving considerable attention, but are not yet developed to the same level of completeness and sophistication as computer-aided structural analysis methods.

The purpose of the present paper is to review computer-aided methods for structural analysis and synthesis which are being developed by Langley Research Center in-house efforts and by related grants and contracts. Methods for sizing structures to meet both strength and stiffness (flutter) requirements have been emphasized in this work and are described. Because of the strong interaction among the aerodynamic loads, structural stiffness, and member sizes of supersonic cruise aircraft structures, these methods have been combined

into systems of computer programs to perform design studies. These programs include static and dynamic structural analyses, steady and unsteady aerodynamics, static aeroelastic and flutter analyses, and methods for sizing structural members.

The finite-element structural analysis program is the central focus in developing such a system. The "SPAR" computer program is currently being used for this purpose at Langley, and its capabilities and features are presented. The theoretical basis for SPAR is given in reference 5.

Both optimality criteria and mathematical programming procedures have been used to size structures to meet strength requirements. These procedures involve iterative processes, and the analysis and design methods have been tailored for efficient use in such processes. A methodology is described which includes these procedures and which results in simultaneous calculation of aircraft design loads and structural member sizes. Efficient analysis and reanalysis methods and approximation techniques are used with mathematical programming procedures to provide capability to size large-scale structural models to meet flutter requirements. The initial implementation of these methods in a pilot computer program and subsequent incorporation into SPAR is discussed.

The method of organization of these various computer programs into systems necessary for structural studies in supersonic cruise aircraft research is an important consideration in terms of time and cost required for development and ease and flexibility of use of the software product. Several approaches were used in organizing the systems described herein and their relative merits are discussed.

STRUCTURAL ANALYSIS

The emphasis in this paper is on structural synthesis or sizing. However, a fundamental part of a structural synthesis system is the program used for structural analysis. The SPAR program is currently being used for this purpose at Langley, and its technical capabilities and features which facilitate its incorporation into a synthesis system are presented in this section. The actual use of SPAR in structural synthesis systems is discussed in subsequent sections.

SPAR Technical Capabilities

SPAR is a system of computer programs capable of computing static deflections and stresses, natural vibration frequencies and modes, and buckling loads and mode shapes of linear finite-element simulations. The system is composed of a group of individual software "processors" which are used in a logical sequence to perform a desired analysis. Each processor is designed to perform a limited, yet distinct and complete, function. Therefore, a very high degree of modularity and user flexibility is provided by this system. These processors are able to communicate directly and automatically with a

data base complex which contains the information generated by or used by other processors during a computer run. A schematic of the organization of the SPAR system is shown in figure 1.

The technical processors are operational on UNIVAC-1100 and CDC 6000/CYBER series computers. On UNIVAC systems, the processors are separate, absolute programs which are executed sequentially. On CDC systems, all the processors are designated as primary overlays in a single, absolute program which has a zero level overlay to call the processors for execution. This zero level overlay is configured to simulate UNIVAC operation; that is, the required input stream or file is identical to that used on UNIVAC systems. This input file, shown on the left-hand side of figure 1, is designed to provide for effective interactive operation. In interactive operation, the @XQT statements which calls a selected processor for execution and the related input data for that processor are typed in sequentially at a user console keyboard after successive prompts from the operating system. The computational sequence is continued by using another @XQT statement to call the next desired processor.

The SPAR program is organized into two functional processor groups: technical processors and utility processors. The functions of each of the SPAR processors are given in table 1. (Table 1 applies explicitly to a recent version of SPAR, denoted level 10.) The technical processors can be used in any logical sequence to perform a desired analysis such as static stress, vibration analysis, etc. A general characteristic of the technical processors is that they are very efficient with respect to both core storage and central processing time requirements. The method for handling the large, sparse matrices encountered in finite-element structural analysis in a manner to achieve this efficiency is described in reference 5. All of the technical processors make extensive use of auxiliary disk storage and operate with computer memory which is automatically allocated so that large structural simulations can be analyzed. The method used for eigenvalue and eigenvector calculations (ref. 6) makes it possible to perform a vibration analysis without first reducing the number of degrees of freedom being considered. This capability is useful in structural synthesis since a single simulation can be used for both static and dynamic calculations. Finite elements which are currently available in SPAR include axial bars, beams of general cross section, triangular and quadrilateral plates having an option to specify coupled or uncoupled membrane and bending stiffness, and quadrilateral shear panels. The provision for warping of the quadrilateral plates and an option to specify plate properties as layers in a laminate of composite materials are recent additions.

Three types of utility processors are available in SPAR; (1) the data complex utility, DCU, which is used to input, output, and manage data sets on the data complex, (2) the arithmetic utility system, AUS, which provides general matrix arithmetic capability and data set construction, and (3) on-line or off-line plotting. All of these utilities provide the user with an interface to the data complex. The contents and features of this data complex is discussed in the following section.

SPAR Data Complex

The organization of the data complex provides ready access to the data which is produced by the various processors during an analysis run. This ready access of data is an important feature since it greatly facilitates the use of SPAR in a structural synthesis system. The data complex is composed of a group of up to 20 libraries, as shown at the bottom of figure 1. Data needed to communicate among the processors during an analysis run are stored on these libraries. User input to each processor specifies the library from which the processor will retrieve needed data and the library on which the processor will store the data it generates. For many analysis runs, only a single library is used. These libraries are direct access files which contain both the data and a directory to the data. Hence, they are separate, self-contained files which can be saved without alteration on disk storage at the end of an analysis run and used in subsequent runs. These files are recognized by the computer operating system as having names of SPARLA . . . SPARLT, as indicated on figure 1.

Each library contains data sets which are produced by the SPAR processors. Each data set has a four-word identifying name. For example, the set of static displacements for load case 10 and boundary condition set 1 would be named STAT DISP 10 1. Through such names, the SPAR processors are able to locate and access automatically all of the information needed to perform a particular analysis. A directory, or table of contents, is stored on each of the libraries in order to determine the size characteristics and location on disk of a data set with a specified name. An example of such a table of contents is shown in table 2.

Each line in the table denotes a data set and gives the sequence it was written on the file, the location on disk, date and time of creation, error code, size and data type information, along with the name used to reference the data set. The data complex utility provides the capability to print these tables of contents, as well as individual data sets. A COPY command is provided to transfer specified data sets between libraries. This capability is very useful in saving selected information between runs. The XCOPY and the XLOAD command are used to copy data sets from the direct access libraries to sequential files and vice versa. These sequential files can then be used to interface other programs to the SPAR system. The arithmetic utility system provides for input of user defined data sets into the library, as well as general matrix arithmetic operation on the data sets.

The flexibility of use of the technical processors and the ability to access and manage data readily in the SPAR system were very useful in developing structural synthesis or sizing systems. The next section of this paper describes two structural synthesis systems which use SPAR.

STRUCTURAL SYNTHESIS

Structural synthesis is the sizing (determination of areas or thickness) of members in a structure to satisfy a prescribed objective, for example

minimum mass. Design constraints such as allowable material strength and flutter boundaries, which also must be satisfied by the structure, are imposed during this process. In this section, methods are described for the synthesis of structures to meet static strength requirements and flutter requirements.

These methods were developed to perform studies of different structural concepts in a supersonic cruise aircraft research project. During these studies, the structural members are sized to meet strength requirements and subsequently analyzed for flutter and stiffened, if necessary. The finite-element representation used in these studies is shown in figure 2 to characterize the level of complexity for which the methods were intended. A half model composed of one side of the simulation is used in the structural analysis with proper boundary conditions at the centerline to represent symmetric behavior of the complete vehicle. The half model contains 746 grid points with a total of 2138 unrestrained degrees of freedom and 2369 elements. Attention is focused on the design of the wing box structure which is modeled in greater detail than the remainder of the structure. During structural sizing, only thicknesses of members in the wing structural box (384 wing rib and spar shear webs and 334 wing cover panels) are calculated. Sizes of all other structural members are fixed at predetermined values to represent correct overall stiffnesses for the remainder of the aircraft. The mass of payload, fuel, and other items making up the total mass of the vehicle are distributed over the model by the analyst to provide both the correct inertia relief loads during maneuver and the correct mass distribution for calculating free-free vibration characteristics for use in flutter analysis procedures. Numerical results from design studies using this model are contained in reference 7. Herein, a description of the methods is presented.

Synthesis for Static Strength Requirements

Computation in strength sizing.— Supersonic cruise aircraft tend to have thin, large area wings and are, therefore, very flexible. Strength sizing of such structures poses complex computational problems since the element sizes depend on the stresses caused by the aerodynamic loads that are governed by the structural deformations which, in turn, depend on the element sizes. The problem is further complicated by the necessity to consider inertia dependent loads such as those generated while rolling on a rough runway (taxi loads) and proper consideration of the jig shape (the prescribed aircraft shape at construction which will deform to the desired aerodynamic shape at the cruise condition). The interaction of these physical quantities are indicated in figure 3. A computer-aided synthesis system to size a structure for strength inherently has the same interactions among the computer programs used to calculate these physical quantities.

The two principal computational tasks that must be performed during the strength sizing process are (1) the calculation of aeroelastic loads, and (2) sizing of the structural members. These two tasks are illustrated schematically in figure 4. The conventional procedure is first to calculate aeroelastic loads based on initial member sizes and then use these loads to

calculate new member sizes in a separate, sequential operation. Following the calculation of new member sizes, the whole procedure should be repeated because changes in member sizes alter the structural flexibility which impacts the aeroelastic loads. This iteration should continue until the changes in overall structural flexibility become sufficiently small to have a negligible effect on the aerodynamic loads. In conventional preliminary design practice, this iterative process is seldom fully converged because of the time and cost required. The interaction effect can be small if good initial member sizes from a previous, similar design are used in the load calculations. However, to reduce flow time for input preparation during preliminary design, it may be necessary to use crude estimates of the initial member sizes. In this case, large changes in structural flexibility could occur during structural sizing, and significant changes in the design loads could result.

Sizing of Aerospace Vehicle Structures (SAVES).- A system called SAVES has evolved from a continuing effort at the NASA Langley Research Center to develop structural synthesis methods to satisfy strength requirements. An initial version of this system used the conventional, sequential process of calculating design loads and structural member sizes (ref. 8). The SAVES system has been restructured into a parallel organization as shown in figure 5 so that the aerodynamic loads and structural member sizes are both updated at the same time. Simultaneous convergence of compatible design loads and structural member sizes is shown in reference 9 to be achieved with a substantial reduction in computer CPU time from the conventional procedure.

Initially, in this process, the jig shape and maneuver deflected shape are assumed to be the same as the rigid cruise shape, and initial member sizes are specified to be constant over large areas of the structure. The process then proceeds in two simultaneous iterative loops as shown in figure 5. Loop (I), shown by double-line arrows, performs the maneuver aeroelastic load calculation, and loop (II), double dashed-line arrows, iteratively sizes the structural elements. Loop (II) uses the element sizes to generate a structural stiffness matrix in SPAR. Cruise, maneuver, and taxi loads are applied to this stiffness matrix and deflections and stresses are generated. The stresses are used in loop (II) by a resizing algorithm to calculate new element sizes. In loop (I), the deflections from the rigid cruise shape due to cruise loads are used to calculate the jig shape, and the deflections due to maneuver loads are then added to the jig shape to get the maneuver shape. The aerodynamic influence coefficient matrix for the maneuver condition is saved so that updated loads are calculated through multiplication of this matrix by the panel slopes obtained from the maneuver deflections.

There are ten computer programs currently in the SAVES system. The first is a preprocessor for generating finite-element structural models of the type shown in figure 2. A linear aerodynamic lifting surface program (ref. 2), the SPAR structural analysis program, and a structural sizing program are the primary programs used in the simultaneous calculation of design loads and member sizes. The sizing program uses either a weight-strength method or a mathematical nonlinear programming method to size individual structural elements, such as wing cover sandwich panels, while a fully stressed design

is being carried out for the overall structure. Six other programs perform auxiliary functions required in the process such as calculating aerodynamic panel slopes, updating the aerodynamic pressure distributions, trimming the aircraft in flight, computing the jig shape, processing the SPAR stress output, and preparing input data for the resizing program. Graphics programs are used to generate displays of design data. The SPAR structural analysis program is also used to calculate vibration mode shapes and frequencies for use in subsequent flutter analyses.

The SAVES system is tailored to perform the entire strength sizing process with computational efficiency in a single computer run. Using this system, it is feasible to obtain structural design results with converged, compatible loads and member sizes based on sound analytical methods within the cost and time constraints of preliminary design.

Synthesis for Flutter Requirements

Structural synthesis methods to meet flutter requirements are important in supersonic cruise aircraft research as indicated in references 10 and 11. The usual design process for aircraft wing structures consists of performing a structural synthesis to meet strength requirements and, if required, determining the additional stiffness or mass distribution to prevent flutter using the analyst's judgment in a trial-and-error procedure. In the past few years, there has been considerable work done to develop automated structural synthesis methods to satisfy flutter requirements. A comprehensive review of this work is contained in reference 12. In the present paper, work that was performed in this area under a NASA grant (see refs. 13 to 17) will be reviewed. Initially, a pilot program (WIDOWAC) was used to develop, improve, and test methods that were needed. Currently, these methods are being combined with the SPAR program to provide the capacity to handle more complex structural models.

Wing Design Optimization With Aeroelastic Constraints (WIDOWAC).— The WIDOWAC program can be used for the synthesis of minimum mass wing structures which are modeled using finite-elements to represent the rib and spar webs and cover panels as shown in figure 6. A technique for using approximate second derivatives in conjunction with the Newton's method was developed for the optimization procedure. This mathematical programming procedure has the generality to allow any number of constraints to be imposed during the design process. Currently, multiple flutter (subsonic and supersonic) stress, strain, deflection, buckling, and minimum gage constraints can be included. Flutter modes, which exhibit a "hump" characteristic and often cause a discontinuity in flutter speed as the design variables are changed, are considered automatically in the program.

Computation times are reduced during this process by several techniques. The number of degrees of the structural model are reduced by specifying that the wing have a symmetric cross section and modeling only either the upper or lower half of the structure. The finite-element structural analysis program,

which was developed for efficient use in this synthesis system, contains procedures needed for iterative analysis methods to reduce significantly reanalysis times compared with the original analysis of the structure.

The number of design variables is kept small by linking the sizes of several structural elements under the control of a single design variable. Thus, the design variables do not describe the thickness of individual finite-elements, but of segments of the wing, each segment containing several finite-elements as illustrated in figure 6.

The wing planform is divided into a number of triangular or quadrilateral segments. The design variables are the thickness of the cover panels at the vertices of the segments. The cover panel thickness is assumed to vary linearly in the triangular segments. A quadrilateral segment is divided into two triangles, each having a linear thickness variation. Thicknesses of elements representing rib and spar shear webs can also be lumped under single design variables.

Composite materials can be represented in the cover panels by stacking together orthotropic plates with stiffness properties equivalent to a fixed fiber orientation to construct the desired laminates. In this case, the design variables are the thicknesses of each of the laminae making up the laminate.

WIDOWAC has been used as a test bed for evaluating optimization methods, constraint formulations, and analysis algorithms suitable for structural synthesis for flutter. Improvements in efficiency of these synthesis procedures and continuing decrease in computer costs have created an atmosphere where these methods can potentially be used on complex structural models which are encountered in supersonic cruise aircraft research. In the next subsection, a description is given of work being done to study complex models by coupling the large-scale, general-purpose, finite-element and data management capabilities of SPAR with the structural synthesis capabilities of WIDOWAC.

Program for Analysis and Resizing of Structures (PARS).- PARS is being developed by converting the flutter analysis and optimization capabilities in WIDOWAC into new SPAR technical processors. This approach will result in a system having the same advantages of SPAR such as modularity, flexibility of use, etc., which were discussed previously. To date, the first six processors have been developed and are being tested (see fig. 7). The functions of these processors are:

1. AERO - Defines the required aerodynamic input and the interface between the structural and aerodynamic grids.
2. SUBKRN - Calculates aerodynamic matrices which are based on subsonic kernel function aerodynamics and are independent of vibration modes.
3. GAF - Calculates generalized aerodynamic forces corresponding to the vibration modes.

4. DKM - Defines the design variables for use in optimization and calculates the derivatives of the generalized stiffness and mass matrices with respect to these design variables.

5. OPT - Performs a flutter analysis of a specified structure or performs a structural optimization to achieve a minimum mass design that satisfies the flutter constraints.

6. DGRA - Calculates the derivatives of displacement vectors with respect to the design variables.

The first five processors provide a flutter analysis capability for subsonic Mach numbers. A V-g flutter analysis can be performed at a given altitude or the altitude can be determined at which the flutter velocity and specified Mach number are compatible, or matched, in a given atmosphere. The flutter synthesis option currently in PARS uses the same set of vibration modes all through the resizing process. This requirement limits the application to moderate differences between the initial design and final optimized design. The limitation will be removed by adding capability to make it convenient to return to SPAR to calculate updated vibration modes after significant changes in the structure have occurred and then repeat the optimization in PARS. The last processor, DGRA, calculates the sensitivity of static displacements and stresses to changes in design variables. These quantities are needed to add displacement and stress constraints to the optimization procedure.

The CDC version of PARS is organized in a separate program using the same input/output and data management routines as SPAR and communicating to a common data library as shown in figure 7. This arrangement is desirable during program development because as programing changes are made in the PARS processors, the entire SPAR system need not be reloaded in the computer. The modularity of the system has expedited the development and testing of PARS and forms the basis for continued developments in structural synthesis.

ORGANIZATION OF STRUCTURAL SYNTHESIS SYSTEMS

Structural synthesis systems are characteristically quite large because of the number of programs and procedures necessary to represent all the disciplines which interact in the sizing process. Thus, the organization of these large systems is an important consideration. Two types of organization represented by SAVES and PARS have been used for the synthesis systems presented herein, with the principal difference being the method used to transfer data among programs and processors. Both of these systems are implemented on the CDC Network Operating System, NOS, and PARS is also implemented on UNIVAC EXEC 8. SAVES makes extensive use of operating system capabilities such as the permanent file system, procedure files, and utilities to change data files which are in the form of card images.

The organization of the SAVES system is indicated on figure 8 which depicts a portion of the total system. The bottom level of the system is a

collection of permanent and temporary sequential data files. Primary or basic input data, including finite-element structural model, aerodynamic paneling data, and load case information, for the system are stored on permanent disk files in the form of card images which are copied to local files during program execution. Data which are generated by one program and used by another such as deflections, stresses, and aerodynamic pressures are handled as temporary local files during a run. These temporary files can be saved and used for restart purposes in a later run.

The next level of the system consists of decks containing file manipulation instructions which alter and combine files to form input files for the analysis programs. Some of the analytical programs used for calculating aeroelastic loads in SAVES are shown on the next level. In this organization, the SPAR program must interact with other separate programs and data which are not part of the data library. An example of the data flow which occurs in the series of programs shown in figure 8 will be given to illustrate the method of interfacing the data.

The process is initiated using the cruise shape geometry in the program AEROIN to calculate angles of attack of the aerodynamic panels for use in the subsequent program PRESS which calculates the corresponding pressure distribution. The aerodynamic influence coefficients which are generated in PRESS are saved for subsequent calculations. Equilibrated loads for the aircraft in flight are calculated in TRIM based on these pressure distributions. These loads are output in the proper form of input card images for the SPAR program, and "modify instruction" decks are used to merge these data into the finite-element model data. SPAR is then executed to calculate deflections which are stored on the SPAR data library. The SPAR utility, XCOPY, is then used to transfer these deflections to a named sequential file which can be then used by JIG to calculate the jig shape and by AEROIN to calculate a new maneuver shape. The process is then repeated with the data files containing the deflections, jig shape, and maneuver loads being updated during each iteration.

These programs are executed in a prescribed manner by procedure files, which are sequences of executable control cards, as indicated by LLOOP and XQINIT in figure 8. A job control deck, which is the highest level procedure file, is used to control the overall process. Other procedure files indicated by the dotted lines and boxes control other portions of SAVES such as structural sizing, vibration analysis, and subsequent flutter analysis.

A system with the same organization as SAVES can be developed quickly and inexpensively on the basis of standard operating system features as indicated in reference 18. However, as the capabilities of a structural synthesis system are increased, the number of program and data files could become quite large and, hence, difficult to manage and document.

The organization of the PARS system, on the other hand, uses directly the data file management capabilities of the SPAR program as was indicated on figure 7. This bookkeeping system provides a standard form for storing or retrieving data sets by name using direct access files. A limited number of subroutines (user is primarily concerned with two) are used to read or write a

data set identified by a four-word name from or into a data library. The size (number of words), along with other descriptive information for the data sets, are contained in tables of contents embedded in the data libraries. Documentation involves only specifying the physical meaning of the contents of each data set and specifying which of these data sets are input to or output from each of the processors.

The capability for performing loops within a single input deck is currently not available in SPAR or PARS. Procedure files such as used in SAVES can be used to accomplish this needed function with the common data libraries being retained between multiple executions of SPAR or PARS. This organization provides a flexible framework on which to add improved or extended structural synthesis methods.

FUTURE DEVELOPMENTS

On-going and planned improvements to the structural synthesis systems include continued work on incorporating methods to size structural components made of composite materials. This work will augment development of methods for synthesis of structures to meet overall stiffness constraints, as well as strength constraints. Testing of the flutter synthesis methods on large, complex structural models will be continued along with development of any needed improvements in these methods that may become apparent in a large problem environment.

Improved calculation of the required aerodynamic quantities for these synthesis systems will be obtained by incorporating the capabilities of the SOUSSA (Steady, Oscillatory, Unsteady Subsonic and Supersonic Aerodynamics) program of reference 19. This program will augment or replace the steady lifting surface aerodynamics and unsteady subsonic kernel function aerodynamics currently being used. SOUSSA will provide the capability to handle complex three-dimensional configurations with a single, common aerodynamic paneling arrangement for both subsonic and supersonic flight regimes. Some alterations of the program will probably be required for efficient operation in an iterative structural synthesis environment. This improved aerodynamic capability will then be organized and implemented in the form of processors for use in the PARS system to take advantage of the SPAR data handling and utility functions.

The capability to assess the effects of including active control systems is becoming an important consideration in the development of structural analysis and synthesis systems. This capability will be initially introduced into the PARS system by including the effect of active controls in the flutter analysis. Additional processors associated with formulating the flutter analysis in the proper form will be required for this work.

As new procedures and new processors are developed for SAVES, SPAR, and PARS, they will provide a basic framework and flexibility of use to test and develop other structural synthesis methods and strategies. Therefore, the

consideration of modularity, efficiency, and ease of use and modifications must be planned and incorporated into the system so new development can concentrate on what is new technically and not have to rebuild or restructure existing programs or processors.

CONCLUDING REMARKS

Computer-aided design methods have been developed by incorporating sound theoretical procedures from a variety of disciplines into systems which have the capacity to handle the detailed simulations required for the analysis and synthesis of supersonic cruise aircraft structures. Finite-element structural analysis methods are available to analyze the linear behavior of a given structure efficiently and in great detail. Structural synthesis methods for sizing structures to meet strength requirements have been developed based on a fully stressed criterion. Compatible member sizes and aircraft design loads can be calculated using a simultaneous iteration procedure during this structural sizing process. Synthesis methods to size the members of large-scale structural simulations to meet flutter requirements have been developed by incorporating efficient analysis and reanalysis methods, approximation techniques, and design variable linking with mathematical programming procedures. The development of these systems has improved the design process by allowing more interacting disciplines to be considered in greater depth and with a decrease in overall flow time.

Flexibility, efficiency, and ease of modification of these systems are important for use in advanced design applications such as supersonic cruise aircraft research because new demands are continually being made on these systems. These requirements have brought into focus the desirability of modular systems which make effective use of capabilities available on time-share operating systems. Needed technical capabilities are being developed for incorporation into these design systems. These capabilities include improved structural resizing methods (especially for stiffness considerations) and improved aerodynamics, as well as capability to consider composite materials and active controls in the structural design.

REFERENCES

1. Butler, Thomas G.; and Michel, Douglas: A Summary of the Functions and Capabilities of the NASA Structural Analysis Computer System. NASA SP-260, 1971.
2. Carmichael, Ralph L.; and Woodward, Frank A.: An Integrated Approach to the Analysis and Design of Wings and Wing-Body Combinations in Supersonic Flow. NASA TN D-3685, 1966.
2. Watkins, Charles E.; Woolston, Donald S.; and Cunningham, Herbert J.: A Systematic Kernel Function Procedure for Determining Aerodynamic Forces on Oscillating or Steady Finite Wings at Supersonic Speeds. NASA TR R-48, 1959.
4. Donato, V. W.; and Huhn, C. R., Jr.: Supersonic Unsteady Aerodynamics for Wings With Trailing Edge Control Surfaces and Folded Tips. AFFDL TR-68-30, U.S. Air Force, August 1968.
5. Whetstone, W. D.: Computer Analysis of Large Linear Frames. Journal of the Structural Division, ASCE, November 1969, pp. 2401-2417.
6. Whetstone, W. D.: Vibrational Characteristics of Linear Space Frames. Journal of the Structural Division, ASCE, October 1969, pp. 2077-2091.
7. Sobieszczanski, J.: Structural Design Studies of a Supersonic Cruise Arrow-Wing Configuration. Supersonic Cruise Aircraft Research (SCAR) Conference, Hampton, Virginia, November 9-12, 1976.
8. Giles, G. L.; Blackburn, C. L.; and Dixon, S. C.: Automated Procedures for Sizing Aerospace Vehicle Structures (SAVES). Journal of Aircraft, Vol. 9, No. 12, December 1972, pp. 812-819.
9. Giles, G. L.; and McCullers, L. A.: Simultaneous Calculation of Aircraft Design Loads and Structural Member Sizes. AIAA Paper No. 75-965, August 1975.
10. Sakata, I. F.; Davis, G. W.; Robinson, J. C.; and Yates, E. C., Jr.: Design Study of Structural Concepts for an Arrow-Wing Configuration Supersonic Cruise Aircraft. AIAA Paper No. 75-1037, August 1975.
11. Robinson, J. C.; Yates, E. C., Jr.; Turner, J. M.; and Grande, D. L.: Application of an Advanced Computerized Structural Design System to an Arrow-Wing Supersonic Cruise Aircraft. AIAA Paper No. 75-1038, August 1975.
12. Stroud, W. J.: Automated Structural Design With Aeroelastic Constraints: A Review and Assessment of the State of the Art. In AMD, Vol. 7, published by ASME, 1974.

13. Haftka, Raphael T.: Automated Procedure for Design of Wing Structures to Satisfy Strength and Flutter Requirements. NASA TN D-7264, 1973.
14. Haftka, R. T.; and Starnes, J. H., Jr.: WIDOWAC (Wing Design Optimization With Aeroelastic Constraints): Program Manual. NASA TM X-3071, October 1974.
15. Haftka, R. T.: Parametric Constraints With Application to Optimization for Flutter Using a Continuous Flutter Constraint. AIAA Journal, Vol. 13, No. 4, April 1975, pp. 471-475.
16. Haftka, R. T.; and Starnes, J. H., Jr.: Applications of a Quadratic Extended Interior Penalty Function for Structural Optimization. AIAA Paper No. 75-764, May 1975.
17. Haftka, R. T.; and Yates, E. C., Jr.: On Repetitive Flutter Calculations in Structural Design. AIAA Paper No. 74-141, January 1974.
18. Sobieszczanski, J.: Building a Computer-Aided Design Capability Using a Standard Time Share Operating System. Presented at the ASME Winter Annual Meeting, Houston, Texas, December 1975, and published in the ASME special publication "Integrated Design and Analysis of Aerospace Structures."
19. Yates, E. C., Jr.; and Bland, S. R.: Developments in Steady and Unsteady Aerodynamics for Aeroelastic Analysis and Design. Supersonic Cruise Aircraft Research (SCAR) Conference, Hampton, Virginia, November 9-12, 1976.

TABLE 1.- SPAR PROCESSORS

<u>Name</u>	<u>Function</u>
TAB	Creates data sets containing tables of joint locations, section properties, material constants, etc.
ELD	Defines the finite elements making up the model.
E	Generates sets of information for each element including connected joint numbers, geometrical data, material and section property data.
EKS	Adds the stiffness and stress matrices for each element to the set of information produced by the E processor.
TOPO	Analyzes element interconnection topology and creates data sets used to assemble and factor the system mass and stiffness matrices.
K	Assembles the unconstrained system stiffness matrix in a sparse format.
M	Assembles the unconstrained system mass matrix in sparse format.
KG	Assembles the unconstrained system initial-stress (geometric) stiffness matrix in a sparse format.
INV	Factors the assembled system matrices.
EQNF	Computes equivalent joint loading associated with thermal, dislocational, and pressure loading.
SSOL	Computes displacements and reactions due to loading applied at the joints.
GSF	Generates element stresses and internal loads.
PSF	Prints the information generated by the GSF processor.
EIG	Solves linear vibration and bifurcation buckling eigenproblems.
DR	Performs a dynamic response analysis.
SYN	Produces mass and stiffness matrices for systems comprised of interconnected substructures.
STRP	Computes eigenvalues and eigenvectors of substructured systems.

TABLE 1.- SPAR PROCESSORS (Concluded)

<u>Name</u>	<u>Function</u>
AUS	Performs an array of matrix arithmetic functions and is used in construction, editing, and modification of data sets.
DCU	Performs an array of data management functions including display of table of contents, data transfer between libraries, changing data set names, printing data sets, and transferring data between libraries and sequential files.
VPRT	Performs editing and printing of data sets which are in the form of vectors on the data libraries.
PLTA	Produces data sets containing plot specifications.
PLTB	Generates the graphical displays which are specified by the PLTA processor.

TABLE 2.- TABLE OF CONTENTS FOR SPAR DATA LIBRARY

TABLE OF CONTENTS, LIBRARY 1

SEQ	RR	DATE	TIME	E R	WORDS	NJ	NI*NJ	T Y	DATA SET N1 N2	NAME N3	N4
1	7	761022	081237	0	18	1	18	0	JDF1 BTAB	1	8
2	-8	761022	081237	0	250	250	250	0	JREF BTAB	2	6
3	-12	761022	081237	0	12	1	12	1	ALTR BTAB	2	4
4	13	761022	081237	0	30	2	30	4	TEXT BTAB	2	1
5	14	761022	081237	0	10	1	10	1	MATC BTAB	2	2
6	15	761022	081237	0	48	4	48	1	ALTR BTAB	2	4
7	16	761022	081237	0	750	250	750	1	JLOC BTAB	2	5
8	28	761022	081237	0	250	250	250	0	JREF BTAB	2	6
9	32	761022	081237	0	25	1	25	1	SA BTAB	2	13
10	33	761022	081237	0	250	250	250	0	CON	1	0
11	37	761022	081237	0	2250	250	2250	1	QJJT BTAB	2	19
12	73	761022	081241	0	3136	196	896	0	DEF E43	11	4
13	129	761022	081241	0	2	1	2	0	GD E43	11	4
14	130	761022	081241	0	15	1	15	0	GTIT E43	11	4
15	131	761022	081241	0	12	12	12	0	NELZ BTAB	1	11
16	132	761022	081241	0	5	1	5	0	KE	0	0
17	133	761022	081241	0	7	1	7	0	NS	0	0
18	134	761022	081241	0	1	1	1	3	ELTS NAME	0	0
19	135	761022	081241	0	1	1	1	0	ELTS LTYP	0	0
20	136	761022	081241	0	1	1	1	0	ELTS NNOD	0	0
21	137	761022	081241	0	1	1	1	0	ELTS ISCT	0	0
22	138	761022	081241	0	1	1	1	0	ELTS NELS	0	0
23	139	761022	081241	0	1	1	1	0	ELTS LE3	0	0
24	140	761022	081244	0	1500	250	1500	-1	APPL FORC	1	1
25	164	761022	081244	0	1500	250	1500	-1	APPL FORC	2	1
26	188	761022	081244	0	1500	250	1500	-1	UNIT VEC	1	1
27	212	761022	081244	0	1500	250	1500	-1	APPL MOTI	5	1
28	236	761022	081244	0	1	1	1	-1	TOT FORC	5	1
29	237	761022	081244	0	1	1	1	-1	CONV AUS	1	1
30	238	761022	081244	0	1500	250	1500	-1	DISP INC	1	1
31	262	761022	081245	0	6272	250	896	0	KMAP	1087	17
32	360	761022	081245	0	8960	250	1792	0	AMAP	1675	28
33	506	761022	081254	0	62720	196	320	4	E43 EFIL	11	4
34	1486	761022	081248	0	20	20	20	0	DIR E43	11	4
35	1487	761022	081248	0	1500	250	1500	-1	DEM DIAG	0	0
36	1511	761022	081302	0	42560	250	2240	1	K SPAR	36	0
37	2176	761022	081323	0	50176	250	3584	1	INV K	1	0
38	2960	761022	081333	0	1500	250	1500	-1	STAT DISP	100	1
39	2984	761022	081333	0	1500	250	1500	-1	STAT REAC	2	1
40	3008	761022	081345	0	10780	196	5555	-1	STRS E43	100	1

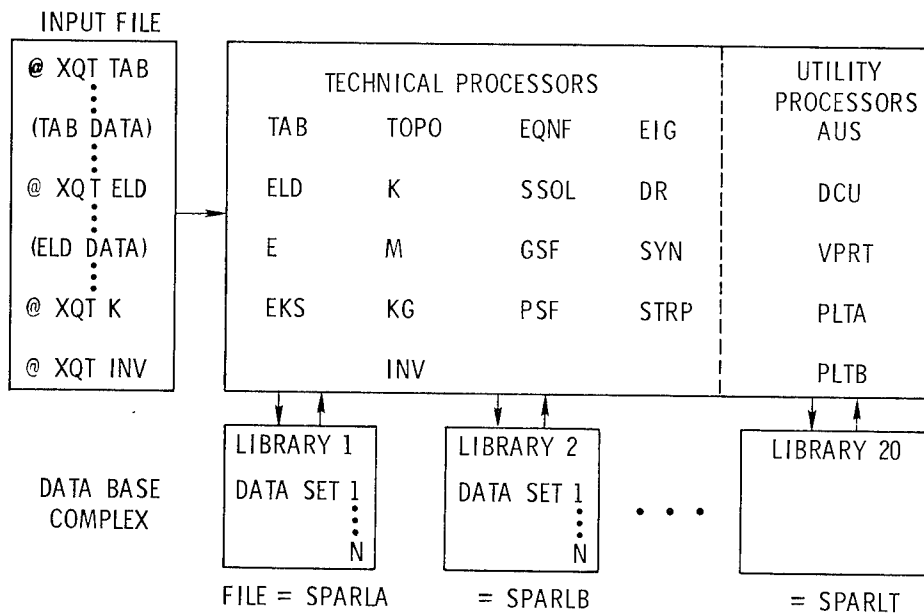


Figure 1.- Organization of SPAR computer program.

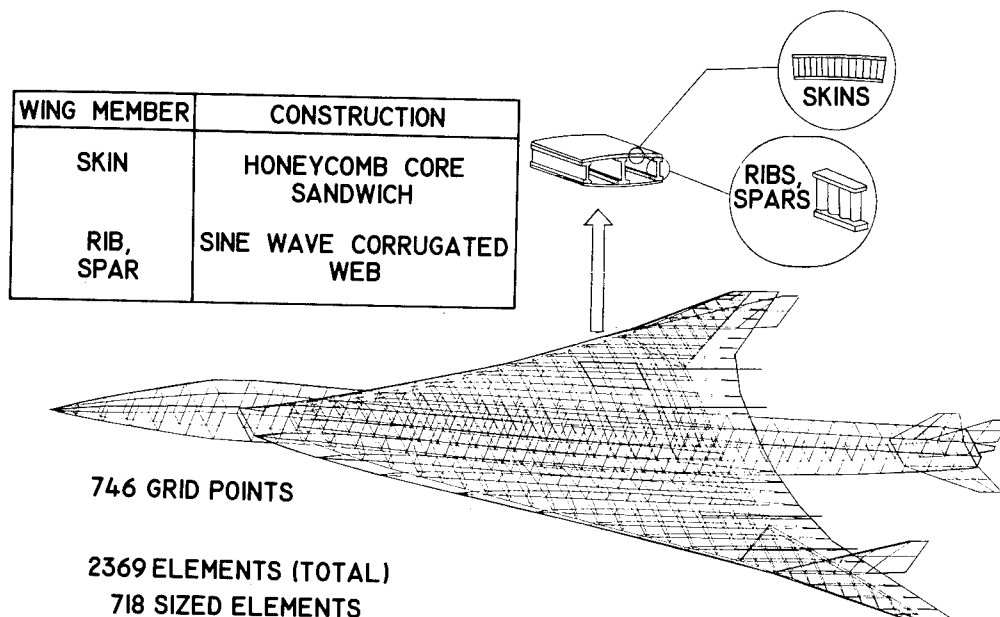


Figure 2.- Finite-element simulation of a supersonic cruise aircraft configuration.

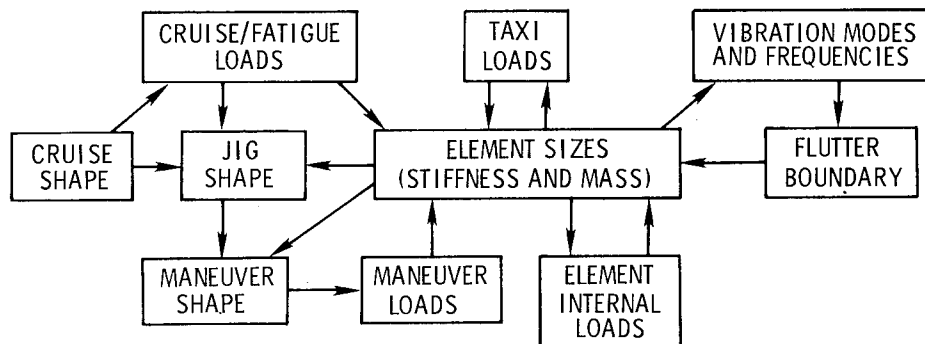


Figure 3.- Interaction of data which is calculated during structural sizing of flexible aircraft.

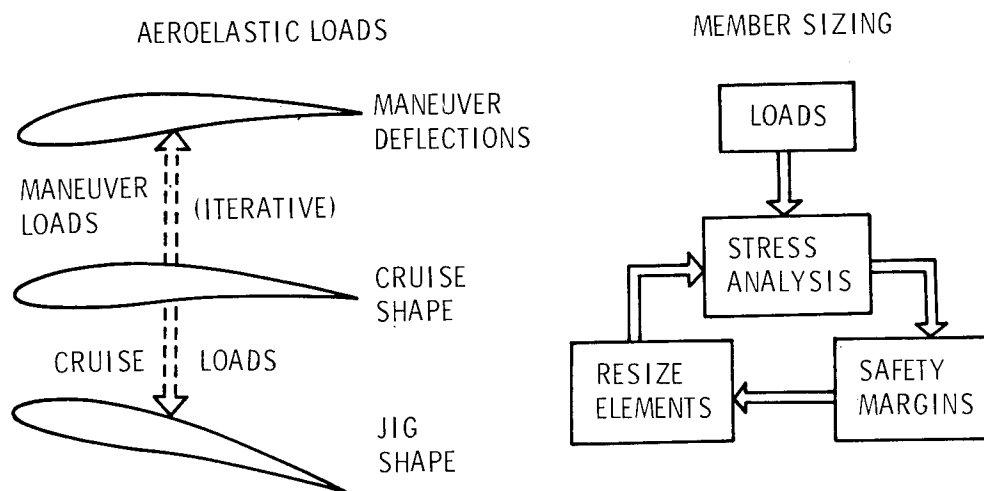


Figure 4.- Iterative procedures to sequentially calculate aeroelastic loads and to size structural members.

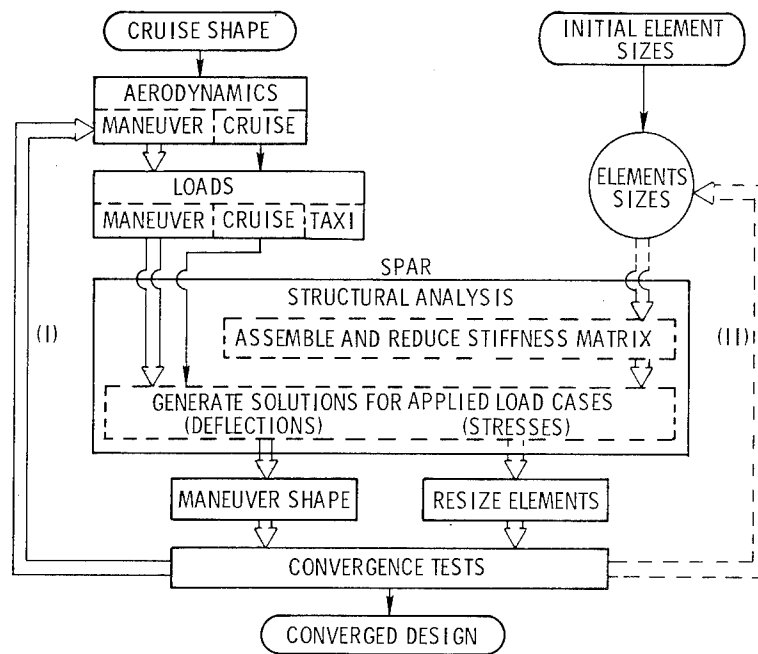


Figure 5.- Schematic of procedure for simultaneous calculation of aircraft design loads and structural member sizes.

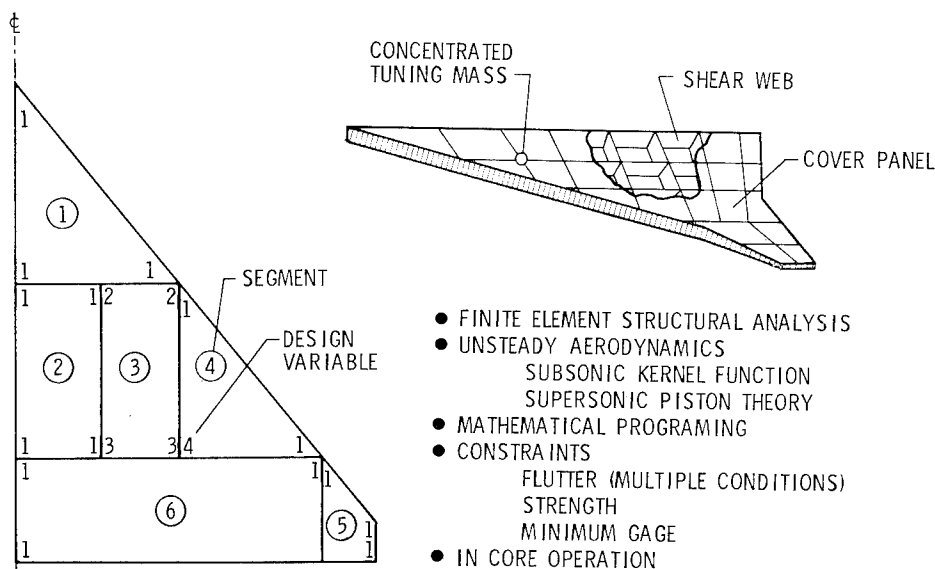


Figure 6.- Characteristics of WIDOWAC flutter synthesis computer program.

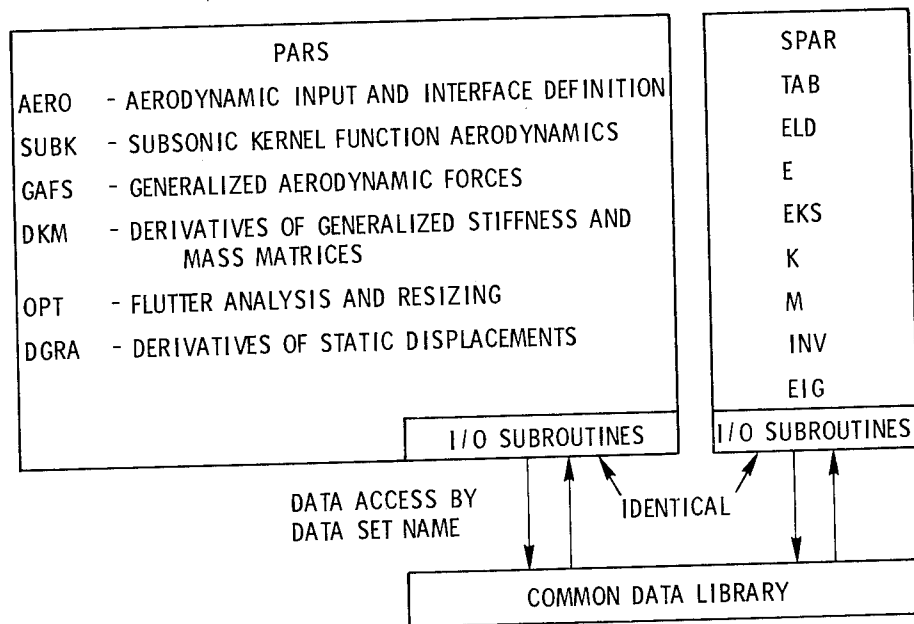


Figure 7.- Schematic showing processors contained in PARS computer program and its interaction with SPAR program.

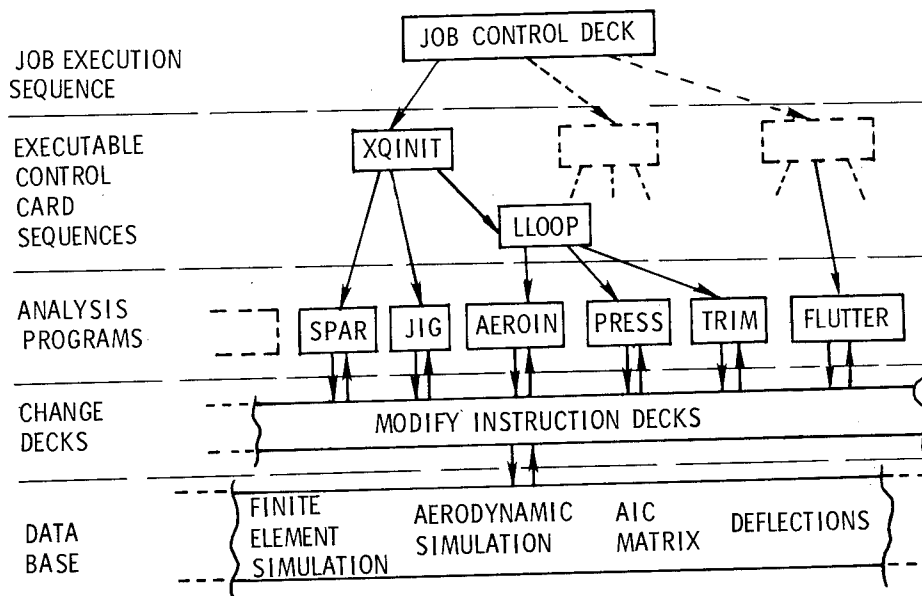


Figure 8.- Organization of a portion of SAVES structural sizing system.

STRUCTURAL DESIGN STUDIES OF A
SUPERSONIC CRUISE ARROW WING CONFIGURATION

Jaroslav Sobieszczanski
NASA Langley Research Center

and

L. Arnold McCullers, Rodney H. Ricketts, Nick J. Santoro,
Sharon D. Beskenis, and William L. Kurtze
Vought Corporation Hampton Technical Center

SUMMARY

Structural member cross sections were sized with a system of integrated computer programs to satisfy strength and flutter design requirements for several variants of the arrow wing supersonic cruise vehicle. The resulting structural weights provide a measure of the structural efficiency of the plan-form geometry, structural layout, type of construction, and type of material including composites.

A study was conducted to determine the material distribution for a baseline metallic structure. The results of this study indicated that an approximate fatigue constraint has an important effect on the structural weight required for strength but, in all cases, additional material had to be added to satisfy flutter requirements. It also proved to be more difficult to satisfy flutter requirements with lighter mass engines with minimum fuel onboard.

A study was performed on a reduced wing area configuration which indicated that although the wing loading was higher than the baseline, the structural mass required to satisfy strength and flutter requirements decreased.

The use of composite materials on the baseline configuration was explored and indicated increased structural efficiency. In the strength sizing, the all-composite construction provided a lower weight design than the hybrid construction which contained composites only in the wing cover skins. Subsequent flutter analyses indicated a corresponding lower flutter speed.

INTRODUCTION

The reported studies are part of the current Langley Supersonic Cruise Aircraft Research (SCAR) program. One of the primary goals of this program is to investigate the design technology for minimum weight supersonic aircraft, strength and flutter requirements for metallic and composite primary structure being considered. The arrow wing configuration, shown in figure 1, in a subsonic

leading-edge wing optimized for low drag due to lift at supersonic speeds. The uniqueness of this planform precludes the use of only statistical data for a reliable estimate of the primary structural mass. Therefore, structural mass estimates have to be supplied by analytical studies such as reported in this paper. Inputs to this work, such as geometric shape, weight breakdown, and material data, were provided by other in-house studies and contractor studies.

This paper devotes separate sections to the development of the baseline configuration, the effect of reducing the wing area, and the influence of composite materials.

An associated goal of the SCAR program involves the development and integration of the computerized tools needed for aircraft structural design. An abbreviated discussion of the tools used to generate the results presented in this paper is given in the appendix.

BASELINE CONFIGURATION (AST 9)

A study was conducted to determine the material distribution for the baseline configuration meeting strength and flutter criteria and utilizing titanium construction. This structural baseline was developed by exploring a number of variants and is used as a basis of comparison for subsequent designs. The study method, the analytical model, and the results of this study are discussed in the following subsections.

Analytical Approach

In general, the exploration of a variant of the configuration consists of the following operations:

(1) Static structural analysis is performed by using a finite-element method accounting for the aeroelastic loads and the jig shape. Trimming the aircraft at each design flight condition is included in the static structural analysis.

(2) Cross sections of selected structural components, usually the wing cover panel skins and the rib and spar shear webs, are sized to satisfy the static strength requirements with minimum structural mass. The techniques used here are the weight-strength method for metal construction, and the more general mathematical nonlinear programming method whenever composite material is involved. Operations (1) and (2) are collectively referred to as the strength design.

(3) Flutter analysis is performed on this strength design in the complete operational velocity-altitude envelope.

(4) The cross sections are resized for greater overall stiffness and minimum additional structural mass (flutter penalty) to eliminate any flutter deficiency.

The methodology involved in these operations and the computer implementation are outlined in the appendix.

All four operations are not always necessary to evaluate the variant under study. Operation (4), the most costly, is frequently omitted if the first three operations do not indicate a major advantage for that variant.

Structural mass is adopted as an ultimate figure of merit to judge the configuration studied, except in the cases when operation (4) is not carried out. In such cases, both structural mass and flutter speed deficiency are used to judge the potential structural efficiency.

Baseline Analytical Model

The basic information for the baseline configuration, shown in the table on figure 1, includes the take-off gross weight (TOGW), operational empty weight (OEW), and payload (PL) which serve as references for quoting the structural weight results. The finite-element model representation of this configuration and the type of construction are shown in figure 2. The wing is built up of corrugated web spars and ribs with caps supporting honeycomb sandwich covers. Conventional stringer-skin-frame construction is used in the fuselage.

Finite-element model. In the finite-element model, the covers are simulated by membrane elements, spar and rib webs by shear panels, and caps by rod elements. Beam elements are used to represent the engines, the engine mounts, and the supports for leading- and trailing-edge devices. Plate elements are used to model the vertical fins and horizontal stabilizers. Nonstructural components are represented by appropriate lumped and distributed masses. For computation economy, the fuselage model is simplified to a rectangular cross-section box with overall bending stiffness and mass equivalent to the fuselage. This simplification is consistent with the study's emphasis on the primary wing structure; as a result the rest of the airframe is excluded from the resizing process, but not from the analysis. The construction material is titanium throughout the primary structure. The resulting half airplane finite-element model has 746 grid points, 2141 degrees of freedom, and 2369 finite elements.

Material properties and allowables. The titanium data used in this study are displayed in the first row of table 1. The allowable stress level for cruise is restricted to the value designated FAC (for Fatigue Allowable Cruise) in order to approximately account for fatigue requirements. In titanium construction, this value corresponds to a notch factor of 4.0. The data for the honeycomb core and core-face sheet bonding are also included in table 1.

Loading cases. From the multitude of loading cases considered in the design of airframes, the three cases shown in table 2, together with their limit load factors, were selected for use in the strength sizing. These three cases are judged to be sufficiently representative for the purpose of this study. The cruise case defines the jig shape and accounts approximately for fatigue,

the maneuver case generates the largest wing root bending moment, and the taxi loads expose the wing lower surface covers to compression. A safety factor of 1.5 is used to define the ultimate (design) load factors.

Four fuel conditions are used in the analyses: (1) full fuel for taxi (TF), (2) heavy fuel (HF) at the maneuver design point during climb, (3) cruise fuel (CF) at the start of cruise, and (4) light fuel (LF) at the maneuver design point during descent. The appropriate fuel inertia forces are included in the design loads for each load condition.

Baseline Results

A number of strength designs, flutter analyses, and flutter designs were performed on the baseline configuration. The results are discussed in the subsequent sections.

Strength design results. A total of 334 wing cover panels and 384 shear webs are subject to sizing in this operation. The spar and rib cap areas and other parts of the airframe are held constant. In the cover panels, the sandwich depth is also kept constant, 2.54 cm (1 in.), so that the face sheet thicknesses are the only variables. A contour map of the resulting skin thickness distribution is shown in figure 3. It shows characteristic islands of thickness which reflect the local stress concentrations in the vicinity of the vertical fin (A), the rear spar crank (B), and the wheel well (C). These concentrations are also evident in the contour map of the upper surface principal stress distribution for the maneuver case, illustrated in figure 4.

Distribution of the critical loading conditions over the upper cover of the wing is shown in figure 5. The outboard part of the wing is dominated by the cruise-fatigue requirements, whereas the maneuver condition is critical for the inboard aft part of the wing box. The influence of the taxi condition is limited to the vicinity of the wheel well. Large areas of the wing have minimum gage thickness covers.

The mass of the strength design is 27 266 kg (60 120 lbm) for the wing structure of the airplane. This includes load-carrying material comprised of the sandwich cover's face sheets, rib and spar caps, and shear webs, and additional mass due to corrugations in the shear webs, core, and bonding.

In order to account for the mass of joints, fasteners, padding, and so forth, an incremental nonoptimum factor is applied to the mass of load-carrying material. To conform to the statistical weight data available as input to these studies, a factor of 0.3125 is present in all mass results reported, unless indicated otherwise.

Results of auxiliary analyses. The strength design was analyzed for thermal stress, extended flap loads, and reduced fuel mass inertia relief in order to check for critical conditions not included in the basic loading cases. The results were as follows:

(1) Thermal analysis revealed that the thermal stress increments in the wing cover panels are relatively small in comparison with the maneuver loading

case stress. The largest thermal stresses are 9 to 10 percent of the maneuver stresses in about 5 percent of the panels.

(2) The extended flap analysis was conducted for a load factor of 1.65 (landing with gust) with flap deflections varying from 24° inboard to 5° at the wing tip. This indicated no overstressed elements.

(3) Analysis with the lightweight fuel showed no overstressed elements and confirmed the criticality of the heavy weight fuel maneuver condition for the strength design.

Flutter analysis. Symmetric flutter analyses of the strength designed wing showed that the structure did not meet the flutter speed requirement of 1.2 V_D (dive velocity) for various combinations of fuel loadings and engine weights. In figure 6, a typical set of results for the original 10 431 kg (23 000 lbm) engines (designated E23) shows that the structure is more deficient in the subsonic region than in the supersonic region and has three distinct flutter modes that can be critical. Also, the analyses showed that the lightweight fuel condition with alternate 7 483 kg (16 500 lbm) engines (designated E16) provided the worst combination for flutter fixing.

Results of the flutter fix. Subsequent to the strength design, a flutter fix was carried out by means of a trial-and-error procedure (outlined in the appendix) for the E23 baseline engine. The additional thicknesses of the wing covers needed to meet the flutter requirements were combined with the strength designed thicknesses by means of a "minimum gage technique" described in the appendix. Combining the two sets of thicknesses has a smoothing effect on the distribution as illustrated by figure 7. The three flutter modes which were critical during the flutter analysis of the strength-sized structure were removed beyond the required envelope as shown in figure 8. A "hump" flutter mode which appeared and disappeared during the flutter fix operation made the flutter resizing more difficult. The final wing design has a total structural mass of 28 810 kg (63 524 lbm). The mass increment (flutter penalty) of 1 544 kg (3 404 lbm) comes entirely from the increased cover thickness and represents a 5.7-percent increase in the structural mass.

A similar flutter fix for the alternate engine (E16) produced a structural mass increase to a total of 30 166 kg (66 514 lbm), a flutter penalty of 2 900 kg (6 394 lbm). Comparison of the structural masses for the cases with engines E23 and E16 shows that the decrease in engine mass more than offsets the structural mass increase (10.6 percent) due to flutter penalty for a net mass decrease of 10 436 kg (23 010 lbm). Because of the lower overall mass and the increased difficulty in flutter sizing, the alternate engine case (E16) was selected for subsequent flutter analyses.

Antisymmetric flutter analysis. The flutter fixed design was analyzed for flutter by using antisymmetric vibration modes and airloads. The results showed that the structure was slightly deficient in flutter speed (0 to 3.3 percent) in the subsonic region. This deficiency was judged to be too small to justify another flutter fix resizing cycle. However, it demonstrated that the antisymmetric flutter modes must be checked for this type of vehicle.

Influence of aeroelastic loads and fatigue allowable. Three additional strength designs were performed to explore the impact of aeroelastic effects in the maneuver load condition and the effect of the cruise-fatigue condition on structural mass. In the first additional design, the baseline configuration was resized with rigid maneuver loads, that is, the maneuver load vector was not updated to include aeroelastic effects. Because of the lack of aeroelastic load relief, this resulted in a structural weight increase of 12.8 percent with almost the entire wing designed by the maneuver condition.

The second and third designs were used to study the effect of the fatigue allowable. The second was performed with flexible maneuver loads and a 33-percent increase in the fatigue allowable. The structural weight dropped 4.5 percent with very few structural elements designed by the cruise-fatigue condition. In the third design, removing the cruise-fatigue condition entirely resulted in only an additional 0.1 percent (total 4.6 percent) structural weight decrease.

Influence of modified carry-through design. The baseline configuration has only the spar caps, typical of floor beams, continuous across the fuselage ahead of the wheel wells. To study the design impact of these moment carrying members, the wing structure was redesigned with these spar caps deleted.

This variant is of interest for two reasons. First, it allows the wing root chord and the fuselage to be longitudinally shaped independent of each other. Thus, the wing root camber may be designed solely by aerodynamic considerations, and the fuselage may be designed by both aerodynamic and passenger comfort considerations. (The fuselage is not forced to assume a form with excessive passenger floor slopes due to cruise angle of attack.) Secondly, it opens the possibility to design the wing-fuselage intersection along the section marked 1 in figure 9 so that the wing's highest temperature area will have the freedom to expand thermally and thus reduce the thermal stress. Strength design of the airframe modified in this manner resulted in a structural mass increase of 1.7 percent over the baseline strength sized configuration.

Subsequent flutter analysis of this design revealed that there is a change in the flutter modes and frequencies but no appreciable change in the lowest flutter speed. It was concluded that the variant is structurally viable and may be adopted in the vehicle design if desired.

Influence of structural box planform geometry. In order to relieve the stress concentration shown in figure 4 in the vicinity of the rear spar crank, the modified planform shown in the figure 9 inset with a "double crank" was strength sized. Even though there was some stress relief in the area of the crank, there was a negligible difference in the structural mass that indicated further study of this variant was not warranted.

Selection of structural baseline. Based on the results discussed in the preceding paragraphs, the material distribution generated by strength sizing the baseline configuration with the E23 engines and the heavy weight maneuver (HF) fuel was selected as the strength sized baseline for comparison with other configurations. The mass and material distribution resulting from

the flutter fix with the lightweight maneuver (LF) fuel and the alternate E16 engines was used for flutter design comparison since this is a more severe case from a flutter standpoint.

REDUCED WING AREA CONFIGURATION (AST 10)

A configuration with a smaller wing was studied because of its improved aerodynamic performance. It is geometrically similar to the baseline with a 15.3-percent reduction in wing area and no change in the fuselage. The relative position of the wing on the fuselage is changed, however, because of aircraft balance requirements. Propulsion system requirements for this variant call for an engine weight of 6 647 kg (14 656 lbm), designated E14. The configurations TOGW and OEW are reduced to 325 624 kg (718 000 lbm) and 139 507 kg (307 612 lbm), respectively, with the payload unchanged. A strength design, a flutter analysis, and a flutter fix were executed for this configuration in a manner similar to that used in the baseline configuration study. Comparison of the results with those given in the subsection "Results of the Flutter Fix" for the baseline configuration shows a strength design structural mass decrease of 10.5 percent (this is less than the area reduction because of higher wing loading) and a flutter penalty decrease of 35.5 percent. This results in a total primary structural mass decrease of 12.9 percent for AST 10.

COMPOSITE MATERIALS CONFIGURATION (AST 11)

The composite material effect on the primary structural mass has been studied by examining a configuration identical with the baseline (AST 9) with composite primary structure. The composite design problem is more difficult since with composite materials each mechanical property can assume several possible values depending on material selection; there are a number of ways in which the fibers can be laid out; and the degree to which the composite is combined with metal can be varied. A number of variants of the composite configuration have been explored to assess the broad range of the available combinations of these factors.

Material Properties and Allowables

Graphite-polyimide is an attractive composite material for supersonic cruise applications because of its relatively good retention of mechanical properties at elevated temperatures. The material properties, displayed in table 1, were supplied by The Boeing Company. In order to establish upper and lower bounds, the properties anticipated to be commonly available in 1986 are included with those available in 1975. In addition, a pessimistic allowable strain is considered to establish a lower and safer bound on the stress allowables. The fiber volume is assumed to be 60 percent throughout. Note that the composite is available in a low Young's modulus and high strength version and a high Young's modulus and low strength version. In the discussion to follow, use of the low modulus version is assumed unless otherwise indicated. Insofar as the fatigue

stress allowables for cruise are concerned, no data similar to those used for titanium construction exist for composites. However, for consistency, the ratio of the allowable cruise stress to the design limit stress for composites has been set equal to the ratio of the fatigue allowable to the design limit stress for titanium.

Both room temperature, 21° C (70° F), and elevated-temperature, 232° C (450° F), properties are provided for the graphite-polyimide composite in table 1. The differences between the two sets of values are not large; they range from under 10 percent for stress to zero for modulus. Since the 1986 room-temperature data are the most optimistic ones available, they were used unless indicated otherwise for the sake of establishing a consistent upper bound on the results reported.

Hybrid Composite-Titanium Construction (AST 11.1)

In this construction variant, the titanium spars and ribs are retained and the composite is used for the wing covers only. The hybrid construction is of interest as an interim stage between the metal and composite technologies. The composite layup used for strength design is shown in figure 10. It is an orthotropic layup that has the plies oriented at four different filament angles: (0°, $\pm\phi$, 90°) and has the thicknesses in the ϕ -direction set equal (that is, $t_\phi = t_{-\phi}$). In addition to ϕ and t_ϕ , the design variables for this type of construction include the following: thickness, t_0 and t_{90} ; depth of the sandwich panel, h ; and the orientation angle of the complete laminate, γ . The design variables are used in a mathematical optimization technique to size the composite sandwich panels as outlined in the appendix. The titanium caps are protected from overstress by strain constraints applied to the composite skins in the optimization procedure.

Hybrid construction baseline. In the basic variant (designated 11.1.1), the three thicknesses, t_0 , t_ϕ , and t_{90} , are free design variables. The other variables are frozen as follows: $\phi = 45^\circ$, $\gamma = 0^\circ$, and h is 2.54 cm (1 in.) over most of the wing and 4.45 cm (1.75 in.) where additional depth is required for panel stability.

The results of the strength design, shown as skin-thickness contour maps, are shown in figure 11. The mass of the strength design is 21 825 kg (48 125 lbm), a decrease of 20 percent from the metal baseline strength design. The mass includes previously defined nonoptimum incremental factors. For the titanium parts, a factor of 0.3125, the same as for metal construction, is applied. For the composite parts, a higher value of 0.50 is used in order to compensate conservatively for the smaller pool of weight data available for composite structures. Flutter analysis showed that this variant has a large flutter speed deficiency as illustrated in figure 12. This deficiency is about twice as large as the one for the metallic baseline strength design shown in figure 6.

A subsequent flutter fix, using the "small model and large model" trial-and-error technique explained in the appendix, produced a flutter-free design at the price of a sandwich skin structural mass increment of 4 172 kg (9 200 lbm). The

total structural mass is 25 997 kg (57 325 lbm) which is smaller than the value for the metal, flutter-fixed baseline by 4 169 kg (9 189 lbm) or 14 percent. This is the only composite design to be resized for flutter to date.

Influence of the choice of design variables. Six variants (11.1.2-7) of different groupings of the free and frozen design variables were strength designed and flutter analyzed in addition to the basic variant. The results in terms of the structural mass and flutter speed increments compared with the metal, flutter-fixed baseline are shown in table 3. It is evident that the influence of the choice of the design variables on both structural mass and flutter speed is significant. As expected, the larger the number of free design variables, the lower the structural mass, and the higher the computer cost. From table 3, one can identify case 11.1.5 as the most promising based on the ratio of the mass saved to flutter speed deficiency ($\Delta M/\Delta V$).

Since the sandwich cover panels are optimized individually (see the appendix), the variants with free orientation angles and sandwich depth may be unacceptably difficult and costly to fabricate by using the standard manufacturing methods. Investigation of these variants has been carried out in order to explore potential benefits. If these benefits are large enough, a revision of the fabrication methods may become justified. The fabrication requirements can also be incorporated in the design itself, at the price of some departure from the minimum mass, by averaging the core depth and orientation variables over large areas of the wing.

Influence of using the high modulus composite. As shown in table 1, the high Young's modulus and relatively lower strength graphite-polyimide is an alternative to the low modulus version used to generate these results. Substitution of the alternative properties in the strength design of the basic variant 11.1.1 showed the structural mass to be 8.3 percent larger than that for the low modulus material. However, the flutter analysis indicated less flutter speed deficiency for the high modulus design, as seen in the right half of figure 12, and lift the issue of which version is more efficient to be settled by the flutter fix operation.

Influence of using conservative allowables. Relatively low allowables are sometimes imposed on the fiber strain to produce a conservative design in order to account for many unknown behavior characteristics of composite materials. A strength design of the basic variant (11.1.1), with an ultimate fiber strain limit of 0.006 for the strength constraint, produces a structural mass increase of 7.2 percent. The flutter speed is also higher (73 percent against 63 percent of the required speed) so that the mass cost of using conservative allowables must be provided by the results of the flutter-fix operation.

Pure Composite Construction (AST 11.2)

The relatively high contribution of the titanium caps and webs to the total structural mass of the hybrid construction points to the complete replacement of the titanium by composites as a means to realize potentially large mass savings. The titanium caps not only contribute mass, but also, as mentioned

before, have to be protected from overstress that would prevent the composite from reaching its full load-carrying capacity in many cases.

The pure composite construction consists of composite sandwich cover panels and composite rib and spar shear webs without caps. The only titanium parts retained were the local reinforcements such as engine mounts, and so forth.

The strength design resulted in structural masses of 11 990 kg (26 437 lbm) for the low modulus material and 13 807 kg (30 445 lbm) for the high modulus material, 45.1 percent and 36.7 percent savings, respectively, over the hybrid baseline AST 11.1.1. Flutter analysis results for this construction using low modulus and high modulus material are presented in figure 13. These results show a decrease in flutter speed from AST 11.1.1, 52 percent against 63 percent of the required speed for the low modulus material and 87 percent against 91 percent for the high modulus material.

DISCUSSION OF THE RESULTS

A bar chart comparing the primary variants is shown in figure 14. The wing structural mass from the strength design of the metallic baseline configuration (AST 9) was 17 percent of the operational empty weight (OEW) and 99 percent of the payload (PL). With the flutter-fix penalty mass added to the strength design mass, the structural mass increased to 19 percent of OEW and 109 percent of PL. Replacing the E23 engines by the E16 engines for this configuration added to the flutter-fix penalty mass but not enough to offset the engine mass savings. This resulted in a decrease of 6.6 percent of OEW and 37.7 percent of PL.

For the reduced wing area configuration (AST 10), the wing structural mass decreased by 2 percent of OEW and 14 percent of PL including the flutter-fix penalty mass.

The change from the metallic baseline configuration (AST 9) to the hybrid configuration (AST 11.1) gave a strength- and flutter-sized structural mass of 16 percent of OEW and 94 percent of PL, a savings of 2 percent of OEW and 10 percent of PL. There is a large decrease in mass due to the strength design, but it is partially offset by a relatively larger flutter-fix penalty mass. Substitution of the high modulus and low strength composite material for the low modulus and high strength composite material gave a strength design structural mass increase of 8 percent of the low-modulus, high-strength design. The use of a more conservative allowable for the low modulus composite material resulted in a strength design structural mass increase of 7 percent compared with the hybrid composite baseline, AST 11.1. Significant structural mass savings for the hybrid configuration were realized by including the sandwich depth as a design variable in the optimization procedure.

To realize fully the mass saving potential of composite materials, an all-composite construction variant (AST 11.2) was explored. The decrease in mass after strength design was 56 and 49 percent of the metallic baseline

configuration for the low and high-modulus composite material, respectively. These are 36 percent larger savings than those of the strength-sized hybrid configurations. Because of the increased flexibility of the all-composite configurations, the flutter-fix penalties would probably be larger than those for the hybrid configurations. Therefore, some of the gain in mass savings would be offset by the increase in the flutter penalty.

CONCLUDING REMARKS

In the main body of the paper, the results were compared on the basis of the total wing structural mass to highlight the large decrease in structural mass when all-composite construction was used (deleting the titanium spar caps). In the discussion of the results, the masses were compared with the operational empty weight and the payload to emphasize the impact on the aircraft. In all studies, the fuselage and control surface masses were held constant. Redesign and/or application of composites to these areas would generate additional weight savings.

Since the wing skins were of primary interest in the resizing, the following observations are based on the mass of the wing skins only.

1. For titanium construction, the arrow wing configurations being studied were made flutter free by increasing the wing skin mass by 15 to 28 percent of the strength-sized skin mass. This increment provides a target mass for the design of an active controls flutter-suppression system.

2. The flutter behavior and the associated mass penalty were significantly affected by the engine mass.

3. Wing-tip washout aeroelastic effects provided load relief savings of about 24 percent of the skin mass for the strength design.

4. Imposition of the fatigue allowable stress on the cruise condition increased the skin mass by 14 percent.

5. Use of composite materials with titanium substructure (webs and caps) saved 55 percent of the skin mass for the strength designs but only 33 percent of the skin mass for the flutter-free designs.

6. The all-composite construction has a much higher mass savings potential as indicated by the strength design results.

7. The use of a high modulus, low strength composite material increased the skin mass by 41 percent for the strength design. This trend may be reversed when a flutter-free design is generated.

8. The methods outlined in the appendix for strength design and flutter analysis proved to be efficient and reliable tools for this application. They also have potential applicability to similar studies of advanced aircraft.

APPENDIX

ANALYSIS AND SYNTHESIS METHODS

The methods used to produce the results reported in this paper are discussed in this appendix. The building blocks of the methodology consist of computer programs for aerodynamic analysis, stress-deflection-vibration analysis, flutter analysis, and data preparation as well as optimization and data handling techniques. Computer graphics are used to display the results. All programs are integrated into a system, as described in reference 1; this integration allows a hands-off data flow among the programs and interactive, as well as batch, executions of sequences of programs.

The study consists of two basic phases: (1) strength analysis and synthesis, and (2) flutter analysis and synthesis.

Strength Analysis and Synthesis

Phase 1 consists of two iterative procedures, one for converging the aeroelastic loads, and the other for resizing the structural cross sections. The two iterations are performed simultaneously as illustrated in figure 15 and described in reference 2. They involve aerodynamic loads computation (ref. 3) stress-deflection analysis, computation of a jig shape, and resizing of the wing individual cover panels and shear webs. Spar and rib caps remain constant in the resizing procedure. The titanium covers are resized by the weight-strength method considering stress, local buckling, and minimum gage (ref. 4). For the composite wing cover panels, the resizing is performed by means of a mathematical programming method applied to each panel separately, as discussed in reference 5, by using the feasible-usable directions technique. Structural mass is the object function in all cases. A comprehensive list of stress, strain, fiber-matrix interaction, local buckling, and geometry constraints for the composite layups are handled by this technique.

Flutter Analysis and Synthesis

The flutter analysis begins with the generation of the vibration mode and frequency data by using the structures finite-element analysis computer program, SPAR. These modes are used to calculate subsonic and supersonic unsteady aerodynamic forces (refs. 6 and 7) which, in turn, are used in the usual k-method flutter analysis. The analysis is entirely automated to produce vibration mode plots, V-g and V- ω plots, and matched point flutter speeds.

The vibration-flutter analysis sequence has been validated by means of wind-tunnel experiments of an arrow wing aeroelastic model undertaken in support of these studies. Resizing to meet the flutter speed requirements (flutter fix) is performed in a trial-and-error manner based on engineering judgment formed by comparing the flutter boundaries with the required flutter free envelope on the velocity-altitude graph and by inspecting the flutter modes. The selected

stiffening is implemented, and the vibration-flutter analysis is repeated in an iterative manner, characterized in figure 16, until a satisfactory result is obtained.

Three different methods of flutter fix stiffening were evaluated:

(1) scaling the strength designed wing cover thickness, (2) adding patches on top of the strength designed thicknesses, and (3) adding the thickness as a new minimum gage to the strength design. The last method has been found to produce the least flutter-fix penalty and was adopted as a flutter-fix tool.

Flutter Synthesis of the Composite Wing

In the case of composite wing covers, the flutter speed deficiency can be removed not only by means of increasing the overall skin thickness in the manner described above, but also by increasing thicknesses at selected orientations, adding plies of a new orientation, or changing the existing ply orientation angles.

Because of the intrinsically large number of possibilities that need to be explored in order to define a flutter-free composite structure, it is prohibitively expensive to use the same finite-element model which is used in the strength analysis in the trial-and-error loop (fig. 16). Therefore, that model is replaced in the flutter analysis by a different model having the degrees of freedom and finite elements reduced to 387 and 77, respectively. This "small model," shown in figure 17, was made dynamically similar to the large model by means of (1) retaining the overall geometry, (2) using plate elements (representing the full-depth wing) with bending stiffness matrices equivalent to those of the corresponding areas of the large model, (3) defining the fuselage as a stiffness equivalent beam, and (4) retaining the concentrated and distributed masses. Transfer of the stiffnesses (by the cover ply thicknesses and orientation angles) between the two models is fully automated. The flutter-free designs are produced by the same, previously outlined, trial-and-error procedure (fig. 16) by using the small model whose vibration-flutter analysis is more than an order of magnitude less expensive than that for the large model. Final results of each trial-and-error iterative sequence are analyzed for flutter and strength upon transfer to the large model.

REFERENCES

1. Sobieszczanski, Jaroslaw: Building a Computer-Aided Design Capability Using a Standard Time Share Operating System. Proceedings of the ASME Winter Annual Meeting, Integrated Design and Analysis of Aerospace Structures, Houston, Texas, November 30-December 5, 1975, pp. 93-112.
2. Giles, Gary L.; and McCullers, L. A.: Simultaneous Calculation of Aircraft Design Loads and Structural Member Sizes. Presented at the AIAA 1975 Aircraft Systems and Technology Meeting, Los Angeles, California, August 4-7, 1975. (AIAA Paper No. 75-965.)
3. Carmichael, Ralph L.; and Woodward, Frank A.: An Integrated Approach to the Analysis and Design of Wings and Wing-Body Combinations in Supersonic Flow. NASA TN D-3685, 1966.
4. Giles, Gary L.: Procedure for Automating Aircraft Wing Structural Design. Journal of the Structural Division, ASCE, January 1971, pp. 99-113.
5. Sobieszczanski, Jaroslaw: Sizing of Complex Structure by the Integration of Several Different Optimal Design Algorithms. AGARD Lecture Series No. 70 on Structural Optimization, AGARD-LS-70, September 1974.
6. Watkins, Charles E.; Woolston, Donald S.; and Cunningham, Herbert J.: A Systematic Kernel Function Procedure for Determining Aerodynamic Forces on Oscillating or Steady Finite Wings at Supersonic Speeds. NASA TR R-48, 1959.
7. Donato, Vincent W.; and Huhn, Charles R., Jr.: Supersonic Unsteady Aerodynamics for Wings With Trailing Edge Control Surfaces and Folded Tips. AFFDL-TR-68-30, U.S. Air Force, Aug. 1968. (Available from DDC as AD 840598.)

TABLE 1.- MATERIAL PROPERTIES USED IN THE STUDIES

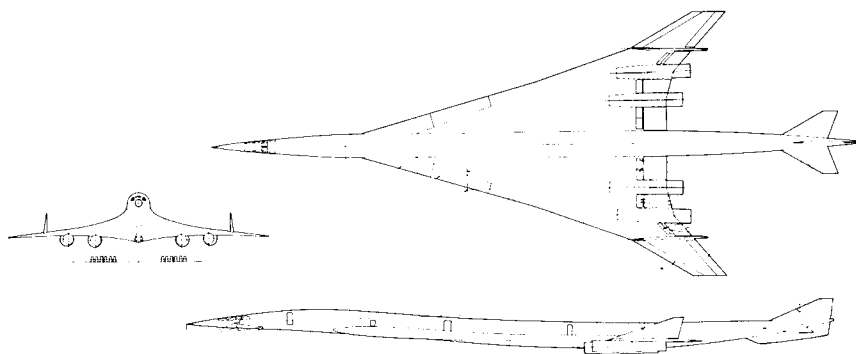
	E GN/m ² (ksi)	ν	F _{tu}	F _{cu}	FAC	Y
			MN/m ² (ksi)			kg/m ³ (lb/in. ³)
TITANIUM ALLOY						
	110 (16.10 ³)	0.3	827 (120)	869 (126)	155 (22.5)	4429 (0.16)
GRAPHITE-POLYIMIDE, AVAILABLE IN 1986, FIBER VOLUME 60%, LOW MODULUS (LM)						
//	138 (20)	0.31	2034 (295)	1999 (290)	352 (51)	1550 (0.056)
⊥	7.8 (1.13)	0.18	115 (16.7)	113 (16.4)		
GRAPHITE-POLYIMIDE, AVAILABLE IN 1986, FIBER VOLUME 60%, HIGH MODULUS (HM)						
//	276 (40)	0.29	1020 (148)	869 (126)	177 (25.6)	1605 (0.058)
⊥	12.4 (1.8)	0.013	46 (6.7)	39.3 (5.7)		
GRAPHITE-POLYIMIDE, AVAILABLE IN 1975, FIBER VOLUME 60%, LOW MODULUS (LM)						
//	13.8 (20)	0.31	1186 (172)	1186 (172)	205 (29.8)	1550 (0.056)
⊥	15.2 (2.2)	0.18	61 (8.8)	101 (14.7)		
GRAPHITE-POLYIMIDE, AVAILABLE IN 1975, FIBER VOLUME 60%, HIGH MODULUS (HM)						
//	179 (26)	0.29	1020 (148)	869 (126)	177 (25.6)	1605 (0.058)
⊥	13.8 (2.0)	0.013	41 (5.9)	110 (16)		
GRAPHITE-POLYIMIDE, AVAILABLE IN 1975, FIBER VOLUME 60%, LOW MODULUS (LM) WITH ULTIMATE STRAIN RESTRICTED TO 0.006						
//	138 (20)	0.31	1420 (206)	1393 (202)	352 (51)	1550 (0.056)
⊥	15.2 (2.2)	0.18	115 (16.7)	113 (16.4)		
	HONEYCOMB CORE kg/m ³ (lb/ft ³)					89 (0.0032)
	ADHESIVE BONDING FACE SHEETS TO CORE, MASS PER AREA, kg/m ² (lb/ft ²)					0.036 (0.288)
LEGEND : E YOUNG MODULUS F _{tu} , F _{cu} ULTIMATE TENSILE, COMPRESSIVE STRENGTH FAC STRESS ALLOWABLE FOR CRUISE ALL VALUES - ROOM TEMPERATURE 20 °C (68 °F) // — PARALLEL TO FIBER ⊥ — PERPENDICULAR TO FIBER						

TABLE 2.- DEFINITION OF THE LOADING CASES

LOAD CASE	LOAD FACTOR [g]	MACH	ALTITUDE m, (ft)	GROSS MASS kg, (lbm)	FUEL MASS kg, (lbm)	REMARKS
CRUISE	1.0	2.7	18 288 (60 000)	313 626 (691 545)	127 212 (280 503)	AIRCRAFT BUILT TO A JIG SHAPE DEFORMS TO A SHAPE AERODYNAMICALLY MOST EFFICIENT FOR CRUISE
MANEUVER	2.5	1.2	10 668 (35 000)	340 823 (751 514)	154 410 (340 473)	SYMMETRIC PULL-UP
TAXI	-2.0	0	0	345 578 (762 000)	158 654 (349 833)	SUPPORT ON THE NOSE AND MAIN GEAR, NO AERODYNAMIC LIFT

TABLE 3.- INFLUENCE OF THE CHOICE OF DESIGN VARIABLES ON MASS AND FLUTTER SPEED

CASE	FREE VARIABLES	MASS, kg (lb)	FLUTTER SPEED DEFICIENCY ΔV , km/hr (knots)	$\frac{\Delta m}{\Delta V}$, $\frac{\text{kg}}{\text{km/hr}}$ ($\frac{\text{lb}}{\text{knots}}$)
11.1.1	$t_0, t_{\pm 45}, t_{90}$	21829 (48125)	309 (167)	27.0 (110.0)
.2	$t_0, t_{\pm 45}, t_{90}, \gamma$	21748 (47947)	335 (181)	25.1 (103.0)
.3	$t_0, t_{\pm \phi}, t_{90}, \phi$	21453 (47297)	411 (222)	21.2 (86.6)
.4	$t_0, t_{\pm \phi}, t_{90}, \gamma, \phi$	21274 (46902)	411 (222)	21.6 (88.3)
.5	$t_0, t_{\pm 45}, t_{90}, h$	20363 (44894)	309 (167)	31.7 (129.0)
.6	$t_0, t_{\pm \phi}, t_{90}, h, \phi$	19908 (43889)	456 (246)	22.5 (92.0)
.7	$t_0, t_{\pm \phi}, t_{90}, h, \phi, \gamma$	19784 (43616)	456 (246)	22.8 (93.1)



TAKE-OFF GROSS WEIGHT	346 363 kg	(762 000 lb)
OPERATION EMPTY WEIGHT	159 608 kg	(351 139 lb)
PAYLOAD	27 740 kg	(61 028 lb)
LENGTH	96 m	(315 ft)
SPAN	42 m	(138 ft)
CRUISE SPEED	$M = 2.7$	

Figure 1.- Basic characteristics of the arrow wing supersonic cruise vehicle.

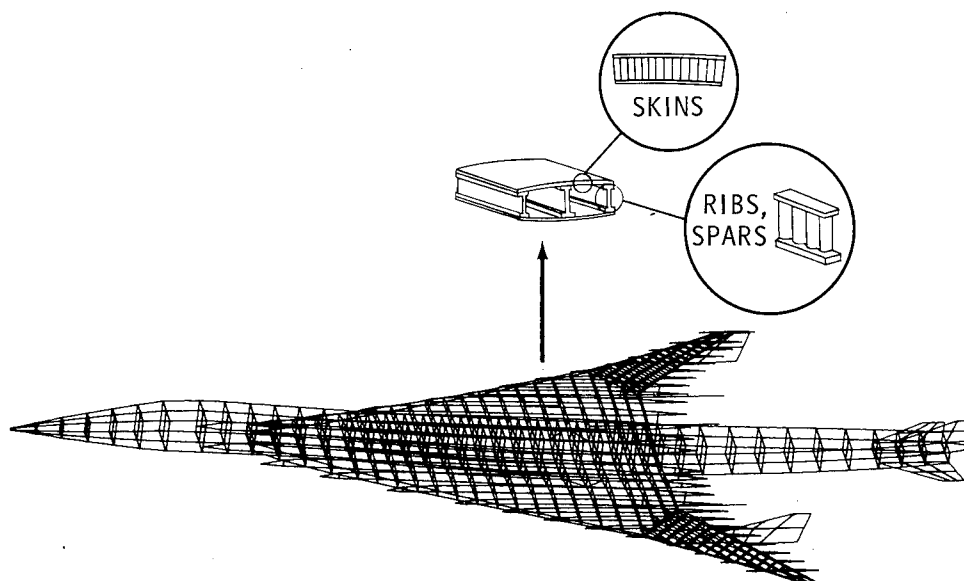


Figure 2.- Finite-element model with details of the wing construction.

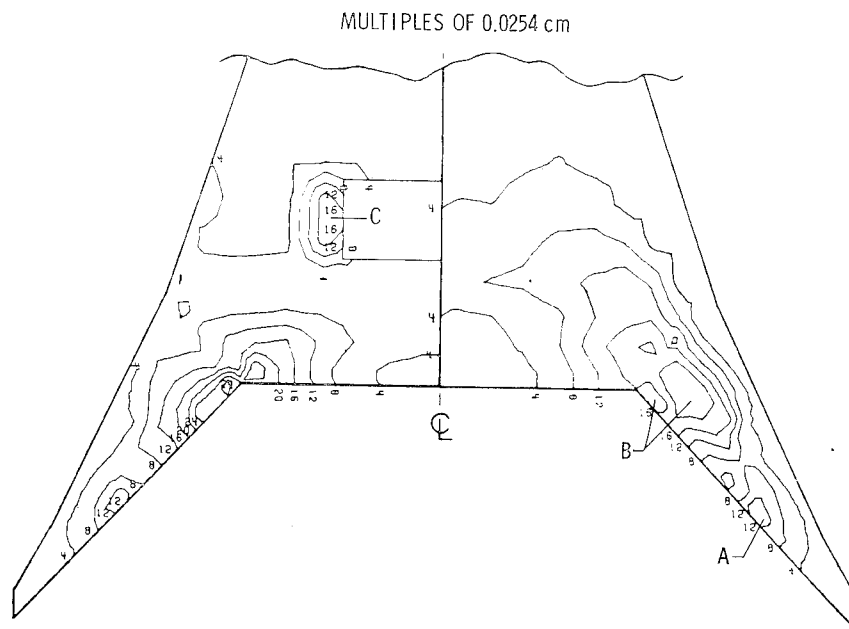


Figure 3.- Strength design thickness distribution.

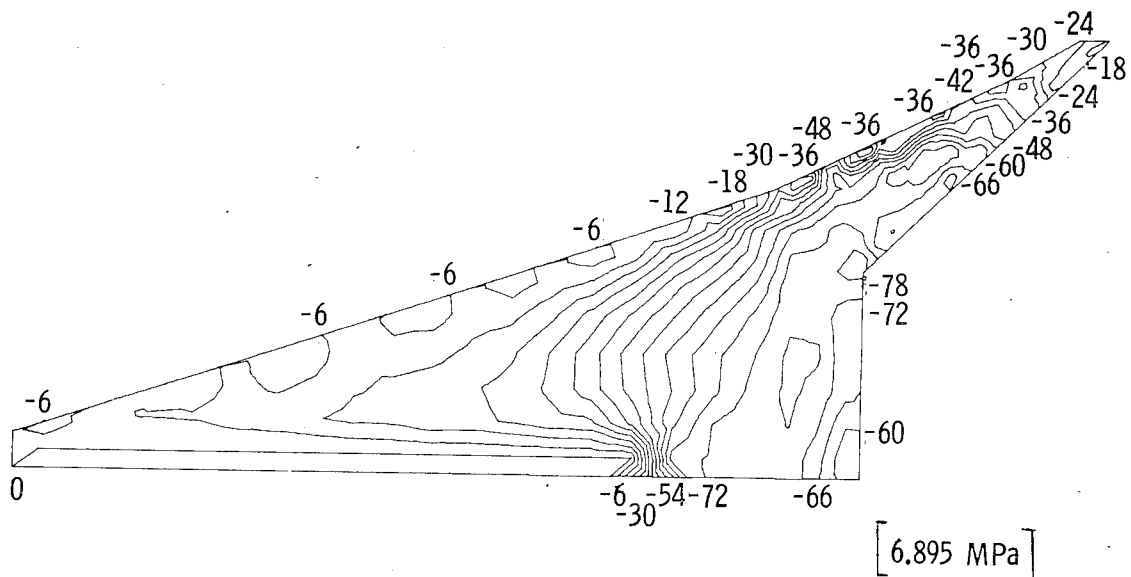


Figure 4.- Minimum (maximum compression) principal stress distribution in the upper cover for the maneuver condition.

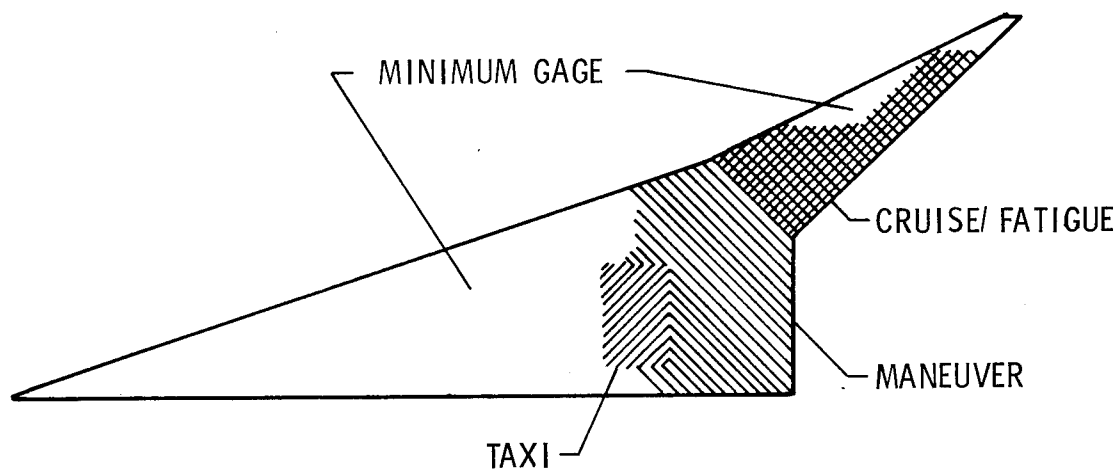


Figure 5.- Critical loading cases for defined wing areas.

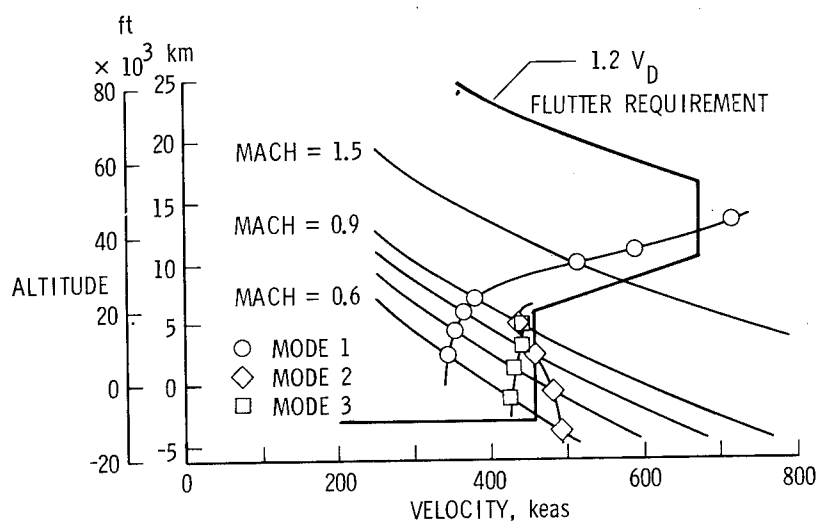


Figure 6.- Flutter boundaries for the strength sized baseline (9.1, E23) configuration, and the required flutter-free envelope.

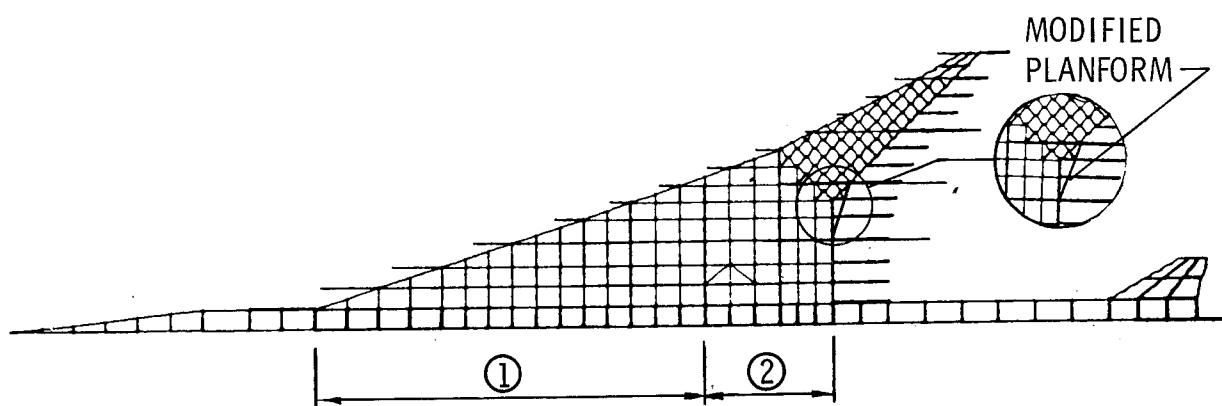


Figure 9.- Modified carry-through and "double crank" (inset) configuration.

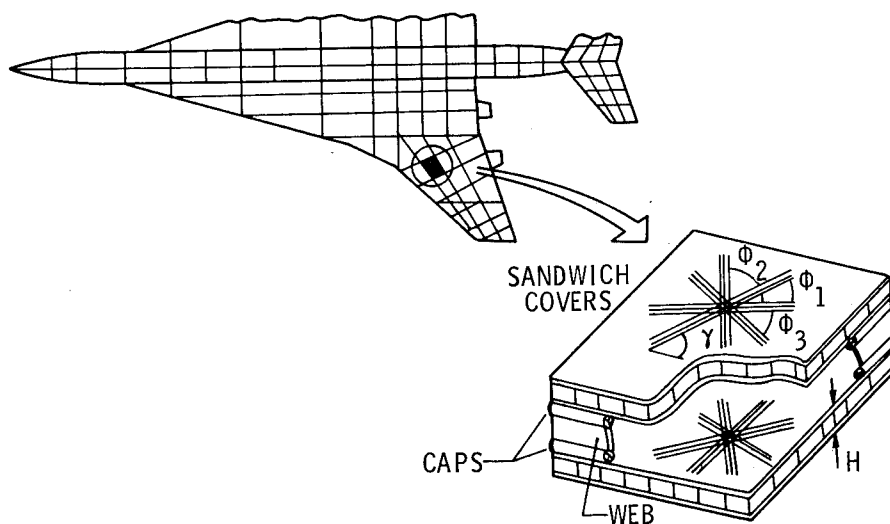


Figure 10.- Composite sandwich wing covers.

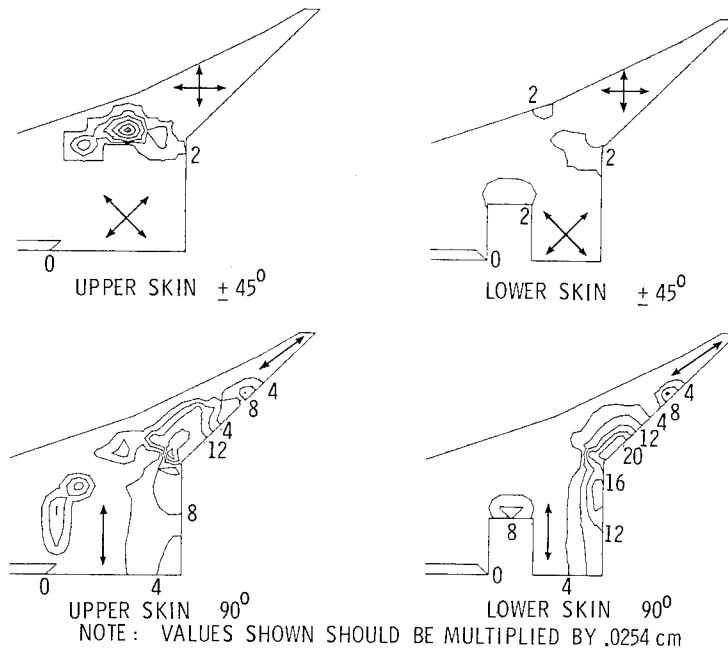


Figure 11.- Strength design thickness distributions of the composite material layers.

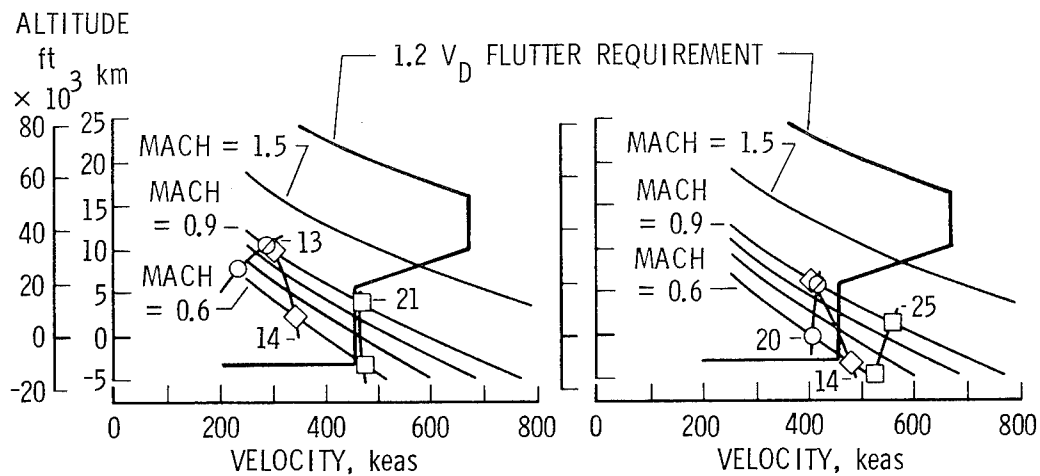


Figure 12.- Flutter deficiency of the strength sized hybrid configuration (variant 11.1.1) for low Young's modulus material (left) and high Young's modulus material (right).

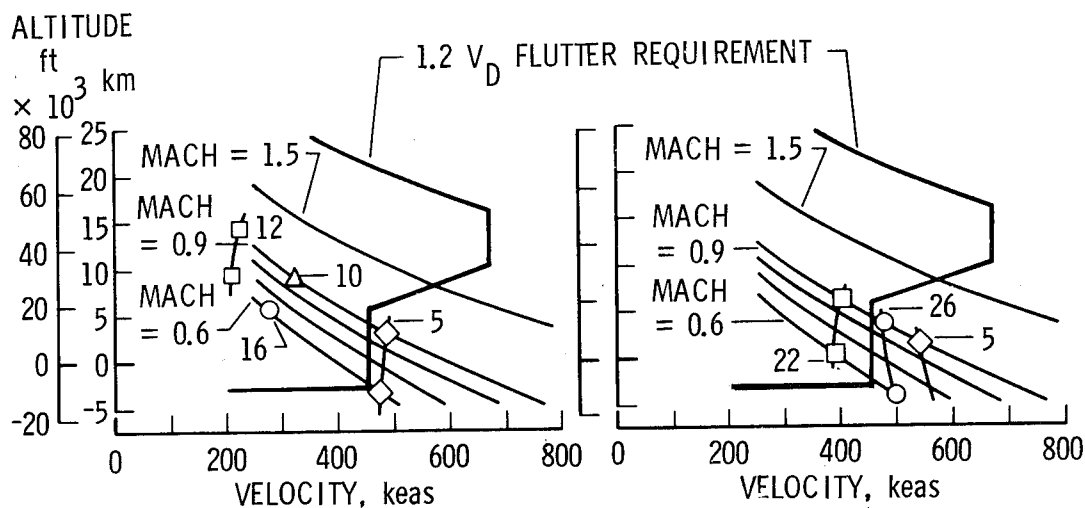


Figure 13.- Flutter deficiency of the strength sized pure composite configuration (11.2) for low Young's modulus material (left), and high Young's modulus material (right).

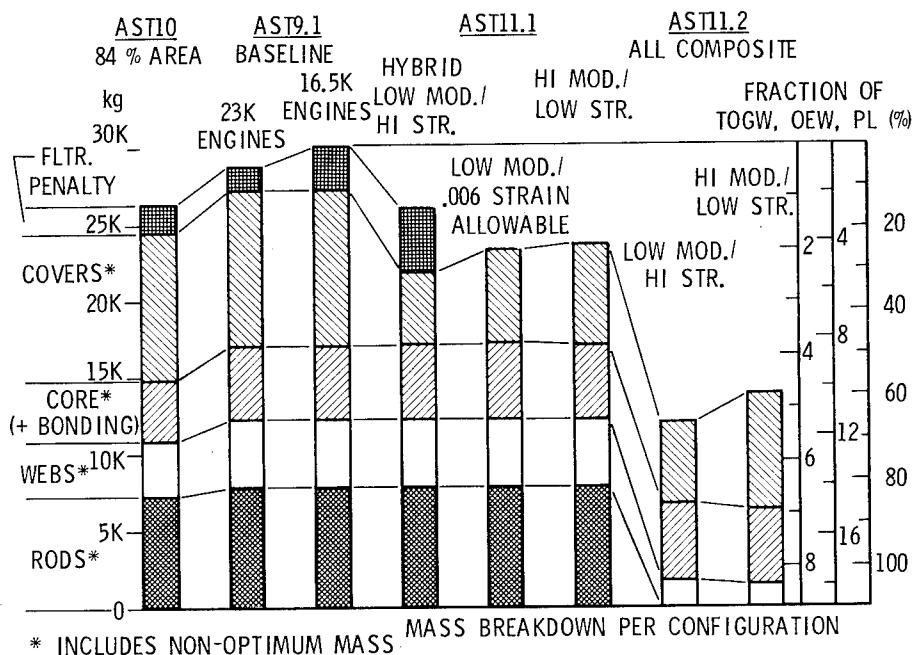


Figure 14.- Comparison of the total structural masses and their components.

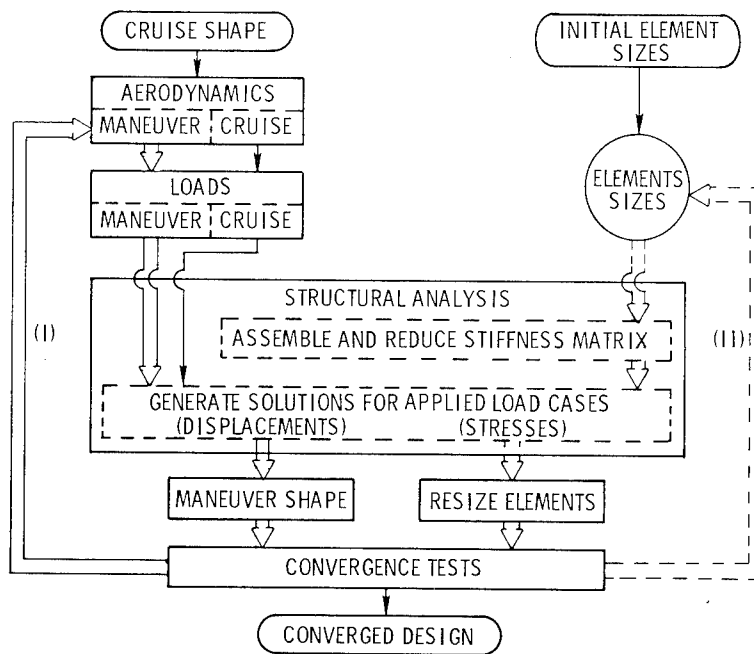


Figure 15.- Iterative procedures for aeroelastic loads computation (loop I) and wing cover resizing (loop II).

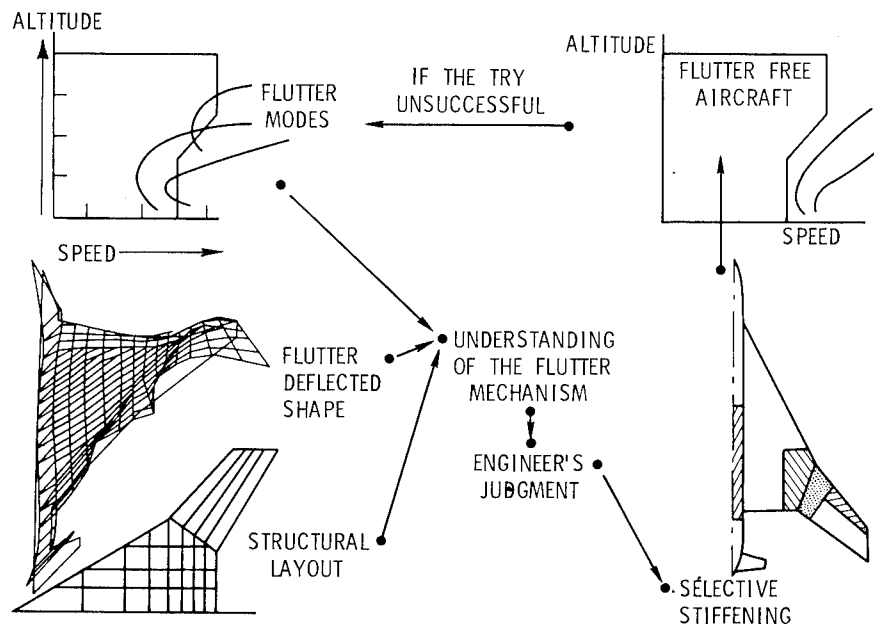


Figure 16.- Trial-and-error flutter fix procedure.

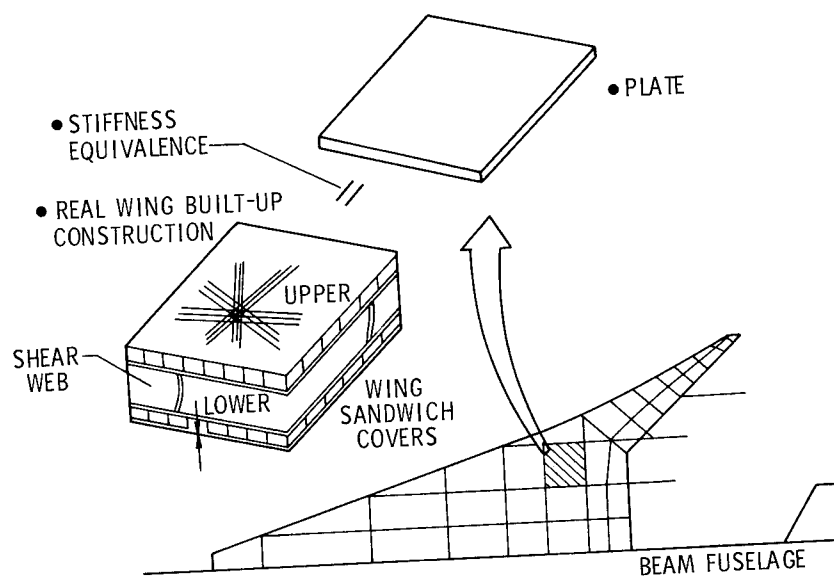


Figure 17.- "Small" model equivalent to "large" model with respect to mass and bending stiffness.

LOADS TECHNOLOGY FOR SUPERSONIC CRUISE AIRCRAFT

Robert C. Goetz
Langley Research Center

SUMMARY

A SCAR Loads Technology Program was initiated in 1973 and includes research in aeroelastic loads, landing loads, acoustic loads, and the measurement of atmospheric turbulence. This paper presents the current status and some results obtained to date for the latter three research areas.

Specifically, a flight program to measure atmospheric turbulence at high altitudes (long wavelengths) in a variety of meteorological conditions is described and some results obtained in high-altitude wind shear are discussed. Results are also presented from wind-tunnel test programs to measure fluctuating pressures associated with over-the-wing engine configurations. Two analyses, a flexible aircraft take-off and landing analysis and an active control landing-gear analysis, have been developed and their capabilities are described. Efforts to validate these analyses with experimental data are also discussed as well as results obtained from parametric studies.

INTRODUCTION

Efficient structural design of a supersonic cruise aircraft is predicated by the accurate knowledge of the critical design loads. Earlier design studies (ref. 1) have indicated the types of critical flight and ground load conditions for the design of typical supersonic cruise aircraft structure and control systems. It was apparent that the critical design conditions for most of the aircraft structure occurred in the transonic speed regime. Critical conditions included balanced maneuvers, abrupt maneuvers, and gusts. Unfortunately, the load prediction methodology is least reliable in this speed regime. Additionally, for high-speed flight, the slender more flexible configurations require more emphasis on landing loads and response, aeroelastic effects, dynamic response to atmospheric turbulence, and fatigue life considerations.

Consequently, a loads program was undertaken to provide an expanded technology which will permit more efficient supersonic cruise aircraft structural design by improved loads and aeroelastic predictive methodology. The SCAR Loads Technology Program is comprised of four elements which include research in aeroelastic loads, landing loads, acoustic loads, and the measurement of atmospheric turbulence. The long range goal of each of these areas is to provide aeroelastic load prediction methodology, develop and validate a take-off and landing analysis including aircraft flexibility and active landing gear design methodology, improved fatigue life prediction methodology, and

to provide a description of the high altitude turbulence environment in a wide variety of meteorological conditions for improved gust loads prediction methodology, respectively. A review of the aeroelastic loads element is given in references 2 to 6. This paper will discuss the remaining three program elements and present the current status and summarize some results obtained to date.

ATMOSPHERIC TURBULENCE

A number of earlier programs have been devoted to measurements of atmospheric turbulence. Results from these programs have, in general, yielded the conclusion that the von Karman description of atmospheric turbulence spectra is valid for the slope of the power spectrum ($-5/3$) at reduced frequencies above about 10^{-3} cycles/m. In the von Karman equation (shown in fig. 1), a value L essentially defines the location of the "knee" in a curve of power spectral density Φ against frequency and thus if σ , the root mean square or intensity level, and L are known, the power spectrum is completely defined. Limitations in both instrumentation and data reduction procedures prevented acquiring data at wavelengths long enough to identify appropriate values of L for the von Karman equation. An example of the significance of the L value for aircraft designers is shown by the vertical bands in figure 1. The primary aircraft response to turbulence is in the rigid body, short period, and Dutch roll modes. For subsonic aircraft such as the 707, B-52, and 747 airplanes which cruise at Mach 0.8 and at altitudes, h , of 11 to 12 km (35 000 to 40 000 ft), the primary response to turbulence is to the right of the knee of the spectral curves for all values of L in the range believed appropriate for consideration. However, for supersonic cruise aircraft, that is, cruise at Mach 2.7 at an altitude of approximately 18 km (60 000 ft), the predicted response is more significantly affected by the L value as can be seen in the figure. Fatigue and ride quality are also important aspects of the aircraft response to atmospheric turbulence. Consequently, a flight measurement program was initiated to determine whether the von Karman equation is appropriate to represent turbulence at the high altitudes (long wavelengths) in various meteorological conditions, and, if so, to define the appropriate L values.

Measurement of Atmospheric Turbulence

The Measurement of Atmospheric Turbulence (MAT) program, being conducted by the Langley Research Center in cooperation with the Dryden Flight Research and Johnson Space Centers, was established to measure all three components of turbulence (vertical, lateral, and longitudinal) over a wide altitude range in different meteorological conditions. It was decided that two sampling aircraft would be required for measurements over the entire range of interest — one airplane covering the range from sea level to 15 km (50 000 ft) altitude and a special high altitude airplane for altitudes above 15 km. The sensors selected required sampling to be done at subsonic

speeds. A B-57B Canberra shown in figure 2 was selected for the sampling up to 15 km and it was decided that a B-57F would be the preferred aircraft for use above 15 km.

The basic measurements of vertical and lateral turbulence components are made by utilizing lightweight balsa vanes mounted on a stiff nose boom. Aircraft motion corrections are accomplished by using onboard inertial platform and rate gyros. The longitudinal turbulence component is made by utilizing a specially designed instrument measuring small pressure fluctuations superimposed on a relatively large nominal pressure. Incremental static pressure is recorded in addition to incremental total pressure in order to be able to account for changes in total pressure which result from airplane altitude variations during a data acquisition period of the flight test.

The equations used for determining time histories of gust velocity are given in reference 7. To obtain power estimates at the extremely low frequencies required (i.e., long wavelengths), narrow spectral "windows" (bandwidths) on the order of 0.02 Hz must be used in the data processing procedure. Such narrow spectral windows introduce wild statistical fluctuations in the power estimates unless relatively long data samples can be obtained. The statistical reliability believed necessary requires on the order of 2^4 to 30 statistical degrees of freedom for the spectral values, which translates to data samples of at least 10 minutes duration. Details concerning the power spectral algorithms employed, and the justification for not prewhitening the time histories for long wavelength analysis are given in reference 8. Instrumentation details and measurement accuracies are given in reference 9. An assessment of the overall instrumentation performance by means of inflight maneuvers, together with assessment of possible low frequency trend-type errors based upon post-flight performance of the inertial platform system, is given in reference 10. A unique feature of this program is the fact that the same instrumentation and data reduction procedure is employed for all measurements covering altitudes from near sea level to about 18 km (60 000 ft) and the various meteorological conditions.

Sampling flights with the B-57B were made in the March 1974 to September 1975 time period. A total of 46 flights were made, 30 in Eastern U.S. within range of the airplane based at Langley AFB, VA, and 16 in Western U.S. within range of the airplane based at Edwards AFB, CA. A full-time project meteorologist provided functions of coordinating and planning flights, observing from the rear seat during the flights, and conducting post-flight analyses to document pertinent meteorological parameters and to define the meteorological condition where turbulence was encountered.

A summary of data obtained is given in table I with the number of data runs to be processed associated with six meteorological conditions. Data processing is currently under way. A typical sample of turbulence categorized as high-altitude wind shear, which is a predominate type of encounter expected for high-altitude supersonic cruise aircraft, will be discussed.

High-Altitude Wind Shear Result

The time histories for the high-altitude wind shear case are presented in figure 3. The intensity of the turbulence for all three components u ,

v, and w is gradually increasing with time. Such nonhomogeneous (or nonstationary) behavior has generally been believed to be responsible for considerable rounding or smoothing of the spectral knee. The recent work of reference 11, however, indicates that unless the change in intensity is considerably more abrupt than shown here, little effect should be observable in the spectra. It is obvious that significant low frequency power is present in the horizontal components. This is assumed to be directly attributable to the changing horizontal wind field. The low frequency content can be thought of as a modulation of the mean value with a typical high-frequency amplitude-modulated random process superimposed. (A model of turbulence which includes mean modulation has been suggested by Reeves, et al. in ref. 12.) No pronounced low frequency power is noted in the vertical component. These observations are substantiated in the corresponding power spectra shown in figure 4.

The power spectra curves presented in figure 4 are comparable with those of figure 1 except that the results have not been normalized; i.e., the area under the curve is equal to the variances, or σ^2 . The abscissa values were obtained by converting Hz to inverse wavelength by using the average true airspeed for each data run of the flight test. Superimposed on the data are shown theoretical von Karman type curves with selected L values. Note that the slopes of the curves match at the higher frequencies. Although an L value of 300 m (1000 ft) appears to be appropriate for the vertical component, L values of greater than 1800 m (6000 ft) would apply for the horizontal components directly reflecting the large power content at low frequencies. Additional data from this program are presented and discussed by Rhyne, et al. for terrain-related rotor, thermal convective, and mountain wave turbulence cases in reference 13.

Presently, a B-57F aircraft is being modified to accept the MAT instrumentation system and sampling flights above 15 km (50 000 ft) are scheduled during the first part of 1977.

ACOUSTIC LOADS

Supersonic cruise aircraft configurations with engines located over the wing and forward have been proposed to obtain increased lift for low speed flight, decreased ground noise by wing shielding, improved flutter behavior, and improved center-of-gravity locations. Location of the engines over the wings has the disadvantage of exposing the fuselage and wing upper surface to intense fluctuating pressures from the high-velocity engine exhaust. Acoustic fatigue and excessive cabin noise may then be difficult to prevent. In order to provide information on the fluctuating pressures, several small-scale model investigations have been conducted.

Test Program

Figure 5 indicates two of the models tested. The model on the left was used by Willis in an investigation conducted in the Langley anechoic facility. The model was a 0.03-scale planform of the SCAT-15. The jet was a Mach 1.5,

fully expanded, convergent-divergent nozzle operating on cold air and at zero forward speed. The jet exit was located near the wing leading edge, one exit diameter above the wing surface and directed 3° downward toward the wing surface. The model on the right has a Mach 1.4 plug nozzle and is currently being tested statically and with forward velocity to determine the effects of engine location and engine exhaust impingement angle on the resulting fluctuating pressure loads on the wing surface.

Results

Figure 6 shows fluctuating pressure loadings measured on the SCAT-15 wing with the $M = 1.5$ engine model. Also shown on the figure are calculated loadings for the same engine model mounted beneath the wing at the trailing edge. These noise loading contours were calculated using AGARD design data charts. The maximum 130 dB loadings for the trailing edge engine location is below the predicted levels that would be generated by a supersonic boundary layer and therefore of little interest to the designer. However, the 167 dB loading with the over-the-wing location is high; therefore, design attention will be required to provide a reasonable fatigue-life design and it also suggests that additional design attention will be required to achieve acceptable cabin noise levels. The jet velocity for this test was about 440 m/s; current considerations are for supersonic jets having velocities of 845 m/s. Therefore, scaling the data to this higher velocity by using a semiempirical method in reference 14 indicates a maximum level for the scaled loads of 181 dB. Figure 7 shows a sample one-third-octave spectrum of measured data that has been scaled to full-scale aircraft frequency, a jet velocity of 845 m/s, and corrected to cruise altitude density. The levels shown for the 50 to 1000 Hz range usually considered in fatigue life design are high enough to indicate that a serious penalty is incurred for over-the-wing engine location if a high velocity engine is used.

LANDING LOADS

Dynamic loads in aircraft resulting from the landing impact phase and the rollout and take-off phases of aircraft operations on rough runways, are recognized as significant in contributing to structural fatigue. In addition, the associated induced vibrations contribute to ground handling problems and crew and passenger discomfort. Such vibration problems have been encountered with conventional transport aircraft and have required modifications to the landing gear systems to improve ride and handling qualities subsequent to the aircraft's entry into service. Ground-induced dynamic loads and vibrations and the resulting problems will be magnified for supersonic cruise aircraft because of the increased structural flexibility of the slender-body, thin-wing configuration and the higher take-off and landing speeds. Consequently, an accurate prediction of the ground-induced loads and vibrations and a method for alleviating excessive loads and motions applied to the airframe are needed. The application of active control landing-gear systems in the design of supersonic cruise aircraft could help to alleviate these dynamic loads and vibrations and provide the aircraft with longer operational

life, safer ground handling characteristics, and more acceptable ride quality.

Active control systems have been applied to ground vehicle suspension systems and are being extensively investigated for application to aircraft aerodynamic controls. Some analytical studies have also been conducted to determine the feasibility of applying active controls to aircraft landing-gear systems. These studies have been primarily concerned with the rollout or taxiing modes of aircraft operations. There is a dearth of information available, however, for actively controlling loads transmitted to the airframe by the landing gear during the impact phase, and no published information is available containing experimental data on actively controlled landing gears.

Experimental and analytical research and development is being conducted by McGehee and Carden of the Langley Research Center to obtain accurate predictions of ground-induced loads and vibrations and to develop the design methodology for active control landing-gear concepts. This section of the paper will describe the prediction methods developed, the validation results to date through comparison with experiment, and planned work in this area.

Flexible Aircraft Take-off and Landing Analysis (FATOLA)

Improved prediction of the airframe structural response is being accomplished with an analysis called FATOLA which provides a comprehensive simulation of the aircraft take-off and landing modes. As illustrated in figure 8, impact loads, runway induced loads, steering loads, perturbation or operational loads (including thrust reversal, braking, aerodynamic loads and asymmetric impact capability) and airframe flexibility characteristics, are combined to make up the total aircraft response analysis. Basically, the analysis can simulate an aircraft either as a six-degree-of-freedom rigid body or as a flexible body over a flat planet. In the flexible body option, the airframe flexibility is represented by the superposition of from one to 20 free-free vibratory modes (input to the program) on the rigid body motions. In the rigid body option, comprehensive information on the airframe, state of maneuver logic, autopilots and control response, and dynamics of the landing gears are output. In the flexible body option, elastic body and total (rigid body plus elastic body) displacements, velocities, and accelerations at up to 20 points on the aircraft are also obtained. Complete details of the computer program are given in references 15 and 16.

Rigid body simulation for X-24B vehicle.— To verify the simulation capabilities of the FATOLA computer program rigid body option, the X-24B manned lifting body research vehicle was selected since unpublished experimental landing loads and motions data were available for this vehicle. As shown in figure 9, this vehicle is delta-shaped with blended wings and a flat bottom. The X-24B was used in a joint NASA/USAF flight research program to explore the subsonic to low supersonic performance characteristics with emphasis on the landing maneuver.

Flight test data from an asymmetric landing of the X-24B were selected for the X-24B simulation study. Pertinent touchdown parameters for the unpowered X-24B landing were: a sink rate of 0.49 m/s (1.6 fps); a ground speed of 87.1 m/s (286 fps); a pitch angle of 13.4° with a nose-over pitch rate of $-0.8^\circ/\text{sec}$; a roll angle of 2° right with a $4.4^\circ/\text{sec}$ right roll rate. The landing surface was assumed to be flat since the actual landing surface inclination and perturbations were undefined.

Typical analytical vertical loads and the associated gear strokes predicted by using the rigid body option of FATOLA are compared with experimental flight test data in figure 10. In figure 10, the results for the right main and nose gears show that the levels of load generally compare well throughout the first 3.5 seconds of impact and rollout time history. However, the predicted loads indicate a slightly higher initial peak and a slightly lower second peak for the main gear as compared with the experimental data. Also included in figure 10 are the analytical and experimental time histories of gear strut stroke for the right main and nose gears. The overall agreement of both magnitude and variation with time between the predicted strut strokes and flight test data is excellent. Comparison of other parameters such as pitch rate, etc. can be found in reference 16.

Flexible body simulation for YF-12 aircraft.— The aircraft used to validate the capabilities of the FATOLA flexible body option and to verify the analysis was the YF-12 aircraft shown in figure 11. This aircraft has a modified delta wing planform and is powered by two jet engines. This fully instrumented, large, flexible, supersonic research vehicle was used in a joint DFRC/LaRC landing loads and motions program recently completed at the Dryden Flight Research Center (DFRC).

The flexibility of the aircraft was represented with the first 10 modes available from a two-dimensional finite-element representation of an aircraft in the YF-12 series. The flexible modes are only generic for the YF-12 class of aircraft and have just vertical modal deflections; they are limited in the wing directions to symmetric modes. Work is currently underway to obtain both symmetric and antisymmetric modal data from a three-dimensional finite-element model of the specific test aircraft for which landing data have been obtained.

Flight test data for an asymmetric landing of the YF-12 aircraft were also selected for the YF-12 simulation study. The touchdown parameters for the flight were: a sink rate of 0.305 m/s (1.0 fps); a pitch angle of 8.3° with a nose-over pitch rate of $-0.2^\circ/\text{sec}$; and a roll angle of 1.2° right. The landing surface was the Edwards Air Force Base runway and the surface perturbations as a function of runway distance were measured prior to the test program.

Typical predictions of the YF-12 aircraft nose gear vertical load are presented in figure 12. Predictions using the rigid body option indicate three almost complete unloadings with six major peaks between 6-1/2 and 10 seconds in time. However, using the flexibility option altered the predicted load pattern to only four major peaks over the same time span. Comparison of the flexible prediction with flight test data indicates excellent agreement in magnitude and

loading pattern and illustrates the importance of structural flexibility in altering the loading behavior of this type of aircraft. Good correlation was also obtained for structural accelerations along the body of the aircraft, as well as for other parameters.

Active Control Landing Gear Analysis (ACOLAG)

An analysis has been developed for the study of actively controlled landing-gear systems. This analysis considers the following parameters shown in figure 13: sinusoidal or random runway roughness; empirical tire-force deflection characteristics; automatic (anti-skid) braking; oleo-pneumatic strut with fit and binding friction; closed-loop, series-hydraulic control with feedback; first-mode wing bending and torsional structural elastic characteristics; and theoretical subsonic aerodynamics. This model has been validated for conventional (passive) gears by comparing calculated results with experimental data obtained from vertical drop tests in reference 17.

The shock strut force computed by using the active control landing gear analysis, for a passive gear, is in good agreement with the experimental data (within the accuracy limits cited for the experimental shock strut force of ± 2.224 kN (± 500 lbf)). Other comparisons of computed and experimental ground forces and the relative motions of the airplane and gear show as good or better agreement as that shown for the shock strut forces. The active control landing-gear analysis is, therefore, valid for predicting landing loads and motions of an airplane during symmetric impact or rollout.

A study has been conducted for the series-hydraulic control gear concept shown in figure 14. This gear employs a hydraulic control actuator in series with a simply modified version (modified orifice tube and strut static extension) of a passive gear from a 2721.6 kg (6000 lb) class general aviation aircraft.

Figure 15 presents computed results from landing impact and rollout simulations of passive and modified version active gears. As shown on the figure, the active control gear reduced the wing force by 18 percent during the initial landing impact and 80 percent during secondary impact of the main gear, due to nose gear impact and rollout, and required an increase in strut stroke of 25 percent. If an aluminum wing structure with a full-reversed stress of 269 MPa (39 000 psi) is assumed when employing the passive gear, the fatigue life would be approximately 20 000 cycles. For the aluminum wing structure, the 18-percent reduction in wing force would correspond to a fatigue life of 54 000 cycles, a factor of approximately 2.7 times that of the passive gear accounting only for the impact phase. The maximum control flow rates required during this simulation were 0.31 m^3 (83 gallons) per minute for removal of fluid from the strut and 0.23 m^3 (60 gallons) per minute for the addition of fluid to the strut.

Presently, a passive gear shown in figure 16 is undergoing modifications and the active control electronic system is being designed and fabricated so that these analytically predicted results can be verified through testing at the NASA Langley landing loads track. The actively controlled gear system will subsequently be tested on a full-scale general aviation aircraft to further demonstrate the concept. Concurrent with the experimental effort, another active control gear concept which has the control installed parallel with the shock strut is being analytically investigated.

In addition, the FATOLA computer program is being modified to include ACOLAG; and thus provide a valid, comprehensive, multi-degree-of-freedom landing and take-off analysis for use in the study and design of landing-gear systems for supersonic cruise aircraft.

CONCLUDING REMARKS

Since the SCAR Loads Technology Program was initiated in 1973, accomplishments to date and results in three of the program areas discussed in this paper are as follows:

(1) Measurement of atmospheric turbulence: Data have been collected from 46 flights for 76 turbulence encounters between 0.3 and 15 km (1000 and 50,000 ft) altitude. The associated meteorological conditions have been identified. The most prevalent meteorological condition for turbulence encountered was the high-altitude wind shear and for this case the following observations are made:

- (a) For all encounters, the $-5/3$ slope of the von Karman turbulence model over the short wavelength region was experimentally confirmed.
- (b) The von Karman turbulence model also appears to be appropriate for the vertical component at the longer wavelengths with an integral scale value of 300 m ($L = 1000$ ft).
- (c) However, for the horizontal components, the very large power obtained at the long wavelengths makes it doubtful whether the von Karman model is applicable in this region. If it is, integral scale values greater than 1800 m ($L > 6000$ ft) are required.

Results from this program should assist in clarifying the nature of the power content of atmospheric turbulence at low frequencies (long wavelengths), and will aid designers of supersonic cruise aircraft.

(2) Acoustic loads: Small-scale static model tests have been conducted on over-the-wing engine configurations to measure fluctuating surface pressures in the jet exhaust impingement area. Variables tested include jet exit Mach number, nozzle deflection angle, engine location above the wing and spanwise and chordwise placement. Results indicate that overall sound pressure levels (OASPL) greater than 160 dB occur in the jet impingement area over large regions of the model surface. These overall levels when extrapolated to full-scale values are high enough to require considerable attention in the design of a wing to achieve acceptable acoustic fatigue lifetime.

(3) Landing loads: A flexible aircraft take-off and landing analysis (FATOLA) has been developed and correlations between X-24B and YF-12 flight test data and analytical results indicate that the analysis is a valid and versatile tool for the study of landing loads and motions of aircraft.

An active control landing gear analysis (ACOLAG) has been developed and verified for passive, conventional landing-gear systems. Parametric studies for a series-hydraulic active control gear concept using ACOLAG indicate the feasibility of the concept and potential load alleviations during the landing phase are shown to improve aircraft fatigue life, ground handling and crew and passenger comfort. Experimental full-scale tests using a series-hydraulic active control gear system are to be performed to validate ACOLAG, and other active control gear concepts are being analytically evaluated. Once ACOLAG has been validated, it is planned to combine this capability into FATOLA.

REFERENCES

1. Manro, M. E.; Moulijn, J. P.; and Knittel, J. D.: SST Technology Follow-On Program - Phase I: Pre-sure Distributions on a Delta Wing Horizontal Stabilizer Combination at Mach Numbers from 0.3 to 2.9 - Volume 1 Summary Report. FAA-SS-72-30-1, July 15, 1972.
2. Manro, M. E.; Tinoco, E. N.; and Bobbitt, P. J.: Comparisons of Theoretical and Experimental Pressure Distributions on an Arrow-Wing Configuration at Transonic Speeds. NASA SP-347, 1975.
3. Manro, M. E.; Manning, K. J. R.; Hallstaff, T. H.; and Rogers, J. T.: Transonic Pressure Measurements and Comparison of Theory to Experiment for an Arrow-Wing Configuration - Summary Report. NASA CR-2610, 1975.
4. Manro, M. E.; Bobbitt, P. J.; and Rogers, J. T.: Comparisons of Theoretical and Experimental Pressure Distributions on an Arrow-Wing Configuration at Subsonic, Transonic, and Supersonic Speeds. AGARD Fluid Dynamics Panel Symposium, Moffett Field, CA, September 27-29, 1976. AGARD Preprint 204.
5. Bobbitt, Percy J.; and Manro, Marjorie E.: Theoretical and Experimental Pressure Distributions for a 71.2° Swept Arrow-Wing Configuration at Subsonic, Transonic, and Supersonic Speeds. Proceedings of the SCAR Conference, NASA CP-001, 1977. (Paper no. 5 of this compilation.)
6. Murrow, H. N.; and Rhyne, R. H.: The MAT Project - Atmospheric Turbulence Measurements with Emphasis on Long Wavelengths. Proceedings of the 6th Conference on Aerospace and Aeronautical Meteorology, American Meteorological Society (El Paso, TX), November, 1976, pp. 313-316.
7. Keisler, S. R.; and Rhyne, R. H.: An Assessment of Prewhitening in Estimating Power Spectra of Atmospheric Turbulence at Long Wavelengths. NASA TN D-8288, 1976.
8. Meissner, C. W., Jr.: A Flight Instrumentation System for the Acquisition of Atmospheric Turbulence Data. NASA TN D-8314, 1976.
9. Rhyne, R. H.: Flight Assessment of Atmospheric Turbulence Measurement System with Emphasis on Long Wavelengths. NASA TN D-8315, 1976.
10. Mark, W. D.; and Fisher, R. W.: Investigation of the Effects as Nonhomogeneous (or Nonstationary) Behavior on the Spectra of Atmospheric Turbulence. NASA CR-2945, 1976.
11. Reeves, P. M.; Joppa, R. G.; and Ganzer, V. M.: A Non-Gaussian Model of Continuous Atmospheric Turbulence Proposed for Use in Aircraft Design. NASA CR-2639, 1976.

12. Rhyne, R. H.; Murrow, H. N.; and Sidwell, K. W.: Atmospheric Turbulence Power Spectral Measurements to Long Wavelengths for Several Meteorological Conditions. Aircraft Safety and Operating Problems, NASA SP-416, 1976, pp. 271-286.
13. Guinn, W. A.; Balena, F. J.; Clark, L. R.; and Willis, C. M.: Reduction of Supersonic Jet Noise by Over-the-Wing Engine Installation. NASA CR-132619, April 1975.
14. Guinn, W. A.; Balena, F. J.; and Soovere, J.: Sonic Environment of Aircraft Structure Immersed in a Supersonic Jet Flow Stream. NASA CR-144996, June 1976.
15. Dick J. W.; and Benda, B. J.: Addition of Flexible Body Options to TOLA Computer Program. NASA CR-132732, September 1975.
16. Carden, H. D.; and McGehee, J. R.: Validation of FATOLA Computer Program Using Flight Landing Data. AIAA Paper No. 77-404, Mar. 1977.
17. McGehee, J. R.; and Carden, H. D.: A Mathematical Model of an Active Control Landing Gear for Load Control During Impact and Rollout. NASA TN D-8080, January 1976.

TABLE I.- SAMPLING SUMMARY OF B-57B FLIGHTS
 [46 FLIGHTS WERE MADE BETWEEN MARCH 1974 AND SEPT. 1975]
 (30 EASTERN U.S. AND 16 WESTERN U.S.)

TURBULENCE CATEGORY	NUMBER OF DATA RUNS
TERRAIN RELATED, ROTOR	14 (6 FLIGHTS)
THERMAL , CONVECTIVE	8 (2 FLIGHTS)
NEAR THUNDERSTORMS	12 (2 FLIGHTS)
JET STREAM AND HIGH-ALTITUDE WIND SHEAR*	27 (6 FLIGHTS)
MOUNTAIN WAVES	8 (4 FLIGHTS)
ISOLATED SITUATIONS	7 (2 FLIGHTS)

* CASE SELECTED FOR REVIEW IN THIS PAPER

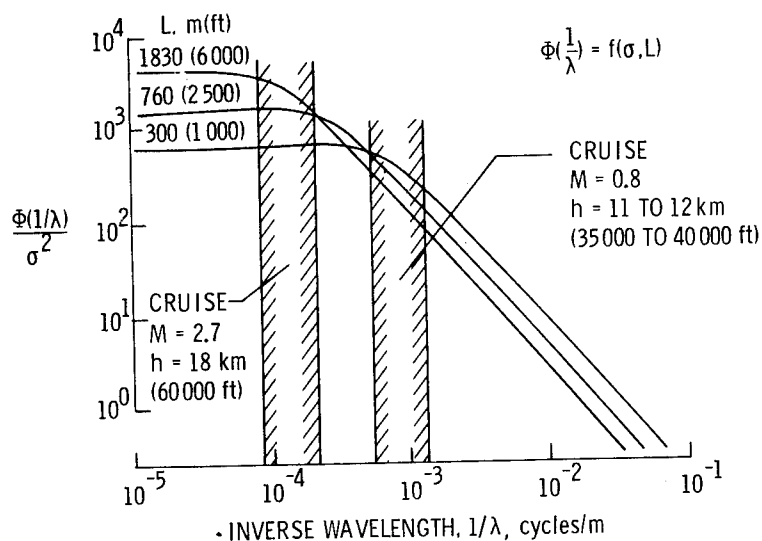


Figure 1.- Theoretical power spectra. Von Karman turbulence model.

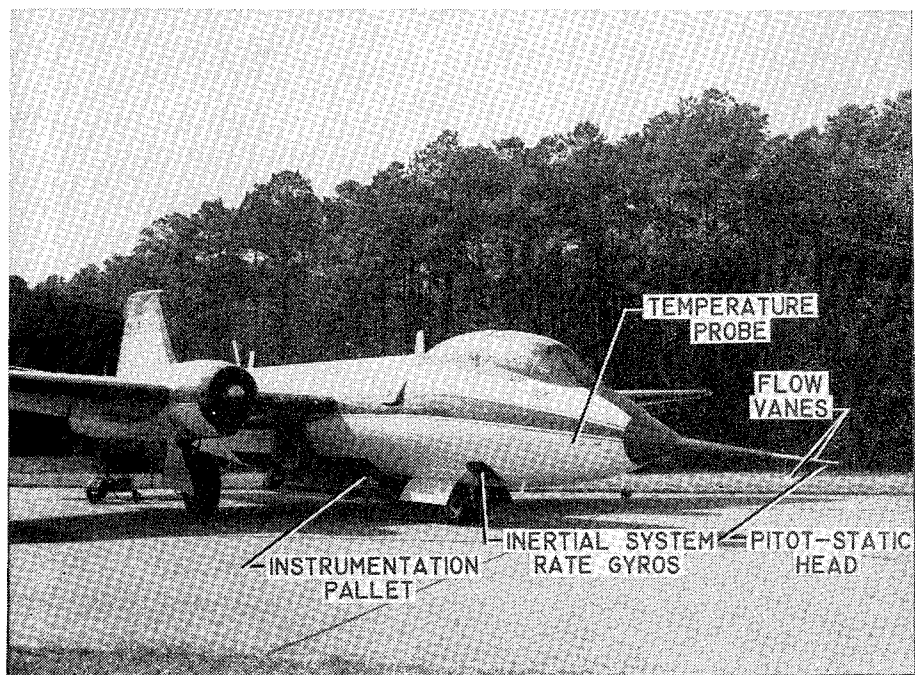


Figure 2.- B-57B instrumented airplane.

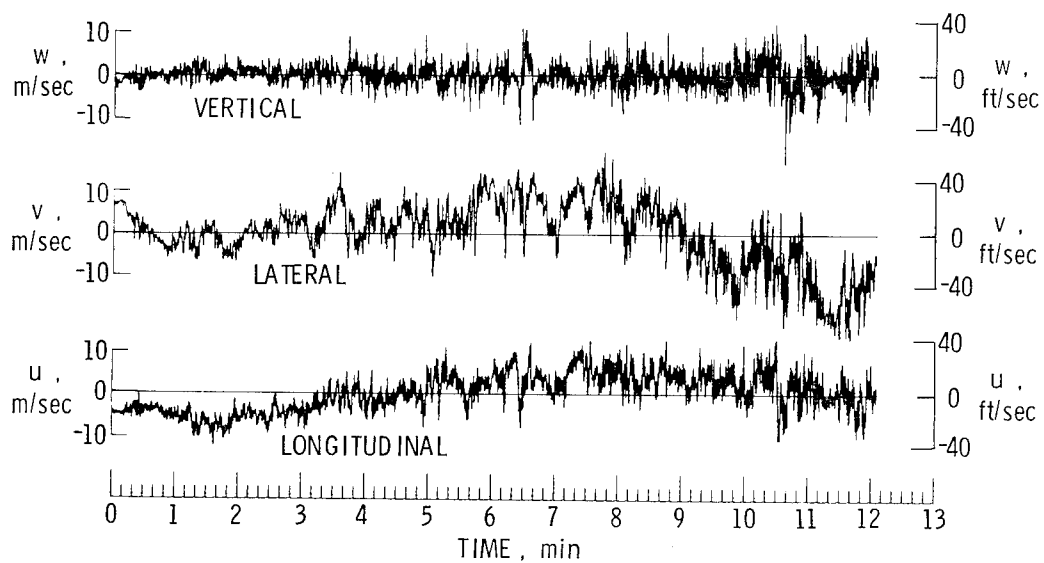


Figure 3.- Turbulence time histories. High altitude wind shear.

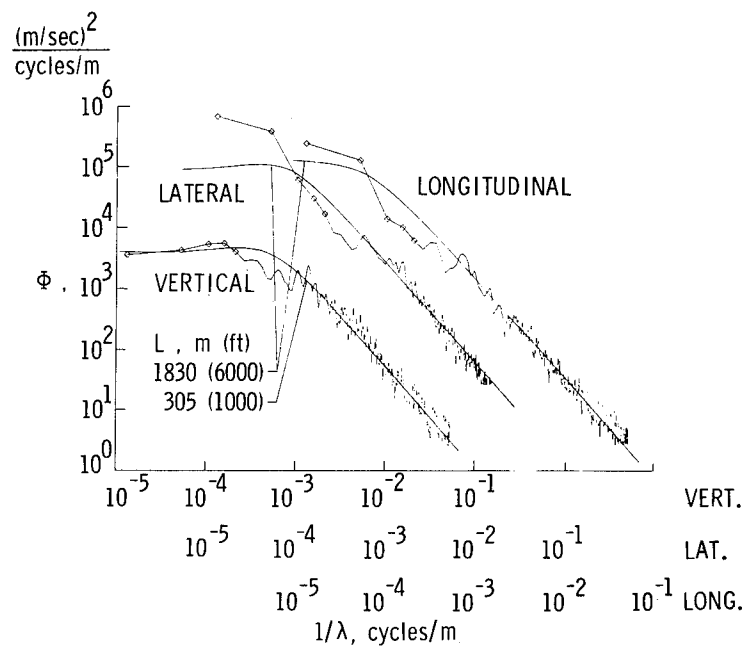
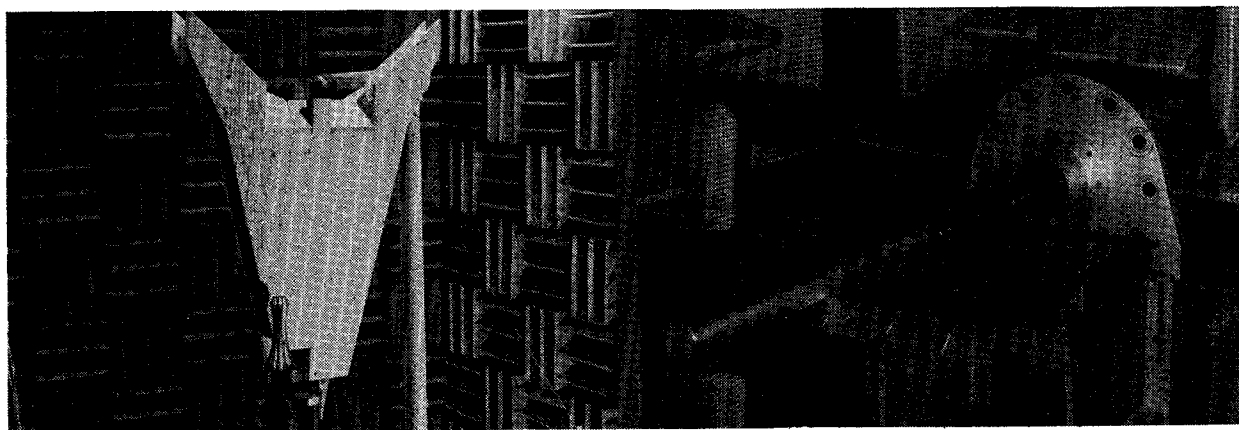


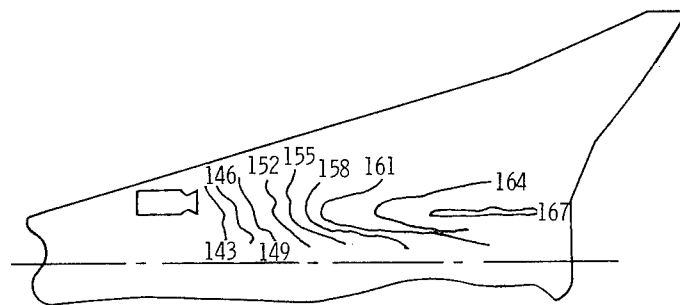
Figure 4.- Power spectral density. High altitude wind shear.



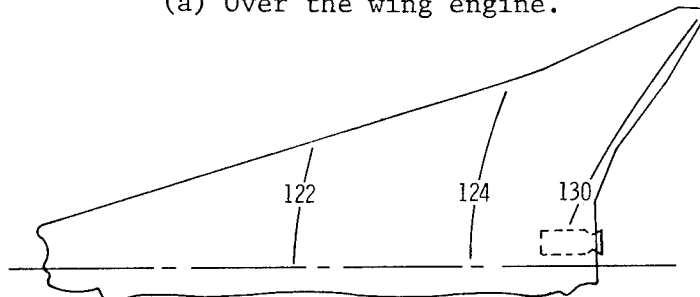
M = 1.5 convergent-divergent nozzle

M = 1.4 nozzle

Figure 5.- Acoustic model tests on over-the-wing engine configurations.



(a) Over the wing engine.



(b) Under the wing engine.

Figure 6.- Fluctuating pressure contours, dB.

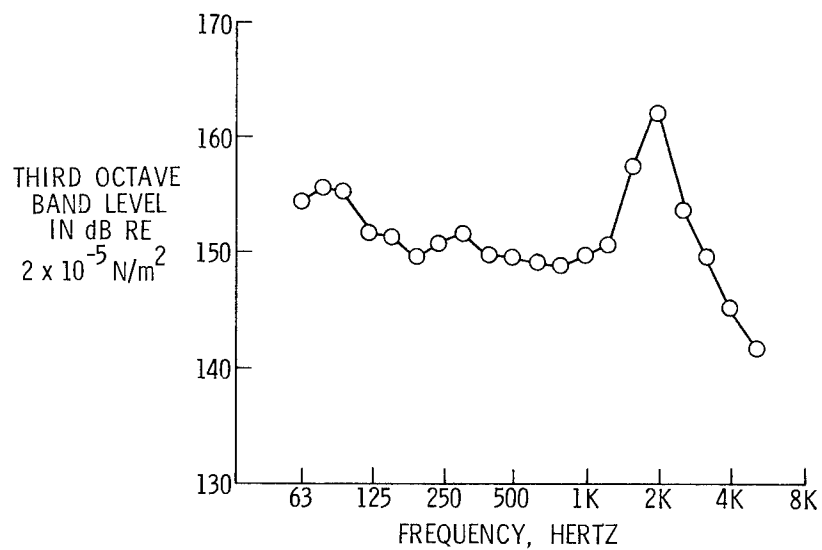


Figure 7.- Full-scale spectrum of measured data.

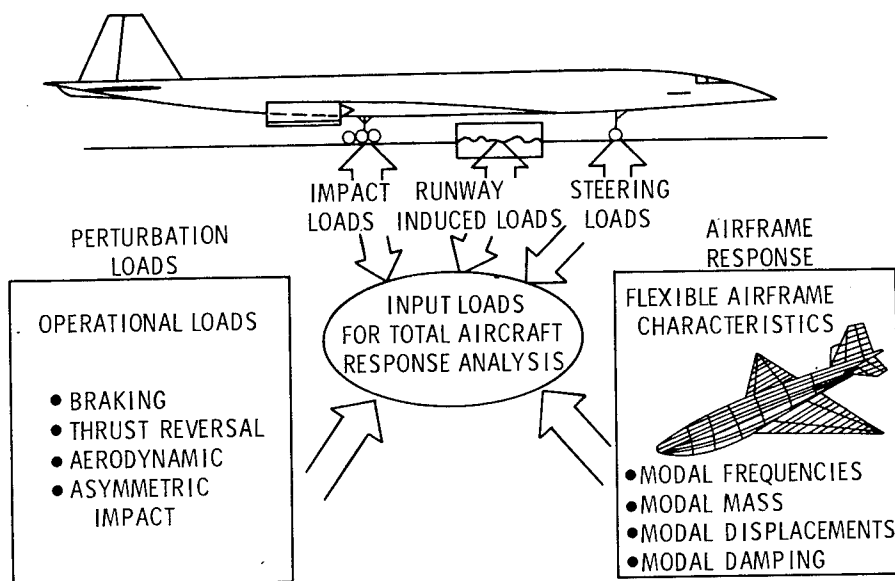


Figure 8.- Flexible aircraft take-off and landing analysis (FATOLA).

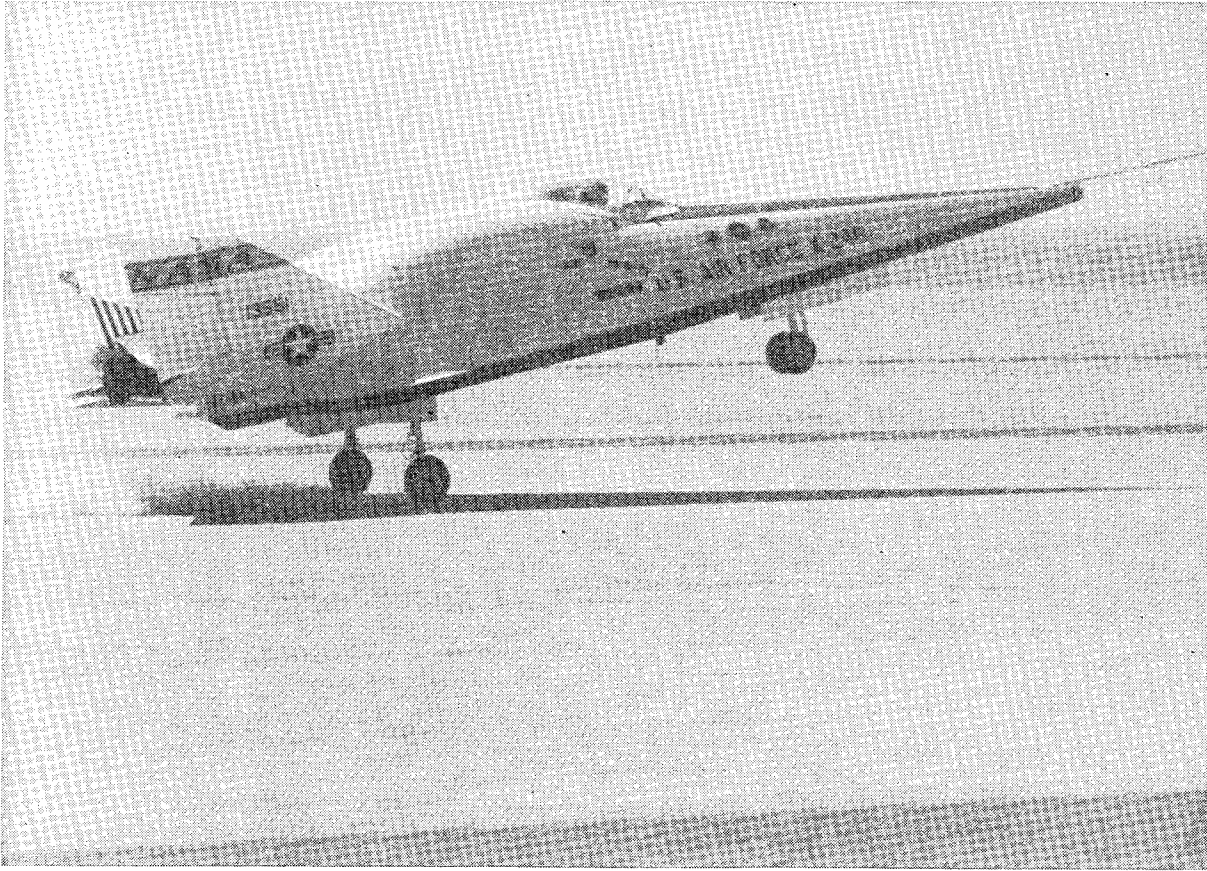


Figure 9.- X-24B landing flight test.

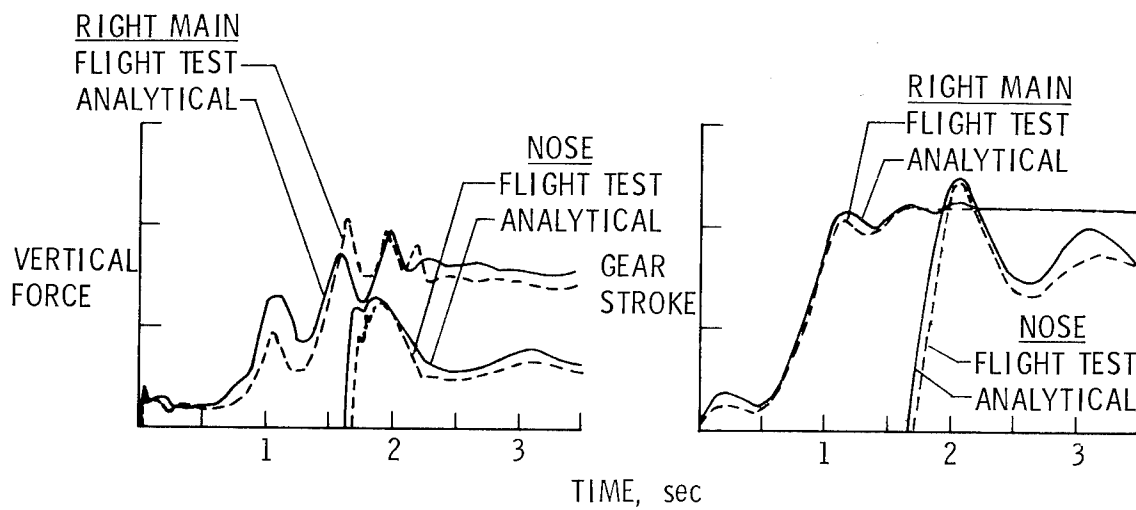


Figure 10.- X-24B experimental compared with analytical results.

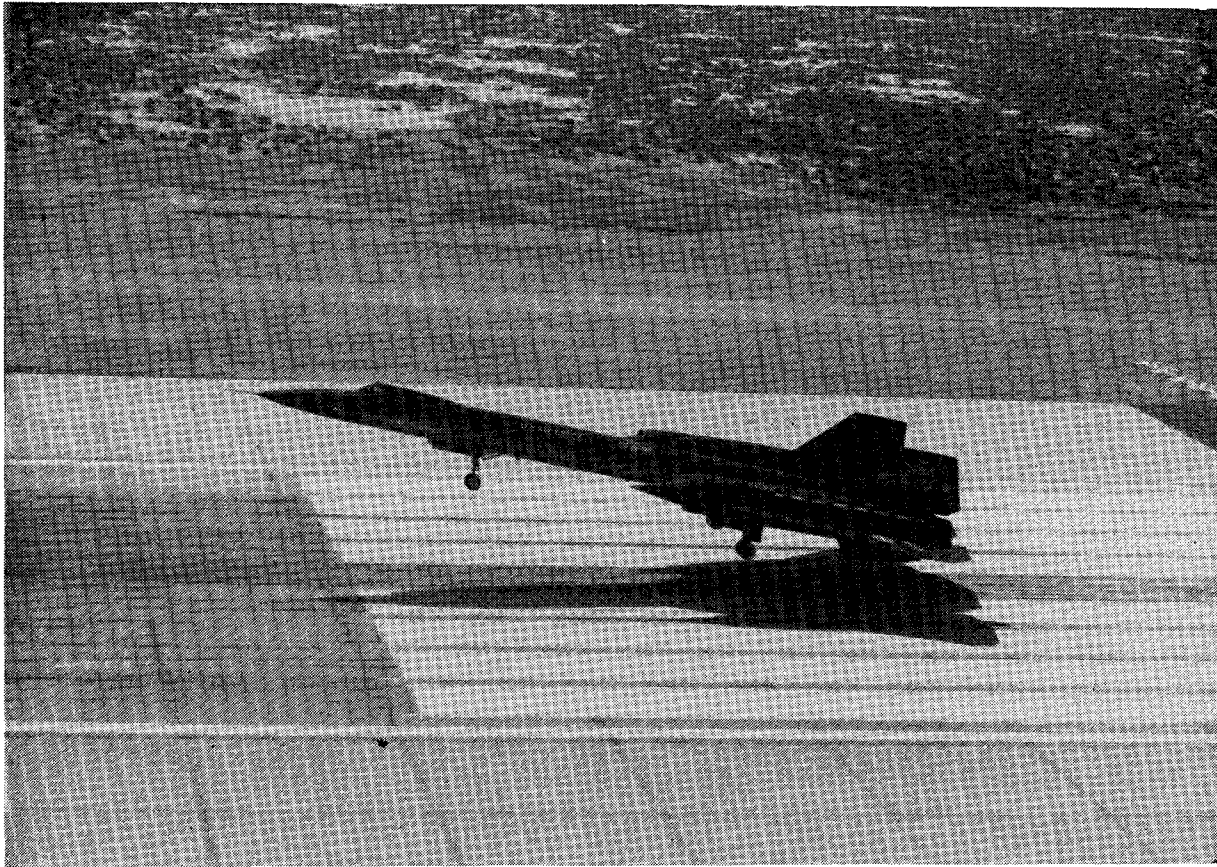


Figure 11.- YF-12 landing flight test.

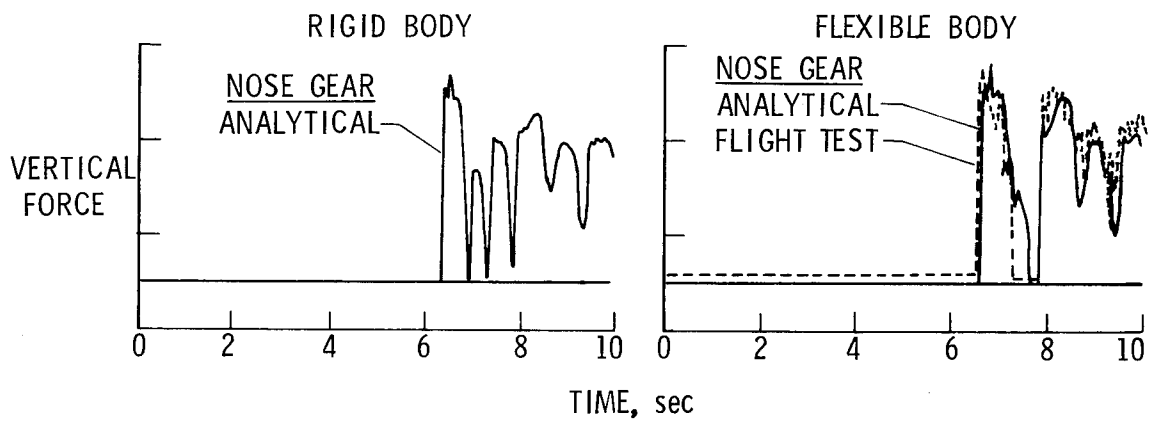
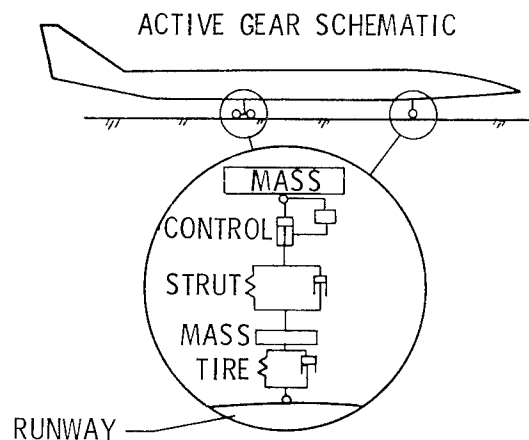


Figure 12.- YF-12 experimental compared with analytical results.



ANALYTICAL CAPABILITIES
 RUNWAY UNEVENNESS
 NONLINEAR TIRE FORCES AND ANTI-SKID BRAKING
 OLEO-PNEUMATIC STRUT WITH FRICTION
 CLOSED-LOOP, SERIES-HYDRAULIC CONTROL
 FIRST MODE WING BENDING AND TORSION
 THEORETICAL SUBSONIC AERODYNAMICS

Figure 13.- Active control landing-gear analysis (ACOLAG).

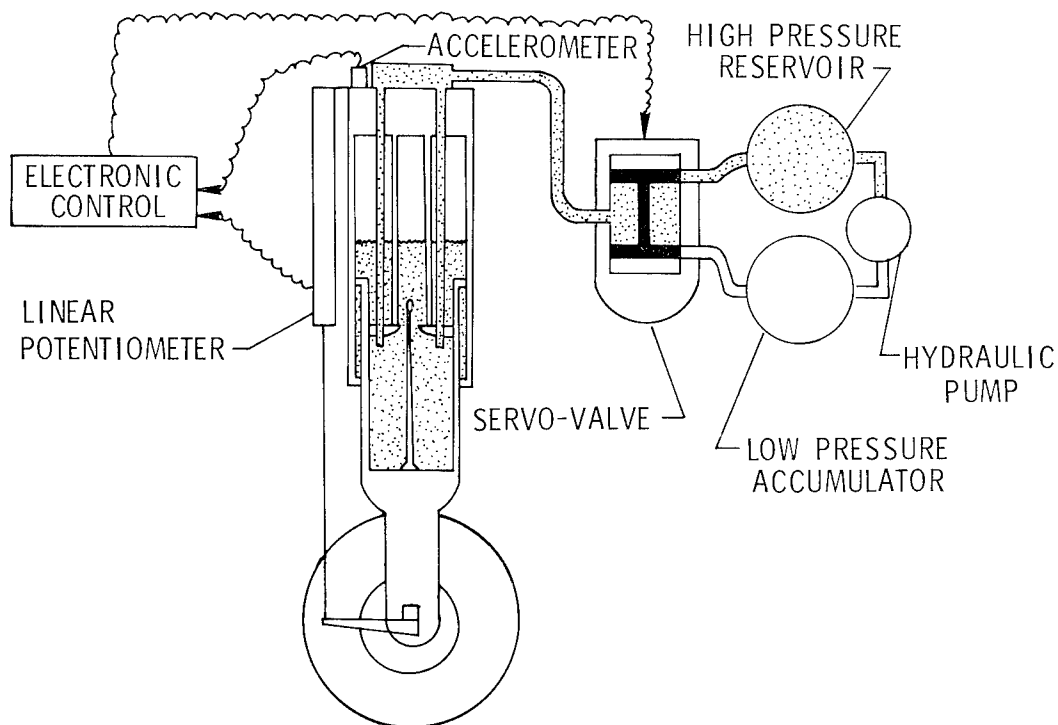


Figure 14.- Series-hydraulic active control concept.

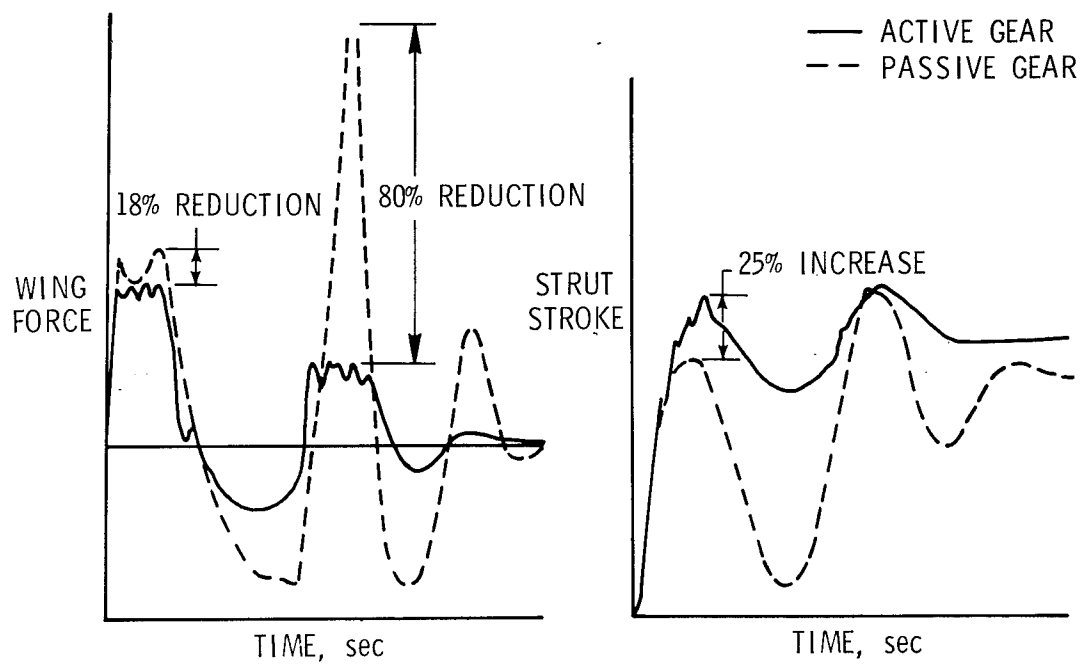


Figure 15.- Analytical results for active and passive gears.

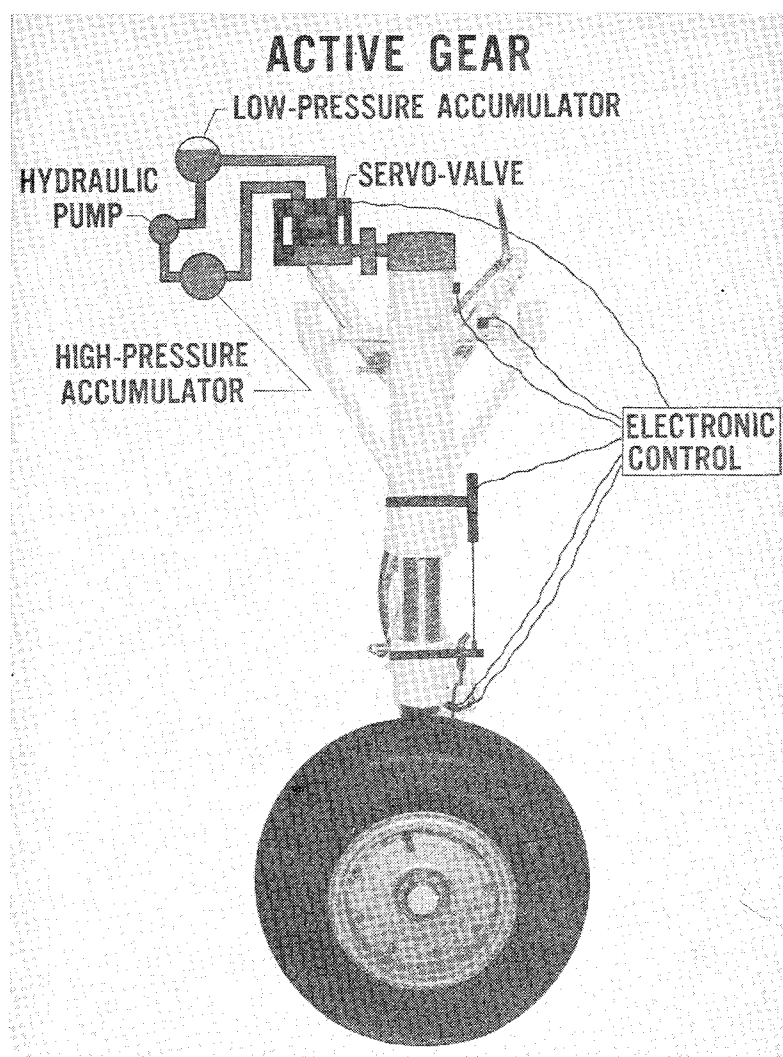


Figure 16.- General aviation aircraft landing gear modified with series-hydraulic active control.

DEVELOPMENTS IN STEADY AND UNSTEADY AERODYNAMICS

FOR USE IN AEROELASTIC ANALYSIS AND DESIGN

E. Carson Yates, Jr., and Samuel R. Bland
NASA Langley Research Center

SUMMARY

A review is given of seven research projects which are aimed at improving the generality, accuracy, and computational efficiency of steady and unsteady aerodynamic theory for use in aeroelastic analysis and design. These projects indicate three major thrusts of current research efforts: (1) more realistic representation of steady and unsteady subsonic and supersonic loads on aircraft configurations of general shape with emphasis on structural-design applications, (2) unsteady aerodynamics for application in active-controls analyses, and (3) unsteady aerodynamics for the frequently critical transonic speed range. The review of each project includes theoretical background, description of capabilities, results of application, current status, and plans for further development and use.

INTRODUCTION

Aeroelastic problems that are encountered in the analysis and design of high-performance aircraft such as supersonic cruise aircraft require consideration of structures and dynamics, as well as aerodynamics of lifting surfaces, control surfaces, and complete aircraft at subsonic, transonic, and supersonic speeds and for steady, oscillatory, and general unsteady motion. Among the technical disciplines involved (i.e., structures, dynamics, and aerodynamics), aerodynamics has always been in the least satisfactory state and has received the greatest emphasis in aeroelastic research and study. Moreover, the development of computer-aided design technology in recent years has imposed even more stringent requirements for comprehensive, accurate, and efficient aerodynamic tools inasmuch as many aerodynamic and aeroelastic analyses must be performed in the repetitive process of designing a minimum-mass aircraft structure that will satisfy a variety of design requirements such as strength, buckling, minimum gage, and aeroelastic requirements such as prescribed minimum flutter speed. (See, e.g., refs. 1 to 3.) In addition to flutter, other static and dynamic aeroelastic characteristics must be assessed. The former include load distribution and associated structural deformation, control effectiveness and reversal, and divergence, whereas the latter include response to gusts, turbulence, control transients, engine failure, and active control systems for the suppression of one or more of these responses.

High-performance, low-load-factor airplanes, such as supersonic cruise aircraft, are usually stiffness-critical to a significant degree. Since mass added to provide required stiffness can be a sizable fraction of payload (refs. 4 to 9), it is essential that it be accurately predictable during the design process. The aeroelastic calculations required for this purpose will, of course, be no more accurate than the aerodynamics used in them.

Requirements for the formulation and use of aerodynamics in aeroelastic analysis and design are in several respects more complicated and more severe than for the more conventional steady-state aerodynamics. For example: (1) The aeroelastician deals with flexible structures so that even in steady-state conditions, the aerodynamic load is a function of structural deformation, and vice versa. (2) The unsteady aerodynamic formulations required in dynamic aeroelasticity involve complex quantities (e.g., velocities, aerodynamic influence functions, and pressure) that manifest time- or frequency-dependent attenuations and phase shifts relative to steady state. (3) In dynamic aeroelasticity - flutter, for example - the aeroelastician must evaluate pressure distributions for vibration mode shapes that are much more wiggly than a typical steady-state mean-camber surface. The corresponding pressure distributions will also be more wiggly than those for steady state so that computational convergence requirements are usually more severe than for steady state. (4) Flutter analyses, as well as iterative structural resizing, require evaluation of pressure distributions for a multiplicity of mode shapes, frequencies, aircraft loading conditions, etc. Consequently, computational efficiency is vital, and it is essential to minimize the amount of recomputation required when mode shapes and/or frequencies are changed.

This paper reviews seven research projects, sponsored by the Langley Research Center, which should help to provide the capabilities in steady and unsteady aerodynamics needed for the aeroelastic analysis and design of high-performance aircraft such as supersonic cruise aircraft. These projects fall into three general categories which indicate the major thrusts of current research efforts: (1) more realistic representation of steady and unsteady subsonic and supersonic loads on aircraft configurations of general shape with emphasis on structural-design applications, (2) unsteady aerodynamics for application in active-controls analyses, and (3) unsteady aerodynamics for the frequently critical transonic speed range. The present review includes theoretical background, description of capabilities, results of application, current status, and plans for further development and use.

SYMBOLS

a_{∞}	free-stream speed of sound
C_L	lift coefficient
C_m	pitching-moment coefficient

C_N	normal-force coefficient
c_n	section normal-force coefficient
C_p	pressure coefficient
ΔC_p	lifting-pressure coefficient
k	reduced frequency
LE, TE	leading edge, trailing edge
M_∞	free-stream Mach number
M_L	local Mach number
s	Laplace-transform variable, i.e., motion exponential (real part defines motion envelope; imaginary part is reduced frequency)
T	thickness ratio
t	time
U	free-stream speed
x, y, z	streamwise, spanwise, and vertical Cartesian coordinates, respectively
α	angle of attack
$\dot{\alpha}$	time rate of change of angle of attack
α_0	initial angle of attack
γ	ratio of specific heats
δ	control-surface deflection angle
δ_{jh}	Kronecker delta
ξ, η	dummy variables for x and y , respectively
Φ	perturbation velocity potential
ϕ	steady-state part of perturbation velocity potential
φ	unsteady part of perturbation velocity potential
ω	frequency

ANALYSIS METHODS

The analysis methods being developed in connection with the seven research projects mentioned previously are listed in table 1, along with an indication of the relevance of each to the three general categories of current research interest, i.e., loads for use in structural design, aerodynamics for active-controls analyses, and aerodynamics for the transonic speed range. With the exception of "transonic aerodynamics for oscillating wings with thickness," all the methods are applicable to the steady-state limit condition. In table 1, the word "Present" indicates applicability of the method in its current state of development; whereas "Future" indicates capability that is still under development.

General Unsteady Compressible Potential Aerodynamics

Objective.— The primary objective of this development (refs. 10 to 19) is an accurate, general, unified method for calculating steady and unsteady loads on complete aircraft with arbitrary shape and motion in subsonic and supersonic flow. Emphasis is on efficient application in aeroelastic analyses (including active-controls analyses) and in computer-aided structural design.

Approach.— Green's theorem has been used to formulate the exact integral equation for the perturbation velocity potential Φ at an arbitrary point (x, y, z) in the fluid at time t in terms of the potential and its derivatives on the fluid boundary (ref. 10).

$$\begin{aligned} \Phi(x, y, z, t) = & \iiint\!\!\!\int GF \, dV_1 \, dt_1 + \iiint [\nabla_1 S \cdot (G \nabla_1 \Phi - \Phi \nabla_1 G) \\ & - \frac{1}{a_\infty^2} \frac{dS}{dt_1} (G \frac{\partial \Phi}{\partial t_1} - \Phi \frac{\partial G}{\partial t_1})] |\square S|^{-1} \, dS \, dt_1 \end{aligned} \quad (1)$$

where

G is Green's function (subsonic or supersonic source potential)

F represents nonlinear terms (products of derivatives of potential)

$S(x_1, y_1, z_1, t_1) = 0$ defines the body surface, and

$$|\square S| = \sqrt{S_{x_1}^2 + S_{y_1}^2 + S_{z_1}^2 + S_{t_1}^2}$$

S_{x_1} , S_{y_1} , S_{z_1} , and S_{t_1} are derivatives of S with respect to the subscript variable. The quadruple integral extends over the entire fluid volume; whereas, the triple integral extends over the surface bounding the fluid, i.e., the body surface, since disturbances must vanish at infinity. To find the potential

and hence the pressure at a point (x,y,z) on the body surface, equation (1) is used in conjunction with the exact boundary conditions and the Bernoulli equation. Note that no small-perturbation assumption has been made. The present computer program SOUSSA (Steady, Oscillatory, and Unsteady Subsonic and Supersonic Aerodynamics), however, does not include the nonlinear terms represented by the quadruple integral in equation (1).

Solution of equation (1) is by spatial discretization with arbitrary nonplanar quadrilateral surface panels and time solution by Laplace transform (ref. 16). The resulting set of simultaneous equations for the potential at a finite number of points on the body surface in terms of the normalwash at the surface can be expressed as

$$\begin{bmatrix} \tilde{Y}_{jh} \end{bmatrix} \begin{Bmatrix} \tilde{\Phi}_h \end{Bmatrix} = \begin{bmatrix} \tilde{Z}_{jh} \end{bmatrix} \begin{Bmatrix} \tilde{\psi}_h \end{Bmatrix} \quad (2)$$

where

$\tilde{\Phi}_h$ is Laplace transform of perturbation velocity potential

$\tilde{\psi}_h$ is Laplace transform of normalwash at body surface

$$\tilde{Y}_{jh} = \delta_{jh} - (C_{jh} + sD_{jh})e^{-s\Theta_{jh}}$$

$$-\sum_n (F_{jn} + sG_{jn})S_{nh} e^{-s(\Theta_{jn} + \pi_n)} \quad (3)$$

$$\tilde{Z}_{jh} = B_{jh} e^{-s\Theta_{jh}}$$

Θ_{jh} and π_n are lag functions, S_{nh} is ± 1 depending on which side of the wake the point is on,

and

$$B_{jh} = \frac{-1}{2\pi} \iint_{\Sigma_B} N_h \frac{1}{R} d\Sigma_B \quad C_{jh} = \frac{1}{2\pi} \iint_{\Sigma_B} N_h \frac{\partial}{\partial N} \left(\frac{1}{R} \right) d\Sigma_B$$

$$D_{jh} = \frac{-1}{2\pi} \iint_{\Sigma_B} N_h \frac{1}{R} \frac{\partial R}{\partial N} d\Sigma_B \quad F_{jh} = \frac{1}{2\pi} \iint_{\Sigma_W} L_h \frac{\partial}{\partial N} \left(\frac{1}{R} \right) d\Sigma_W$$

$$G_{jh} = \frac{-1}{2\pi} \iint_{\Sigma_W} L_h \frac{1}{R} \frac{\partial R}{\partial N} d\Sigma_W \quad (4)$$

where

Σ_B and Σ_W indicate integration over body and wake surfaces, respectively,

$N_h(x,y,z)$ and $L_h(x,y,z)$ are shape functions,

R is elliptic ($M_\infty < 1$) or hyperbolic ($M_\infty > 1$) distance between influenced and influencing points, and

N is direction normal to body or wake surface.

Note that the integrals in equations (4) are independent of deformation or mode shape and are also independent of the transform variable s (and hence frequency in the oscillatory case). Consequently, these integrals need to be evaluated only once for a given Mach number unless the paneling arrangement is changed. Moreover, \tilde{Y}_{jh} and \tilde{Z}_{jh} are also independent of deflection shape and contain only simple functions of the transform variable. Hence, equation (2) can be solved efficiently for a variety of deflection shapes and frequencies. For example, adding modes in a flutter analysis or changing modes in structural design requires alteration only of the normalwash matrix in equation (2) and does not require reevaluation of the coefficient matrices $[\tilde{Y}_{jh}]$ and $[\tilde{Z}_{jh}]$.

A further advantage of this method results from use of arbitrary non-planar quadrilateral surface panels. If desired, the aerodynamic paneling can exactly fit a structural finite-element paneling arrangement so that interpolations between structural model and aerodynamic model can be minimized or avoided.

This formulation provides a unified surface-panel method for arbitrary motion of complete aircraft in subsonic and supersonic flow in which bodies, stores, lifting surfaces, and control surfaces are all paneled alike, i.e., with source panels having strength proportional to normalwash (usually specified) and doublet panels having strength proportional to Φ obtained by solution of equation (2).

Status.— The final version of the proof-of-concept computer program has been completed and is being documented as an interim SOUSSA code. Its capabilities are indicated in figure 1. An intermediate form of SOUSSA is also being used in FCAP (Flight Controls Analysis Program) (refs. 20 and 21) which is being developed primarily for analysis and synthesis of active control systems.

The interim SOUSSA program, in effect, solves the linearized velocity-potential equation with exact boundary conditions. The current development effort is directed primarily toward adaptation of SOUSSA for application in the transonic range. Several approaches are being pursued to incorporate the dominant effects of the nonlinear character of transonic flow without requiring brute-force numerical evaluation of the volume integral in equation (1).

Inclusion of the nonlinear influence of wake deformation in subsonic flow has also been demonstrated (ref. 17).

The interim SOUSSA program uses constant-potential (zeroth-order) surface elements which were adequate for demonstration of capability. However, a dominant objective throughout this work has been to use elements sophisticated enough to converge solutions for complicated shapes and motions with a number of elements small enough for the solution to be computationally tractable and economical. Consequently, higher order elements are being developed, along with special elements that have potential distributions which are appropriate for paneling adjacent to normalwash discontinuities such as at control-surface hinge lines and edges.

Reference 22 presents a finite-element approach to the analysis of rotational flow. The method is still under development. In combination with SOUSSA, it may offer a means for representing viscous-flow influence.

Applications.— Figure 2 (reproduced from ref. 18) shows the magnitude and phase angle of supersonic lift coefficient for an oscillating rectangular wing. Results are shown for converging, diverging, and harmonic oscillation. The latter are in good agreement with results from the acceleration-potential lifting-surface method of Laschka (ref. 23).

Figure 3 (also from ref. 18) shows chordwise pressure distribution on the wing of a wing-body-tail configuration in a diverging oscillation in incompressible flow. For simplicity in this demonstration calculation, both wing and tail have been taken to be rectangular with aspect ratio 6 and thickness ratio 0.09. No comparable calculations are available for comparison.

Plans*.— The additional capabilities that are under current development (fig. 1) will be incorporated into SOUSSA as they become available. Several approximations that were employed for computational expediency in the development program will be eliminated or revised in order to improve the accuracy, efficiency, and generality of the method. These broadened capabilities and improvements will also be incorporated into a modular "production" program SOUSSA that will be structured for efficient application to large-order flutter analysis and design problems.

SOUSSA aerodynamics will be combined with the SPAR finite-element structural-analysis program (ref. 24) and with the WIDOWAC structural-optimization program (refs. 1 to 3) in order to produce an efficient program PARS (Program for Analysis and Resizing of Structures) for generating minimum-mass structures for complete aircraft that will satisfy a number of static and dynamic structural and aeroelastic design requirements such as multiple flutter-speed constraints. FCAP (refs. 20 and 21) may eventually be used in combination with PARS for design of structures for aircraft with active control systems.

*All sections entitled "Plans" in this paper contain statements of current intentions. These, of course, are subject to change as time progresses.

Thus, SOUSSA will find application in flutter analyses, in active-controls analyses, and in computation of static and dynamic loads for computer-aided structural design.

Subsonic Kernel-Function Analysis for Wings With Oscillating Controls

Objective.— The objective of this work is accurate representation of the pressure distribution on lifting surfaces with oscillating leading-edge and trailing-edge controls. Emphasis is on applications to flutter analyses and active-controls studies.

Approach.— The well-known kernel-function analysis of reference 25 provides an integral equation representation of the linear potential equation for harmonic oscillations of a thin lifting surface. This equation

$$\frac{w(x,y)}{U} = \iint_S \Delta C_p(\xi,\eta) K(M_\infty, k, \xi-x, \eta-y) d\xi d\eta \quad (5)$$

relates the known downwash velocity $w(x,y)$ at a point on the surface to the unknown lifting pressure distribution $\Delta C_p(\xi,\eta)$. The kernel function K is defined by a singular integral. The integration region S includes only the wing surface. This integral equation is solved by the procedure of reference 26 as follows: The unknown pressure distribution is expanded in a series of known functions θ_n with unknown coefficients a_n as

$$\Delta C_p(\xi,\eta) = \sum_{n=1}^N a_n \theta_n(\xi,\eta) \quad (6)$$

The functions θ_n are chosen to satisfy the known edge conditions on the lifting surface (e.g., the Kutta condition at the trailing edge). Equation (6) is substituted into equation (5) and the integration performed for a set of N points (x_i, y_i) at which the downwash is known from the boundary condition. The resulting set of N simultaneous linear equations is then solved for the coefficients a_n .

Recent research (refs. 27 to 30) has provided an improved kernel-function procedure for wings with leading- and/or trailing-edge controls. In linear potential flow, the surface slope discontinuity at a control-surface hinge line or side edge leads to a downwash discontinuity which causes a logarithmic singularity in the lifting pressure at the hinge line and a $y \log y$ type variation in lifting pressure at the control surface edge (y measured from the control edge). The present method treats these singularities meticulously by using a set of pressure functions θ_n containing appropriate logarithmic terms. Within the framework of thin-wing theory, this kernel-function method provides the most accurate treatment of control-surface aerodynamics currently

available to the aeroelastician.

Status.— Program refinements and delivery should be completed in 1976.

Application.— An example of the results obtainable is shown in figure 4 (taken from ref. 27). The calculated lifting pressure distributions on a swept wing with oscillating partial-span control are compared with the experiment of reference 31. The agreement is excellent except near the control edges--the analysis treats the edge gaps as sealed.

Plans.— No further development is contemplated. The completed computer program will be used in studies of active control systems.

Unsteady Loads on Lifting Surfaces with Sharp-Edge Separation

Objective.— The objective of this development (refs. 32 to 38) is accurate evaluation of steady and unsteady aerodynamic loads on lifting surfaces of general shape at moderate to high angles of attack. Emphasis is on representations of structural design loads and flutter aerodynamics for high-load-factor conditions that are more realistic than those obtained from linearized (small disturbance) aerodynamic theory.

Approach.— Sharp edges are assumed in order to fix the location of flow separation. Kutta condition is imposed along all edges on which separation occurs. No assumptions of small perturbations are involved. A vortex model is established in which a mean-camber surface (or alternatively, wing upper and lower surfaces) of arbitrary shape is overlaid with a vortex grid from which discrete free vortices extend into the fluid across all edges on which separation occurs. The vortices are constrained to cross perpendicular to wing edges in order to satisfy the Kutta condition. The shape of each free vortex is approximated by a sequence of contiguous straight-line segments. The requirement that the free vortex system be force-free is satisfied approximately by aligning each free vortex segment with the local flow velocity at one point along its length. Solution is by Biot-Savart law which is imposed in conjunction with an assumed position of the free vortices and exact normalwash boundary conditions on the mean-camber (or wing) surface in order to calculate the strengths of the bound vortices. After these strengths have been determined, Biot-Savart law is employed iteratively to find a new force-free location of the free vortices. The process is repeated until convergence tests are satisfied.

Status.— Current computer programs calculate steady load distributions and flow field for nonplanar and interfering lifting surfaces with flow separation from sharp leading edges, tips, and trailing edges, and also for general unsteady motion of lifting surfaces with separation from tips and trailing edges. Unsteady capability is currently being extended to include leading-edge separation. In figure 5, the present models are compared with the previously used flat-wake model of Belotserkovskii (ref. 39) and the incompressible-flow model of Djojodihardjo and Widnall (ref. 40) which accounts only for vorticity issuing from the trailing edge.

As presently formulated, compressibility is accounted for approximately by a Prandtl-Glauert type transformation which is based on the linearized potential-flow equation. The present problem becomes approximately linear, and hence this type of transformation becomes reasonable only when either Mach number or flow perturbation (e.g., angle of attack) is small. Comparisons of steady-state calculated lift and pitching moment with experimental values for several wings at several Mach numbers (e.g., ref. 35) have indicated that the present procedure gives good results for angles of attack (in degrees) up to at least $20\sqrt{1 - M_\infty^2}$. Use of local Mach number instead of free-stream Mach number in the transformation may extend the usefulness of the method to higher angles of attack in the middle-to-upper subsonic range.

Current activity is concerned with the effect of several internal parameters (e.g., vortex grid spacing, length of free vortex segments, etc.) on convergence of the calculations. In addition, artificial viscosity is being incorporated as a means of avoiding erratic behavior when vortices come close together, although this has not been a problem up to this time. Also, vorticity distribution functions are being investigated as a possible means for improving the efficiency of the calculations.

Applications.— Figure 6 (taken from ref. 36) shows a typical calculated vortex flow pattern around the tip of a rectangular wing. Only a coarse grid pattern is shown here for clarity. Figure 7 (also from ref. 36) shows the vorticity pattern for the same wing at the end of a ramp-type increase in angle of attack from 11° to 15° . Figure 8 (taken from ref. 38) illustrates lift lag as angle of attack is increased from 11° to 15° and conversely decreased from 15° to 11° . Figure 9 (from ref. 35) presents calculated spanwise load distributions for a rectangular wing in comparison with values calculated by linear theory and with experimental values. The large increase in load intensity, particularly near the tip, has significant implications for the structural designer since aircraft design loads occur at large angle-of-attack (limit load factor) conditions. Finally, figure 10 (from ref. 35) shows calculated normal force and pitching moment for a swept wing and includes comparisons with linear-theory results and with experiment.

Plans.— Pertinent results from the previously described current study will be incorporated into the computer program to improve its efficiency and generality. The program will be used to calculate aerodynamic characteristics, stability derivatives, and structural loads for several wing and wing-tail configurations, including deflected and deflecting control surfaces, and for the arrow-wing SCAR configuration. Generalized aerodynamic forces will be generated for flutter calculations to determine the effect of sharp-edge flow separation on flutter boundaries at moderate to high angles of attack. The changes in steady-state load distribution caused by edge separation indicate that the effect on flutter is probably detrimental. Note that linearized theory predicts no effect on flutter of angle of attack, twist, camber, or thickness.

Finite-Difference Method for Oscillating Transonic Flow

Objective.— The objective of this work is accurate solution of the transonic small-perturbation potential equation for harmonic oscillation. Current emphasis is on accurate "benchmark" type calculations that can serve as a standard for assessing the accuracy of approximate methods that are computationally more economical.

Approach.— Many aeroelastic problems, flutter in particular, are most severe in the transonic speed regime. In contrast with the steady transonic potential-flow problem which is inherently nonlinear, it is possible to linearize the unsteady problem and decouple it from the steady problem if oscillation frequencies are sufficiently high. Reference 41 presents many such linear-theory solutions in detail. Unfortunately, this linearization is not generally possible for accurate aeroelastic calculations at the low to moderate frequencies that are of usual interest and in the presence of varying local flow velocity and shock waves which characterize transonic flow.

The simplest equation which can properly describe the essential features of the flow is the transonic small-disturbance potential equation

$$\left[1 - M_{\infty}^2 - (\gamma + 1)M_{\infty}^2 \phi_x - (\gamma - 1) \frac{M_{\infty}^2}{U} \phi_t \right] \phi_{xx} + \phi_{yy} + \phi_{zz} - 2 \frac{M_{\infty}^2}{U} \phi_{xt} - \frac{M_{\infty}^2}{U^2} \phi_{tt} = 0 \quad (7)$$

Subscripts x , y , z , and t indicate derivatives of the potential with respect to the subscript variable. The nonlinear terms involving ϕ_x and ϕ_t are retained because they are of the same order as $1 - M_{\infty}^2$. It is possible to effect a linearization for the unsteady flow by expressing the perturbation potential ϕ as a sum of steady and unsteady parts

$$\Phi(x, y, z, t) = \phi(x, y, z) + \varphi(x, y, z) e^{i\omega t} \quad (8)$$

where harmonic motion has been assumed. It is further assumed that the unsteady motion is a small perturbation of the mean, steady flow so that $\varphi \ll \phi$. Substitution of equation (8) into equation (7) leads to a partial separation of the steady and unsteady flow effects. The usual small-perturbation equation results for the mean steady flow

$$\left[1 - M_{\infty}^2 - (\gamma + 1)M_{\infty}^2 \phi_x \right] \phi_{xx} + \phi_{yy} + \phi_{zz} = 0 \quad (9)$$

and the equation for unsteady flow is

$$\left[1 - M_\infty^2 - (\gamma + 1)M_\infty^2\phi_x\right]\phi_{xx} + \phi_{yy} + \phi_{zz} - M_\infty^2\left[i2k + (\gamma + 1)\phi_{xx}\right]\phi_x + M_\infty^2\left[k^2 - i(\gamma - 1)k\phi_{xx}\right]\phi = 0 \quad (10)$$

This is a linear equation for the unsteady potential ϕ . However, the equation has nonconstant coefficients which depend on the mean, steady flow potential ϕ . Equation (10) is of the same type as equation (9); that is, the unsteady-flow problem is elliptic (subsonic) or hyperbolic (supersonic) at any point in accordance with the character of the mean, steady flow at that point.

There is current interest in a variety of attacks on the unsteady transonic flow problem. The significant successes of finite-difference methods for steady flow led to the application of these methods to the unsteady flow problem. Some of this research is reported in references 42 to 45. In the present procedure, the steady flow equation (9) is first solved on a rectangular finite-difference mesh. The unsteady equation (10) is then solved on the same mesh using values from the steady solution to provide the values of the nonconstant coefficients required at the mesh points. The large system of algebraic equations (one for each mesh point) is solved by a relaxation procedure. Central differences are used in subsonic portions of the flow, and backward differences are used in supersonic portions.

Status.— Initial calculations have been made for several airfoils and for a pitching rectangular wing. However, numerical difficulties have imposed an upper limit on frequency that becomes more severe as free-stream Mach number approaches 1.0. Work is still in progress.

Application.— The results of the first application of this method to a three-dimensional flow problem (ref. 44) are given in figure 11. The real part of the lifting pressure for a rectangular wing oscillating in pitch is presented. There were 18 304 mesh points used. In general, the finite-difference calculation agrees well with the linear theory (uniform flow). However, the flow is supercritical, and a shock wave is evident over inboard portions of the wing in the finite-difference result (nonuniform flow).

Plans.— Development of this method will continue and should lead to a documented computer program for isolated lifting surfaces.

Although finite-difference methods have promise for providing accurate solutions to transonic-flow problems, the computational task is enormous in comparison with conventional lifting-surface or surface-paneling methods. Two approximate, but perhaps more widely useable methods are described in the following two sections. A discussion of several proposed methods is given in reference 46.

Transonic Aerodynamics for Oscillating Wings with Thickness

Objective.— The objective of this development (refs. 47 to 49) is an approximate method for calculating unsteady transonic aerodynamic forces that is more accurate than linear theory, especially in the range of reduced frequency that is of usual interest in lifting-surface flutter problems. Emphasis is on a method that accounts for the dominant effects of nonuniform mean flow and is at the same time theoretically and computationally suitable for use in flutter analyses.

Approach.— If local Mach number does not vary much from 1.0, the transonic equation for small-perturbation velocity potential can be written in terms of local Mach number

$$\varphi_{yy} + \varphi_{zz} - M_L^2(2ik\varphi_x - k^2\varphi) = 0 \quad (11)$$

As in the previous section, the unsteady perturbation is assumed to be small relative to the steady state so that local Mach number can be taken to be that for the mean steady flow. If the nonuniform coordinate transformation

$$\tilde{x} = x \quad \tilde{y} = M_L(x,y)y \quad \tilde{z} = M_L(x,y)z \quad (12)$$

is imposed, equation (11) becomes

$$\tilde{\varphi}_{\tilde{y}\tilde{y}} + \tilde{\varphi}_{\tilde{z}\tilde{z}} - 2ik\tilde{\varphi}_{\tilde{x}} + k^2\tilde{\varphi} = 0 \quad (13)$$

where $\tilde{\varphi}(\tilde{x}, \tilde{y}, \tilde{z}) = M_L(x,y)\varphi(x,y,z)$.

Equation (13) is a linear equation with constant coefficients and has exactly the same form as the conventional linearized unsteady transonic-flow equation. (See, e.g., ref. 41.) Solutions of the latter involve propagation of pressure disturbances along straight ray paths. The coordinate transformation (eq. (12)) therefore is equivalent to distorting the space so that ray paths that are curved in the physical space x,y,z are straightened out in the transformed space $\tilde{x}, \tilde{y}, \tilde{z}$. Consequently, the problem can be solved in the transformed space by any method that is suitable for the conventional linearized equation—e.g., sonic kernel function (refs. 25 and 50) or sonic box (refs. 51 to 53). The latter method has been used for current implementation.

Figure 12 illustrates the distortion of wing planform caused by the coordinate transformation. If the transformation is to be single valued, equations (12) imply limitations on how rapidly Mach number can vary in a direction lateral to the free stream. Thus, shock waves must not impinge upon the wing. Another limitation on usefulness of this method is the requirement that a steady-state solution be available to provide local

Mach number values for the coordinate transformation.

Status.— The coordinate-transformation method has been demonstrated (refs. 47 to 49) by modification of the sonic box computer program (refs. 51 to 53). The accuracy, efficiency, and generality of the demonstration program is currently being improved. The final documented program should be available early in 1977.

Applications.— The method has been used to calculate aerodynamic parameters for several wings with finite thickness, and the results have been compared with calculations for zero thickness (conventional linear transonic theory) in references 47 and 48. The calculated detrimental effect of finite thickness on transonic flutter speed is illustrated in figure 13 (taken from ref. 47) for a 45° delta wing with elliptical cross section. For a 0.04 thickness-chord ratio, flutter speed is 15 percent below the zero-thickness value.

Plans.— The improved computer program will be documented and further evaluated by comparison of results with measured unsteady air forces and by application to transonic flutter analyses. Use of the coordinate transformation in conjunction with other linear-theory methods is contemplated.

Mixed Subsonic-Supersonic Kernel-Function Analysis for Oscillating Wings

Objective.— The objective of this effort (refs. 54 to 56) is an approximate method for calculating unsteady transonic aerodynamic forces that accounts for the presence of shock waves and the mixed subsonic-supersonic character of the flow. Emphasis is on a method that includes variations in local Mach number and is suitable for use in flutter analyses.

Approach.— The present method was synthesized by patching together linear subsonic and supersonic kernel-function analyses to simulate the mixed subsonic-supersonic character of transonic flow. The wing is divided into a few subsurfaces on which the flow is either subsonic or supersonic. Either subsonic or supersonic kernel-function aerodynamics, as appropriate, is used on each subsurface. In addition, the local Mach number is used at each collocation point. This method requires this mean (steady-flow) local Mach number as input from another source. A doublet singularity is included to represent the unsteady shock condition.

The mixed-flow method should be attractive to the aeroelastician since it is composed of methods which are generally familiar and which are relatively efficient computationally. However, extensive testing will be required to assess its limitations and reliability.

Status.— The computer program is being debugged and documented.

Application.— Measured and calculated pressure distributions for a wing oscillating in bending are shown in figure 14. The calculations are from reference 56; the measurements are from reference 57. The local Mach number

distribution, shown for a section near midsemispan, was used as input. The uniform-flow calculation (dash line) was carried out with the subsonic kernel function at $M_\infty = 0.997$. The mixed-flow calculation, which includes the shock condition, provides somewhat better agreement with experiment than the uniform-flow calculation.

Plans.— The method will be applied in transonic flutter calculations as time permits.

Oscillatory Supersonic Lifting-Surface Panel Method

Objective.— The objective of this effort is a general, linear-theory method for calculating supersonic aerodynamic forces on thin oscillating lifting surfaces with a panelling scheme that fits planform boundaries exactly and is independent of Mach number. Emphasis is on developing a method that is suitable for routine use in flutter analyses.

Approach.— This method is a reformulation of the work reported in references 58 to 61. The method is applicable to configurations of the type illustrated in figure 15. Each lifting surface (e.g., wing segment, vertical tail, control surface) is represented as a plane defined by the locations of its four corners. Each of these zero-thickness surfaces is panelled with parallelograms which have two edges parallel to the surface leading edge and two edges parallel to the free stream. As can be seen in the figure, this geometry must be adjusted at the surface trailing edge.

The analytical method is based on an integral equation solution of the linear potential equation for harmonic motion. The unknowns are the streamwise gradients of the jump in velocity potential across each panel. Within each panel, the velocity potential varies linearly in the streamwise direction and is constant in the spanwise direction. Specification of the downwash in each panel leads to a collocation solution for the unknown potential-gradient values.

This method should lead to an efficient procedure for applying linearized supersonic flow theory to thin lifting surfaces. It should be useful for flutter analyses and active-control analyses. It represents a significant advance over the earlier Mach box lifting-surface procedures.

Status.— A documented computer program should be available by the end of 1976.

Plans.— No additional development effort is contemplated.

CONCLUDING REMARKS

High-performance, low-load-factor airplanes, such as supersonic cruise aircraft, are usually stiffness-critical to a significant degree. Consequently,

to satisfy stiffness and aeroelastic stability requirements without undue mass penalty, it is essential that the static and dynamic aeroelastic characteristics and stiffness requirements of such aircraft be accurately and reliably assessable by efficient analytical means. Since the aerodynamic methods available for such purposes are in a much less satisfactory state than are the structures and dynamics techniques, considerable importance is placed upon improving the generality, accuracy, and computational efficiency of steady and unsteady aerodynamics.

This paper has reviewed seven research projects which indicate three major thrusts of current research efforts: (1) more realistic representation of steady and unsteady subsonic and supersonic loads on aircraft configurations of general shape with emphasis on structural-design applications, (2) unsteady aerodynamics for application in active-controls analyses, and (3) unsteady aerodynamics for the frequently critical transonic speed range. The projects reviewed herein should help to broaden significantly the aerodynamic capabilities available for aeroelastic analysis and design.

REFERENCES

1. Haftka, Raphael T.: Automated Procedure for the Design of Wing Structures to Satisfy Strength and Flutter Requirements. NASA TN D-7264, 1973.
2. Haftka, Raphael T.; and Starnes, James H., Jr.: WIDOWAC (Wing Design Optimization with Aeroelastic Constraints): Program Manual. NASA TM X-3071, 1974.
3. Haftka, Raphael T.; and Yates, E. Carson, Jr.: Repetitive Flutter Calculations in Structural Design. J. of Aircraft, vol. 13, no. 7, July 1976, pp. 454-461.
4. Sakata, I. F.; Davis, G. W.; Robinson, J. C.; and Yates, E. C., Jr.: Design Study of Structural Concepts for an Arrow-Wing Supersonic Cruise Aircraft. AIAA Paper 75-1037, 1975.
5. Sakata, I. F.; and Davis, G. W.: Evaluation of Structural Design Concepts for an Arrow-Wing Supersonic Cruise Aircraft. NASA CR-2667, 1976.
6. Sakata, I. F.; and Davis, G. W.: Substantiating Data for Arrow-Wing Supersonic Cruise Aircraft Structural Design Concepts Evaluation. NASA CR-132575, vols. 1 to 4, 1976.
7. Robinson, James C.; Yates, E. Carson, Jr.; Turner, M. Jonathan; and Grande, Donald L.: Application of an Advanced Computerized Structural Design System to an Arrow-Wing Supersonic Cruise Aircraft. AIAA Paper 75-1038, 1975.
8. Grande, D. L.; and Turner, M. J.: Study of Structural Design Concepts for an Arrow-Wing Supersonic Cruise Aircraft. NASA CR-2743, 1976.
9. Boeing Staff: Study of Structural Design Concepts for an Arrow-Wing Supersonic Transport Configuration. NASA CR-132576. vols. 1 and 2, 1976.
10. Morino, L.: A General Theory of Unsteady Compressible Potential Aerodynamics. NASA CR-2464, 1974. (Supersedes Boston University Report TR 72-01, June 1972).
11. Morino, L.: Unsteady Compressible Potential Flow Around Lifting Bodies: General Theory. AIAA Paper 73-196, 1973.
12. Kuo, C. C.; and Morino, L.: Steady Subsonic Flow Around Finite-Thickness Wings. NASA CR-2616, Nov. 1975.
13. Morino, L.; and Kuo, C. C.: Unsteady Subsonic Compressible Flow Around Finite Thickness Wings. AIAA Paper 73-313, March 1973.
14. Morino, L.; and Kuo, C. C.: Subsonic Potential Aerodynamics for Complex Configurations: A General Theory. AIAA J., vol. 12, no. 2, Feb. 1974, pp. 191-197.

15. Morino, L.; Chen, L. T.; and Suciu, E. O.: Steady and Oscillatory Subsonic and Supersonic Aerodynamics Around Complex Configurations. AIAA J., Vol. 13, No. 3, March 1975, pp. 368-374.
16. Morino, L.; and Chen, L. T.: Indicial Compressible Potential Aerodynamics Around Complex Aircraft Configuration. In Aerodynamic Analyses Requiring Advanced Computers, NASA SP-347, Paper No. 38, 1975, pp. 1067-1110.
17. Suci, E. O.; and Morino, L.: A Nonlinear Finite-Element Analysis of Wings in Steady Incompressible Flows with Wake Roll-up. AIAA Paper 76-64, 1976.
18. Tseng, K.; and Morino, L.: Fully Unsteady Subsonic and Supersonic Potential Aerodynamics of Complex Aircraft Configurations for Flutter Applications. Proceedings of the AIAA/ASME/SAE 17th Structures, Structural Dynamics, and Materials Conference, King of Prussia, PA., May 5-7, 1976.
19. Tseng, K.; and Morino, Luigi: A New Unified Approach for Analyzing Wing-Body-Tail Configurations with Control Surfaces. AIAA Paper No. 76-418, July 1976.
20. Noll, R. B.; and Morino, L.: FCAP-A New Tool for the Evaluation of Active Control Technology. AIAA Paper No. 75-1059, 1975.
21. Noll, R. B.; and Morino, L.: Flutter and Gust Response Analysis of Flexible Aircraft With Active Control. Proceedings of the AIAA/ASME/SAE 17th Structures, Structural Dynamics and Materials Conference, King of Prussia, Pa., May 5-7, 1976.
22. Morino, L.: A Finite Element Method for Rotational Incompressible Aerodynamics. Boston University, College of Engineering, TN-74-04, December 1974.
23. Laschka, B.: Zur Theorie der Harmonisch Schwingenden Tragenden Fläche bei Unterschallstromung. Zeitschrift für Flugwissenschaften, 11 (1963), Heft 7, pp. 265-292.
24. Giles, Gary L.: Computer-Aided Methods for Analysis and Synthesis of SCAR Structures. Presented at the Supersonic Cruise Aircraft Research (SCAR) Conference, Hampton, Virginia, November 9-12, 1976.
25. Watkins, Charles E.; Runyan, Harry L.; and Woolston, Donald S.: On the Kernel Function of the Integral Equation Relating the Lift and Downwash Distributions of Oscillating Finite Wings in Subsonic Flow. NACA Rep. 1234, 1955.
26. Watkins, Charles E.; Woolston, Donald S.; and Cunningham, Herbert J.: A Systematic Kernel Function Procedure for Determining Aerodynamic Forces on Oscillating or Steady Finite Wings at Subsonic Speeds. NASA TR R-48, 1959.

27. Rowe, W. S.; Winther, B. A.; and Redman, M. C.: Prediction of Unsteady Aerodynamic Loadings Caused by Trailing Edge Control Surface Motions in Subsonic Compressible Flow - Analysis and Results. NASA CR-2003, June 1972.
28. Rowe, W. S.; Winther, B. A.; and Redman, M. C.: Unsteady Subsonic Aerodynamic Loadings Caused by Control Surface Motions. J. Aircraft, vol. 11, no. 1, Jan. 1974, pp. 45-54.
29. Rowe, W. S.; Sebastian, J. D.; and Redman, M. C.: Some Recent Developments in Predicting Unsteady Loadings Caused by Control Surface Motions. AIAA Paper 75-101, Jan. 1975.
30. Rowe, W. S.; Redman, M. C.; Ehlers, F. E.; and Sebastian, J. D.: Prediction of Unsteady Aerodynamic Loadings Caused by Leading Edge and Trailing Edge Control Surface Motions in Subsonic Compressible Flow - Analysis and Results. NASA CR-2543, 1975.
31. Försching, H.; Triebstein, H.; and Wagner, J.: Pressure Measurements on an Harmonically Oscillating Swept Wing with Two Control Surfaces in Incompressible Flow. Symposium on Unsteady Aerodynamics for Aeroelastic Analyses of Interfering Surfaces - Part II, AGARD CP-80-71, Apr. 1971.
32. Mook, D. T.; and Maddox, S. A.: Extension of a Vortex-Lattice Method to Include the Effects of Leading-Edge Separation. J. of Aircraft, vol. 11, no. 2, Feb. 1974, pp. 127-128.
33. Kandil, O. A.; Mook, D. T.; and Nayfeh, A. H.: Nonlinear Prediction of Aerodynamic Loads on Lifting Surfaces. AIAA Paper 74-503, June 1974, also in Journal of Aircraft, vol. 13, no. 1, January 1976, pp. 22-28.
34. Kandil, O. A.; Mook, D. T.; and Nayfeh, A. H.: Subsonic Loads on Wings Having Sharp Leading Edges and Tips. J. Aircraft, vol. 13, no. 1, Jan. 1976, pp. 62-63.
35. Kandil, O. A.: Prediction of the Steady Aerodynamic Loads on Lifting Surfaces Having Sharp-Edge Separation. Ph.D. Dissertation, Engineering Science and Mechanics Department, Virginia Polytechnic Institute and State University, December 1974.
36. Atta, E. H.: Unsteady Flow Over Arbitrary Wing-Planforms, Including Tip Separation. M.S. Thesis, Dept. of Engineering Science and Mechanics, Virginia Polytechnic Institute and State University, Mar. 1976.
37. Kandil, Osama A.; Mook, Dean T.; and Nayfeh, Ali H.: New Convergence Criteria for the Vortex-Lattice Models of the Leading-Edge Separation. Vortex-Lattice Utilization. NASA SP-405, 1976.
38. Atta, E. H.; Kandil, O. A.; Mook, D. T.; and Nayfeh, A. H.: Unsteady Flow over Wings Having Sharp-Edge Separation. Vortex-Lattice Utilization. NASA SP-405, 1976.

39. Belotserkovskii, S. M.: Gust Effects on Wings of Complex Planform at Subsonic Speeds. *Izv. ZN SSSR, Mekhanika Zhidkosti i Gaza*, vol. 4, 1966, pp. 129-138.
40. Djojodihardjo, R. H.; and Widnall, S. E.: A Numerical Method for Calculation of Nonlinear Unsteady Lifting Potential Flow Problems. *AIAA Journal*, vol. 7, no. 10, Oct. 1969, pp. 2001-2009.
41. Landahl, Marten T.: *Unsteady Transonic Flow*. Pergamon Press, Inc., 1961.
42. Ehlers, F. Edward: A Finite Difference Method for the Solution of the Transonic Flow Around Harmonically Oscillating Wings. NASA CR-2257, 1974.
43. Ehlers, F. Edward: A Finite Difference Method for the Solution of the Transonic Flow Around Harmonically Oscillating Wings. AIAA Paper 74-543, June 1974.
44. Weatherill, Warren H.; Ehlers, F. Edward; and Sebastian, James D.: Computation of the Transonic Perturbation Flow Fields Around Two- and Three-Dimensional Oscillating Wings. NASA CR-2599, Dec. 1975.
45. Weatherill, Warren H.; Sebastian, James D.; and Ehlers, F. E.: On the Computation of the Transonic Perturbation Flow Fields Around Two- and Three-Dimensional Oscillating Wings. AIAA Paper 76-99, Jan. 1976.
46. Bland, Samuel R.: Recent Advances and Concepts in Unsteady Aerodynamic Theory. In *Aerodynamic Analyses Requiring Advanced Computers, Part II*, NASA SP-347, 1975, pp. 1305-1326.
47. Ruo, S. Y.; Yates, E. Carson, Jr.; and Theisen, J. G.: Calculations of Unsteady Transonic Aerodynamics for Oscillating Wings with Thickness. *Journal of Aircraft*, vol. 11, no. 10, Oct. 1974, pp. 601-608.
48. Ruo, S. Y.; and Theisen, J. G.: Calculation of Unsteady Transonic Aerodynamics for Oscillating Wings with Thickness. NASA CR-2259, June 1975.
49. Ruo, S. Y.: Calculation of Unsteady Transonic Aerodynamics for Oscillating Wings with Thickness (Computer Program). NASA CR-132477, Sept. 1974.
50. Runyan, Harry L.; and Woolston, Donald S.: Method for Calculating the Aerodynamic Loading on an Oscillating Finite Wing in Subsonic and Sonic Flow. NACA Rep. 1322, 1957.
51. Rodemich, E. R.; and Andrew, L. V.: Unsteady Aerodynamics for Advanced Configurations, Part II - A Transonic Box Method for Planar Lifting Surfaces. FDL-TDR-64-152, Part II, May 1965, Air Force Flight Dynamics Lab., Wright-Patterson Air Force Base, Ohio.

52. Olsen, J. J.: Demonstration of a Transonic Box Method for Unsteady Aerodynamics of Planar Wings. AFFDL-TR-66-121, Oct. 1966, Air Force Flight Dynamics Lab, Wright-Patterson Air Force Base, Ohio.
53. Stenton, T. E.; and Andrew, L. V.: Transonic Unsteady Aerodynamics for Planar Wings with Trailing Edge Control Surfaces. AFFDL-TR-67-180, Aug. 1968, Air Force Flight Dynamics Lab, Wright-Patterson Air Force Base, Ohio.
54. Cunningham, Atlee M., Jr.: The Application of General Aerodynamic Lifting Surface Elements to Problems in Unsteady Transonic Flow. NASA CR-112264, 1973.
55. Cunningham, Atlee M., Jr.: An Oscillatory Kernel Function Method for Lifting Surfaces in Mixed Transonic Flow. AIAA Paper 74-359, Apr. 1974.
56. Cunningham, Atlee M., Jr.: Further Developments in the Prediction of Oscillatory Aerodynamics in Mixed Transonic Flow. AIAA Paper 75-99, Jan. 1975.
57. Becker, J.: Vergleich gemessener und berechneter instationärer Druckverteilungen für den hohen Unterschall an einem elastischen gepfeilten Flügel. EWR-Bericht Nr. 403-69, Messerschmitt-Bolkow-Blohm, Sept. 1969.
58. Appa, Kari; and Smith, G. C. C.: Further Developments in Consistent Unsteady Supersonic Aerodynamic Coefficients. J. Aircraft, Vol. 9, No. 2, Feb. 1972, pp. 157-161.
59. Appa, Kari; and Smith, G. C. C.: Development and Application of Supersonic Unsteady Consistent Aerodynamics for Interfering Parallel Wings. NASA CR-2168, Aug. 1972.
60. Appa, Kari; and Smith, G. C. C.: Finite Element Supersonic Aerodynamics for Oscillating Parallel Wings. J. Aircraft, Vol. 11, No. 8, Aug. 1974, pp. 433-434.
61. Appa, Kari; and Jones, William P.: Integrated Velocity Potential Formulation of Unsteady Supersonic Aerodynamics for Interfering Wings. AIAA Paper 75-762, May 1975.

TABLE 1.- SUMMARY OF ANALYTICAL METHODS

Analysis method	Design loads	Active controls	Transonic range
General unsteady compressible potential aerodynamics (SOUSSA)	Present	Present	Future
Subsonic kernel-function analysis for wings with oscillating controls		Present	
Unsteady loads on lifting surfaces with sharp-edge separation	Present	Future	
Finite-difference method for oscillating transonic flow			Present
Transonic aerodynamics for oscillating wings with thickness			Present
Mixed subsonic-supersonic kernel-function analysis for oscillating wings			Present
Oscillatory supersonic lifting-surface panel method	Present	Present	

GENERAL SURFACE-PANEL METHOD:

- ARBITRARY COMPLETE A/C CONFIGURATION
- STEADY AND GENERAL UNSTEADY MOTION
- SUBSONIC AND SUPERSONIC
- COMPUTATIONAL EFFICIENCY

CURRENT DEVELOPMENTS:

- NONLINEAR EFFECTS (TRANSONIC FLOW, WAKE DEFORMATION)
- IMPROVED SURFACE ELEMENTS (HIGHER ORDER, SPECIAL PURPOSE)
- ROTATIONAL FLOW (TURBULENCE, VISCOSITY)

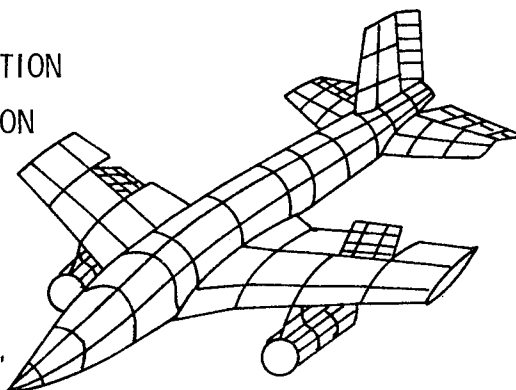


Figure 1.- Status of design-oriented potential-flow aerodynamics (SOUSSA).

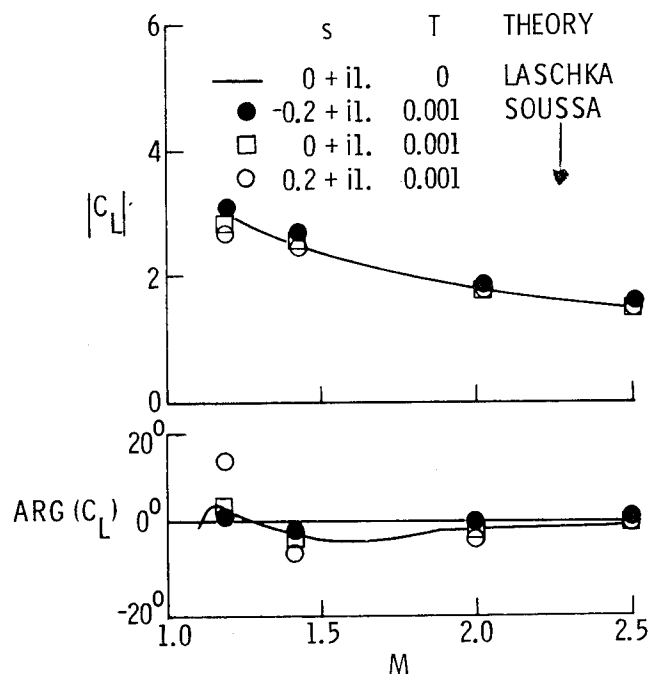


Figure 2.- Lift coefficient for aspect-ratio-2 rectangular wing oscillating in pitch.

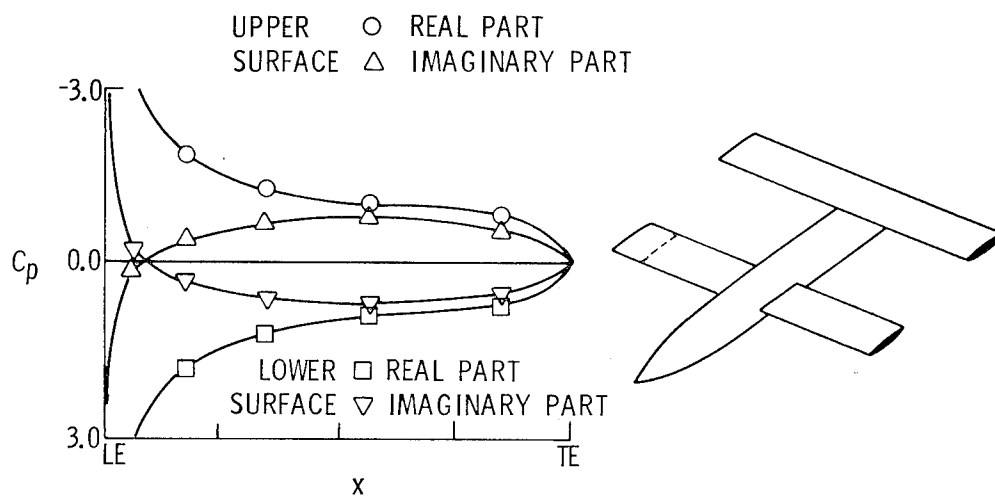
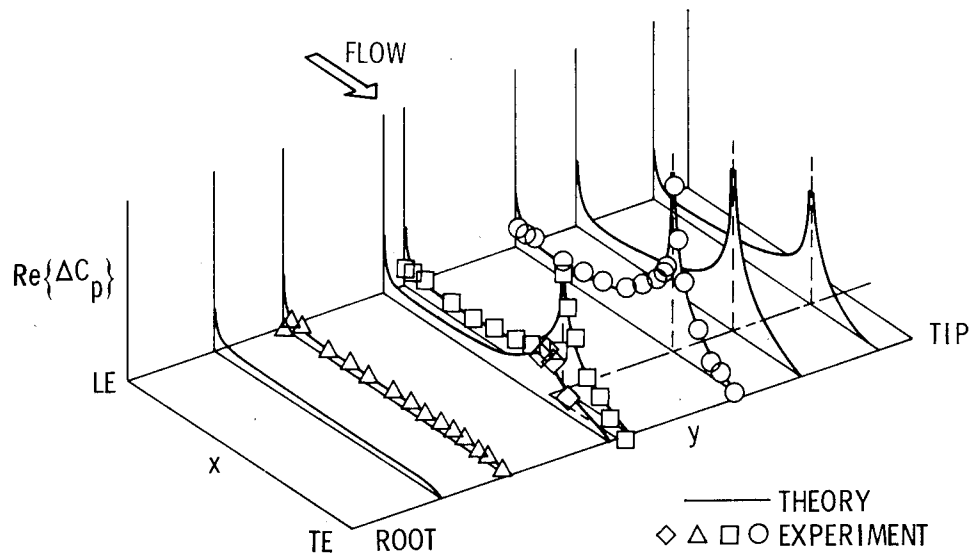
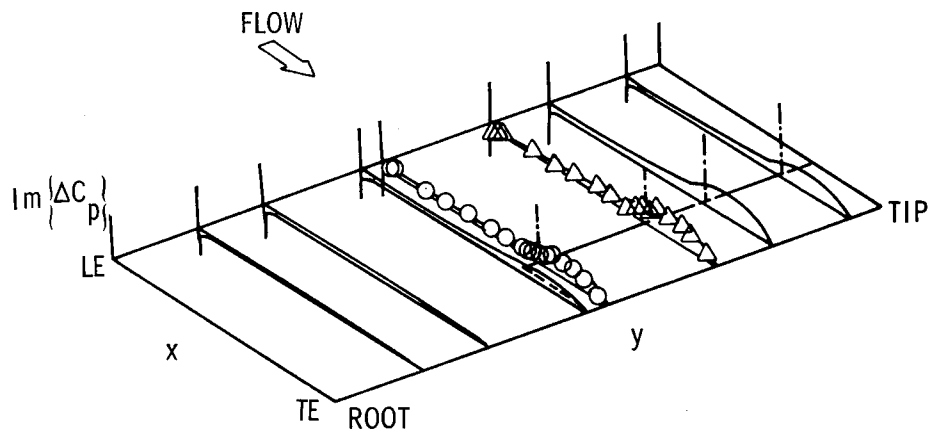


Figure 3.- Pressure distribution at wing spanwise station 0.78 on wing-body-tail in diverging pitch oscillation about wing midchord. $s = 0.1 + i1.5$, wing and tail aspect ratio = 6.0, $T = 0.09$.



(a) Real part.



(b) Imaginary part.

Figure 4.- Lifting pressure distribution on swept wing with oscillating control surface. $M_\infty = 0$; $k = 0.372$; $\delta = 0.66^\circ$.

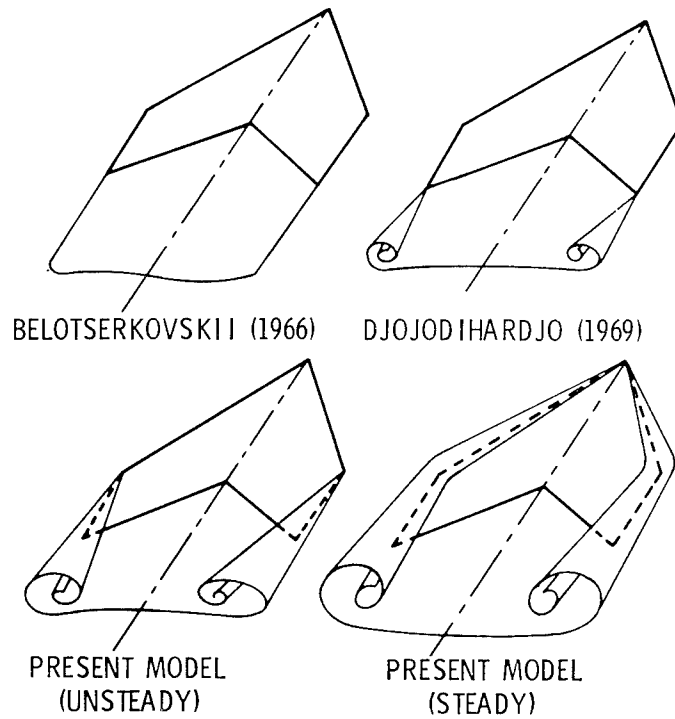


Figure 5.- Comparison of present models and previous models.

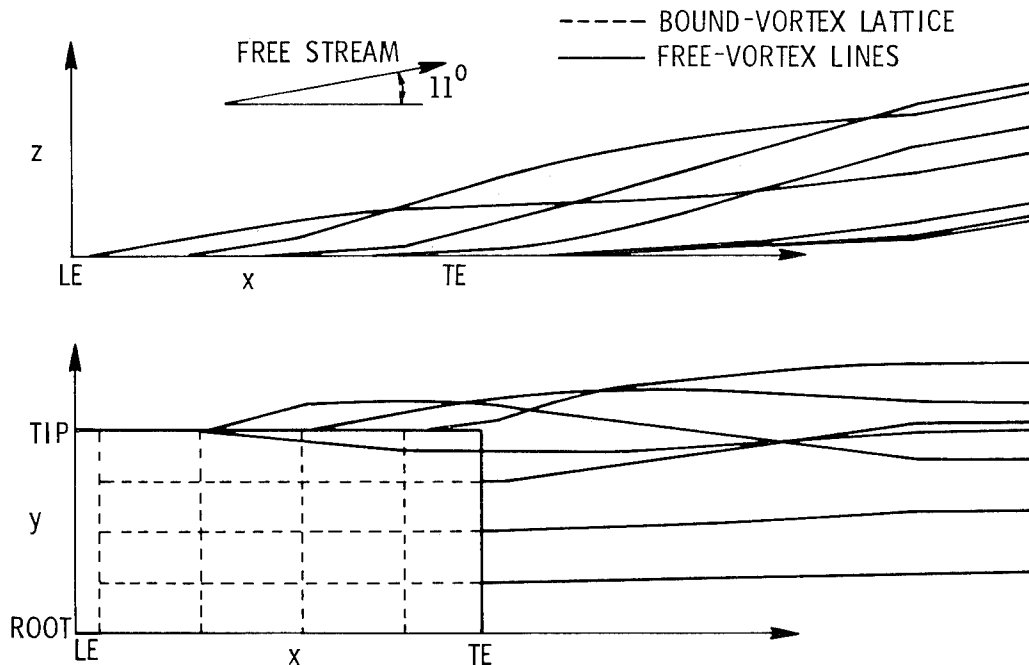


Figure 6.- Wake shape for aspect-ratio-1.0 rectangular wing in steady flow. $\alpha = 11^\circ$.

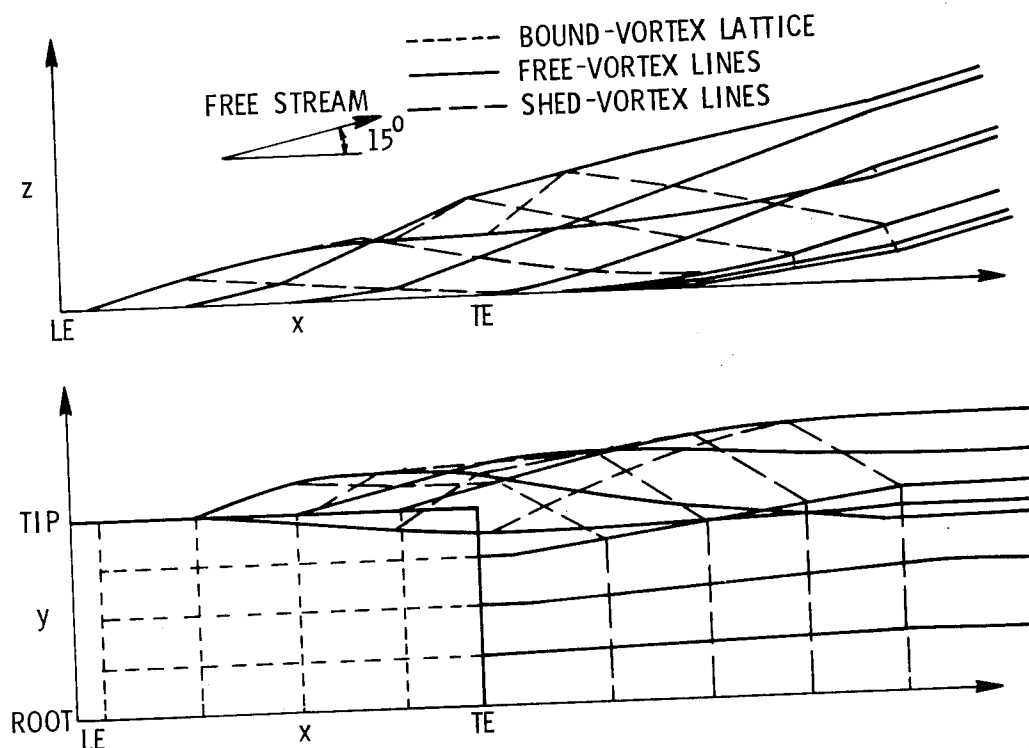


Figure 7.- Wake shape for aspect-ratio-1.0 rectangular wing in unsteady flow.
 $\alpha(t) = \alpha_0 + \dot{\alpha}t$; $\alpha_0 = 11^\circ$; $\dot{\alpha} = 1.0$; $t = 4$.

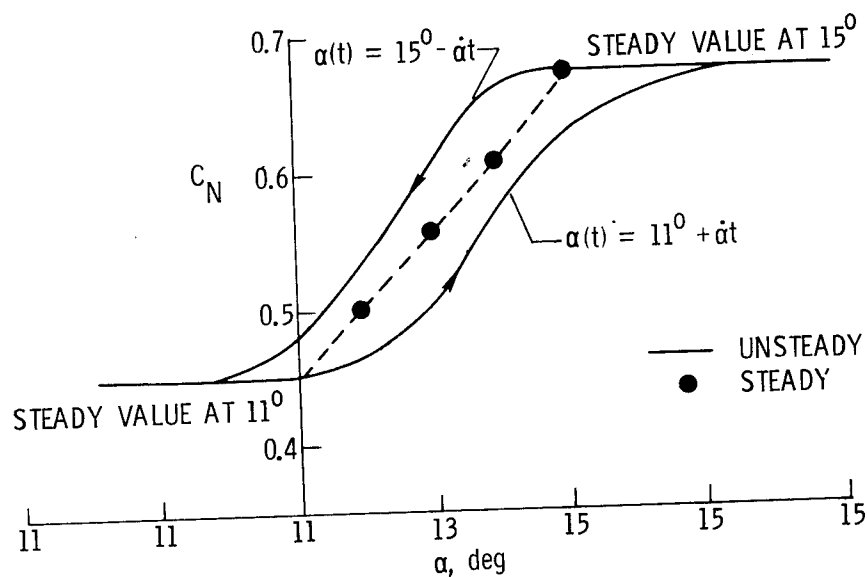


Figure 8.- Normal-force coefficient for aspect-ratio-1.0 rectangular wing in unsteady flow. $\dot{\alpha} = 1$.

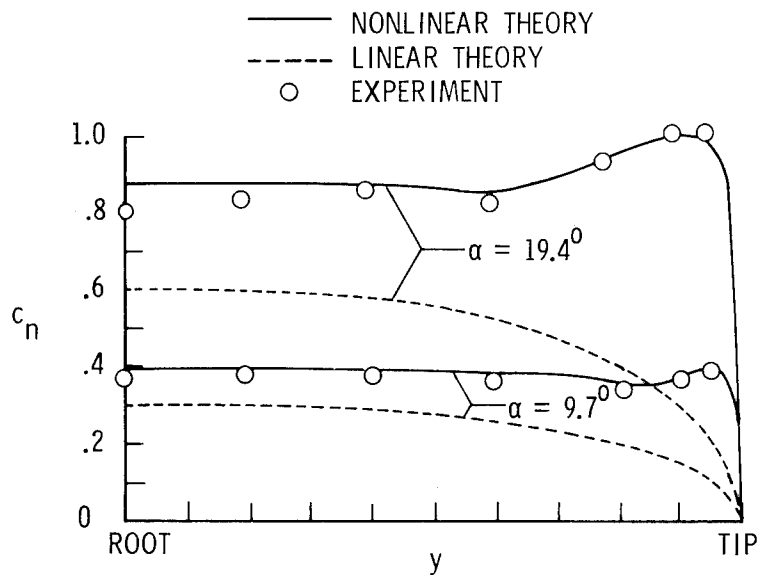


Figure 9.- Spanwise distribution of normal-force coefficient for aspect-ratio-1.0 rectangular wing.

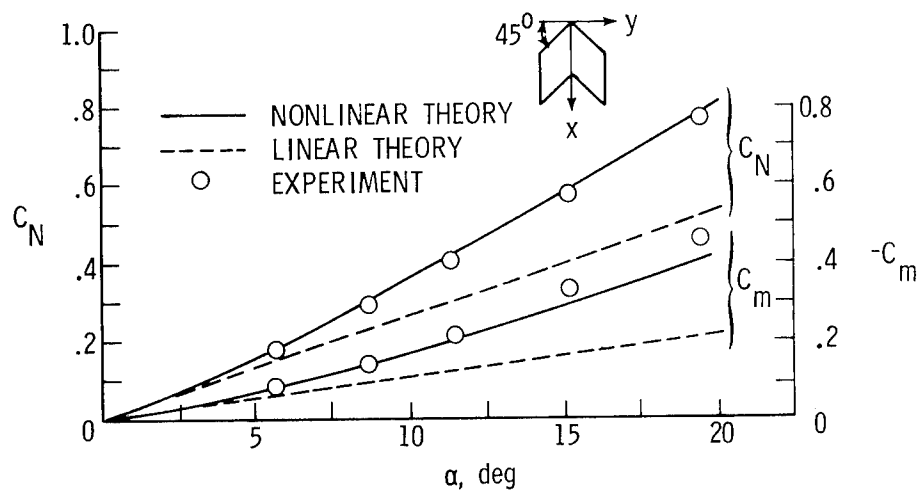


Figure 10.- Normal-force and pitching-moment coefficients for aspect-ratio-1.0 swept wing.

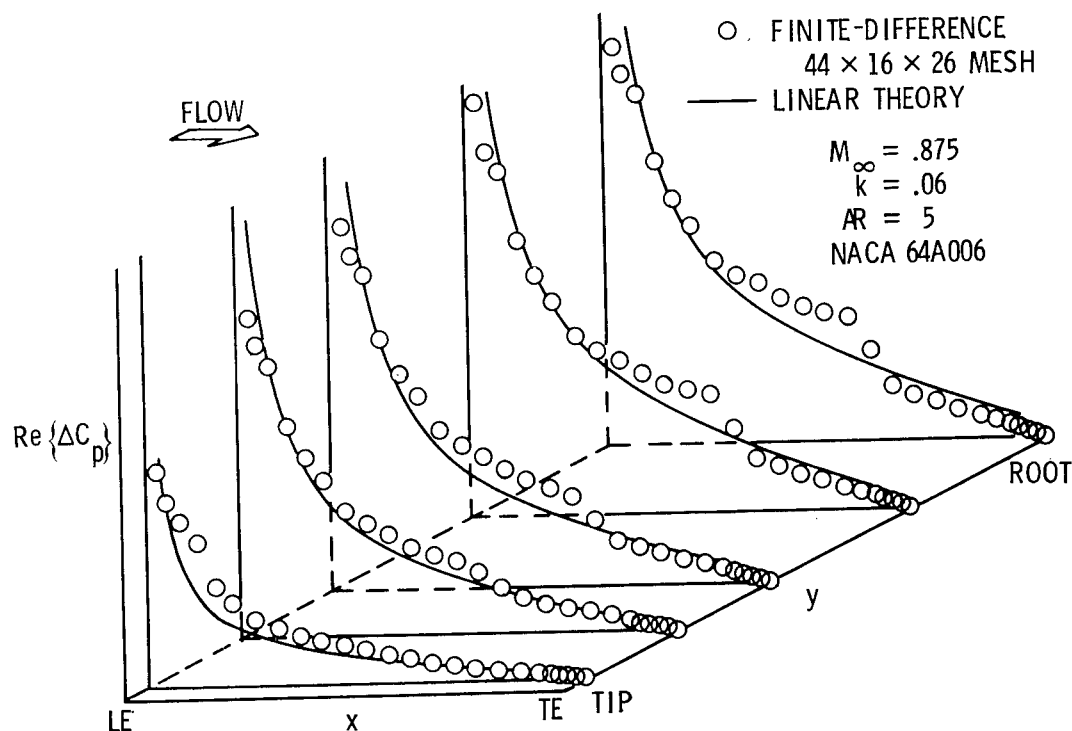


Figure 11.- Real part of pressure distribution on aspect-ratio 5. rectangular wing with NACA 64A006 airfoil oscillating in pitch. $M_\infty = 0.875$, $k = 0.06$.

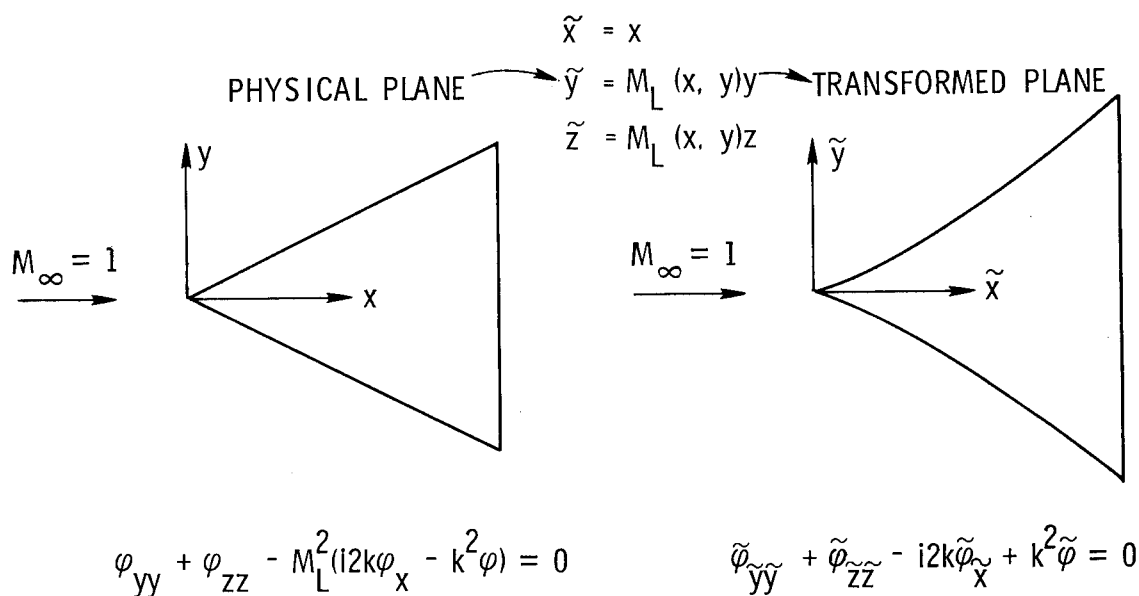


Figure 12.- Coordinate transformation for transonic flow.

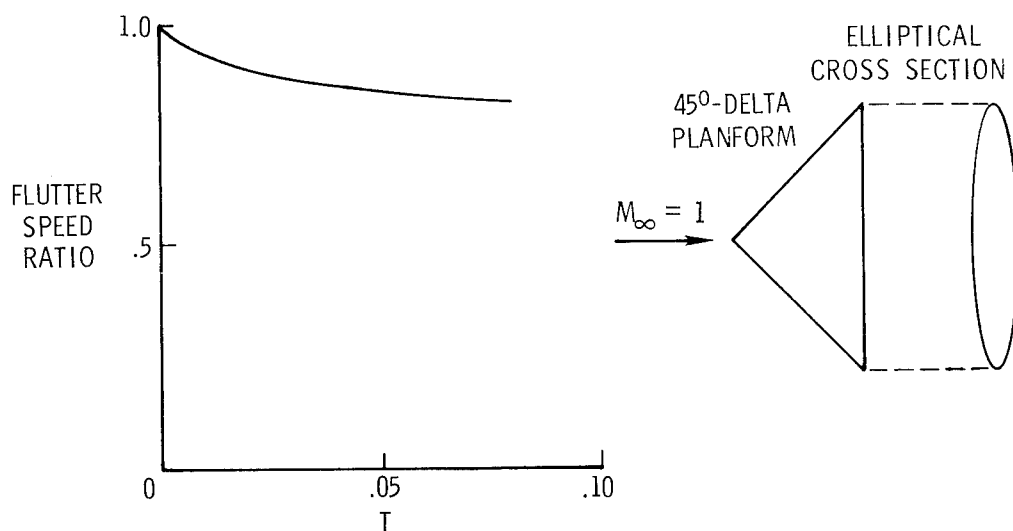


Figure 13.- Effect of thickness on transonic flutter speed.

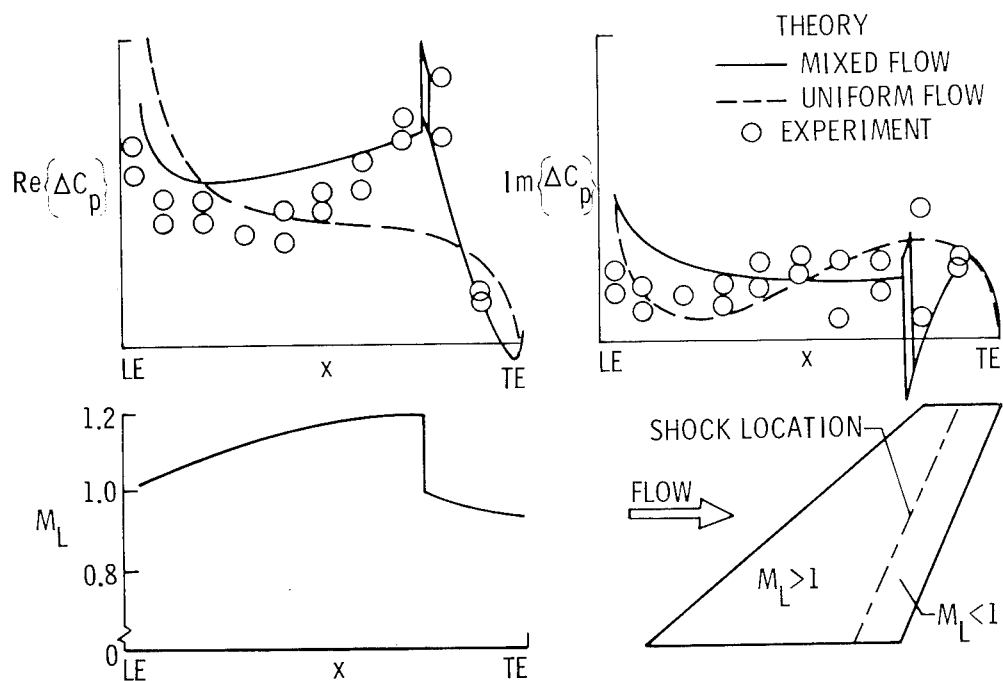


Figure 14.- Pressure distribution at spanwise station 0.556 on wing oscillating in bending. $M_\infty = 0.997$, $k = 0.207$.

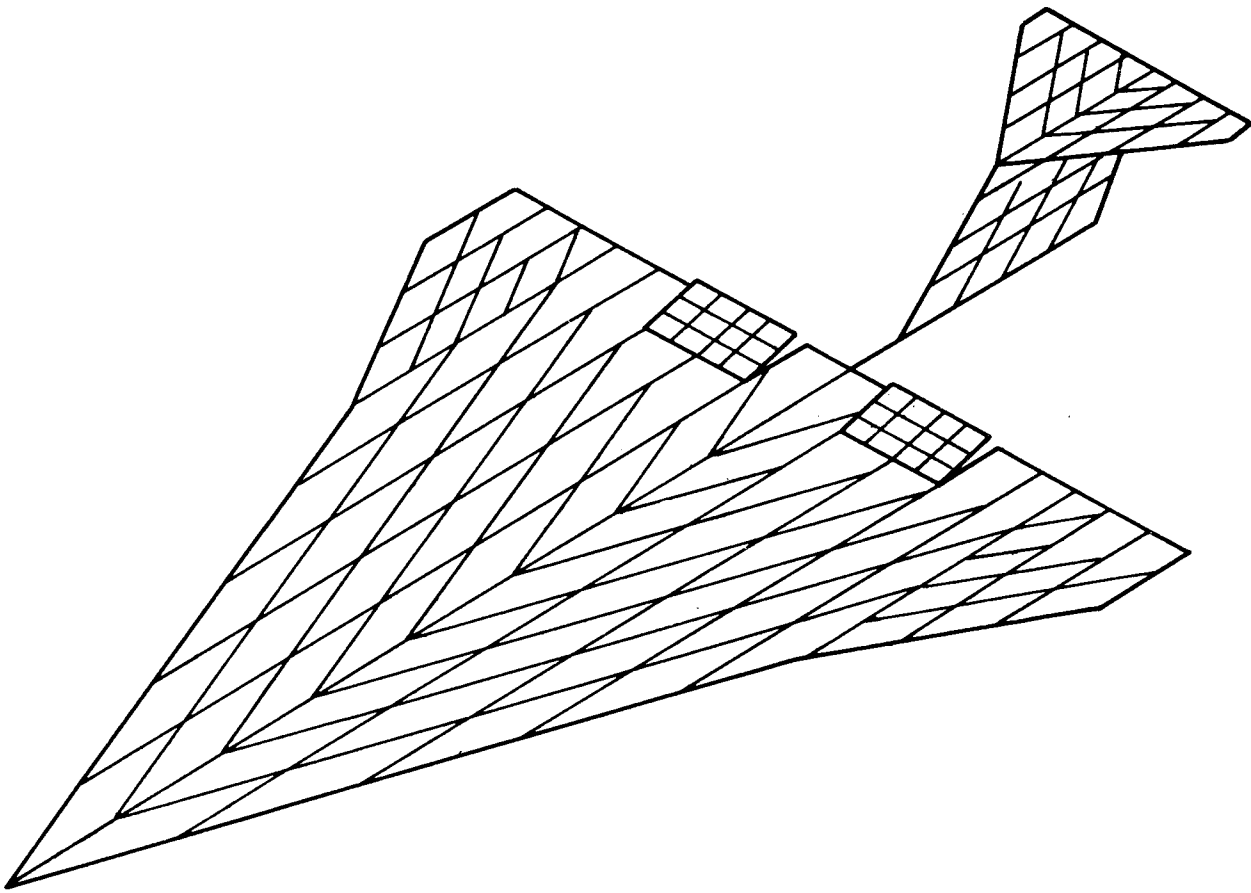


Figure 15.- Geometrical capabilities of oscillatory supersonic lifting-surface panel method.

FATIGUE OF TITANIUM ALLOYS IN A SUPERSONIC- CRUISE AIRPLANE ENVIRONMENT

L. A. Imig
NASA Langley Research Center

SUMMARY

Many fatigue tests have been conducted to explore thermal effects on structural materials in the time since supersonic commercial flight first received serious consideration. Most of the testing has been conducted with coupons of structural materials because large numbers of realistic simulated structures are prohibitively expensive. The test programs conducted by several aerospace companies and NASA, summarized in this paper, studied several titanium materials previously identified as having high potential for application to supersonic-cruise airplane structures. These studies demonstrate that the temperature (560 K) by itself produced no significant degradation of the materials. However, the fatigue resistance of titanium-alloy structures, in which thermal and loading effects are combined, has been studied insufficiently. The predominant topic for future study of fatigue problems in Mach 3 structures should be the influences of thermal stress — particularly, the effects of thermal stress on failure location.

INTRODUCTION

In the early 1960's, worldwide anticipation of supersonic commercial flight prompted extensive study of materials and thermal effects for supersonic airplane structures. The predominant questions were: Will materials stably withstand the prolonged exposure to elevated temperature? How will structures respond to prolonged temperature and thermal stresses? What test procedures will be required to verify structural fatigue resistance to the loads, temperatures, and thermal stresses experienced by a transport airplane during supersonic flight? Since then, many tests have been conducted by NASA and the aerospace industry to study thermal effects on materials. But structural response to temperature and thermal stress has received little study in the United States because the cost of sample structures is very high, and because the driving force, development of a U.S. supersonic transport, was removed. The only continuing research uses coupon specimens to study test procedures to account for the loading, temperature, and thermal stress expected in supersonic-cruise airplanes.

This paper summarizes the NASA/industry research and discusses the results insofar as they address the development of simplified testing procedures for supersonic-cruise airplane materials and structures. The research programs discussed here all used titanium alloys. Much more recently, composite material development has produced materials showing potential sufficient

to warrant study of their applicability to supersonic-cruise airplane structures. Such studies have not yet been conducted.

SYMBOLS

The units for physical quantities used in this paper are given in the International System of Units (SI); however, measurements during the investigations were made in U.S. Customary Units.

E	modulus of elasticity, GPa
K_{Tg}	gross-area stress-concentration factor
M	Mach number
S	stress, MPa
S_d	one-g design stress on gross section (stress on gross section for level unaccelerated flight at maximum gross mass), MPa
S^*	maximum gross stress in most frequently occurring simulated flight, MPa
T	temperature, K
T_s	stagnation temperature, K
T_{sol}	solidus temperature, K
ΔT	temperature range, K
α	coefficient of linear thermal expansion, 1/K

Abbreviations:

CA	constant amplitude
DA	duplex annealed
FBF	flight-by-flight
MA	mill (single) annealed
STA	solution treated and aged
SW	spotwelded
TA	triplex annealed
6-4	titanium alloy Ti-6Al-4V
8-1-1	titanium alloy Ti-8Al-1Mo-1V

MATERIAL SELECTION AND TESTING OPTIONS

Extensive material characterization studies (refs. 1-10) identified titanium alloys as leading candidates for structural applications at a Mach number of 3. These studies were organized to screen a large number of titanium alloys, stainless steels, superalloys, and for comparison, some aluminum alloys. The studies considered such diverse topics as availability, fabricability, mechanical properties, corrosion resistance, and thermal effects. Thus, titanium alloys were selected only after very broad deliberations.

Most of the research discussed in this paper was initiated at least 10 years ago when Ti-8Al-1Mo-1V was the leading titanium-alloy candidate so the early research programs used that alloy. Since then, alloy Ti-6Al-4V has proven to have better salt-corrosion resistance than Ti-8Al-1Mo-1V. Except where salt is an important part of the test environment, trends in data from one alloy seem representative for the other alloy, as discussed later in this paper.

Material selection has an important influence on the procedures employed for structural fatigue tests. For example, figure 1 shows that Mach 3 structures of the stainless steel, superalloy, or titanium alloy shown would operate at much lower temperatures relative to their ultimate thermal capabilities than would be the case for the aluminum alloy in a Mach 2 structure. Thus, thermal effects on the materials are likely to be much more important for the Mach 2 aluminum alloy structure than for Mach 3 structures of the other materials. Consequently, the rigorous simulation of thermal effects is likely to be much more important in fatigue tests of Mach 2 aluminum alloy structure than for structures of the other three materials shown.

Such thermal considerations for supersonic-cruise-related fatigue tests lead to several options as shown in the following table:

Thermal options		Test objectives			Speed	Expense
		Verify service life	Identify failure locations	Account for temperature and thermal stress effects		
Cyclic		Yes	Yes	Yes	Slow	Most
C o n s t a n t	Hot	Not directly	?	Some	Fast	<div style="text-align: center;"> ↓ Least </div>
	Presoaked			Some		
	Ambient			No		

The first option, cyclic temperature, provides the best simulation of supersonic-cruise airplane operation. Such a test is likely to satisfy the predominant test objectives shown in the table, but will be very slow and expensive — especially for large test articles and for temperature cycles as are being employed in fatigue tests of Concorde (refs. 11 and 12).

The other three options listed avoid temperature cycles. Thus, these constant-temperature options would fail to simulate the cyclic temperatures and temperature effects of repeated supersonic-cruise flights. To recommend or undertake a constant-temperature test would require an independent justification that the procedure was acceptable.

The three constant-temperature options would allow testing speeds nearly as fast as for subsonic airplanes. Such tests would obviously be much less expensive than cyclic-temperature tests, but carry the risk of compromising some important test objectives. To insure acceptable compromises, the test procedures for the American SST were planned to rely heavily on empirical and analytical techniques developed from extensive preliminary testing programs (refs. 13 and 14).

The obviously high cost of cyclic-temperature structural fatigue tests and the low relative temperature for a titanium structure at $M = 3$ justify exploration for relatively fast and inexpensive fatigue tests, perhaps constant-temperature fatigue tests, which would provide suitable information about the life and failure locations of the test article. Such exploratory research has been in progress for more than 10 years. Most of the effort has employed coupon specimens or small components, but some early work was conducted with larger specimens. In most of the work, thermal stresses were simulated mechanically or purposely minimized; thus, little information about thermal stress influences on failure locations has been derived.

The remainder of this paper will discuss previous studies that addressed the simplification of testing procedures from the prolonged cyclic-temperature conditions experienced by a supersonic-cruise airplane. Wing structure was considered in all of these investigations.

FATIGUE RESEARCH PROGRAMS

The research programs discussed in this section originated after the decision to construct an American SST from predominantly titanium alloys; thus, these programs all used titanium materials. The programs were conducted at the Lockheed-California Company, The Boeing Commercial Airplane Company, the LTV Aerospace Corporation, and the Langley Research Center. The important aspects of the gust and maneuver spectrums employed for these studies were nearly the same; thus, the results of the studies may be compared directly.

Tests at the Lockheed-California Company

In a recently completed series of flight-by-flight fatigue tests, the Lockheed-California Company explored potential thermal simplifications in fatigue tests (refs. 15 and 16). Their program included a variety of material and specimen combinations, and test conditions as shown in the following tabulations:

Sheet material	Specimen configuration	Kind of fatigue test	Test temperatures
8-1-1 MA 8-1-1 DA 8-1-1 TA 6-4 MA	Central-hole coupon	Accelerated	Ambient (300 K) Hot (530 K) Cyclic (300 K to 530 K)
(Extrusions) 8-1-1 MA 6-4 STA	Central-hole coupon	Real-time	Cyclic (300 K to 530 K)
8-1-1 DA	Coupon with single-spotweld tab		

As shown in figure 2, an accelerated simulated flight required only 5 sec (19 sec for accelerated tests with cyclic temperature), compared with about 65 min for real-time flight simulation. In all these tests, a mechanical tensile stress increment during cruise and a compressive stress increment during descent were added to the one-g stress to simulate the thermal stress for wing substructure. All of the tests were conducted at a gross-area one-g design stress of 172 MPa. As a rule, four replicate tests were conducted for accelerated test conditions and six for real-time test conditions.

The median fatigue lives from Lockheed's accelerated tests are shown in figure 3 normalized by the median lives from their real-time tests. The top row of bars is for constant elevated-temperature tests, the middle row is for room-temperature tests, and the bottom row is for cyclic-temperature tests.

None of the accelerated-test methods produced a consistent ratio of fatigue life to real-time life. Within each row, the bars differ in height by at least a factor of 3.

Room-temperature and cyclic-temperature accelerated tests of some materials produced fatigue lives that were longer than the real-time lives; for other materials, these accelerated tests produced fatigue lives that were shorter than the real-time lives. For a given material, the fatigue life from cyclic-temperature accelerated tests was about equal to the life from room-temperature accelerated tests. Thus, the added experimental complication attendant to the temperature cycles for these accelerated tests proved of little value.

Only the constant elevated-temperature tests produced a consistent result: their fatigue lives were always shorter than for the corresponding real-time test.

Tests at NASA

NASA has conducted a separate series of flight-by-flight fatigue tests (refs. 17 and 18) which complement Lockheed's program. The following table contains the major components of each:

Test condition	Lockheed	NASA
Design stress	172 MPa	138, 165, 195 MPa
Materials	7	3
K_{Tg}	3	5
Load spectrum	only slightly different	
Real-time tests	1 hr per flight, 1 stress profile	1.5 hr per flight, 3 stress profiles

In the NASA tests, the stresses in each flight simulated thermal stresses for the substructure (as in the Lockheed tests), or thermal stresses for the skin (fig. 4), or simulated a reference flight without thermal stress. Accelerated tests were conducted at constant temperatures of 300 K and 560 K. In real-time tests, the temperature was cycled within each flight from 300 K to 560 K. Gross-area one-g design stresses for these tests were 138, 165, and 193 MPa.

For the schematic flights shown in figure 4, the blocks represent, in sequence, the cyclic stresses for climb, cruise, and descent segments of flight (ref. 17). The minimum stress in all these flights was -0.50 of the one-g design stress.

The NASA results are summarized in figure 5 for both accelerated and real-time tests with the two thermal-stress simulations, and for the reference stress profile. These data are plotted against S^* (see fig. 5), which established the range of the present ground-air-ground (GAG) cycles, because much previous research has shown that range to be the predominant source of fatigue damage for this type of flight-simulation loading. The lower left of the figure, for accelerated tests at 560 K, shows that the results of tests at all three design stresses fall reasonably well on a smooth curve. The dashed curve in the plot represents the results of room-temperature tests (ref. 18). The lives from room-temperature tests were about twice as long as for tests at 560 K. The curves for both temperatures indicate that the test results correlated well with only the GAG cycles. Thus, these results are consistent with extensive earlier data that establish the importance of GAG cycles (see

refs. 13 and 19 for examples). In the present tests, the only effect of the simulated thermal stresses was to change the GAG-cycle range. In structures, the predominant influence of thermal stresses is also likely to be on GAG cycles. Thus, the good correlations shown on figure 5 suggest that the influence of thermal stresses on fatigue can be simply accounted for by calculating their contribution to GAG cycles.

The lower right part of figure 5 shows that the lives of all the real-time tests were longer than for accelerated tests at 560 K for corresponding stress levels. The data include the effects of quite different thermal stress conditions and include the cumulative effects of the long cyclic thermal exposure. The constant-elevated-temperature data provide a very good lower bound for the results under the more complicated test conditions. These observations suggest that these constant-elevated-temperature data could be used as design data for all of the real-time conditions represented in the figure.

Tests at The Boeing Commercial Airplane Company

Specimens with somewhat more realistic structural features than the Lockheed and NASA specimens were prepared for Boeing's study of test simplification procedures (ref. 20). Boeing's specimen, figure 6, consisted of two components joined by commercially available threaded fasteners. Boeing conducted flight-by-flight fatigue tests in which the stress sequences were identical to those in the NASA tests. Five specimens were tested in each of three accelerated-test series conducted at a one-g design stress of 207 MPa.

The first series included cyclic differential heating of the two specimen components to simulate Mach 3 temperature conditions (at one flight per min) and to provide a set of reference fatigue lives. The other two series of tests were conducted to evaluate two simpler test procedures. These series were conducted at two flights per minute and at constant temperature. Of the two series, one was conducted entirely at room temperature, but specimens for the other were presoaked for 500 hours at 560 K before being tested at room temperature as had been proposed in reference 13 for the American SST.

The results of all three series of tests, figure 6, indicate only small differences among the fatigue lives. Boeing's data show that the cyclic-temperature (reference) tests produced lives about equal to those from their room-temperature tests — a result very similar to that from Lockheed's tests.

Tests at the LTV Corporation

The LTV Corporation tested large titanium-alloy box-beam covers representing structure for commercial supersonic-cruise airplanes (refs. 21 and 22). Their specimens, of Ti-8Al-1Mo-1V, were about 300 cm by 58 cm (see fig. 7). Four covers each were fabricated by riveting, spotwelding, and fusion welding. They contained a transverse splice, a hand hole, and a structural door to represent typical structural features.

Specimens for each fabrication method were tested in three ways. For one test, only constant-amplitude GAG cycles were applied. The cycles ranged from the one-g stress of 172 MPa to -86 MPa, and the entire test was at room temperature. In another test, only constant-amplitude cruise cycles were applied. The mean stress during these cruise cycles included a positive increment of stress to simulate mechanically a thermal stress for a spar cap or a similar interior component. The alternating stresses applied about that mean resulted in test stresses of 241 ± 43 MPa, and the entire test was at 560 K. The remaining two covers of each type were tested in a composite test combining both flight-by-flight and block loading as follows. The climb and GAG stresses for 240 flights were applied flight-by-flight at room temperature; the cruise stresses for 240 flights were then applied in a randomly arranged block at 560 K. Descent stresses were neglected because they were below the fatigue limit. Such blocks of this composite loading were repeated until the covers failed or the tests were terminated for other reasons.

For the riveted and spotwelded covers, constant-amplitude tests identified the same critical crack locations as the block tests. But for fusion-welded covers the crack locations were different in the three kinds of tests. Thus, the adequacy of these simplified (constant-amplitude) tests for identifying the critical failure locations depended on the fabrication method.

DISCUSSION OF RESULTS

All of the data reviewed in earlier sections of this paper are combined in figure 8 to permit broader discussion of the results than was permissible when discussing only the individual investigations.

The NASA results shown are for tests of all three titanium materials. The results of accelerated tests of all three materials at 560 K are represented by the solid curve shown. The fatigue lives of these materials were about the same in these tests. The fatigue lives from real-time tests of the three materials were also about equal (see open circles, fig. 8). These results demonstrate that the fatigue resistance of these three materials is substantially the same, and suggest that the fatigue design allowable stresses for these materials would be the same — a conclusion similar to that given in reference 23 for several aluminum alloys.

Lockheed's data from coupons tested at 530 K are represented by the diamond symbol and the dashed curve. The symbol is plotted at the average life (see ref. 15 for data) of their seven kinds of specimens. The curve is shown simply to approximate a trend from their data.

The large separation between the two curves reflects the influence of the stress-concentration factors for the coupons in the two series of tests. The stress-concentration factor, or more generally, a structural-quality index, is widely recognized as one of the major factors upon which structural fatigue life depends. The large separation between these curves quantifies the importance of that index.

The Boeing and LTV data in figure 8 each relate to the coupon data in a way consistent with considerations of their specimen qualities. The small Boeing components were very carefully fabricated, and their tests produced fatigue lives very close to the lives from Lockheed's open-hole coupons when their test temperatures are accounted for. The Boeing datum point represents room-temperature tests. Their report (ref. 20) shows that elevated temperature tests produced lives only one-half as long as at room temperature. Adjusting the data point in figure 8 to account for constant elevated temperature would put it very close to Lockheed's diamond. The LTV data, on the other hand, represent much larger specimens, in which uniformly high structural quality is much more difficult to maintain. Thus, the fatigue strength of the box-beam covers fell within the lower group of data. These limited data for titanium coupons and structure are consistent with other publications (refs. 24 and 25) reporting that the fatigue behavior of aluminum-alloy structures approximated that from notched aluminum-alloy specimens of $K_T = 4$ to 5, but more data would be required to confirm that result for titanium structures.

The data in figure 8 were obtained from tests that employed substantially the same load spectrum, and these results inherently reflect that spectrum. The gust and maneuver stresses derived in reference 17 were for a hypothetical but realistic supersonic-cruise airplane. Assuming that these stresses will be representative for future supersonic-cruise airplanes, the results of figure 8 will have useful applicability to future supersonic-cruise airplanes.

Design Stresses

Figure 8 leads to interesting speculation about the use of such data to determine design stresses. Using the flight stresses of references 15 and 17 as examples, calculation of one-g design stresses from the S^* values shown indicates one-g design stresses of only about 120 MPa (17 ksi) up to 180 MPa (26 ksi) for a design life of 20,000 flights. For comparison, the following table shows values of one-g design stress currently being considered for wing structure of supersonic-cruise airplanes:

Airplane	One-g wing stress	Payload fraction
Boeing arrow-wing (ref. 26)	172 MPa (25 ksi)	0.065
Lockheed arrow-wing (ref. 27)	165 (24)	.065
LTV study (ref. 28)	155 (22.5)	.085

These design stresses are within the range of values determined from figure 8. But the selection of a particular value of design stress depends strongly on the assumed level of structural quality.

A Concept for Design and Testing

The data in figures 5 and 8 show that if a structure were designed from constant-elevated-temperature fatigue data, but tested at room temperature, an appropriate factor would be required to establish the duration of the room-temperature test. Data from Boeing, Lockheed, and NASA show that the fatigue lives from room-temperature tests were about twice the lives from tests at 560 K. Therefore, a factor of 2 would be required to account for the temperature difference and an additional factor would be required beyond that, as is conventional in such fatigue tests, to account for experimental uncertainties.

A constant-temperature concept of design and testing recommends itself by its simplicity. But a major deterrent to adopting that concept is the risk that a constant-temperature test would fail to identify the critical structural failure locations. To remove that deterrent would require assurance from many tests of large components, showing that constant-temperature tests correctly identify the failure locations found to be critical in service-simulation tests. Insufficient funding has been available to conduct such an investigation in a generic way; if the adequacy of constant-temperature tests requires verification to support a future airplane development, the cost would then be more easily justified.

Thermal Stress Considerations

Thermal stresses resulting from differential structural temperature have caused much concern about their potentially harmful effects on fatigue. Simple calculations of thermal stress ($E\alpha \Delta T$) produce the values in the following table for the materials and applications shown:

Material Application	Temperature range, K		Calculated thermal stress range $E\alpha \Delta T$, MPa	Reported thermal stresses, MPa
	Max.	Min.		
Aluminum Subsonic	320	220	170	20 to 80 (estimated)
Titanium Mach 3 cruise	560	220	340	35 to 140 (ref. 13)
Aluminum Mach 2 cruise	375	220	270	55 to 140 (ref. 29)

The calculated thermal-stress ranges in the third column represent theoretical limits for the temperature ranges shown. Practical considerations prevent such large stresses from developing. More realistic values calculated in references 13 and 29 by accounting for the practical restraints are listed in the fourth column. These values are only 0.1 to 0.5 of the theoretical values. How far below the theoretical values they are depends on thermal conductivity through joints, fabrication techniques to relieve thermal strains, adjacent

heat sinks, and other factors. The "practical fractions" of the theoretical values reflect that thermal stresses develop to a larger or smaller degree depending on the structural location.

Conventionally, aerodynamically induced thermal stresses are not directly accounted for in the design of subsonic airplane structure. Yet applying the "practicality factors" to the theoretical range for subsonic-flight temperatures indicates that thermal stresses of 20 to 80 MPa might realistically develop in subsonic airplane structure.

The upper values of thermal stress for the subsonic aluminum and Mach 3 titanium applications (80 and 140 MPa) are of about the same size as the respective one-g design stresses. That observation provokes some very interesting discussion. If one-g-sized thermal stresses can be practically ignored, as they have been for subsonic airplanes, perhaps they can also be ignored for Mach 3 titanium airplanes. On the other hand, if such thermal stresses constitute a serious problem for Mach 3 structures, perhaps they must also be deliberately accounted for in subsonic-airplane structure. Of course, the larger the thermal stresses, the less advisable ignoring them becomes; thus, for a Mach 2 aluminum structure (Concorde) thermal stress considerations dictated that very elaborate thermal simulations be employed during fatigue testing. But even for Concorde, reference 29 suggested the possibility of safely ignoring thermal stresses in some structural locations.

CONCLUDING REMARKS

Many fatigue tests have been conducted to explore thermal effects on structural materials in the time since supersonic commercial flight first received serious consideration. Most of the testing has been conducted with coupons of structural materials because large numbers of realistic simulated structures are prohibitively expensive. The test programs summarized in this paper, conducted by several aerospace companies and NASA, studied several titanium materials previously identified as having high potential for application to supersonic-cruise airplane structures. These studies demonstrate that the temperature (560 K) by itself produced no significant degradation of the materials. However, the fatigue resistance of titanium-alloy structures, in which thermal and loading effects are combined, has been studied insufficiently. The predominant topic for future study of fatigue problems in Mach 3 structures should be the influences of thermal stress — particularly, the effects of thermal stress on failure location.

REFERENCES

1. Raring, Richard H.; Freeman, J. W.; Schultz, J. W.; and Voorhees, H. R.: Progress Report of the NASA Special Committee on Materials Research for Supersonic Transports. NASA TN D-1798, 1963.
2. Anon.: Proceedings of NASA Conference on Supersonic-Transport Feasibility Studies and Supporting Research. NASA TM X-905, 1963.
3. Braski, David N.; and Heimerl, George J.: The Relative Susceptibility of Four Commercial Titanium Alloys to Salt Stress Corrosion at 550° F. NASA TN D-2011, 1963.
4. Illg, Walter; and Castle, Claude B.: Fatigue of Four Stainless Steels and Three Titanium Alloys Before and After Exposure to 550° F (561° K) up to 8800 Hours. NASA TN D-2899, 1965.
5. Illg, Walter; and Imig, L. A.: Fatigue of Four Stainless Steels, Four Titanium Alloys, and Two Aluminum Alloys Before and After Exposure to Elevated Temperatures for up to Three Years. NASA TN D-6145, 1971.
6. Phillips, Edward P.: Effect of Outdoor Exposure at Elevated Temperature on the Fatigue Life of Ti-8Al-1Mo-1V Titanium Alloy and AM 350 Stainless Steel Sheet. NASA TN D-5362, 1969.
7. Phillips, Edward P.: Effect of Outdoor Exposure at Ambient and Elevated Temperatures on Fatigue Life of Ti-6Al-4V Titanium Alloy Sheet in the Annealed and the Solution-Treated and Aged Condition. NASA TN D-7540, 1974.
8. Peterson, John J.: Fatigue Behavior of AM 350 Stainless Steel and Titanium 8Al-1Mo-1V Sheet at Room Temperature, 550° F, and 800° F. NASA CR-23, 1964.
9. Gideon, D. N.; Marschall, C. W.; Holden, F. C.; and Hyler, W. S.: Exploratory Studies of Mechanical Cycling Fatigue Behavior of Materials for the Supersonic Transport. NASA CR-28, 1964.
10. Healy, M. S.; Marschall, C. W.; Holden, F. C.; and Hyler, W. S.: The Fatigue Behavior of Materials for the Supersonic Transport. NASA CR-215, 1965.
11. N'Guyen, V. P.; and Ripley, E. L.: Design Philosophy and Fatigue Testing of the Concorde. Mann, J. Y.; and Milligan, I. S., eds.: Aircraft Fatigue—Design, Operational, and Economic Aspects. Pergamon Press, c. 1972. Pergamon Press (Australia) Pty Limited, pp. 403-436.
12. Ripley, E. L.: The Philosophy Which Underlies the Structural Tests of a Supersonic Transport Aircraft With Particular Attention to the Thermal Cycle. Advanced Approaches to Fatigue Evaluation. NASA SP-309, 1972, pp. 1-91.

13. Donaldson, D. R.; and Kenworthy, K. J.: Fatigue Design and Test Program for the American SST. Mann, J. Y.; and Milligan, I. S., eds.: Aircraft Fatigue—Design, Operational, and Economic Aspects. Pergamon Press, c. 1972. Pergamon Press (Australia) Pty Limited, pp. 437-476.
14. Doty, Ralph J.: Fatigue Design Procedure for the American SST Prototype. Advanced Approaches to Fatigue Evaluation. NASA SP-309, 1972, pp. 365-404.
15. Anon.: Fatigue Strength Evaluation of Titanium Materials for the Supersonic Transport Under Flight-by-Flight Loading Spectra. Lockheed-California Company Technical Report SST-66-2, 1966.
16. Lunde, Ted: Real-Time Testing of Titanium Sheet and Extrusion Coupon Specimens Subjected to Mach 2.7 Supersonic-Cruise Airplane Wing Stresses and Temperatures. NASA CR-2754, 1977.
17. Imig, L. A.; and Illg, Walter: Fatigue of Notched Ti-8Al-1Mo-1V at Room Temperature and 550° F (560° K) With Flight-by-Flight Loading Representative of a Supersonic Transport. NASA TN D-5294, 1969.
18. Imig, L. A.; and Garrett, L. E.: Fatigue-Test Acceleration With Flight-by-Flight Loading and Heating to Simulate Supersonic Transport Operation. NASA TN D-7380, 1973.
19. Naumann, Eugene C.: Evaluation of the Influence of Load Randomization and of Ground-Air-Ground Cycles on Fatigue Life. NASA TN D-1584, 1964.
20. Watanabe, R. T.: Acceleration of Fatigue Tests for Built-up Titanium Components. NASA CR-2658, 1976.
21. Peterson, John J.: Fatigue Behavior of Ti-8Al-1Mo-1V Sheet in a Simulated Wing Structure Under the Environment of a Supersonic Transport. NASA CR-333, 1965.
22. Peterson, John J.: Fatigue Behavior of a Fusion Welded Ti-8Al-1Mo-1V Simulated Wing Structure Under the Environment of a Supersonic Transport. NASA CR-881, 1967.
23. Templin, R. L.; Howell, F. M.; and Hartman, E. C.: Effect of Grain Direction on Fatigue Properties of Aluminum Alloys. Product Engineering, Vol. 21, No. 7, July 1950, pp. 126-130.
24. Spaulding, E. H.: Design for Fatigue. Soc. Auto. Engr. Trans., Vol. 62, 1954, pp. 104-116.
25. Crichlow, Walter J.: On Fatigue Analysis and Testing for the Design of the Airframe. Fatigue Life Prediction for Aircraft Structures and Materials. LS-62, AGARD Lecture Series 62, Section 6. Printed by Technical Editing and Reproduction LTD. Harford House, 7-9 Charlotte St., London W1P1HD.

26. Turner, M. J.; and Grande, D. L.: Study of Metallic Structural Design Concepts for an Arrow-Wing Supersonic-Cruise Configuration. NASA CR-2743, 1976.
27. Sakata, I. F.; and Davis, G. W.: Evaluation of Structural Design Concepts for an Arrow-Wing Supersonic Cruise Aircraft. NASA CR-2667, 1976.
28. Baber, Hal T., Jr.; and Swanson, E. E.: Advanced Supersonic Technology Concept AST-100 Characteristics Developed in a Baseline-Update Study. NASA TM X-72815, 1976.
29. Atkinson, R. J.: The Testing of Supersonic Transport Structures in Fatigue. Dexter, Robert R., ed.: Proceedings of the Fourth Congress of the International Council of the Aeronautical Sciences. Spartan Books, Inc., Washington, D.C., 1965, pp. 259-279.

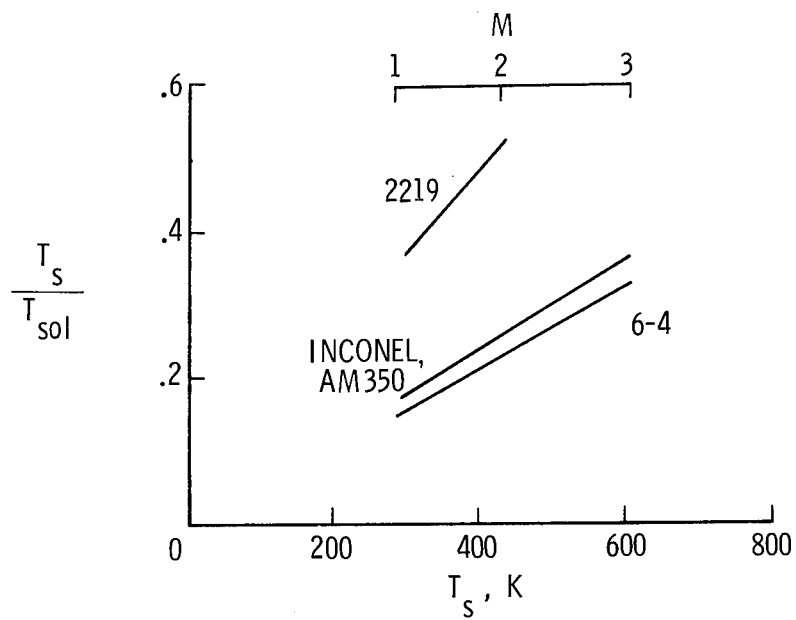


Figure 1.- Relative temperatures for skin materials.

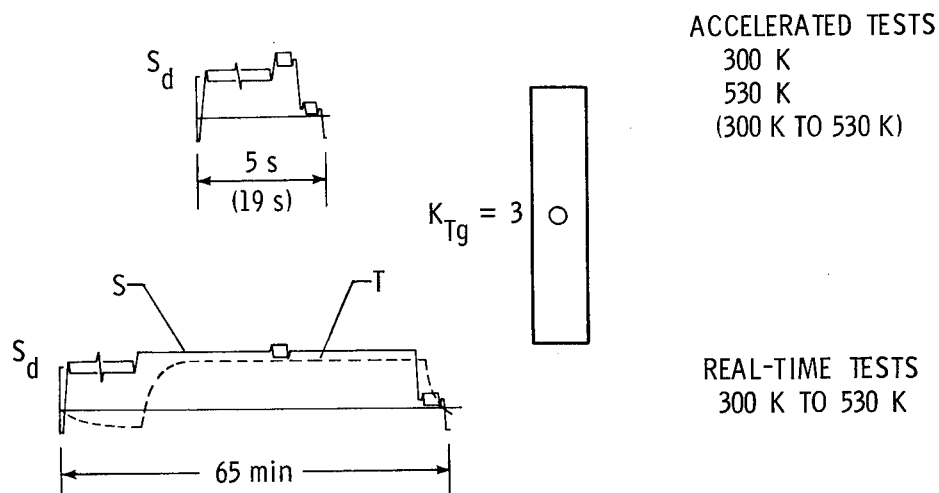


Figure 2.- Lockheed fatigue tests with simulated thermal stress (refs. 15 and 16). Gross-area one-g design stress. $S_d = 172$ MPa.

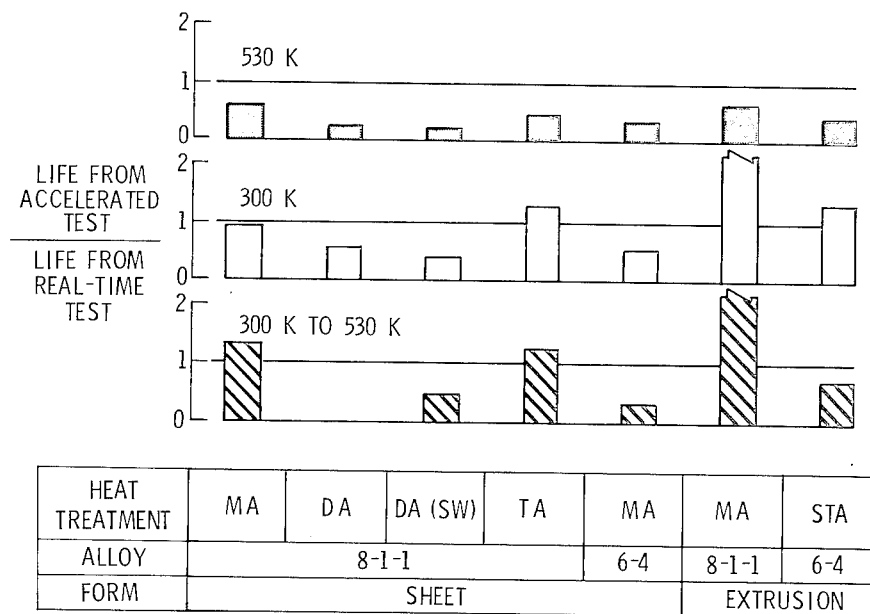


Figure 3.- Summary of Lockheed's fatigue tests. Crack initiation; $K_{Tg} = 3$.

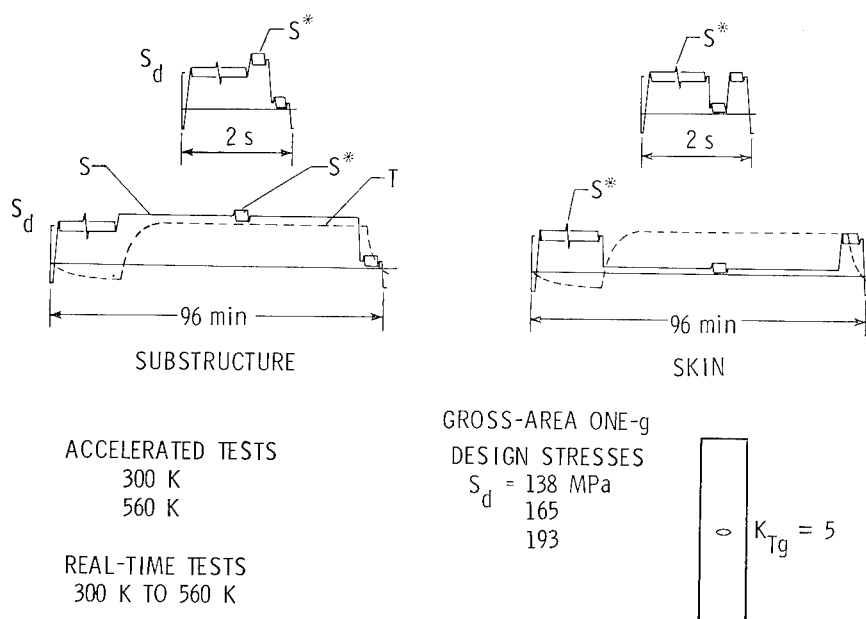


Figure 4.- NASA fatigue tests with simulated thermal stress (refs. 17 and 18).

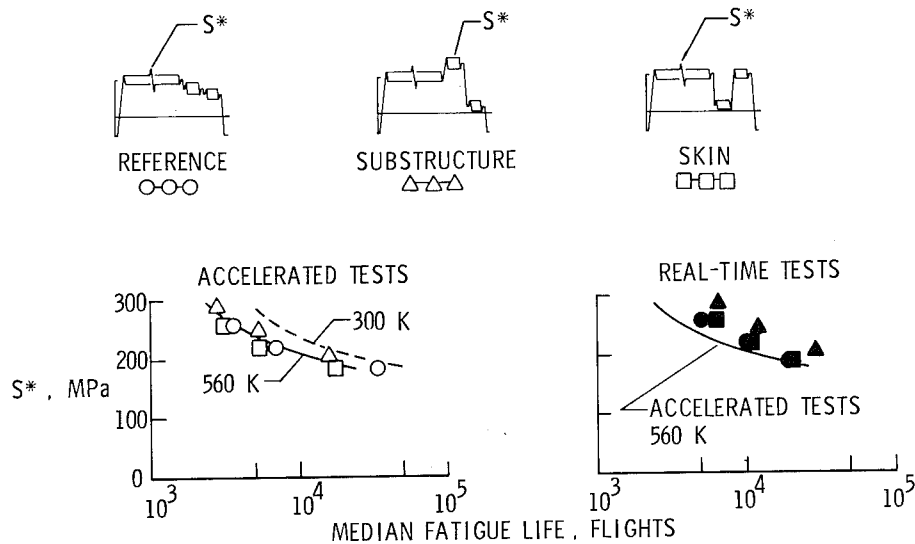


Figure 5.- Summary of NASA fatigue tests. Specimen failure; DA Ti-8Al-1Mo-1V; $K_{Tg} = 5$.

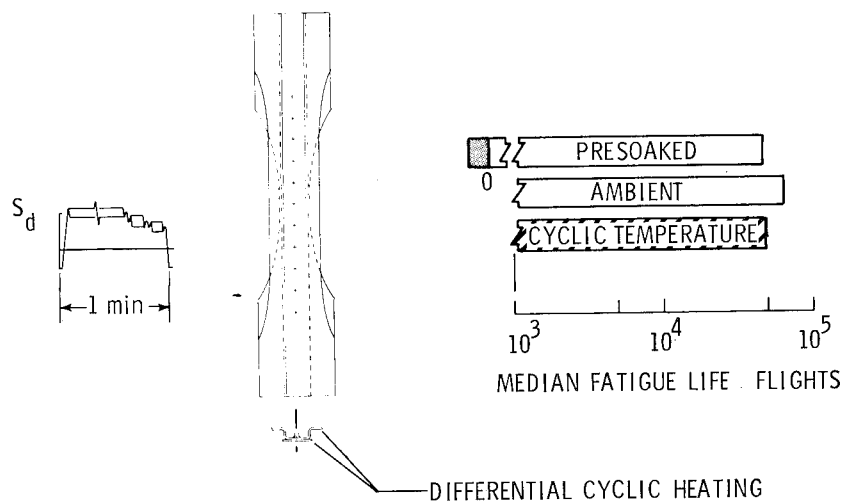
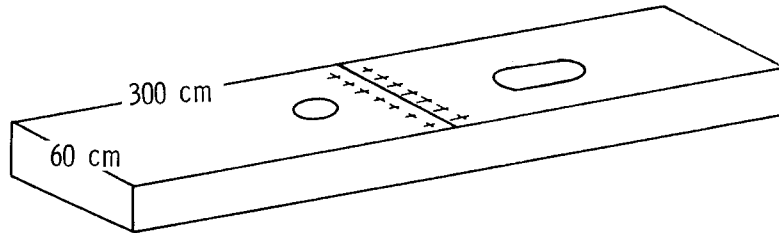


Figure 6.- Boeing accelerated fatigue tests (ref. 20). MA Ti-6Al-4V sheet; gross-area one-g design stress $S_d = 207$ MPa.



TESTS OF RIVETED ,
SPOTWELDED, AND
FUSION-WELDED BOX
COVERS

LOADING	TEMPERATURE
CA 172 , -86	300 K
CA 240 ± 43	560 K
FBF/BLOCK , $S_d = 172$	300 K/560 K

RESULTS

- CONSTANT AMPLITUDE TESTS OF RIVETED AND SPOTWELDED COVERS IDENTIFIED FAILURE LOCATIONS OF SPECTRUM TESTS; BUT NO CORRELATION FOR FUSION-WELDED COVERS
- ADEQUACY OF CONSTANT AMPLITUDE TESTS TO IDENTIFY CRITICAL FAILURE LOCATIONS DEPENDED ON METHOD OF FABRICATION

Figure 7.- LTV fatigue tests of box beams (refs. 21 and 22).
Ti-8Al-1Mo-1V; gross area one-g design stress $S_d = 172$ MPa.

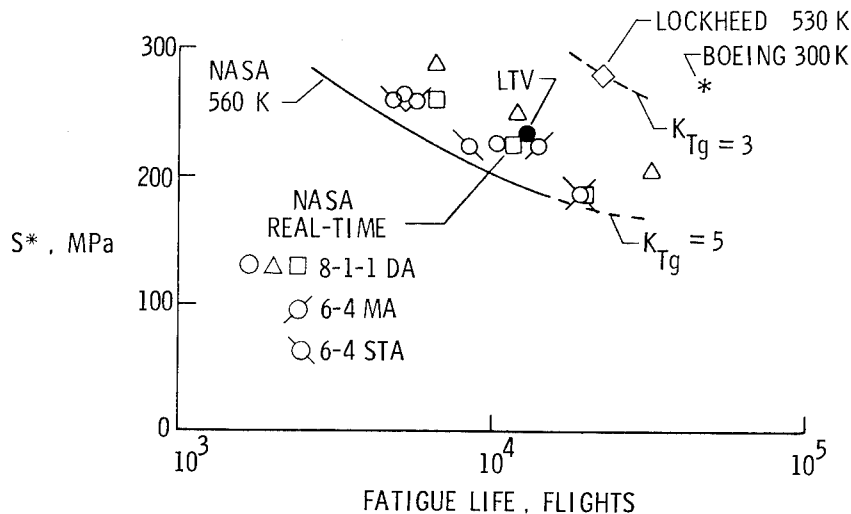


Figure 8.- Summary of coupon and component fatigue tests with specimen loads.

NEW ADVANCEMENTS IN TITANIUM TECHNOLOGY AND THEIR

COST AND WEIGHT BENEFITS

Leonard A. Ascani and John K. Pulley
Rockwell International

SUMMARY

A new technology is emerging that promises to revolutionize the field of metal fabrication and design, particularly that of titanium. A process that combines both the superplastic and diffusion bonding properties of metal into one concurrent operation is being developed at Rockwell International. Estimates using this technology have indicated that this combined process will result in cost savings up to 70 percent when compared to conventional construction methods, while also saving weight. Many structural forms are possible including sandwich structures made by expanding face sheets and core against die forms. The classic difficulties normally associated with fabricating sandwich structures, such as parts fit-up, close tolerances, adhesive or braze alloy strength, do not exist with this technique. The total potential of Rockwell's patented new processes is limited only by the ingenuity of the designer and is expected to effect significantly future airplane concepts and criteria.

INTRODUCTION

The science of aircraft technology is continually being pressured to develop new and innovative concepts to produce aircraft with higher performance and lower cost. This is particularly true in the field of aircraft structures, since this discipline represents a large fraction of the cost and weight of aircraft. A new technology is emerging in the field of titanium fabrication which promises substantial progress in the state-of-the-art towards meeting the challenge of reducing airframe costs. These new and inventive processes combine superplastic forming and diffusion bonding (SPF/DB) into a single process that promises to revolutionize titanium fabrication and structural design.

New design concepts heretofore considered impractical because of high costs and fabrication difficulties are now possible using the SPF/DB process. These concepts include sandwich structures in which face sheets, core, and

edge members can be formed and bonded into a practical structure, all in one operation. Other structures such as beaded panels, corrugated or sine wave spars and frames, panels with integral frames, etc, are now possible, at low cost, with these processes.

These complex configurations have been produced in titanium by the SPF/DB processes in a single cycle which could otherwise not be fabricated by conventional methods. Manufacturing feasibility and cost savings potential have been established through both Rockwell IR&D efforts and Air Force contracts. Cost savings of up to 70 percent and weight savings up to 40 percent have been estimated when compared to conventional titanium fabrication methods, because of the large reduction in labor costs and the ability to design more efficient structure made available by SPF/DB technology.

PROCESS DESCRIPTIONS

Superplasticity in titanium is a phenomenon in which very large tensile elongations may be realized because local thinning (necking) does not occur under the proper conditions of temperature and strain rate (figure 1). Diffusion bonding is the joining of titanium under pressure at elevated temperature without melting or use of bonding agents. Fortunately, through a natural occurrence, superplastic forming and diffusion bonding of titanium can be accomplished under identical parametric conditions. This is the basis for the combined SPF/DB processes.

Superplastic Process

Rockwell has pioneered the superplastic forming (SPF) of titanium alloy sheet components. Much additional work was done, under Air Force contract, with the Air Force Materials Laboratory (ref. 1). It has been shown that SPF monolithic components can replace designs requiring numerous details and large numbers of fasteners while realizing significant cost and weight savings (figure 2). In this example, a superplastic frame was redesigned to replace a conventional frame composed of eight separate hot-sized and machined parts and 96 fasteners. As shown in the figure, cost estimates indicating savings of 55 percent are possible, accompanied by weight savings of 33 percent. SPF is an approved process for the B-1, with Aircraft 1 through 3 having several superplastically formed components. Aircraft 4 will incorporate much more additional SPF structure. Space shuttle components, also being made by SPF, include windshield seal frames which replace an aluminum design using formed

sheet and machined details. Six SPF/DB frames replace 25 machined fittings, 72 sheet metal details, 30 splice plates, and 396 each of screws, washers, and nuts (figure 3).

In the Rockwell patented SPF process, a metal diaphragm, possessing superplastic properties, is placed across a die (figure 4) containing the desired part configuration, and sealed by the top plates in an hydraulic press. Argon gas is introduced and heat applied through ceramic platens to heat the diaphragm to temperatures at which the material becomes superplastic. For titanium, this temperature is 925° C (1,700° F). Argon gas pressures up to a maximum of 2×10^3 kPa (300 psi) are varied to produce stretching at the material's proper strain rate. This is an arbitrary pressure limit and is a function of tooling limitations rather than forming limitations. The actual forming time at temperature is a function of the part configuration and strain rate limitations and can be as low as 20 minutes. The resulting part will exactly match the die configuration, since there is no springback associated with the process.

Structural configurations which were previously considered impossible with conventional forming methods are easily fabricated with this process. Figure 5 shows a sine wave beam made using SPF which is an efficient structural shear member, particularly in lifting surface structure. The frame shown previously in figure 2 also produces an efficient shear-resistant structure, with beads or corrugations forming an integral part of the structure.

Superplastic Forming Combined with Diffusion Bonding (SPF/DB)

Titanium temperatures required for diffusion bonding are fortunately coincidental with those required for superplasticity. The inventive combination of these two processes has yielded impressive results. The Rockwell SPF/DB patented process allows not only the forming of complex sheet metal structure, but, by preplacing details in the tooling, selected areas of the structure can be reinforced, padded, or otherwise joined to functional fittings or attachments, as shown in figure 6. The argon gas provides the pressure required for diffusion bonding of the details, while the plasticity of the materials ensures a perfect part fit to produce highly reliable, repetitive components.

A further extension of the process utilizes diffusion bonding and expansion forming, as shown in figure 7. This illustrates the formation of a waffle or beaded-type structure into a die cavity by inserting a gas pressure source between two sheets, thereby expanding the material superplastically into a die cavity. Prior to this operation, the interfaces are diffusion bonded together either by applying die pressure where desired, or by using gas pressure to diffusion bond the interfaces.

The gas pressure method requires the use of an interface material (stop-off compound) to prevent diffusion bonding where desired. This material is applied to the sheets by either spraying or through the use of a silk screen process. This stop-off, then, prevents diffusion bonding in selected areas where applied and controls the shape of the finished part through the applied stop-off pattern and forming die. A more reliable part is produced in this manner because the gas pressure is uniformly distributed and die fit-up is not critical as would be the case using the die pressure approach. This procedure is explained in more detail later in this paper under "B-1 APU Door."

Expanded Sandwich

A particularly important development in SPF/DB is the method of expanded sandwich structure. In this Rockwell patented process, at least three titanium alloy sheets are diffusion bonded in selected areas and then expanded apart by internal pressure into the containment tooling. Thus, an integrally stiffened sheet metal structure may be produced in one operation.

The process (figure 8) is similar to that described in the foregoing except that the stop-off compound is applied to both sides of a core sheet to prevent diffusion bonding. The multiple sheet pack is inserted into the die, heated to SPF/DB temperatures, gas pressure applied to one side of the pack to diffusion bond the interfaces, and then applied between the face sheets (on both sides of what will become the core sheet), and expanded to final shape. No differential pressure is applied across the core sheet during this cycle. The core sheet is formed into final shape by pulling of the core apart through the diffusion bonds at the face sheets. This effectively stretches the core sheet superplastically into final shape as the face sheets are forced into the die cavities by the argon gas pressure. The final shape of the part is dictated by the die shape and the stop-off pattern applied to the core sheet.

The sandwich core produced by this process is a function, therefore, only of the pattern produced by the stop-off prior to stretching of the core. No tooling is required to produce the core, no inserts requiring removal are used, no fit-up problem exists, and all edge members are produced simultaneously with the core forming process. Additionally, other structural forms can be pre-placed in the die as desired and concurrently diffusion bonded to form attachment angles, fittings, etc (figure 9). Compound contours are not a problem with this technique since fit-up problems are nonexistent and the forming and bonding are done in a superplastic state. A large variety of sandwich core configurations are also possible with this technique. Since no tooling is required to form the core, its final configuration is strictly dependent on the

stop-off compound pattern and the ability to stretch the core from its original flat sheet configuration. Figure 10 shows typical representative core configurations that have been fabricated to date. These include a truss core, dimpled core (core bonded to face sheets in intermittent spot pattern), and sine wave core (core bonded in a parallel sine wave pattern). The process also readily permits core variations within the same panel; i.e., all types of core can be utilized within the same panel by varying the stop-off pattern if an advantage can be gained with this approach.

MATERIAL PROPERTIES

Experience accumulated on SPF/DB hardware to date indicates (1) that the strength levels resultant in the hardware are equivalent to that obtained with the SPF cycle only, and (2) diffusion bonds have been 100-percent complete to the limit of NDT detection, and possess essentially parent metal properties.

Under a current Air Force SPF/DB program (ref. 2) and under a Rockwell IR&D program on sandwich development, a variety of strength data has been obtained. Property comparisons were made among the data from DB and SPF areas of a SPF/DB-processed part, data from superplastic-formed parts, and data from diffusion-bonded parts. The comparison indicates that the mechanical properties of the Ti-6Al-4V parts subjected to SPF, DB, or SPF/DB processes are similar.

The results of single lap-shear tests showed 5.44×10^5 kPa to 6.1×10^5 kPa (79.0 to 89.5 ksi) ultimate shear strength at the DB interface (table I). The shear values agree well with those obtained on double lap-shear tests of 5.522×10^5 kPa to 5.93×10^5 kPa (80.1 to 86.1 ksi) for the fully bonded interface, indicative of parent metal strengths. The slightly larger scatter in test results for the single lap-shear tests is believed to be caused by the off-centered or asymmetric loading of the specimen.

Static peel tests resulted in parent metal fracturing without evidence of peeling at the bond plane (table II). The sheet gage used and the part geometry simulated in the test parts are representative of the SPF/DB full-scale parts to be fabricated. The peel test fracturing mode signifies that the DB joint strength exceeds that of the SPF metal.

The strength tests to date on sandwich, limited to the truss core type, are summarized in table III. In all tests, load fall-off resulted from predictable buckling, wrinkling, or crushing of the structure, as delineated in the table. No separation of diffusion bond joints occurred in the tests. No

cracks were developed in the metal at maximum load. Maximum load was a function of the structure geometry and the properties of the 6Al-4V titanium alloy. Loading deflections far beyond the deflection at maximum load were required to develop cracks in the structure. The tests showed that the diffusion bond joints were sound and did not reveal any indication of material degradation by the process used to produce the structure.

At present, prediction of the structural capability of discrete designs will require specific verification. However, generalizations emerging from current and future work will allow increasing ability to predict structural behavior with confidence.

B-1 APU DOOR DEMONSTRATION

A significant milestone for the application of the SPF/DB process to a full-scale B-1 part was accomplished as a function of a present Rockwell/AFML development contract (ref. 2). A 0.39 m^2 (600 square inch plan area expanded laminate part was bonded and formed in a single operation. Figure 11 shows the door configuration after trimming. A picture-frame doubler in between the two face sheets and a smaller doubler were required as part of the basic door. In addition, the smaller doubler was bonded to the diaphragm prior to forming and was subsequently superplastically expanded into a female cavity. The SPF/DB cycle was applied with a predetermined pressure time cycle in a 40×10^6 newton (4500 ton) hydraulic press with existing heating platens. The door configuration obtained was well defined and the hollow sections fully formed, including the one area where two diffusion-bonded sheets were also weld joined. The demonstration of the concurrent SPF/DB concept on a complicated expanded section of the 0.39 m^2 plan area door was successful. Subsequent ultrasonic inspection indicated diffusion bonding continuity with no detectable disbands.

Tooling

Tooling consists of an upper plate, an insert, and a container. The upper plate incorporated a projection to effect the seal during the process cycle. The container was a thick block of steel with a machined cavity to receive the insert. Ramps were provided around the interior periphery of the container to ease removal of the insert. The container has two main purposes: (1) To act as a venting cavity for the argon gas to escape as forming progresses which prevents gas entrapment, and (2) to provide the means for gas pressure diffusion bonding to the lower side of the diaphragm. In addition, the container

becomes a universal holder for other expanded laminates by the utilization of different inserts.

The container and insert were machined using numerically controlled methods, while the top plate was conventionally machined. Figure 12 shows the machining being accomplished, and figure 13 shows the three completed tooling sections.

Stop-Off Application

An important consideration in assembly of the titanium sheet metal details is the application of stop-off material to those areas of the diaphragm which are not to be bonded. Locating the stop-off pattern for correct alignment with the tool cavity requires the use of templates indexed to the titanium sheet and the tool. A recently developed method of applying stop-off utilizes a silk screen process. The application of the stop-off and the resulting pattern on the titanium sheet are shown in figure 14. The stop-off slurry must, of necessity, be of a specific consistency and able to retain wetness. Dimensional accuracy can be maintained by use of the silk screen through proper locating points.

Door Fabrication

The completed door shown in figure 11 was highly successful both in quality of bonds and accuracy of forming. As stated previously, the basic door consisted of two sheets formed into a hat-stiffened structure with a doubler required around the periphery and one in an area of the center section where a fire access door is added later.

The picture-frame doubler was made up of four individual sheets welded together with a rectangular opening. The interior edge incorporated a 60-degree chamfer to allow the preforming of the diaphragm during the bonding cycle, as shown in figure 15.

The full-scale APU door was fabricated by diffusion bonding in selected areas, as determined by the stop-off pattern, and superplastically expanded to complete the part. Diffusion bonding time and pressure were determined by an analytical prediction curve which had been verified through previous subscale tests. For this part, the diffusion bonding cycle used 2×10^3 kPa (300 psi) argon gas pressure applied for 1-1/2 hours.

The forming, or superplastic expansion cycle, was selected on the basis of two separate tool depths (cavities). A cycle was selected so as to allow the material to form into the shallow cavity bottom surface without rupturing. At this point, the pressure-time profile was changed to form effectively the deeper cavity.

After completion of the SPF/DB cycle, the pack was allowed to cool to 650° C (1200° F) with a continuous flow of argon gas through the tooling and the formed part. The part was removed with ease at a temperature of approximately 600 - 650° C (1100° - 1200° F).

Part Evaluation

The APU door was cleaned and evaluated visually and by NDT. The following observations resulted:

- (1) The part was fabricated in a manufacturing environment using production facilities.
- (2) Full forming occurred on the diaphragm side and conformed to the die configuration.
- (3) Part cleanliness was good, verifying that shielding during elevated temperature exposure was adequate.
- (4) Ultrasonic inspection showed satisfactory bonds throughout.

COST/WEIGHT IMPACT

Evaluations conducted to date have shown significant cost/weight reductions using this process, when compared to conventional construction methods. Additionally, substantial reductions in part count, fasteners, and tool quantities have resulted. Some examples of types of estimated savings are as follows.

Typical Fuselage Structure

A comprehensive conceptual study was conducted on a typical fuselage-type structure consisting of titanium sheet metal and machined ribs, longerons, and chem-milled skins fastened together with a standard riveting system. This

design is illustrated in the exploded view of figure 16. An alternate design using a concept similar to the expanded waffle, where diffusion bonded skins with hat-section stiffeners form the basic skin panel, was designed to include integral frame structures. This is shown in figure 17. The structure is expanded into a die in a manner similar to the procedure used in the APU door. Except for the fact that deeper drawn sections and larger panels are required, the concept is very similar to the APU door configuration with doublers bonded to the integral frame as it is formed into the die cavity. Sine wave webs are formed in the frames to provide shear-resistant structure. The results of this conceptual design study are shown in table IV. As indicated, estimated weight savings of approximately 40 percent and cost savings approaching 50 percent can be realized with the SPF/DB concept.

Cost and weight savings were also estimated for the APU door previously described to determine the impact of SPF/DB. Figure 18 illustrates the potential cost savings of the SPF/DB concept over that of the original design which was machined from a titanium plate. Weight savings of 30 percent were realized while cost savings of 50 percent were estimated for production B-1 aircraft.

Equivalent cost savings were also estimated for sandwich structure. Figure 19 shows sandwich structure savings when compared to other S-O-A sandwich structures. One of the structures of figure 19 is a welded sandwich panel compared to a truss core SPF/DB panel. Savings of 45 percent were realized. Figure 19 also shows a comparison of an engine shroud with the original design a brazed-titanium honeycomb panel. Cost savings of 45 percent can be realized using the SPF/DB concepts.

All of the foregoing estimates were based on production quantities of 240 aircraft. They were estimated from drawings using Rockwell cost estimating procedures and are used for comparison purposes only and are not intended to represent absolute cost data.

Advanced Supersonic Aircraft Studies

SPF/DB can obviously impact a large airplane such as an advanced high-speed transport aircraft since this aircraft will use large amounts of titanium. To determine its impact, a study was undertaken under a NASA contract (ref. 3) to evaluate its potential cost and weight savings on an arrow wing supersonic transport commercial aircraft. The evaluation used as a baseline a brazed-titanium honeycomb wing structure and a skin/stringer titanium fuselage. Trade studies were conducted comparing this baseline with several

types of SPF/DB concepts including integral frames, truss core, dimpled core, superplastic spars, and superplastic frames. A typical concept applicable to both wing and fuselage is shown in figure 20. This concept consists of a truss core expanded sandwich for the fuselage skin and wing skins. Sine wave frames for the fuselage and full depth sine wave spars for the wing spars were used. As expected, large cost savings and substantial weight savings were realized. The results of the studies are shown in figures 21 and 22 for this and several other concepts. Potential cost savings up to 60 percent can be realized with potential weight savings up to 30 percent.

CONCLUDING REMARKS

The effort expended to date on the SPF/DB processes has definitely proven the design advantages and manufacturing feasibility of this technology. Cost evaluations conducted on a variety of concepts producible by these techniques have indicated substantial savings over present state-of-the-art means of titanium construction and, in some instances, over aluminum construction. It appears inevitable that SPF and SPF/DB will be extensively applied to future aircraft.

However, much work remains to be accomplished. Although small hardware parts have been demonstrated to actual aircraft requirements, application to large-scale hardware remains to be accomplished. A giant step in this direction will be the successful fabrication of a large B-1 engine access door some time during the first quarter of 1977. This contract has recently been signed to design, fabricate, and test one of these doors for the B-1 to demonstrate the transferability of SPF/DB technology to large-scale hardware. Figure 23 illustrates the door configuration and structural concept that will be pursued. This structure will be a corrugated sandwich using SPF/DB techniques and will be fabricated in one operation using expanded sandwich structure, including concurrently diffusion bonded hinge fittings as well as latch structures. Estimates have shown the SPF/DB design will be 40 percent less costly than an equivalent aluminum honeycomb design and 20 percent lighter. The successful culmination of this effort into a 1.22 x 2.74 m (4 x 9 ft.) structural section will conclusively demonstrate the feasibility of SPF/DB technology for large-scale aircraft hardware.

The potential impact of this technology on advanced transports and military aircraft can obviously be very significant. However, the data base for this technology does not presently exist to permit the design and fabrication of a complete aircraft. Although some structural design data are available, much

more work must be accomplished before an airplane can be completely designed with this technology. Such structural design data as static allowables for new structural concepts must be developed. Fatigue data, fracture mechanics data, new materials applications, crack stopping techniques, and long-term environmental effects are among those requiring characterization.

The SPF/DB technology is expected to revolutionize the field of aircraft structural design and fabrication. New design concepts heretofore impossible or extremely difficult with state-of-the-art methods are relatively easily made with SPF/DB technology. To date, the potential of these patented processes has only been scratched. The future will see new concepts, as yet unthought of, limited only by the ingenuity of the design/producibility team.

REFERENCES

1. Superplastic Forming of Titanium Structures, AFML-TR-75-62, April 1975.
2. Manufacturing Methods for Superplastic Forming/Diffusion Bonding Process. IR 798-5 (I, II, III, IV, V) 1975. Air Force Contract No. F33615-75-C-5098.
3. Evaluation of Low Cost Titanium Structure for Advanced Aircraft. NASA CR-145111, 1976.

TABLE I.- RESULTS OF SINGLE LAP-SHEAR TESTS

Test area	Grain direction	Specimen ID	Test thickness		Shear ultimate strength	
			mm	(in.)	MPa	ksi
DB	L	4-19	5.8	0.230	555	80.6
		4-20	5.8	.230	588	85.3
	LT	15-15	3.9	.155	595	86.3
		15-16	3.9	.155	552	80.1
		15-17	2.56	.101	617	89.5
		15-18	2.56	.101	569	82.6
	L	8-23	2.1	.084	561	81.4
		8-24	2.1	.084	600	87.1
		16-35	2.6	.103	576	83.5
		16-36	2.6	.103	581	84.3
	LT	8-21	2.1	.084	545	79.0
		8-22	2.1	.084	588	85.3

TABLE II.- PEEL TEST RESULTS, SPF/DB CORNER INTERSECTION

Test area	Specimen ID	Gage		Peel strength	
		mm	(in.)	N/mm	lb/in.*
DB/SPF juncture	15-1	1.8	0.071	258	1475
	15-2	§	§	251	1435
	15-3	1.8	.071	229	1310
	15-4			262	1495
	13-1	1.8	.071	224	1278
	13-2	§	§	230	1312
	13-3	3.2	.125	236	1350
	13-4			232	1325

*Parent metal (SPF member) failed.

TABLE III.- MECHANICAL PROPERTIES OF EXPANDED SANDWICH STRUCTURES

Type test	Specimen size mm (in.)	Thickness		Test direction	Maximum stress MPa (psi)	Failure description
		Face sheets mm (in.)	Core mm (in.)			
Flatwise tension	12.7 x 44.5 x 44.5 (1/2 x 1 3/4 x 1 3/4)	1.8/1.5 (0.070/0.060)	0.3 (.012)	-	>3.287 (>476.8)	Adhesive bond between specimen and test fixture failed
Flatwise compression	12.7 x 50.8 x 50.8 (1/2 x 2 x 2)	1.65 (.065)	.3 (.012)	-	1.15 (167.4)	Core buckling
	10 x 76 x 76 (.4 x 3 x 3)	.81 (.032)	.3 (.012)	-	2.2 (319.3)	Core buckling
Edgewise compression	12.7 x 76 x 76 (1/2 x 3 x 3)	.46/.4 (.018/.016)	.3 (.012)	Transverse	79 (11,458)	Face sheet buckling
	12.7 x 76 x 76 (1/2 x 3 x 3)	.48/.46 (.019/.018)	.3 (.012)	Transverse	79 (11,523)	Face sheet buckling
	12.7 x 76 x 76 (1/2 x 3 x 3)	.46/.43 (.018/.017)	.3 (.012)	Longitudinal	653 (94,728)	Core and face sheet buckling
	12.7 x 76 x 76 (1/2 x 3 x 3)	.48/.46 (.019/.018)	.3 (.012)	Longitudinal	702 (101,927)	Core and face sheet buckling
Core shear	12.7 x 38 x 127 (1/2 x 1 1/2 x 5)	1.65 (.065)	.3 (.012)	Transverse	1.047 (151.9)	Core buckling
	12.7 x 50 x 101 (1/2 x 2 x 4)	1.65 (.065)	.3 (.012)	Longitudinal	6.16 (894.7)	Core wrinkling
Beam bending	11.9 x 66.6 x 232 (.47 x 2 5/8 x 9 1/8)	.43/.5 (.017/.020)	.43 (.017)	Transverse	110 (16,000)	Face sheet buckling
	11.9 x 50 x 229 (.47 x 2 x 9)	.46/.5 (.018/.020)	.3 (.012)	Transverse	110 (16,200)	Face sheet buckling
	10.9 x 76 x 178 (.43 x 3 x 7)	.48/.5 (.019/.020)	.3 (.012)	Longitudinal	>643 (>93,300)	Core crushing at a loading point

TABLE IV.- POTENTIAL BENEFITS FROM NEW TECHNOLOGY

	EXISTING DESIGN	PROPOSED DESIGN
• NUMBER OF PARTS	680	84
• NUMBER OF FASTENERS	9940	1112
• NUMBER OF TOOLS	400	100
• ASSEMBLY WEIGHT	75 kg (600 lb)	41 kg (360 lb)
• ASSEMBLY COST	\$ 295,336	\$154,726

DEFINITION: CAPABILITY OF TITANIUM ALLOYS TO DEVELOP
EXTREMELY HIGH TENSILE ELONGATIONS AT
ELEVATED TEMPERATURES AND CONTROLLED
STRAIN RATES

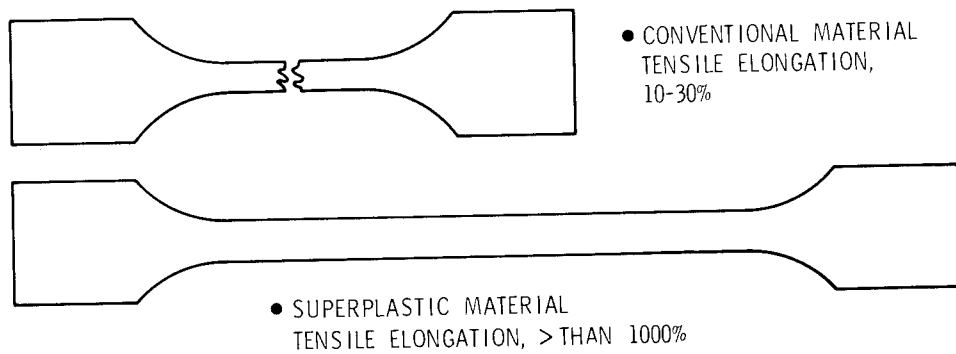


Figure 1.- The superplastic phenomenon.

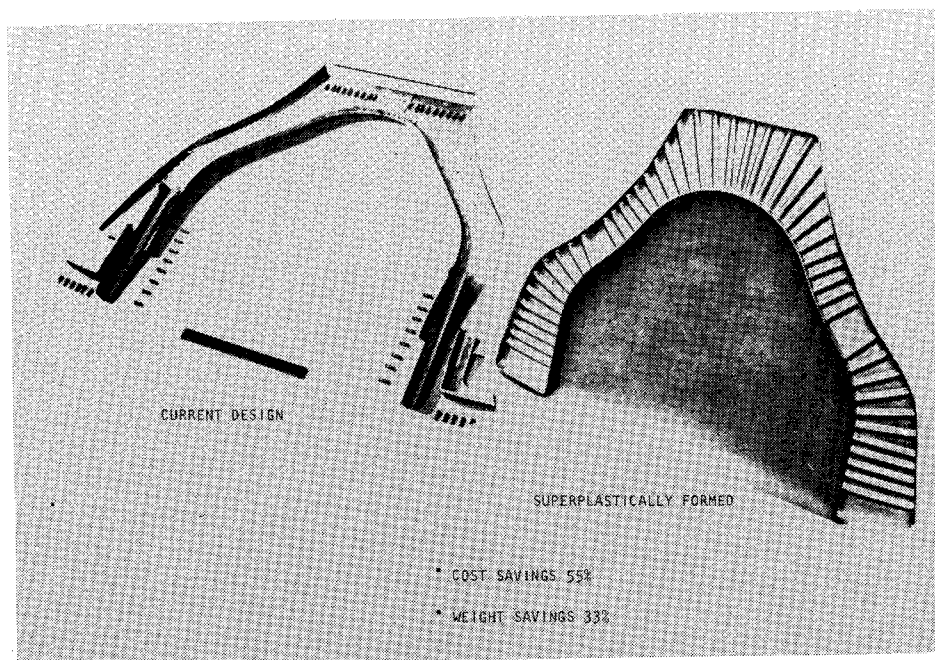


Figure 2.- Nacelle frame redesign comparison.

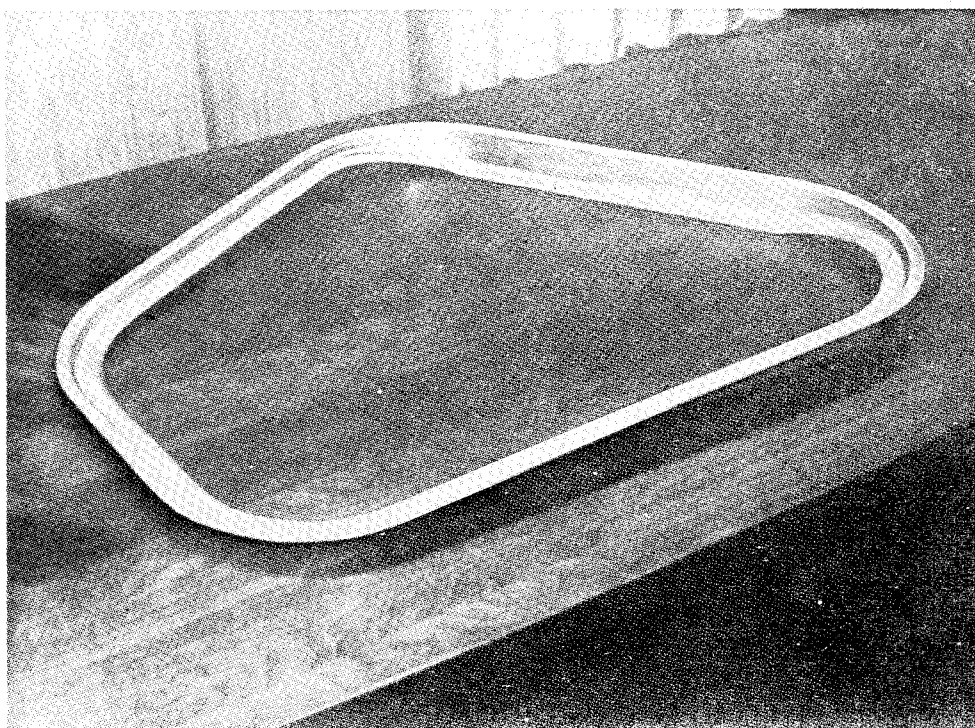


Figure 3.- Superplastically formed space shuttle windshield frame.

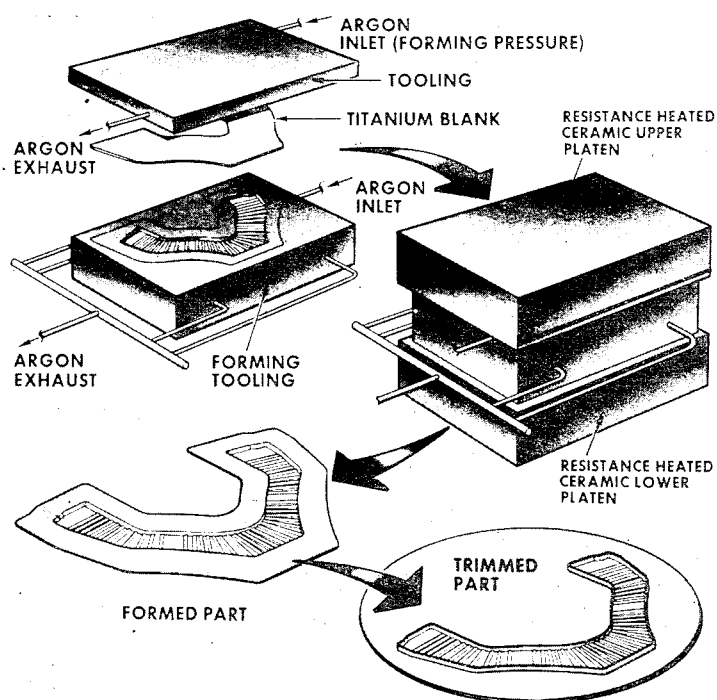


Figure 4.- Superplastic forming of titanium.

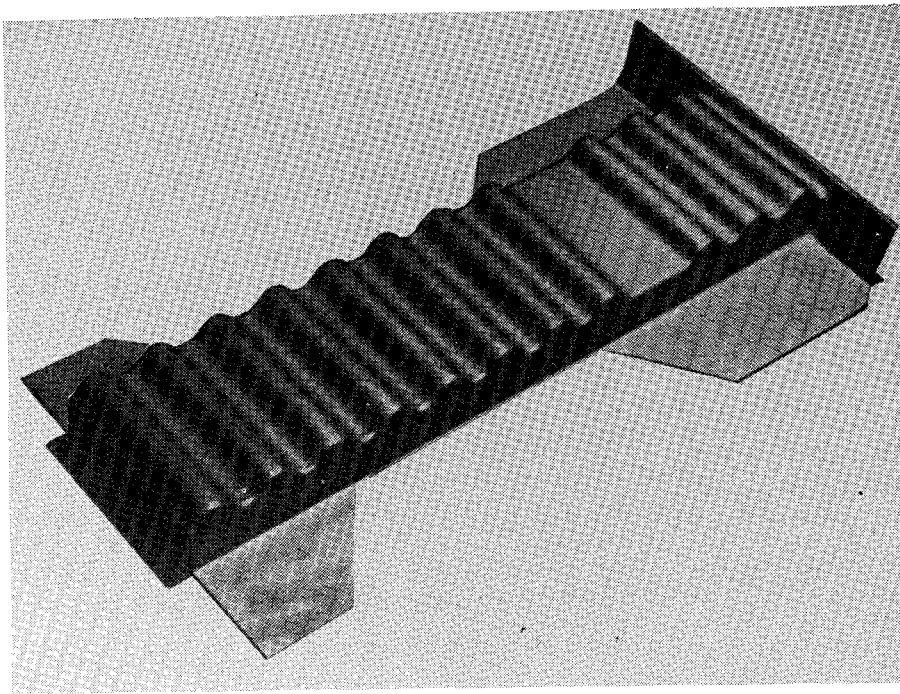


Figure 5.- Superplastically formed sine wave beam.

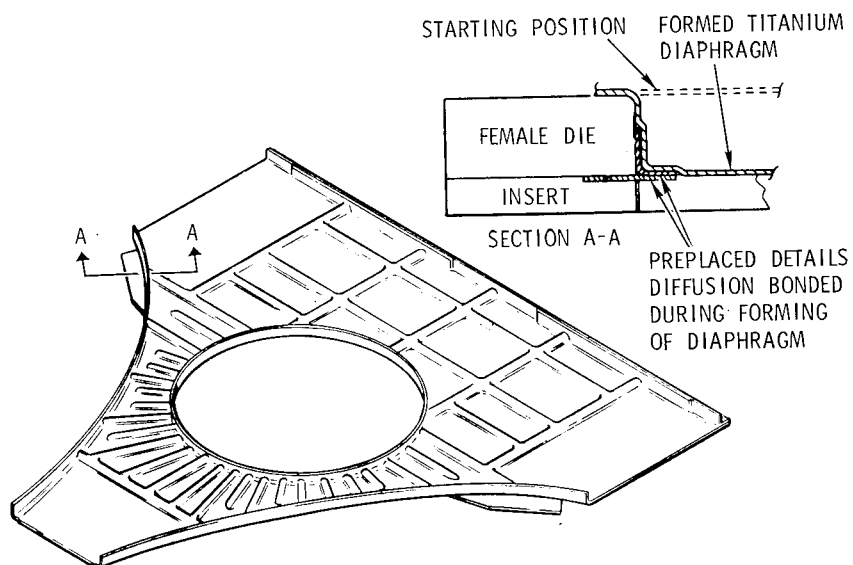


Figure 6.- Concurrent superplastic-formed/diffusion bonding cycle.

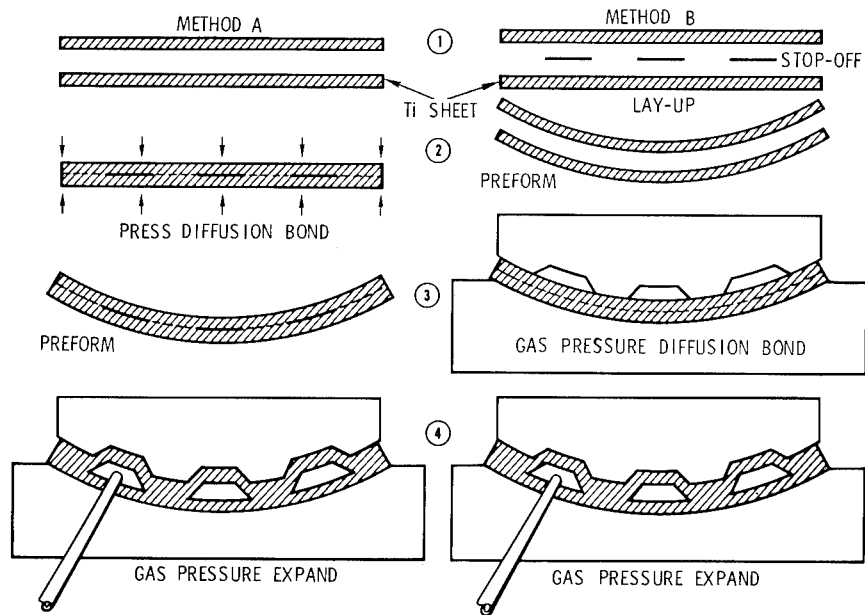


Figure 7.- Superplastic-formed/diffusion bonding expansion process.

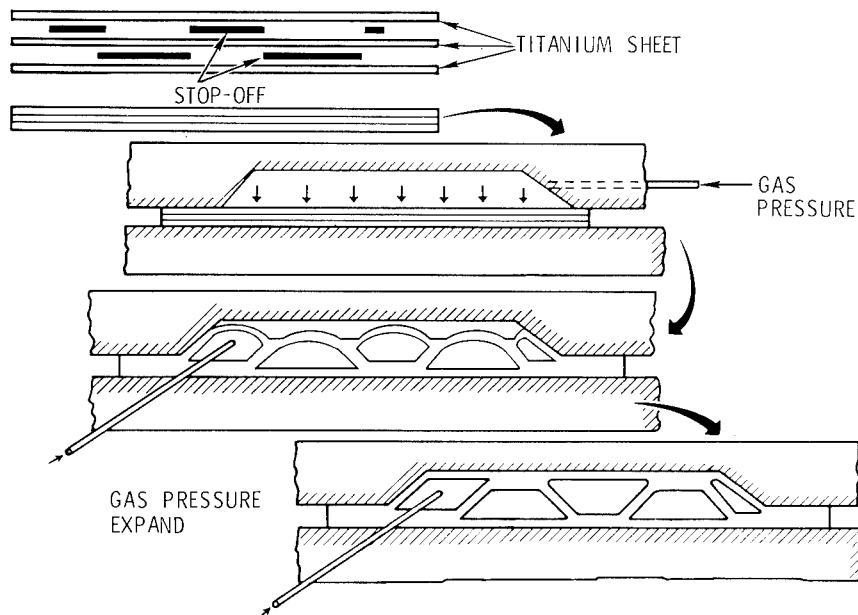


Figure 8.- Expanded sandwich process.

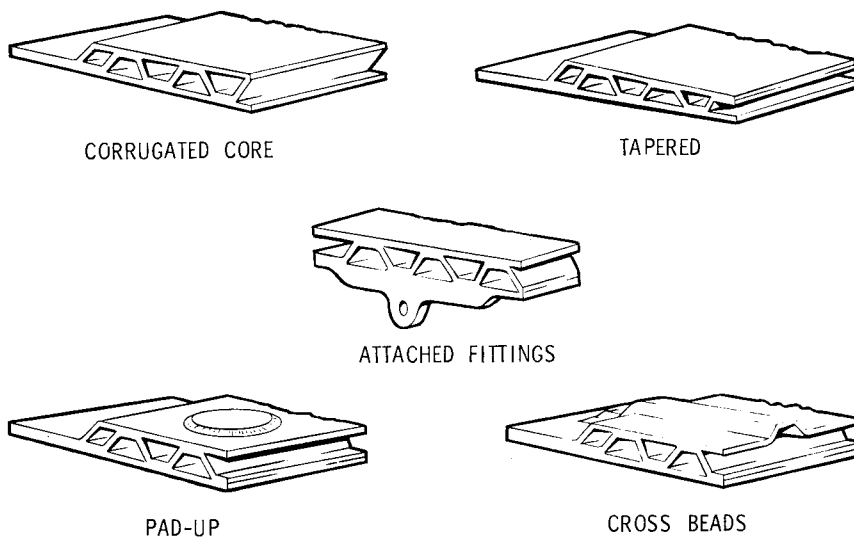


Figure 9.- Possible superplastic-formed/diffusion bonding configuration.

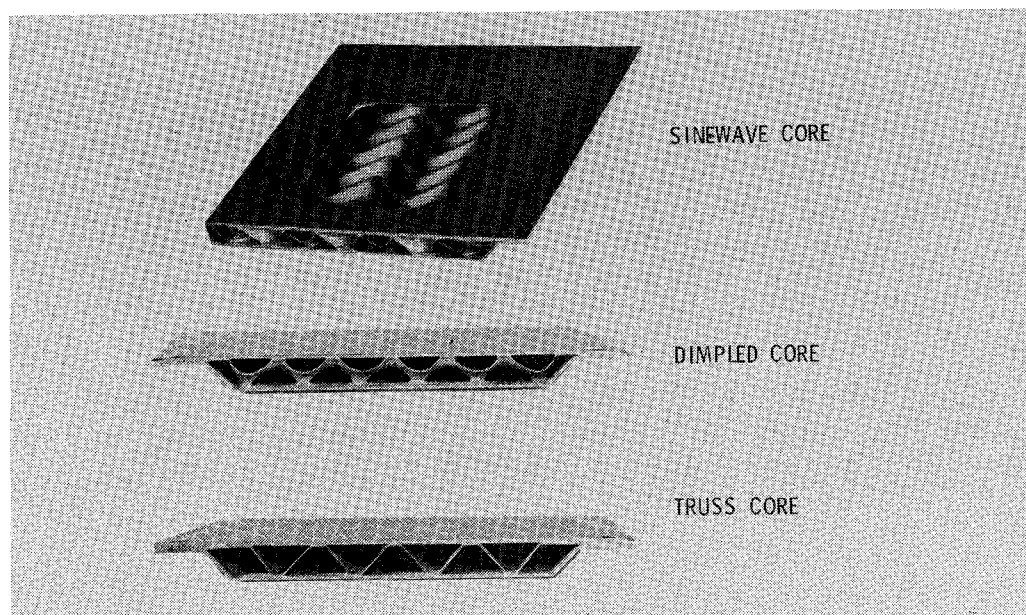


Figure 10.- Examples of actual expanded sandwich hardware.

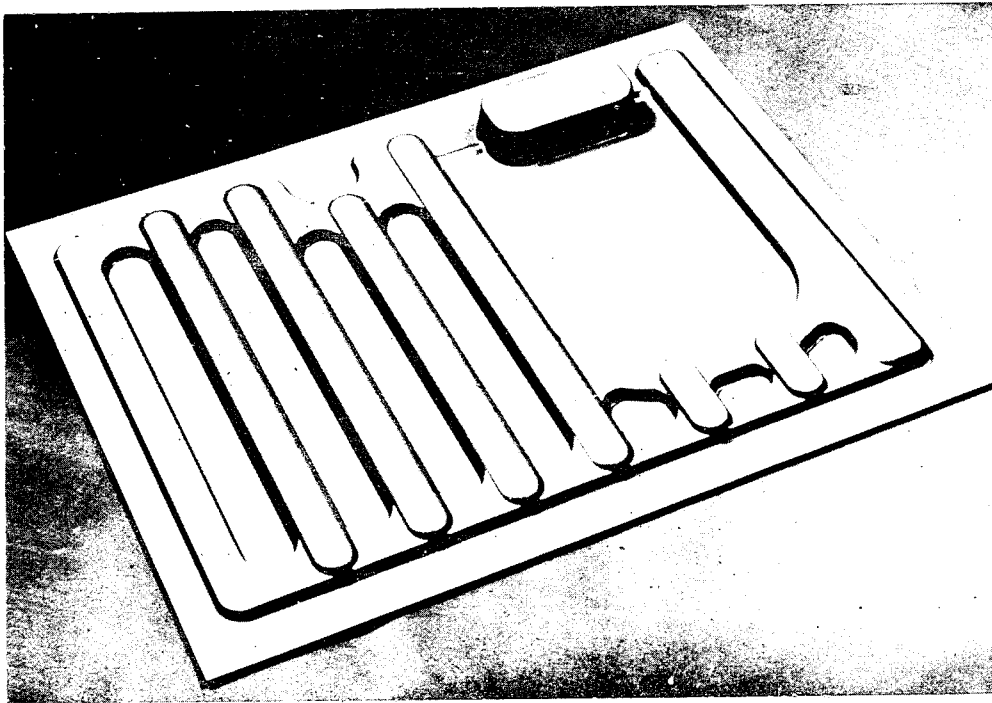


Figure 11.- B-1 superplastic-formed/diffusion-bonded APU door.

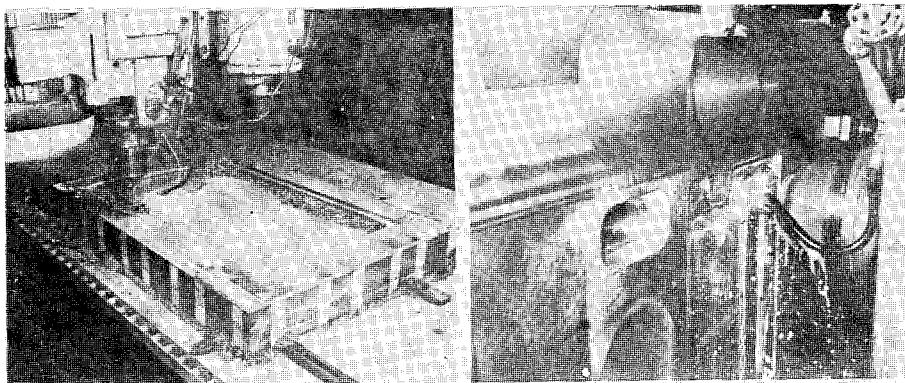


Figure 12.- Machining of APU door tool insert and container.

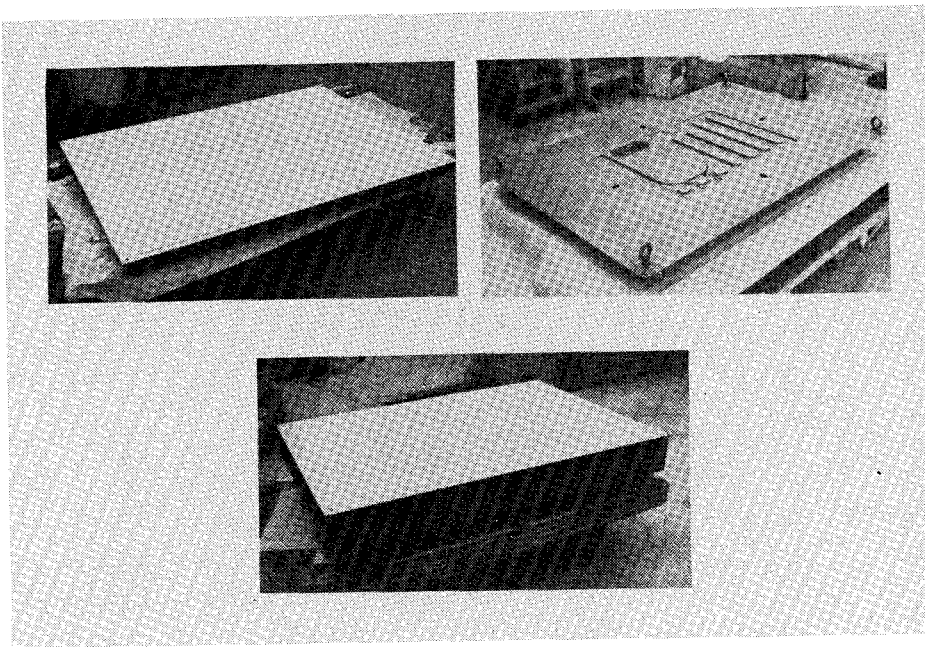


Figure 13.- Tooling subsequent to machining.

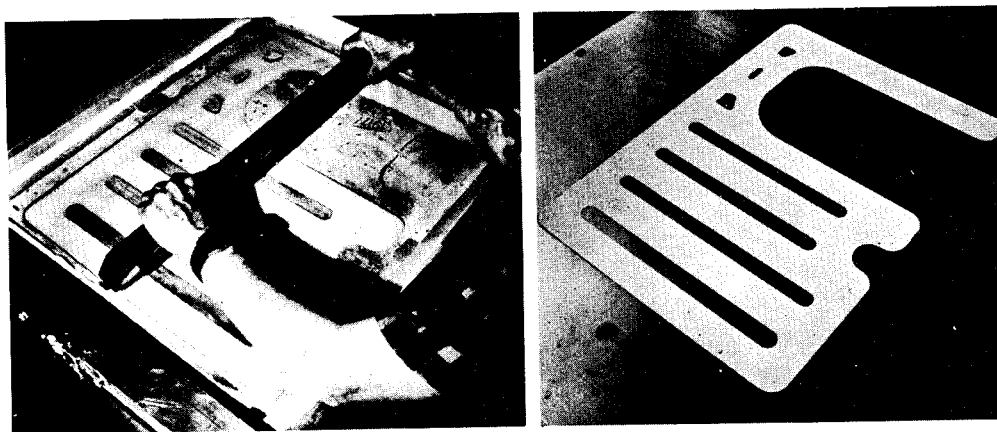


Figure 14.- Silk screen operation for APU door stop-off pattern.

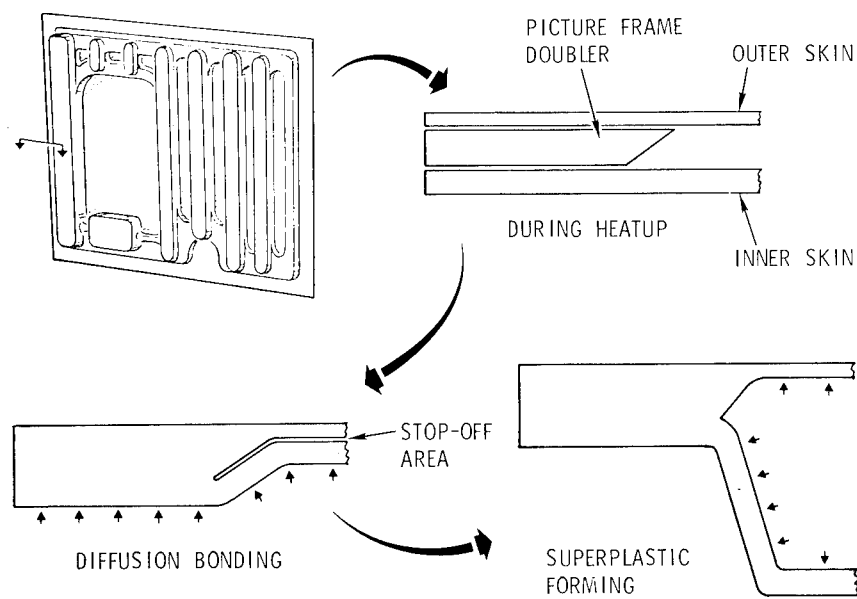


Figure 15.- Preforming of titanium sheet during diffusion bonding cycle.

- FRAME & SKIN CONSTRUCTION
- MECHANICALLY FASTENED
- Ti MATERIAL
- APPROX 112 cm X 325 cm
(44 in. X 128 in.)

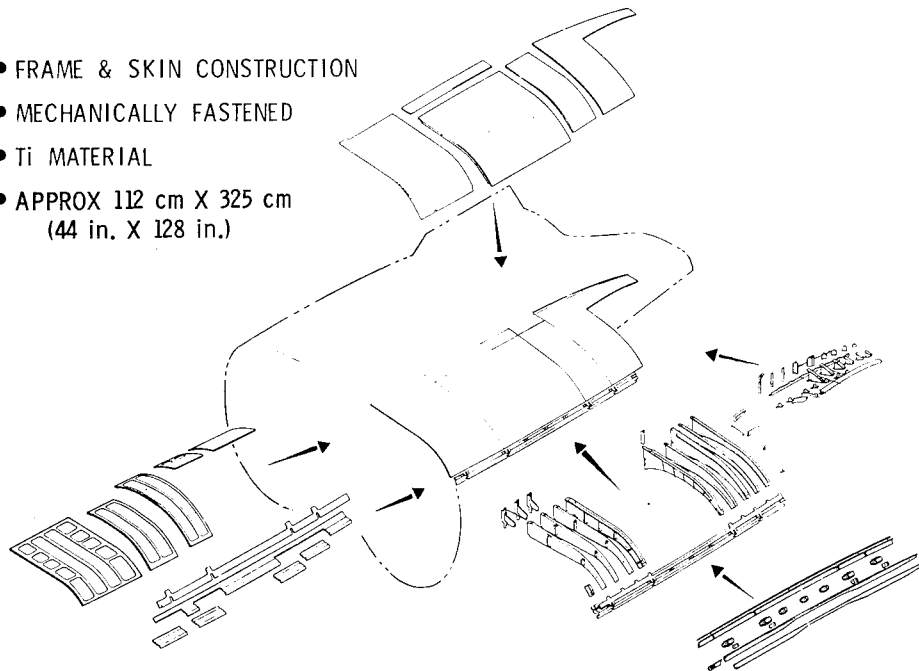


Figure 16.- Typical state-of-the-art sheet metal fuselage assembly.

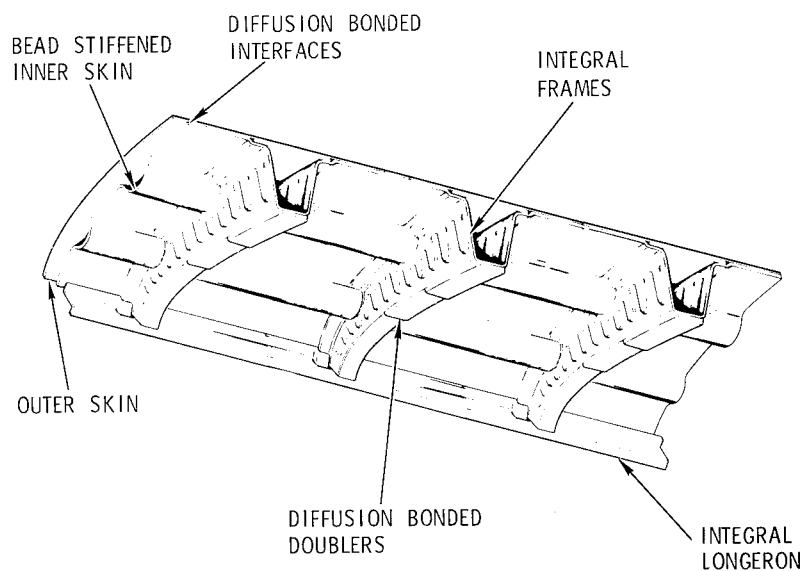
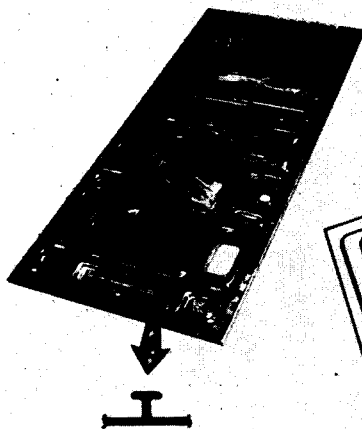


Figure 17.- Fuselage-type structure using SPF/DB with integrally formed frames.

PRESENT DOOR

- Machined Ti
- Cost: \$18,746



REDESIGNED DOOR

- Superplastic-formed /
Diffusion-bonded Ti
- Cost: \$9,290
- Wt Savings: 31%

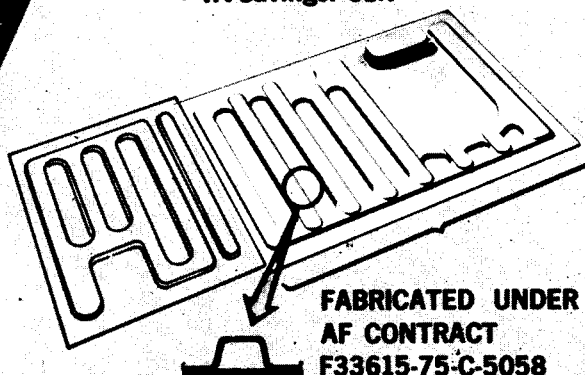


Figure 18.- SPF/DB APU door saves 50 percent.

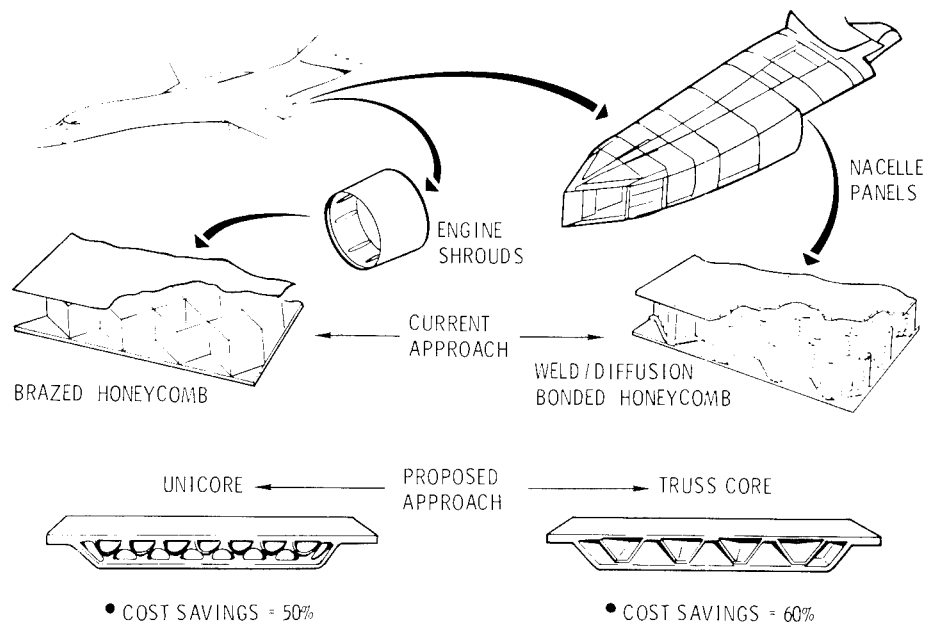


Figure 19.- Expanded sandwich comparison to present state-of-the-art methods.

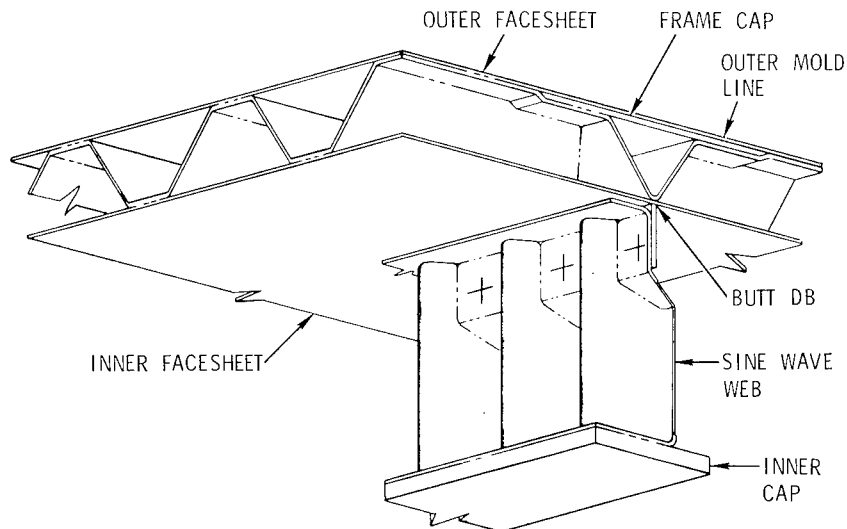


Figure 20.- Typical wing/fuselage structure using SPF/DB process.

CONCEPT	HAT	TRUSS	DIMPLE	DIMPLE	TRUSS	HAT	HAT	D-T	TRUSS
% WT SAVINGS	-22	-14	-6.4	-31	-14	-33	+22	-18	-20
% COST SAVINGS (100 AIRCRAFT)	-61	-51	-43	-48	-47	-45	-49	-50	-53

FORWARD

INBOARD

OUTBOARD

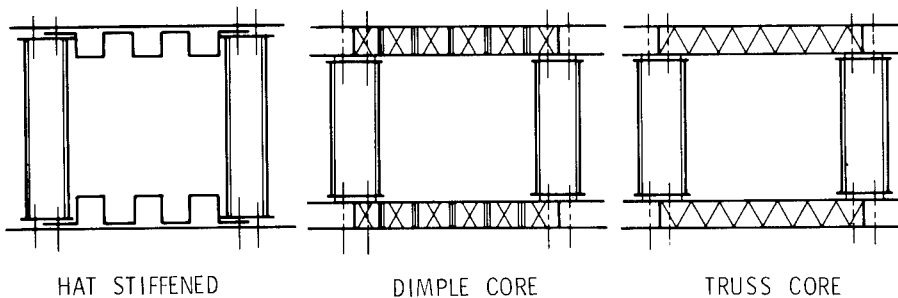


Figure 21.- Advanced supersonic aircraft wing cost/weight comparison.

CONCEPT	SANDWICH	HAT	INTEGRAL	SANDWICH	HAT	INTEGRAL
% WT SAVINGS	-8	+2	+3	-15	-2	-4
% COST SAVINGS (100 AIRCRAFT)	-22	-9	-28	-59	-49	-65

FORWARD

AFT

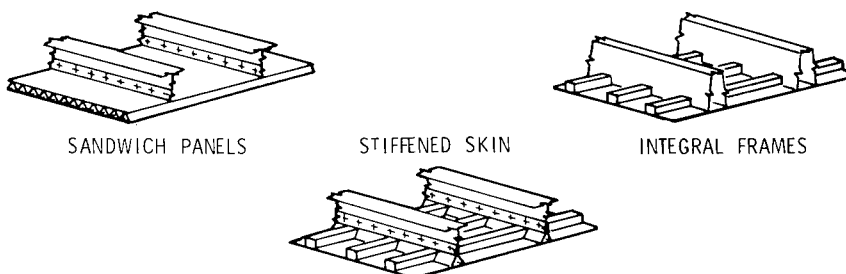


Figure 22.- Advanced supersonic aircraft fuselage cost/weight comparison.

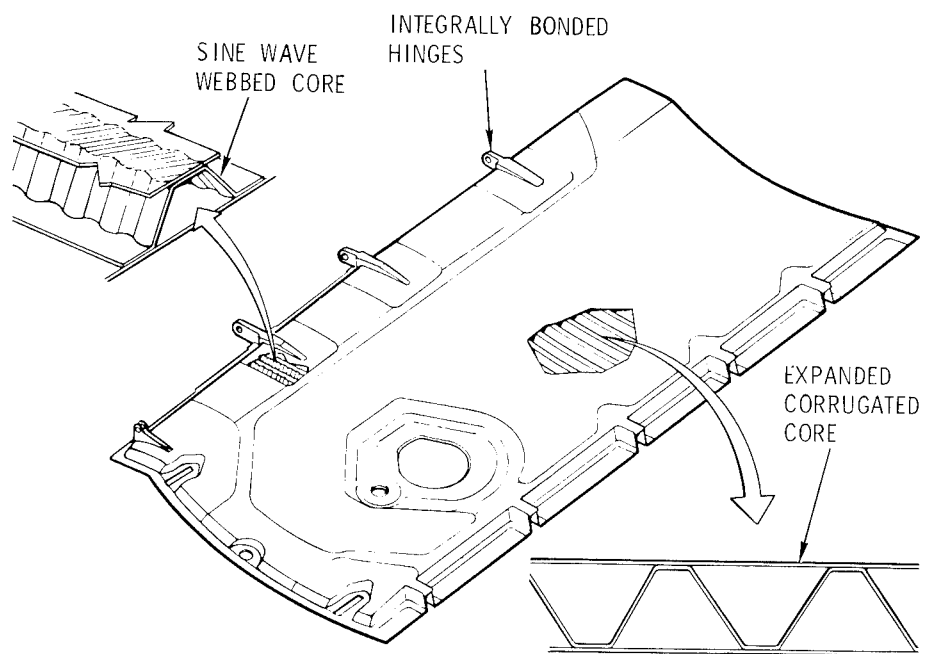


Figure 23.- Proposed engine door design.

FABRICATION AND EVALUATION OF ADVANCED
TITANIUM AND COMPOSITE STRUCTURAL PANELS

Thomas T. Bales and Edward L. Hoffman
NASA Langley Research Center

Lee Payne
Lockheed-California Company

Alan L. Carter
NASA Dryden Flight Research Center

SUMMARY

Advanced manufacturing methods for titanium and composite material structures are being developed and evaluated by NASA in support of the Supersonic Cruise Aircraft Research Program. The focus for the manufacturing effort is the fabrication of full-scale structural panels which replace an existing shear panel on the upper wing surface of the NASA YF-12 aircraft. The program, with the Lockheed-California Company, Advanced Development Projects Division, as prime contractor and support from the Dryden Flight Research Center, involves design, fabrication, ground testing, and Mach 3 flight service of full-scale structural panels and laboratory testing of representative structural element specimens.

Results discussed include the manufacturing methods and test results for weldbrazed and RohrBond titanium panels fabricated by aerospace contractors and the development of fabrication methods for producing Borsic/aluminum and graphite/PMR-15 polyimide panels at LaRC. Test data presented on the titanium panels include results obtained from flight service on the YF-12 aircraft and from ground-exposure to 589 K (600°F) for 10,000 hours. In-house fabrication studies include the development of a satisfactory brazing process for Borsic/aluminum and an expandable rubber process for forming graphite/polyimide components. Test results are also presented for a Borsic/aluminum design verification panel.

INTRODUCTION

The development of efficient future supersonic aircraft is dependent on an advanced technology base in many areas. In order to develop this technology, NASA has initiated a multidisciplined Supersonic Cruise Aircraft Research (SCAR) program. In support of SCAR, the Manufacturing Technology Section at the Langley Research Center has implemented studies on the development and evaluation of advanced fabrication methods for titanium and high temperature

composite materials. To insure that viable fabrication methods were being studied, primary structure shear panels for the upper wing surface of the Mach 3 NASA YF-12 aircraft (fig. 1) were selected for manufacturing development. Panels were designed to the YF-12 criteria and were extensively ground tested and evaluated in flight service on the YF-12 aircraft. Exposure and testing of specimens was a joint activity of NASA Langley Research Center, NASA Dryden Flight Research Center, and Lockheed's Advanced Development Projects Division (ADP). Results discussed include the manufacturing methods and test results for weldbrazed and RohrBond titanium panels fabricated by aerospace contractors and the development of fabrication methods for producing Borsic/aluminum and graphite/PMR-15 polyimide panels at LaRC.

SPECIMENS AND TEST CONDITIONS

The test program consists of exposure of element-type specimens and full-scale wing panels to various temperature environments for up to 10,000 hours and subsequent static testing. The types of specimens and tests are depicted in figure 2. For skin-stringer panel designs, lap shear and compression crippling specimens were investigated to determine the integrity of the joining process used to attach the stringers to the panel face sheet. For honeycomb-core panel designs, flatwise tension specimens were used. The full-scale 406 x 711 mm (16 x 28 in.) wing panels were tested in shear, which is the primary type of loading experienced on this component on the YF-12 aircraft.

The ground exposure program and test schedule are outlined in figure 3. The element type specimens were tested at room temperature after constant temperature or cyclic exposure. The titanium specimens were exposed at constant temperatures of 478, 589, 700, and 811 K (400°, 600°, 800° and 1000°F) for periods up to 10,000 hours. Exposure temperatures for the composite specimens were 431, 478, 533 and 589 K (300°, 400°, 500° and 600°F) because this class of materials is considered to have a lower use temperature than titanium. For cyclic exposure, the titanium specimens were exposed for 1000 cycles of the temperature profile shown on the lower portion of figure 3. This temperature profile simulates a three hour flight with two hours at supersonic cruise. Composite specimens were exposed to a similar profile with the exception that the maximum temperature was 533 K (500°F) rather than 589 K (600°F). Cyclic exposures were conducted both in an environmental chamber at constant sea level pressure and in a chamber which simulates the pressure associated with supersonic flight.

Full-scale wing panels were tested in shear at room temperature following exposure for up to 10,000 hours at a constant temperature of 589 K (600°F) for the titanium panels and 533 K (500°F) for the composite panels and after cyclic exposure for 1000 cycles. In addition, flight qualification panels were tested at ambient and elevated temperature to verify compliance with design requirements.

FABRICATION METHODS

The program to date includes four different YF-12 wing panel designs; two of titanium and two of high temperature composites as follows: (1) weldbrazed titanium skin-stringer, (2) RohrBond titanium with honeycomb-core, (3) Borsic/aluminum with titanium honeycomb-core, and (4) graphite/PMR-15 with polyimide glass honeycomb-core. Fabrication and testing of the two titanium panel designs have been completed while the fabrication of the composite panels are still under development.

Titanium Panels

Weldbrazed skin-stringer panel.- Weldbrazing is a process developed in the Manufacturing Technology Section at the Langley Research Center which combines resistance spotwelding and brazing to produce a continuous high strength joint (ref. 1). Following in-house development, the technology was transferred to Lockheed-ADP who successfully designed and fabricated the weldbrazed skin-stringer panels which are represented schematically in figure 4. The titanium "Z" stiffeners were first spotwelded to the face sheet, aluminum braze alloy was placed along the edge of the stiffeners, and the assembly was brazed in a vacuum furnace at a brazing temperature of 950 K (1250°F) for 10 minutes in a vacuum of 1.3 mPa (10^{-5} torr). Under these conditions, the braze alloy melts and flows by capillary action into the faying surface gap. The weldbrazed panel weighed 3.9 kg (8.5 lb), the same as the integrally stiffened panel it was designed to replace.

RohrBond titanium honeycomb-core panel.- RohrBond is a Rohr Industries, Inc. titanium joining method that uses a "proprietary" Liquid Interface Diffusion (LID) process consisting of selectively electroplating the components to be joined with several layers of material which act as an eutectic to aid diffusion bonding (ref. 2). Bonding, or diffusion, is accomplished in a vacuum of 6.7 mPa (5×10^{-5} torr), at 1208 K (1715°F) for 1.5 hours. Construction details for the YF-12 panels, designed and fabricated by Rohr Industries, are shown in the lower portion of figure 4. The panel consists of a titanium frame, fabricated from four machined edge members and fusion welded at the corners, a titanium honeycomb-core, and titanium face sheets. The honeycomb-core is positioned in the frame, cell walls are resistance welded to the frame, face sheets are positioned, and the assembly is placed on the vacuum furnace hearth. Tungsten pellets are used for dead weight loading to provide the pressure required for bonding. The RohrBond panels weighed 3.2 kg (7.1 lb), 12 percent less than the weldbrazed and integrally stiffened panels.

Composite Panels

Borsic/aluminum titanium honeycomb-core panels. The design and fabrication of the Borsic/aluminum (B_{SC}/Al) panels is an in-house program at the Langley Research Center. The design concept selected to meet the YF-12 panel requirement is shown in the upper portion of figure 5. The concept consists of upper

and lower skins of B_{sc}/Al brazed to a titanium honeycomb-core and frame assembly. The orientation of the Borsic filaments in the composite is +, -, -, +, $\pi/4$ rad (45°) to sustain the shear load requirements. The ramp of the Ti-6Al-4V titanium alloy frame was capered at an angle of $\pi/6$ rad (30°) to aid in the introduction of load into the inner skin. Titanium Ti-3Al-2.5V alloy honeycomb-core was selected because of its mechanical properties and its amenability to brazing. The braze alloy selected to join the B_{sc}/Al skins to the honeycomb-core frame assembly was 718 aluminum. This alloy was selected because of its favorable melting temperature and its wetting and strength characteristics. In order to minimize the effect of interaction of the braze alloy with the 6061 aluminum alloy matrix and Borsic filaments of the composite, the skin material contained a 0.127 mm (0.005 in.) layer of 1100 aluminum alloy on the braze surface to serve as a diffusion barrier. A panel of this design is approximately 30 percent lighter than the original YF-12 titanium panel.

Graphite/PMR-15 polyimide glass honeycomb-core panel.- Design and fabrication of graphite/PMR-15 polyimide (Gr/PI) composite panels are also underway in-house at Langley. The design concept is similar to that of the Borsic/aluminum panel and is shown in the lower portion of figure 5. The panel consists of an HT-S graphite/PMR-15 polyimide upper skin and pan assembly bonded to a glass/polyimide honeycomb-core using LaRC-13AI adhesive which was developed at LaRC. The ply orientations shown in the figure were chosen to carry the required loads. The estimated weight of this design is approximately 1.9 kg (4.25 lb) or about 50 percent less than the original YF-12 titanium panel.

Borsic/aluminum braze tooling.- The tooling used for the successful fluxless brazing of the B_{sc}/Al titanium honeycomb-core panel is shown in figure 6. Shown are an upper and lower platen, a caul sheet, a pressure bladder, fiberfrax insulation, and titanium honeycomb-core tooling. Following assembly, the panel and tooling are placed in a vacuum furnace for brazing. Brazing is accomplished in a vacuum of a 0.67 mPa (5×10^{-6} torr) and a temperature of 860 K ($1090^\circ F$). During brazing the bladder was pressurized using inert gas to a pressure of 27.6 kPa (4 psi) to maintain alignment of mating parts. Since the bladder concept has a low thermal mass compared to other concepts, such as dead weight loading, the time at temperature and degradation of the composite materials from the thermal exposure were minimized.

Gr/PI rubber compaction process.- The tooling utilized to consolidate the contoured Gr/PI pans using the rubber compaction process is shown in figure 7. The graphite/PMR-15 polyimide is first "B" staged over the male die and the RTV expandable rubber is precast to fit the tooling. Following assembly of components the tooling is placed between heated platens in a hydraulic press. As the assembly is heated, the rubber expands and exerts a uniform hydrostatic pressure on the composite. At the cure temperature of 589 K ($600^\circ F$) a pressure of approximately 4.1 MPa (600 psi) was applied. This concept has the advantage of applying uniform pressures over a contoured surface and is less expensive than matched die molding for a limited number of parts.

RESULTS AND DISCUSSION

The results reported herein consist of those obtained from full-scale panel tests and observations concerning the development of manufacturing methods for composite structures. Data obtained from the representative element tests for the weldbrazed and RohrBond processes are reported in references 3 and 4.

Titanium Panels

Weldbrazed panels.— Results obtained from shear tests of the full-scale weldbrazed panels are presented in figure 8. Shear tests were conducted at ambient temperature and 589 K (600°F) for exposed and as-fabricated panels. Exposures for the ambient temperature tests were as follows:

- no exposure
- 100 hr at 589 K (600°F)
- 1000 cycles at 219 K to 589 K (-65° to 600°F) constant pressure
- 1000 cycles at 219 K to 589 K (-65° to 600°F) varying pressure
- 10,000 hr at 589 K (600°F)
- 106 hr flight service on YF-12, 31.7 hr above Mach 2.6

As shown in the figure the ambient-temperature strength of all panels exceed the design ultimate shear strength of 680.3 kN/m (3885 lb/in.) by approximately 30 percent and the elevated temperature strengths exceeded the design allowable by approximately 70 percent. Based on these results, weldbrazing is considered to be a satisfactory process for fabricating structures suitable for use on supersonic aircraft.

RohrBond panels.— The results of shear tests of the full-scale RohrBond honeycomb-core sandwich panels are shown in figure 9. Exposure conditions for the panels were the same as for the weldbrazed panels with the exception of flight service testing. The panel flown on the YF-12 aircraft accumulated 40 hours of flight service exposure, with 14.3 hours at speeds above Mach 2.6. Panel strengths at ambient temperature exceeded the design ultimate by approximately 20 percent while those tested at 587 K (600°F) exceeded the design value by approximately 30 percent. These results indicate no degradation following either long term thermal exposures or flight service.

Panel cost estimates.— Cost estimates for machined titanium integrally stiffened panels, weldbrazed panels, and RohrBond panels are compared in figure 10 in terms of unit selling price in 1975 dollars. Data for the machined panel are based on a learning curve of approximately 90 percent, while data for the weldbrazed and RohrBond panels are based on learning curves of 88 percent. For 100 panels, the data show the RohrBond panels cost approximately 3.5 percent more than the machined-integrally stiffened panels, while the weldbrazed panels cost approximately 15 percent less. However, the mass of the RohrBond panel (3.2 kg (7.1 lb)) was less than that of the weldbrazed and original machined panels (3.9 kg (8.5 lb)).

Composite Panels

Borsic/aluminum titanium honeycomb-core panels.- Development of a successful brazing process for fabricating Borsic/aluminum has only recently been completed; therefore, the only full-scale test to date is for a design verification panel. The results of this test are shown in figure 11 where the applied load is plotted against shear strain. The shear strains were calculated as the sum of the absolute readings of two $\pi/4$ rad ($\pm 45^\circ$) gages located in the center of the panel. The panel was tested by loading to design limit 267 kN (600 kips), unloading to 89 kN (20 kips), and reloading incrementally to failure. As shown, the shear stiffness on first loading was approximately 50 percent below that obtained on second loading. This inelastic behavior is apparently characteristic of crossplied metal matrix composites and has been attributed to the state of residual stresses in the composite material (ref. 5). On second loading, the panel failed at 125 percent of design ultimate load or approximately 434 MPa (63 ksi) ultimate shear stress in the composite skin. This panel failure shear stress compares favorably with test results on as-received material which indicates that the B_{SC}/Al was not degraded by exposure to the brazing environment.

The adequacy of the brazing process for fabricating B_{SC}/Al was also investigated by metallurgical analysis. Two photomicrographs showing the brazed joint between the B_{SC}/Al skin and the titanium honeycomb-core of the panel are shown in figure 12. The needlelike or acicular silicon particles of the 718 aluminum braze alloy are shown to stop at the 1100 aluminum surface of the B_{SC}/Al , indicating that interaction between the braze material and the constituents of the composite has been avoided. Therefore, degradation of the composite properties associated with exposure to a brazing environment have been minimized. A more detailed description of the braze-composite interaction is presented in reference 6.

Based on these results the brazing process developed for joining B_{SC}/Al composite appears satisfactory. Using this process, a B_{SC}/Al panel has been fabricated which fully complies with the ambient temperature design requirements of the YF-12 aircraft.

Gr/PMR-15 PI glass honeycomb-core panels.- The technology development for Gr/PI panels is at the process verification panel fabrication stage. A design verification panel has not been fabricated to date due to problems associated with obtaining consistent quality prepreg. However, recent results indicate that the problems can be rectified. Employing the technology developed to date, the process verification panel shown in figure 13 has been fabricated. This technology includes development and application of the rubber compaction process to polyimide materials for consolidating the Gr/PMR-15 PI inner pan of the panel and the development and application of LaRC-13AI polyimide adhesive for bonding Gr/PI to glass/polyimide honeycomb-core. NDE results indicate that consolidation of the composite by the rubber compaction process and the bonding between the composite laminates and honeycomb-core were successful.

CONCLUDING REMARKS

An overview of the SCAR YF-12 Panel program has been presented. This program is a joint activity between NASA Langley Research Center, NASA Dryden Flight Research Center and Lockheed. Manufacturing methods for fabricating advanced titanium structures have been evaluated and methods for fabricating high temperature composite materials are being developed. Evaluation of the structures fabricated include both flight service on the Mach 3 YF-12 aircraft and ground testing after exposure to a simulated supersonic aircraft environment. The following comments are based on the results obtained to date:

Evaluation of two advanced titanium panel concepts has been completed. Panels fabricated by weldbraze and Rohrbond processes have performed successfully in Mach 3 flight service and in ground tests after ground exposure to 587 K (600°F) for 10,000 hours.

A satisfactory process has been developed in-house at LaRC for the fluxless brazing of B_{Sc}/Al using 718 aluminum alloy braze which minimizes degradation of the composites mechanical properties. This process has been used to fabricate a B_{Sc}/Al titanium honeycomb-core structural panel that meets the ambient temperature design requirements of the SCAR YF-12 panel program.

Fabrication processes have been developed that appear capable of producing full-scale graphite/PMR-15 polyimide glass honeycomb-core panels for inclusion in the structural panel program.

REFERENCES

1. Bales, Thomas T.; Royster, Dick M.; and Arnold, Winfrey E., Jr.: Development of the Weld-Braze Joining Process. NASA TN D-7281, 1973.
2. Swartz, M. M.: Rohrbond. 5th National SAMPE Technical Conference, Kiamesha Lake, New York, October 1973.
3. Hoffman, Edward L.; Payne, Leroy; Carter, Alan L.: Fabrication Methods for YF-12 Wing Panels for the Supersonic Cruise Aircraft Research Program. 7th National SAMPE Technical Conference, Albuquerque, New Mexico, October 1975.
4. Payne, Leroy: Fabrication and Evaluation of Advanced Titanium Structural Panels for Supersonic Cruise Aircraft. NASA CR-2744, 1976.
5. Broutman, Lawrence J.; and Krock, Richard H.: Composite Materials. Volume IV-Metallic Matrix Composites, Edited by Kreider, Kenneth G., 1974.
6. Bales, Thomas T.; Wiant, H. Ross.; Royster, Dick M.: Brazed Borsic/Aluminum Structural Panels. NASA TMX-3432, 1976.

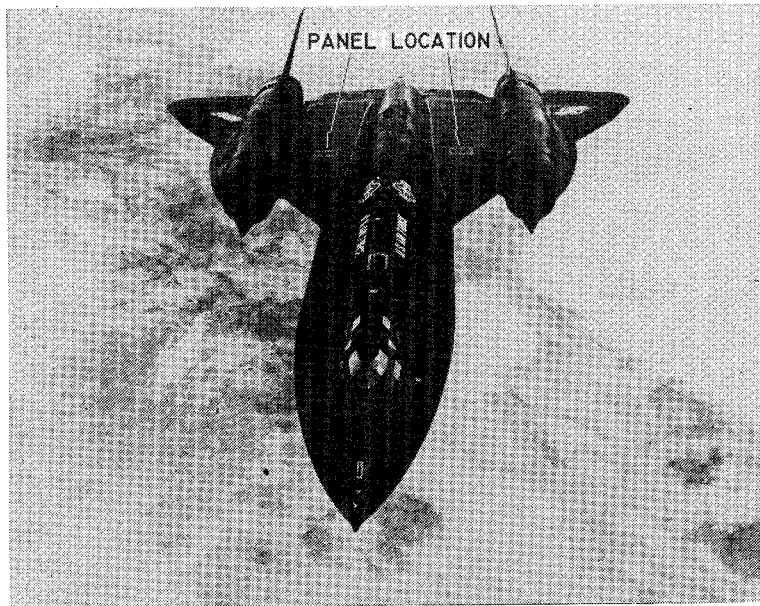


Figure 1.- Panel location on NASA YF-12.

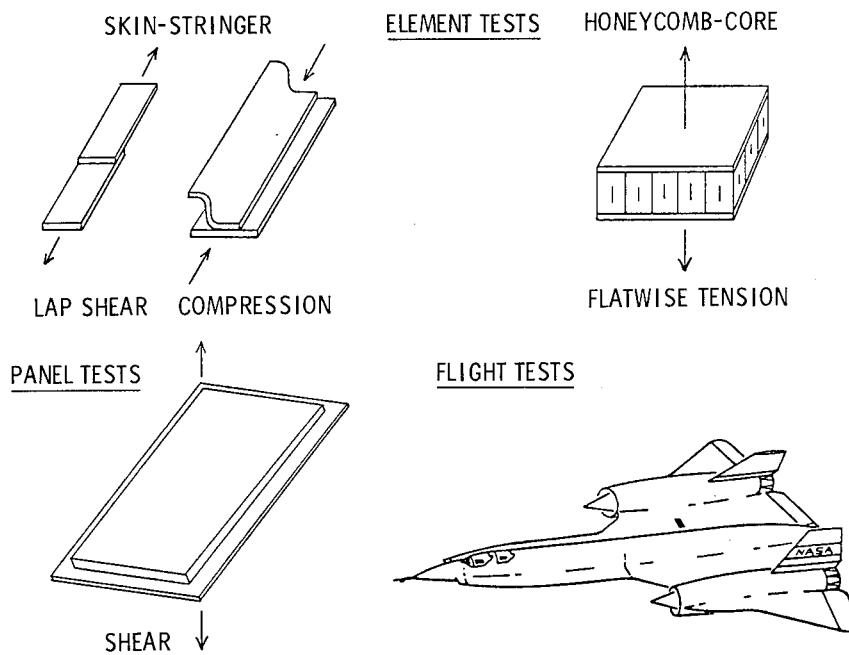


Figure 2.- Specimen types and test methods.

CONSTANT EXPOSURE			
SPECIMEN TYPE	TEST TEMP., K (°F)	EXPOSURE TEMP., K (°F)	EXPOSURE TIME, hr
STRUCTURAL ELEMENTS	297 (75)	498, 589, 700, 811 (400, 600, 800, 1000)	0, 100, 1000, 5000, 10 000
FULL-SCALE PANELS	297 (75) 589 (600)	589 (600) 589 (600)	0, 100, 10 000 0, 100

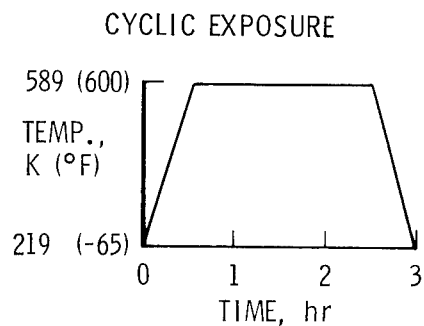


Figure 3.- Ground exposure and test schedule.

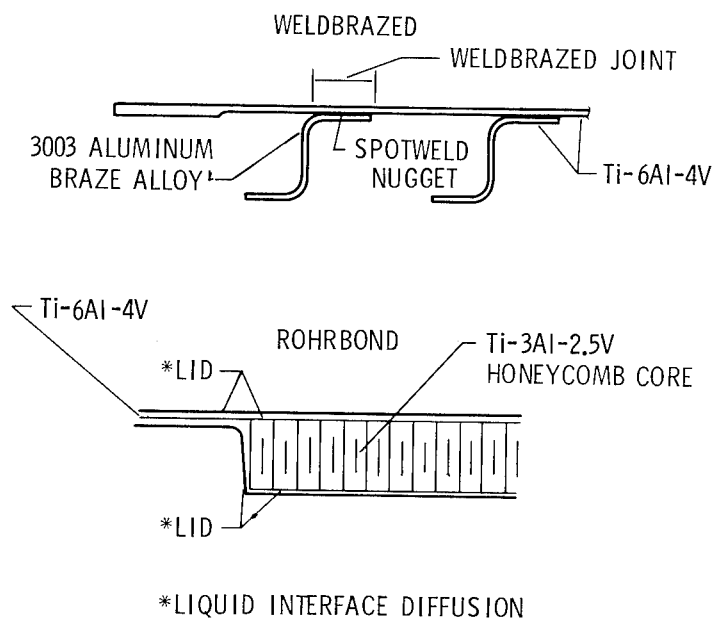


Figure 4.- Titanium panel concepts.

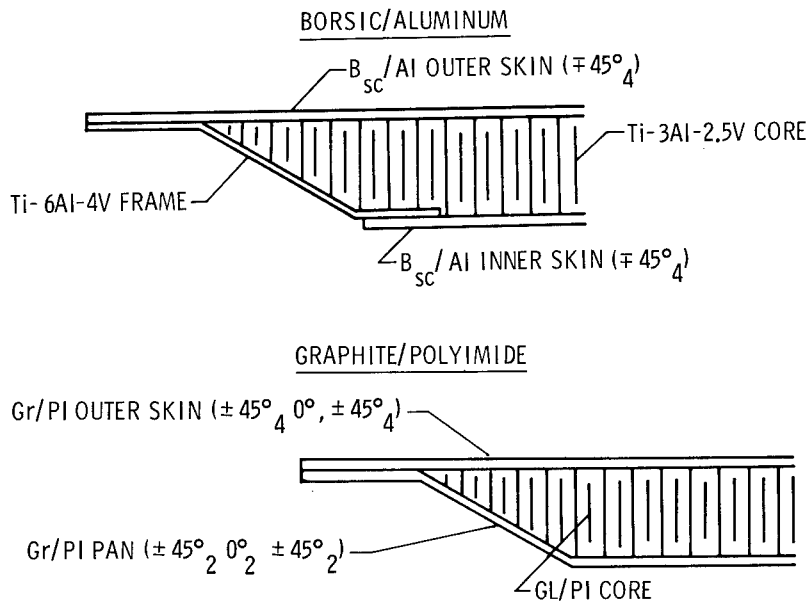


Figure 5.- Composite panel concepts.

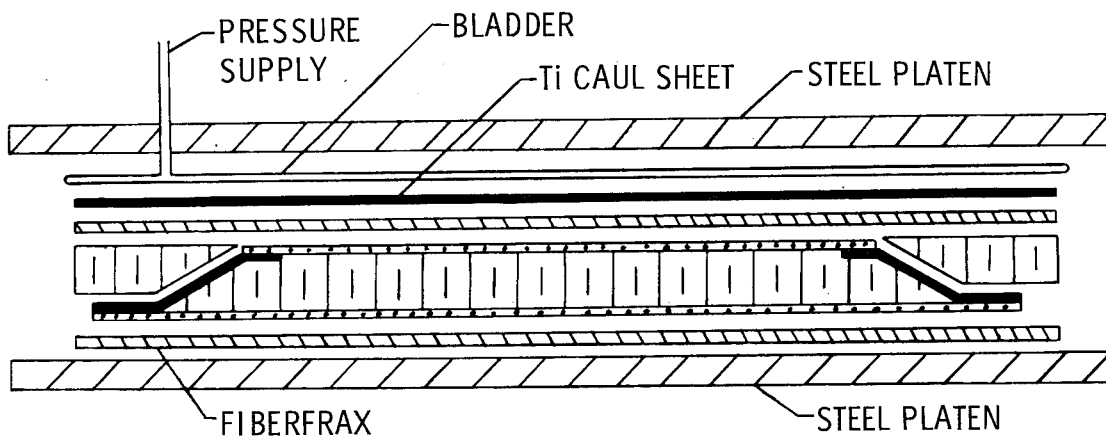


Figure 6.- Brazing fixture for B_{SC}/Al panels.

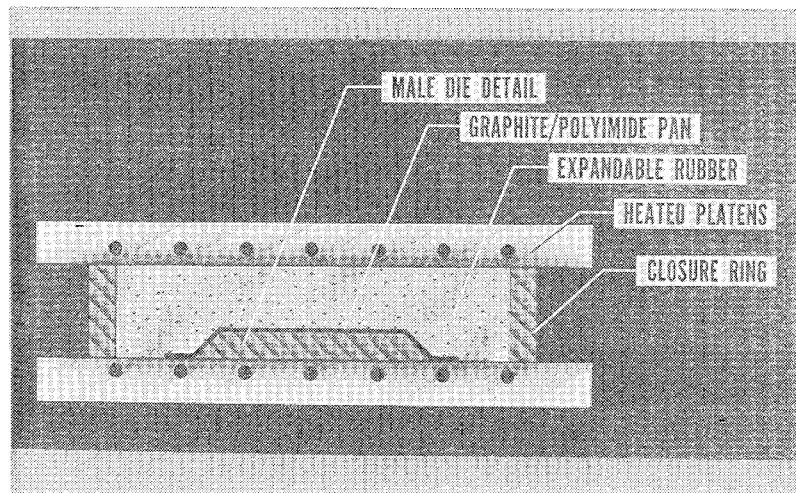


Figure 7.- Rubber compaction process for Gr/PI.

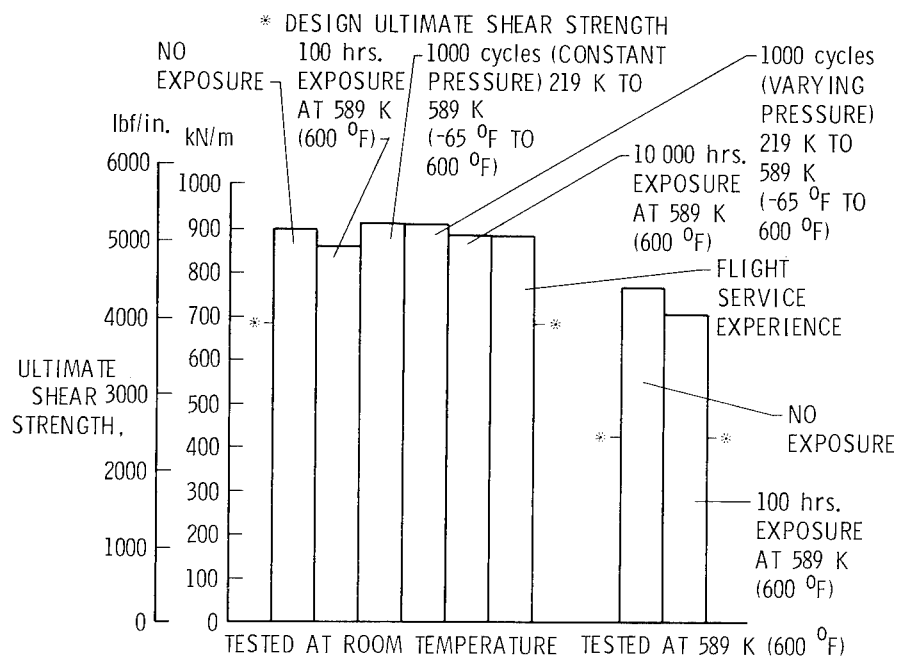


Figure 8.- Weldbrazed panel shear test results.

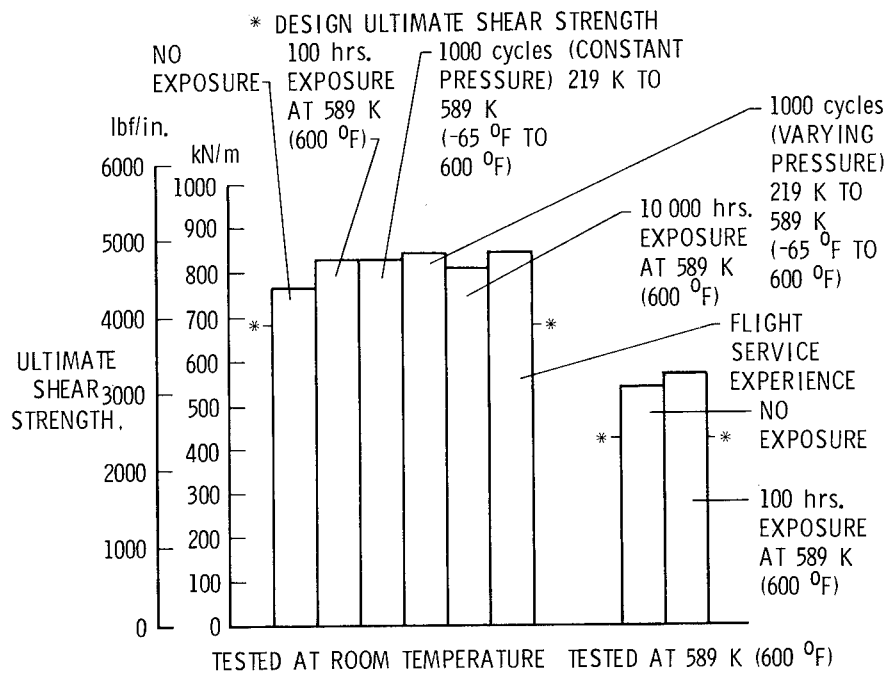


Figure 9.- RohrBond panel shear test results.

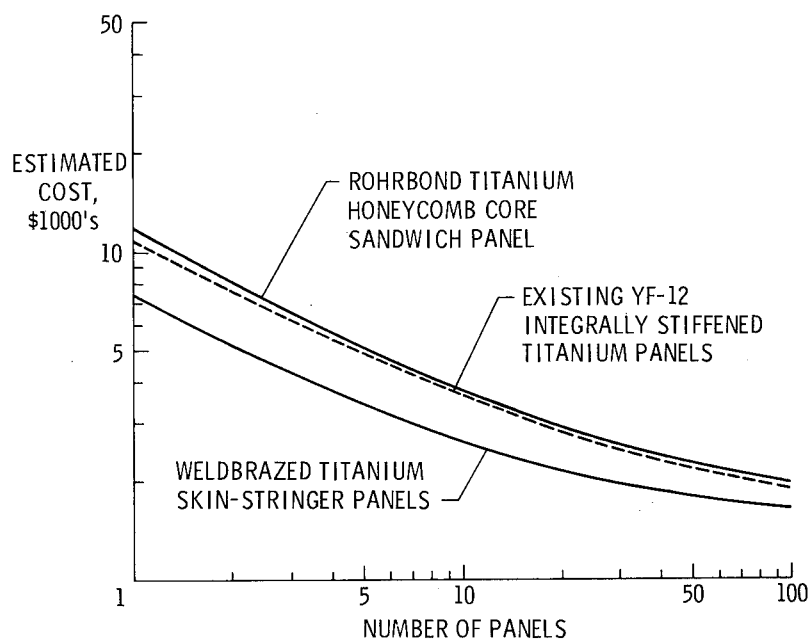


Figure 10.- Estimated costs of titanium panels.

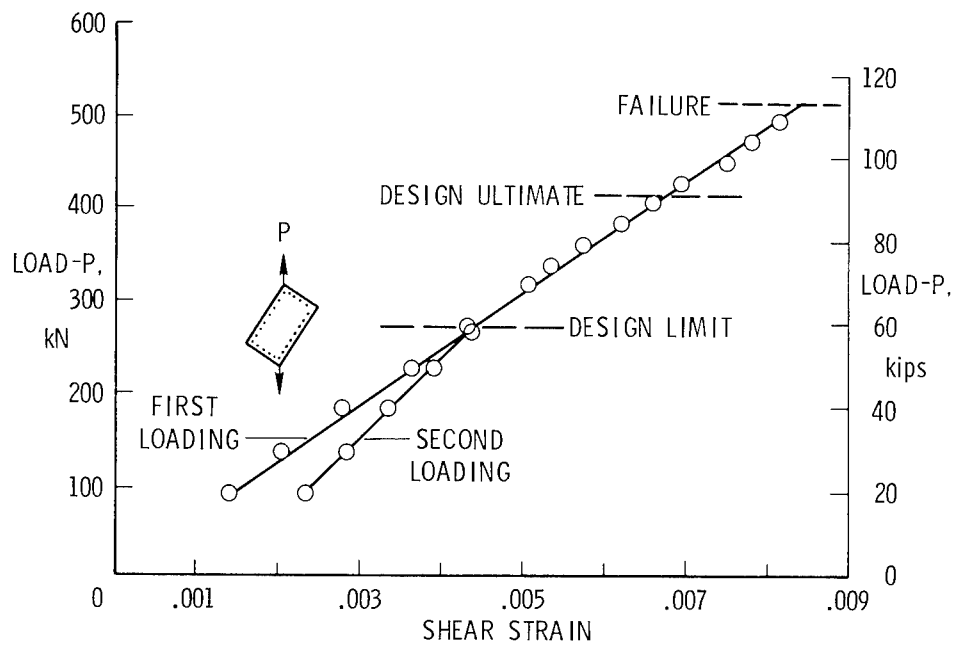


Figure 11.- B_{sc}/Al panel shear test results.

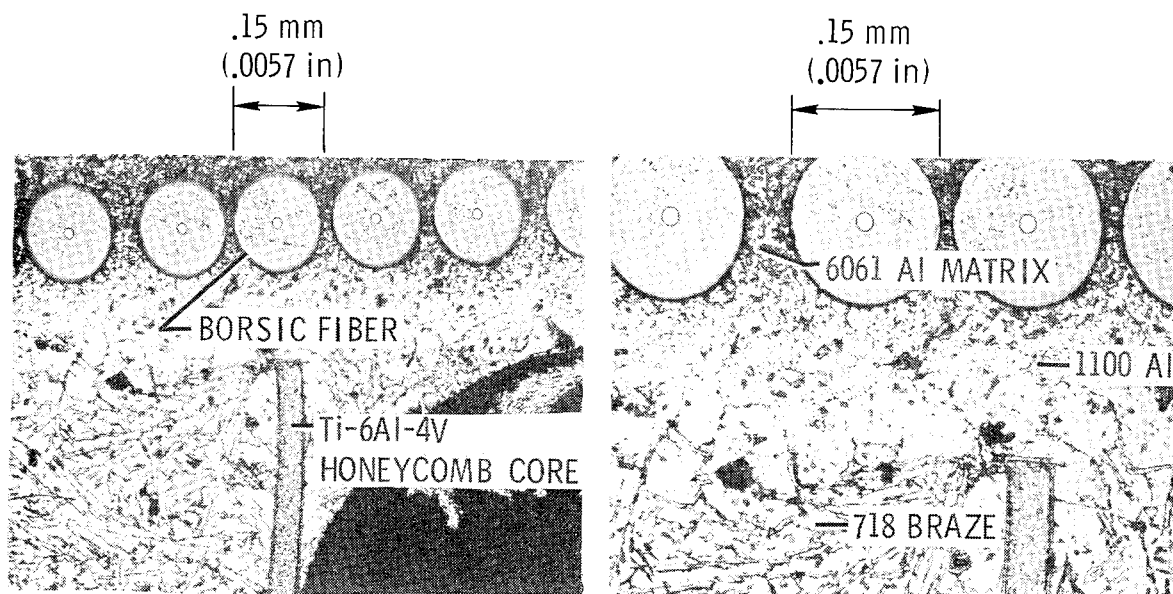


Figure 12.- B_{sc}/Al Ti honeycomb-core joint.

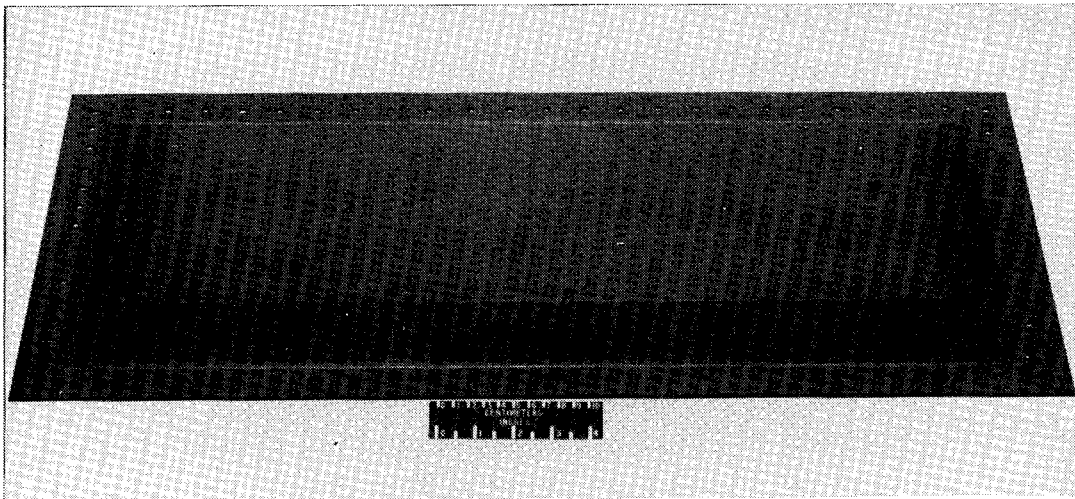


Figure 13.- Gr/PMR-15 PI process verification panel.

TIME-TEMPERATURE-STRESS CAPABILITIES OF COMPOSITES FOR SUPERSONIC CRUISE AIRCRAFT APPLICATIONS*

J. F. Haskins and J. R. Kerr
General Dynamics Corporation
Convair Division

B. A. Stein
NASA-Langley Research Center

ABSTRACT

Advanced composite materials have the potential of reducing the weight of future supersonic cruise aircraft structures. However, information on the effects of long-time, cyclic exposure to environments, and loadings representative of long-time supersonic cruise aircraft service for the composite materials of interest is not available. A program to generate such information was initiated in 1973. A range of baseline properties was determined for representatives of 5 composite materials systems: B/Ep, Gr/Ep, B/PI, Gr/PI, and B/Al. Long-term exposures are underway in static thermal environments and in ones which simultaneously combine programmed thermal histories and mechanical loading histories. Material behavior during these exposures and post exposure residual property tests will provide exposure effects and reveal material degradation mechanisms.

Much of the baseline property data including tensile, notched tensile, shear, fatigue and creep that have been obtained on this program have been published previously. This paper presents selected results from the environmental exposure studies with emphasis placed on the 10,000-hour thermal aging data. Results of residual strength determinations and changes in physical and chemical properties during high temperature aging are discussed and illustrated using metallographic, fractographic and thermomechanical analyses. Some initial results of the long-term flight simulation tests are also included.

* Sponsored by NASA Langley Research Center under Contract NAS1-12308.

INTRODUCTION

In the materials portion of the SCAR program, NASA's goal is to advance the technology and establish a data base so that sound technical decisions may be made in the future regarding the use of advanced composite materials in supersonic cruise aircraft structures. This paper reviews the objectives and status of the on-going study to determine the time-temperature-stress characteristics of five classes of composite materials: boron/epoxy, graphite/epoxy, boron/polyimide, graphite/polyimide, and boron/aluminum.

This is the fourth in a series of papers (ref. 1, 2, 3) presenting data developed during this study at General Dynamics Convair under NASA Contract NAS1-12308. The general objective of this study is to assess the suitability of these advanced filamentary reinforced composite materials for future supersonic cruise aircraft structures. The study has two phases. The first includes all material property determinations and aging and simulation exposures up through 10,000 hours. The second continues these tests up to 50,000 hours.

Figure 1 is a schematic diagram of the study. The changes in baseline tensile, notched tensile, shear, fatigue, and fracture properties that occur during times out to 50,000 hours are being measured for ambient and thermal aging conditions, as well as random cyclic loading with cyclic temperature variations. These latter tests are intended to simulate the conditions experienced during supersonic flight. In the previous reports some data have been presented on the effects of thermal aging and ambient aging on mechanical properties. These reports contain extensive baseline data and some of the preliminary results of the fatigue and creep portions of the study. The design and construction of the flight simulation equipment have also been discussed in a previous paper (ref. 3).

This paper updates the results of residual mechanical property tests and discusses in some detail the analysis to date on the graphite/epoxy thermal aging specimens and provides some explanation for their loss in strength after 10,000 hours of elevated temperature exposure at ambient and reduced pressures. Some preliminary results of the flight simulation tests are also included.

MATERIALS

Of the multitude of advanced composite material systems that have been developed and evaluated, five have generally been accepted as the most promising for aerospace structural design applications: boron/epoxy (B/E), graphite/epoxy (G/E), boron/polyimide (B/PI), graphite/polyimide (B/PI), and boron/aluminum (B/Al). Within each of these five classes there are several types of matrix materials and different types of filaments. Table I lists the specific advanced composite systems evaluated in this program. The selection of these particular composite systems was based on cost, current availability and manufacturing maturity, existing data base, fabrication history, good thermomechanical and physical properties, and material suppliers' continuing interest in producing a particular system.

The organic matrix composites were fabricated by Convair from vendor supplied prepreg material using conventional autoclave processing methods. The B/Al, which was purchased in the form of finished sheet material, was fabricated by diffusion bonding at approximately 800 K (975°F) using a single-step hot pressing technique. Both unidirectional and $[0^\circ \pm 45^\circ]$ laminates were evaluated for each system. Six-ply laminates were used for all tests except flexure, short beam shear, transverse tensile, and $R = -1$ fatigue for which 12-ply panels were required. Diamond impregnated saws were used for specimen cutting, and all holes and notches were prepared by rotary ultrasonic drilling, electrical discharge machining, or ultrasonic impact grinding.

Since the beginning of this contract, many new advanced composite systems have been developed, and of these several are now commercially available. One of the goals of the overall program was to follow this progress and to add new materials if sufficiently promising ones appeared. This will be done by choosing a material from the group of recently developed high temperature graphite fiber reinforced polyimide systems listed in table II. In order to select the best materials system of these emerging graphite reinforced polyimides, a preliminary screening test will be conducted. The criteria for selecting the best system will include:

- a. Availability and cost of prepreg material.
- b. Ability to fabricate both full-size 12-ply panels and a simple structural shape.

- c. Moisture resistance.
- d. High temperature thermal stability and oxidation resistance.

PROGRAM STATUS AND INTERIM RESULTS

Because of the length of this contract, it was thought to be desirable to provide periodic reports on the program status. In this way, results can be presented as they become available rather than waiting until the end of the study for a complete presentation of the data. The program is currently nearing the end of Phase 1, the 10,000-hour portion, and considerable data have been obtained. Table III summarizes the type and number of tests included and also shows the number of tests that have been completed at this time. Customary units rather than the International System of Units (SI) were used as the working units of measurement for all tests. The following sections describe these tests and test procedures and, in addition, present and discuss some of the recently obtained results. Much of the earlier data has been presented in previous papers, and these references have been noted.

Quality Assurance

Quality assurance testing was conducted on the epoxy and polyimide preregs and on all fabricated panels of all materials. These acceptance tests included ultrasonic C-scans, volume percentage determinations, mechanical property testing, and for the organic matrix composites flexural testing before and after 24-hour water boil.

While all five materials passed the acceptance tests, one, B/PI, was later dropped from the program because of extensive thermal degradation observed during thermal aging and short term flight simulation testing at 505 K (450F). Later tests by the resin producer, Ciba Geigy, substantiated Convair's data and reinforced the conclusion that the resin was not suitable for this application.

Baseline Testing

The purpose of the baseline tests is threefold. First, these data will serve to characterize the composite materials and add to any existing data bases. Second, the baseline tests will provide the scale and shape parameters necessary to define the statistical distribution of the ultimate tensile strengths for each of the material systems. These, in turn, are used to set the loads for the short term tests, and with the short term results, are used in a wear out analysis model to relate static and fatigue strengths. Finally, the baseline tests will provide a rational starting point against which the various environmental effects may be measured.

Tests that were conducted included: ultimate tensile, tensile modulus, Poisson's ratio, notched tensile ($K_t = 3$), transverse tensile (unidirectional laminates only), shear, and fracture. Testing was performed over the temperature range from 218 K (-67°F) to 450 K (350°F) for the epoxy specimens, to 616 K (650°F) for the polyimide specimens, and to 700 K (800°F) for the boron aluminum specimens. These data have been presented previously, reference 1, and are not included in this paper.

Environmental Aging

Most of the data generated to date on advanced composite materials have been initial strength data without regard to environmental conditions. The small amount that is available is generally for only relatively short periods of exposure compared to the lifetime of a commercial airliner. This portion of the program was intended to evaluate the composite systems as a function of exposure to moisture, ambient aging, and atmospheric contaminants over relatively long periods of time.

For the resin matrix composites, 24-hour water boil, 6-week humidity, and 20-week and 52-week ambient aging tests were conducted as accelerated means of simulating long-term ambient exposure. Residual strength testing (flexure) of these specimens was performed to determine the effects of exposure. The results are summarized in table IV. For the epoxy systems the room temperature flexural strengths were nearly unaffected, while those at 450 K (350°F) were, in general, severely degraded. The effects of the moisture exposures on the polyimide specimens were generally less damaging than for the epoxy systems. Some decreases in flexural strength of the crossplied material were observed at

450 K (350°F) after the 24-hour water boil and 6-week humidity tests, but no significant effects were observed as a result of the 20- and 52-week ambient ages. Absorption of moisture is the primary cause for the deterioration in high temperature properties. The water plasticizes the resin which subsequently lowers the glass transition temperature of the resin and, thereby, decreases the high temperature mechanical properties. Complete results for the epoxy and polyimide systems can be found in reference 2.

Significant efforts exist at several laboratories in this country to determine moisture effects on mechanical properties of polymer matrix composites. Many results have been recently presented at U.S. Air Force Materials Laboratory and Society of Aerospace Materials and Process Engineers workshops, while some initial data have been published (see, for example, references 4 and 5). A general conclusion based on this information is that epoxy matrix composites should generally be limited to less than 394 K (250°F) for supersonic cruise aircraft applications.

Another environmental study is being conducted to determine the effects of corrosion and atmospheric contaminants on the four composite systems. Tensile specimens of the epoxy and polyimide systems and tensile and shear specimens of coated and bare B/Al have been placed in an outdoor industrial-seacoast atmosphere corrosion test facility maintained by Convair in San Diego, California. A high temperature coating with a maximum use temperature of about 589 K (600°F) was applied to one-half of the B/Al specimens. The coating consisted of a chemical conversion coating followed by an epoxy primer and a polyimide topcoat. No coatings were used on any of the organic matrix composites. The specimens are tested after 10,000 and 50,000 hours of exposure for the B/Al and 50,000 hours for the epoxy and polyimide specimens.

To date, the 10,000-hour B/Al exposure tests have been completed with the remaining specimens having approximately 25,000 hours of exposure. For the 10,000-hour B/Al exposure, the coated specimens have shown no change in either appearance or mechanical properties. The uncoated specimens, on the other hand, have experienced significant surface corrosion and decreases in matrix controlled properties, i. e, transverse tensile and shear strength. Results of the 10,000-hour exposures are available in reference 3.

Thermal Aging

All of the composite materials are being thermally aged for periods up to 50,000 hours. At various times during the 50,000 hours, specimens are removed for examination and determination of residual tensile strength. Both unidirectional and $[0^\circ \pm 45^\circ]$ crossply materials are included. The aging temperatures are: epoxy, 394 K (250°F) and 450 K (350°F); polyimide, 505 K (450°F) and 561 K (550°F); and B/Al 450 K (350°F), 561 K (550°F) and 700 K (800°F). The organic matrix composites are aged at one atmosphere (101 kN/m²) and at a reduced pressure of 13.8 kN/m² (2 psi) to simulate high altitude flight conditions. Previous work has shown a direct correlation of thermal aging and oxygen pressure on residual strength of resin matrix composites (reference 6). The B/Al system is aged at atmospheric pressure (101 kN/m²) only.

Exposures were conducted as described in reference 1. The effects of moisture were eliminated from all tests by carefully baking-out each of the specimens before test. Thermal aging tests are currently in progress with exposure times of just under 25,000 hours for several of the systems. Residual strength data are available for all of the composites out to at least 10,000 hours. Table V and figure 2 show the thermal aging data for A-S/3501 graphite/epoxy. Those specimens aged at 394 K (250°F) and one atmosphere and those aged at 450 K (350°F) and 13.8 kN/m² (2 psi) show no loss in strength out to 10,000 hours for either the unidirectional or $[0^\circ \pm 45^\circ]$ crossply materials. The G/E aged at 450 K (350°F) and one atmosphere showed a 20 percent loss in strength for the unidirectional materials, and a 60 percent loss in strength for the $[0^\circ \pm 45^\circ]$ crossply material after 10,000 hours. Photomicrographs and fractographs of this material during thermal aging will be discussed later in the paper. The data shown in table VI are for B/5505 boron/epoxy and are very similar to the graphite/epoxy data except for the 30 percent loss in strength of the crossply material after 10,000 hours exposure at 450 K (350°F), and 13.8 kN/m² (2 psi). In summary of these data, A-S/3501 graphite/epoxy and B/5505 boron/epoxy should be limited to 394 K (250°F) for exposures greater than 10,000 hours because of loss of residual tensile strength during thermal aging.

Table VII and figure 3 show the data for HT-S/710 graphite/polyimide after aging at 505 K (450°F) and 561 K (550°F). The results are analogous to those for boron/ and graphite/epoxies in that the lower temperature exposures had little effect, while the high temperature aging caused a considerable decrease in tensile strength. It should be noted that the aging temperatures for the polyimide system were 111 K (200°F) higher than those used for the epoxies. In like manner to the crossply boron/epoxy, the reduced pressure

aging of unidirectional graphite/polyimide at the higher temperature also lowered the tensile strength significantly. In summary of these data, HT-S/710 graphite/polyimide should be limited to 505 K (450°F) for exposures greater than 10,000 hours because of loss of residual tensile strength during thermal aging.

In general, strength degradation during aging in all organic matrix composites tested appears to be matrix related. Subsequent sections will discuss organic matrix degradation in more detail.

Table VIII and figure 4 show the thermal aging results for boron/aluminum at three aging temperatures and times out to 10,000 hours. The 5,000-hour data were presented and discussed previously in reference 3. The 10,000-hour data show a further decrease in tensile properties at all aging temperatures for both unidirectional and crossply material and substantiate the results described in reference 3. Based on transverse tensile and shear data (not shown) for boron/aluminum specimens, the decrease in properties appears to be primarily fiber related. Boron filaments have apparently become embrittled and weakened as a result of interdiffusion between the boron and 6061 aluminum alloy at the fiber matrix interface during thermal exposure. In summary of these data, B/6061 boron/aluminum should be limited to 450 K (350°F) for supersonic cruise aircraft cumulative exposures greater than 10,000 hours because of loss of residual tensile strength during thermal aging.

Microscopic Examination of the Thermal Aging Specimens - After tensile testing, many of the thermal aging specimens were sectioned and mounted for study using both an optical microscope (metallograph) and scanning electron microscope (SEM).^{*} These studies were intended to detect changes which occurred in the composites during exposure in order to assist in identifying degradation mechanisms. Additional examinations were conducted of the fractured surfaces (primarily with the SEM) to determine failure modes and to further study the degradation processes. As these investigations have been completed for only the graphite/epoxy, the following discussion will be limited to this system.

Figure 5 shows photomicrographs using a metallograph and a SEM at 100X and 500X magnifications. These pictures are for 10,000 hours exposure at 450 K (350°F) and 13.8 kN/m² (2 psi) pressure. Close examination of these photomicrographs shows only surface changes in the resin and some

^{*} The photomicrographs used in this paper were provided by M. Featherby of General Dynamics.

cracking which probably occurred during post exposure tensile testing. Some of the cracks are located at boundaries between lamina and others within a particular lamina, as shown in the upper two photomicrographs. The lighter cast at the specimen edges in the SEM pictures will be shown later to be oxidation. In this case, it has only occurred at the surfaces exposed to oxygen.

The pictures in figure 6 taken at 100X with the metallograph show good examples of how oxidation of the epoxy resin can proceed inward as a function of time and temperature. The upper pictures show that there is little difference between the as-received material and that aged for 10,000 hours at 394 K (250°F) in one atmosphere air. The lower pictures, on the other hand, show extensive degradation in the outside plies after 5,000 hours at 450 K (350°F), and considerable degradation in both the inner and outer layers after 10,000 hours. The SEM pictures in figure 7 taken from the same specimens show the identical effects, but even more clearly than the metallographic pictures. For example, the slight amount of surface oxidation after 10,000 hours at 394 K (250°F) is easily distinguished in the SEM photograph in figure 7, while scarcely visible in figure 6.

The changes from light to dark for pictures taken using the metallograph and dark to light using the SEM are explained by the amount of relief polishing around the individual fibers that increases with the degree of oxidation. When the epoxy resin oxidizes, it is more prone to crumble and differences in the amounts of oxidation in the polished mounts can easily be detected using the SEM at higher magnifications.

Figure 8 shows typically how this occurs. The as-received specimen has little and uniform relief for all plies as shown at 2500X using the SEM to examine a typical polished surface. The inner plies of a specimen aged for 10,000 hours at 394 K (250°F) look much the same except for the filaments being oriented at 45° to the surface. If one moves to the outer ply, the relief has increased as shown at the lower right of figure 8. This effect becomes more pronounced for specimens aged at 450 K (350°F) and 10,000 hours as shown in the lower left picture. The magnification was lowered to a 1,000X for clarity.

Fractographs - In addition to the metallographic cross sectional examinations, a study was also made of the fracture surfaces of several of the specimens. Examples are presented in figures 9 and 10. Typical fractographs of graphite/epoxy unaged and aged at 394 K (250°F) for 10,000 hours are shown in the upper portion of figure 9. As might be predicted from the tensile results, the appearance of the fracture surfaces are very similar for the two specimens. The matrix is relatively intact and there is little fiber pull out. For specimens aged at 450 K (350°F) for either 5,000 or 10,000 hours, it was not possible to

get a good SEM picture of the fracture. The very brittle resin had crumbled away from the filaments in the area of the fracture so that only a few filament ends would have appeared in the field of view.

The pictures in the lower portion of figure 9 show some of the filaments near the fracture locations in specimens aged at 450 K (350°F). The filaments are quite different in appearance than those in the upper two photographs in the amount of resin adhering to the surface. The presence of this much resin on the graphite filaments indicates a severe degradation of the epoxy matrix which accounts for the failure within the matrix rather than at the fiber/resin interface.

An interesting example of the gradient of oxidation into the specimens is illustrated in the fractographs of figure 10. These pictures were taken from areas near the surface of specimens aged at 394 K (250°F) and ambient pressure and at 450 K (350°F) and reduced pressure. As shown in figures 5 and 7, only a slight amount of oxidation (only at the outer surfaces) had occurred in these specimens in 10,000 hours. In figure 10 the depth to which the oxidation had progressed is readily visible. The resin near the outer surface has been embrittled by oxidation and has broken away from the filaments during tensile testing. Deeper into the specimen the fracture surface more closely resembles that of an unaged specimen.

Glass Transition Temperature Studies - Further studies of the changes in the epoxy resin were made by measuring the glass transition temperature (T_g) of small samples cut from the thermal aging specimens. These tests were performed using a DuPont 942 Thermomechanical Analyzer module in conjunction with a DuPont 990 Thermal Analyzer. The results are tabulated in table IX. For aging at 394 K (250°F) no change was observed for aging times out to 10,000 hours, in agreement with the tensile results. For the reduced pressure, 13.8 kN/m² (2 psi), exposures at 450 K (350°F), however, significant increases in T_g were found. These changes in the resin were not detected by either the mechanical property tests or microscopic examinations. No measurements could be made on the 5,000-hour and 10,000-hour specimens aged at ambient pressure and 450 K (350°F) because of the damage which occurred during tensile testing. The full significance of the changes in the T_g values and their relationship to the changes in the resin systems during aging are not clearly understood at this time. It is hoped, however, that this analytical technique will assist in the study of the processes which take place during elevated temperature exposure.

The last entry in table IX is for a flight simulation specimen (aging plus random fatigue loading) which failed in approximately 4,500 hours. The rather large increase in T_g obtained from this specimen is the first indication that the combined effects of heat and load may be much larger than one would predict.

Creep and Fatigue

The creep and constant amplitude fatigue testing portions of Phase I have recently been completed. Creep tests were conducted at two temperatures for each system for exposure times of 100 and 1,000 hours. The fatigue tests were performed at room and one elevated temperature at stress ratios of 0.1 and -1. Both flawed and unflawed fatigue specimens were included in the study. Details of the test procedures for both creep and fatigue have been described in reference 1. Data reduction, curve plotting, and analysis of the results of both the creep and fatigue tests are currently in progress. Because these tasks are unfinished at this time, only a small portion of the data is included in this paper. The completed results will be presented in a later publication.

Creep data for graphite/polyimide tested at 561 K (550°F) are shown in figure 11 for both unidirectional and $[0^\circ \pm 45^\circ]$ crossply specimens. The amount of creep (plastic strain) after 100 hours was less than 0.1 percent. This small amount of creep is typical of composites with unidirectional plies. Figure 12 compares the results of fatigue testing $[0^\circ \pm 45^\circ]$ graphite/polyimide at 505 K (450°F) at stress ratios of $R = 0.1$ and $R = -1$. The data show the fatigue life for a stress ratio of $R = -1$ to be much lower than for $R = .1$. Similar results have been observed for the other composite systems at room and elevated temperatures and for both unnotched and notched specimens. The fatigue properties of unnotched and notched $[0^\circ \pm 45^\circ]$ B/Al tested at 297 K (75°F) and 561 K (550°F) are compared in figure 13. The effect of raising the test temperature from 297 K (75°F) to 561 K (550°F) is to significantly reduce the fatigue strength at 10^7 cycles. For fatigue lives of 10^5 cycles or less, however, the effect of temperature is not very great.

Examination of the B/Al specimens that were fatigue tested at 561 K (550°F) has revealed severe degradation of the aluminum matrix material, as shown in figure 14. The surface of the specimen showed multiple cracks and roughness caused by localized deformation. The surface appearance suggests that the degradation may have been caused by grain growth and embrittlement at the grain boundaries. Specimens tested at 505 K (450°F) showed none of this surface degradation. Tests at 561 K (550°F) in either argon or nitrogen atmospheres gave significant decreases in surface degradation, an indication that environment plays an important role in the degradation process. In view of these results, boron/aluminum should be limited to 505 K (450°F) applications where it will be subjected to fatigue loading in air.

Flight Simulation

The major task of this program, the flight simulation tests, is the one for which the least amount of data are available at this time. These tests involve evaluation of the composite materials after they have been subjected to simulated supersonic flight environments for 10,000, 25,000 and 50,000 hours. The 50,000 hours are composed of 25,000 flight cycles similar to the one presented in figure 15. Exposures are performed in the General Dynamics Convair flight simulator shown in figure 16. This apparatus is capable of long time automatic testing using random loading and realistic flight temperature profiles. Both load level and maximum temperature are adjusted to suit the particular capabilities of each composite system. Following exposure residual tensile, notched tensile, fatigue, and notched fatigue strength will be determined. Details of (a) the design, construction, and checkout of the flight simulator, (b) the specimen configuration, and (c) the test plan have been covered extensively in references 2 and 3.

The flight simulation tests are in progress, but no residual strength results will be available until the first 10,000 hours have been completed. At the time of this writing, the boron epoxy and graphite epoxy systems have completed 7,500 hours of exposure and the graphite polyimide and boron aluminum systems 4,500 hours.

There have been, however, four unnotched graphite epoxy specimens that have failed in less than 5,000 hours, a rate well in excess of that predicted from the wearout theory used to set the test load levels and temperature. Three of these specimens are shown in figure 17. Fracture has occurred in the 5 cm (2 inch) long heated zone located at each end of the specimen. The fourth fractured in a manner which suggested an equipment problem rather than a material failure. A study is now in progress to determine the degradation mechanisms responsible for these early failures. Preliminary results indicate that the compression load which occurs once per flight cycle may be an important factor in the failure of the specimens. This is shown by the delaminations visible in the edge view in figure 18. The photograph is of the heated zone of a specimen which has not failed. Another mechanism which may be important is the accelerated oxidation that occurs as filaments in the outer plies fail, thereby exposing the underlying resin to the oxidizing environment. This is clearly shown in figure 19. SEM and optical examinations, residual compression and tensile strength, and chemical and thermomechanical analyses are currently in progress to resolve the difference between predicted and experimental failure for the graphite epoxy system. If compression continues to be the failure mode of these long term flight simulation specimens,

then wearout model predictions of failure (based on short term flight simulation specimens which failed in tension) are not applicable. Analyses based on more complex wearout plus oxidation mechanisms will need to be developed to predict long term flight simulation test failures.

CONCLUDING REMARKS

This paper describes a long term study to characterize the properties of several types of advanced filamentary reinforced composite material systems and to determine the effects of long time supersonic flight simulation on these properties. A status report on the progress to date has been presented along with some detailed results and analysis of the thermal aging phase of the program. While the investigation is still in progress, interim conclusions have been drawn on the basis of the data generated to date concerning the capabilities of these composite materials for supersonic cruise aircraft applications. These conclusions are in the form of exposure time and temperature limits; stress limits cannot be suggested until more results of simulated flight service testing are available. The interim conclusions are:

Graphite/epoxy (A-S/3501) and boron/epoxy (B/5505) should be limited to temperatures lower than 394 K (250°F) for cumulative exposures greater than 10,000 hours because of:

1. Moisture effects on elevated temperature strength (due to matrix degradation).
2. Loss of residual tensile strength during thermal aging (due to oxidation induced matrix degradation).
3. Early flight simulation test failures (due to compression loading combined with oxidation induced matrix degradation).

Boron/aluminum (B/6061) should be limited to 450 K (350°F) for exposures greater than 10,000 hours because of:

1. Loss of residual tensile strength during thermal aging (due to interface diffusion induced fiber degradation).
2. High temperature fatigue effects (matrix surface cracking and oxidation).

Boron/polyimide (B/P105AC) is not suitable for this application (because of lack of thermal exposure stability for 1000 hours at 505 K (450°F)).

Graphite/polyimide (HT-S/700) should be limited to 505 K (450°F) for exposures greater than 10,000 hours because of loss of residual tensile strength during thermal aging (due to oxidation induced matrix degradation).

REFERENCES

1. Kerr, J. R., Haskins, J. F. and Stein, B. A.: Program Definition and Preliminary Results of a Long-Term Evaluation Program of Advanced Composites for Supersonic Cruise Aircraft Applications. Environmental Effects on Advanced Composite Materials, Spec. Tech. Publ. 602, American Soc. Testing and Materials., 1976, pp. 3-22.
2. Haskins, J. F. Wilkins, D. J. and Stein, B. A.: Flight Simulation Testing Equipment for Composite Material Systems. Environmental Effects on Advanced Composite Materials, Spec. Tech. Publ. 602, American Soc. Testing and Materials, 1976, pp. 23-36.
3. Haskins, J. F. and Kerr, J. R., Time-Temperature-Stress Capabilities of Composite Materials for Advanced Supersonic Technology Applications, Third Conference on Fibrous Composites in Flight Vehicle Design, November 4-6, 1975, NASA TMX-3377, April 1976.
4. McKague, E. L.; Reynolds, J. D. and Halkias, J. E.: Life Assurance of Composite Structures, Vol. I - Moisture Effects, AFML-TR-75-51, May 1975.
5. Hertz, J.: Investigation Into The High Temperature Strength Degradation of Fiber-Reinforced Resin Composites During Ambient Aging, NASA CR-124290, June 1973.
6. Chase, V. and Beeler, D., Manufacturing Methods for Large High-Temperature Sandwich Structures, Technical Report AFML-TR-70-211, Air Force Materials Laboratory, Dayton, Ohio 1970.

TABLE I. LIST OF ADVANCED COMPOSITE SYSTEMS.

MATERIAL SYSTEM	TYPE	VENDOR	NOMINAL FIBER VOLUME (%)	SPECIFIC GRAVITY
BORON/EPOXY	RIGIDITE 5505 4.0-MIL BORON	Avco	58	2.0
GRAPHITE/EPOXY	A-S/3501	HERCULES	60	1.6
BORON/POLYIMIDE	B/P105AC 4.0-MIL BORON	Avco	50	2.0
GRAPHITE/POLYIMIDE	HT-S/710	HERCULES	63	1.5
BORON/ALUMINUM	DIFFUSION BONDED 5.6-MIL BORON; 6061 ALUMINUM	Avco	50	2.6

TABLE II. SCREENING EVALUATION CANDIDATES.

MATERIAL SYSTEM	POTENTIAL VENDORS
HT-S/NR-150B2	NARMCO, FIBERITE, U. S. POLYMERIC
HT-S/PMR-15	U. S. POLYMERIC, FERRO
HT-S/HR-600	FIBERITE
HT-S/5230	NARMCO
HT-S/F-178	HEXCEL
HT-S/4397	HERCULES

TABLE III. SUMMARY OF PHASE I TEST PROGRAM.

TEST TYPE	TOTAL TESTS	TESTS COMPLETED	PERCENT COMPLETED
QUALITY ASSURANCE	356	356	100
TENSILE	558	558	100
SHEAR	56	56	100
FRACTURE	24	8	33
ENVIRONMENTAL AGING	189	189	100
THERMAL AGING	297	297	100
CREEP	90	90	100
FATIGUE	495	495	100
FLIGHT SIMULATION	200	160	80
A. RESIDUAL TENSILE	550	160	29
B. RESIDUAL FATIGUE	160	0	0
C. RESIDUAL SHEAR	20	0	0
	2,995	2,369	79

TABLE IV. SUMMARY OF EFFECTS OF MOISTURE AND AMBIENT AGING ON RESIN-MATRIX COMPOSITES

Retention of Flexural Strength (Percent) after Indicated Exposure*					
Orient	Temp Deg K (Deg F)	24 Hour H ₂ O Boil	6 Week Humidity	20 Week Ambient	52 Week Ambient
B/5505 Boron/Epoxy					
[0]	297 (75)	94	103	105	110
[0]	450 (350)	23	39	59	53
[0 ± 45]	450 (350)	63	74	102	94
A-S/3501 Graphite/Epoxy					
[0]	297 (75)	100	100	110	96
[0]	450 (350)	34	30	54	46
[0 ± 45]	450 (350)	54	41	81	57
HT-S/710 Graphite/Polyimide					
[0]	297 (75)	85	85	103	100
[0]	450 (350)	105	106	85	107
[0 ± 45]	450 (350)	75	81	111	93

*Average of 3 Tests

TABLE V-A. THERMAL AGING DATA FOR UNIDIRECTIONAL A-S/3501 GRAPHITE/EPOXY.

Aging Temp K (F)	Pressure kN/m ² (psi)	Test Temp K (F)	Aging Time (HR)	Tensile Strength MN/m ² (ksi)	
394 (250)	101 (14.7)	450 (350)	0	1,590	(230)
				1,520	(220)
				1,590	(230)
				1,540	(224)
				Avg 1,550	(225)
			500	1,260	(182)
				1,270	(184)
				1,470	(213)
				Avg 1,330	(193)
			1,000	1,480	(214)
				1,560	(227)
				1,450	(210)
				Avg 1,500	(217)
			5,000	1,630	(236)
				1,600	(232)
				1,440	(209)
				Avg 1,560	(226)
			10,000	1,650	(240)
				1,650	(239)
				1,850	(268)
				Avg 1,720	(249)
			100	1,500	(218)
				1,650	(239)
				1,460	(212)
				Avg 1,540	(223)
			500	1,630	(236)
				1,620	(235)
				1,550	(225)
				Avg 1,600	(232)
			1,000	1,260	(182)
				1,500	(218)
				1,540	(223)
				Avg 1,430	(208)
			5,000	1,210	(175)
				1,370	(199)
				1,300	(188)
				Avg 1,290	(188)
			10,000	1,360	(198)
				1,270	(184)
				1,210	(176)
				Avg 1,280	(186)
450 (350)	101 (14.7)	450 (350)	100	1,730	(251)
				1,740	(252)
				1,560	(227)
				Avg 1,680	(243)
			5,000	1,770	(257)
				1,870	(271)
				1,760	(255)
				Avg 1,800	(261)
			10,000	1,730	(251)
				1,740	(252)
				1,560	(227)
				Avg 1,680	(243)

TABLE V-B. THERMAL AGING DATA FOR [0° ± 45°] CROSSPLY A-S/3501 GRAHPITE/EPOXY.

Aging Temp K (F)	Pressure kN/m ² (psi)	Test Temp K (F)	Aging Time (HR)	Tensile Strength MN/m ² (ksi)	
394 (250)	101 (14.7)	450 (350)	0	500	(72.5)
				496	(72.0)
				542	(78.6)
				483	(70.0)
				Avg 507	(73.5)
			100	475	(68.9)
				492	(71.4)
				494	(71.7)
				Avg 487	(70.7)
			500	494	(71.6)
				552	(80.0)
				626	(90.8)
				Avg 557	(80.8)
			1,000	589	(85.4)
				559	(81.1)
				536	(77.7)
				Avg 561	(81.4)
			5,000	559	(81.1)
				593	(86.0)
				585	(84.9)
				Avg 579	(84.0)
			10,000	494	(71.6)
				608	(88.2)
				559	(81.1)
				Avg 554	(80.3)
			450 (350)	552	(80.0)
				501	(72.6)
				563	(81.6)
				Avg 539	(78.1)
			500	485	(70.3)
				440	(63.8)
				474	(68.7)
				Avg 466	(67.6)
			1,000	265	(38.5)
				60	(8.7)
				238	(34.5)
				Avg 188	(27.2)
450 (350)	13.8 (2)	450 (350)	5,000	584	(84.7)
				596	(86.4)
				571	(82.8)
				Avg 584	(84.6)
			10,000	535	(77.6)
				498	(72.3)
				548	(79.5)
				Avg 527	(76.5)

TABLE VI-A. THERMAL AGING DATA FOR UNIDIRECTIONAL B/5505 BORON/EPOXY.

Aging Temp K (F)	Pressure kN/m ² (psi)	Test Temp K (F)	Aging Time (HR)	Tensile Strength MN/m ² (ksi)			
394 (250)	101 (14.7)	450 (350)	0	1,380 (200)			
			100	1,390 (202)			
				1,350 (196)			
				1,370 (198)			
				Avg 1,370 (199)			
			500	1,460 (212)			
				1,360 (197)			
				1,340 (194)			
				Avg 1,390 (201)			
			1,000	1,330 (193)			
				1,390 (201)			
				1,380 (200)			
				Avg 1,370 (198)			
			5,000	1,480 (214)			
				1,450 (210)			
				1,520 (220)			
				Avg 1,480 (215)			
			10,000	1,410 (204)			
				1,430 (208)			
				1,450 (211)			
				Avg 1,430 (208)			
450 (350)	101 (14.7)	450 (350)	5,000	1,230 (179)			
				1,240 (180)			
				1,250 (182)			
				Avg 1,240 (180)			
			10,000	1,010 (146)			
				1,010 (147)			
				1,080 (156)			
				Avg 1,030 (150)			
			450 (350)	13.8 (2)	450 (350)		1,520 (220)
							1,290 (187)
10,000	1,400 (203)						
	Avg 1,400 (203)						
	1,390 (201)						
	1,340 (195)						
				1,400 (203)			
				Avg 1,380 (200)			

TABLE VI-B. THERMAL AGING DATA FOR [0° ± 45°] CROSSPLY B/5505 BORON/EPOXY.

Aging Temp K (F)	Pressure kN/m ² (psi)	Test Temp K (F)	Aging Time (HR)	Tensile Strength MN/m ² (ksi)
394 (250)	101 (14.7)	450 (350)	0	550 (79.8)
			100	510 (73.9)
				496 (71.9)
				493 (71.5)
				Avg 500 (72.4)
			500	478 (69.4)
				428 (62.1)
				474 (68.7)
				Avg 460 (66.7)
			1,000	512 (74.2)
				504 (73.1)
				539 (78.2)
				Avg 518 (75.2)
			5,000	535 (77.6)
				527 (76.4)
				533 (77.3)
				Avg 532 (77.1)
			10,000	538 (78.1)
				534 (77.4)
				522 (75.7)
				Avg 531 (77.1)
450 (350)	101 (14.7)	450 (350)	500	544 (78.9)
				461 (66.9)
				517 (75.0)
				Avg 507 (73.6)
			1,000	581 (84.2)
				508 (73.7)
				493 (71.5)
				Avg 527 (76.5)
			5,000	310 (44.9)
				319 (46.3)
				309 (44.8)
				Avg 313 (45.3)
			10,000	339 (49.2)
				342 (49.6)
				314 (45.6)
				Avg 332 (48.1)
450 (350)	13.8 (2)	450 (350)	5,000	519 (75.3)
				529 (76.7)
				590 (85.6)
				Avg 546 (79.2)
			10,000	379 (54.9)
				367 (53.2)
				381 (55.3)
				Avg 376 (54.5)

TABLE VII-A. THERMAL AGING DATA FOR UNIDIRECTIONAL HT-S/710 GRAPHITE/POLYIMIDE.

Aging Temp K (F)	Pressure kN/m ² (psi)	Test Temp K (F)	Aging Time (HR)	Tensile Strength MN/m ² (ksi)	
505 (450)	101 (14.7)	505 (450)	0	1,210	(176)
			500	827	(120)
				752	(109)
				758	(110)
				Avg 779	(113)
			1,000	1,210	(175)
				990	(144)
				1,370	(198)
				Avg 1,190	(172)
			5,000	1,190	(173)
				1,420	(206)
				1,240	(180)
				Avg 1,280	(186)
			10,000	1,280	(185)
				1,390	(201)
				1,350	(196)
				Avg 1,340	(194)
505 (450)	13.8 (2)	505 (450)	5,000	1,370	(198)
				1,210	(175)
				1,480	(215)
				Avg 1,350	(196)
			10,000	1,280	(185)
				1,140	(166)
				1,180	(171)
				Avg 1,200	(174)
			0	1,320	(191)
				1,290	(187)
				1,280	(185)
				1,350	(196)
				Avg 1,310	(189)
			500	1,170	(170)
				1,300	(189)
				1,200	(174)
				Avg 1,220	(178)
			1,000	1,100	(159)
				1,170	(169)
				1,190	(173)
				Avg 1,150	(167)
			5,000	1,170	(169)
				1,070	(155)
				1,010	(147)
				Avg 1,080	(157)
			10,000	1,117	(162)
				876	(127)
				807	(117)
				Avg 933	(135)
561 (550)	101 (14.7)	561 (550)	0	1,320	(191)
				1,290	(187)
				1,280	(185)
				1,350	(196)
				Avg 1,310	(189)
			500	1,170	(170)
				1,300	(189)
				1,200	(174)
				Avg 1,220	(178)
			1,000	1,100	(159)
				1,170	(169)
				1,190	(173)
				Avg 1,150	(167)
			5,000	1,170	(169)
				1,070	(155)
				1,010	(147)
				Avg 1,080	(157)
			10,000	1,117	(162)
				876	(127)
				807	(117)
				Avg 933	(135)
561 (550)	13.8 (2)	561 (550)	5,000	1,300	(188)
				980	(142)
				1,300	(188)
				Avg 1,190	(173)
			10,000	1,060	(154)
				1,010	(146)
				970	(140)
				Avg 1,010	(147)

TABLE VII-B. THERMAL AGING DATA FOR [0° ± 45°] CROSSPLY HT-S/710 GRAPHITE/EPOXY.

Aging Temp K (F)	Pressure kN/m ² (psi)	Test Temp K (F)	Aging Time (HR)	Tensile Strength MN/m ² (ksi)	
505 (450)	101 (14.7)	505 (450)	0	470	(68.2)
			1,000	521	(75.5)
				443	(64.3)
				328	(47.5)
				Avg 431	(62.4)
			5,000	435	(63.1)
				501	(72.6)
				576	(83.5)
				Avg 504	(73.1)
			10,000	335	(48.6)
				525	(76.2)
				454	(65.9)
				Avg 438	(63.6)
			0	434	(63.0)
				443	(64.2)
				474	(68.7)
				394	(57.1)
				Avg 437	(63.3)
			5,000	276	(40.0)
				276	(40.0)
				258	(37.4)
				Avg 270	(39.1)
			10,000	192	(27.8)
				211	(30.6)
				274	(39.7)
				Avg 226	(32.7)
561 (550)	101 (14.7)	561 (550)	0	434	(63.0)
			1,000	443	(64.2)
				474	(68.7)
				394	(57.1)
				Avg 437	(63.3)
			5,000	276	(40.0)
				276	(40.0)
				258	(37.4)
				Avg 270	(39.1)
			10,000	192	(27.8)
				211	(30.6)
				274	(39.7)
				Avg 226	(32.7)

TABLE VIII-A. THERMAL AGING DATA FOR UNIDIRECTIONAL BORON/ALUMINUM.

Aging Temp K (F)	Pressure kN/m ² (psi)	Test Temp K (F)	Aging Time (HR)	Tensile Strength	
				MN/m ²	(ksi)
450 (350)	101 (14.7)	297 (75)	0	1,430	(208)
			5,000	1,320	(191)
				1,230	(179)
				1,070	(155)
				Avg 1,210	(175)
			10,000	1,007	(146)
				986	(143)
				869	(126)
				Avg 954	(138)
561 (550)	101 (14.7)	297 (75)	5,000	841	(122)
				855	(124)
				889	(129)
				Avg 862	(125)
			10,000	855	(124)
				703	(102)
				786	(114)
				Avg 781	(113)
700 (800)	101 (14.7)	297 (75)	5,000	327	(47.4)
				631	(91.5)
				315	(45.7)
				Avg 424	(61.5)
			10,000	263	(38.1)
				320	(46.4)
				318	(46.1)
				Avg 300	(43.5)

TABLE VIII-B. THERMAL AGING DATA FOR [0° ± 45°] CROSSPLY BORON/ALUMINUM.

Aging Temp K (F)	Pressure kN/m ² (psi)	Test Temp K (F)	Aging Time (HR)	Tensile Strength	
				MN/m ²	(ksi)
450 (350)	101 (14.7)	297 (75)	0	516	74.8
			5,000	430	62.3
				467	67.7
				535	77.6
				Avg 477	69.2
			10,000	459	66.6
				444	64.4
				428	62.1
				Avg 444	64.4
561 (550)	101 (14.7)	297 (75)	5,000	276	40.1
				251	36.4
				257	37.3
				Avg 261	37.9
			10,000	184	26.7
				214	31.1
				210	30.4
				Avg 203	29.4
700 (800)	101 (14.7)	297 (75)	5,000	168	24.4
				185	26.8
				198	28.7
				Avg 184	26.6
			10,000	142	20.6
				143	20.7
				154	22.3
				Avg 146	21.2

TABLE IX. GLASS TRANSITION TEMPERATURE, TG, DATA FOR [0° ± 45°] A-S/3501 GRAPHITE/EPOXY.

CONDITION	Tg, K (F)
AS-RECEIVED	463 (374)
AGED 5,000 HR. AT 394K, 101 kN/m ²	463 (374)
AGED 10,000 HR. AT 394K, 101 kN/m ²	464 (375)
AGED 5,000 HR. AT 450K, 13.8 kN/m ²	490 (422)
AGED 10,000 HR. AT 450K, 13.8 kN/m ²	505 (449)
AGED 5,000 HR. AT 450K, 101 kN/m ²	*
AGED 10,000 HR. AT 450K, 101 kN/m ²	*
FLIGHT SIMULATION, 4,5000 HR. AT 408K	498 (436)

* SPECIMENS WERE UNSUITABLE FOR Tg DETERMINATION.

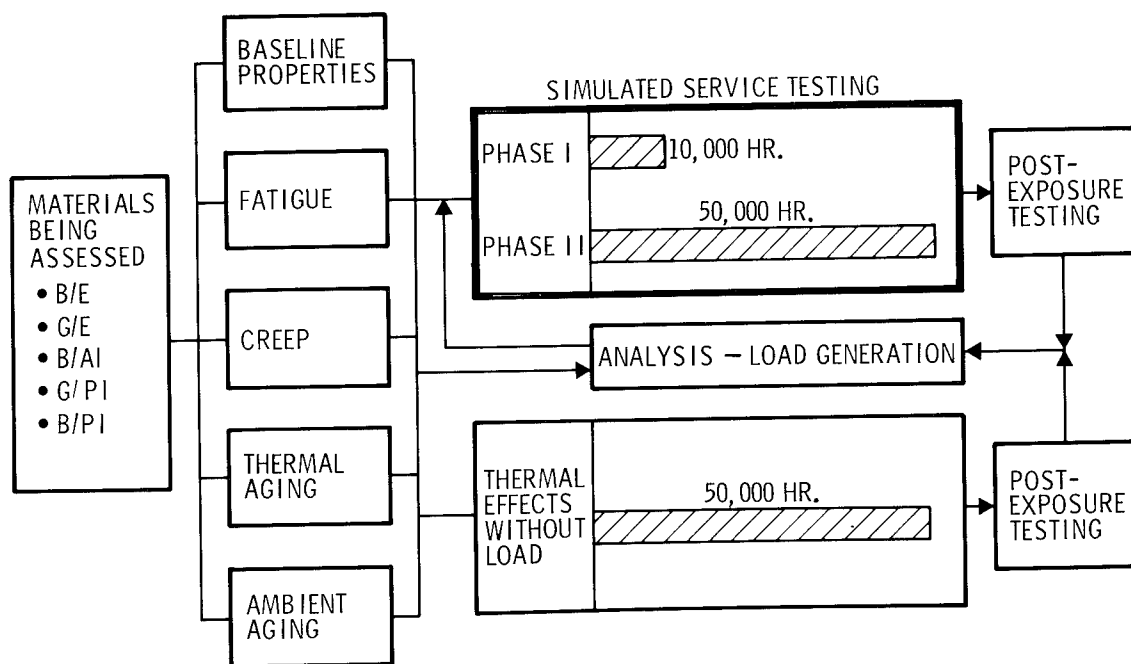


Figure 1.- Time-temperature-stress capabilities of composite materials.

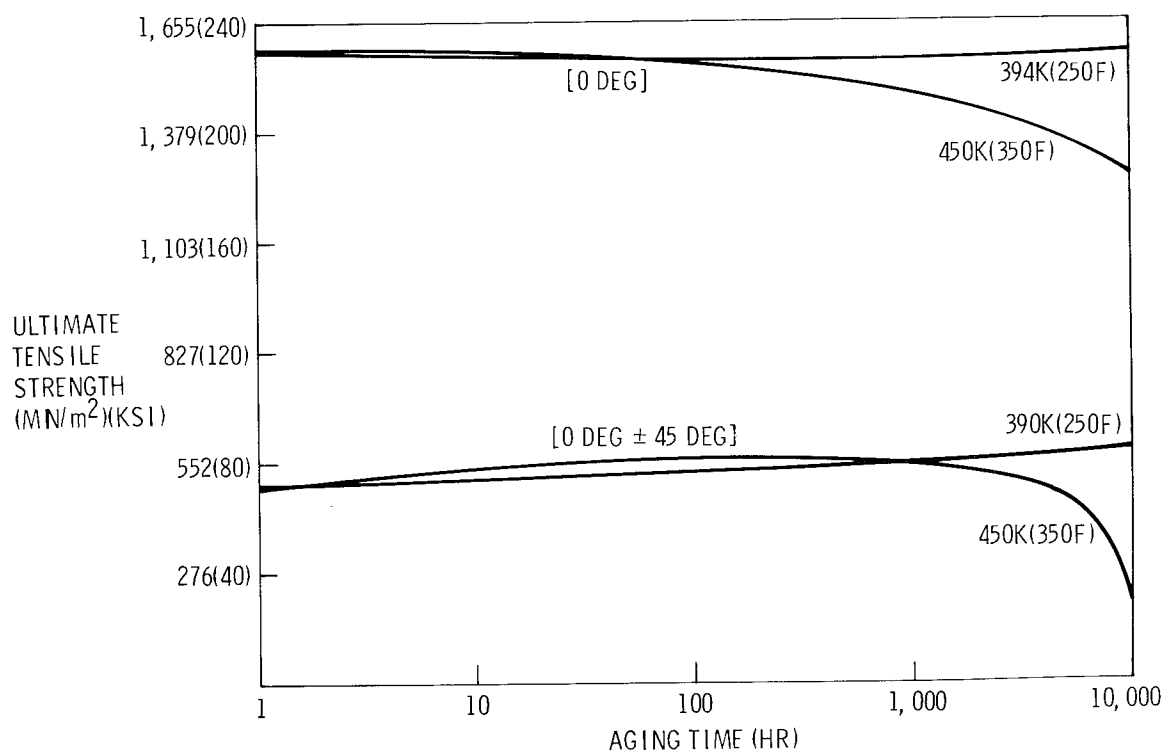


Figure 2.- Tensile strength of A-S/3501 graphite/epoxy at 450 K (350°F) after thermal aging at indicated temperature.

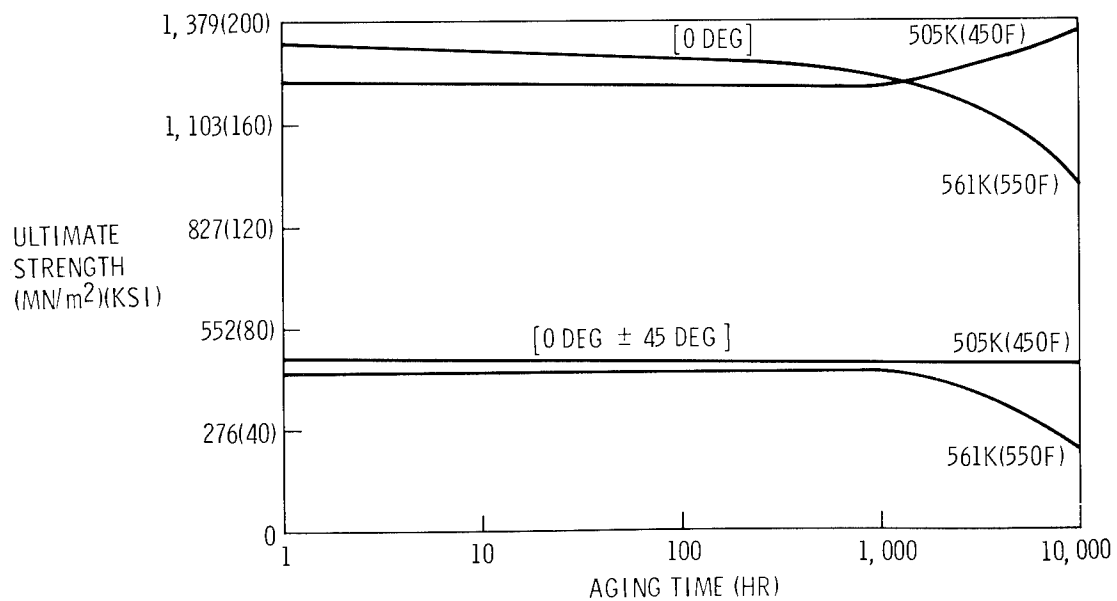


Figure 3.- Tensile strength of HT-S/710 graphite/polyimide at 505 K (450°F) and 561 K (550°F) after thermal aging at the same temperature.

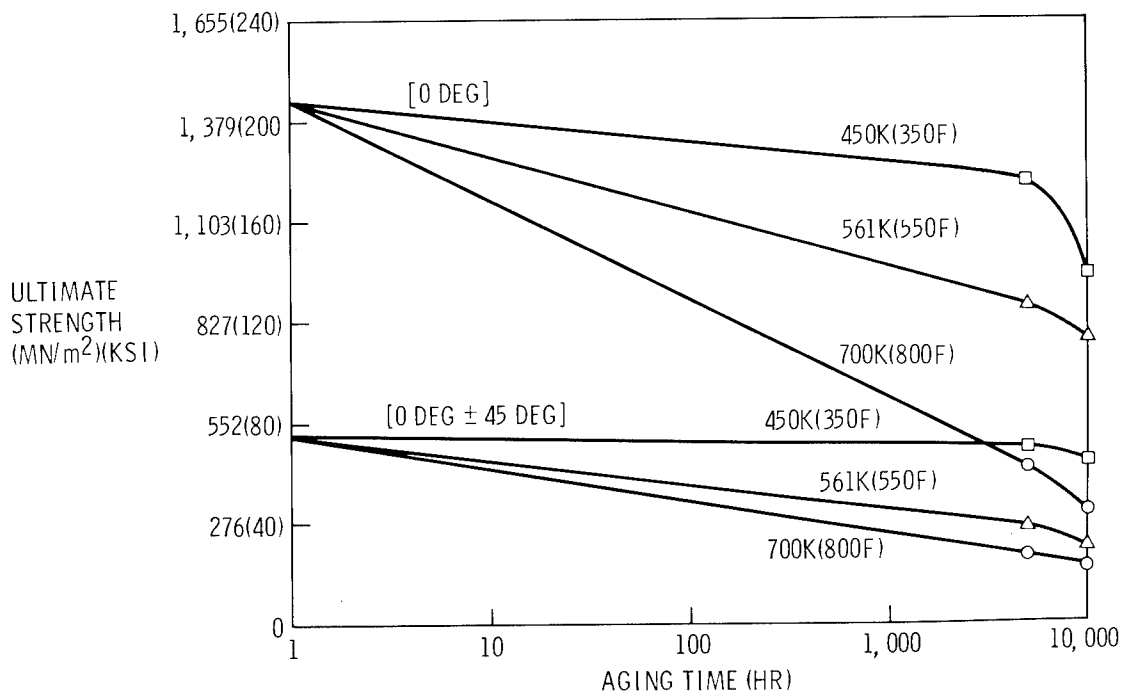


Figure 4.- Tensile strength of diffusion-bonded boron/aluminum at 297 K (75°F) after thermal aging at indicated temperature.

ARROWS INDICATE SPECIMEN EDGES

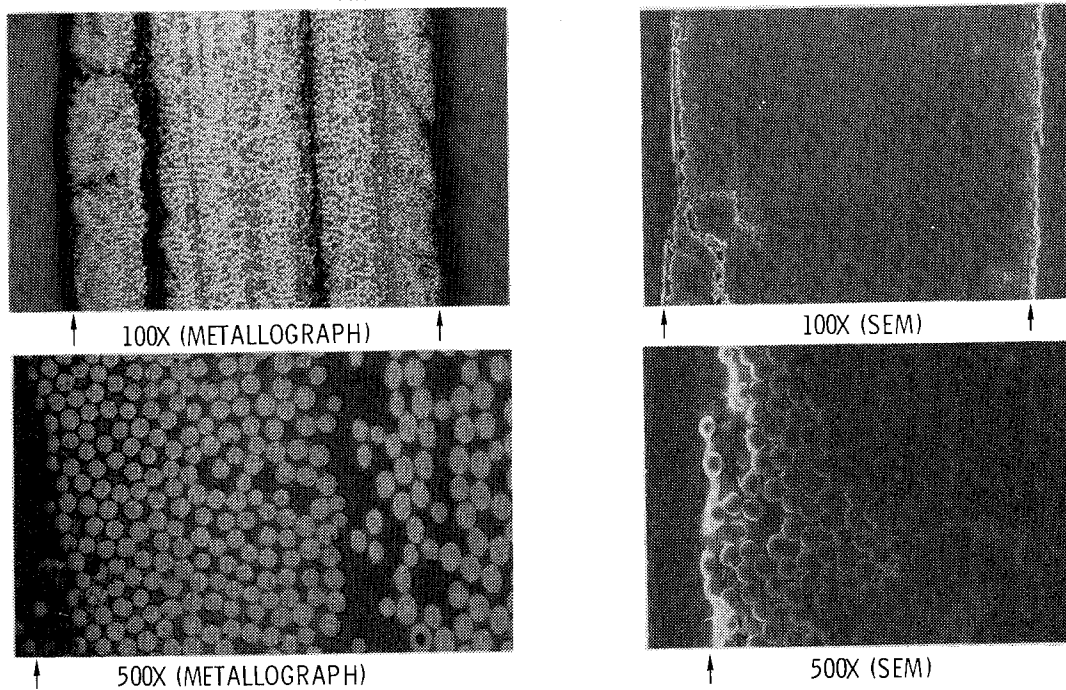


Figure 5.- Photomicrographs of A-S/3501 graphite/epoxy after thermal aging at 450 K (350°F) and 13.8 kN/m² (2 psi) for 10,000 hours.

ARROWS INDICATE SPECIMEN EDGES

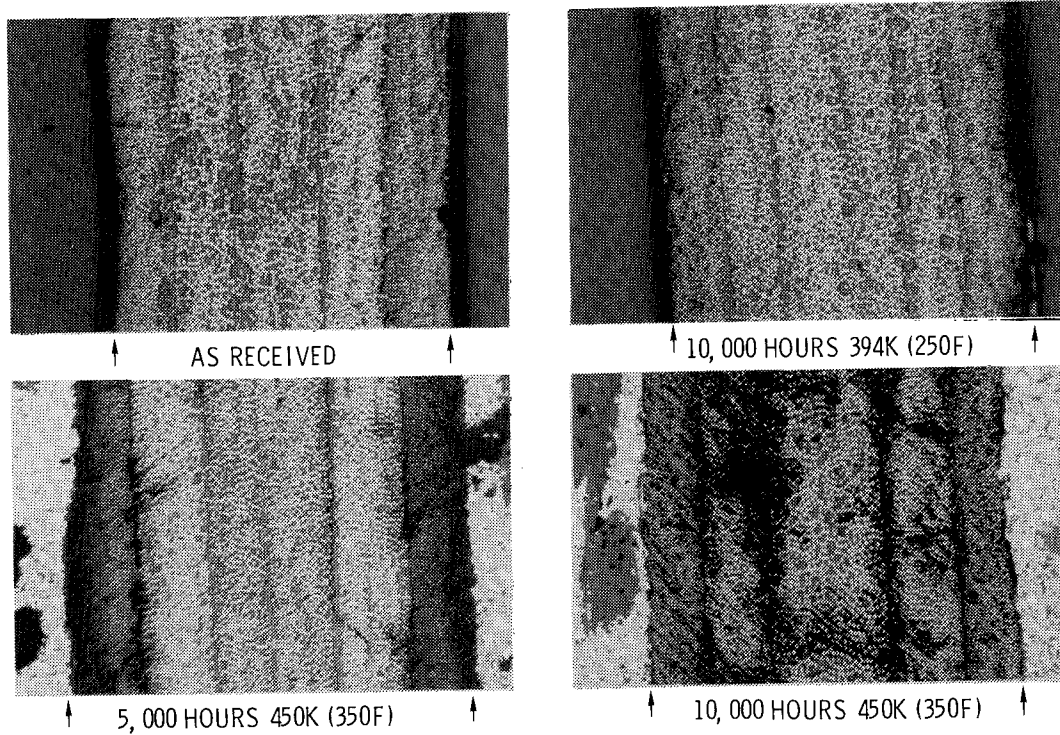
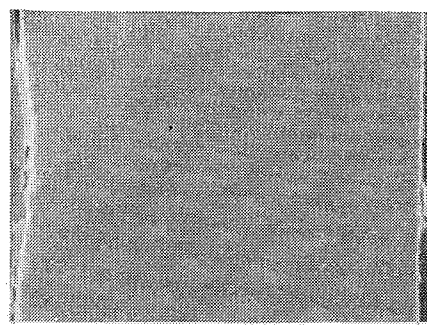
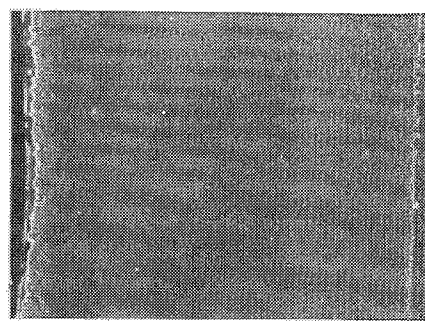


Figure 6.- Photomicrographs (metallograph) of A-S/3501 graphite/epoxy at 100X magnification.

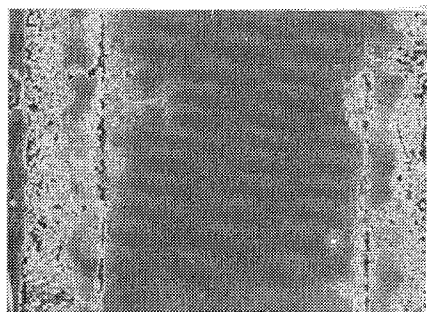
ARROWS INDICATE SPECIMEN EDGES



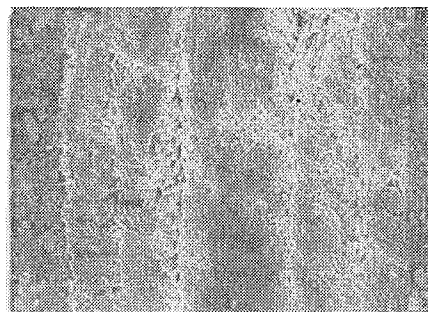
AS RECEIVED



10,000 HOURS 394K (250F)

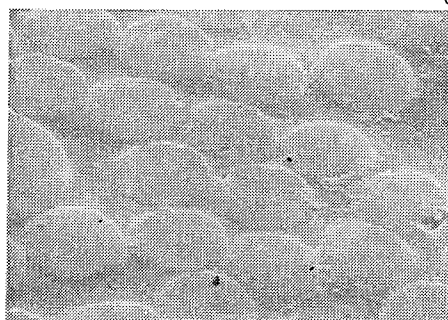


5,000 HOURS 450K (350F)

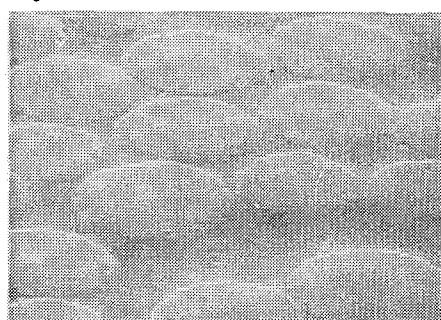


10,000 HOURS 450K (350F)

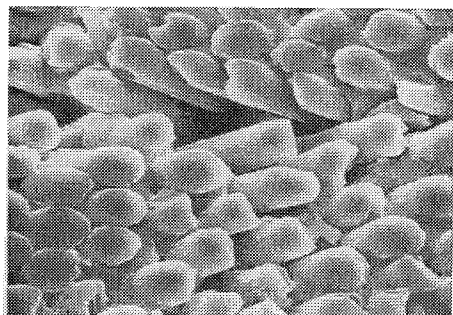
Figure 7.- Photomicrographs (SEM) of A-S/3501 graphite/epoxy at 100X magnification.



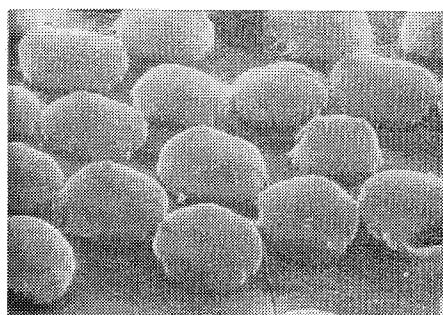
AS RECEIVED (2500X) ANY PLY



10,000 HOURS 394K (250F) (2500X) INNER PLY

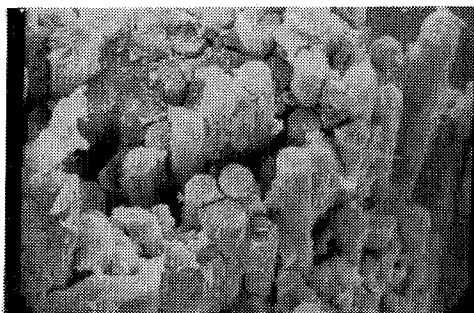


10,000 HOURS 450K (350F) (1000X)
INNER PLIES

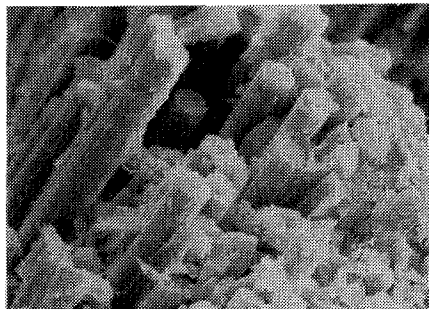


10,000 HOURS 394K (250F) (2500X)
OUTSIDE PLY

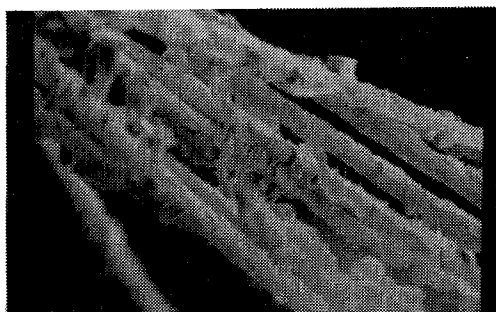
Figure 8.- Photomicrographs (SEM) of A-S/3501 graphite/epoxy.



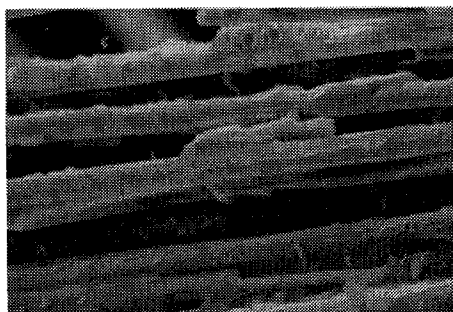
- AS RECEIVED TESTED AT 450K (350F) (900X)



10, 000 HOURS 394K (250F) (1000X)

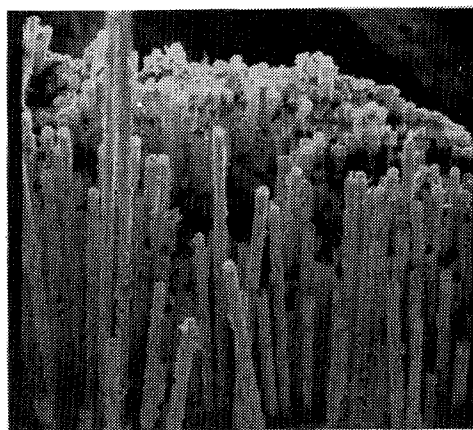


5, 000 HOURS 450K (350F) (500X)

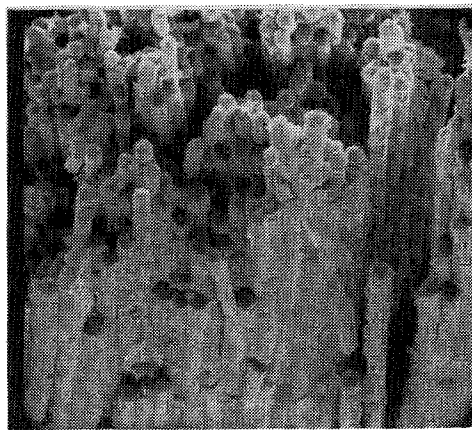


10, 000 HOUR 450K (350F) (600X)

Figure 9.- SEM fractographs of A-S/3501 graphite/epoxy. 101 kN/m^2 .



10, 000 HOURS 394K (250F), 101 kN/m^2 (14.7 psi)



10, 000 HOURS 450K (350F), 13.8 kN/m^2 (2 psi)

Figure 10.- SEM fractographs of A-S/3501 graphite/epoxy.

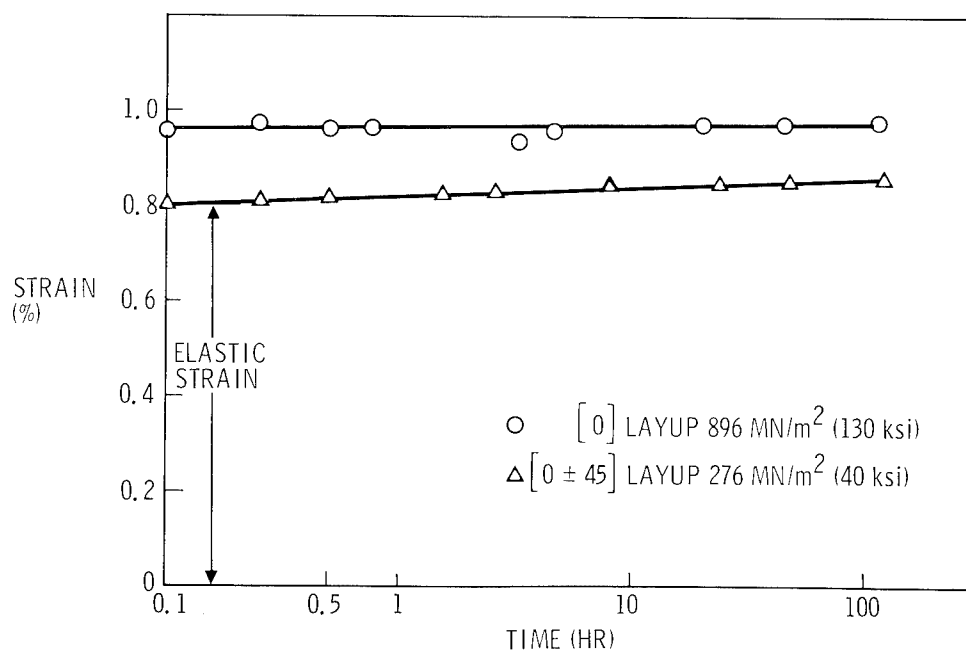


Figure 11.- Creep strain versus time for HT-S/710 graphite polyimide at 561 K (550°F).

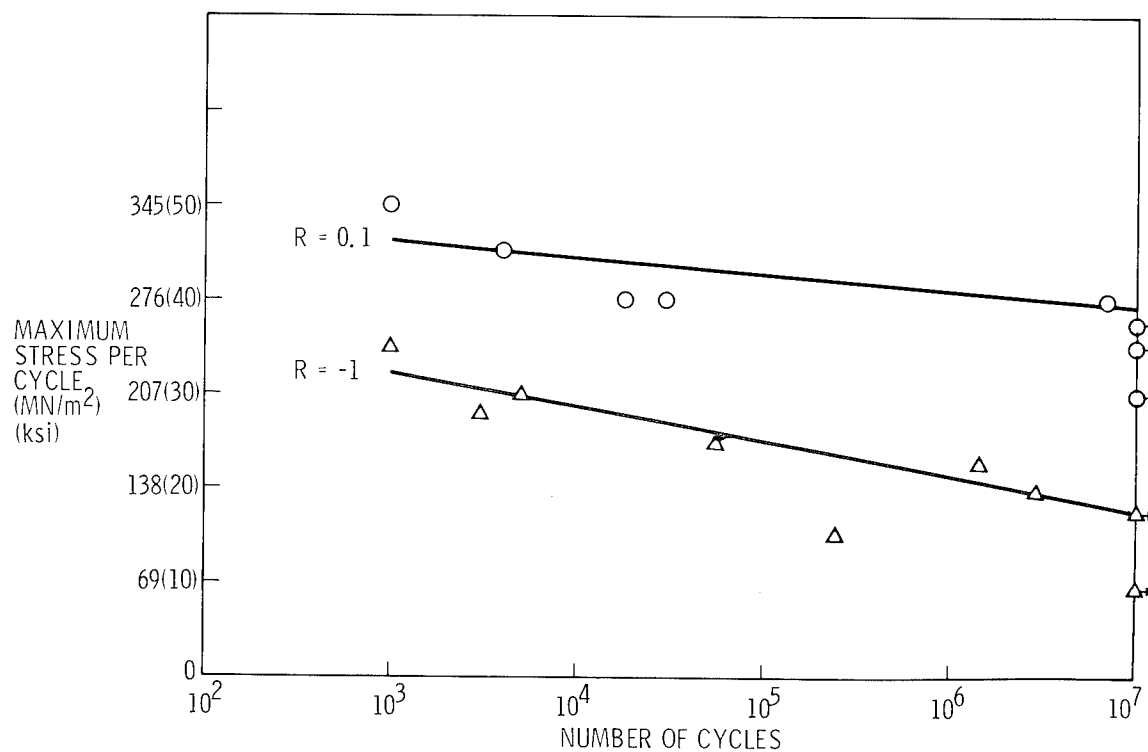


Figure 12.- Axial fatigue properties of [0 ± 45] HT-S/710 graphite polyimide at 505 K (450°F).

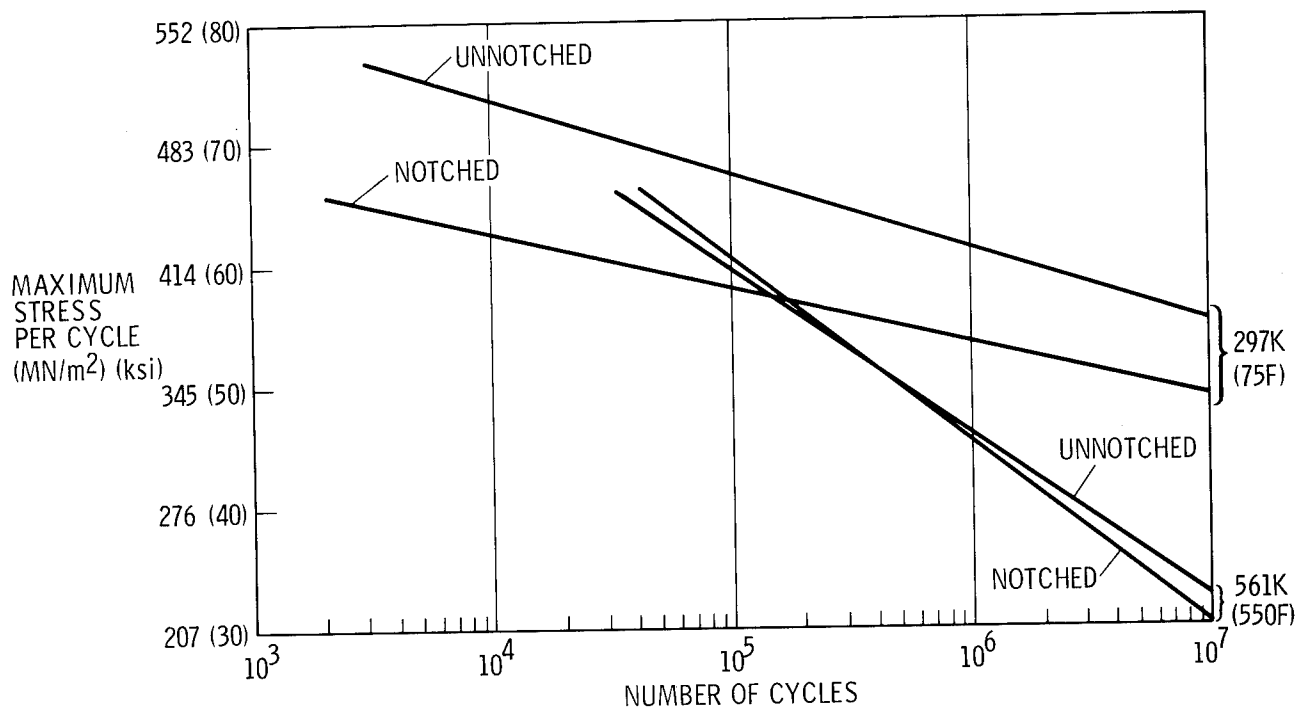


Figure 13.- Axial fatigue properties of $[0 \pm 45]_s$ boron/aluminum, for a stress ratio, R , of 0.1.

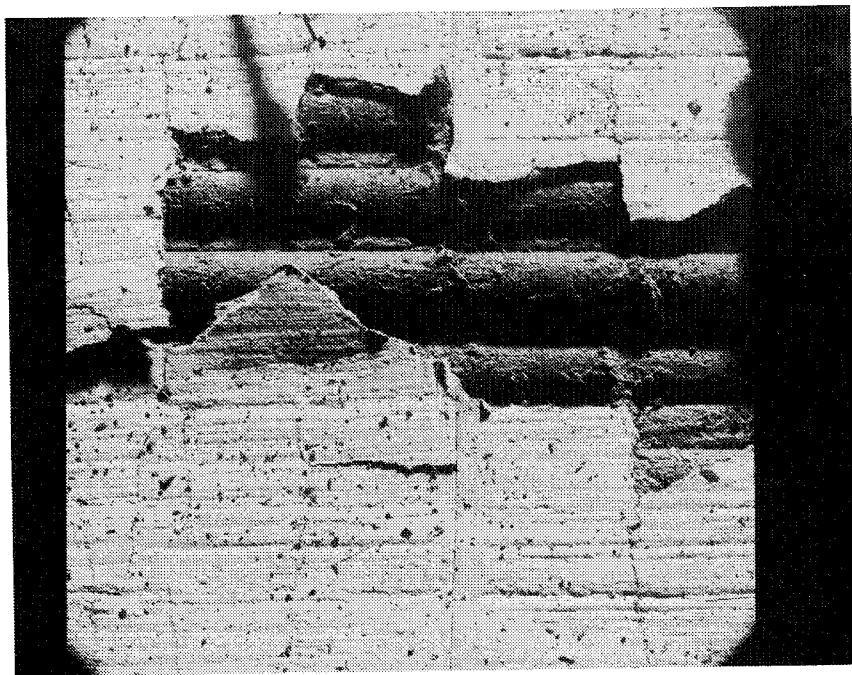


Figure 14.- Area of degraded boron aluminum surface showing reticulation and exposed boron fiber.

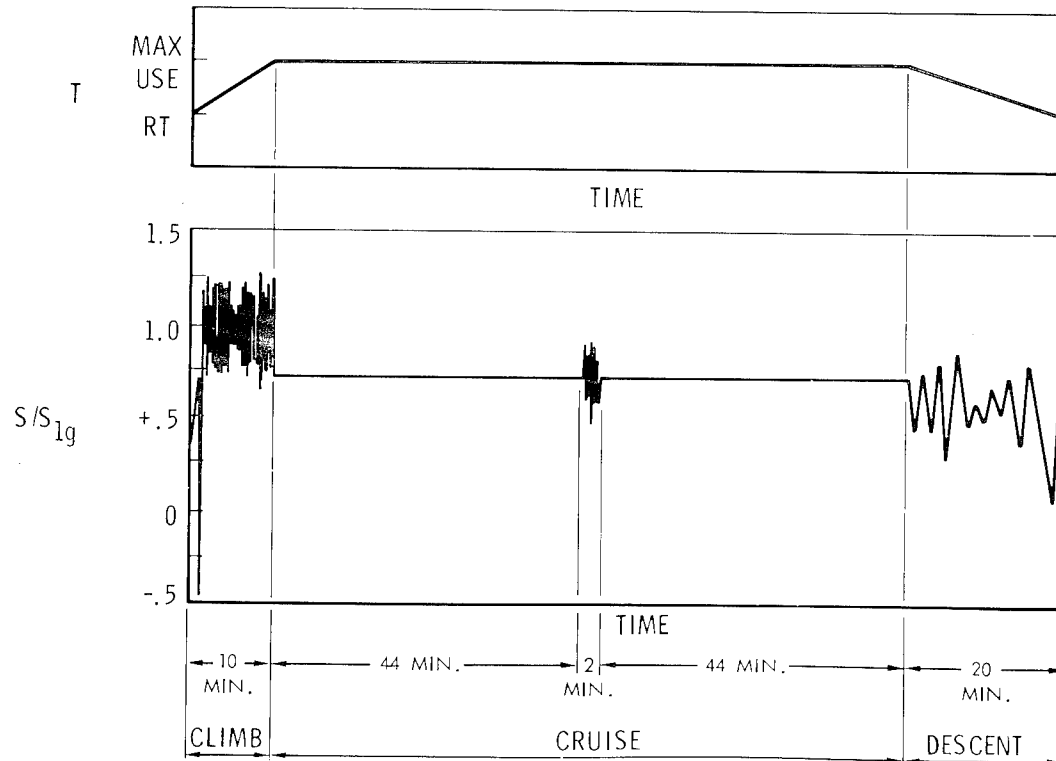


Figure 15.- Typical flight simulation cycle showing load and temperature profile.

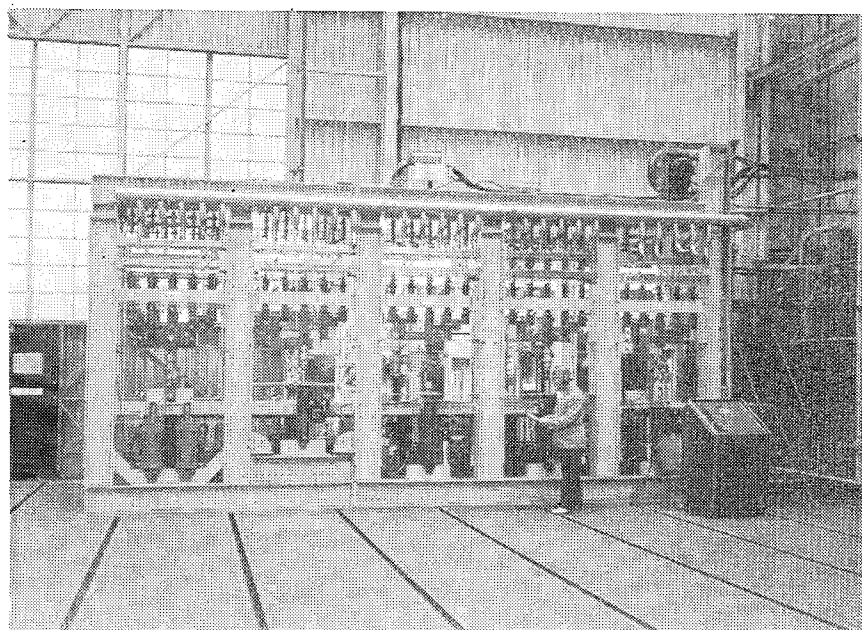


Figure 16.- Flight simulation equipment.

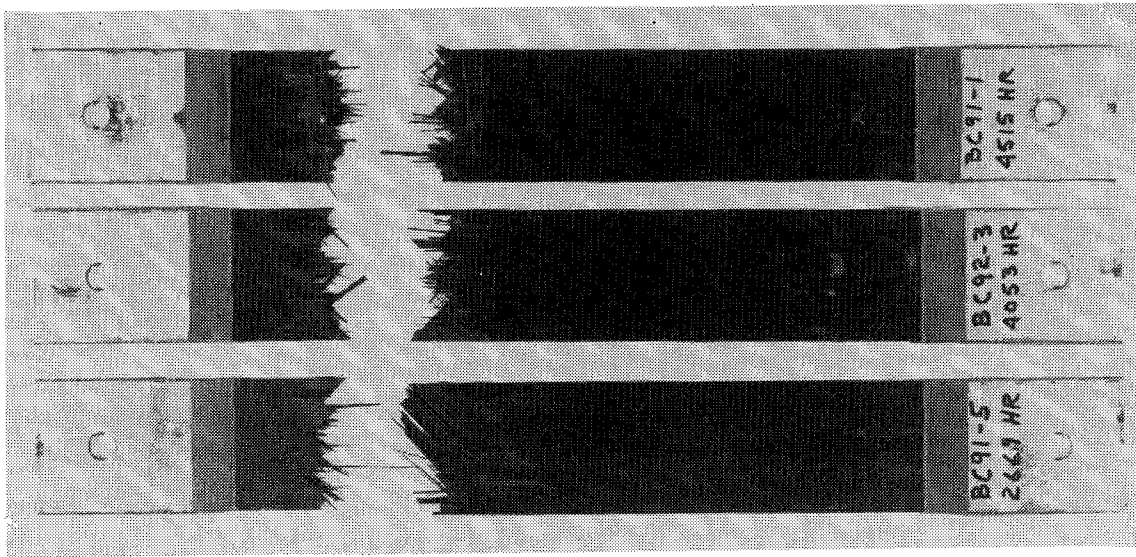


Figure 17.- A-S/3501 graphite/epoxy specimens after flight simulation exposure.

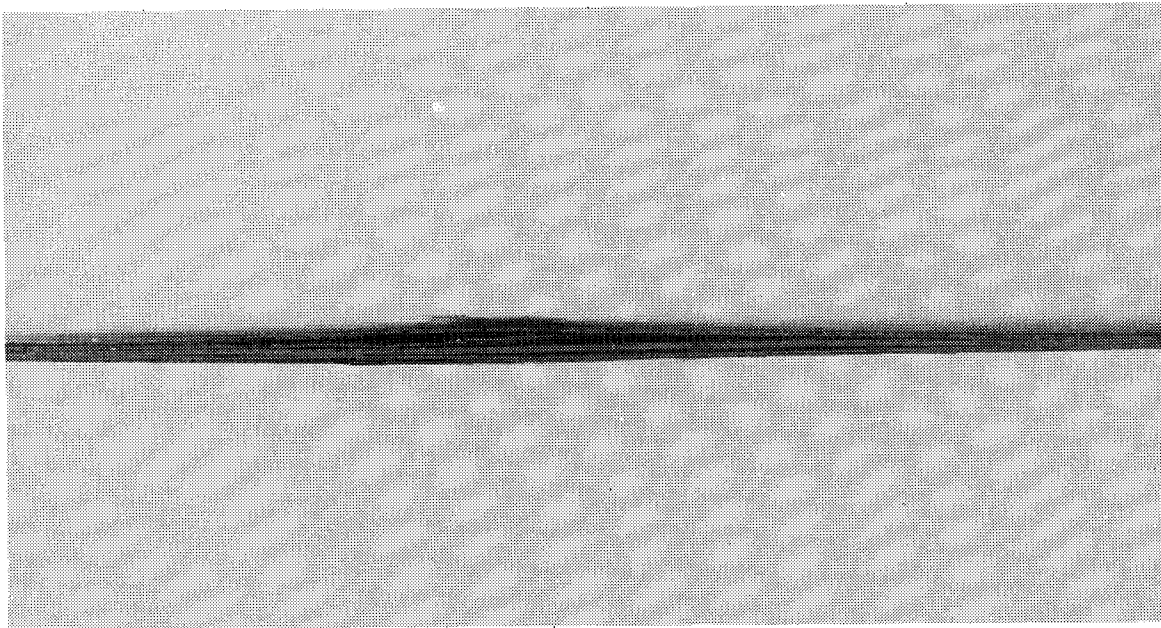


Figure 18.- A-S/3501 graphite/epoxy flight simulation specimens showing edge delaminations.

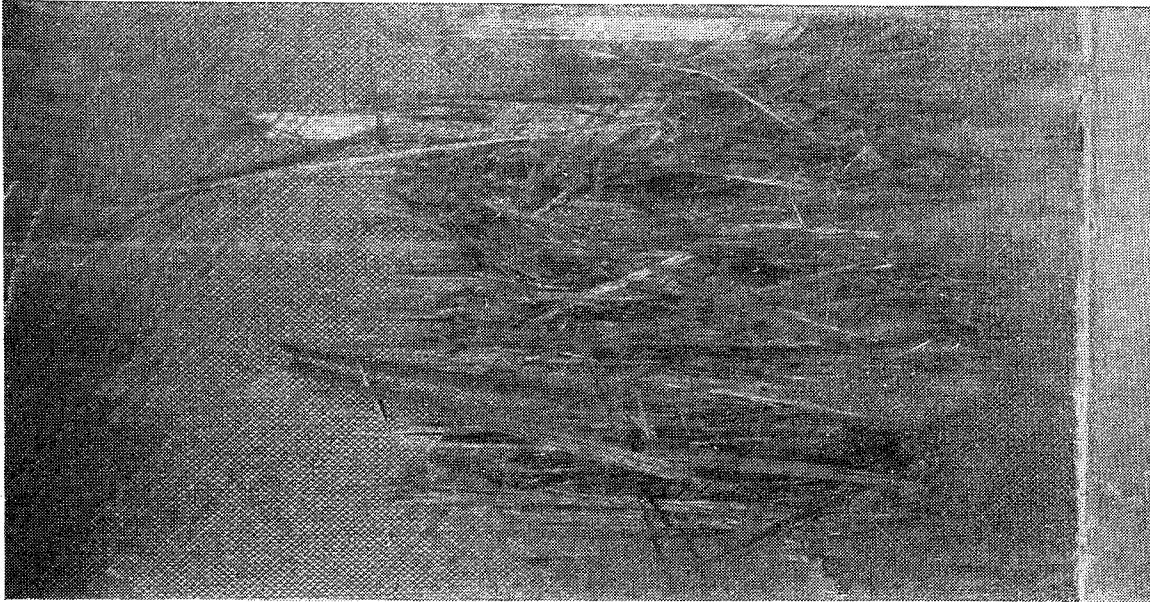


Figure 19.- A-S/3501 graphite/epoxy flight simulation specimen showing surface damage in 5 cm (2 inch) heated zone.

ADVANCED SUPERSONIC TECHNOLOGY FUEL TANK SEALANTS

Robert W. Rosser and John A. Parker
NASA Ames Research Center

SUMMARY

The Advanced Supersonic Technology (AST) Fuel Tank Sealants Program is reviewed. Status of the fuel tank simulation and YF-12A flight tests utilizing a state-of-the-art fluorosilicone sealant is described. New elastomer sealant development at Ames Research Center is detailed, and comparisons of high and low temperature characteristics are made to baseline fluorosilicone sealants.

INTRODUCTION

The continuing search for improved candidates for high temperature fuel tank sealants was begun at the NASA Ames Research Center in the Chemical Research Projects Office with the new incentives of both NASA's supersonic cruise aircraft research (SCAR) program and continuation of DOT's effort to evolve an advanced supersonic technology base.

A review of what had been accomplished synthetically suggested that the Dow Corning (DC) developmental sealant 77-028, a fluoroalkylsiloxane, and derivatives of the perfluoroethers offered opportunities for further development and exploitation. Although Boeing studies had shown that DC77-028 has a tendency to degrade, it might, with the appropriate predictive analysis, be useful in meeting the high-performance sealant requirements. Research has suggested that with appropriate modifications to reduce the glass transition temperature and to improve the efficiency of crosslinking processes these basic materials have the potentiality of providing sealants with marked improvements in stability in extreme environments (ref. 1).

The overall goal of the AST Fuel Tank Sealant Program is to produce a flight-proof, fully characterized, predictable fuel tank sealant that meets high-performance supersonic aircraft requirements. Figure 1 indicates the various interrelated activities of the fuel tank sealants program. These activities comprise synthesis and characterization of new fluoroether elastomers, processing and scale-up activities, sealant-metal system development, sealant prediction studies, flight simulation, and actual flight testing of the best state-of-the-art sealants.

For advanced sealant elastomers, both new extension and new branching reactions that can be carried out with hexafluoropropylene oxide oligomers are under consideration. The reactions of these polymeric intermediates through nitrile cyclizations to give triazines, and nitrile co-reactions with acid fluorides to give polyoxadiazoles are two principal systems being studied. Early work indicated promising results for the two systems under investigation.

Both high and low temperature applications appeared feasible in spite of the initial deficiencies in physical properties. Thus, molecular weight and crosslinking control are currently the primary areas of investigation.

In principle, the desired predictive method can be developed from a suitable combination of viscoelastic measurements (leading to the construction of a characteristic failure "property surface" for the elastomer) and stress-relaxation measurements (which assess the extent and contribution of chemical degradation in these materials). Work at the Jet Propulsion Laboratory (JPL) has led to the development of short-time test methods that enable predictions to be made of the lifetime of elastomers under operating conditions, but in the absence of chemical degradation. From other studies, methods were also developed for measuring network degradation kinetics for elastomers exposed to a fuel environment at elevated temperatures; these were principally adaptations of classical chemorheological techniques. Efforts have been made to show that these methods can be combined to yield a satisfactory prediction of long-term aging using short-term tests.

Actual time simulated tank studies were conducted at Boeing. The experimental fluorosilicone sealant was installed in a test chamber where it was subjected to the pressures and temperatures of the supersonic cruise aircraft flight cycle. Simultaneously, the tank was subjected to spanwise and chordwise loading representative of the fatigue spectrum expected under the most severe flight conditions.

The fluorosilicone DC77-028 is considered the state-of-the-art sealant candidate to date and efforts have been made to correlate its behavior in prediction studies and flight simulation. The DC77-028 is currently being tested on the YF-12A NASA aircraft, and correlation with the prediction and simulated tank studies will then provide a baseline for future testing of new elastomeric candidates in subsequent flight cycles.

FAILURE MODES

Several years ago NASA, DOT, and Boeing visited most of the NASA Centers and talked with the principal investigators who had been concerned with supersonic cruise vehicle fuel tank sealant developments. To guide future developments, the specific deficiencies of the baseline DC77-028 sealant were identified. Three failure modes were evident from these discussions: (1) reversion, (2) low tear strength, and (3) lack of reproducibility of adhesion to titanium. These failure modes are discussed below.

Reversion

It is well accepted and proven that the root cause of the observed degradation of the base-line sealant DC77-028 is due to polymer reversion with the formation of cyclic tetramer from the principal chains. The practical result of this degradation process is the loss of sealant from the seal

rather than significant degradation in polymer bulk properties. For this reason, compounded sealant shrinks in the joints. This phenomenon of reversion is generally characteristic of silicones and is a limiting factor in their application for continuous service at temperatures above 204° C (400° F). Fluorosilicone hybrids, a family of new derivatives which have been proposed and synthesized for military applications, have virtually eliminated reversion but have introduced the possibility of dehydrofluorination followed by oxidative chain scission. The new perfluoroether candidates suffer from none of these deficiencies.

Mechanical Tearing of Sealant

Failure of sealant installation by the formation of cracks due to tearing of the sealant in the joint seems to be the most common failure mode. It seems to be an inherent difficulty with state-of-the-art formulated sealants, that they possess a rather large thermal coefficient of expansion and also exhibit a significant loss in tensile strength at elevated temperatures. These two properties couple to provide the tearing mechanism. A good possibility for eliminating this difficulty is the development of polydisperse blends and graft or block polymer systems.

Adhesion Failure

Difficulties with the sealant-primer-titanium interfaces manifest themselves in total lack of reproducibility in the measured peel strengths which can vary by as much as two orders of magnitude. Just how significant peel strength is as related to failure is not clear. When coupled with chemically induced stress corrosion in the joint, the lack of integrity could completely degrade the interface structure.

From the foregoing considerations, some constraints on the evolution of new polymer types can be defined. The siloxane group is a weak link and should be reduced in concentration or blocked against reversion. Cyano substitution in siloxanes degrades stability. Vicinal substitution with HF may lead to instability and chemical stress corrosion. The perfluoroether derivatives begin to meet most of these constraints, but they require innovations to reduce glass transition temperatures (T_g), by chain extension and crosslinking control.

TEST RESULTS

Flight Simulation

In 1973, NASA-Ames contracted with The Boeing Company to design, fabricate, and subject to supersonic flight environment a small tank representative of the materials and structure of a supersonic transport fuel cell. The tank was sealed using the best known sealant for supersonic use and was periodically examined and tested for leaks. Another part of the program was to conduct

studies of sealant adhesion to titanium. Lap shear specimens were subjected to elements of supersonic fuel tank environment and tested after 6 weeks of such exposure.

Table I lists the condition of the seal in the simulated fuel tank after 861 flight cycles and after 1389 cycles. Inspection after 861 flight cycles disclosed no noticeable degradation; there were no tank leaks and no perceptible cracks in the sealant. However, after 1389 flight cycles there were numerous hairline cracks in the sealant, the tank leaked badly at the corners, and minor leaks were observed in other locations. Lack of adhesion was observed at some of the cracks. The results demonstrate the importance of combining simultaneously all elements of the environment, including loads, that the material being tested would encounter in service. It is believed that stressing the sealant while at high temperature (227°C, 441°F), together with stresses due to high thermal expansion, caused it to tear.

Figure 2 is a photograph of the tank after inspection at 1389 flight cycles. The cracks are characteristic of failure under high-temperature stress. A lower modulus (higher elongation to failure) material would perhaps overcome the problem.

YF-12A Flight Tests

The objectives of the NASA-Ames program for flight testing on the YF-12A aircraft are (1) to correlate JPL prediction studies and the Boeing simulated tank test to actual flight testing, (2) to provide side-by-side comparisons of the various fluorosilicone candidate sealants, and (3) to provide a baseline for future testing of new NASA developed sealant elastomer candidates.

During the second week of January 1975, test specimens of DC77-028 sealant were mounted in a YF-12A. Some of these were from JPL and had been made with Lockheed cooperation. There were four perforated stainless steel boxes mounted on the wall of the center wing tank: two were mounted forward and two aft. In each case, one of the two was mounted near the bottom of the tank and the other near the top. Thermocouples are on the surface near each box. In each of the boxes are 22 tensile elongation specimens, 2 weight and volume loss specimens, 2 lapped titanium specimens with a fillet over the lap and a deflection of 0.01 inch at the fillet, a strip of titanium with primer only on the surface, and four strips of molded DC77-028 wrapped and clamped around a 0.32-cm (0.125 in.) rod. A sheet of titanium, coated with 0.25 cm (0.1 in.) of DC77-028, is mounted outside the boxes. One end is straight and rigid and the other is wrapped and clamped to put a variable strain in the sealant. Also, primer and sealant are applied to numerous sealant-free areas of the tank surface.

Figure 3 is a photograph of two of the mounted boxes containing the sealant specimens. The only sealant failures were some stress rings mounted in the boxes, part of a JPL test. There were no failures in the outboard forward box, the two rings of the greatest stress had broken in the aft

outboard box, and in each of the other two boxes only the ring with next to the greatest stress had broken. Adhesion to all surfaces was good except to the old sealant.

Table II summarizes the four phases of the YF-12A flight test. In Phase 1, the test fillets now in the YF-12A will be damaged and repairs effected according to Boeing's instructions. A new "saddle" block with higher stressed sealant than the existing one will also be installed in the tank.

During Phase 2 of the YF-12A flight tests, the No. 5 tank of the YF-12A will be stripped and resealed after completion of thermodynamic (cold wall) tests. The expected completion date, after 12 to 15 more supersonic flights, is January 1977. Tank stripping will be contracted for by NASA-DFRC and performed by Lockheed. Stripping is not routinely done on the No. 5 tank and there will be some equipment costs. After initial preparation stripping takes about 24 hr. Resealing will then be carried out by NASA-DFRC technicians with assistance from Boeing. Future plans, Phases 3 and 4, call for the testing of the new NASA fluoroether sealant candidate(s) after all baseline and correlative information has been established.

Advanced Polymers

General. - The availability of hexafluoropropylene oxide and the research on the polymerization of tetrafluoroethylene oxide at the DuPont Co. (ref. 2) prompted us to consider the possibility of building long-chain perfluoroalkylene ethers that would yield a combination of properties for severe environmental applications that were not possible with any other polymer system. Our goal, then, was to obtain high molecular weight elastomers that have good low-temperature mechanical properties, high thermal stability, and high chemical resistance, while maintaining sufficient flexibility over a wide temperature range. It should be mentioned here that, until now, perfluoroether synthesis has been limited by inadequate molecular weights.

The unusual resistance of highly fluorinated materials to high temperatures, oxidation, and a variety of organic solvents has been known since Plunkett's discovery of Teflon in 1938. Efforts since then have centered on the synthesis of partially and completely fluorinated polymers designed to retain the thermooxidative and chemical stability of polytetrafluoroethylene, while adding elastomeric character, low-temperature flexibility, processibility, etc. The literature reveals many attempts to prepare fluorinated ether polymers (refs. 3-6). It is to be noted that by incorporating ether backbones one can design materials that will maintain flexibility below -30°C (-28°F). For example, nitroso rubber has a T_g of -50°C (-58°F), but its high-temperature stability is limited. The fluorosilicone comes nearest to meeting the requirements of a high-temperature sealant. It has excellent low- and high-temperature properties, but it tends to undergo reversion and has low tear strength.

We at NASA, together with scientists at PCR, Inc., reopened the question of how to chain extend these fluoroether systems. The objectives were to prepare long-chain difunctional polyperfluoroethers and investigate chain

extension mechanisms, as well as to convert these materials to stable cross-linked polymers for sealant applications. The nitrile, acetylene, and isocyanate groups were considered. Each of these is capable of both trimerization reactions and cycloadditions. From this base line, one could then evoke both chain extension and cross-linking with a variety of reaction schemes (ref. 7).

The general characteristics of the sealant elastomer required before formulation and mechanical property testing can begin are as follows: thermal stability from 227°C (450°F) to 316°C (600°F); low temperature flexibility to -46°C (-50°F); chemical resistance; and adhesion to metals. Our initial efforts were then directed toward increasing the molecular weights of the fluoroethers by chain extension reactions. This was to be achieved through thermally stable anchor points which could serve as "hard domains" to improve high temperature mechanical properties as well as provide the necessary crosslink sites and molecular weight control.

Two systems were selected based upon the same nitrile terminated fluoroether prepolymer backbone. The difunctional nitrile could be trimerized, that is, reacted with itself to form triazine or co-reacted with aromatic nitrile oxides to give aromatic 1, 2, 4-oxadiazoles. Both systems were investigated and results indicated good thermal stability and low temperature flexibility, but both were lacking in mechanical properties. Deficiencies in processing and molecular weights appeared to be principal reasons for achieving inadequate sealant elastomer characteristics. These materials are compared to recently developed polymers in a later section.

Model studies. — Simultaneously, we embarked upon a detailed polymer model study which would enable us to design polymers based on relating structural parameters to performance. Specifically examined were the relative effects of degradation in selected environments on the heterocyclic ring structures and ring substituents (ref. 8).

Table III shows simplified chemical models representative of four (4) ring systems which might be synthesized from the base nitrile-fluoroether prepolymer as mentioned above. Left to right they are the s-triazine; 1, 2, 4-oxadiazole; 1, 2, 4-triazole and 1, 3, 4-oxadiazole. R, R_f and Ar indicate various substituent molecules which can be synthesized into a polymeric structure. The purpose was to degrade and analyze the materials in fuel tank environments. The investigation determined on specific model compounds the relative thermal, thermal oxidative, and hydrolytic stability of potential chain extension moieties and crosslinks useful for curing perfluoroalkyl ether elastomers. Initial results emphasized the importance of structures 1 and 2 relative to 3 and 4.

Table IV indicates that terephthalonitrile-bis-N-oxide derived oxadiazoles decomposed extensively at 325°C (617°F). Although the effect of substituents cannot be discerned, subsequent data reinforce the idea that an aromatic group adjacent to the oxadiazole leads to lessened thermal stability.

By going to a fully fluorinated 1, 2, 4-oxadiazole (compound A) as shown in table V, a significant increase in thermal stability in an inert atmosphere can be demonstrated. Moreover, at the indicated temperature of 325°C (617°F), there is adequate thermal oxidative and hydrolytic stability of the 1, 2, 4-oxadiazole for projected high-performance sealant applications. Contrast this with the 1, 3, 4-oxadiazole (compound B) where thermal-oxidative stability is lower. Subsequent runs indicate erratic behavior of the 1, 3, 4-oxadiazole in oxidative environments. Recent data reflect equal stability characteristics for the fluoroether-1, 2, 4-oxadiazole as for (compound A) which contains no ether groups.

Table VI shows the results of the alternate system, the triazine-fluoroether models. Both triazine models exhibit excellent thermal and thermal-oxidative stabilities at 325°C (617°F). However, an examination of the degradations performed under thermal-hydrolytic conditions indicates a very high sensitivity to the unbranched fluoroaliphatic group attached to the triazine nucleus (compound A). A dramatic turn around in hydrolytic stability of the triazine containing the branched fluoroether group (compound B) can be clearly seen from the data. This information points to an important structural detail in designing a stable fluorinated triazine polymer. Our polymer work utilized this result to tailor-make triazine-fluoroethers having a -CF- and not a $\text{-CF}_2\text{-}$ adjacent to the CF_3

triazine nucleus. Apparently this is due to steric reasons (that is, a crowding at the site of hydrolytic attack of the triazine) rather than to electronic effects. This represents the first time that a thorough model study has been used to establish criteria for tailoring structural details in polymer synthesis design.

Synthesis of new fluoroether polymers. — Guided by the model stability studies described in the previous section, two promising sealant elastomer candidates have emerged from synthetic investigations. The candidates are a fluorinated ether triazine and a fully fluorinated ether-1, 2, 4-oxadiazole. Recent efforts have concentrated on molecular weight and it now appears that we have achieved molecular weight ranges between 15 000 and 50 000 which should be adequate for a fillet type sealant. Current work involves the determination of the optimum crosslink density for attaining the requisite mechanical properties in a high-performance sealant application.

Table VII compares the relative weight loss of the Ames fluoroether polymers to the best state-of-the-art fluorosilicones. The 77-108 is the Dow-Corning hybrid fluorosilicone designed to improve the thermal stability and reversion tendency of the DC77-028 fluorosilicone currently being flight-tested on the YF-12A.

Note that weight loss does not begin at 300° C (572° F) for the two Ames fluoroether elastomers as it does with both fluorosilicones. Weight loss comparisons are also made at 350°, 400°, 450°, and 500° C (662°, 752°, 842°, and 932° F). Even at 500° C (932° F), the fluoroether -1, 2, 4-oxadiazole at 57-percent weight loss compares favorably with the fluorosilicones while the triazine fluoroether shows a weight loss of only 20-percent.

Figure 4 shows actual traces of the thermogravimetric analyses of both fluorosilicones and the two Ames fluoroether polymers. Also included is a polyphosphazene polymer which has been proposed as a high temperature elastomer. Here again, it is clear that the Ames fluoroether -1, 2, 4-oxadiazole compares very favorably to both fluorosilicones in thermal stability while the Ames fluoroether-triazine is superior.

A summary of Ames materials compared to the fluorosilicones is shown in table VIII. In this table we are comparing the temperatures at which specific weight losses of 1, 10, 50, and 90 percent occurred. Also shown are relative comparisons of the glass transition temperatures which give an indication of the low temperature brittle or use point. Finally, a relative assessment of the elastomeric properties are compared.

The two fluorosilicones are listed on lines 1 and 2 where it can be seen that all properties are reasonably good. Lines 3 and 4 are examples of the early Ames polymers mentioned previously. Points worth mentioning here are that the oxadiazole on line 3 is not quite up to the thermal stability or elastomeric property expectations. This was certainly substantiated in the model studies mentioned earlier. The triazine on line 4, although showing good high and low temperature properties, is deficient in the necessary mechanical properties. Lines 5 and 6 indicate that the two new Ames fluoroether polymers have very good high and low temperature properties as well as very promising elastomeric characteristics.

CURRENT AND FUTURE PLANS

The characterization and vulcanization study that will be carried out this year for polymer selection will determine the best crosslink density and will measure the properties of the polymers. This will include molecular weight and molecular weight distributions, thermal stability, aging studies, glass transition temperatures, and fuel, metal, and hydrolytic stabilities.

Simultaneously, the sealant elastomer will be formulated with the appropriate fillers and its mechanical properties determined. Sheet stocks will then be prepared for sealant-metal system development and actual flight testing in the YF-12A aircraft.

CONCLUSIONS

Preliminary results indicate that new fluoroether polymers developed at Ames Research Center compare favorably with state-of-the-art fluorosilicone sealants. The glass transition temperatures are comparable and the thermal stabilities are equal or superior to the baseline materials. It is anticipated that the fluoroethers will exhibit enhanced resistance to reversion and should provide materials for consideration as serious high-performance sealant candidates.

REFERENCES

1. Rosser, R. W.; and Parker J. A.: Chemical Research Office, Fuel Tank Sealants Review. NASA TM X-62,401, Dec. 1974.
2. Fritz, C. A.; and Warnell, J. L.: U.S. Patent 3,317,484, 1967.
3. Arnold, R. G.; Barney, A. L.; and Thompson, D. C.: Fluoroelastomers. Rubber Chemistry and Technology, vol. 46, July 1973, p. 646.
4. Eleuterio, H. S.: Polymerization of Perfluoro Epoxides. J. Macromol. Sci. Chem., vol. A6, no. 6, Oct. 1972, pp. 1027-1052.
5. Sianesi, Danio; Pasetti, Adolfo; Fontanelli, Renzo; Bernardi, Gian Carlo; and Caporiccio, Gerarde: Perfluoroethers by Photooxidation of Fluoroolefins. La Chimica E L' Industria, vol. 55, no. 2, 1973, pp. 208.
6. Zollinger, J. L.; Throckmorton; J. R., Ting; S. T.; and Mitsch, R. A.: Preparation and Curing of Poly (Perfluoroalkylene Oxides). In Polymers in Space Research. C. L. Segal, et al, ed., Marcel Inc., N. Y., 1970, pp. 409-430.
7. Rosser, R. W.; Parker, J. A.; de Pasquale, R. J.; and Stump Jr., E. C.: Polyperfluoroalkylene Ethers as High Temperature Sealants. American Chemical Society Series No. 6 "Polyethers," 1975, pp. 185-198.
8. Paciorek, D. L.; Kratzer, R. H.; Kaufman, J.; and Rosser, R. W.: Synthesis and Degradations of Fluorinated Heterocyclics. Journal of Fluorine Chemistry, vol. 6, 1975, pp. 241-258.

TABLE I.- BOEING FLIGHT SIMULATION

77-028 FLUOROSILICONE SEALANT

NUMBER OF FLIGHT CYCLES -46°C to 227°C (-50°F to 441°F) 3 HOURS/FLIGHT	FUEL CELL CONDITION
861	NO LEAKS, NO SEALANT CRACKS
1389	NUMEROUS BASELINE AND MOON SHAPED SEALANT CRACKS CORNER LEAKS SOME ADHESION FAILURE

TABLE II.- YF-12A AIRCRAFT FLIGHT TEST

PHASE 1:

SMALL TEST SPECIMENS—FLUOROSILICONES

- TENSILE SPECIMENS
- ADHESION SPECIMENS
- WEIGHT & VOLUME CHANGE SPECIMENS
- CONSTANT STRAIN SPECIMENS

FLIGHT TEST INITIATED MARCH 1975

30 FLIGHTS TO JANUARY 1976

INSPECTION JUNE 1976

PHASE 2:

- STRIPPING OF SEALANT IN NUMBER 5
AFT WING TANK
- RESEALING OF NUMBER 5 TANK WITH
25-30 LB. FLUOROSILICONE SEALANT
(ROOM TEMPERATURE CURE)

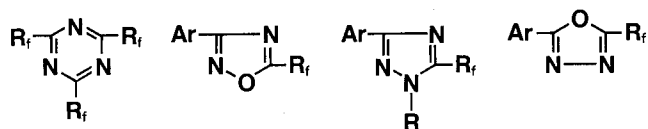
PHASE 3:

- SMALL TEST SPECIMENS—NASA DEVELOPED
FLUOROETHER SEALANT CANDIDATES

PHASE 4:

- RESEALING OF AFT WING TANK WITH
SELECTED NASA FLUOROETHER

TABLE III.- STABILITY OF MODEL COMPOUNDS



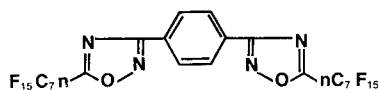
PURPOSE:

TO SIMULATE ACCELERATED DEGRADATION TO PERMIT
EXTRAPOLATION OF DATA TO SEALANT SERVICE
CONDITIONS.

- THE-OXIDATIVE TO 316°C (600°F)
- HYDROLYTIC, 0.25 TO 3% WATER
- ANALYSIS AND MATERIAL BALANCE

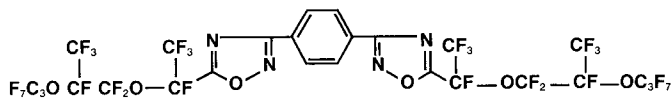
TABLE IV. - MODEL STUDIES

DEGRADATION AND MASS BALANCE AFTER 48 HOURS



COMPOUND A

TEST RESULTS—COMPOUND A		
TEMPERATURE, °C	ENVIRONMENT	WEIGHT, % RECOVERED
235	N ₂	98.8
235	N ₂ /H ₂ O	98.3
325	N ₂	—

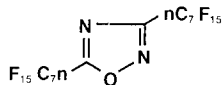


COMPOUND B

TEST RESULTS—COMPOUND B		
TEMPERATURE, °C	ENVIRONMENT	WEIGHT, % RECOVERED
235	N ₂	100
235	N ₂ /H ₂ O	99.1
325	N ₂	—

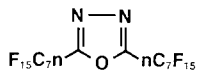
TABLE V.- MODEL STUDIES

DEGRADATION AND MASS BALANCE AFTER 48 HOURS



COMPOUND A

TEST RESULTS—COMPOUND A		
TEMPERATURE, °C	ENVIRONMENT	WEIGHT, % RECOVERED
235	N ₂ /H ₂ O	99.1
325	N ₂	99.7
325	AIR	99.3
325	N ₂ /H ₂ O	98.4



COMPOUND B

TEST RESULTS—COMPOUND B		
235	N ₂ /H ₂ O	100
325	N ₂	99.5
325	AIR	60

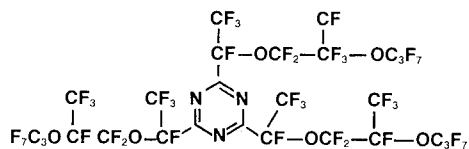
TABLE VI.- MODEL STUDIES

DEGRADATION AND MASS BALANCE AFTER 48 HOURS



COMPOUND A

TEST RESULTS—COMPOUND A		
TEMPERATURE, °C	ENVIRONMENT	WEIGHT, % RECOVERED
235	N ₂	100
235	N ₂ /H ₂ O	—
325	N ₂	99.8
325	AIR	98.3



COMPOUND B

TEST RESULTS—COMPOUND B		
235	N ₂ /H ₂ O	99.4
325	N ₂	98.9
325	AIR	98.5
325	N ₂ /H ₂ O	95.5

TABLE VII.- FLUOROPOLYMERS
THERMOGRAVIMETRIC ANALYSES IN NITROGEN

TEMPERATURE, °C	WEIGHT LOSS, PERCENT			
	HYBRID FLUROSILICONE 77-108	FLUROSILICONE 77-028	OXADIAZOLE FLUOROETHER	TRIAZINE FLUOROETHER
300	3	2	TRACE	—
350	5	3	1.5	0.5
400	7.5	5	3.5	2
450	12	10	11	7.5
500	60	55	57	20

TABLE VIII.- FLUOROPOLYMERS

POLYMER	% WEIGHT LOSS IN NITROGEN				Tg*, °C	ELASTOMERIC PROPERTIES
	1	10	50	90		
77-028 FLUROSILICONE	340°C	450°C	495°C	520°C	-50	GOOD
HYBRID FLUROSILICONE	325	440	485	510	-34	GOOD
1,2,4-OXADIAZOLE-AROM FLUROETHER	295	330	365	450	-40	FAIR
NITRILE TRIMERIZATION (FLUROETHER TRIAZINE)	340	460	535	560	-50	POOR
IMIDOYL AMIDINE (FLUROETHER TRIAZINE)	350	465	540	560	-61	GOOD
1,2,4-OXADIAZOLE FLUROETHER	350	440	490	515	-45	GOOD

* Glass transition temperature

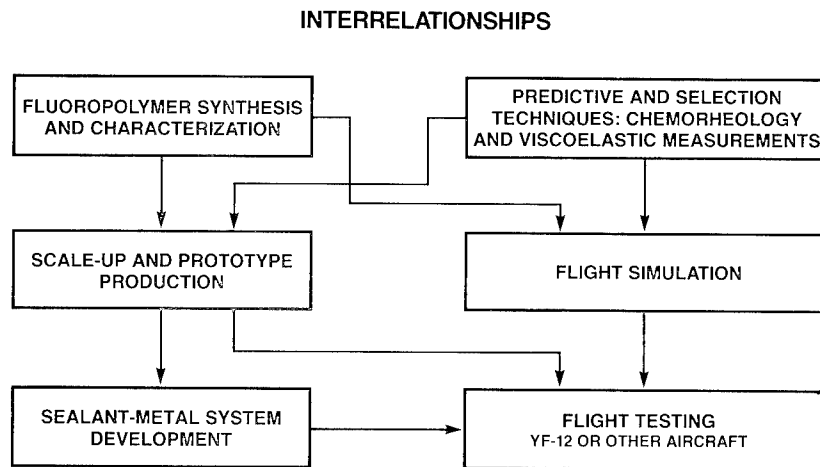


Figure 1.- AST fuel tank sealants program.

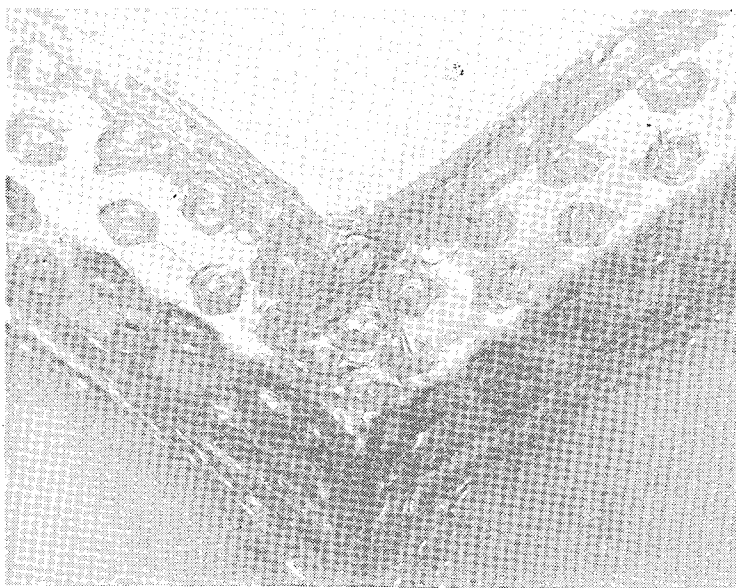


Figure 2.- Small fluorosilicone specimens mounted in fuel tank of YF-12A aircraft.

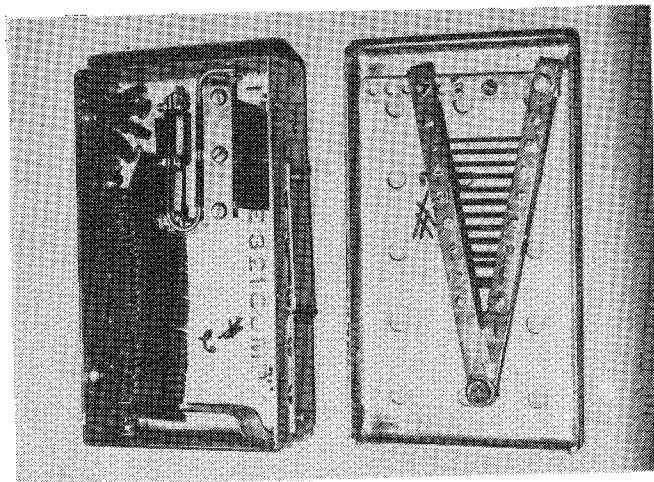


Figure 3.- Fluorosilicone sealant used in fuel tank simulator.

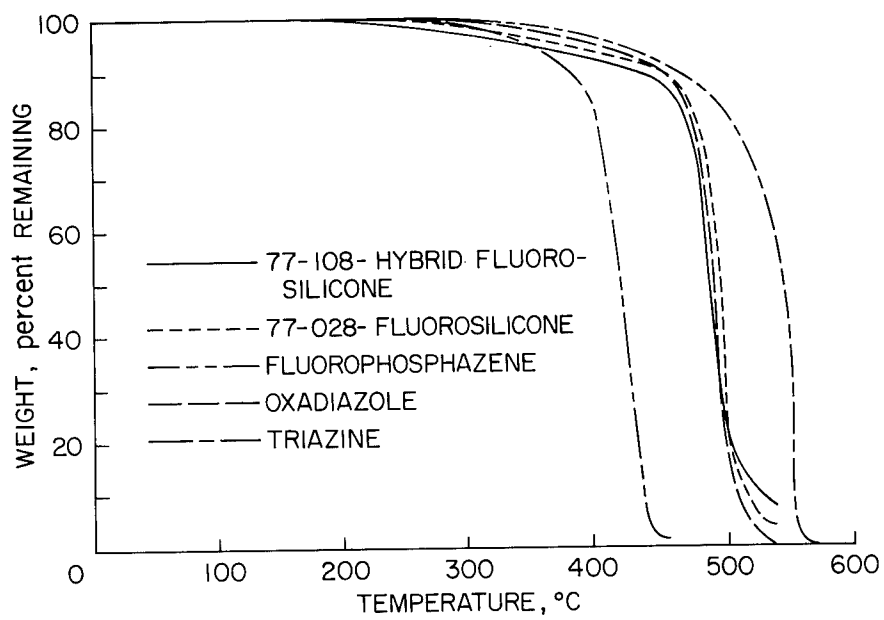


Figure 4.- Thermogravimetric analyses of fluoropolymers in nitrogen.

SESSION VI - DESIGN INTEGRATION

INTRODUCTORY REMARKS

William S. Aiken, Jr.
NASA Headquarters

The papers in this session are intended to demonstrate the integration possibilities resulting from the advances which have been discussed in the previous five sessions. In other words, this is where we get to the punch lines.

As Ed McLean noted during the opening session of the Conference, Douglas, Lockheed, and Boeing have been conducting a continuous series of systems studies under contract to Langley Research Center beginning just about 4 years ago this month.

Each company has taken a different design approach - Boeing concentrating on a blended wing fuselage configuration with variable cycle engines; Douglas, on an arrow-wing with more near-term engine technology; and Lockheed, on an arrow-wing with an over- and under-the-wing engine arrangement.

As noted in your program, there will be a set of papers from each contractor and this afternoon we begin with Boeing.

TOWARD A SECOND GENERATION FUEL EFFICIENT SUPERSONIC CRUISE AIRCRAFT

DESIGN CHARACTERISTICS AND FEASIBILITY

Frank D. Neumann
Boeing Commercial Airplane Company

SUMMARY

Studies at Boeing in recent years have focused on the definition, analysis, and evaluation of the blended wing-fuselage concept. Although blended wing configurations have been examined before, this fresh approach was initiated to reduce airplane drag in response to the increasing need for improved fuel efficiency. Studies to date not only indicate that this type of wing-fuselage integration is conducive to an efficient low fuel consuming airplane with a smaller, less expensive propulsion system that meets noise goals, but also is structurally efficient and practical. This paper reviews the basis and objectives of design improvement studies. Design changes that lead to improved aerodynamic and structural efficiency are presented. Practical design constraints and approaches for a blended wing-fuselage are discussed, as well as the integration of the configuration that leads to aerodynamic and structural efficiency. Highlighted are new approaches used to provide for structural efficiency, airline/passenger acceptance, passenger evacuation, and subsystem integration. Results of full-scale passenger cabin mock-up evaluations are presented showing the feasibility of the concept.

BACKGROUND

The construction of two prototype U.S. SST airplanes by Boeing was well under way at the time the program was cancelled in 1971. The design characteristics of these prototype aircraft represented the culmination of more than a decade of engineering and technology development, analysis and experimental testing on a grand scale. The results of this program and the DOT technology follow-on program have provided an extensive, invaluable and accessible data base. This base is a logical starting point for useful development work towards definition of future advanced supersonic cruise aircraft. Therefore, a small Boeing team, in its technology assessment and design improvement studies, both in-house and under the SCAR program, has departed incrementally from this 1971 design (fig. 1). Studies have focused on improvement in areas where the potential payoff appeared greatest and where the results could be validated with confidence. Airplane size was kept fixed while the benefits of incremental design improvements have been measured in terms of increased range or fuel efficiency.

DESIGN OBJECTIVES

The design objectives for future supersonic cruise aircraft have been changed greatly by external factors which are much different now than they were for both Concorde and the original U.S. SST design. Goodmanson in reference 1 has dealt with this concept of a moving target. Among these factors fuel efficiency is now paramount to meet the imperatives of an energy-conscious era and to counter the ever-increasing burden of fuel cost on operating economics.

Transatlantic range is no longer enough and transpacific capability of over 7500 km (4000 N. Mi.) is required to create new non-stop city pairs, offering more travelers the ultimate benefit of supersonic flight. This points to the need for much improved aerodynamic efficiency for supersonic cruise in addition to other advances in propulsive efficiency, structural efficiency, plus those improvements that can be effected by advances in systems technology. In 1973 a vigorous program was initiated at Boeing to reduce the supersonic drag of the 1971 design. Looking at the supersonic drag buildup in figure 2, wave drag at transonic speed accounts for 40% of the total drag while during cruise it accounts for about 25%. Substantial reductions in wave drag were sought. These would also cut down the engine size and weight which severely compromised the performance of the 1971 design.

REDUCING SUPERSONIC WAVE DRAG

During initial design studies drag reduction features were incorporated into the 1971 wing. These are shown in figure 3:

- . Thickness to chord ratio of the outboard wing was reduced effectively by changing from a biconvex airfoil to a modified double wedge shape, reducing maximum thickness while retaining structural depth at front spar and rear spar.
- . Weight/drag trades indicated that further modifications in span-wise thickness distribution favored a thinner outboard wing with lower drag.
- . Increased strake size is a very powerful drag reduction feature. Incorporation of an "alpha" limiter into the flight control system will make possible this larger strake which increases aircraft pitch-up tendency at low speed. The main wing was sheared aft to retain aerodynamic balance.
- . Aft shearing of the wing further reduced wave drag and also effectively increased the chord of the wing structural box, and, since the engines were not moved, reduced the engine overhang. These wing geometry revisions improved wing flutter characteristics which were marginal on the 1971 design.

Detail structural analyses showed that this newer low drag wing with improved aeroelastic characteristics actually weighs less than the 1971 prototype wing.

- Further studies have shown that favorable trades between transonic and supersonic drag are possible by area-ruling the fuselage at a Mach number lower than cruise. This, in effect, increases volume of the forebody. The larger forebody allows more passengers to be carried efficiently, balancing the weight of the aft-mounted engines as shown in figure 4.

These initial configuration improvement studies reduced transonic drag by 13% and cruise drag by 6%. The effect on engine/airframe matching was favorable, allowing smaller, more efficient multicycle engines to be used yet provide for satisfactory supersonic climb and acceleration of the airplane as shown by Vachal (ref. 2).

WING-FUSELAGE BLENDING

Further drag reductions were seen possible through a blended wing-fuselage arrangement. Using this concept airplane cross-sectional area and total volume are reduced, hence reducing supersonic drag.

The most effective approach was found to be in the minimizing of the combined height of wing and fuselage in the aircraft midsection. This was done by raising the upper surface of the wing from below the passenger cabin floor to the middle of the cabin and then using a wrap-around structural arrangement for the wing carry-through structure as shown in figure 5. Lowering the combined wing-fuselage height to a practical minimum in this manner reduced the cross section by an area equivalent to the proverbial barn door. A 5-abreast passenger seating arrangement was maintained as well as sufficient structural depth for transfer of the wing loads across the top and bottom of the fuselage. The new area distribution of the mid-fuselage section compares to the old distribution as shown in figure 6. Blending brings total lift/drag improvement to 20% transonically and to 18% during supersonic cruise as shown in figure 7.

The corresponding improvement in airplane range (or fuel efficiency) is 30% when considering only the effects of reduced drag and engine size. The configuration that evolved during two years of detailed design and trade studies retains many of the features of the 1971 design such as the forebody, aft body, landing gear, and empennage, along with the wing improvements described above. Sensitivity studies showed that these components, for which an extensive data base either existed or, in the case of the wing, was being developed in parallel, could be integrated efficiently with the new, blended section (ref. 3).

THE QUESTION OF FEASIBILITY

Wing-fuselage blending has been applied successfully to modern military aircraft like B-1 and F-16, increasing both their aerodynamic and structural efficiency. On a passenger airplane these benefits are somewhat more difficult to realize, because what's good aerodynamically and structurally, in this case can affect the passenger. Previous commercial blended designs were not seriously considered and the reasons may be categorized as follows:

- . The technology was not available to solve inherent problems effectively, i.e., in the structures area.
- . Never before were the problems associated with blending worked in enough depth to find satisfactory solutions.
- . The need to make the concept work has been amplified by increased fuel prices.
- . In the past arbitrary ground rules were established that ruled out blending, i.e., everybody needs a window!

To evaluate feasibility and practicality during the present effort, each of the following critical areas of concern was studied in considerable depth and satisfactory solutions were found and/or demonstrated:

Structural efficiency and weight

Manufacturing complexity and cost

Passenger appeal, comfort and outside viewing

Passenger evacuation

Volume limitations

STRUCTURAL EFFICIENCY

Two factors are decisive in making the blended structure react the wing and fuselage bending moments efficiently. First, a gradual transition must be provided between wing and fuselage in the highly loaded wing inboard region (7 meters long) to avoid excessive kick loads. To satisfy this requirement for a gradual transition, the inboard wing thickness was increased substantially. Acceptable aft airfoil closure angles were maintained by extending the wing trailing edge aft, creating the planform fillet which is characteristic of blended configurations as shown in figure 8. Second, the skin covers must be of thick sandwich construction to prevent buckling and in order to work effectively with the deep wing-fuselage frames, which are continuous across the blend area (see figure 5). The technology to manufacture the required, large, heavy gauge, thick sandwich panels has been developed recently.

The cabin pressure shell in the blended region is formed by the upper and lower wing-fuselage skin panels and vertical pressure panels of sandwich construction. The latter also act as a fuel barrier for the wing tanks. Forward and aft of the blend area conventional skin/stringer construction is used. Other features that are unique to the blended structure, and that affect structural efficiency include reduced fuselage height, attachment of the wing strake to the fuselage above the floor beams and the non-circular pressure shell. Hoy (reference 4) describes the detailed analyses that were conducted. The results show a structural weight of 28,000 kg for the airplane blended section, which is only 500 kg more than for the same section of the 1971 design. Unless such items as a longer landing gear and volume requirements for bulk cargo, which have not been evaluated, increase weight significantly, this would be a small penalty to pay for the large drag improvement achieved.

MANUFACTURING COMPLEXITY

In the past, production of the large structural elements of complex shape for the blended wing-fuselage section was believed to increase manufacturing cost substantially. Through the multiple use of the diffusion bonded wing-fuselage frame assemblies, the new design provides significant savings in estimated part numbers. Also, the new design offers a simpler wing-fuselage intersection by merging these two structures into a single structural element. Considering these favorable factors, the design was found to be producible and indeed may reduce manufacturing production costs as compared to a conventional wing-fuselage intersection area as shown in figure 9.

PASSENGER ACCOMMODATIONS

This aspect of blending has received much adverse publicity in the past, primarily because most configurations considered previously have used blending in excess, almost completely burying the fuselage inside the wing and, as a consequence, blocking out most windows and access to the cabin as shown in figure 10.

On the present configuration blending has been limited to the mid-cabin section. The airplane will appear as a conventional design to the passenger who is entering either through the forward entry door or the aft entry door. These floor level doors are unobstructed and will also be used for all galley servicing. Cabin windows and overhead clearance are conventional in the forward and aft two-thirds of the cabin (fig. 11). The interior layout provides seats and services at today's comfort level for 270 passengers. The seating is basically 5-abreast, single aisle with some 6-abreast seating in the wide forebody.

The passenger may notice the effect of blending only in the mid-cabin section. Ceiling height will be the same as on Concorde but there will not be any conventional windows as shown in figure 12. However, this section of

the airplane can be designed to be very spacious and appealing. This has been demonstrated through a full-scale mock-up as shown in figures 13 and 14. The effect of spaciousness was created through the effective use of sculptured panels, recessed between wing-fuselage frames, spaced at 1 meter intervals. Innovative lighting of these recessed panels in the sidewalls and ceiling creates an open atmosphere. Overhead luggage bins are also effectively recessed between the deep fuselage frames similar to the new wide body look of the popular Boeing 727 trijet interior. Raceways for the major systems are integrated into the lower sidewalls with functional armrests for the "window" seats. The result is a pleasant, acceptable, modern cabin interior as confirmed by numerous visitors to the full-scale mock-up.

OUTSIDE VIEWING

Airline/passenger acceptance of a partially windowless cabin will probably be controversial, even though indirect vision systems could offer the passenger outside viewing far superior to that offered by small windows shielded by the large wing of a supersonic airliner. For example, viewing sensors for such systems could be located at the extremities of the airplane, thereby giving excellent field of viewing to the passengers and the flight crew.

One of the limiting factors in previously proposed indirect viewing systems has been the excessive space required by the cathode ray tube display system in the passenger cabin. With the new technology of solid state thin screen television, this constraint has been greatly reduced.

These thin television screens would be inserted into the back of the passenger seats, illustrated in figure 15, or elsewhere. View selection could be multiple, giving the passenger options such as different outside views or videotaped programs. Override control could be available to the flight crew to transmit any desired message. Other symbology could be superimposed for standard information such as: the "fasten seat belt," and "no smoking" messages, as well as emergency drills which normally require separate display systems.

PASSENGER EVACUATION

One critical concern of safety has been the emergency escape over the wing from the cabin mid-section. At this location the top of the wing is above the floor at a height of four normal stair steps. Although overwing doors are generally not suitable for the loading of passengers nor the servicing of galleys because of potential wing damage, these doors must provide for emergency exit of passengers seated in the vicinity, in accordance with Federal Air Regulations.

The overwing doors provide the emergency exit for about 100 passengers in the case of the blended configuration. A full-scale demonstration mock-up was built as shown in figures 16, 17, with a new type of emergency exit, designed specifically for the blended configuration, to demonstrate the

emergency exit feasibility. The size of the door opening reflects the standard of present wide-body jets. The steps are integral with the door and automatically form a low rise stair as the door opens outward. The basic door design employed here is a well proven and safe plug-type, similar in principle to the 737 and Concorde entry doors, 707 and 727 emergency exit doors, and 727-200 cargo doors.

Preliminary exit rate testing was conducted at Boeing in 1968 of a similar exit and stair arrangement. Based on those tests and recent evaluation by our safety staff, we feel that the proposed design could be developed for 100 passengers capability.

Further, the flotation characteristics of the airplane after ditching on water were reviewed and it appears that safe escape for all passengers can be provided should the airplane ever come to rest on water. A concept for integration of the emergency slide and raft was identified.

VOLUME LIMITATIONS

Reducing the fuselage cross-sectional area through blending has increased the airplane volumetric efficiency, or mass-per-unit volume ratio by 13%. This puts a premium on space for aircraft systems--primarily fuel. About 85% of the total fuel for transpacific range is now carried in the wing outboard of the fuselage, taking advantage of the larger inboard wing. The thermal management system of the airplane has been examined. The combination of increased fuel efficiency, increased range and increased volumetric efficiency makes careful thermal management necessary to avoid excessive fuel tank temperatures and to provide an adequate heat sink. However, recent developments in titanium sandwich construction will reduce the thermal conductivity of wing fuel tanks, and use of the heat sink capability of cabin exhaust air will help to preserve the fuel heat sink near the end of long supersonic flights. Thus, the thermal management situation is considered satisfactory for this stage of the design cycle.

The arrangement of systems in the fore and aft fuselage remains nearly identical to that of the 1971 design, including baggage containers, passenger cabin, environmental control system and nose gear. The underfloor space in the blended fuselage section is reserved for systems routing with adequate provisions made for cabin air supply and return ducts.

CONCLUDING REMARKS

Significant progress has been made in the NASA Supersonic Cruise Aircraft Research program toward defining the technology and characteristics of fuel efficient supersonic cruise aircraft. As each element of the blended wing-fuselage concept is evaluated and as a result of the work to date, summarized in figure 18, confidence is increased that the blended wing concept can be one of the most essential elements in reducing drag and fuel consumption for a practical and safe supersonic passenger airliner design (fig. 19).

REFERENCES

1. Goodmanson, L. T. and Williams, B.: Second Generation SST, SAE Paper 730349, Air Transportation Meeting, Miami, Florida, April 24-26, 1975.
2. Vachal, J. D.: Toward a Second Generation Fuel Efficient Supersonic Cruise Aircraft - Performance Characteristics and Benefits. Proceedings of the SCAR Conference, NASA CP-001, 1977. (Paper no. 41 of this compilation.)
3. NASA CR-132723, Advanced Supersonic Configurations Studies Using Multi-cycle Engines for Civil Aircraft, Boeing Commercial Airplane Company - Product Development, September, 1975.
4. Hoy, J. M.: Toward a Second Generation Fuel Efficient Supersonic Cruise Aircraft - Structural Design for Efficiency. Proceedings of the SCAR Conference, NASA CP-001, 1977. (Paper no. 40 of this compilation.)

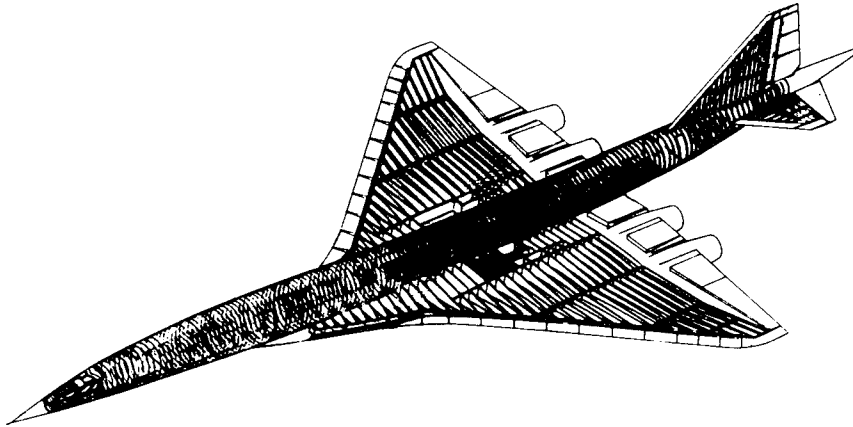


Figure 1.- 1971 U.S. SST.

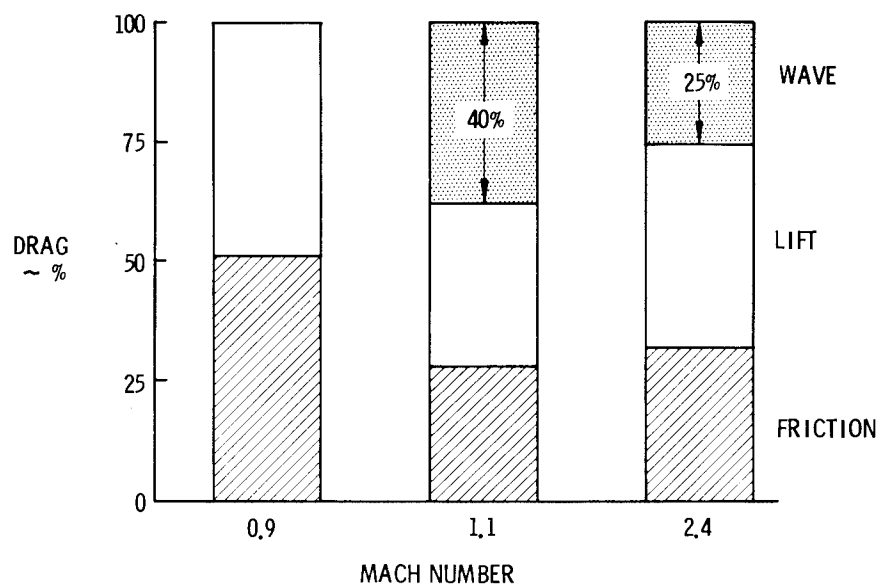


Figure 2.- Drag contributions for 1971 design.

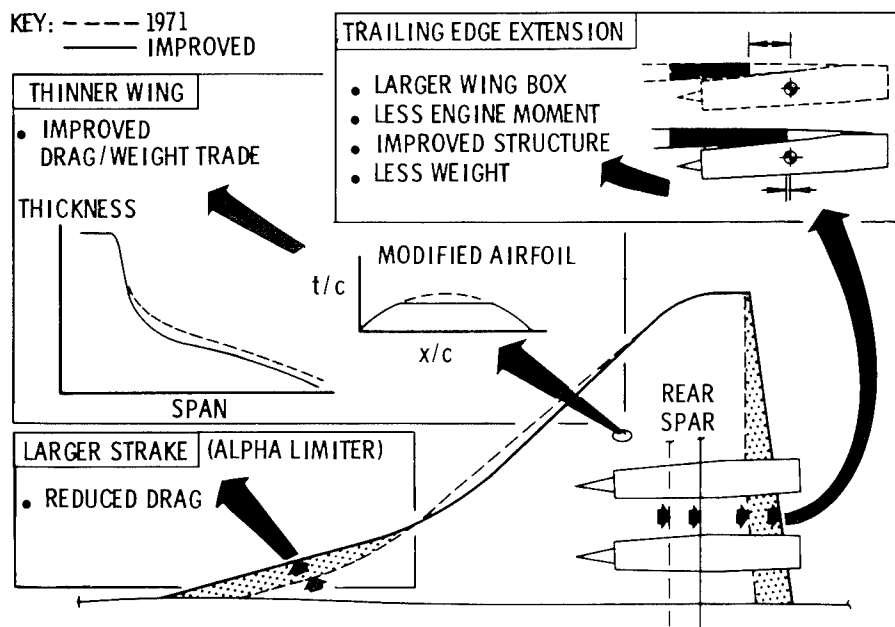


Figure 3.- Wing improvements.

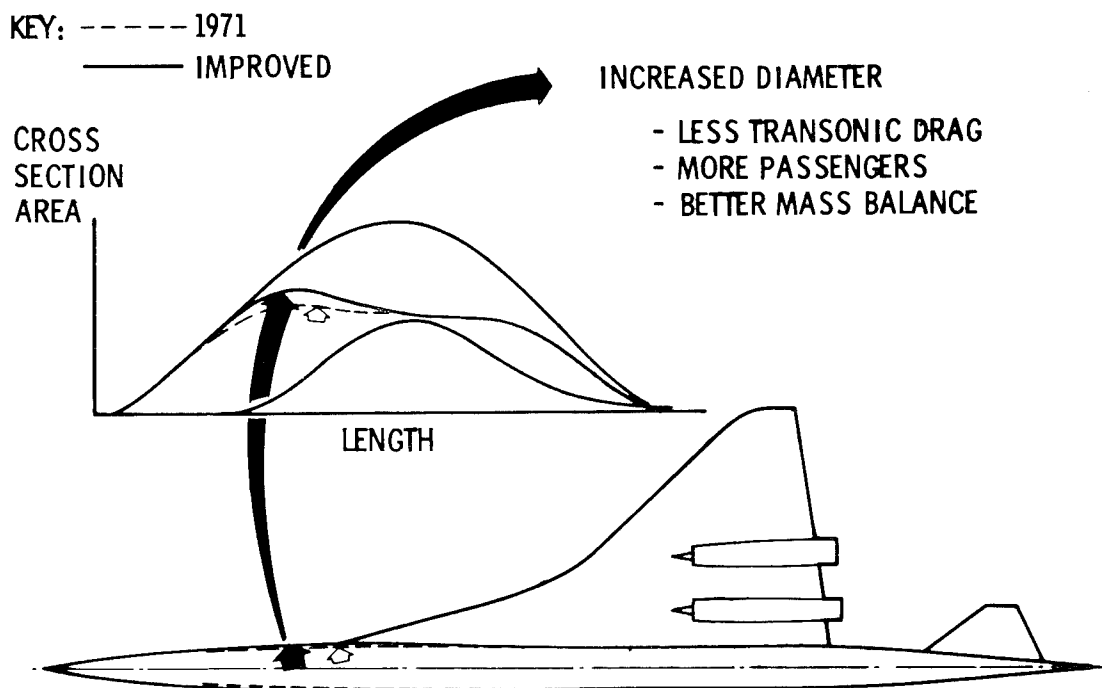


Figure 4.- Fuselage shape improvement.

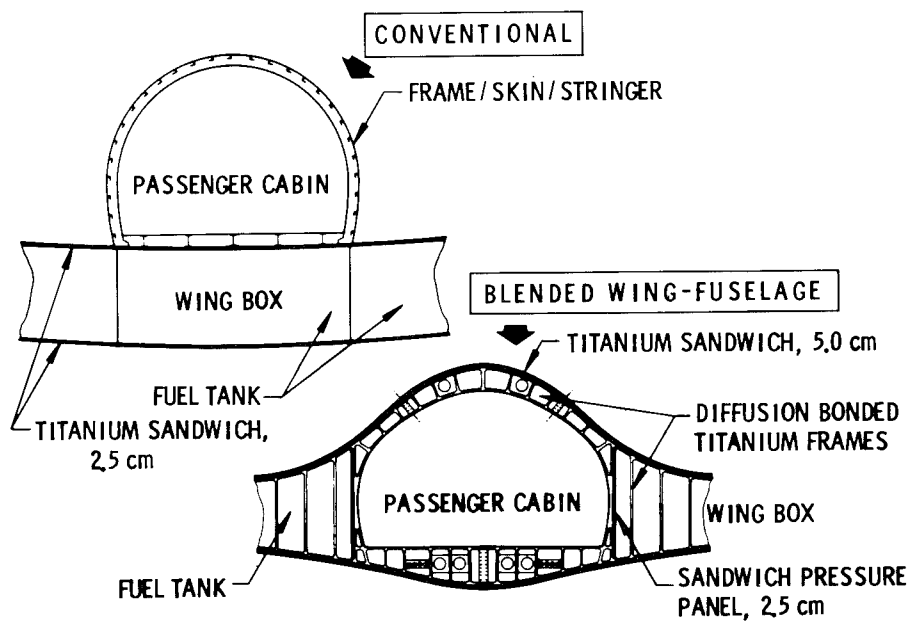


Figure 5.- Fuselage cross-section comparison.

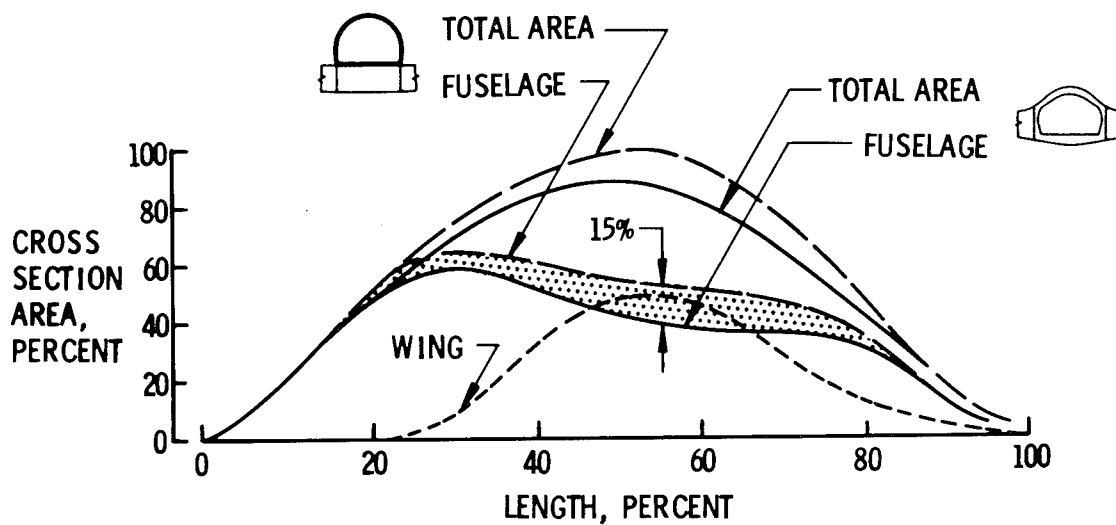


Figure 6.- Effect of wing-body blending on cross-sectional area distribution for Mach number of 2.4.

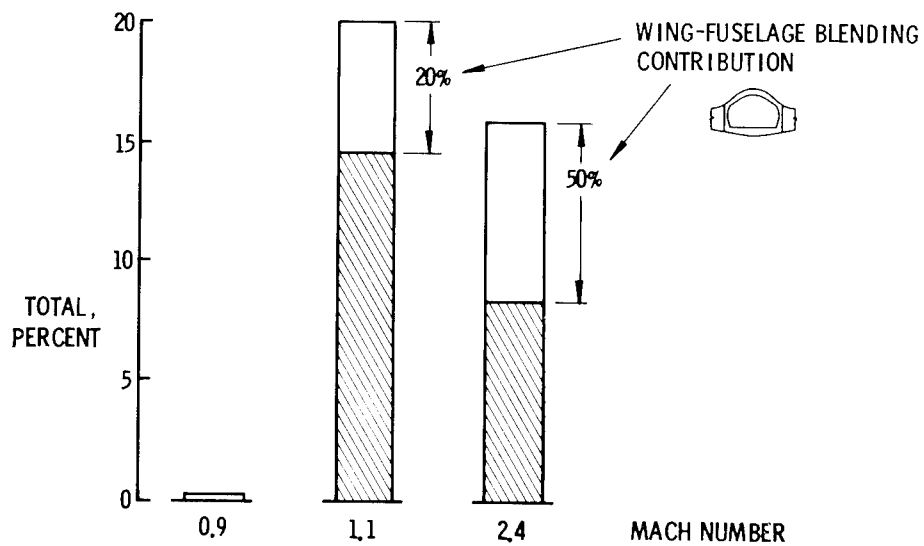


Figure 7.- Recent lift/drag improvement.

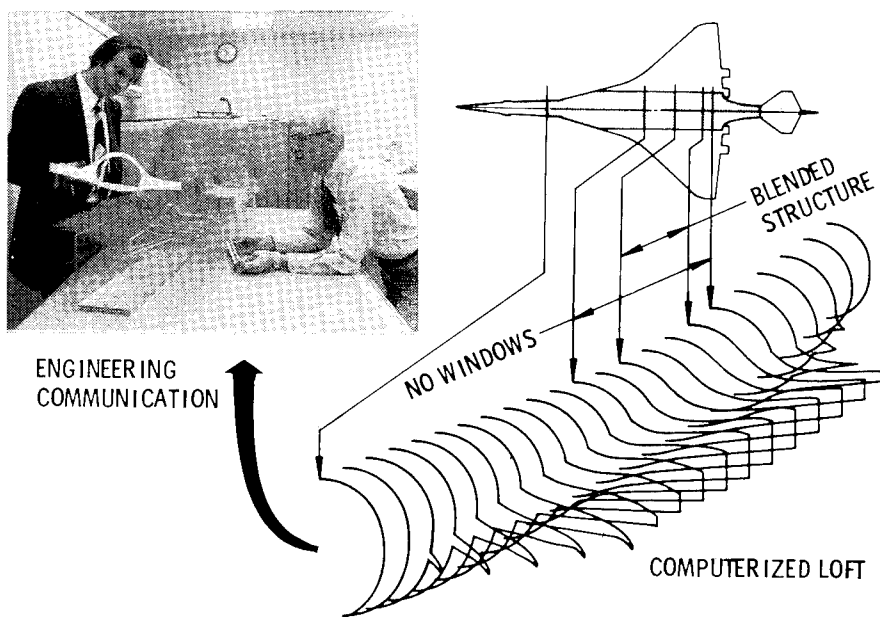


Figure 8.- Geometric definition for blended configuration.

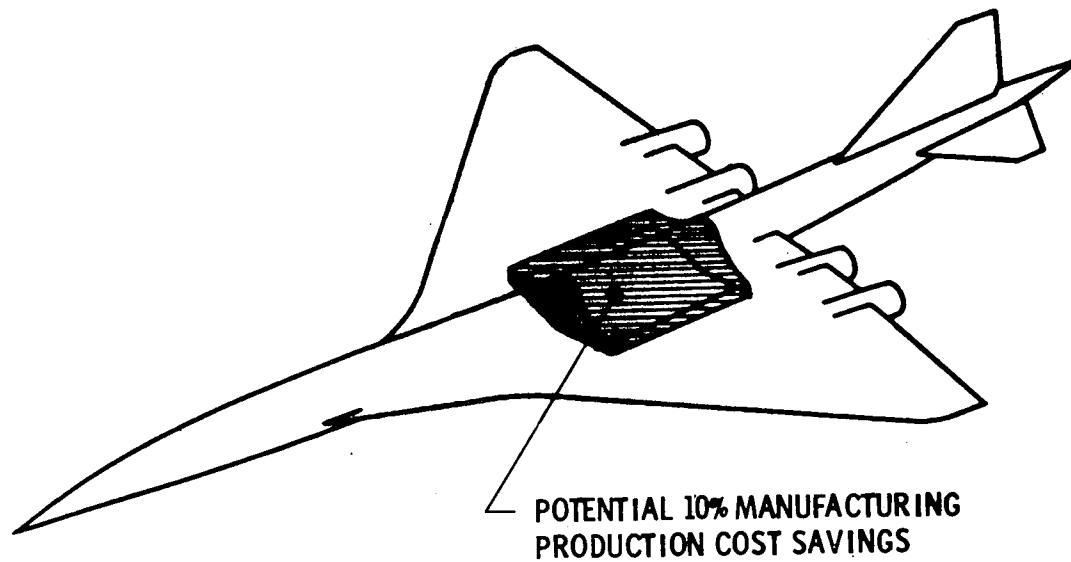


Figure 9.- Manufacturing complexity assessment.

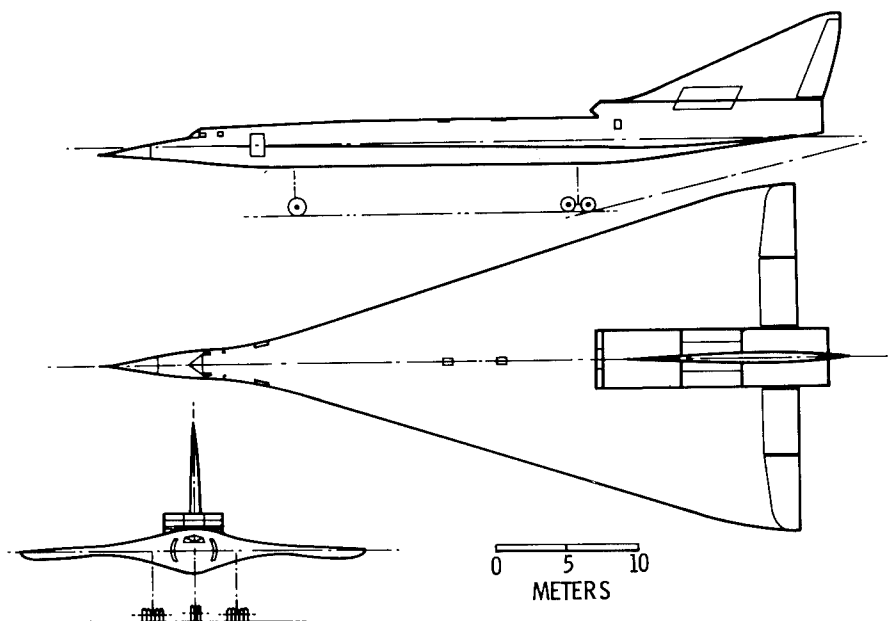


Figure 10.- Blended wing-fuselage concept of the early 1960's.

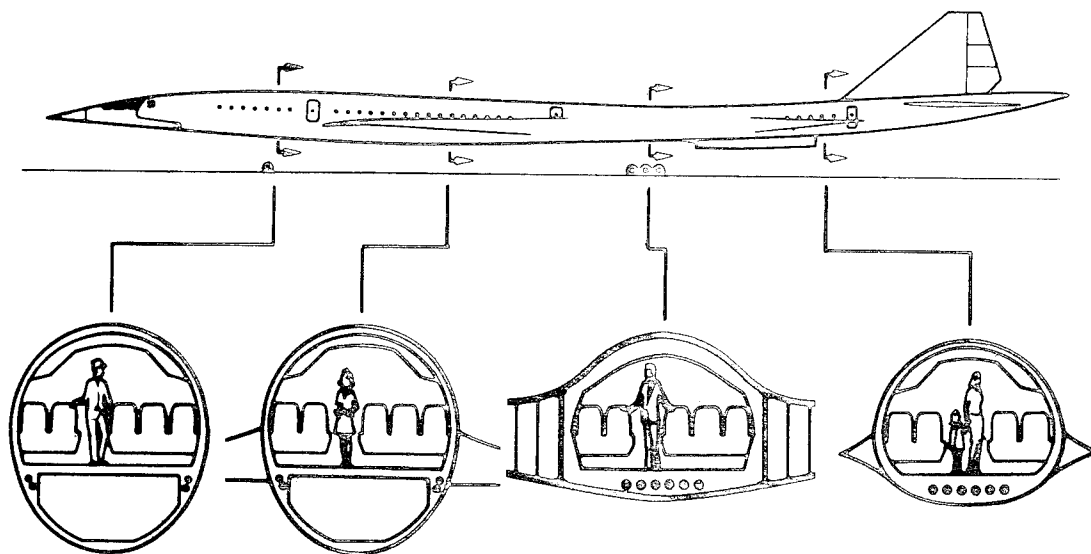


Figure 11.- Passenger cabin arrangement.

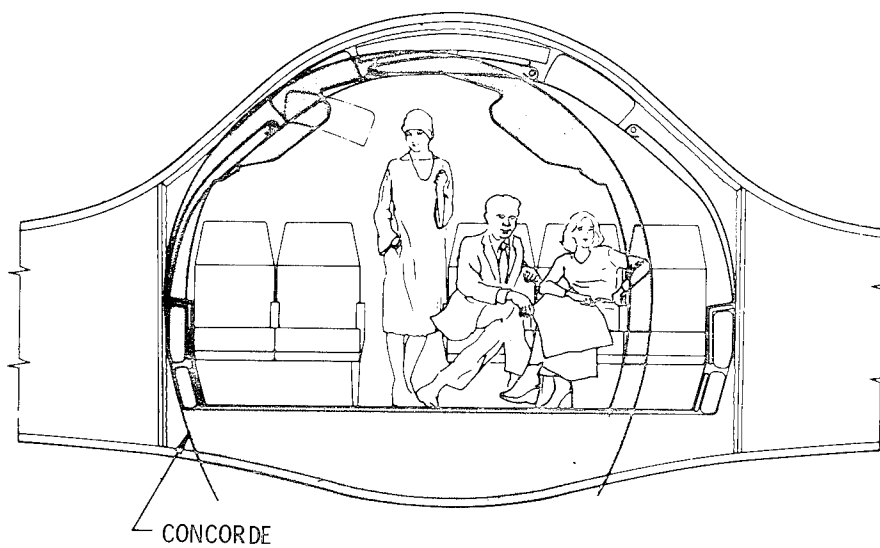


Figure 12.- Fuselage cross-section comparison with Concorde.

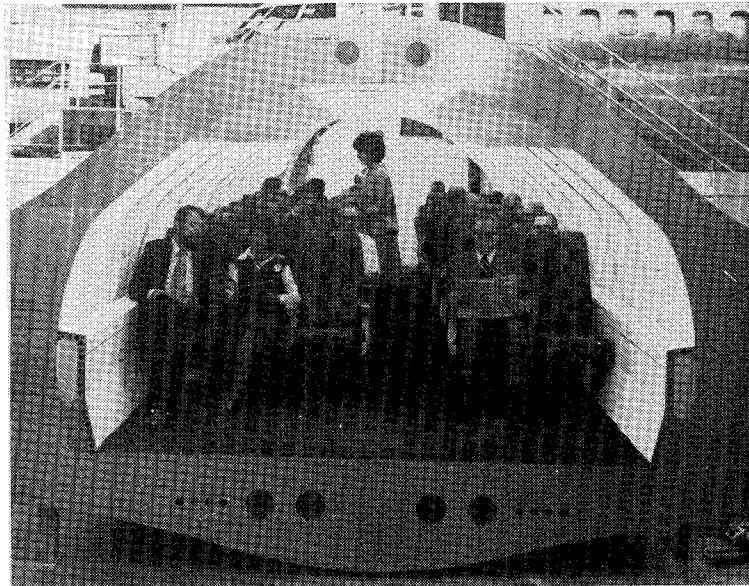


Figure 13.- Display of mock-up of blended cabin section.



Figure 14.- Closeup view of mock-up of blended cabin section.

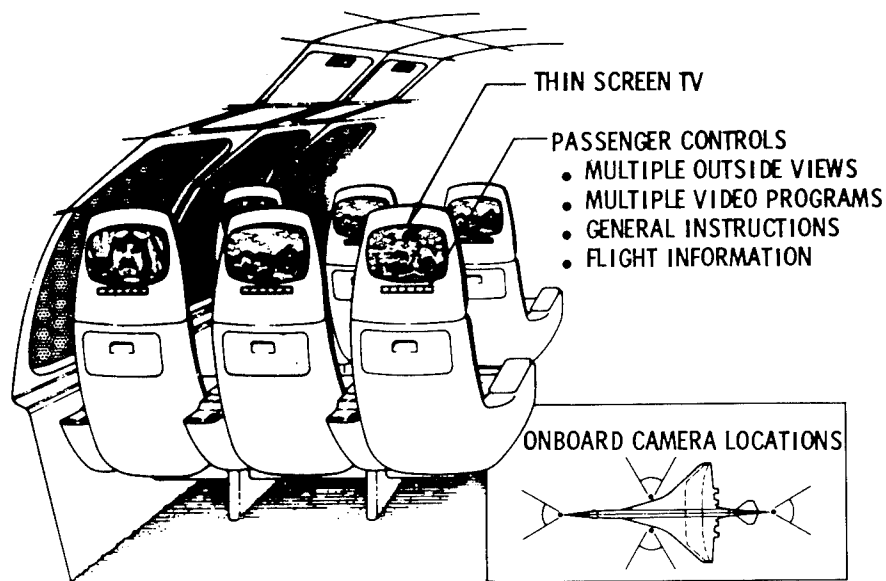


Figure 15.- Indirect outside viewing concept.

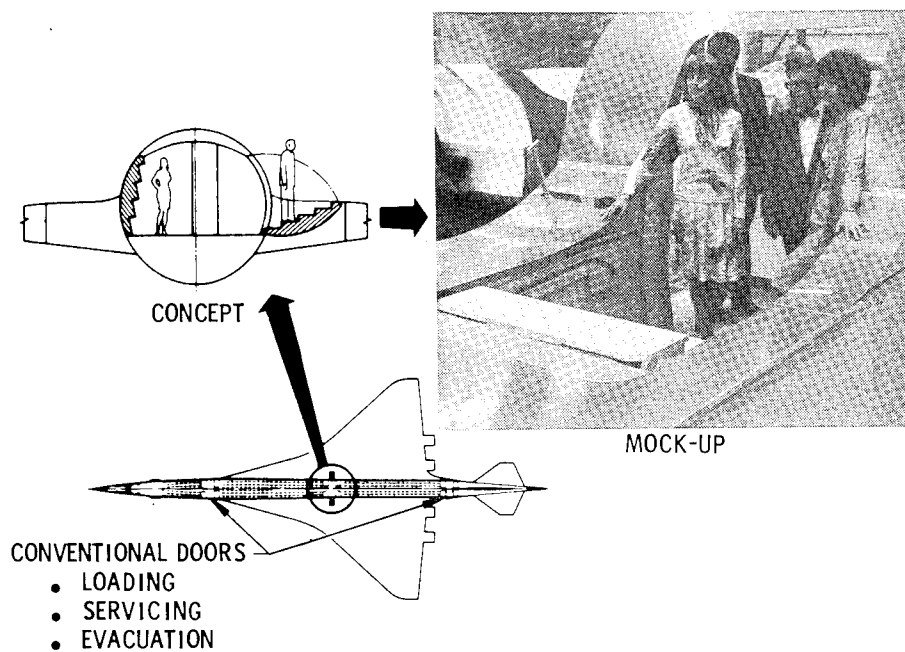


Figure 16.- Overwing passenger evacuation.

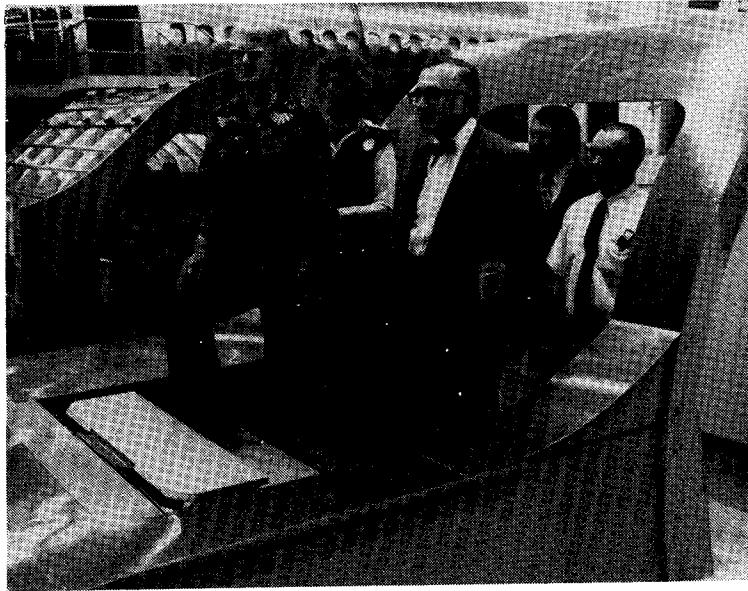


Figure 17.- Emergency exit mock-up.

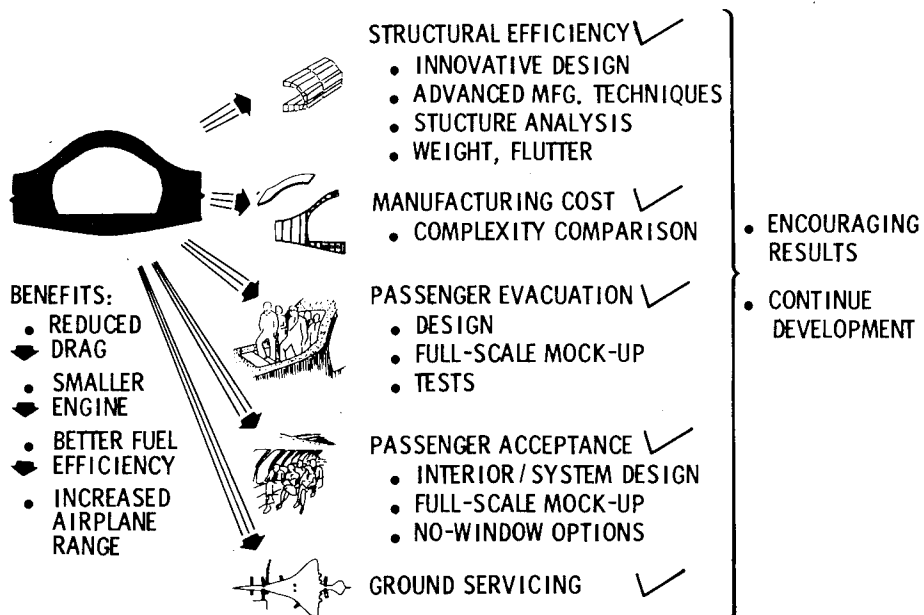


Figure 18.- Progress summary for blended configuration.

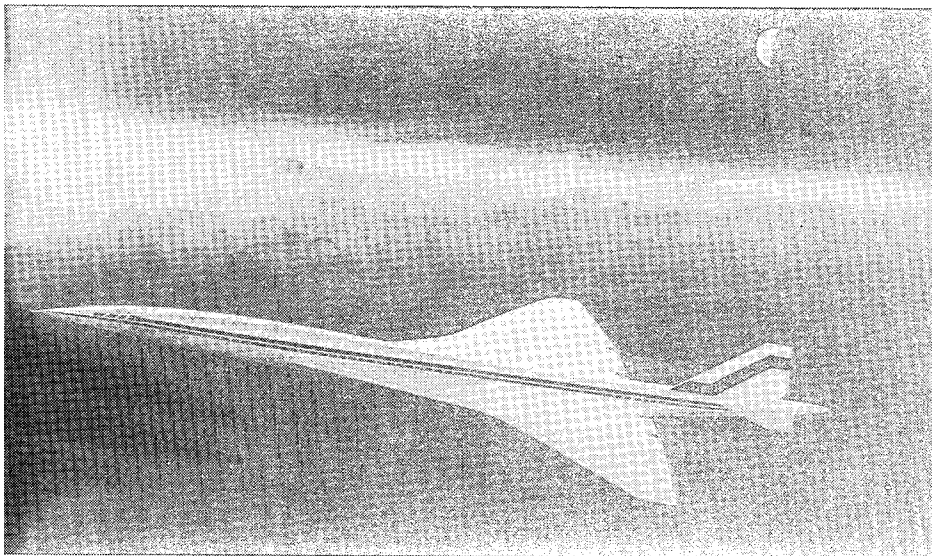


Figure 19.- Artist conception of second-generation, fuel-efficient supersonic cruise airplane.

TOWARD A SECOND GENERATION FUEL EFFICIENT SUPERSONIC CRUISE AIRCRAFT

STRUCTURAL DESIGN FOR EFFICIENCY

James M. Hoy
Boeing Commercial Airplane Company

SUMMARY

The unique challenge of this concept to the structural designer is discussed. The potential of the application of advanced structural design concepts and new titanium fabrication processes is emphasized. Highlighted are the results of a detailed structural analysis, including weight and flutter, showing successful use of the ATLAS structural design and analysis system. It is concluded that blending of the structure may not have an adverse impact on structural efficiency, weight, and manufacturing complexity.

INTRODUCTION

The blended wing-fuselage configuration is of considerable interest for supersonic airplanes because the smaller cross-sectional area of the airframe reduces drag. New manufacturing techniques and stronger efforts to conserve fuel have indicated that a new approach to the problem was justified. This paper examines in some detail a structural design that could be used for the blended wing-fuselage configuration. The analysis involves material and allowable selections followed by the selection of critical load conditions from past studies. An elaborate finite element math model is constructed that is automatically resized. The resulting deflections are examined and finally the estimated weights are determined and flutter speeds calculated.

DESCRIPTION OF STRUCTURE

Figure 1 shows a rear view of a typical frame in the heavily loaded area between the front and rear spars.

Each wing spar blends smoothly into a fuselage frame. This blend is accomplished by a large diffusion bonded titanium assembly. This assembly is spliced into the wing spar at wing station 4.65 and into an opposite hand part at wing station 0.0 at the bottom of the fuselage. A smaller diffusion bonded assembly completes the frame structure across the top of the fuselage with splices at left and right wing station 1.12.

The diffusion bonded process was selected because of efficient use of raw material and the cost effective use of the same parts in several locations with only machining differences.

The selection of a structural concept that could withstand high loads circumferentially as well as longitudinally is an essential part of the success of this study. A well stabilized sandwich structure is one of the most efficient types of structure for carrying biaxial compression loads. Aluminum brazed titanium is presently considered to be the best manufacturing process to make such a sandwich. Several other processes (including superplastic-formed, diffusion bonded) are being considered as alternates for possible cost and weight savings. In this study, these panels are configured as shown in Figure 2. The upper and lower panels splice to basic wing panels at wing station 4.65. They are 5 cm thick except locally where they taper down to 2.5 cm at the outboard end. The upper surface panels have substantial curvature at the side of the body and terminate at a longeron at wing station 1.12. This longeron consists of a heavy plate running fore and aft outside of contour and another inside plate which passed thru a machined step in the frames. Another similar longeron is at wing station .4 for a total of four along the top of the body. Between these longerons are three longitudinal panels, 15 meters long, made of 5 cm deep titanium honeycomb sandwich. The longerons serve three functions, 1) they splice the spanwise panels to the body panels and the body panels to each other, 2) they act as primary members in the fuselage strength and stiffness and 3) they act as fail safe members to arrest any circumferential crack that might start in the panels.

The lower surface wing panels have much less curvature and are continuous between wing station 4.65 and wing station 0 where they are spliced by a keel beam.

The vertical side panels at wing station 1.7 are intercostal to the frames and are mechanically fastened to the upper and lower panels. These panels complete the pressure section and are made of aluminum brazed titanium honeycomb.

The fuselage monocoque forward of the main landing gear wheel well is titanium skin-stringer similar to the 1971 SST. In this section, each wing spar attaches directly to a fuselage frame. The loads from the upper surface of the strake must be carried by bending in the frames. The fuselage aft of sta 64.7 is also skin-stringer construction. Appropriate transition sections are included to blend the non-circular sandwich skin into the circular skin-stringer sections.

ANALYSIS MODELS

The structural analysis and design process is based on mathematical models representing airload distributions, mass distributions and structural members. These models are developed from the geometric arrangement and the structural definition of the airplane. ATLAS, a modular system of computer codes integrated within a common executive and data base framework, is used to perform the structural analysis and design. The external geometry and structure of the wing outboard of the blending was taken from a previous study of a delta wing configuration (Reference 1). The previous study established the structural weight of a wing similar to that of the national SST but with the planform and thickness modified to reduce wave drag. The structural analysis was based on wind tunnel model pressure data from the national SST program and a detailed finite element structural mathematical model.

The finite element structural model for the current study was derived from the model used in the previous study. The model was divided into two substructures to permit the increase in size required for modeling the blended section of the fuselage. The wing substructure, which was modeled using spar and cover elements was taken from the previous study.

A new model was made for the fuselage substructure. Rods were used for the frame caps and plates in pure shear for the webs. Web stiffeners were included in the model to provide a path for kick loads. The honeycomb skin was modeled as plates which carry inplane loads only. Rods were used to represent the longitudinal splices or longerons. The fuselage substructure along with a section of the wing is shown in Figure 3.

Secondary models of small sections were used to augment the primary model where secondary loads or structural details had a significant effect on the material requirements. For example, a section of the fuselage was modeled with a fine grid of bending plates to determine the significance of cabin pressurization on the non-circular honeycomb shell. This analysis also determined the secondary stresses induced in the sandwich skins due to curvature.

The mass model used in the previous study was modified to account for the payload and fuel distribution changes that resulted from blending the wing and fuselage. Weight of structural members such as spars, ribs, frames and cover elements is determined from the material density and member sizes.

The retained nodes from the previous analysis were adequate for distributing the outboard wing loads through the structure. However, there was not a sufficient number of retained nodes on

the fuselage to properly distribute loads through the blended section. Therefore, the loads were redistributed to each frame as shown on Figure 4. Each fuselage nodal load was distributed to the appropriate frames in a manner that would preserve the net shears and bending moments. The total load on each frame was divided among the eight nodes on the lower frame member. Side of body loads and wing loads were also applied to each frame.

The aerodynamic model and the resulting external loads were taken from the previous study. The model included a system of lifting surfaces, slender bodies and interference flow elements. Six flight load conditions and one taxi condition were selected for sizing the blended fuselage structure (table I). These conditions were selected on the basis of a review of the critical design conditions for the national SST and an evaluation of the effect of bi-axial loads in the fuselage shell. The flight conditions are combined with both zero and 1.5 factors on the fuselage pressure of 79.3 kPa. In addition, an ultimate pressure condition of 3 factors on fuselage pressure is considered. This resulted in a total of 14 load cases.

MATERIALS AND ALLOWABLES

The material used for all frame sections and skins is 6Al-4V annealed titanium. The allowables conform with the data of MIL Handbook V. Tension allowables were appropriately reduced to compensate for fastener "hole-out." Theoretical analyses were made to determine the elastic buckling allowables for the "s" shaped honeycomb panels. These calculations showed that the curved panel buckling stresses are higher than for flat panels. For simplicity and conservatism standard flat panel allowables were used.

RESIZE

The resize of the structural elements is automatically done in ATLAS. Element stresses and internal loads (output of the stress modules) are passed on to the design module for sizing. These elements are resized by calculating their margin of safety and modifying their gauges to give a prescribed margin.

Many elements were constrained by a lower bound against resize. Resize constraints include minimum gage requirements, stiffness requirements and structure that would probably be designed by conditions not being considered. Figure 5 shows the minimum gage criteria that was used for this study. It also identifies the sections of rear spar and trailing edge beam that had been stiffened to improve flutter speed in the previous

study. These stiffened sections were constrained to that size. Finally, the upper surface panel above the landing gear wheel well will probably be designed by ground handling type conditions. The gages of this panel were selected based on the 1971 SST data and constrained to that size. Those elements that are constrained from being resized will have those requirements imposed on them by the design program.

The strength designed results are then weighed by the mass subroutine. The analysis of this resized structure is repeated for as many cycles as required for convergence to minimum weight structural elements. For this study, good theoretical weight convergence resulted within three analysis cycles, as shown in Figure 6, where the percentage weight change of the total theoretical structure is plotted vs. resize cycles. The final gages of the elements are then printed out for further analysis. Typical results are shown in Figure 7.

Note that the third rod from the centerline of the inner chord of the upper frame has an area significantly smaller than those on either side. This small area occurs because of an inflection point in the bending moment for the symmetrical load condition. Such areas must be identified and smoothed over before final weight estimates are made.

The stiffness matrix of the final results was used to perform stress and deflection analysis which were printed out for evaluation. The deflection results of the 2.5g balanced maneuver at V_D were used to plot the deflected shape of the rear spar frame as shown in Figure 8. As expected and as shown by the deflection values of wing station 2.67, the load path for the upper spar caps is softer than the lower caps therefore deflecting more and resulting in larger wing tip deflections for the blended wing as compared to the conventional wing. These values are indicated in the wing deflections at the rear spar as shown in Figure 9.

Since the blended wing airplane fuselage is not as deep as the conventional configuration the deflections will be higher for the blended wing airplane. This fact is demonstrated by the crown deflection plot for both airplanes shown in Figure 9.

FLUTTER ASSESSMENT

As shown in the calculated static deflections and confirmed in a review of the vibration mode shapes and frequencies, the blended wing configuration is somewhat more flexible in both body and wing bending.

Figure 10 shows that this additional flexibility results in a flutter speed for the blended wing 20 m/sec EAS below the $1.2V_D$ flutter requirement. The flutter mode also changes from a 2.6 Hz mode on the conventional airplane to a 1.9 Hz mode on the blended wing airplane. Moderate additional wing stiffening would probably restore the 2.6 Hz flutter mode at a speed above the flutter requirement.

WEIGHTS

In the ATLAS analysis process, theoretical member sizes required to carry loads and the associated weight based on the member material density and dimensions are calculated. Determination of the total weight of the structural components requires that weight adjustment factors be developed and applied to the theoretical weight. The total estimated weight of the sized primary structural members is the product of the adjustment factor and the theoretical weight. These factors are incorporated in the aeroelastic analysis cycle to provide an iterative capability for evaluating strength and flutter requirements and related weight effects.

Weight adjustment factors provide for so called "non-optimum" features i.g. reinforcement pad-ups, dense honeycomb core edges, braze material, splices, material tolerances, etc. These factors can represent an appreciable weight as shown by Figure 11 which reflects the adjustment factors to be applied to the theoretical skin weight in a blended titanium honeycomb pressurized body. These are only skin weight adjustments and do not include the core, core edge members, braze etc. Lower surface factors are higher in this case because of the greater number of cut outs in the lower surface.

Total structural weight for the blended body section analyzed includes the primary structure previously discussed and secondary structural items, i.e., bulkheads, doors, decks, etc. The total estimated weight of the structure analyzed was 29,500 kg for an airplane having a design gross weight of 340,200 kg and body length required for 269 passengers. A preliminary comparison of this body section for a mid-wing design versus a comparable section in a low wing design indicates that the mid-wing design body structure is only slightly heavier.

CONCLUDING REMARKS

This study demonstrates that this is a practical, efficient structural design that can be used to achieve the blended wing fuselage configuration that is desirable to improve the performance of a second generation supersonic cruise configuration.

REFERENCE

1. Advanced Supersonic Configuration Studies Using Multi-Cycle Engines for Civil Aircraft. NASA CR-132723, 1975.

TABLE 1.- DESIGN LOAD CASES

CONDITION DESCRIPTION	FLAP SETTING	MACH NO.	ALTITUDE m	GROSS WEIGHT kg	C. G. m	n	U_{de} m/sec	PRESSURE FACTOR
BAL. MAN. AT V_C	SUBSONIC	0.60	2000	335,000	53.5	2.5	0.0	0 & 1.5
POSITIVE GUST AT V_B	SUBSONIC	0.60	4500	202,300	53.4		20.1	0 & 1.5
BAL. MAN. AT V_D	SUBSONIC	0.95	6300	325,900	53.6	2.5	0.0	0 & 1.5
POSITIVE GUST AT V_B	SUBSONIC	0.95	11,000	202,300	53.4		14.9	0 & 1.5
BAL. MAN. AT V_C	SUBSONIC	0.95	8800	325,900	53.6	-1.0	0.0	0 & 1.5
BAL. MAN. AT V_A	TRANSONIC	1.30	11,400	316,800	53.7	2.5	0.0	0 & 1.5
TAXI		0.0	0	339,500	54.4	2.5	0.0	0
ULT. PRESSURE								3

V_C MAXIMUM CRUISE SPEED

V_B ROUGH AIR SPEED

V_D DIVE SPEED

V_A MINIMUM SPEED

U_{de} GUST VELOCITY

n LIMIT LOAD FACTOR

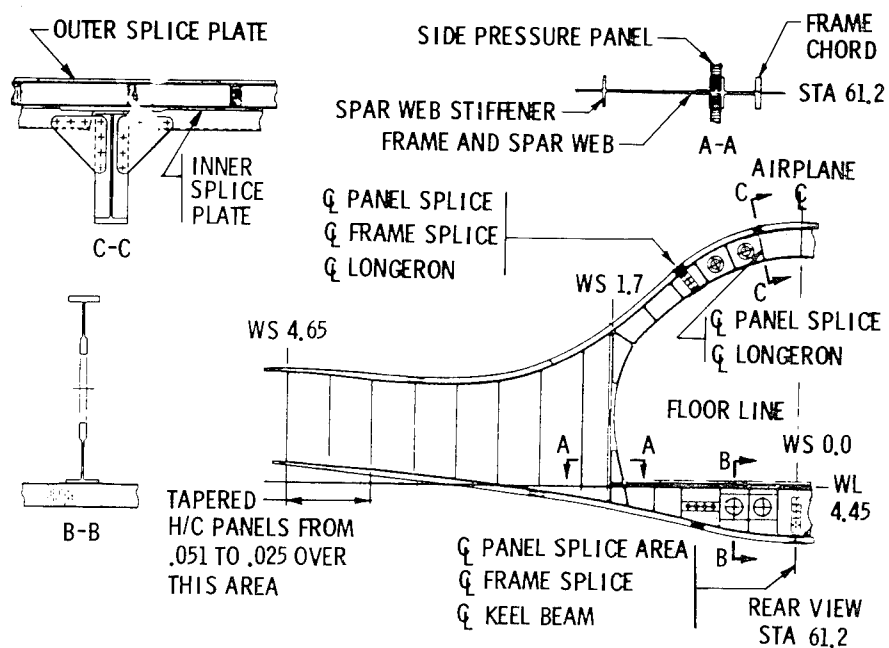


Figure 1.- Frame and spar concept blend area.

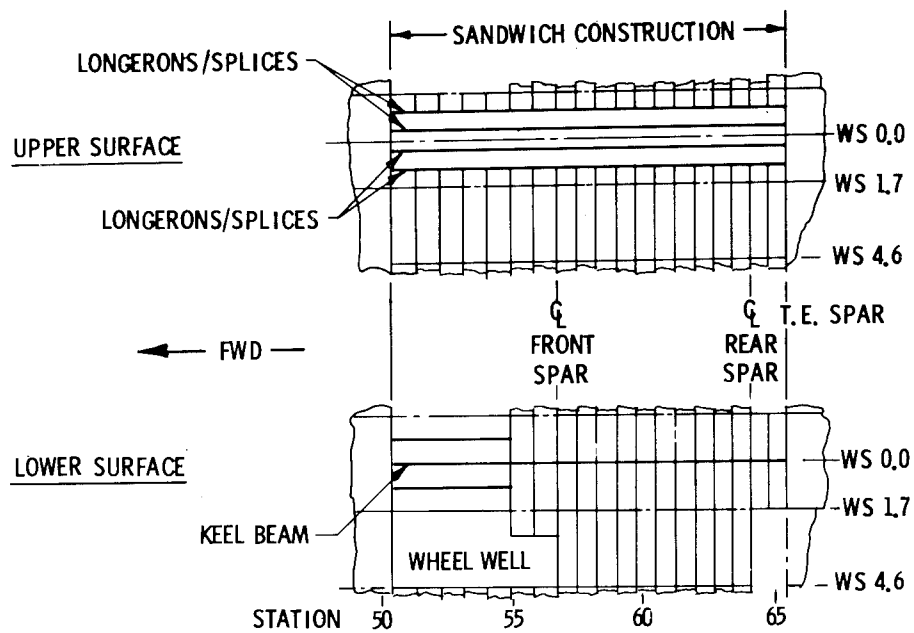


Figure 2.- Panel configuration.

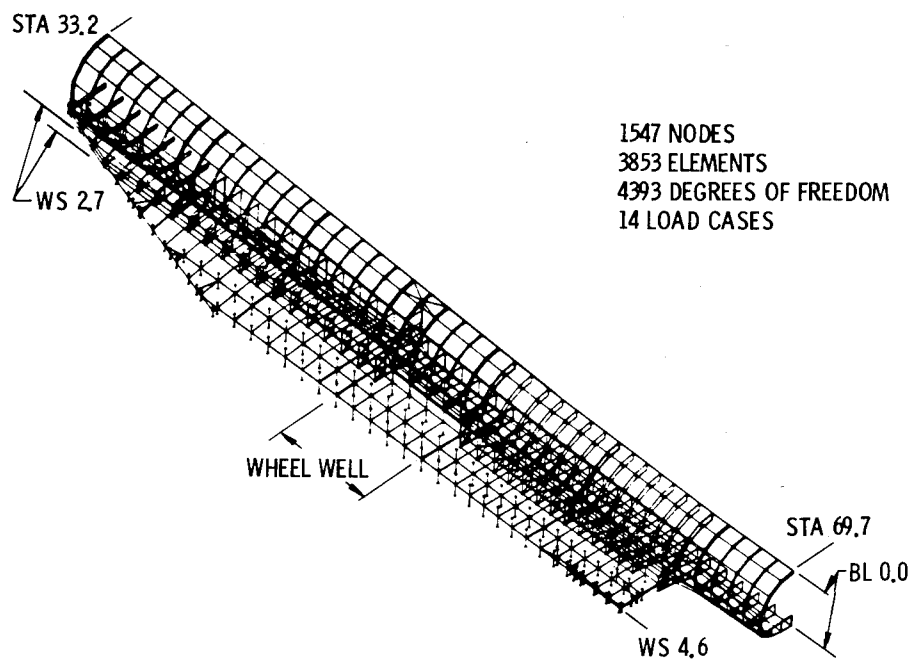


Figure 3.- Resized blended wing/fuselage math model.

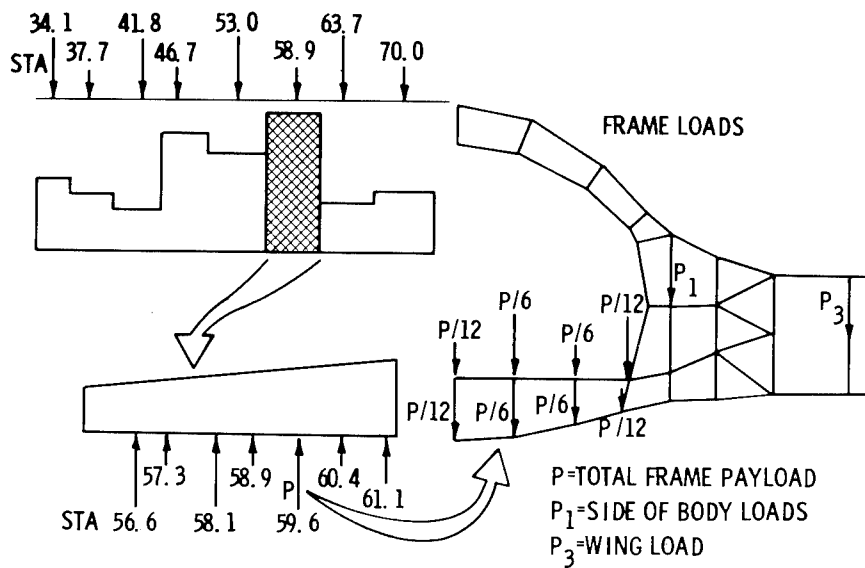


Figure 4.- Fuselage/frame load distribution.

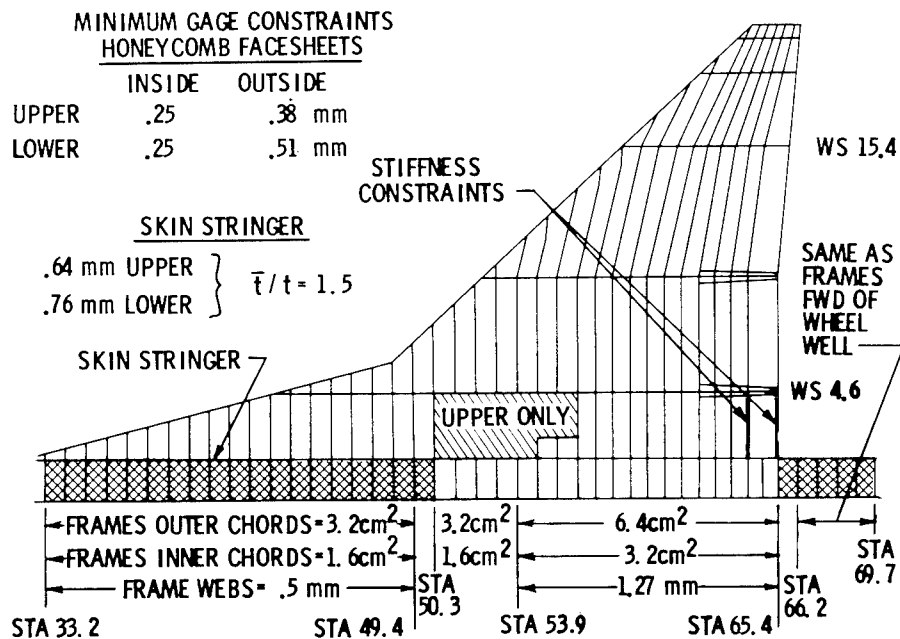
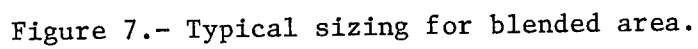
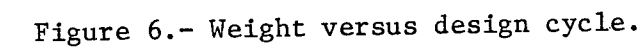


Figure 5.- Resize constraints. (\bar{t}/t is the ratio of skin plus stiffeners area to skin area.)



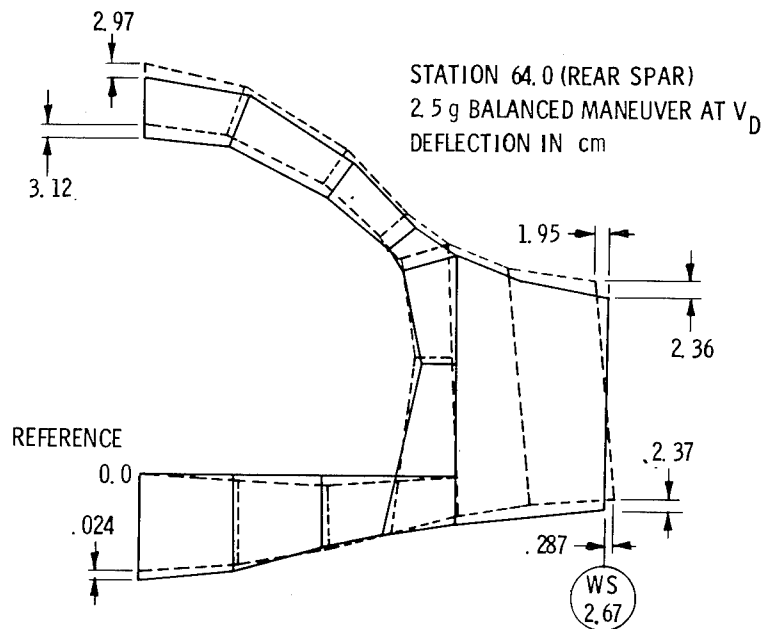
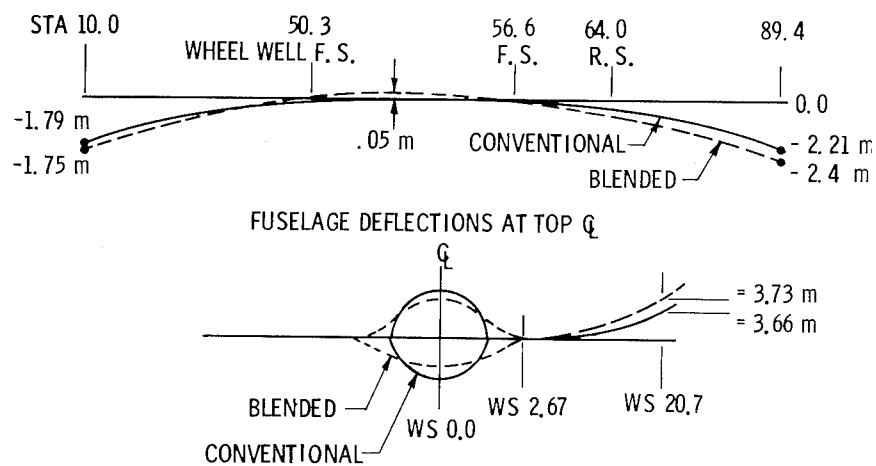


Figure 8.- Frame limit deflections.



WING DEFLECTIONS AT REAR SPAR

Figure 9.- Comparison of limit deflections for blended and conventional wing airplanes. 2.5g balanced maneuver at V_D .

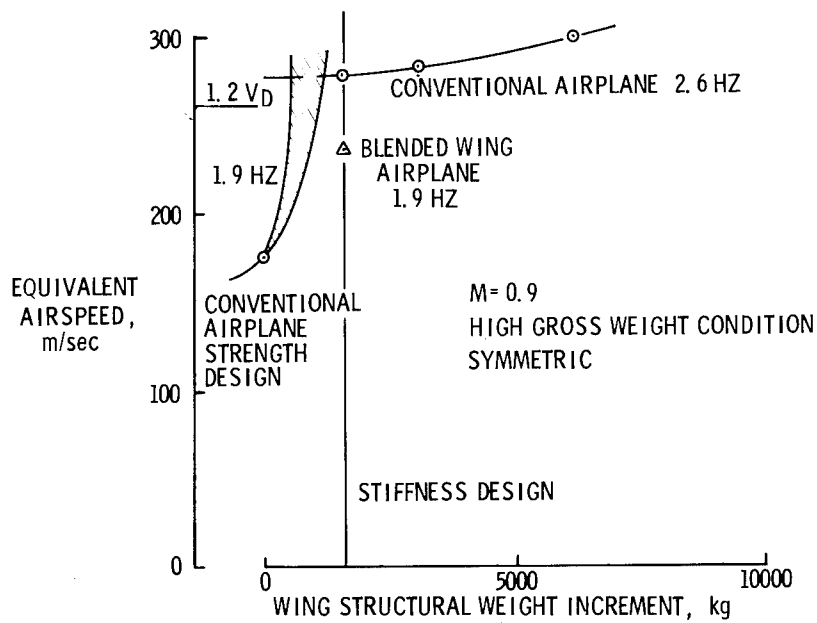


Figure 10.- Flutter speed comparison for blended wing and conventional airplane.

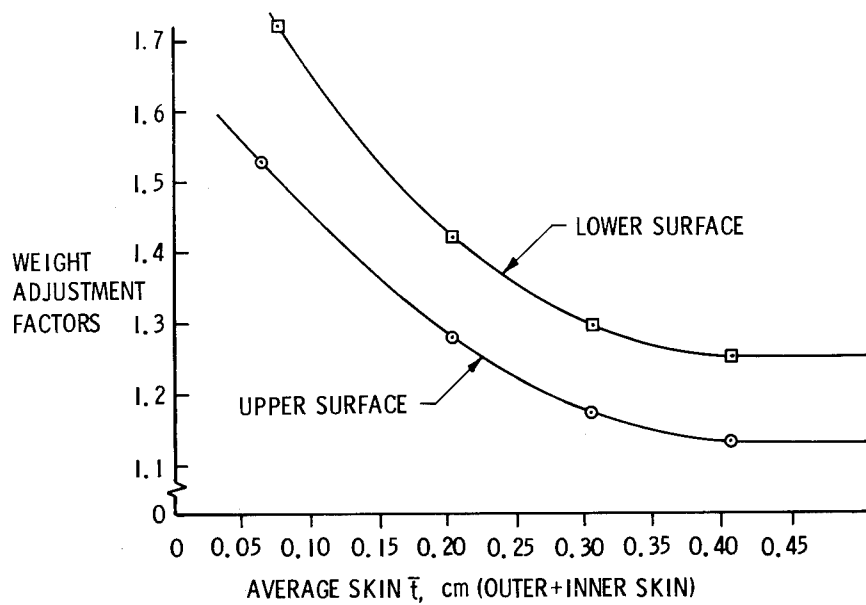


Figure 11.- Skin weight adjustment factor. Body pressurized; titanium honeycomb panels.

TOWARD A SECOND GENERATION FUEL EFFICIENT SUPERSONIC CRUISE AIRCRAFT

PERFORMANCE CHARACTERISTICS AND BENEFITS

John D. Vachal
Boeing Commercial Airplane Company

SUMMARY

The NASA Supersonic Cruise Aircraft Research (SCAR) program has led to the identification of many technological advances applicable to supersonic cruise aircraft. Studies at Boeing in recent years have focused on the integration of these technological advances into a second generation Supersonic Cruise Airliner. This paper briefly reviews the characteristics of the 1971 U.S. SST. The need for greatly improved fuel efficiency and off-design subsonic characteristics is discussed. Engine-airframe matching studies are presented which show the benefits of a configuration designed for much lower supersonic drag levels (blended wing-fuselage) and how well this airframe matches with the new advanced variable-cycle engines. The benefits of advanced takeoff procedures and systems together with the co-annular noise effect in achieving low noise levels with a small cruise-sized engine are discussed. It is concluded that the SCAR technology advances when carefully integrated through detailed engine-airframe matching studies on a validated baseline airplane lead to a much improved supersonic cruise aircraft, i.e., more range, less fuel consumption, noise flexibility and satisfactory off-design characteristics.

INTRODUCTION

At the time of the cancellation of the U.S. SST program in 1971 increased emphasis on low community noise levels had resulted in a configuration which incorporated a large dry turbojet engine with a retractable noise suppressor. This solution to the noise problem caused problems in other areas. The dry turbojet had low thrust capability at supersonic speeds. Oversizing it to provide adequate supersonic thrust resulted in an even larger engine with increased weight, balance, flutter and drag penalties. Furthermore, subsonic performance, already poor, was further degraded by the necessity to operate at lower power settings. The poor subsonic performance meant that on many desirable routes requiring overland subsonic operation, i.e., Rome to New York, extra fuel and/or reduced payloads were necessary. Finally, this poor subsonic performance also meant that even for all-overwater flights, i.e., San Francisco to Honolulu, the necessity to allow for subsonic operation after engine and/or pressurization failure meant carrying extra fuel reserves or off-loading payload.

The need for increased supersonic cruise thrust and much lower subsonic fuel consumption led to investigation of variable cycle engines as well as ways of lowering the supersonic drag levels of the 1971 configuration. The recent emphasis on fuel efficiency has greatly emphasized the latter need, i.e., to achieve the lowest possible airplane drag levels.

SYMBOLS AND ABBREVIATIONS

Values are given in both SI and U.S. Customary Units. The measurements and calculations were made in U.S. Customary Units.

DHTF-CD	duct-heating turbofan, convergent-divergent nozzle
EPNdB	effective perceived noise measured in decibels
FAR	Federal Air Regulation
$F_{N_{REQ}}$	required thrust
G.E.	General Electric
H	pressure altitude
ILS	instrument landing system
L/D	lift-drag ratio
M	Mach number
MTW	maximum taxi weight
OEW	operational empty weight
OEW-ENG	operational empty weight less propulsion pod weight
P&WA	Pratt & Whitney Aircraft
RF	range factor
SCAR	Supersonic Cruise Aircraft Research
SFC	specific fuel consumption
SL	sea level
S/L	sideline
ST^D	standard day
t/c	wing thickness to chord ratio
T-D/D	transonic thrust margin
TOGW	takeoff gross weight
TOFL	takeoff field length

V_{app}	approach speed
VCE	variable cycle engine
VSCE	variable stream control engine

ENGINE-AIRFRAME MATCHING STUDIES

The NASA Supersonic Cruise Aircraft Research (SCAR) program has led to many technology improvements in the key areas of: aerodynamics, variable cycle engines, and advanced takeoff systems and procedures. Integrated engine-airframe matching studies have been carried out on the 1971 Validated Baseline U.S. SST to determine the performance characteristics of a new baseline airplane incorporating the SCAR technology improvements and to assess the benefits in terms of a better matched configuration with lower fuel consumption, increased range, better economics and good "off-design" performance.

Objectives and Constraints

The object of the engine-airframe matching studies was to develop a supersonic cruise airliner with low fuel consumption matched to the characteristics of the multicycle engines developed in parallel NASA studies which met the objectives and constraints noted in table 1. Relative to the 1971 Baseline SST, design range has been increased to include non-stop Pacific flights while speed, payload, field length and noise objectives and requirements are essentially unchanged. In the areas of climb and cruise performance the objectives and requirements were selected to be responsive to Airlines concerns with the characteristics of the 1971 airplane powered by a dry turbojet engine.

Ground Rules

The basic mission profile and the fuel reserves for the "all-supersonic" design mission used in the engine-airframe matching studies are shown in figure 1. It is worth noting that even on this "all supersonic" basic mission about 20 to 25% of the total fuel is required for subsonic flight conditions and reserves. This, together with the necessity to revert to subsonic flight in the event of engine and/or pressurization failure, places great emphasis on efficient subsonic flight for any supersonic airliner.

The basic airplane characteristics used in the engine-airframe matching studies are shown in table 2. The size of the airplane (gross weight, wing area and payload) was fixed and range was allowed to vary as the figure of merit as different engine cycles and aerodynamics changes were evaluated. Wing span was also held constant and this meant a fixed value of engine thrust was required to meet the takeoff field length requirement. The reason wing area and/or span changes were not a part of the engine-airframe matching

studies is shown in figure 2. The 1971 Baseline SST's small wing area and relatively high span were carefully selected to achieve the smallest possible wing area consistent with community noise, approach speed and fuel volume constraints. Full span wing leading and trailing edge flaps plus a separate trimming tail surface provide good lift/drag ratios for takeoff and landing operations.

Effect of Supersonic Aerodynamic Improvements

The achievement of low supersonic drag, consistent with good subsonic and low speed performance characteristics, was an important design goal for the Baseline 1971 SST. Supersonic cruise lift-drag ratios of approximately 7.5 were validated. However, the need for much improved fuel efficiency led to re-evaluation of many aspects of the design. Trade studies were conducted to determine where increases in fuel efficiency could be made, i.e., where drag could be lowered even if the weight effect resulted in no range gain since this does result in less fuel consumed. As a result of these trade studies the following changes have been incorporated into the baseline airplane:

- . Modified wing planform with revised t/c distribution
- . Blended wing-body
- . Low-drag engine nacelle installation

Together, these changes have resulted in an improvement of about 20% in supersonic lift-drag ratio. The improvement in subsonic lift-drag ratio is only about 2%. The performance benefits of this large improvement in supersonic drag are shown in figures 3 and 4. Figure 3 shows the improvement in range and climb characteristics for the airplane powered by a variable-cycle engine. At a constant airframe weight, a range (and fuel usage) improvement of about 30% is achieved with an engine 20% smaller while maintaining adequate transonic thrust margins and time-to-climb capability. Not all of the weight effects are fully analyzed at this time but it is expected that not more than 25% of this range and fuel usage benefit will be offset by increased airframe weight. Figure 4 shows the effect on cruise efficiency. As expected, the 20% improvement in supersonic drag improves the supersonic cruise efficiency about 20%. However, the subsonic cruise efficiency was improved only about 3%, and even including the benefits of a 20% smaller engine size, the ratio of subsonic/supersonic cruise efficiency was lowered from 1.08 to 0.95. Since the objective was a ratio of 1.0, further improvement in subsonic cruise efficiency (either L/D or SFC) is desirable. It is worth noting that had the airplane not been powered by a variable-cycle engine, but rather the original dry turbojet which powered the 1971 SST, the ratio of subsonic to supersonic cruise efficiency would be much worse, about 0.68; i.e., the improvements in supersonic cruise efficiency brought about by airframe changes are made feasible by improvements in subsonic cruise efficiency brought about by a variable-cycle engine.

Effect of Engine Cycle Improvements

The variable cycle engine is one of the major technology advances that the SCAR program has brought forth. Both G.E. and P&WA, under separate contracts to NASA, have produced propulsion data for this type of engine. The effect of these engine cycle improvements on airplane performance have been determined, accounting for the important interactions between the airframe and the propulsion system. A goal of these studies was to develop an efficient airframe that would take advantage of the special characteristics of these engines, i.e., greatly improved subsonic fuel consumption characteristics.

General Electric Engines

The range and climb characteristics of two 1985 technology variable-cycle engines, the initial GE21/J11-B5 and a later improved version, the GE21/J11-B5B, are compared to a 1975 technology dry turbojet engine, the GE4/J6H2, in figure 5. The engines are installed on the blended wing-body configuration. The GE21/J11-B5 and -B5B are "low augmentor temperature rise" double bypass VCE's with 10% oversized front fan blocks, which permit high mass flow operation for takeoff and for subsonic cruise airflow matching. The -B5B variant has a lower bypass ratio and increased supersonic airflow compared to the -B5.

The initial -B5 variable cycle engine showed a substantial improvement in range (and fuel usage), about 12% relative to the GE4/J6H2; however, a larger engine size was necessary to meet the transonic climb thrust margin requirements.

The cruise efficiency characteristics of both engines are shown in figure 6. The initial -B5 variable cycle engine showed a much improved subsonic cruise efficiency, about 20%, and a small improvement in supersonic cruise efficiency, about 2%. The ratio of subsonic to supersonic cruise efficiency was improved from about 0.75 to about 0.85. Note that the larger engine size required to meet the transonic thrust margin degraded the subsonic/supersonic cruise efficiency ratio by about 4%.

Based upon this installed evaluation of the GE21/J11-B5 engine and upon their continuing cycle improvement studies, G.E. identified several areas of potential improvement which resulted in the -B5B variant. As shown in figure 5, the -B5B variant results in a large improvement in range (and fuel usage), about 22% relative to the GE4/J6H2 at a smaller engine size for maximum range. As shown in figure 6, the cruise efficiency characteristics of the -B5B variant are such that the ratio of subsonic to supersonic cruise efficiency has been improved from about 0.75 to about 0.86. Note that the smaller engine size of the -B5B offsets the decreased subsonic cruise efficiency due to a lower bypass ratio.

Pratt & Whitney Aircraft Engines

The range and climb characteristics of two 1985-1990 technology variable cycle engines, the VSCE-502B and VCE-112C, are compared to a 1975 technology duct-heating turbofan engine, the DHTF-C/D, in figure 7. The engines are installed on the blended wing-body configuration. The VSCE-502B is a variable-stream-control duct-heating turbofan engine while the VCE-112C is a tandem dry turbojet with a single rear valve. Both new engine concepts show a large range (and fuel usage) improvement, about 18%, relative to the 1975 DHTF-C/D at a smaller engine size for maximum range.

The cruise efficiency characteristics of all three engines are shown in figure 8. The two new variable cycle engines show substantial improvements in both supersonic and subsonic cruise efficiencies, about 16% and 12% respectively. The ratio of subsonic to supersonic cruise efficiency has been only slightly degraded from about 0.98 to about 0.96 and remains very close to the objective value of 1.0.

One important item of an efficient variable-cycle propulsion system is the nozzle. A variable flap ejector nozzle has been designed as a part of the SCAR program. This nozzle concept has the potential for high installed performance, particularly with regard to the boattail drag at subsonic cruise conditions. Reduced fuel consumption of up to 15% during subsonic cruise operations, appear possible compared to the auxiliary inlet ejector nozzle. While initial study results indicate no range benefit on the all-supersonic mission due to increased weight, the incorporation of this type nozzle into the variable cycle engines discussed above could be very desirable to achieve equal subsonic and supersonic cruise efficiencies.

Advanced Takeoff Systems and Procedures, Coannular Noise Effects

In the previous sections we have shown that small, light variable cycle engines can be integrated with a low supersonic drag airframe to produce a large improvement in range and hence in fuel consumption and economics. The question remained could low noise levels (FAR 36) be met with this engine-airframe combination.

Performance emphasis on the blended wing-body configuration was focused on takeoff and climbout at a gross weight of 340,200 kg (750,000 lb) with engines sized for best range, 318 kg/sec (700 lb/sec). Particular attention was given to estimating the jet noise at the FAR 36 sideline and community noise stations (noise sources other than jet noise have not yet been identified and quantified for these variable-cycle engines). Performance calculations and noise predictions were made for both the basic FAR takeoff and climbout procedures and also for a modified takeoff and climbout using advanced systems and procedures to minimize noise (table 3). The basic jet noise prediction utilized the method from reference 1 for maximum noise level. Directivity angle effects are based upon current Boeing test data. The SAE procedure does not predict the observed co-annular noise reduction effect

associated with the variable-cycle inverted jet velocity profile. Co-annular noise reduction increments from SAE prediction levels based upon P&WA, G.E. and Boeing test data to date are about 7 EPNdB at takeoff power setting at the sideline, to 5 EPNdB or EPNdB at the community, depending upon the power setting. Co-annular noise reduction increments from SAE are less at cutback than for sideline since the peak noise angle at cutback occurs near 90° instead of 140° for the sideline case. Each of the variable cycle engines discussed previously would benefit from the co-annular effect.

The effect on sideline and community levels of using advanced takeoff procedures and systems compared to current FAR 35 procedures is shown in figure 9. The crosshatched area shows the reduced noise levels after the co-annular effects have been applied. These data show that using FAR 36 rules and an engine thrust to achieve a takeoff field length of 3660 m (12,000 ft) the SAE prediction methods gives a sideline noise level of 117 EPNdB and a community noise level of 120 EPNdB. Co-annular benefits reduce the levels to 109 and 115 for the sideline and community respectively. Hence the co-annular effect can reduce sideline noise to FAR 36 "traded" noise levels with a small, cruise-sized variable cycle engine. However, the community noise level is much too high. These data also show that by using advanced systems and procedures to minimize community noise the community noise level can be reduced to only 105 EPNdB (including the co-annular benefit). This advanced takeoff and climbout involves:

- . Maximum thrust (within sideline noise constraints) during ground roll, taking advantage of ground shielding
- . Thrust reduction during climb (programmed throttles) to control sideline noise
- . Flap retraction during climb (programmed flaps) for better lift/drag ratio.
- . Acceleration during climb to improve lift-drag ratio
- . Cutback at community to less than 3 engine level flight thrust. If an engine fails at this point, APR automatically increases thrust to level flight power setting.

Note that the takeoff field length has been decreased from 3660 m (12000 ft) to 3200 m (10500 ft) since power has increased during the ground roll to take advantage of ground shielding. An alternate procedure is shown to minimize sideline noise. Here power is reduced during ground roll consistent with a takeoff field length of 3660 m (12000 ft). Sideline noise is reduced 4 EPNdB. This will result in less acceleration to the community, a lower lift-drag ratio and more noise at cutback, about 5 EPNdB. These data show that advanced takeoff procedures and systems have the potential to achieve community noise levels below FAR 36 and can provide flexibility to trade sideline and community noise levels to suit individual airport requirements.

CONCLUDING REMARKS

The NASA Supersonic Cruise Aircraft Research (SCAR) program has led to the identification of many technology advances which, if pursued, will make possible a much improved Supersonic Cruise Airliner. In particular, the integration of the technology advances in the areas of supersonic aerodynamics, variable-cycle engines, advanced takeoff procedures and systems, and co-annular noise effects through careful engine-airframe matching studies on a well validated baseline configuration has led to a configuration with greatly improved range, fuel consumption, economics and "off-design" characteristics.

REFERENCE

1. Jet Noise Prediction Aerospace Information Report No. 876A, Society of Automotive Engineers, July 10, 1965.

TABLE 1.- OBJECTIVES AND CONSTRAINTS

• CRUISE SPEED		M = 2.2 TO 2.7
• RANGE	NORTH ATLANTIC + INLAND CITIES	≈ 7041.4 km (3,800 nmi)
	PACIFIC	≈ 8338.5 km (4,500 nmi)
• PAYLOAD	NO. OF PASSENGERS	180 TO 360
• TAKEOFF FIELD LENGTH (SL, STD +10°C)		3657.6 m (12,000 ft)
• WING AREA		} AS SMALL AS POSSIBLE
• ENGINE SIZE		
• COMMUNITY NOISE		LOW
• CLIMB PERFORMANCE	TRANSONIC THRUST MARGIN	0.30
	TIME TO CRUISE, HRS	0.75
• CRUISE PERFORMANCE	<u>SUBSONIC RANGE FACTOR</u> <u>SUPERSONIC RANGE FACTOR</u>	1.0

TABLE 2.- AIRPLANE CHARACTERISTICS

TOGW = 340,200 kg (750,000 lb)	}	FIXED SIZE AND PAYLOAD, RANGE IS THE FIGURE OF MERIT
PAYLOAD = 273 PASSENGERS		
WING AREA = 715 m ² (7700 ft ²)		
OEW LESS ENG = 123,340 kg (271,920 lb)		
TOFL = 3,660 m (12,000 ft) (SL, STD + 10 ⁰ C)		
F _{NREQ.} = 198,000 N (44,500 lb) (SL, STD + 10 ⁰ C)		

TABLE 3.- ADVANCED TAKEOFF SYSTEMS AND PROCEDURES

SYSTEM/ PROCEDURE	APPLICATION	PURPOSE	ADVANTAGES
PROGRAMMED THROTTLES	AUTOMATIC THROTTLE MODULATION DURING TAKEOFF AND CLIMB	TAKING ADVANTAGE OF GROUND SHIELDING TO INCREASE THRUST DURING GROUND ROLL	HIGHER ALTITUDE AND/OR SPEED AT COMMUNITY, SHORTER FIELD LENGTH
PARTIAL FLAP RETRACTION	AUTOMATIC PARTIAL FLAP RETRACTION DURING INITIAL CLIMB	IMPROVE CLIMBOUT LIFT / DRAG RATIO	HIGHER ALTITUDE AND L/D AT COMMUNITY, LOWER CUTBACK POWER SETTING
CLIMB ACCELERATION	TRADE CLIMB CAPABILITY FOR ACCELERATION	IMPROVE L/D AT THE EXPENSE OF COMMUNITY ALTITUDE	HIGHER L/D AT COMMUNITY, LOWER CUTBACK POWER SETTING
AUTOMATIC PERFORMANCE RESERVE (APR)	AUTOMATIC INCREASE IN THRUST AFTER ENGINE FAILURE	ALLOWS LOWER 3 ENGINE CUTBACK POWER SETTINGS	LOWER CUTBACK POWER SETTING

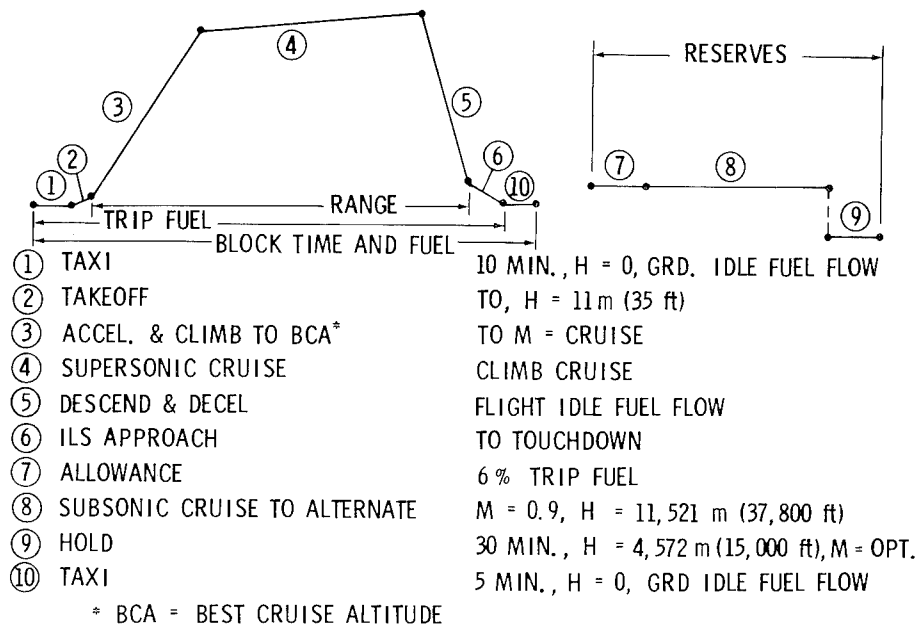


Figure 1.- Flight profile and reserves.

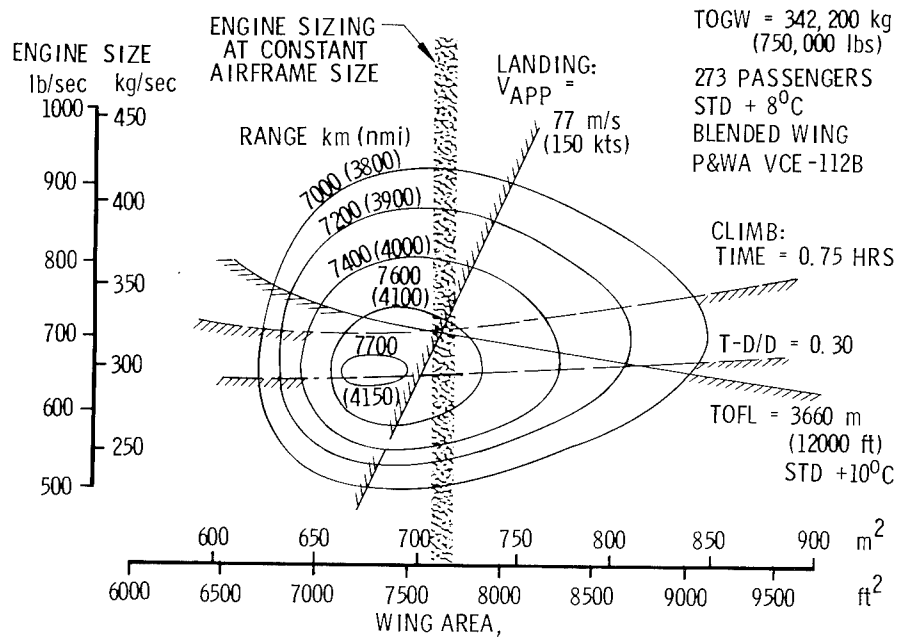


Figure 2.- Engine/airframe matching.

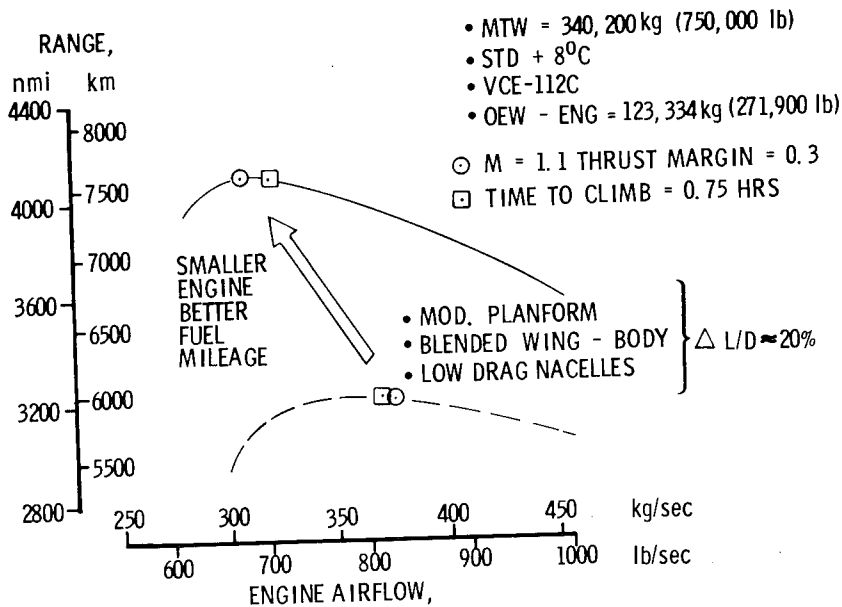


Figure 3.- Effect of supersonic aerodynamic improvements on range and climb characteristics.

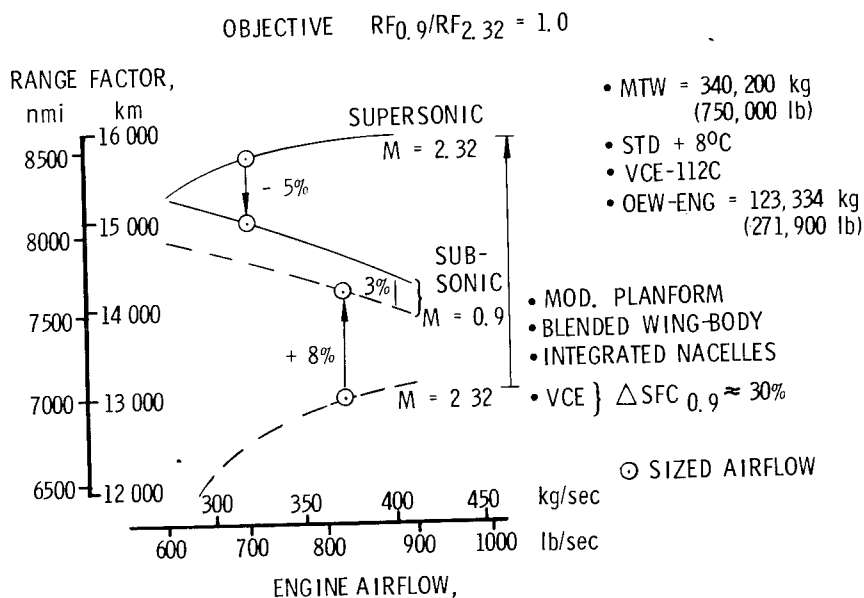


Figure 4.- Effect of supersonic aerodynamic improvements on cruise efficiency characteristics.

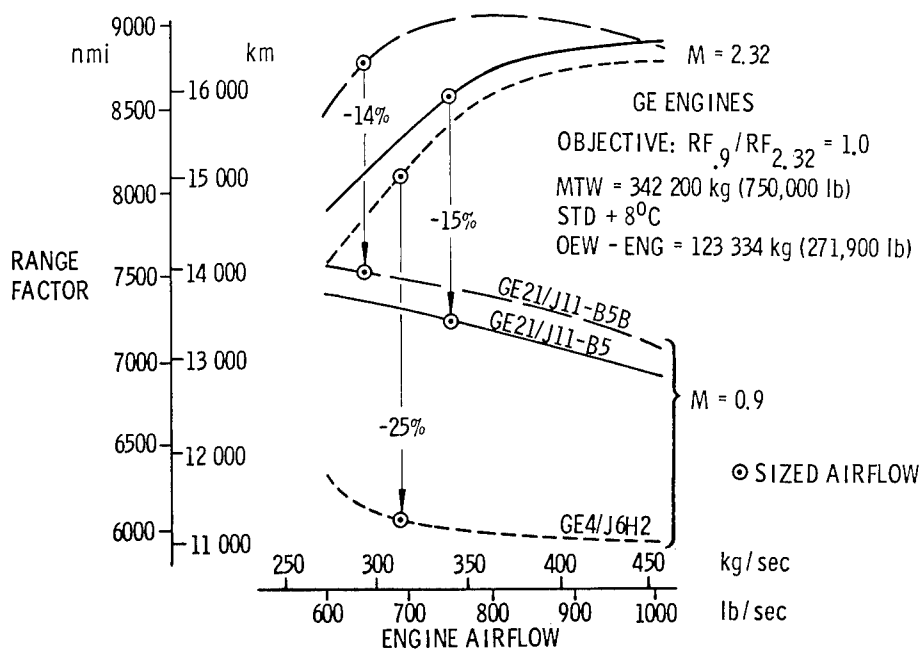


Figure 5.- Effect of engine cycle improvements on range and climb characteristics for GE engines.

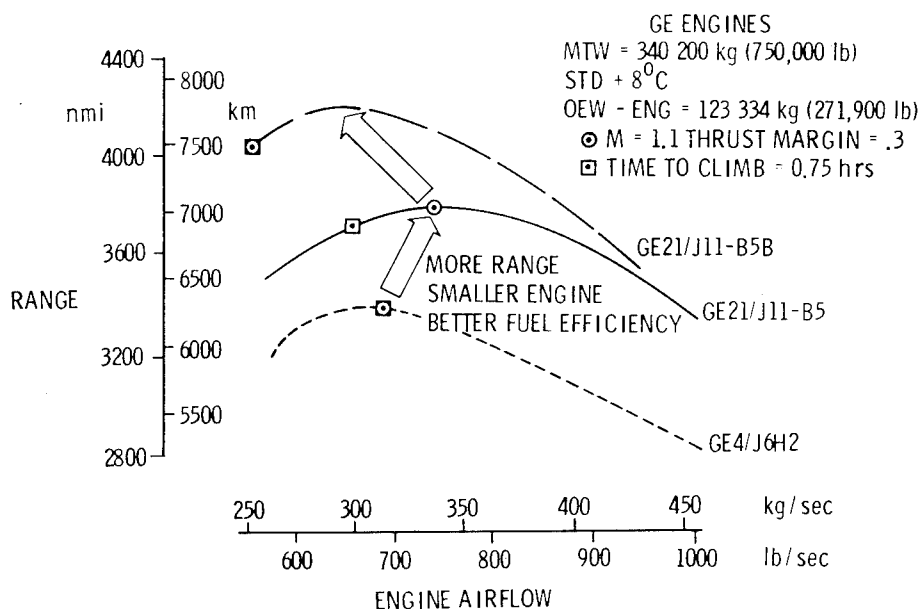


Figure 6.- Effect of engine cycle improvements on cruise efficiency characteristics for GE engines.

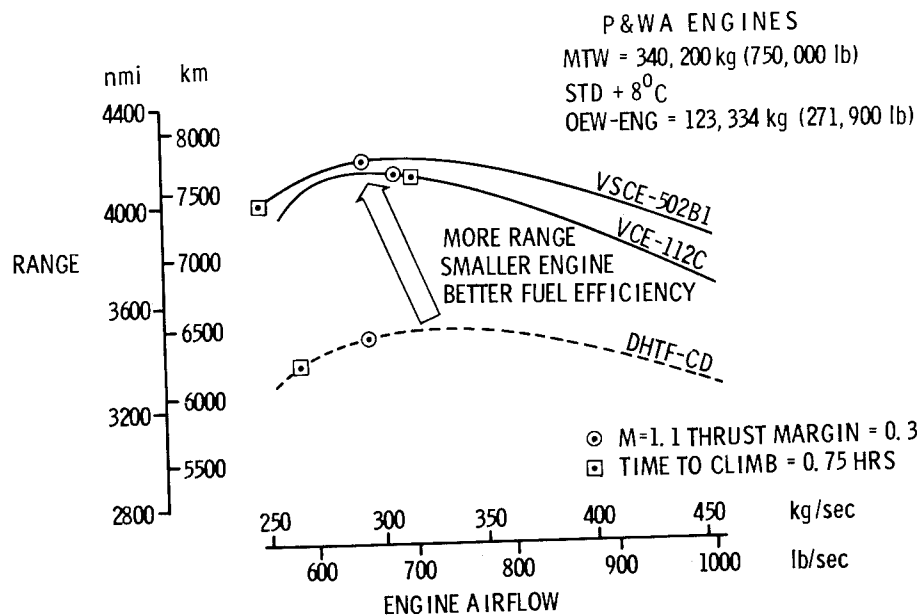


Figure 7.- Effect of engine cycle improvements on range and climb characteristics for P&WA engines.

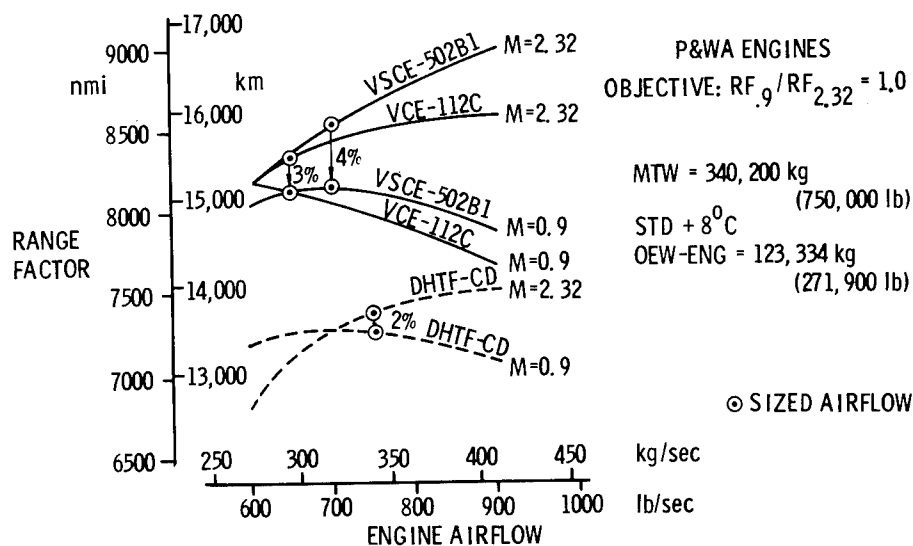


Figure 8.- Effect of engine cycle improvements on cruise efficiency characteristics for P&WA engines.

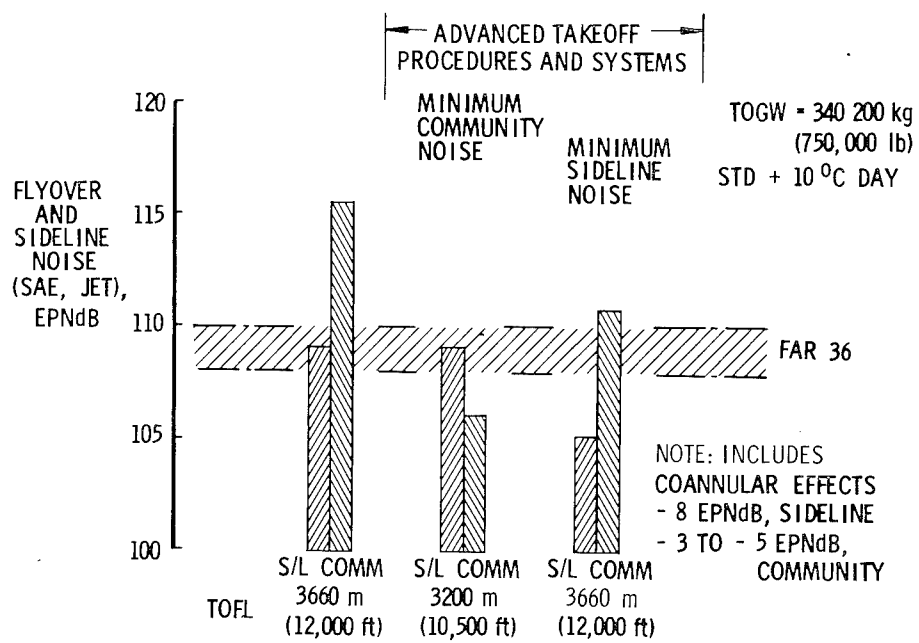


Figure 9.- Effect of advanced takeoff procedures and systems.

DESIGN FEASIBILITY OF AN ADVANCED TECHNOLOGY

SUPERSONIC CRUISE AIRCRAFT

William T. Rowe
McDonnell Douglas Corporation

SUMMARY

Research and development programs by McDonnell Douglas, including both NASA contracted support and company-funded activities, provide confidence that technology is in-hand to design an economically attractive, environmentally sound supersonic cruise aircraft for mid-1980 world-wide commercial operations. The principal results of studies and tests are described including those which define the selection of significant design features. These typically include the results of (a) wind-tunnel tests, both subsonic and supersonic, (b) propulsion performance and acoustic tests on noise suppressors, including forward-flight effects, (c) studies of engine/airframe integration, which lead to the selection of engine cycles/sizes to meet future market, economic, and social requirements, and (d) structural testing.

INTRODUCTION

For four years, McDonnell Douglas (MDC), with both company funds and NASA contracted support, has been conducting advanced supersonic technology application studies, advanced supersonic technology engine integration studies, and development testing. This effort has been to substantiate that the design of an economically attractive, environmentally sound supersonic cruise aircraft for world-wide commercial operations is feasible for the mid-1980 time period.

Three years ago a conceptual baseline supersonic cruise aircraft was designed to evaluate technology problems. The conclusion is that it is now possible to design an advanced technology transport. The technology remaining to be validated consists of completing concentrated efforts to optimize configuration and to accomplish development testing in time for major program decisions.

MDC is continuing the necessary studies and testing to that extent possible with available funding. This paper summarizes some of the results of the advanced design studies which define significant configuration features, wind-tunnel test results, propulsion performance and acoustic testing of mechanical noise suppressors, structural tests, and engine/airframe integration studies.

SYMBOLS

Al	Aluminum
B	Body (Fuselage)
c.g.	Center of Gravity
C_D	Drag Coefficient
DOC	Direct Operating Costs
FAR Part 36	Federal Aviation Regulation for Noise
H	Horizontal Tail
L/D	Lift-Drag Ratio
$(L/D)_{\max}$	Maximum Lift-Drag Ratio
M	Mach Number
SIC	Structural Influence Coefficient
Ti	Titanium
W	Wing
V	Vertical Tail

Technology Evaluation

Four years ago MDC conducted technology assessment studies to determine the feasibility of designing an improved supersonic cruise aircraft. An advanced design team involving the major disciplines (i.e., active controls, aerodynamics, propulsion, structures, materials, acoustics, airport compatibility, economics, etc.) was assigned this task. Analytical tools and experimental data have been used to parametrically derive candidate configurations.

Preliminary designs were completed for configurations at 2.2, 2.7, and 3.2 Mach numbers. These designs included sufficient detail analysis so that the direct operating cost (i.e., overall efficiency) of each design could be determined. The results (fig. 1) show that as the design Mach number increases, the direct operating cost increases rapidly. Also shown is that for an all metal airplane, a mix of titanium and aluminum materials provides the optimum design at the lower Mach numbers and that an all-titanium structure is required to survive

the 2.7 M environment. The increase in the relative direct operating cost between the 2.2 and 2.7 Mach cases is 13 percent. The 2.2 Mach cruise region was selected for further technology evaluation and refinement studies. In 1975 the original study was repeated with greater design depth, including material allowables at each Mach number, thermal stresses, consistent aeroelastic constraints, and flutter fixes. Results again validate the 2.2 Mach speed selection as shown in figure 1.

Figure 2 summarizes the results of the advanced design study in terms of technology risk at each Mach number. In the 2.2 Mach region, the majority of the technologies are in the low risk area. This chart depicts the general variation in technology risk, by discipline, as Mach number increases. These relationships are developed from pertinent technical knowledge gained from over twenty-two years of continuous design, development, production and operation of supersonic fighters and test aircraft, including the D-558-II, X-3, F-101, F5D-1, F-4, and F-15. For a new commercial supersonic aircraft, McDonnell Douglas can see no advantages in departing from the low risk 2.2 Mach number type design.

Baseline Definition

To assess the technology, a 2.2 Mach advanced supersonic cruise point design (baseline) airplane has been defined. The target date for initiation of commercial operation was found to be feasible for the mid-1980's. The analysis and detail design integration is of sufficient depth to identify the geometric features, structural arrangement and concepts, materials, acoustic treatment, systems and sub-systems.

Table I shows the characteristics summary for the baseline airplane. The fuselage is sized for 273 passengers with 15 percent first class and 85 percent economy class accommodations. Engines are mini-bypass turbojets with mechanical suppressors, sized for take-off at less than or equal to FAR Part 36 requirements, compatible with the near-term 1986 time period. Examples of advanced technology application are the incorporation of the arrow-type wing with geometry tailored to optimize performance and weight, use of area-ruled fuselage in combination with arrow wing and placement of engines to minimize wave drag, selection of optimum mix of metals and optimization of structural parameters (strength, fail-safe, aeroelastics, and flutter), and incorporation of acoustic treatment to meet environmental requirements. Single nacelles incorporating axisymmetric inlets were selected for this baseline after careful trade-off studies of options such as dual pods and two-dimensional inlets.

AERODYNAMICS

The advanced technology arrow wing is capable of producing significantly higher lift-drag ratios (L/D) than the delta planforms considered for the early supersonic transports (ref. 1). To validate this improved L/D in an integrated

configuration, a MDC-NASA cooperative wind-tunnel test program was conducted. Figure 3 shows the model in the Ames test facility. The model was instrumented to obtain force and pressure data simultaneously. Some of the results were published in reference 2 and presented earlier in these proceedings (ref. 3). Figure 4 shows a summary of the test results at 2.2 Mach compared with the design point analysis. Also shown is the revised design goal based on possible improvements identified and the $(L/D)_{\max}$ values used for the 2.2 Mach speed study validation. This correlation provides confidence that the analytical methods are sufficiently accurate for the necessary aerodynamic design of an improved supersonic cruise aircraft.

The wind-tunnel program also investigated both external compression and mixed compression inlets as defined in reference 4. Results of an integration study based on the tunnel data are shown in figure 5. The mixed compression inlet provides a 2 percent range improvement and is being adopted as part of the baseline configuration.

Wing-fuselage blending has been studied as applied to the baseline configuration for possible $(L/D)_{\max}$ improvement. A blended configuration, which minimizes fuselage volume to the point where a minimally integratable configuration remained, is developed and analyzed. The 2.2 Mach number area-averaged-body area distributions are shown in figure 6 along with a summary of the aerodynamic analysis. The skin friction and wave drag are reduced; however, the larger wing to fuselage fillet results in an increase in the drag due to lift at the cruise lift coefficient. The resulting 1.2 percent improvement in $(L/D)_{\max}$ is not as significant as has been reported from delta-wing-fuselage blending results. This occurs because a substantial reduction in peak cross-sectional area cannot be achieved with a carefully designed arrow-wing configuration. Because of the location of the wing main torque box the blending required to achieve integration of the wing spar to fuselage frame structure is aft of the maximum area peak.

In the low speed/high lift area MDC is providing the aerodynamic design for a NASA model as depicted in figure 7. This model is scheduled for testing during 1977 and is expected to provide much valuable aerodynamic data on leading edge devices and flaps.

STRUCTURES AND MATERIALS

To insure a reliable structure for commercial operation, an all-metal aluminum and titanium structure is considered for the near term (1980 go-ahead) design. The baseline materials, distribution of materials and possible construction methods are summarized in figure 8. This concept has recently been validated by another in-depth study. Study details are summarized in reference 5. The conclusion in the structural area is that large-scale technology development of manufacturing and long term testing of the titanium concepts must be initiated immediately in order that results may be available in time to support near-term program decisions.

Current company-funded efforts at MDC consist of fabrication and testing of panels of aluminum brazed titanium honeycomb representative of the wing design as shown in figure 9 and of a typical lower fuselage panel of weld-brazed titanium skin and stringers as shown in figure 10. Unfortunately, these programs are not of sufficient scope to identify the degree of risk such designs pose for selection on a near-term commercial supersonic aircraft.

EXHAUST NOZZLE SUPPRESSOR TESTING

Nozzle/suppressor/reverser configurations have been designed which integrate with the turbojet and mini-bypass turbojet engines. Since noise constraints are so critical to engine sizing and to final engine cycle selection, MDC has concluded that the mechanical suppressor development is a critical backup development item in the technology assessment program. It is recognized that coannular suppression is possible but its development and the applicable variable cycle engine to which it can be adapted is considered to be applicable only to a 1985 go-ahead program which may not be soon enough to match customer demand.

To initiate the validation testing for the nozzle/suppressor, MDC has fabricated 12 separate nozzle designs and has completed the propulsion performance testing. Excellent results have been obtained. One of the nozzles which produced a higher nozzle velocity coefficient than observed from previous test programs is shown in figure 11. Also shown in the figure is a smaller scale version of the same nozzle which is currently in test on the Rolls-Royce spin rig at Filton (fig. 12). This acoustic testing is to measure acoustic results on the spin rig to simulate forward flight effects. Also, additional tests are scheduled for the same design in the NASA Ames 40-foot by 80-foot tunnel during 1977.

ENGINE/AIRFRAME INTEGRATION

McDonnell Douglas has found it necessary to perform a rather detailed integration of the emerging advanced technology engine cycles for possible supersonic cruise vehicle application. Engine sizing for cruise must be carefully balanced with take-off noise constraints. Also, a comparison of uninstalled specific fuel consumption is not realistic as installation losses vary from engine to engine, and more importantly, not all engine cycles optimize cruise at $(L/D)_{\max}$.

The procedure used by MDC for engine/airframe integration is outlined in figure 13. Initial sizing is established by FAR Part 36 noise requirements. After engine packaging is complete, a detailed configuration integration is accomplished where tail clearance, landing-gear length, flap clearances, pylon design, and structural and aerodynamic trades are made. The early engine integration work, including the dual valve and the early duct heating turbofan engines, has been reported in reference 6.

Figure 14 presents the detailed model which is used to complete the structural analysis. As shown in the example, for the new engine weight and c.g. location,

the analysis calculates the size of each element for five loading conditions and then integrates to determine the wing and fuselage weight change. For those cases where significant changes are identified, a flutter check is included in the analysis.

Table II presents a summary of wave drags for typical configurations to illustrate the depth of detail involved in the aerodynamic analysis.

The final integration results where the candidate engine is evaluated in terms of range improvement are illustrated in figure 15. Range is plotted against engine airflow (engine size) so that the initial engine size can be modified if a larger engine than that sized for noise constraints is shown to provide maximum range. The advanced technology engines provide range improvements as high as 20 percent over the baseline airplane.

CONCLUSION

Design of an advanced supersonic cruise vehicle is now technically feasible. An expanded and accelerated development program to include the items listed in table III is needed to provide a 1980 go-ahead which could provide an operational airline transport by the mid-1980's.

REFERENCES

1. FitzSimmons, R. D.; and Roensch, R. L.: Advanced Supersonic Transport. SAE Paper No. 750617.
2. Radkey, R. L.; Welge, H. R.; and Roensch, R. L.: Aerodynamic Design of a Mach 2.2 Supersonic Cruise Aircraft. AIAA Paper No. 76-955.
3. Roensch, R. L.: Aerodynamic Validation of a SCAR Design. Proceedings of the SCAR Conference, NASA CP-001, 1977. (Paper 8 of this compilation.)
4. Welge, H. R.; and Henne, P. A.: Nacelle Aerodynamic Design and Integration Study on a Mach 2.2 Supersonic Cruise Aircraft. Douglas Paper No. 6461, presented to AIAA/SAE 12th Propulsion Conference, Palo Alto, California, July 1976.
5. Fischler, J. E.: Structural Design of a Supersonic Cruise Aircraft. Proceedings of the SCAR Conference, NASA CP-001, 1977. (Paper 43 of this compilation.)
6. FitzSimmons, R. D.; and Rowe, W. T.: AST Propulsion Comparisons. SAE Paper No. 750631.

TABLE I.- BASELINE CHARACTERISTICS SUMMARY

GROSS WEIGHT — kg (LB)	340,200 (750,000)
WING AREA — m ² (FT ²)	929 (10,000)
PLANFORM	ARROW WING
PASSENGERS	273
CRUISE SPEED (MACH)	2.2
L/D AT CRUISE	9.6
RANGE — km (N MI)	8500 (4590)
ENGINES	4 MINI-BYPASS TURBOJET*
SFC AT CRUISE — kg/HR/N (LB/HR/LB)	0.138 (1.35) (INSTALLED)
THRUST/ENGINE MAX — N (LB)	332,300 (74,700)
NOISE	< FAR PART 36
STRUCTURAL MATERIAL	70 PERCENT TITANIUM 30 PERCENT ALUMINUM
TAKEOFF FIELD LENGTH — m (FT)	3260 (10,700)
LANDING FIELD LENGTH — m (FT)	1725 (5650)

* ARBITRARY

TABLE II.- EFFECT OF ENGINE ON WAVE DRAG

ENGINE	ZERO LIFT WAVE DRAG ($C_{D0} \times 10^4$)	CHANGE FROM BASELINE ($\Delta C_{D0} \times 10^4$)
BASELINE DRY TURBOJET	26.80	—
GENERAL ELECTRIC MINI-BYPASS	23.88	—2.92
PRATT & WHITNEY 502 B	22.30	—4.50
GENERAL ELECTRIC DB/VCE	22.30	—4.50

TABLE III.- RECOMMENDED NASA TECHNOLOGY

TOP PRIORITY ITEMS

2.2 MACH

- INTEGRATED NOZZLE/SUPPRESSOR/REVERSER
NOISE AND PROPULSION TESTS
- LARGE SCALE TITANIUM HONEYCOMB TESTS (WING)
- LARGE SCALE TITANIUM STIFFENED SKIN TESTS (FUSELAGE)
- COMPREHENSIVE TESTING OF ARROW WING
AERODYNAMICS — CLEAN WING
- LOW SPEED VALIDATION TESTING
- INLET TESTS — PERFORMANCE AND CONTROLS
- ELEVATED TEMPERATURE — TIME TESTING
ALUMINUM AND EPOXY COMPOSITES
- FLUTTER MODEL TESTING

PLUS

ENGINE TESTS

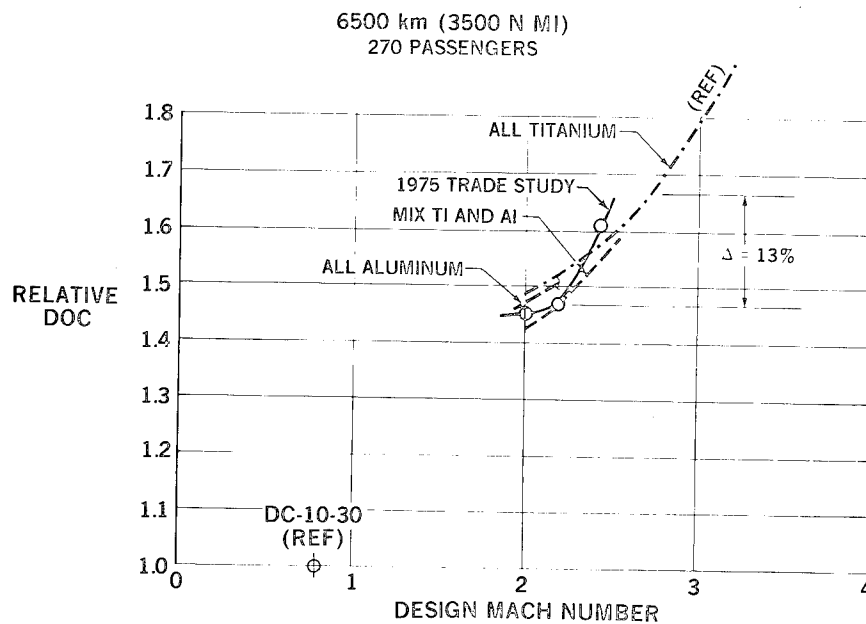


Figure 1.- Effect of design speed on DOC.

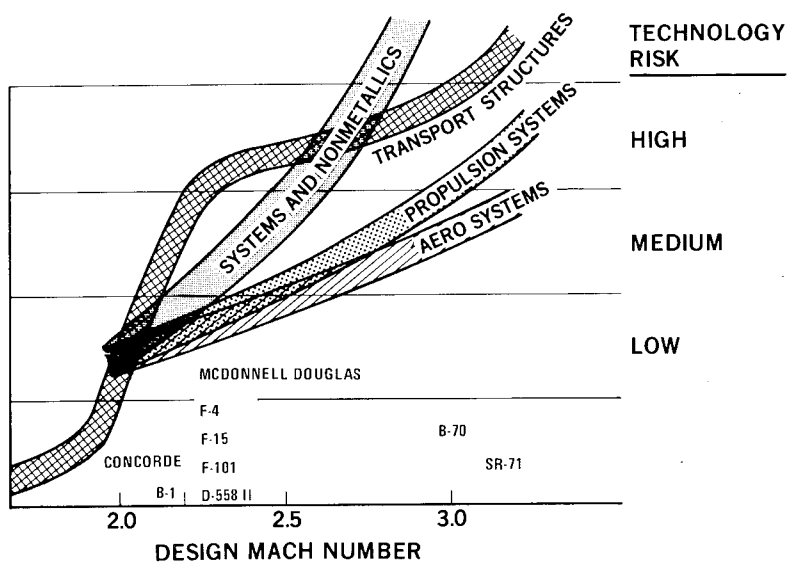


Figure 2.- Technology assessment.

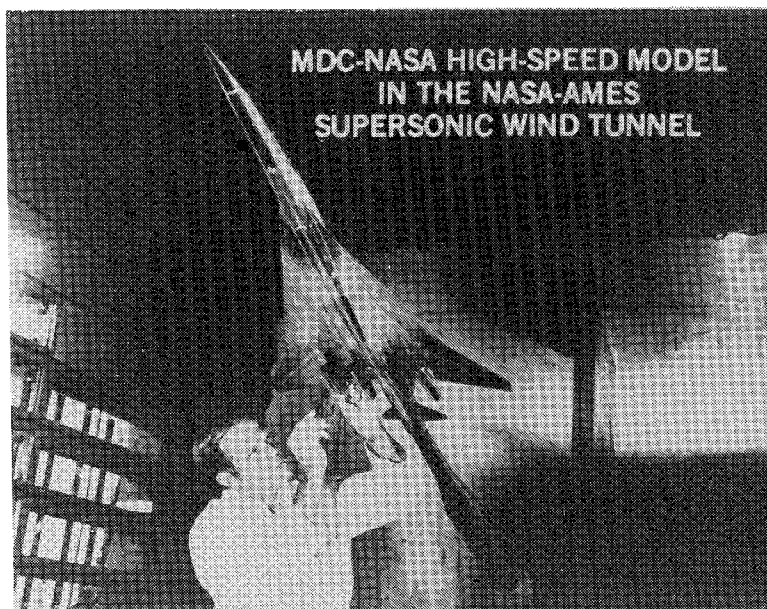


Figure 3.- MDC-NASA high-speed model in the NASA-Ames supersonic wind tunnel.

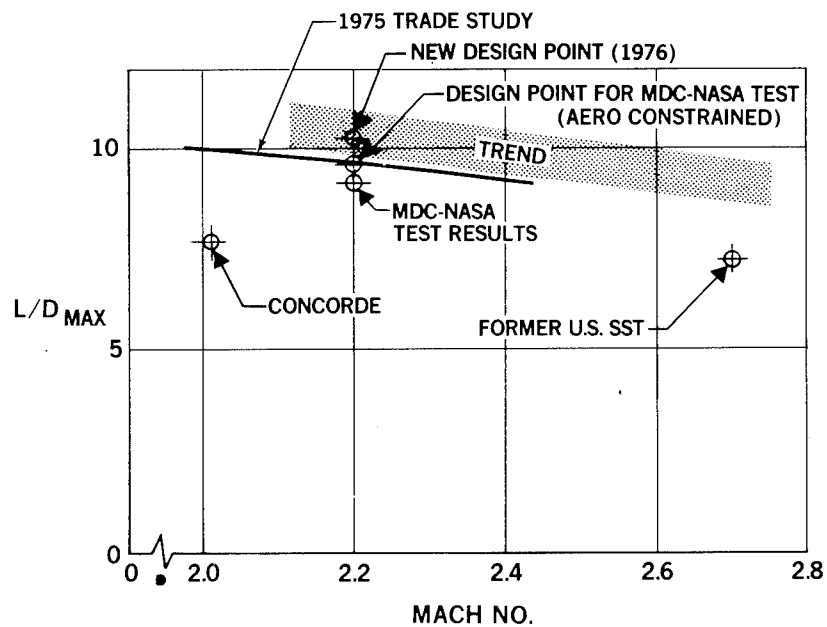


Figure 4.- Aerodynamic efficiency.

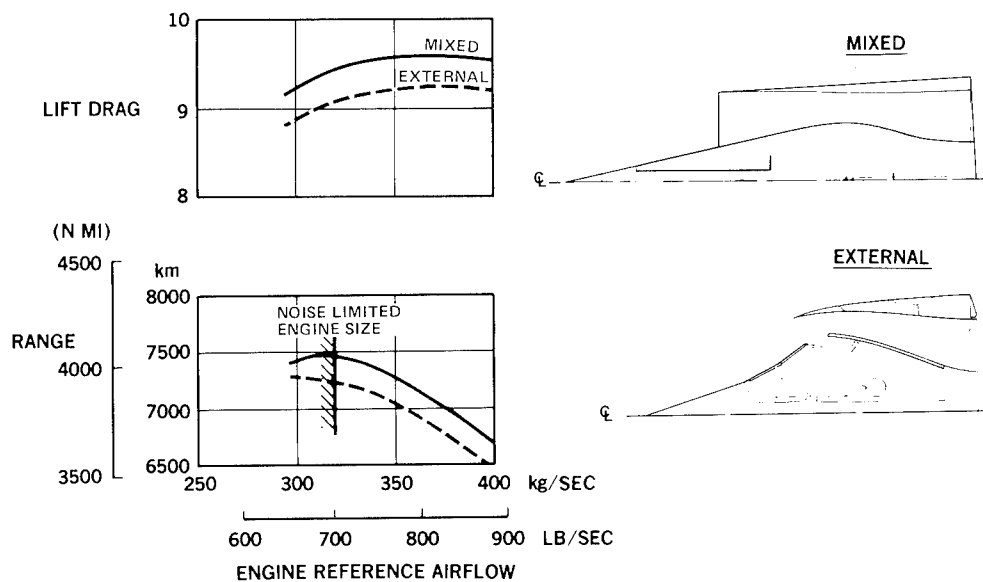


Figure 5.- Effect of mixed and external compression inlets on performance.

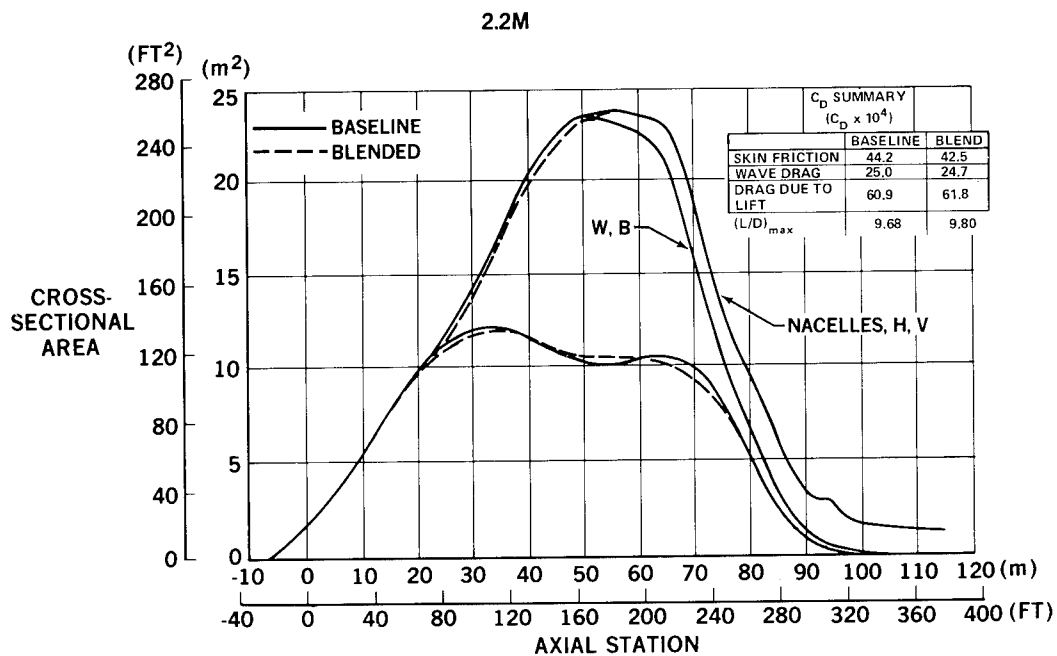


Figure 6.- Area-averaged-body area distributions.

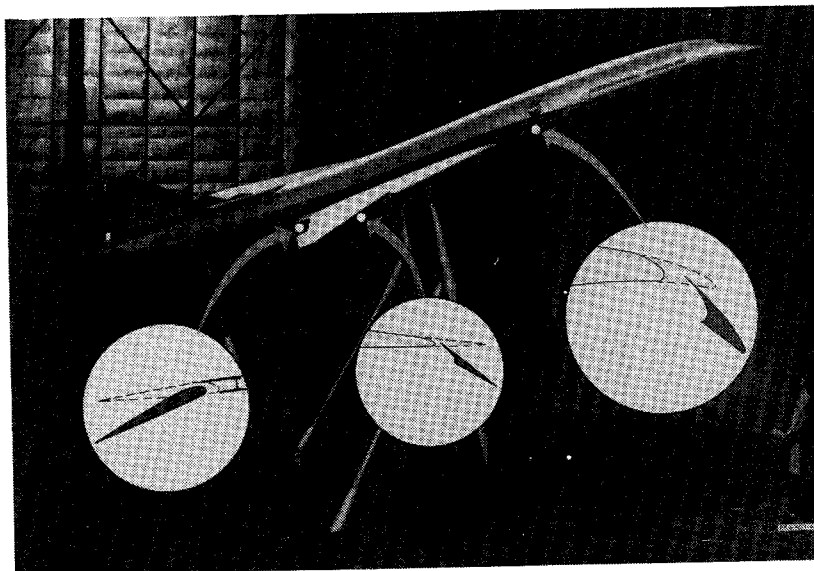


Figure 7.- Artist's rendering of NASA low-speed model.

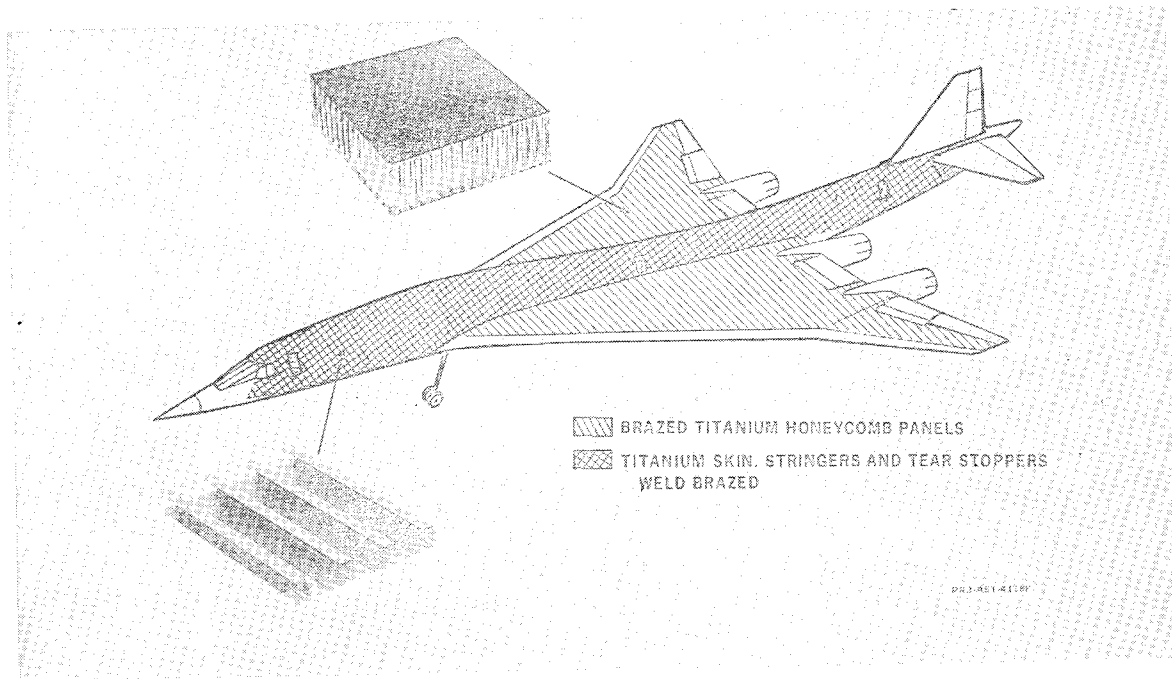


Figure 8.- Baseline materials and constructions.



Figure 9.- Aluminum brazed titanium honeycomb panel.

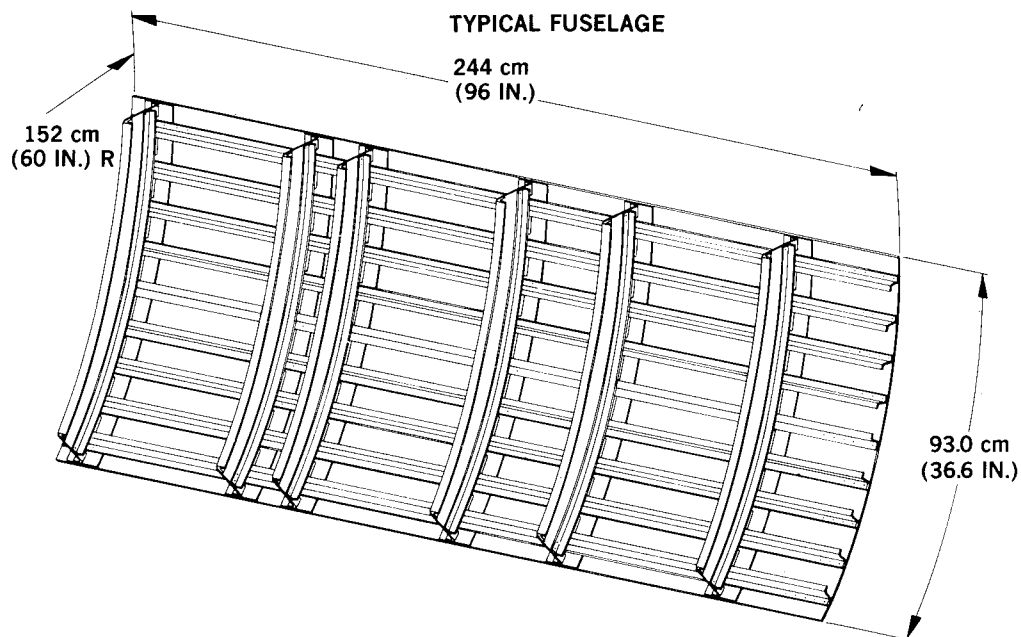


Figure 10.- Weld-brazed titanium panel.

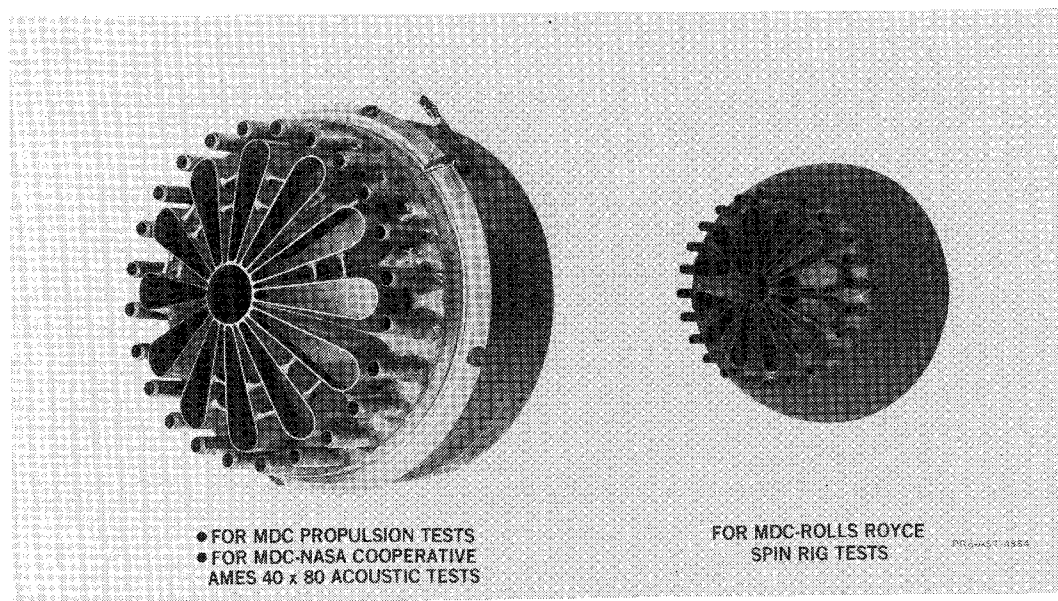


Figure 11.- Mixer nozzle for nozzle/suppressor/reverser design of MOC baseline.

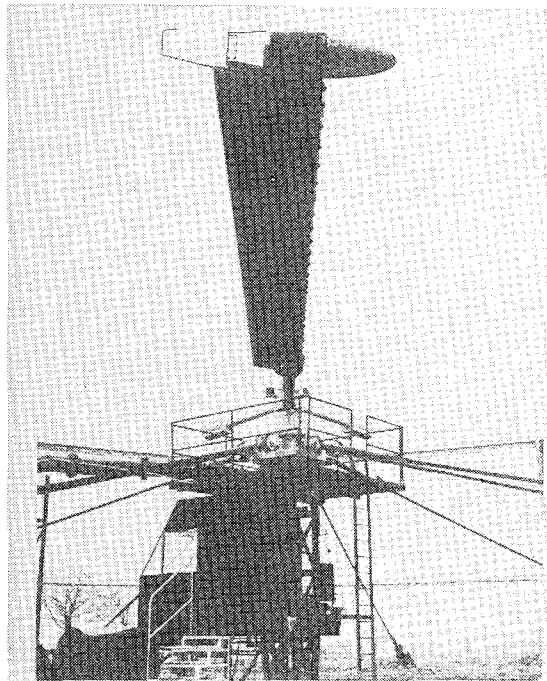


Figure 12.- Rolls-Royce acoustic test facility.

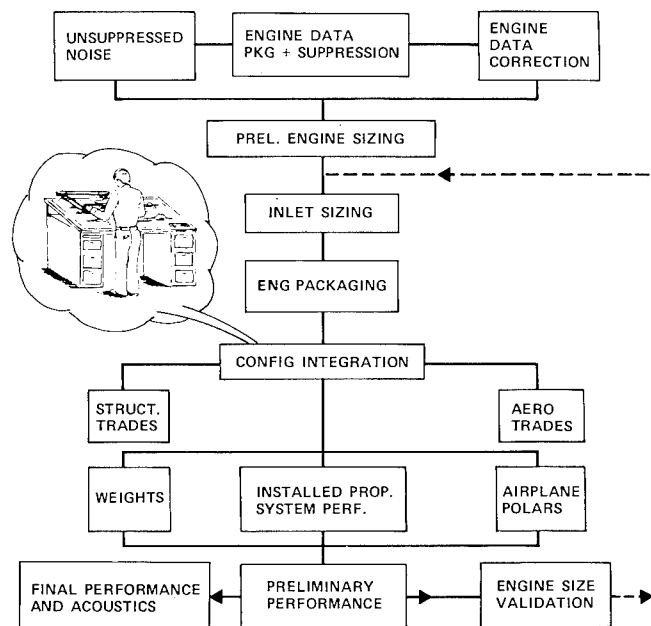


Figure 13.- Engine integration.

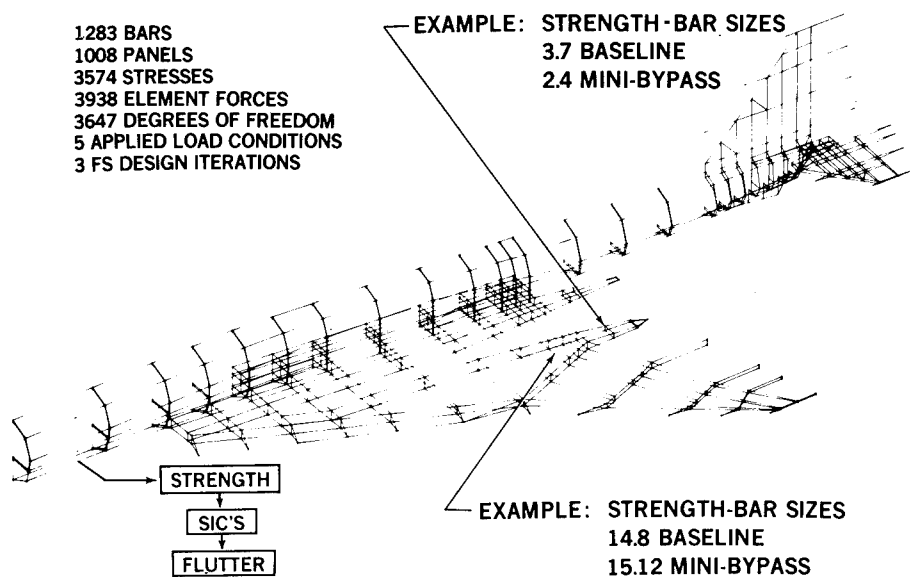


Figure 14.- Typical structures analysis.

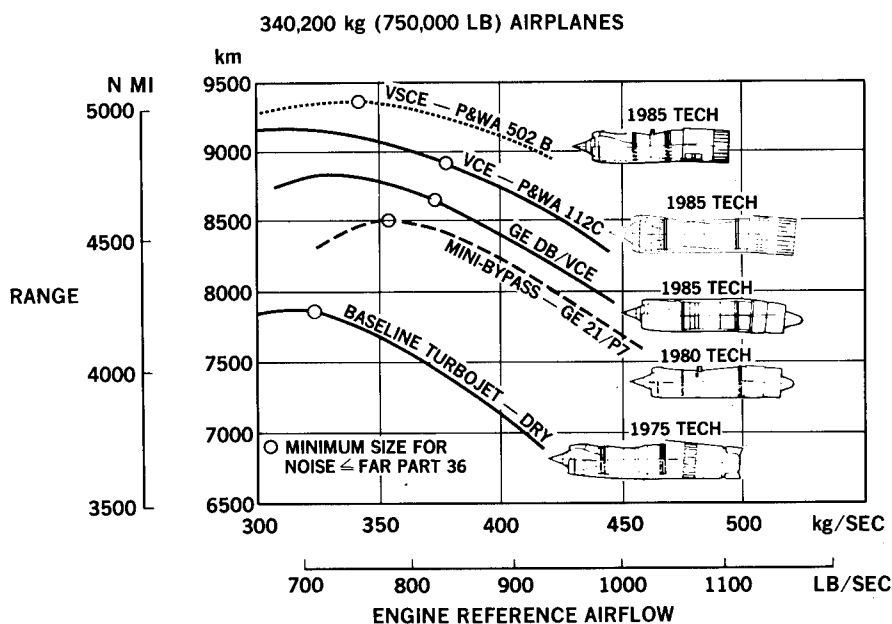


Figure 15.- Engine cycle selection.

STRUCTURAL DESIGN OF SUPERSONIC CRUISE AIRCRAFT

J. E. Fischler
McDonnell Douglas Corporation

SUMMARY

The supersonic cruise aircraft structures efforts have been supported by NASA-contracted studies, reference 1, and McDonnell Douglas-funded research and testing. The major efforts leading to an efficient structural design include (a) the analysis methods used to improve the structural model optimization and compare the structural concepts; (b) the analysis and description of the fail-safe, crack growth, and residual strength studies and tests; (c) baseline structural trade studies to determine optimum structural weights including effects of geometry changes, strength, fail-safety, aeroelastics and flutter; (d) comparison of British, French, and United States aluminum alloys with 6AL-4V annealed titanium in structural efficiency after 70 000 hours at temperature; (e) the study of three structural models for aircraft at 2.0 Mach, 2.2 Mach, and 2.4 Mach cruise speeds; (f) the study of many structural concepts to determine their weight efficiencies; and (g) the determination of the requirements for large-scale structural development testing.

INTRODUCTION

The highlights of the McDonnell Douglas structural study results are presented herein. This includes extensive Company-funded efforts to improve the analytical methodology for use in preliminary design activities. The system studies represent work supported by NASA during the 1973 to 1976 period and Company-funded efforts for research and development for a longer period. An arrow wing has presented a structural design challenge for over a decade. Early studies indicated large weight penalties to solve the aeroelastic and flutter problems. The thin wing, high aspect ratio, thermal stresses and thermal degradation of the materials from the long life at temperature were all important considerations in the design selection process that lead to the use of high percentages of titanium in spite of the higher material and fabrication costs. Direct operating cost studies substantiated the titanium selections. The strength, fail-safe, aeroelastic, and flutter optimization methods developed have enabled McDonnell Douglas to achieve cost effective structure for the 2.2 Mach number selected for the baseline design. With a substantial structural development program in titanium and to a lesser degree in aluminum, the structural integrity can be insured for an early design go-ahead. A longer development period is required for the introduction of composites because minimum time temperature experience is available.

STRUCTURAL ANALYSIS METHODOLOGY

The structural optimization process used by McDonnell Douglas for the supersonic cruise vehicle has a long history of development. In the late 1940's, McDonnell Douglas developed a matrix method of structural analysis (see reference 2). Continued development, with some help from the Air Force Flight Dynamics Laboratory, reference 3, has enabled McDonnell Douglas to create FORMAT, a Fortran Matrix Abstraction Technique. This system has been the foundation for structural analysis development. In the early 1970's at McDonnell Douglas it was formally recognized that the Advanced Design needs are different than Production Design. Drastic reductions in elapsed time for obtaining accurate structural information in the Advanced Design of a supersonic cruise vehicle were required. Improved methods were developed which resulted in the following operational programs and procedures for the supersonic cruise aircraft design activities today:

- A structural optimization program, reference 4, has been developed which uses many options to speed up the resizing process and obtain accurate results. By using combined allowables with the best element representation, the weight for strength is more accurately predicted early in the design phase.

The various types of structural models used for the supersonic cruise vehicle are shown in table I. It can be noted that a 24.3 percent improvement in strength weights result from the improved methods that more accurately represent the structure. The simple bar and panel elements are shown in figure 1. The more sophisticated upper wing and fuselage membrane elements substituted for some of the shear panels are shown in figure 2. The lower wing panels are also used but do not show in this figure. This membrane analyses can be improved by using interaction formulas that account for the combination of the biaxial, shear, thermal degradation, thermal stresses, and size-dependent allowables. This is now done.

- In addition, a sub-program for sandwich panels is used for the wing surfaces that accounts for the local and general stability of the core and sandwich and optimized facings, core depth, and core ribbon thickness. It also accounts for the panel end fixity in the presence of biaxial, shear, thermal gradients, temperature degradation, pressure, and constraints on panel deflection and panel rigidity.
- By establishing wing deflection constraints with a fully stressed design, the structural analysis can be optimized more rapidly. A good estimate of the wing deflection constraint reduces the convergence time. Roll effectiveness, control effectiveness, and aerodynamic center movement with Mach number and dynamic pressure can also be more rapidly optimized by deflection constraints.

The above studies are now used in the advanced design process for the advanced supersonic design. As the design progresses towards production,

larger structural models are used with many more structural elements. The FAA has approved the FORMAT methodology.

For the DC-10 substantiation, 100,000 internal structural elements were used by joining 77 substructures. The degree of accuracy of the FORMAT method has been demonstrated by correlating 10 to 15 full-scale static test airplanes. Test strain gages and deflection readings showed excellent correlation when compared with analysis predictions.

ANALYSIS METHODS FOR FAIL-SAFETY

It is desirable to account for fail-safety, crack growth, and residual strength in the initial sizing for structural design. This can be done by cutting a structure member and using the resulting required sizes as the minimum initial size for further optimization studies.

Studies shown in table II optimized spar cap areas for fail-safe design. This increased the panel sizes, reduced spar cap areas, did not appreciably increase the wing weight, but substantially increased fail-safety. It was also found that by using a 400 finite-element model around a crack on a face sheet of a honeycomb panel, the analysis was able to duplicate the test results of the residual strength for honeycomb panels. Notice that titanium honeycomb panels have high residual strength compared with unstiffened sheet (see figure 3). This residual strength, when corrected for actual panel widths, can be used to help determine the initial allowables, when correlated with the crack growth rate for the actual 2.2 Mach cruise design spectra.

TRADE STUDIES

The ability to trade structural weight against specific complex geometry parameters has been developed. A computer graphics program has been developed which enables the analyst to input critical geometry points and quickly create a structural model. This final detailed model can automatically have all elements listed for further analysis. The aerodynamic box loads, inertia fuel loads, and concentrated loads can quickly be transferred to the structural load vectors by special automated programs. Figure 4 and table III are examples of the complex geometry changes analyzed. Figure 4 shows the geometry changes, specifically of thickness ratio variations with span, and of variations in location of maximum thickness ratio. The results of the trade study depicted in table III have been used to assist in the design of the baseline.

A flutter optimization program that uses as an input, derivatives of the strength optimization program's structural influence coefficients as functions of weight, has been developed. Good results have been obtained for variation of the wing thickness ratio both spanwise and chordwise, and the fuel distribution. The aerodynamics section has created a drag equivalent weight for

combining with the strength, fatigue, fail-safety, roll and control effectiveness, and flutter penalties for a variation in wing thickness ratio. (See figure 5). Estimates of the structural total weight and the equivalent wing weight are shown in table III. To ease the space and the manufacturing problems, the 3 percent thickness ratio wing has been selected for the baseline design. It is recognized that a slightly reduced thickness ratio wing has improved aerodynamic performance and a small range increase, but such a refinement is beyond the scope of present analysis requirements.

ALUMINUM TRADE STUDIES

Aluminums have been investigated for high temperature long time application. See reference 5. British and French data have been compared with NASA, ALCOA, and other data sources. British test data of percent creep strain against hours is from reference 5 and is compared with NASA data in figure 6. The McDonnell Douglas design life requirements of 100,000 hours (two lifetimes) with 70,000 hours at temperature may be achievable with some of the British/French alloys of aluminum that show a creep strain of approximately 0.1% at 120°C (248°F) at a maximum continuous stress of 17,650 N/cm² (25,600 lb/in²). Creep-fatigue and rupture for aluminum alloys for the 2.2 Mach supersonic cruise vehicle also have been investigated. With the best aluminum alloys, a one g stress of approximately 5516 N/cm² (8000 lb/in²) is recommended to account for the long time creep, rupture strength, thermal stresses, and creep-fatigue effects for long-time temperature exposure for 2.2 Mach cruise vehicles. This is approximately a 40% reduction in the one g stress as compared with subsonic wide-body transports. Titanium does not appreciably deteriorate in allowables due to thermal effects for the 2.2 Mach supersonic cruise vehicle (table IV). The comparable one g stress for titanium is 15,223 N/cm² (22,080 lb/in²). The specific one g stress ratio of aluminum is 5516 N/cm² (8000 lb/in²) divided by a density of 0.1 compared with titanium with 15,223 N/cm² (22,080 lb/in²) divided by 0.16 density. The best aluminums are, therefore, only 58% of the structural efficiency of current annealed 6AL-4V titaniums when used for strength design parts for 70,000 hours at temperature at 2.2 Mach number.

CRUISE SPEED TRADE STUDIES

An in-depth trade study of the structural weights of a 2.0 Mach, 2.2 Mach, and 2.4 Mach aircraft with a common payload and range has been accomplished. Table IV shows the results from reference 1. The most important structure variables are the thermal stress differences from the thermal gradients, the allowables in compression, and the allowables in tension that account for fatigue and fail-safety. Aeroelastic and flutter weight penalties for each of the three Mach number aircraft are included. The relative direct operating costs (DOC) are shown. The DOC for the 2.4 Mach design is appreciably higher (9.6%) than that for the 2.2 Mach design.

COMPOSITE TRADE STUDIES

From what has been learned of composites from the McDonnell Douglas system studies (see reference 1), further range improvements are possible.

These composite studies have been shown to increase the range significantly if substantial development of composites occur. Table V shows that the baseline airplane has a range of 8093 km (4730 n. mi.) with 1977 go-ahead and near-term mini-bypass engine. For such a go-ahead in 1977, an all-metal aircraft of 70% titanium and 30% aluminum is recommended. If the go-ahead date is 1980, sufficient time seems to be available to develop an all-composite graphite-epoxy secondary structure for use on floor beams, flaps, elevators, and other nontemperature-critical areas. In addition, it may be possible to utilize some limited applications of composite-reinforced titanium to reduce the thickness ratio of the outboard wing panel, for example. These improvements could increase the range to 9153 km (4942 n. mi.). By post-1985 the variable-stream control engine (VSCE) could probably be available for airline service, and the base airplane could have a range of 9354 km (5051 n. mi.). By 1985 composite reinforcements of the titanium main wing spars and fuselage longerons and frames with unidirectional boron-epoxy could be sufficiently analyzed and tested to provide confidence in this concept. An additional 602 km (325 n. mi.) range can be realized, yielding a total range of 10,605 km (5726 n. mi.).

STRUCTURAL CONCEPTS TRADE STUDIES

Eight structural concepts are being investigated and have been compared with the baseline aluminum-brazed titanium honeycomb sandwich concept for the wing and weld-brazed skin stiffener concept for the fuselage. Results show that the selected baseline concepts are the best for overall efficiency.* Nonetheless, one of the more interesting concepts, the superplastically formed diffusion-bonded concept (SPF/DB), figure 7, has been compared with the baseline aluminum-brazed titanium honeycomb sandwich, figure 7. For a uniaxial loading, the superplastically formed concept can use some of its core weight to relieve the face skin stresses if it were optimized so that the web core would not fail from local or general stability. However, in the honeycomb sandwich concept, the core only serves to stabilize the face sheets and does not sustain any axial loading. Therefore, some small advantage can be obtained for a uniaxial loading for the SPF/DB concept. However, when transverse loads and shear are added, the McDonnell Douglas SPF/DB concept seems to rapidly lose its advantage; see figure 8. The SPF/DB concept face sheet is stabilized by the pitch of the truss core corrugations rather than the small cell size for the honeycomb concept.

Therefore, the skin can buckle from transverse and shear loads if the pitch is too large. However, making the pitch small seems to increase the

*1976 NASA study for Langley Research Center under preparation by the Douglas Aircraft Co., McDonnell Douglas Corp.

weight. The use of SPF/DB would seem to save fabrication costs compared with the baseline honeycomb concept. Further studies are planned to fabricate and test SPF/DB concepts, and determine overall system cost effectiveness. Notice in figure 7 that special inserts are required at the splicing bolt attachments to prevent crushing the truss core. With honeycomb sandwich, figure 7, this is readily accomplished by increasing the core density near the joint.

Another interesting concept considered is integrally stiffened titanium panels. Figure 9 shows two arrangements compared with aluminum-brazed titanium sandwich with the same weight per square foot. When optimized for uniaxial loads only, the integral panel approaches the honeycomb values in the Nx direction but cannot sustain desirable transverse loads. The test values were obtained in the 1976 study and the analysis optimization results are from a five-mode stability analysis developed at McDonnell Douglas.

For high confidence in the candidate selections, a large-scale test and development program is necessary. Additional analyses to determine the required coupon, small test panels, large test panels and components are necessary. Tests are then required to obtain the allowables, weight, and cost values with the realistic operating requirements for a supersonic cruise vehicle. Cutouts for inspection, lightning strikes, foreign object damage, splices, corrosion, crack growth under realistic loadings, are a few of the requirements. The testing should start with small coupons, sheet, and panels and culminate in large panels and components to yield confidence in the structural concept.

CONCLUDING REMARKS

The advanced design studies of the supersonic cruise vehicle show that the near-term structural efficiency of titanium using the structural concepts that can sustain high biaxial and shear loads along with pressure, thermal degradation, and long-time fatigue, is high enough to obtain the desired range with an arrow wing for a 2.2 Mach cruise design. To insure the weight, cost, and structural integrity of the most promising titanium concepts, an early structural development program must be initiated. This program should have reached the large component test phase in the near term to insure low risk for an early go-ahead.

The use of composites shows high payoffs for the intermediate and far term aircraft. Because of the elevated temperature problems, an intensive analysis, ground test, and flight test program is necessary to insure the structural reliability of the composites for secondary structure and for composite-reinforced titanium primary structure for the intermediate term. Composites are sensitive to the long-time cruise temperature. Therefore, an intensive testing program using the 2.2 Mach cruise spectra for 70,000 hours at temperature and for a 100,000 hour design life (two lifetimes) is desired for graphite-epoxy and boron-epoxy composites. This development program must start with the analysis and testing of small composite coupons, built-up composite-reinforced titanium joints, and built-up composite-reinforced

titanium panels. Later phases should include large panels and components that would be static and fatigue tested to the 2.2 Mach cruise vehicles' spectra. This large development test program should run concurrently with a flight test program using various structural concepts of composites and composites reinforcing titanium. The NASA flight test composite programs already completed and those planned are important contributions to test the subsonic environment. However, if a partial composite supersonic cruise vehicle is to be considered for the intermediate term, and it is to have a considerable percentage of composites, the ground structural development test should be supplemented by supersonic cruise flight testing using the composite concepts. Perhaps the near-term all-metal (70% titanium and 30% aluminum) aircraft is the best test bed for the intermediate and far-term partial composite supersonic cruise aircraft since no other vehicle will have the right environment and design life at temperature.

REFERENCES

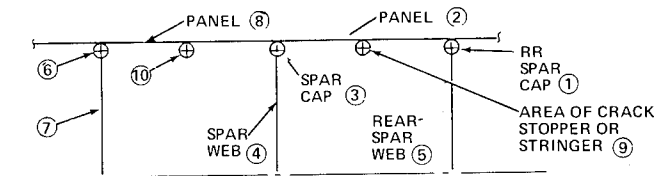
1. NASA CR-144925: Technology Application Studies for Supersonic Cruise Aircraft. Volume 1, prepared under Contract No. NAS1-13612 for Langley Research Center by the Douglas Aircraft Company, McDonnell Douglas Corporation, Douglas Report MDC J4532, November 1975.
2. Denke, P. H.: A Matric Method of Structural Analysis. Proceedings of the 2nd U.S. Congress of Applied Mechanics, June 14-18, 1954.
3. Pickard, J., et al: FORMAT - Fortran Matrix Abstraction Technique. AFFDL-TR-66-207, December 1968.
4. Dodd, A. J.: Specification for a Static Structural Optimization Capability. McDonnell Douglas Report MDC J5442, March 1972.
5. Harpur, N. F.: Concorde Structural Development. British Aircraft Corporation, Filton Division, Bristol, England.

TABLE I.- EXAMPLES OF STRUCTURAL ELEMENTS ANALYSIS FOR
STRENGTH, FATIGUE, AND FAIL SAFETY

DESIGN PHASES		ADVANCED DESIGN		DESIGN	DESIGN SUBSTANTIATION
	MODEL TYPE	NUMBER ELEMENTS	MODEL WT kg (LB)	NUMBER ELEMENTS	NUMBER ELEMENTS
DC-10	BARS AND PANELS	6000	CONSTANT VALUE	60,000	100,000
2.2M SCAR	BARS AND PANELS	3938	17,892 (39,445)	—	—
	MEMBRANES	4555	17,232 (37,989)	—	—
	IMPROVED MEMBRANES ⁽¹⁾	4555	14,163 (31,223)	—	—
	SANDWICH PANELS ⁽²⁾	6365	13,544 (29,859)	—	—

- (1) SIZE OPTIMIZATION — INCLUDES INTERACTION EQUATIONS FOR BIAXIAL AND SHEAR LOADINGS, THERMAL EFFECTS, ETC.
(2) SANDWICH OPTIMIZATION — INCLUDES FACING AND CORE THICKNESSES, CORE DEPTH, THERMAL EFFECTS, PRESSURE, ETC.

TABLE II.- FAIL-SAFE CONDITIONS



FAILURE MODE	STRUCTURAL MODEL EQUIVALENT
OUTER OR INNER PANEL FACING FAILURE OF HONEYCOMB SANDWICH (2)	REDUCE AREA OF PANEL (2) BY 50 PERCENT
OUTER OR INNER PANEL FACING FAILURE OF HONEYCOMB PANEL (8)	REDUCE AREA OF PANEL (8) BY 50 PERCENT
OUTER AND INNER PANEL FACINGS FAILURE OF PANEL (2)	CUT PANEL (2) TO ZERO THICKNESS
OUTER AND INNER PANEL FACINGS FAILURE OF PANEL (8)	CUT PANEL (8) TO ZERO THICKNESS
REAR SPAR CAP FAILURE (1)	CUT AREA OF REAR SPAR CAP (1) TO ZERO
INTERMEDIATE SPAR CAP FAILURE CAP (3)	CUT AREA OF SPAR CAP (3) TO ZERO
FAILURE OF PANEL (2) WITH A FAILURE OF CAP (3)	COMBINE III AND VI
FAILURE OF PANEL (2), PANEL (8), AND INTERMEDIATE CAP (3)	COMBINE CASES III, IV, AND VI

PR5-AST-4581

TABLE III.- WING STRUCTURAL BOX WEIGHT OPTIMIZATION

DESIGN		5	-5 MOD	-5A	-5X
t/c (ROOT, T.E., L.E., TIP)		2.25; 3; 2.5; 2	2.25; 3; 2; 2	2.25; 3; 3; 3	2.25; 3; 4; 4
MAX t/c LOCATION - % C		40 TO 60	60 TO 75	60 TO 75	60 TO 75
STRENGTH + FAIL-SAFE + AEROELASTIC	kg (LB)	28,123 (62,000)	22,226 (49,000)	21,772 (48,000)	21,319 (47,000)
FLUTTER	kg (LB)	2,268 (5,000*)	907 (2,000)	390 (860)	390 (860)
ROLL EFFECTIVENESS	kg (LB)	2,722 (6,000**)	1,814 (4,000**)	907 (2,000**)	680 (1,500**)
ESTIMATED WING BOX	kg (LB)	33,113 (73,000)	24,947 (55,000)	23,069 (50,860)	22,389 (49,360)
DRAG EQUIVALENT	kg (LB)	0 0	2,268 (5,000)	5,216 (11,500)	9,253 (20,400)
EQUIVALENT TOTAL	kg (LB)	33,113 (73,000)	27,215 (60,000)	28,285 (62,360)	31,642 (69,760)

*4,536 kg (10,000 LB) FUEL PER SIDE MOVED INBOARD

**PRELIMINARY ESTIMATE

▲
BASELINE

TABLE IV.- MACH TRADE STUDY SUMMARY

273 PASSENGERS — RANGE 7400 km (4000 N MI)

DESIGN MACH NUMBER		2.0	2.2	2.4
TAKEOFF GROSS WEIGHT	kg (LB)	311,255 (686,200)	320,962 (707,600)	372,388 (820,974)
ENGINE AIRFLOW	kg/SEC (LB/SEC)	299 (660)	320 (705)	397 (875)
CRUISE SFC (INST)	kg/HR/N (LB/HR/LB)	0.1342 (1.316)	0.1403 (1.376)	0.1516 (1.487)
CRUISE L/D		9.73	9.33	8.86
OPERATING EMPTY WEIGHT	kg (LB)	129,410 (285,300)	134,799 (297,182)	153,228 (337,871)
ΔT = THERMAL GRADIENT	$^{\circ}\text{C}$ ($^{\circ}\text{F}$)	49 (120)	71 (160)	93 (200)
ALLOWABLES* IN COMPRESSION	N/cm ² (LB/IN. ²)	-74,939 (-108,690)	-68,644 (-99,560)	-62,039 (-89,980)
ALLOWABLES* IN TENSION	N/cm ² (LB/IN. ²)	75,842 (110,000)	68,948 (100,000)	63,432 (92,000)
FATIGUE PLUS FAIL-SAFE				
RELATIVE DOC		0.988	1.00	1.096

*INCLUDES INTERACTION EQUATIONS, SIZE DEPENDENT ALLOWABLES, THERMAL STRESSES, AND DEFORMATION CONSTRAINTS (NASA CR-144925)

PAGE 38/40

TABLE V.- EFFECT ON AIRCRAFT RANGE BY ADDING COMPOSITES

		1977	1980	POST-1985
BASLINE AIRPLANE RANGE	km (N MI)	8093 (4370)	8504 (4592)	9,354 (5,051)
ENGINE TYPE		NEAR TERM MINI-BYPASS	ADV TECH MINI-BYPASS	ADV TECH VSCE-502BD
COMPOSITE SECONDARY STRUCTURE	km (N MI)	—	232* (125*)	232* (125*)
NEW OUTBOARD WING PANEL WITH LOWER t/c 'S AND COMPOSITES	km (N MI)	—	417* (225*)	417* (225*)
COMPOSITE REINFORCED METAL WING SPARS AND RIBS	km (N MI)	—	—	380* (205*)
COMPOSITE REINFORCED METAL FUSELAGE LONGERONS AND FRAMES	km (N MI)	—	—	185* (100*)
COMPOSITE LANDING GEAR BRACES	km (N MI)	—	—	37* (20*)
TOTAL RANGE	km (N MI)	8093 (4370)	9153 (4942)	10,605 (5,726)

*RANGE INCREASE

PR6-AST-4858

1283 BARS
1008 PANELS
3574 STRESSES
3938 ELEMENT FORCES
3647 DEGREES OF FREEDOM
5 APPLIED LOAD CONDITIONS
3 FS DESIGN ITERATIONS

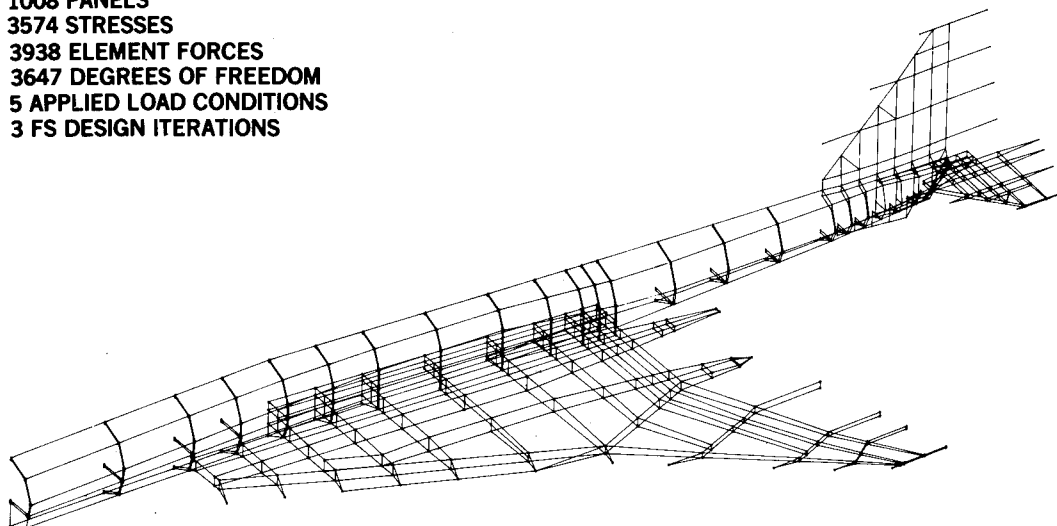


Figure 1.- Typical structural analysis.

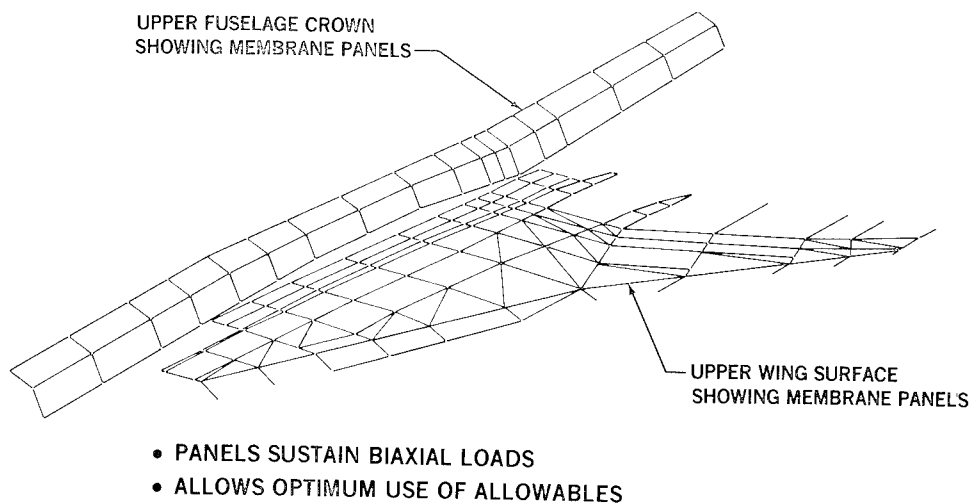


Figure 2.- -5A structural model.

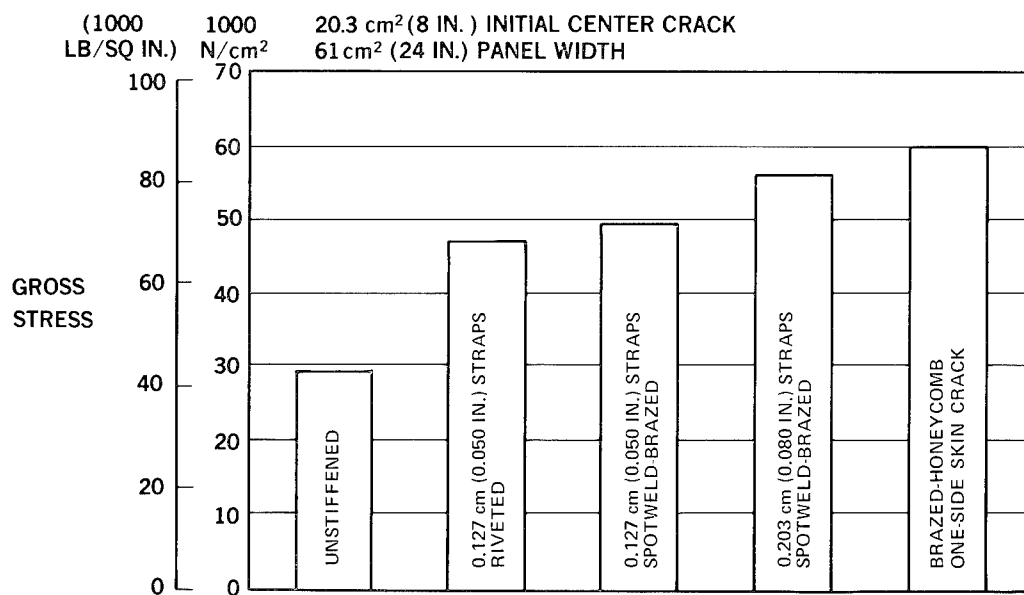


Figure 3.- Residual strength tests of Ti panels.



Figure 4.- Inboard panels thickness distribution study.



Figure 5.- Structural box weight optimization for AST wing.

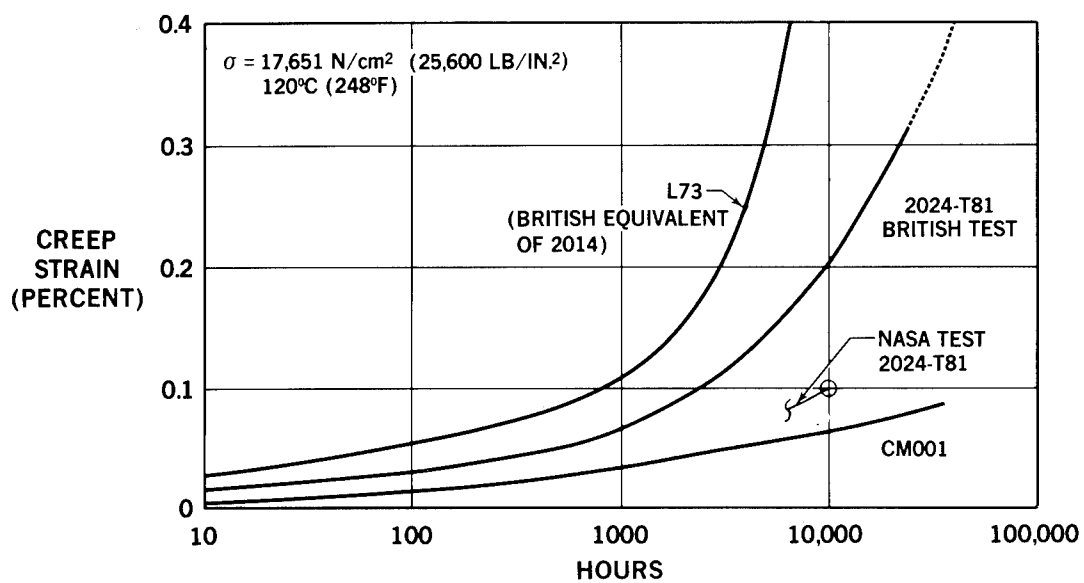


Figure 6.- Creep strain of aluminum materials.

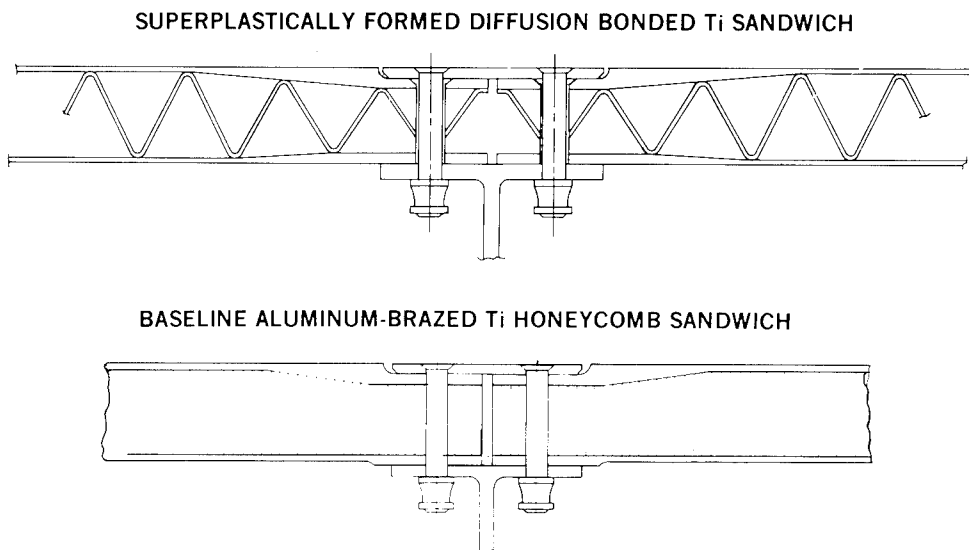


Figure 7.- Candidate structural concepts.

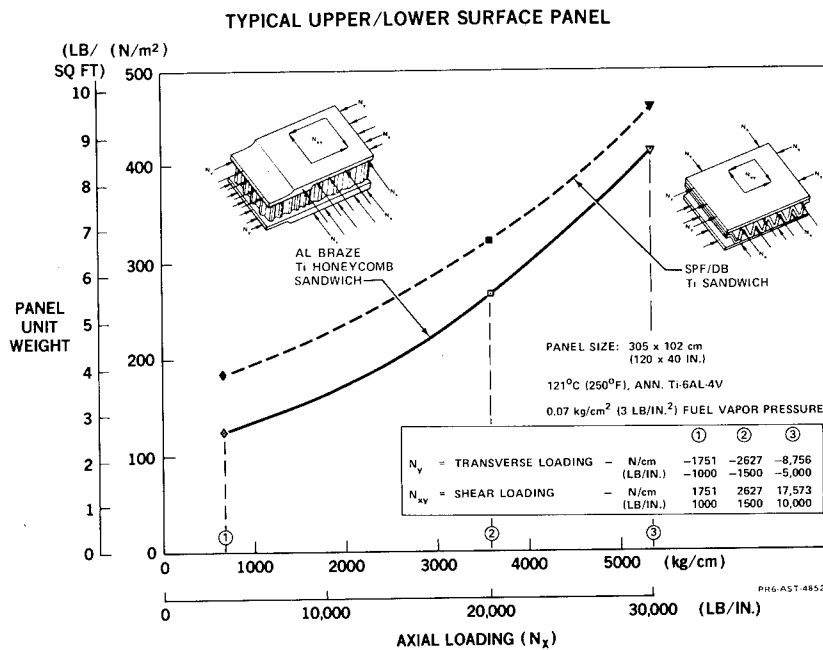


Figure 8.- Panel weights for candidate concepts.

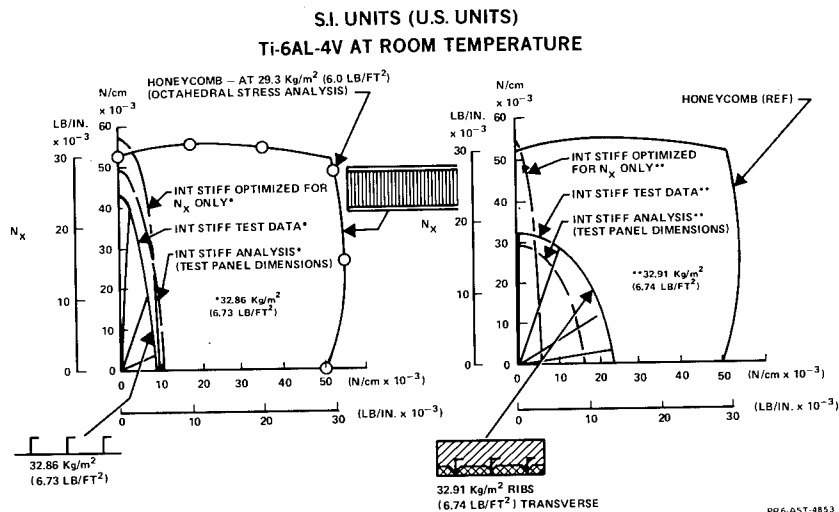


Figure 9.- Comparison of ultimate loads of aluminum brazed Ti honeycomb and integrally stiffened Ti panels.

PERFORMANCE AND BENEFITS
OF AN
ADVANCED TECHNOLOGY SUPERSONIC CRUISE AIRCRAFT

Richard D. FitzSimmons
McDonnell Douglas Corporation

SUMMARY

The results of four years research on technology are synthesized in an advanced supersonic cruise aircraft design. Comparisons are presented with the former United States SST and the British-French Concorde, including aerodynamic efficiency, propulsion efficiency, weight efficiency, and community noise. Selected trade study results are presented on the subjects of design cruise Mach number, engine cycle selection, and noise suppression. The critical issue of program timing is addressed and some observations made regarding the impact that timing has on engine selection and minimization of program risk.

INTRODUCTION

Since 1972, McDonnell Douglas (MDC) has been conducting systems studies for NASA Langley, coupled with extensive Company-funded efforts, to identify technology requirements for an economical, environmentally satisfactory, supersonic cruise commercial airplane. These efforts were unencumbered by preconceived notions of what should be a proper design. A configuration evolved, based on extensive trade studies, that represents all the advanced technologies deemed applicable to a second generation supersonic passenger airplane.

In order to understand how technology has progressed in the last four years, comparisons are shown with the former U.S. SST design and with the world's first operational supersonic transport, the British-French Concorde. Updating of earlier published data is included.

In addition, important data on several trade studies are presented to enable others to participate in the design selection process. Cruise speed selection and engine cycle selection are both controversial issues at present. At McDonnell Douglas, the cruise speed trade studies seem to confirm the results found separately in over twenty-two years of continuous design, development, and production of military supersonic aircraft. The engine cycle trade studies and important data results are shown. The issue of noise-suppression variations between coannular and mechanical suppression is presented inasmuch as understanding these relationships is so critical to eventual engine cycle selection.

The results presented reflect comprehensive analysis, utilizing extensive computer and detail design iterations, capabilities only recently validated for use in the preliminary design process.

MDC BASELINE DEFINITION

The early research at NASA Langley on the former U.S. SST program identified the fact that a large increase in the aerodynamic efficiency of a supersonic transport could be realized. This was validated in 1965 by the tests of SCAT 15F, a mid-wing design with an arrow wing identified by a notch cutout of the trailing edge of the wing planform. Unfortunately, at that time, satisfactory solutions could not be found for the structural aeroelastic and flutter questions or for the passenger requirements for the fuselage with its impact on fuselage wing intersections. The arrow wing was dropped.

In 1972, following the demise of the U.S. SST, a fresh look at the arrow wing was undertaken. McDonnell Douglas wing planform trade studies, unencumbered by previous design selections, showed that the early delta-wing designs, typical of the Concorde and the former U.S. SST (fig. 1), were not optimum. By keeping a large subsonic leading-edge inner panel, a rather small supersonic leading-edge outer panel, and utilizing a moderate notch in the trailing edge, a result was found that was optimum for minimum operating cost. Some small penalties were paid in aerodynamic cruise efficiency to satisfy the structural demands for strength, aeroelasticity, safe-life, fatigue, damage tolerance, and flutter. Fortunately, improved computer-aided design techniques had become available which were not available in the mid-sixties; thus, much could be done to understand a specific airplane design. The result is that the structural stiffness and flutter questions, which hurt the competitiveness of arrow-wing designs in the late 1960's, can now be allayed and efficient arrow wings designed with confidence.

The four engines were located under the wing, aft of the rear spar and separate from the fuselage based on careful optimization trade studies involving complete airplane structural modeling, detail nacelle design, aerodynamic wave drag, and including even the impacts of changes in landing-gear length as required for engine ground clearance during rotation. Studies indicated that the tail could be reduced in size to match neutral static stability requirements, but that reducing the tail size further was not consistent with the low risk demanded for the other airplane variables.

The McDonnell Douglas baseline airplane that resulted is a 340 200 kg (750 000 lbm) design, with a 929 m^2 ($10\,000 \text{ ft}^2$) wing (table I). As compared to the last U.S. SST, the design cruise speed has been selected at 2.2 Mach number. The resulting range is 4590 nautical miles, a 48 percent improvement over the last U.S. SST, most of which is from the increase in aerodynamic cruise efficiency, lift to drag (L/D), which improved 34 percent. This then is the big difference in SST design between 1971 and 1976, a 34-percent increase in aerodynamic efficiency.

Much has been written about the advancements required for the propulsion system to make a supersonic airplane viable. There was nothing wrong with the cruise

propulsion efficiency of the 1971 engine on the U.S. SST. The big problem was the noise. Thermodynamics is a well-known subject and the ideal engine cycle for cruise has not changed much. The component efficiencies of the 1971 engines were high; thus improvements have not come easily. The big advancements made in the recent NASA-funded U.S. engine studies have been in noise and in weight. Much of the weight improvement results from increased turbine temperatures and improved materials. The challenge really has been to meet or exceed the community noise requirements without losing supersonic cruise propulsion efficiency and this challenge has been met by the engine manufacturers.

One other interesting result is that the structure optimizes with titanium wherever elevated temperatures and highly loaded conditions exist. This is because of the long range payload sensitivity of the supersonic airplane design. On the other hand, studies show that lower cost aluminum is more cost effective on all secondary structures, or on components that have no temperature problem or are lightly loaded.

Two trade studies on cruise speed have been completed, one in 1973, and a more sophisticated second analysis in 1975 (table II). The 1975 results show a slight penalty in gross weight required at 2.2 Mach as compared with 2.0 Mach although the range factor is actually higher at 2.2 Mach. A large penalty is shown for designing for the higher Mach number of 2.4. The designs have all been configured to carry 273 passengers for 7408 kilometers (4000 nautical miles). There are small variations in aerodynamic cruise efficiency and in propulsion efficiency; however, the large variations that result are in the cruise engine thrust requirement. Because the 2.4 Mach number design has to cruise both higher and faster, a significant increase in engine thrust is required. The engine thrust also has to be increased due to a higher take-off speed, and lower climbout lift-drag ratio, whereas the FAR noise requirement remains constant. The structural design for each airplane has been analyzed in detail, including considerations for temperature and thermal stress where appropriate. The weights reflect all these conditions.

The 1975 study results make the case even stronger for selecting a moderate design cruise speed as compared with a higher cruise speed design.

For over twenty-two years McDonnell Douglas has been in continuous design, development, and production of supersonic fighter aircraft (fig. 2). Steady pressure by the customers has been applied over these many years, to try to justify supersonic aircraft with higher speeds like Mach 2.7 or Mach 3.0 but with no success. The latest McDonnell Douglas fighters, the F-18 and the F-15, reflect the results of extensive trade studies on the optimum solution for design speed. (They are more equivalent to 2.2 Mach cruise supersonic transport designs than to 2.5 Mach.) Higher speeds do not seem to be proven to be cost effective. Similar studies on early B-1 designs have shown the same type results. At McDonnell Douglas, no justifiable case can be made for designing an airline transport for a cruise speed above about 2.2 Mach number. At the same time, at McDonnell Douglas it is recognized that much of the technical knowledge gained from these U.S. military programs can be applied to the development of a 2.2 Mach advanced supersonic cruise commercial airplane.

A comparison with the Concorde shows a few additional items of importance (table III). Here, in addition to improvements in aerodynamics and noise, improvements in payload and in cruise speed can be shown, both of which are powerful variables in the economics equation. All hourly operating costs are divided by speed and by payload to obtain operating costs per passenger mile, and of course, tickets are priced by cents per passenger mile. Compared with the Concorde, the 9-percent increase in speed and the 150-percent increase in payload offer dramatic improvements in economy, equivalent to a 60-percent reduction in direct operating costs due to these two parameters alone.

The Concorde today is doing an outstanding technical job, except it is noisy (fig. 3). In the future, any second generation supersonic passenger aircraft must meet society's needs regarding noise. The McDonnell Douglas baseline design meets or exceeds FAR Part 36 noise requirements. Two additional items are of significance. By designing the supersonic airplane for 8334 kilometers (4500 nautical miles), the actual noise will be reduced significantly for most average missions as the gross weight will be lower, and the take-off performance much improved. Also there is good reason to believe that current emphasis on jet noise research is proving to be the most rewarding and further reductions in noise can be envisioned for supersonic designs. Fortunately, for supersonic designs, variable area nozzles are required for thrust recovery at cruise, which means that the variability is already available; there are possibilities for future clever designs for noise suppression at take-off nozzle positions.

The payload range of an airplane is all important for International airlines. The payload range that results for the MDC baseline shows that 273 passengers can be flown 8445 kilometers (4560 nautical miles) in an all metal design utilizing a 1980 state-of-art mini-bypass engine cycle (fig. 4). For a 1980 go-ahead, prudent use of graphite epoxy composite secondary structure is reasonably insured. For a 1985 go-ahead, the state of the art may well allow use of additional composites to reinforce the metal airframe in critical areas, probably in uniaxial loading type applications. Also, for a 1985 go-ahead, the variable cycle engine can be considered applicable and the resulting range of such a design becomes 10,649 kilometers (5750 nautical miles), equivalent to the very longest of the routes being considered today by airlines for subsonic operations. It looks as if a second generation supersonic cruise airplane inherently should possess good growth potential and not be range limited.

The ability to fly long ranges and open up the Pacific to supersonic travel will do much to save unproductive travel time. Such service should stimulate much travel.

A derivative of the Rolls-Royce Olympus is shown, based upon utilizing present core developments coupled with an additional turbine driving a low pressure compressor and fan. Such an engine is marginal for the 273 passenger size McDonnell Douglas design, but for a slightly smaller version it offers much promise. Further work here is active today both in England and at McDonnell Douglas.

The engine cycle selection is critical as engine development time from go-ahead to certification is the pacing item for a supersonic cruise airplane program, as the airplane development actually can take less time. Accordingly, the specific engine cycle and size must be selected early, and this requires selection by the airlines. This means airlines will have placed initial orders, specific engines will have been offered, airplane detail specifications will have been defined, and firm prices will have been established. This process does not come easily. Pacing all these conditions may well be the results of forward-flight tests on coannular and/or mechanical sound suppressors.

The variations in airplane range that result from engine technology readiness dates are shown (fig.5). The 1975 technology engine would require a relatively heavy multi-tube flow breakup nozzle with an acoustically lined ejector for meeting FAR Part 36 noise levels. The 1980 engine also incorporates a mechanical noise suppressor, although lighter. The 1985 technology designs utilize the inherent noise reduction benefits predicted for the coannular jet exhausts which are unique to the variable cycle engine designs. The weight variations between the engines tend to be the dominant reason for the range variations shown.

At present, it is not possible to narrow the engine selection process as the important variables of timing and noise suppression cannot be defined accurately. A comparison of the existing noise suppressor variations between coannular and mechanical suppressor as used by McDonnell Douglas is shown (fig. 6). As compared with conventional unsuppressed nozzles, mechanical suppressors are competitive, especially as the jet velocity is reduced. It can be shown that both mechanical suppressor and coannular suppressor airplane designs can result in airplane noise levels below the 108 EPNdB of FAR Part 36 if the jet velocity can be held low.

NASA could do the industry a great service if they would adequately fund validation testing of large-scale noise-suppression tests of both competitive design approaches that would accurately portray noise-suppression levels corrected for forward flight.

There are engine considerations being given additional study (table IV). The weight variations that result from the McDonnell Douglas engine sizing studies are as shown, with the VSCE showing a 14 515 kg (32 000 pound) advantage in operating empty weight. In addition, the VSCE shows a reduction in fuel reserve of 9 545 kg (21 000 lbm), which is significant, but has only a secondary effect on reducing direct operating costs. It is interesting that the Double Bypass and VSCE engines both optimize for designs that result in long climb schedules relative to more conventional cycles. The analysis includes optimizing the augmentation schedule as well as varying engine size. The average range factors vary more than by differences in specific fuel consumption. This is because most augmented-engine cycle-powered airplane designs optimize for flight at or near the altitude for maximum lift-drag ratio, whereas nonaugmented cycle designs seem to optimize for a slightly smaller engine size and cruise at an altitude that results in a slightly reduced lift-drag ratio.

The engine results show rather significant variations in direct operating costs. These are preliminary results only, uncorrected for changes such as 1976 fuel

costs. Further efforts are required to better understand the trades between technology readiness dates, range, and direct operating costs. Airline guidance is needed in this area.

CONCLUDING REMARKS

Four years of systems studies, coupled with important validation wind-tunnel test results of an airline design, indicate that the technology is in-hand to develop an economical, environmentally satisfactory supersonic cruise commercial airplane (table V). No inventions are required. The extensive twenty-two years of continuous design, development, and production of McDonnell Douglas supersonic fighter designs including present F-4, F-15, and F-18 aircraft provide credibility to the McDonnell Douglas baseline supersonic cruise aircraft design. Selection of a 2.2 Mach number for cruise comes from this background of supersonic experience and offers low-risk improved airline economics and lower development costs. Program timing will dictate engine cycle selection and noise testing may also impact on engine selection. Inasmuch as no actual aircraft experience exists in the United States for (1) supersonic performance of arrow wings, (2) brazed titanium honeycomb and skin/stringer primary structures, or (3) flight effects for engine noise suppression, such tests will pace a U.S. second generation transport. Extensive validation testing is required to minimize the inordinately high risk that these areas represent. Only then can a low-risk production program be initiated. Should the U.S. government move out on these tests in FY 1978, then an engine selection is possible in 1980-81 and an economical, environmentally sound advanced supersonic aircraft can be in airline service in 1986.

TABLE I.- SUPERSONIC TRANSPORT TECHNOLOGY COMPARISON

	SST (1971)	MDC BASELINE (1976) *	IMPROVEMENT
SPEED	MACH 2.7	MACH 2.2	
RANGE	5741 km (3100 N MI)	8500 km (4590 N MI)	48% FARTHER
PASSENGERS	261	273	5% MORE
ENGINE	TURBOJET WITH AFTERBURNER MINI-BYPASS TURBOJET — DRY		
PROPULSION EFFICIENCY (M/SFC)	1.74	1.74	NO CHANGE
AERO EFFICIENCY (L/D)	7.2	9.6	34% INCREASE
STRUCTURAL WEIGHT EFFICIENCY	100% TITANIUM 216°C (420°F)	70% TITANIUM + 30% ALUMINUM 116°C (240°F)	4% BETTER
TAKEOFF AND LANDING NOISE	112 EPNdB AVERAGE	105 EPNdB AVERAGE	BETTER THAN FAR PART 36

★ 1980 GO-AHEAD

TABLE II.- CRUISE SPEED STUDY SUMMARY

	$R = K \frac{L}{D} \frac{M}{SFC} \ell_g \frac{W_{TO}}{W_L}$			R = 7408 km (4000 N MI)
		2.0M	2.2M	2.4M
L/D MAX		9.74	9.49	8.97
L/D CRUISE		9.73	9.33	8.86
SFC UNINSTALLED		1.23	1.27	1.33
SFC INSTALLED		1.32	1.38	1.49
M/SFC		1.52	1.59	1.61
L/D x M/SFC (RANGE FACTOR)		14.8	15.0	14.3
W _{TO} * kg (LB)	311,909 (686,200)	321,636 (707,600)	373,182 (821,000)	
W _L kg (LB)	182,798 (403,000)	189,874 (418,600)	214,368 (472,600)	
SLS THRUST/ENGINE kN (LB)	287.4 (64,600)	302.9 (68,100)	376.3 (84,600)	

* MATERIAL SELECTION AND ALLOWABLES INCLUDE TEMPERATURE AND THERMAL STRESS CONSIDERATIONS

REF: NASA MDC 1975 STUDIES

TABLE III.- SUPERSONIC TRANSPORT TECHNOLOGY COMPARISON

	CONCORDE	MDC BASELINE (1976) *	IMPROVEMENT
SPEED	MACH 2.02	MACH 2.2	9% FASTER
RANGE	5834 km (3150 N MI)	8500 km (4590 N MI)	46% FARTHER
PASSENGERS	108	273	2.5 TIMES
ENGINE	TURBOJET WITH AFTERBURNER MINI-BYPASS TURBOJET — DRY		
PROPULSION EFFICIENCY (M/SFC)	1.70	1.74	2% INCREASE
AERO EFFICIENCY (L/D)	7.6	9.6	26% INCREASE
STRUCTURAL WEIGHT EFFICIENCY	ADVANCED ALUMINUM 93°C (200°F)	70% TITANIUM + 30% ALUMINUM 116°C (240°F)	4% DECREASE
TAKEOFF AND LANDING NOISE	116 EPNdB AVERAGE	105 EPNdB AVERAGE	BETTER THAN FAR PART 36

★ 1980 GO-AHEAD

TABLE IV.- ENGINE CONSIDERATIONS

	TECHNOLOGY READINESS	Δ OWE kg (LB)	Δ FUEL RESERVE ⁽¹⁾ kg (LB)	Δ T. O. AND CLIMB ⁽²⁾ kg (LB)	Δ RANGE FACTOR	Δ DOC ⁽³⁾
BASLINE WITH MECHANICAL SUPPRESSOR (MDC)	1975	REF	REF	REF	REF	REF
MINI-BYPASS WITH MECHANICAL SUPPRESSOR (GE)	1980	-5,910 (-13,000)	-4,545 (-10,000)	-3,182 (-7,000)	+1%	-5-1/2%
DOUBLE BYPASS VCE	1985	-5,000 (-11,000)	-5,910 (-13,000)	+5,000 (+11,000)	+6%	-6-1/2%
VCE 112C	1985	-8,636 (-19,000)	-6,364 (-14,000)	+455 (+1,000)	+2%	-2-1/2%
VSCE 502B	1985	-14,545 (-32,000)	-9,545 (-21,000)	+9,545 (+21,000)	+6%	-7%

(1) CORRECTED FOR SAME RANGE
(2) SAME TAKEOFF WEIGHT
(3) 1973 COSTS

TABLE V.- CONCLUSIONS

- 2.2 MACH DESIGN SEEMS OPTIMUM (VERSUS 2.4)
 - MORE CURRENT STATE OF THE ART (F-15, F-18, F-4, ETC)
 - SMALLER ENGINE
 - SMALLER AIRPLANE
 - LOWER DIRECT OPERATING COST
 - LOWER CAPITAL INVESTMENT
- PROGRAM TIMING DICTATES ENGINE SELECTION
 - CRUISE PERFORMANCE SAME
 - COMMUNITY NOISE
 - VCE ADVANTAGES MOSTLY IN LIGHTER WEIGHT
 - VCE REQUIRES 400°F INCREASE IN TURBINE TEMPERATURE
(8 YEARS?)
- VALIDATION OF NOISE SUPPRESSION CRITICAL TO ENGINE SELECTION

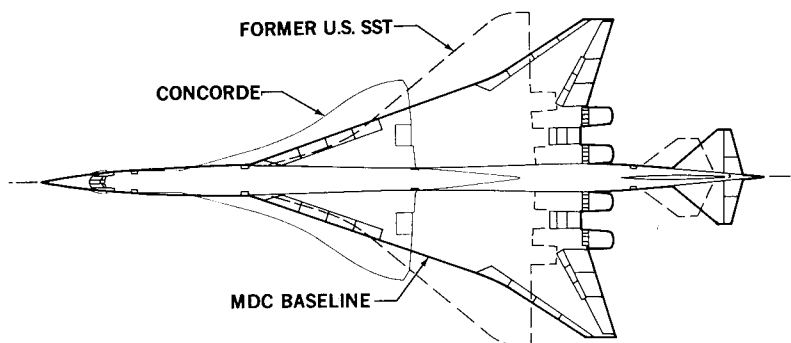


Figure 1.- McDonnell Douglas baseline.

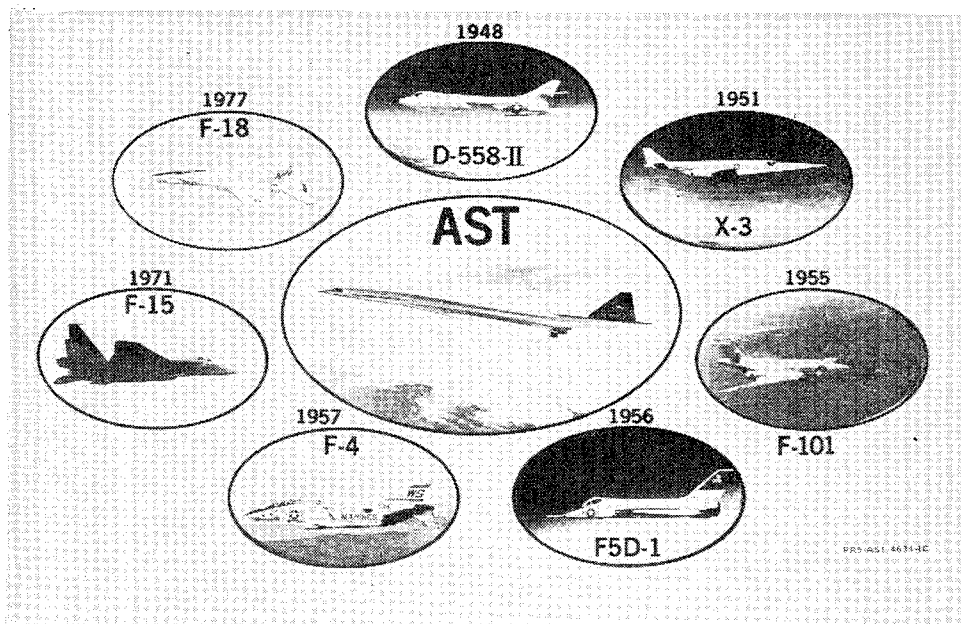
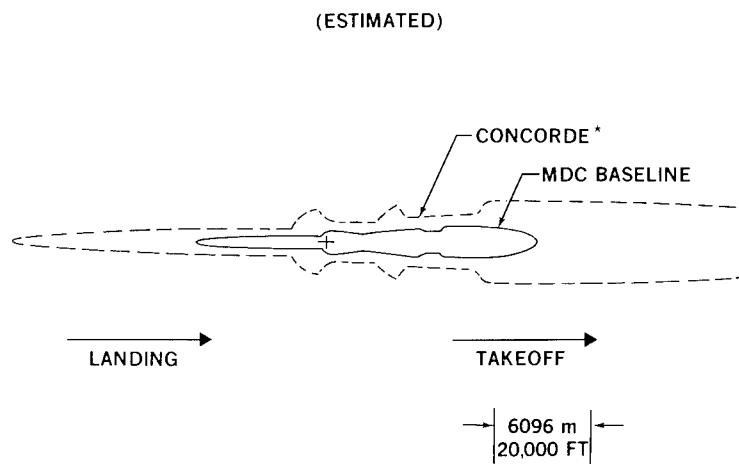


Figure 2.- MDC supersonic aircraft.



*CONCORDE REFERENCE: ENVIRONMENTAL IMPACT STATEMENT ATTACHMENTS

Figure 3.- Comparison of MDC baseline and Concorde 100-EPNdB contours.

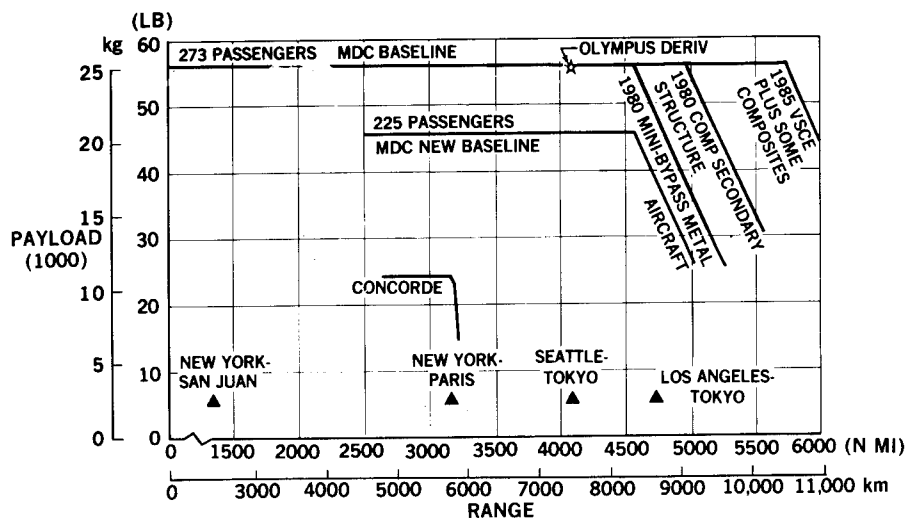


Figure 4.- Payload - range curves.

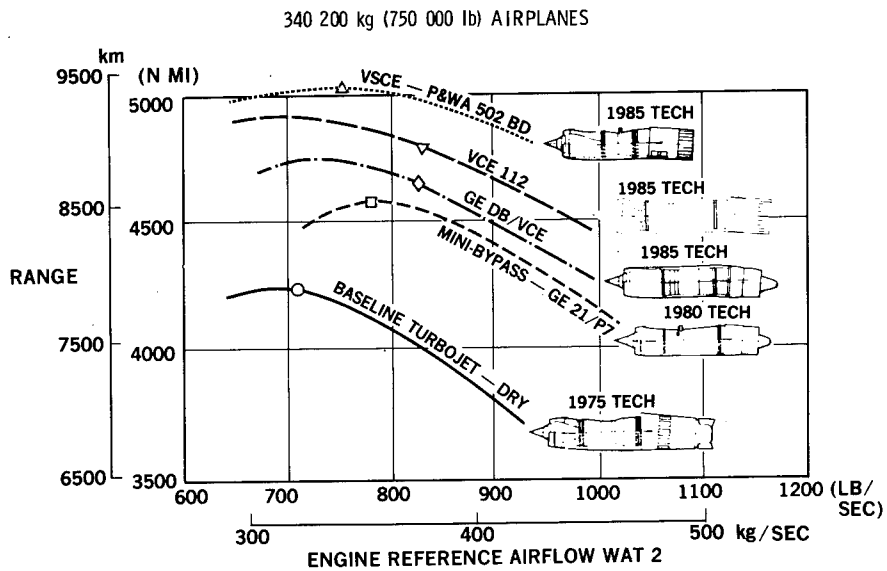


Figure 5.- Engine cycle selection.

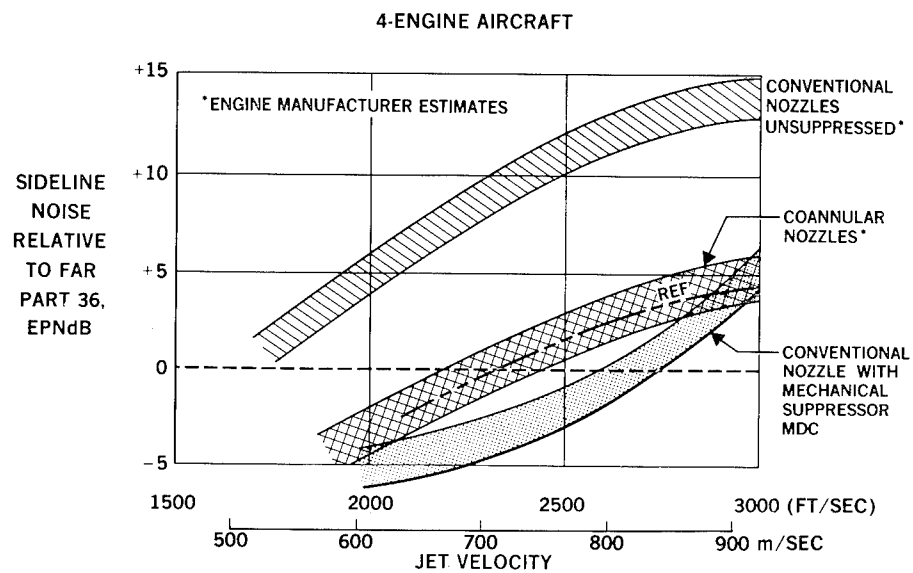


Figure 6.- Noise suppression comparisons.

AN ADVANCED CONCEPT THAT PROMISES ECOLOGICAL

AND ECONOMIC VIABILITY

Bruce R. Wright, Thomas A. Sedgwick, and David M. Urie
Lockheed-California Company

SUMMARY

Economical and ecologically acceptable supersonic travel throughout the world can be a reality in the 1990's. The actuality of supersonic commercial service being provided by Concorde is demonstrating to the world the advantages offered by supersonic travel for both business and recreation. Public acceptance will gradually and persistently stimulate interest to proceed with a second generation design that meets updated economic and ecological standards. This paper identifies an advanced technology supersonic cruise vehicle, developed under the NASA SCAR program, that could be available for commercial service in the 1990's. It is estimated that this concept could operate profitably on world-wide routes with a revenue structure based upon economy fares. This airplane will meet all present day ecological requirements regarding noise and emissions.

INTRODUCTION

The National Supersonic Transport Program was canceled in 1971 after a considerable investment of the national resources, both material and human. The major factors which contributed to the program demise were the ecological and economic deficiencies due to marginal range-payload characteristics. In the same time period, attractive subsonic wide-body aircraft were being introduced into the long-haul aircraft market. At the close of the program, it was clear to both Government and industry that significant improvements in supersonic technology were required to make a second generation aircraft economically viable and ecologically acceptable.

In 1972, the National Aeronautics and Space Administration (NASA) initiated an Advanced Supersonic Technology (AST) program. The intent of the program was, and still is (in the form of the SCAR program), to give the industry of the country the technology data base needed to proceed with development of a second generation supersonic cruise vehicle, when that decision is made.

TECHNOLOGY - WHY?

At the present time, it is not proper to ask "Why a civil supersonic cruise vehicle?" but rather "Why technology studies?"

For the past several years, NASA Langley Research Center has been pursuing a Supersonic Cruise Aircraft Research (SCAR) program to provide sound technical bases for future civil and military supersonic vehicles. Under NASA sponsorship, various engine and airframe companies have been conducting technology assessment or impact studies to identify and assign priorities to important research and development programs and provide guidance and support to see that the critical needs are implemented. This program has provided industry with funds to perform contract studies, and has defined a flagpole around which industry could gather its own privately funded supersonic technology studies and research. An integrated program approach, as illustrated in Figure 1, has been formed because of this stimulus. Without an integration team monitoring the various on-going programs and assessing the technology impact, guidance for updating programs or identifying new programs would be missing. The all important technology and economic feedback would also be missing. In earlier aircraft development programs, these kinds of advancements in the various technologies were largely stimulated by general NASA research and military aircraft studies, contracts, and development.

The present SCAR impact studies have drawn together inputs from NASA research efforts, industry independent research and development (IRAD), FAA/SST follow-on tasks, and various Climatic Impact Assessment Program (CIAP) and airline inputs. Such studies provide the only valid means of assessing the worth of the discrete technical advances resulting from the research and technology

programs. Such efforts are beneficial in reducing risk and building experienced design teams necessary to permit successful program expansion from the research and technology phase to a development/production program at a later date. It should also be noted that these studies give emphasis to the need for experimental programs and correlation of results with parallel theoretical programs.

TECHNOLOGY - WHEN?

The point in time when technology readiness must be established depends upon what degree of technology advancement is required, what funding support is to be made available to establish these advances, when the airplane that results from these technology improvements can be made available, and finally, and most importantly, when the marketplace is in a position to accept and successfully employ this new advanced technology airplane.

Early introduction of a Supersonic Cruise Vehicle (SCV) into the marketplace does not seem likely at this time because of the current economic status of the airline industry, its need to replace aging subsonic long range equipment with new quiet fuel-efficient replacements, and the political adversity to new aircraft designs that are claimed to threaten the ecological well-being of all citizenry.

The 1980's are most likely to be the era of the subsonic transport derivative (Figure 2). In the middle 1980's, airlines will be replacing 727-100's, 707's and DC-8's. The projected economic viability of the airline industry will not be able to support two aircraft programs such as subsonic derivatives and a supersonic cruise vehicle. Airline management must opt for the derivative aircraft first.

Time is therefore available to perform further SCV technology studies. With adequate funding, this time can be used to develop much improved airframes and propulsion systems, and demonstrate their viability as well. This program would establish for this country a supersonic airplane technology readiness status by mid 1980 that would permit low-risk development of economic and

ecologically viable commercial supersonic cruise vehicles and superior advanced supersonic military tactical and long range cruise aircraft.

SCV DESIGN OBJECTIVES

A successful second generation SCV must properly meet market needs in terms of range and size. To insure economic viability, the design should emphasize the smallest aircraft size possible, cruise speeds commensurate with best possible utilization, and payload fractions at least twice that of Concorde. Lockheed marketing studies performed in 1973, with market projections carried out to the year 2000, suggested that the most attractive designs adopt trans-Atlantic range with approximately a 300-passenger payload capability. Such a concept benefits from small airplane size, with resultant improvements in development/production costs and operating expenses. A later growth version of the concept appears as a logical follow-on derivative that would provide nonstop trans-Pacific operation. A modest payload growth to 11 - 12 percent appears reasonable (Figure 3).

Cruise speed studies suggest operation at Mach 2.5, with the capability of achieving these speeds under representative high-altitude, hot-day operations.

Range

The Lockheed concept has been designed to achieve a zero-wind, hot-day range of 7400 km (4000 nautical miles). This goal provides a design concept that can achieve world-wide operations as shown in Figure 4. The aircraft can readily accommodate the North Atlantic with nonstop operation. The aircraft will be practical for North-South American operations. It can operate satisfactorily in the Pacific using Honolulu as a stopover for east/west flights. Nonstop Pacific operation requires a range of 8900 km (4800 nautical miles); an aircraft with this capability would increase gross mass approximately 68,000 kg (150,000 lb) and be more costly for most service operations. It may be possible to develop this size airplane as a later growth version of the basic 7400 km (4000 nautical mile) design.

Speed

Task III of the NASA-Lockheed technology assessment study carefully examined cruise speed options. TWA added airline experience by assisting in a separate Lockheed-funded cruise speed study. Figure 5 reveals that Mach numbers greater than 2 permit four flights per day across the Atlantic with reasonable allowances made for turnaround time. The studies indicated that increasing speed offered greater potential with regard to utilization and scheduling flexibility.

Beyond Mach 2.5, temperature effects prohibit use of practical composite materials (Figure 6). SCV's must use polyimide type composites. The epoxy versions being developed for subsonic aircraft cannot be employed for elevated temperature SCV application because of structural deficiencies brought on by moisture absorption.

Capacity

During the Lockheed economic studies conducted in Task II of the SCAR studies, the question of payload size was studied. The results, shown in Figure 7, indicate an economic plateau around 300 passengers. Below this number, return on investment (ROI) decreases due to increasing direct operating cost (DOC). Above this number the forecast traffic potential is not great enough to sustain utilization and would result in decreased flight frequency.

SCV MAJOR CONCERNS

The aforementioned design goals must be realized while fully recognizing the demands of other vital issues: cost, risk, noise, emissions (Figure 8). Performance advances can be obtained by two methods: improved flight efficiency in terms of lift-to-drag ratio and fuel consumption; and reduced airplane mass fractions, defined as the ratio of operating mass empty (OME) to takeoff gross mass (TOGM). Using today's technology an aircraft sized to 7400 km (4000 nautical miles) is not competitive. Mass and size need to be

reduced in order to reduce development costs, facility costs, first costs, and support costs. The reduced size aircraft also reduces noise and emissions. To minimize risk, the aircraft must reflect simplicity in design wherever possible. A simple aircraft design reduces unknowns.

Technology advancements required to produce a viable supersonic cruise concept must encompass all the related disciplines of propulsion, aerodynamics, structures, and controls.

PROPULSION

Lockheed considers the propulsion technology as one of the most important areas that can benefit from research and development. Propulsion technology encompasses long-lead-time, high-risk items. This technology offers improvements in fuel economy and economics along with reductions in noise and emissions. Propulsion involves not only the engine but inlet, nozzle, and propulsion/airframe integration.

Advanced Engines

Throughout the SCAR program, attention has been given to engine cycle studies. Lockheed has maintained a continuous exchange with the two engine manufacturers involved in the SCAR program: the Pratt and Whitney Aircraft Company and the General Electric Company. Many advanced engine cycles have been studied since 1973 as indicated in Figure 9. The number of cycles have been narrowed down from eight in 1973 to two in 1976. Turbojets, various-bypass-ratio turbofans, and various combinations of forward, rear, and dual-valved variable cycle engines (VCE) have been investigated. The two most promising cycles that have emerged are a medium-bypass-ratio turbofan, designated as a variable stream control engine (VSCE), and a double-bypass, dual-cycle engine. The valve concepts look complex with marginal benefits.

Performance results from these cycle development efforts are compared in Figure 10 with the 1971 SST engine. The best turbojet and fan are compared

along with three VCE concepts. Only small supersonic cruise fuel consumption benefits are offered by the more modern engines. The 1971 SST turbojet engine reflects near optimum cruise efficiency, whereas the modern engines reflect recognition of noise constraints which limit operating temperatures and require tailored exhaust profiles.

Subsonic fuel consumption for the SCAR engines are improved due to better off-design airflow schedules that result in less spillage and boattail drag. Large payoffs have come in improved engine mass due to advanced materials and lowered operating temperatures. The fan cycle offers the most attractive options to date due to its light mass and superior subsonic fuel consumption.

Noise

The critical airport noise problem for an SCV is jet exhaust noise. This problem, while not relevant for current subsonic transport design, is a major problem for Concorde. The SCAR studies have revealed four new potential schemes for relieving the jet noise problem. These schemes are shown in Figure 11 along with the mechanical suppressor which was available for first generation SST's. The shaded areas of the figure suggest areas of uncertainty for the various noise reduction methods. The mechanical suppressor, while offering the largest reduction potential, is the least attractive because of maintenance, stowage, and loss of nozzle efficiency. The coannular effect looks very attractive but to date has only been verified using small scale models. Full scale forward flight effects are required.

Optimization of the flight profile is a noise reduction method that is additive to the other schemes. Lift-to-drag ratio refinements brought about from high lift refinements, powered lift, and wing shape modifications, can be used to improve take-off and climb performance. Active controls can be employed for flight profile management.

Jet noise shielding provided by an above-wing engine installation appears to offer a new noise relief prospect.

Two airframe-engine arrangements that may offer this jet noise shielding potential are shown in Figure 12. The over-under engine arrangement could provide flyover noise benefits of 3 to 5 EPNdB while the acoustical staggered engine arrangement could provide sideline noise benefits of up to 3 EPNdB. The experimental results obtained from two recent independent test programs are summarized in Figure 13. The twin jet noise studies indicate a 3 EPNdB noise reduction beneath the path of the aircraft as compared to the noise levels 90 degrees to the plane of the twin jets. This data was obtained from University of Tennessee tests (Ref. 1) at relatively low jet velocities. General Electric Company data (unpublished) at higher jet velocities indicate noise reduction levels of 5 EPNdB.

Wing shielding benefit studies were made jointly by Lockheed and NASA to examine the use of wing structure as the shielding medium. A photograph of the configuration is shown in Figure 14. The effort stressed use of engines on top of the wing positioned to obtain noise shielding in combination with upper surface blowing to achieve aerodynamic improvements. The shielding benefits proved to be small. Erosion and corrosion problems plus sonic fatigue problems appear to be sizeable. Therefore the concept is not considered to be attractive.

Advanced Inlets

A serious propulsion need exists to develop advanced technology inlets to match and integrate with the development of advanced cycles. The B-70 and YF-12 are the only mixed compression inlets designed and built for supersonic aircraft. Both of these inlets incorporate technology of the 1960's.

The major areas of needed effort for advanced engine inlet technology are presented in Figure 15. Advanced control technology being developed today will allow for digital integrated propulsion controls for the inlet, engine, and nozzle package. The need for self-starting capability of the inlet must be verified. Inlet hardware commonality and simplicity have to be design goals for inlets even if designed for slightly different local Mach numbers at the inlet face.

An example of inlet airflow matching between inlet and engine for the General Electric double-bypass, dual-cycle engine is shown in Figure 16. Corrected airflow is plotted versus Mach number. The dashed lines indicate the initial SCAR inlet design using axisymmetrical inlets with translating centerbodies. These inlets are of the 1960 technology type. The final design features 2-D inlets with articulated centerbodies which allow for large throat area for transonic operation. All of the inlets are designed to have identical corrected airflow at cruise.

It should be noted that the over-wing inlet, due to its larger local Mach number, must have a 14 percent larger capture area at cruise to deliver the same corrected airflow to the engine. However, because of the airflow flexibility of the new proposed engines, the engines need only have different engine/inlet controls in order to be adaptable to either below-wing or over-wing installations. The mass increase of the larger over-wing inlet is offset by the ability of the inlet to supply increased transonic airflow resulting in a 25 percent thrust increase transonically with a corresponding 7 percent reduction in fuel consumption. These benefits offset partially the mass and friction drag penalties paid for the larger inlet.

Engine Location

SCV engine integration with the airframe is a complex design task that affects performance, flying quality, maintenance, and noise characteristics. A comprehensive engine location study was undertaken to identify the airplane performance, mass, and noise characteristics of several engine location arrangements (Figure 17). This study included over-the-wing, tail-mounted, and fuselage-mounted engines. Configurations incorporating three engines, T-tails, staggered engines, and canards were examined. Two configurations evolved which had superior performance characteristics: the over-under engine arrangement and the more conventional four-engines-under wing arrangement.

The over-under engine installation offers some unique characteristics that warrant more detailed investigation (Figure 18). High lift enhancement results

from increased flap span. Inlet unstart isolation is provided by wing structural shielding. Mass reduction is created by a more efficient engine support structure. Vertical tail size is reduced due to movement inboard of the critical engine-out moment arm. Flyover noise reduction is produced by jet noise shielding.

Concerns were expressed regarding engine/inlet airflow matching, hardware commonality for inlet and engine, and above-wing engine-out incremental forces and moments. These concerns were the basis for high speed wind tunnel tests. The tests examined the supersonic characteristics of an engine mounted over the wing as shown in Figure 19. No problems were revealed. Aerodynamic disturbances of inlet unstart for over-wing mounted engines were reduced over that for a conventional four-engines-under-wing arrangement, since the critical engine was further inboard and experienced reduced local dynamic pressure over the top of the wing. Favorable sidewash at the vertical tail was generated by the inlet flow disturbance.

AERODYNAMICS

An SCV concept must be configured to favor cruise efficiency. In recognition of this, much wind tunnel testing and analysis, together with analytic tools employing elaborate computer programs, have been developed over the years by both NASA and industry. A respectable data base regarding the importance and understanding of wing planform shape, equivalent body shape and fineness ratio, drag-due-to-lift minimization using twist and camber, and trim drag alleviation has been amassed. Further work is in progress in these areas. Nacelle-airframe integration, elements of which have already been discussed, also forms an important part of this current activity.

A critical problem with all aircraft designed for efficient high speed operation relates to the flight characteristics that these swept wing, slender body aircraft generate at subsonic speeds, and during take-off and landing operations. The design challenge is to seek out design features and refinements that improve these deficiencies.

For these reasons, Lockheed has spent much of its SCAR aerodynamic efforts on low speed studies, wind tunnel tests, and analysis. A photograph of the low speed model is shown in Figure 20.

Wing Development

The first generation SST developed by Lockheed during the FAA/SST program of the 1960's featured a low wing loading, double delta planform, tailless concept. The philosophy of this design was to aerodynamically eliminate aerodynamic center movement due to Mach number change (double delta planform); eliminate cruise trim drag with proper wing shape and center of gravity location to enhance cruise L/D (tailless configuration); and utilize a large wing area to permit higher altitude, lower sonic boom cruise operations, and at the same time allow operations in the terminal area without need for high lift devices. Fundamentally, the concept stressed simplicity.

Technology advancements made since that time suggest that alternatives to that design philosophy may offer attractive potential. In addition, different, and in some cases, more demanding design requirements are imposed by today's scenario. Noise is a more critical consideration and forces the aerodynamicist to develop better subsonic lift-drag ratio levels for airport operation. Vortex lift cannot be relied upon because of attendant vortex drag and resultant low levels of L/D. Camber lift and the L/D benefits of high lift flaps must be utilized.

The added complexity of high lift devices is measurably offset by the benefits in wing mass savings, achieved because the high lift devices permit adoption of a higher design wing loading (smaller wing). The wing mass savings has a significant favorable impact on design range or gross mass for a given range. The best wing loading for achieving maximum payload range characteristics is always higher than the wing loading desired for airport performance needs. All subsonic transports in operation today adopt wing loadings that favor cruise performance, and adopt high lift devices to tailor the wing aerodynamic characteristics to provide good airport performance characteristics. A similar philosophy applied to an SCV therefore seems like an attractive prospect.

Figure 21 depicts the major considerations affecting wing area selection for a given payload range supersonic cruise airplane. The incremental range gain with decreasing wing area shows the benefit for cruise operation at wing loadings for best cruise efficiency. A 1970 technology design wing area is identified. The range benefit obtainable from improved lift augmentation is indicated by the 199X objective wing size.

Takeoff field length and approach speed sensitivity to reduced wing area are shown in the side plots. These figures serve to indicate the need for advancements in high lift required to achieve satisfactory speeds and field lengths, when taking the high wing loading option.

High Lift Assessment

Lift enhancement is made difficult by the very features which are responsible for its high cruise efficiency - leading edge sweep and reduced span. Large wing leading edge sweep angles are desired so that the leading edge falls behind the Mach line in cruise. This geometry relationship produces benefits in cruise L/D, and allows for rounded wing leading edge shapes that benefit low speed L/D. Trailing edge sweep also improves supersonic L/D levels. Hence for best supersonic cruise efficiency, the highly swept arrow wing offers the greatest potential.

Extreme sweep, combined with low span, offers very poor low speed aerodynamic characteristics, and requires auxiliary means for achieving desired levels of performance. One potential solution to the problem is to adopt the variable sweep wing design concept - configure a wing with an inboard pivot that will allow for rotation of an outer wing panel, so as to reduce its sweep and increase wing span for low speed operations. This novel design idea was thoroughly explored in the FAA/SST program of the 60's, and was abandoned because of extreme design complexity and mass bogies.

Use of a fixed wing with supersonic leading edge sweep offers some relief to the low speed problem, but the benefits do not totally eliminate the need for

auxiliary geometry changes. The exception to this would be use of large wing areas (the Lockheed approach of the 1960's).

The present Lockheed philosophy is to recognize the need for high lift devices (Figure 22), and accept the challenge that these auxiliary flaps be developed so as to provide satisfactory low speed aerodynamic characteristics while adopting the most efficient high speed wing shape - the arrow wing.

The development task that needs to be done can and should include the following considerations:

Angle of attack - high values produce more lift, but also more vortex drag, worsen flight station visibility, and require a longer landing gear.

Active controls - offer the potential for using relaxed static stability as a means for alleviating the trim drag normally associated with flap deflection (it should be noted that the notch of the arrow wing also helps alleviate flaps-down trim problems, since the flap is located in a more forward location than would be the case with an unnotched planform).

Powered lift - the high thrust-weight ratio of the SCV suggests the use of vectored thrust, or engine bleed air for BLC, as a further means for achieving lift for takeoff.

Folding wing tips - can be employed to provide tip extensions for low speed operation, and retract during normal flight regimes.

Figure 23 illustrates how flaps and relaxed static stability help improve the low speed characteristics. The flaps generate camber lift producing an increased lift at constant angle of attack. The flaps also generate additional nose down pitching moment. However, the trim requirement needs are alleviated by moving the center of gravity aft. Tail loads are not needed for trim but, as indicated, the aircraft will operate with a negative static margin. Results from NASA and Lockheed low speed wind tunnel tests indicate that a trimmed

approach lift coefficient compatible with the wing loading desired for best payload and range can be attained at an acceptable angle of attack. These data show that the incremental pitching moment coefficient from the trailing edge flaps requires a relaxation of inherent static stability requirements by about 6-8 percent. Relaxed Static Stability (RSS) is predicated on the continued development of necessary active control stability augmentation systems.

Additional lift enhancement is proposed for the Lockheed SCAR baseline configuration by means of folding wing tips (Figure 24). During cruise these panels are vertical, adding to the directional stability. At low speed, when the trailing edge flaps are extended, the wing tips are redeployed horizontally. Wind tunnel tests verify that the added span improves the lift curve slope so that at approach angle of attack, a supplemental lift increment of approximately 10 percent can be realized by reasonably sized tip extensions.

The use of powered lift to enhance arrow wing lift characteristics has received serious attention. One application, using upper surface blowing as a means for supplementing flap lift, was discussed early in connection with Figure 14. Other means studied were vectored thrust and BLC. Analytic studies and large scale NASA wind tunnel tests have been carried out. Lockheed assisted in the data analysis of these tests.

Findings are summarized in Figure 25. Shown is the thrust increase needed to provide added lift, as a function of the reduction in approach speed permitted by the lift increment, assuming fixed approach attitude. Compared are the relationships using simple flap deflection, flaps with hinge line chordwise blowing, and thrust vectoring by means of tilting exhaust nozzles. The figure shows that in the range of flap effectiveness linearity ($\delta_f = 0^\circ - 30^\circ$), use of powered lift requires greater levels of approach thrust to achieve a given decrement in approach speed. Greater thrust means higher approach noise. Therefore, these results do not suggest any advantage for powered lift. However, the potential of this idea has not yet been fully explored, and further study of powered lift appears to be warranted.

STRUCTURES

Advances in aircraft structures offer significant potential when applied to supersonic cruise vehicles, with the prospect that the "1960 all-titanium structure" vehicle mass can be decreased by ten percent. This will be achievable because of new developments in materials, controls technology, manufacturing processes, and analytic methods.

As part of the NASA SCAR activities, Lockheed performed a one year structural design contract study of an arrow wing planform SCV. This program exercised the latest computer aided analytic techniques and advanced materials options, and studied numerous structural design concepts. Design criteria, design conditions, stress allowables, loads, structural arrangements, masses, aero-elastic characteristics, and flutter behavior were all established during this detailed study. Results are presented in Reference 2.

Materials

A new structural advancement receiving great attention at present is the prospect of using new composite materials to replace metal alloys. These composites are formed from filaments of metal or carbon imbedded in a formable matrix. The orientation of the fibers can be arranged to produce any desired structural property with regard to load intensity and direction. Strength/mass properties exceed conventional metal alloys. Therefore, these new materials have the potential of offering lighter, more efficient structures for advanced aircraft.

Figures 26 and 27 show Lockheed aircraft that are being used to obtain flight service experience with these new materials. The L-1011 is being used to examine epoxy type composites in support of the NASA ACEE program. The YF-12 shown is a NASA research vehicle operated by Dryden Research Center, and is being used to obtain real world high temperature advanced materials characteristics in the actual flight environment of future SCV concepts.

Adoption of these new materials for commercial transport application will require an extensive, time consuming, development program. Current projections are shown in Figure 28. Most emphasis is being directed towards the epoxy subsonic aircraft type materials. Adoption of the high temperature materials for SCV use will require accelerated program activity, if these new materials are to see extensive application in basic structures.

Projected benefits of high temperature composites in reducing SCV size are shown in Figure 29. Using 1985 technology, take-off gross mass decreases 6 percent over 1980 technology, reducing the aircraft cost by \$8 million (based on a production run of 300 aircraft).

Manufacturing Technology

A very significant technology emerging from the SCAR program is new manufacturing techniques such as high temperature forming (superplastic forming) and no-draft forming (Figure 30). These techniques significantly impact fabrication cost by eliminating machining operations, and by providing large structural assemblies with fewer detailed parts. Figure 31 shows a typical cost comparison to indicate the savings of using the no-draft precision forging method. Ninety percent less material is used with the total cost reduced by 75 percent. This real-world component, a titanium tail bumper forging used on the L-1011, is shown in Figure 32. Further applications and development will offer even greater opportunities to save mass and reduce production costs for 1990 airplanes.

Analytic Methods

Many new analytic methods have emerged since the first generation SST program (Figure 33). The benefits from these new analytic methods include accelerated design processes, more efficient structure, greater accuracy, improved correlation of theory and experimental tests, all at reduced cost. The structural design iteration process requires involved analyses and many technical disciplines (Figure 34). The ability to use computer programs which are properly

interfaced and combined with computer graphics, measurably helps to improve response time and accuracy of results.

Shown in Figure 35 is a typical arrow wing structural model used for analysis. A computer derived map of temperature contours for one particular design condition is presented in Figure 36. A graphic representation of static deformation of the wing is shown in Figure 37.

CONTROLS

The most promising advanced technology that will see early implementation on future subsonic transport aircraft will involve use of advanced controls. These advances will pave the way for extensive application on SCV's in the 1990's. This belief is highlighted by the milestone chart of Figure 38. Certified use of active controls for load relief on the L-1011 is projected by 1982.

Potential active controls benefits are illustrated in Figure 39. Throttle management, programmed flaps, and relaxed stability will produce better climb profiles, less trim drag, and resulting noise relief. Maneuver load control, gust load alleviation, elastic mode suppression, and relaxed stability are means for mass savings that will be developed in the 1980's on subsonic aircraft. Flight station ride quality and envelope limiting are safety items needed for long-body aircraft. Relaxed stability, fuel management, and inlet controls will improve performance by reducing trim drag and improving engine performance.

The projected impact of active controls on take-off gross mass is presented in Figure 40. The benefits are the result of analyses performed using the arrow wing structure studies results presented in Ref. 2. The benefits shown may appear to be small. However, it should be appreciated that the mass savings indicated follow benefits already realized by propulsion, aerodynamics, and materials advanced technology.

CONCEPT DEVELOPMENT

A vital need of the SCAR program has been to assess technology advances to indicate the impact, relative benefit, and research priorities for the various emerging improvements. The following paragraphs describe a potential 1990 SCV design that adopts the technology advances discussed in previous paragraphs.

Figure 41 presents a summary of the advanced technology items that were adopted. An advanced turbofan is employed in an over-under engine arrangement. Potential noise relief options are envisioned as allowing the engine to be sized for maximum payload and range while meeting noise standards. The wing can be optimized for cruise while being tailored to meet low speed needs by use of a high lift system combined with relaxed static stability. New materials and fabrication techniques are employed along with active controls.

To meet the 290 passenger, 7400 km (4000 n. mi.) design requirement using 1970 technology would require a 385,500 kg (850,000 lbm) aircraft, as shown in Figure 42. Advanced technology reduces take-off gross mass by 117,000 kg (260,000 lbm). The mass reduction is distributed between the various technologies of propulsion, aerodynamics, and structures. The cross-hatched area indicates potential attainable with more optimistic advancements.

Concept Description

The concept, shown in Figure 43, is 89.5 m (294 ft) long with a 36.4 m (119.5 ft) wing span.

A summary of the concept characteristics is shown in Figure 44. The takeoff gross mass is 268,500 kg (592,000 lbm) with a payload fraction of 9 percent or 26,300 kg (58,000 lbm). The engine airflow size at take-off is 270 kg/s (600 lbm/sec). This is approximately the same engine size as employed by today's wide-body transports. The approach speed is 81 m/s (158 knots). The wing area of 624 m² (6720 ft²) corresponds to a wing loading of 430 kg/m² (88 PSF) at takeoff. FAR part 36 noise levels are met.

Payload-range characteristics are shown in Figure 45. The 26,300 kg (58,000 lbm) payload reflects only passengers and their baggage with no provisions for cargo. The total fuel load is approximately 136,000 kg (300,000 lbm) with the reserve fuel being 70 percent of the payload. The aircraft requires a 3350 m (11,000 foot) takeoff field length on a hot day and a 3050 m (10,000 foot) landing field length.

Figure 46 compares the advanced SCV concept with the first generation Lockheed L-2000 design. The concept has increased range and carries more passengers at a slightly slower speed. It employs a smaller wing, and has a longer fuselage to accommodate the increased payload. There is no projected improvement in sonic boom. The masses are about the same.

Operating Costs

Prediction of real operating economics for a 1990 aircraft is impossible to do reliably. However, some meaningful trends are illustrated in Figure 47. Total operating cost (TOC) is plotted as a function of seat cost using 1973 dollars and 8.7¢/liter (33¢/gallon) fuel cost. An SCV will have higher cost per seat than for subsonic transports - it is a more technology intense airplane. The operating cost will be higher because of increased fuel requirements, increased engine maintenance, and lack of cargo revenue. However, Lockheed studies indicate the possibility of an attractive realization of return on investment (ROI) even if the operating costs are 10 - 20 percent higher than the subsonics. What is presumed is that SCV's will provide all one-class passenger accommodations, that is, first class supersonic service with fare levels between present day tourist and first class rates.

CONCLUDING REMARKS

Technology accomplishments that strongly benefit economics have been identified (Figure 48). Small wing size, composite materials, and active controls provide improved performance with a smaller airframe-engine combination. Advanced

manufacturing techniques and refined analytic tools show promise of providing lower development and fabrication costs.

The technology accomplishments that benefit ecology are presented in Figure 49. Engine cycle development and coannular noise relief have led to a light mass, reduced exhaust velocity turbofan. Jet and structural shielding benefits support the use of the over-under engine concept.

Future SCAR effort should follow the guidelines indicated in Figure 50. In propulsion, a scaled engine demonstrator is needed to verify predicted cycle characteristics. In-flight noise relief tests are critical and need more priority. Inlet research is needed to keep pace with cycle development. In aerodynamics, more wind tunnel testing is needed to verify emerging analytical methods. In structures, development of materials and manufacturing techniques should be accelerated. Large scale hardware programs should be implemented.

REFERENCES

1. Goethert, B.H.; Maus, J.R.; and Dunnill, W.A.: Investigation of Feasible Nozzle Configuration for Noise Prediction in Turbofan and Turbojet Aircraft. FAA-RD-75-162, July 1975.
2. Sakata, I.F.; and Davis, G.W.: Advanced Structures Technology Applied to a Supersonic Cruise Arrow-Wing Configuration. Proceedings of the SCAR Conference, NASA CP-001, 1977. (Paper No. 29 of this compilation.)

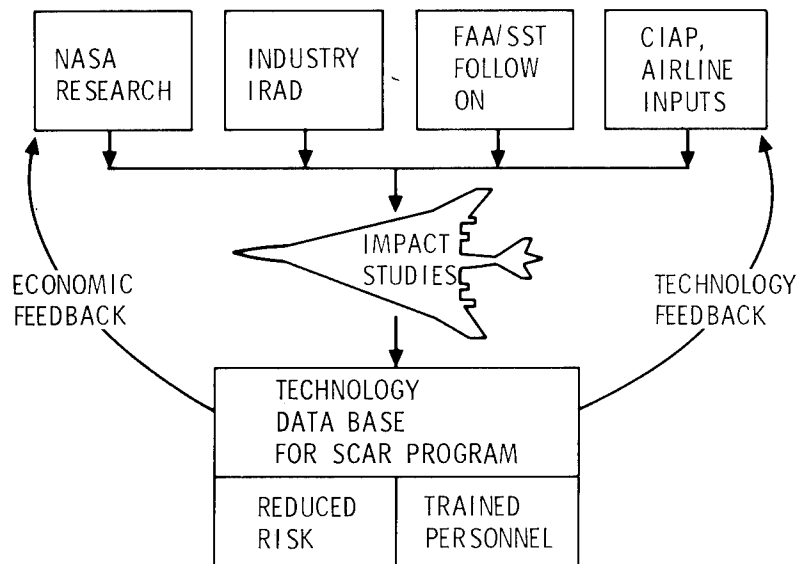


Figure 1.- Technology - why?

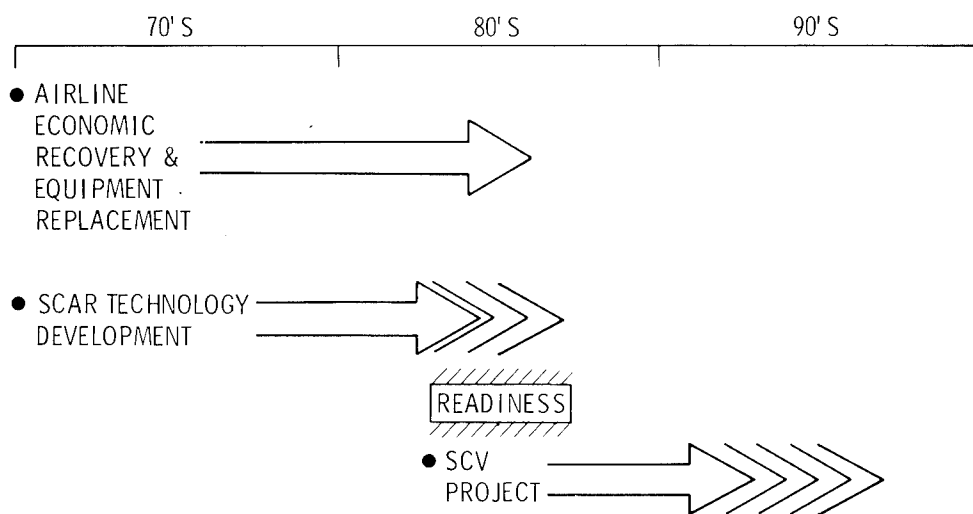


Figure 2.- Technology - when?

	INITIAL PRODUCTION	GROWTH DERIVATIVES
RANGE	TRANS-ATLANTIC	TRANS-PACIFIC (GROSS MASS STRETCH)
SPEED	2.55 \pm <u> </u>	2.55 \pm <u> </u>
PAYLOAD	9%	11%

Figure 3.- Performance philosophy.

4000 N.MI. PROVIDES OPERATIONAL SERVICE BETWEEN THE
FOLLOWING CITY PAIRS:

	GREAT CIRCLE DISTANCE	
	<u>km</u>	<u>(N. MI.)</u>
NEW YORK - LIMA	6945	(3750)
ANCHORAGE - COPENHAGEN	6936	(3745)
NEW YORK - ROME	6862	(3705)
HONOLULU - TOKYO	6188	(3341)
TOKYO - ANCHORAGE	5563	(3004)
ANCHORAGE - NEW YORK	5430	(2932)

Figure 4.- Range.

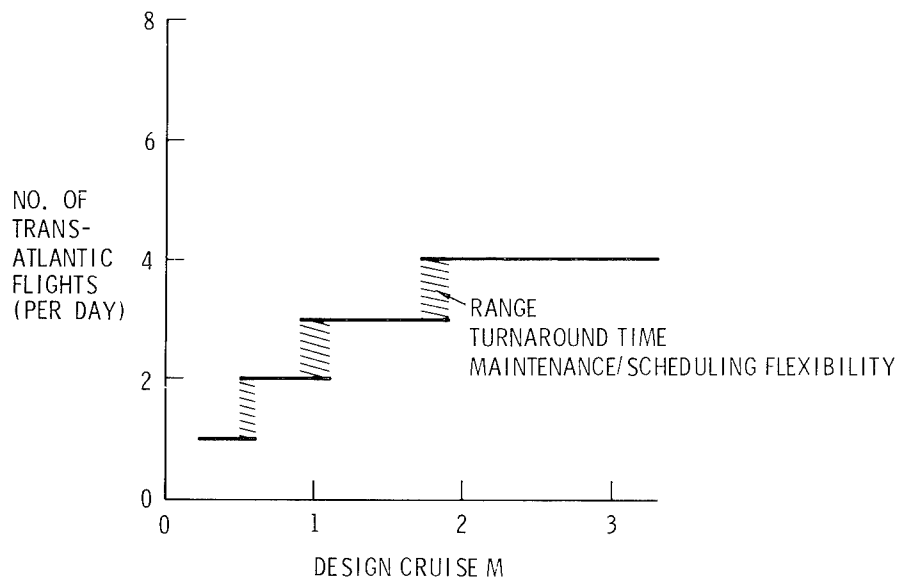


Figure 5.- Speed - scheduling impact.

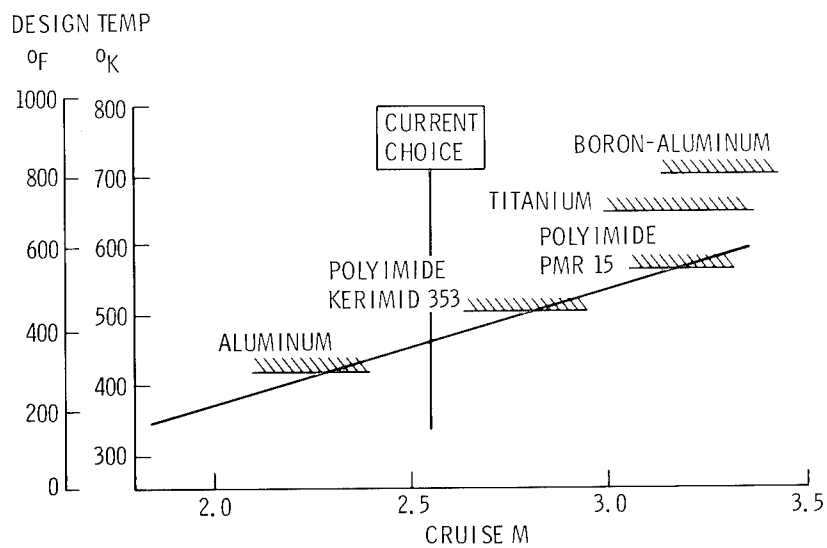


Figure 6.- Speed - materials impact.

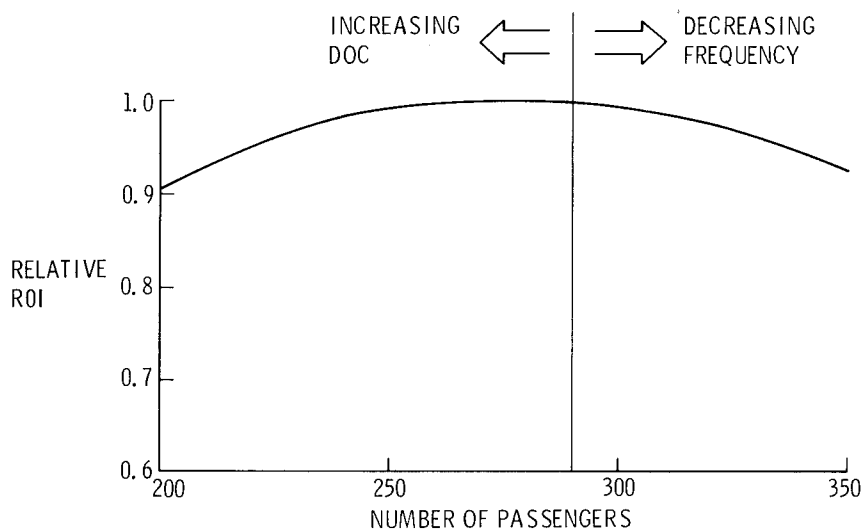


Figure 7.- Capacity.

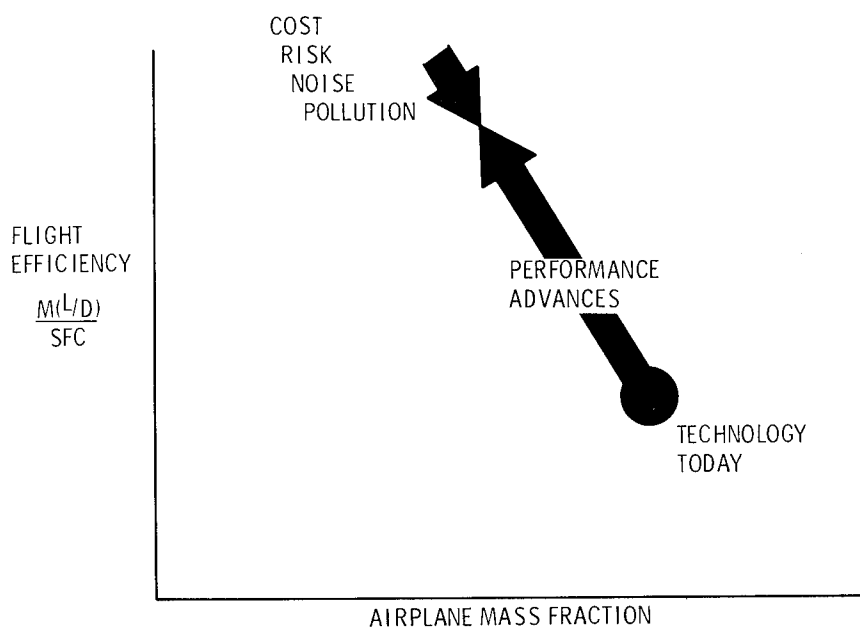


Figure 8.- SCV major concerns.

<u>1973</u>	<u>1974</u>	<u>1975</u>	<u>1976</u>
● MINI-B/P TJ	● LOW BPR A/B TJ	● LOW BPR A/B TJ (NEAR TERM)	
● LOW BPR VSCE	● MED BPR VSCE	● MED BPR VSCE	● MED BPR VSCE
● MED BPR VSCE	● MED BPR VSCE (IMP BURNER)	● DBL BYPASS DUAL CYCLE VCE	● DBL BYPASS DUAL CYCLE VCE
● HIGH BPR DBTF	● HIGH BPR DBTF	● REAR VALVE VCE	
● LOW BPR MIXED A/B TF	● SGL VALVE VCE		
● SGL VALVE VCE	● DBL BYPASS DUAL CYCLE VCE		
● DBL VALVE VCE	● REAR VALVE VCE		
● DBL VALVE VCE MIXED FLOW			

Figure 9.- Advanced engines.

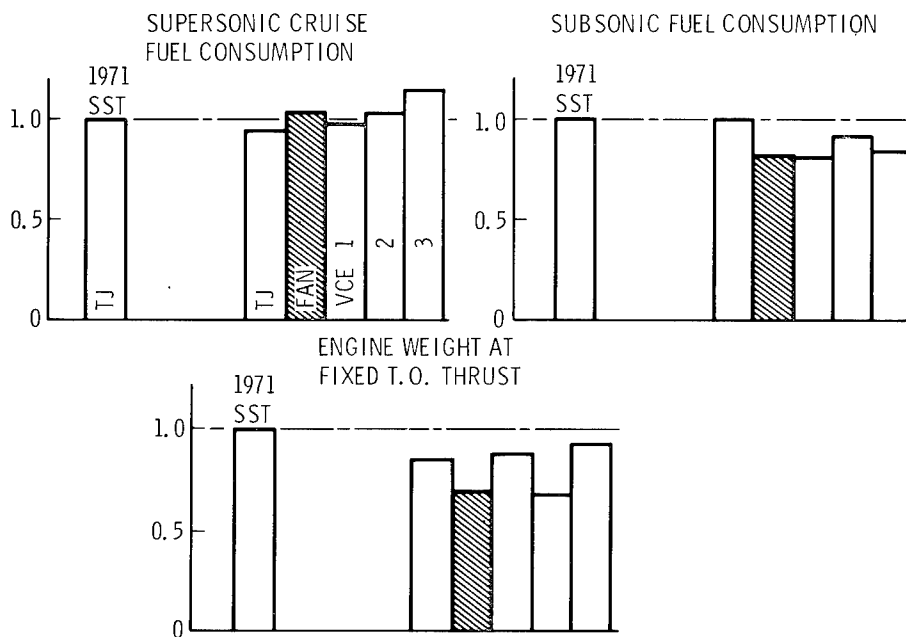


Figure 10.- Engine cycle comparisons.

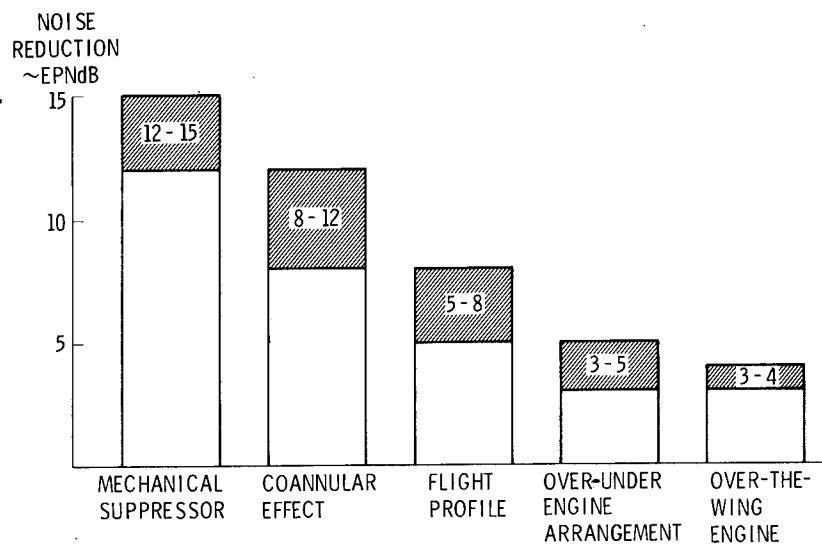


Figure 11.- Noise reduction potential.

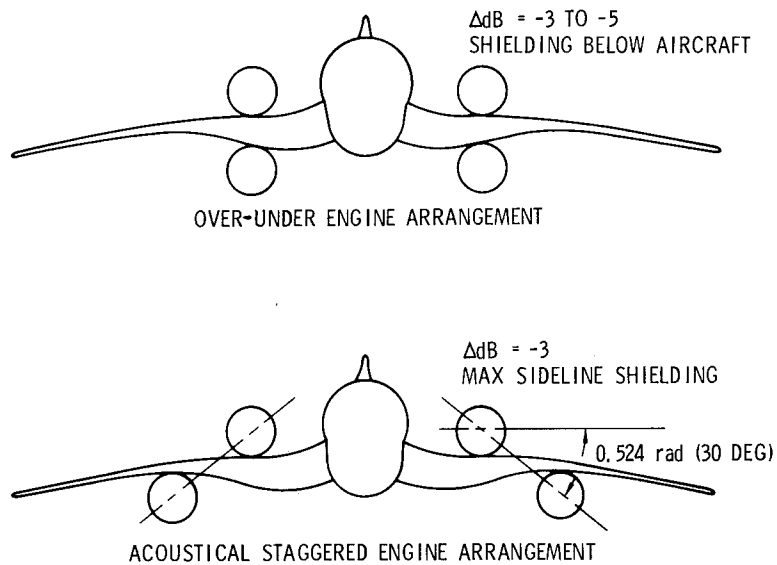


Figure 12.- Engine arrangement shielding benefits.

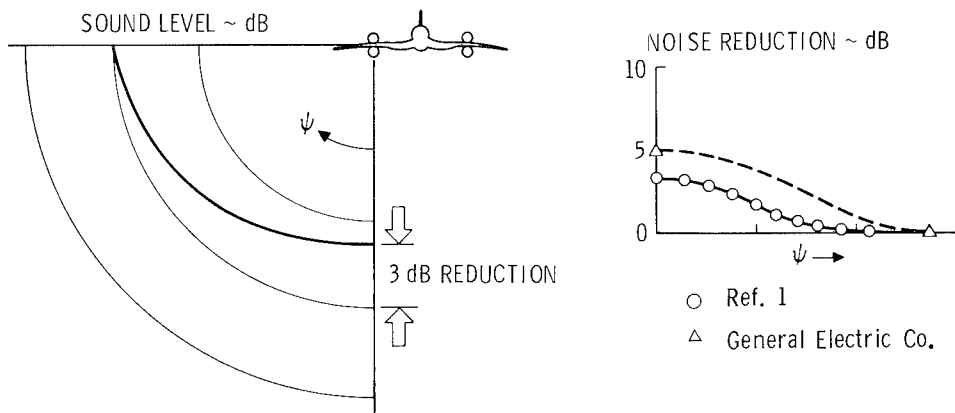


Figure 13.- Twin jet noise studies.

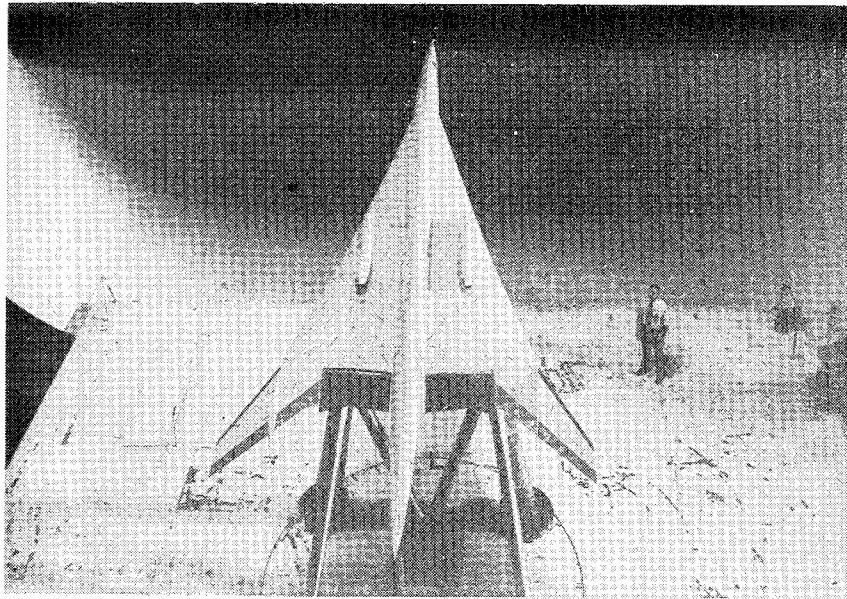


Figure 14.- Over-the-wing shielding benefits.

- ENGINE/INLET AIRFLOW MATCHING FOR MAXIMUM PROPULSION SYSTEM PERFORMANCE
- VARIABLE PERFORMANCE/STABILITY TRADEOFF
- DIGITAL INTEGRATED PROPULSION CONTROLS
- SELF-STARTING CAPABILITY
- ENGINE/INLET COMPATIBILITY
- HARDWARE COMMONALITY AND SIMPLICITY

Figure 15.- Advanced engine inlets.

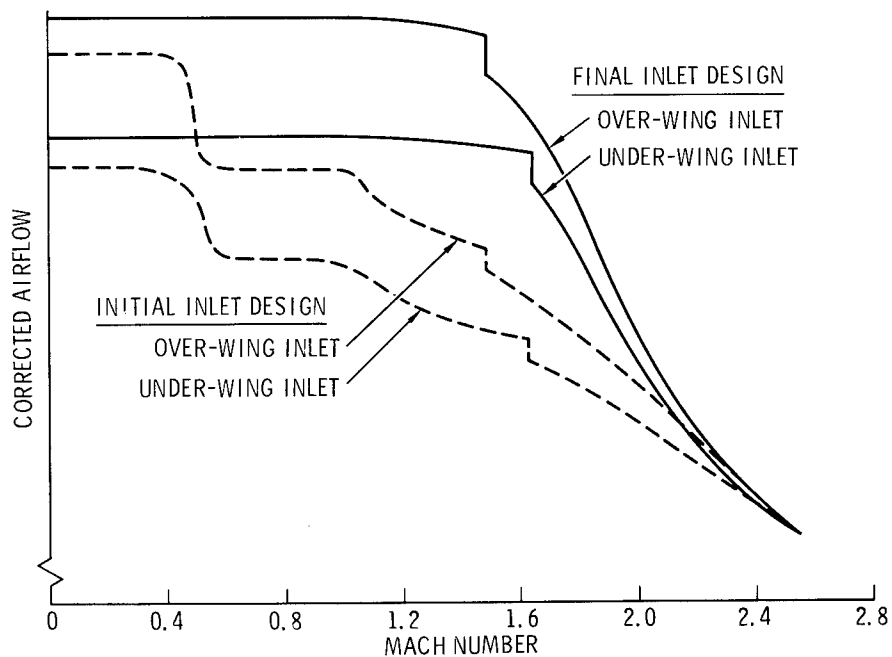


Figure 16.- Inlet airflow optimization.

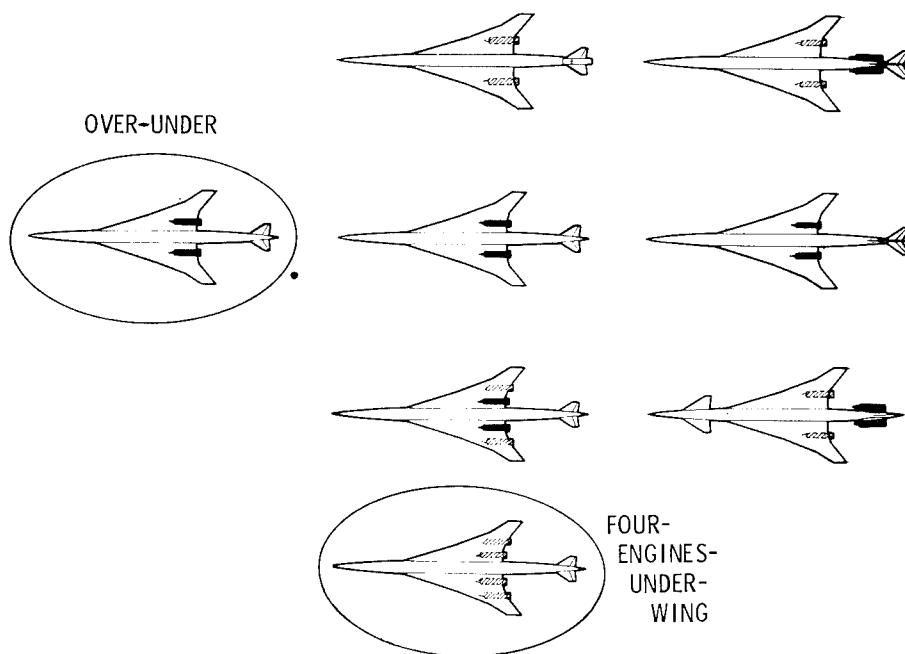


Figure 17.- Engine location study.

- HIGH LIFT ENHANCEMENT
- INLET UNSTART ISOLATION
- WEIGHT REDUCTION
 - ENGINE SUPPORT STRUCTURE
 - VERTICAL TAIL
- FLYOVER NOISE REDUCTION
- INSTALLATION CONSIDERATIONS
 - ENGINE/INLET AIRFLOW MATCHING
 - HARDWARE COMMONALITY
 - INCREMENTAL FORCES AND MOMENTS

Figure 18.- Over-under engine installation.

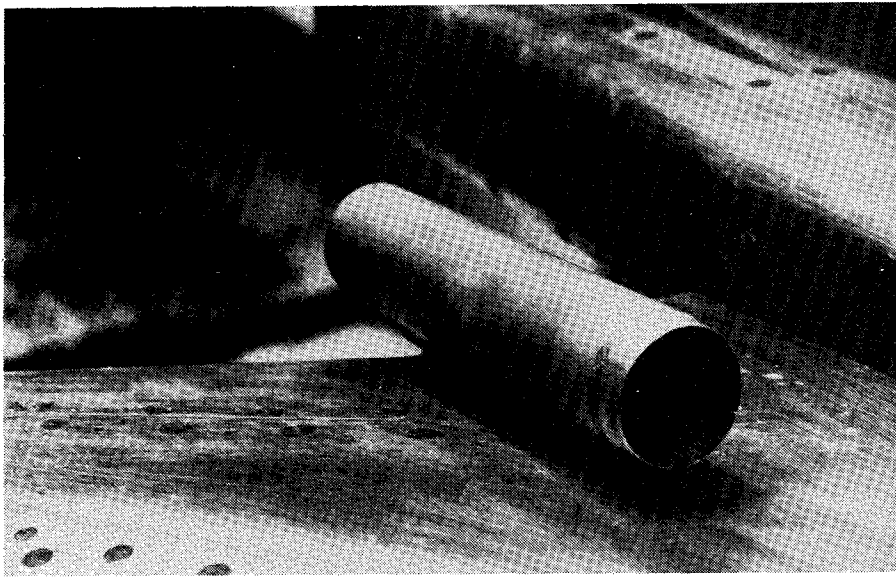


Figure 19.- Inlet unstart test.

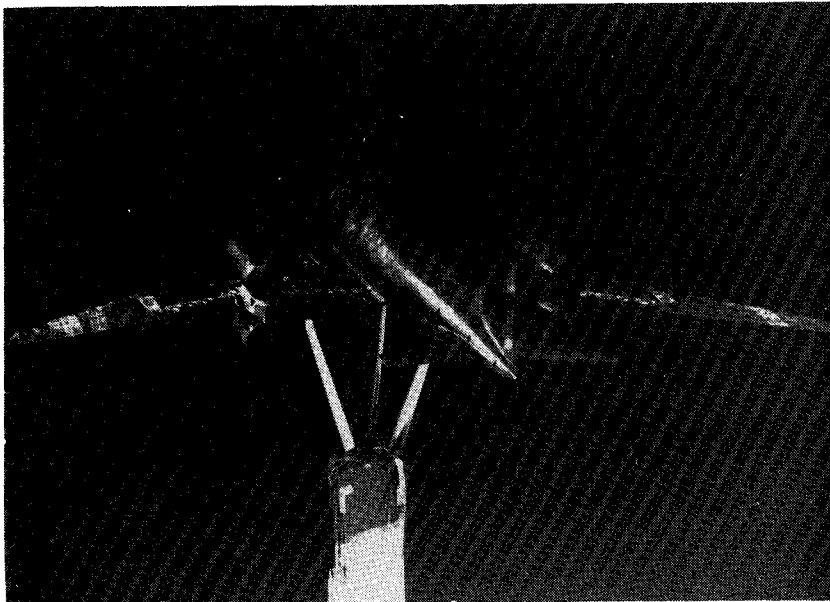


Figure 20.- High lift development model.

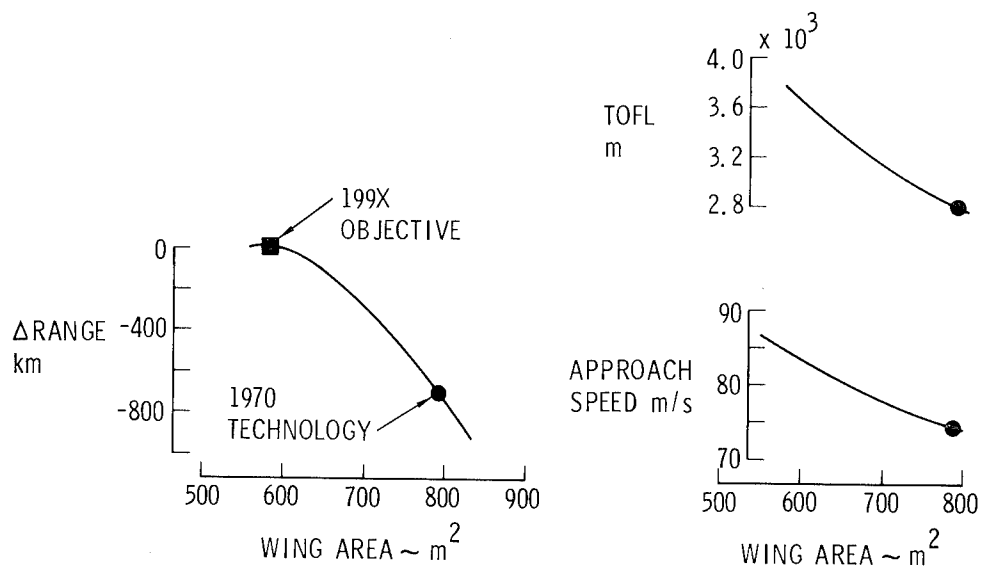


Figure 21.- Wing area selection.

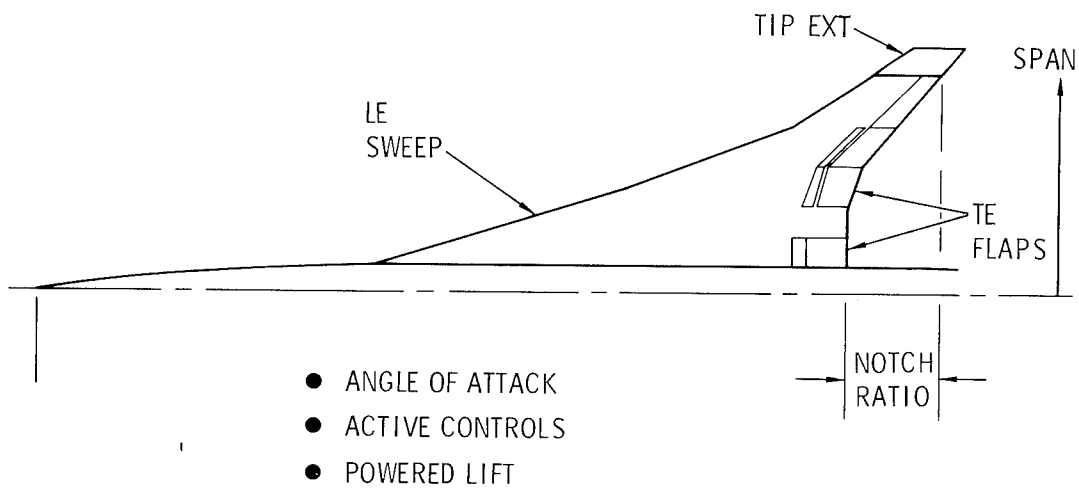


Figure 22.- Low speed lift enhancement.

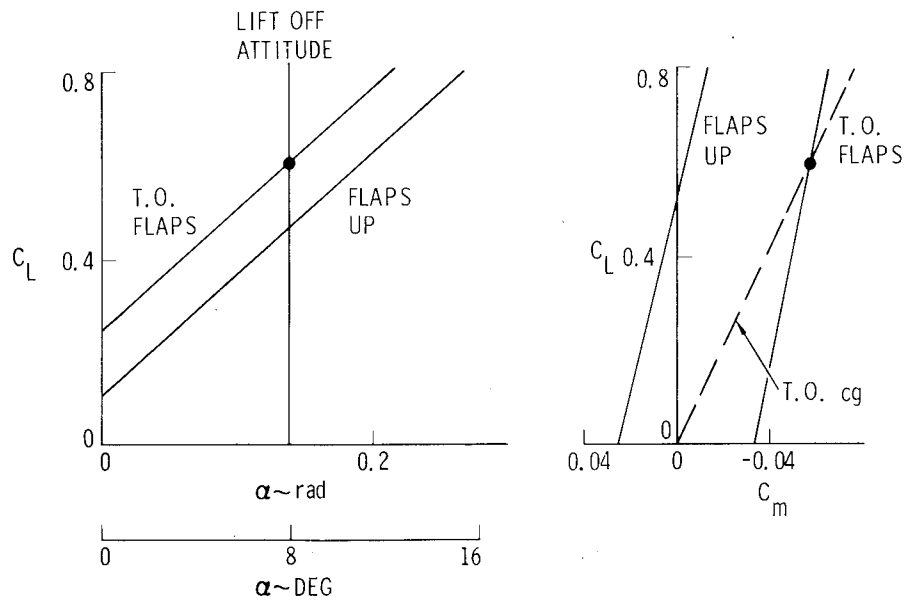


Figure 23.- Benefits of flaps and RSS.

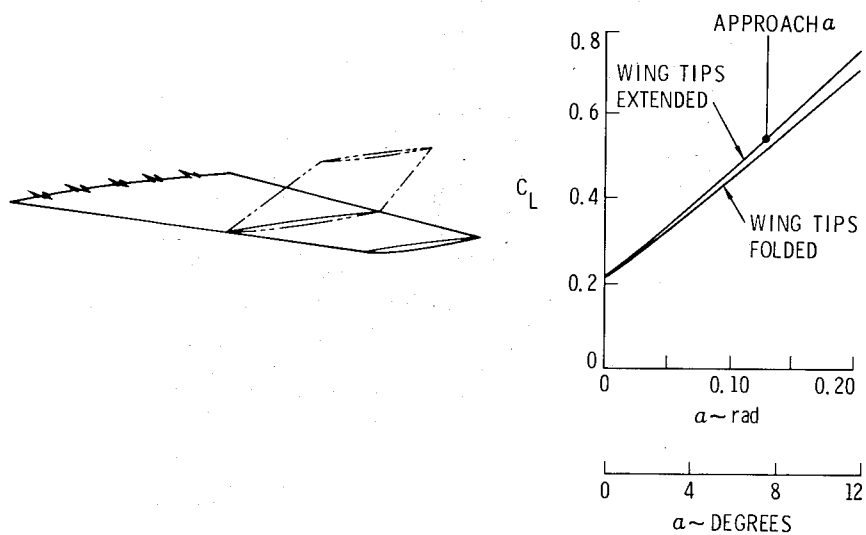


Figure 24.- Folding wing tips.

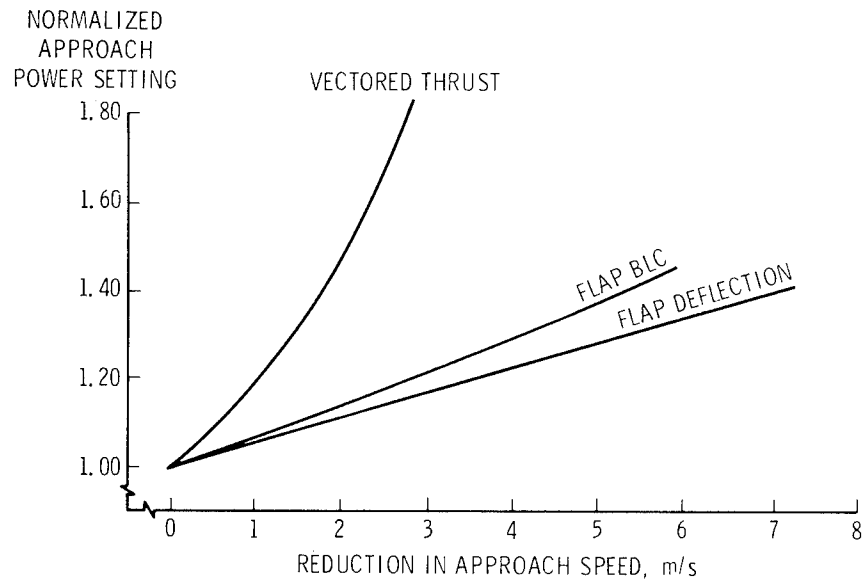


Figure 25.- Powered lift.

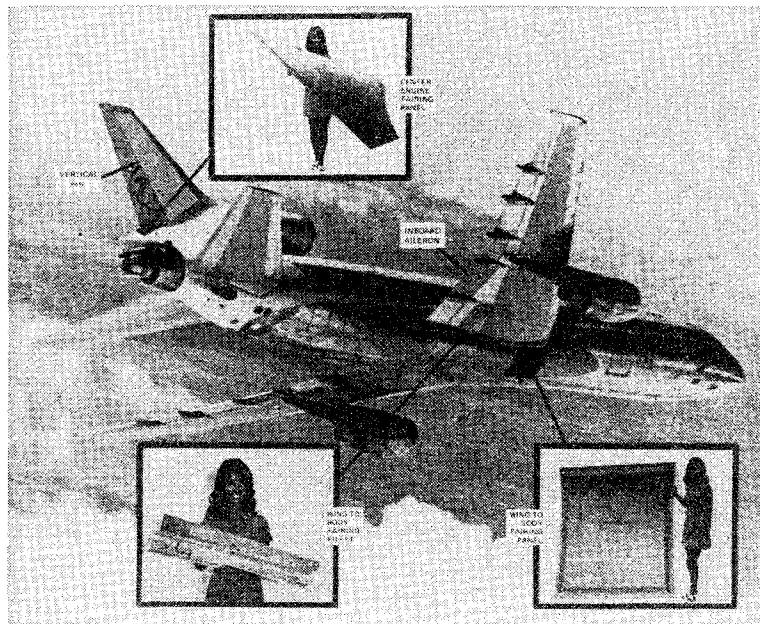


Figure 26.- Advanced material development.

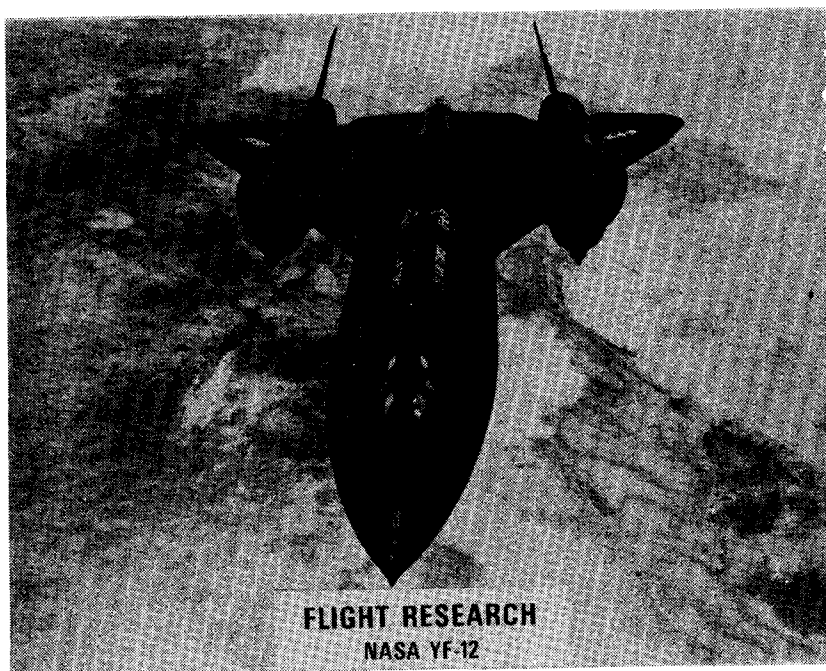


Figure 27.- YF-12 panel tests.

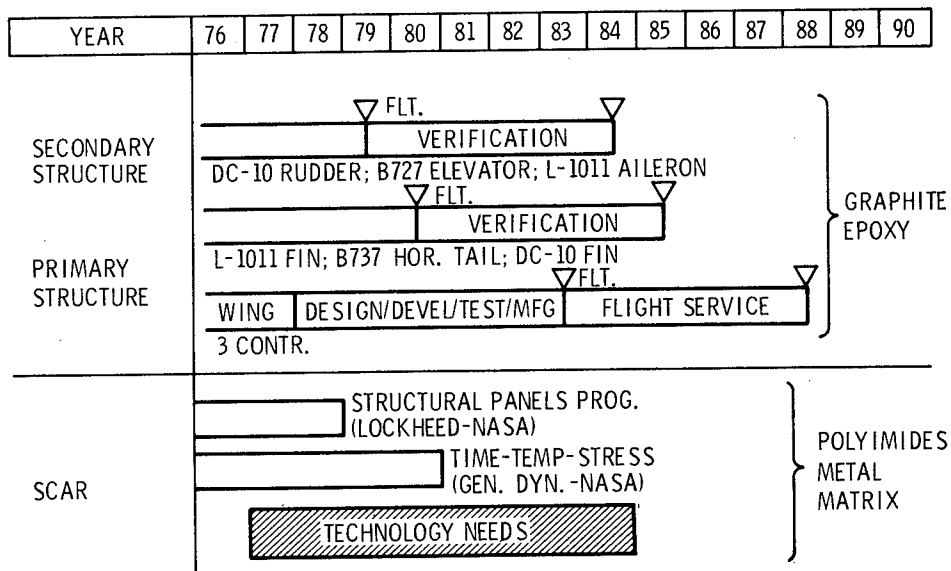


Figure 28.- Advanced composites technology schedule.

TAKEOFF GROSS MASS

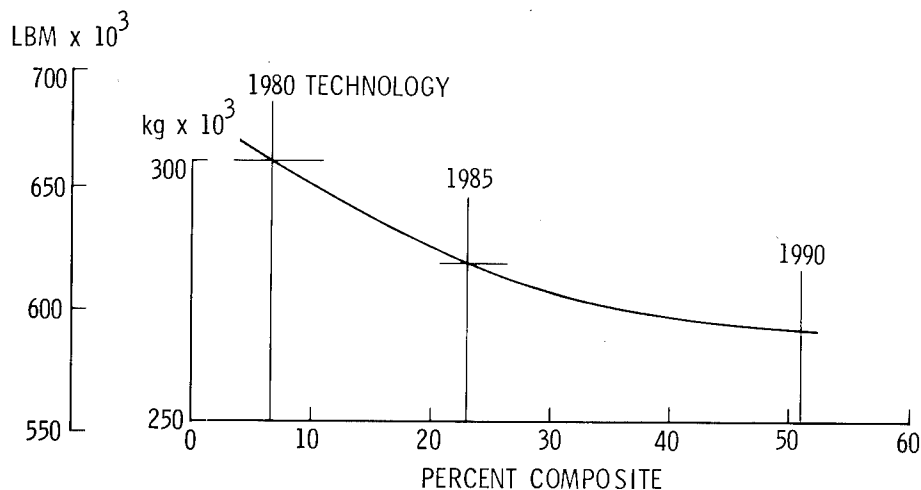


Figure 29.- Composite materials impact.

NEW TECHNIQUES

- LOW-COST—NO-DRAFT PRECISION TITANIUM FORGING
- SUPERPLASTIC FORMING

PAYOFF

- ELIMINATES MACHINING
- MINIMIZES NUMBER OF PARTS
- REDUCES MASS AND COST

Figure 30.- Advanced manufacturing technology.

L-1011 TAIL BUMPER SUPPORT

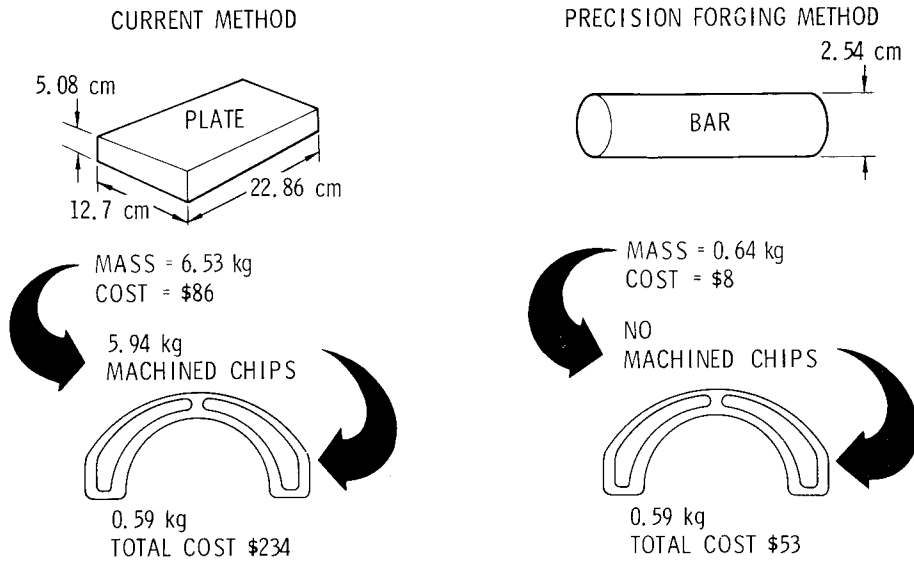


Figure 31.- Low-cost—no-draft precision titanium forging.

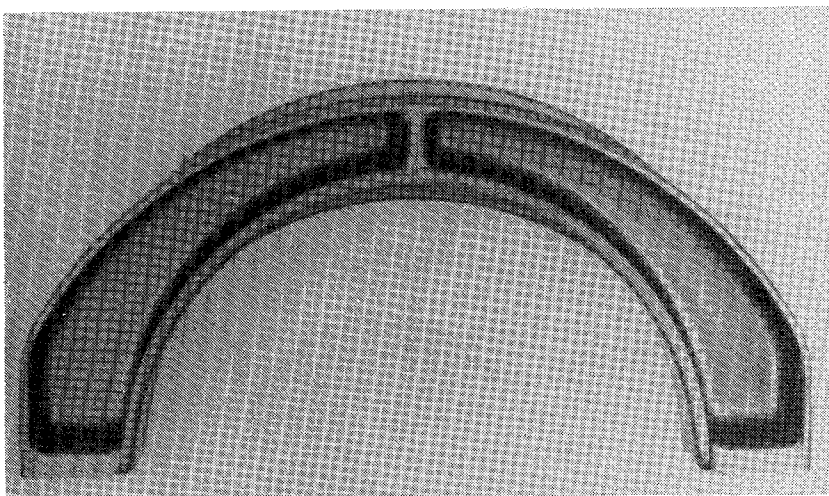


Figure 32.- Titanium manufacturing.

- NASTRAN-FAMAS SYSTEM
AUTOMATED STRENGTH SIZING

- CADAM
- CSMP
- GFAM

- ACCELERATED DESIGN PROCESS
- ENGINEER-IN-THE-LOOP
- EFFICIENT STRUCTURE
- REDUCED COST

Figure 33.- New analytic methods.

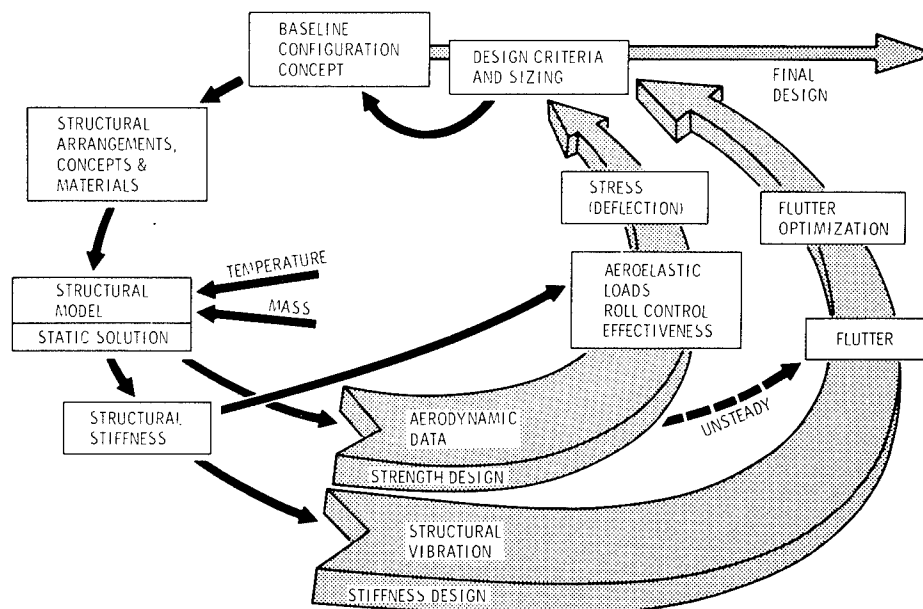


Figure 34.- Structural design methodology.

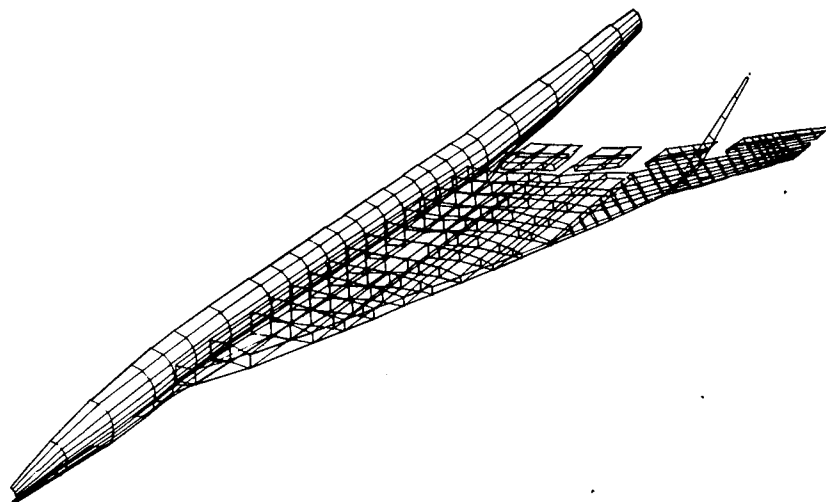


Figure 35.- Finite element structural model.

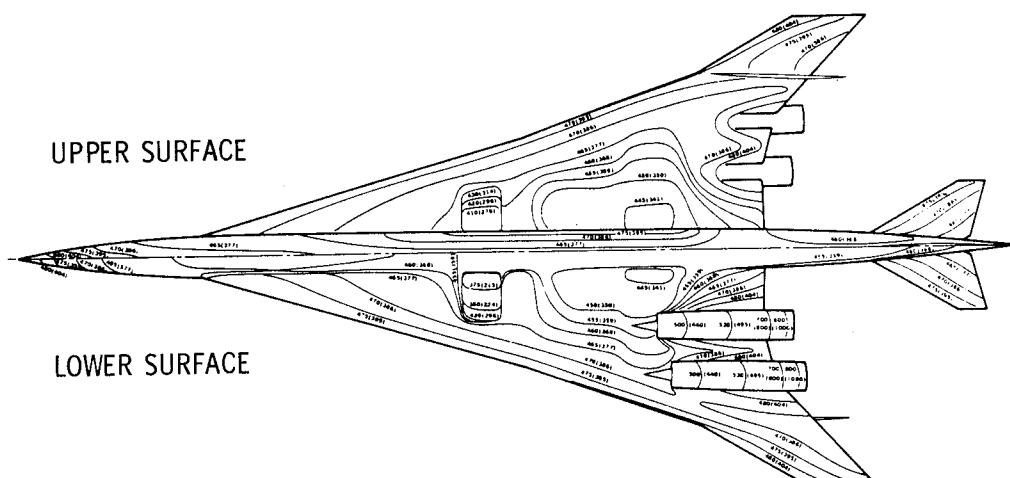


Figure 36.- Temperature contours.

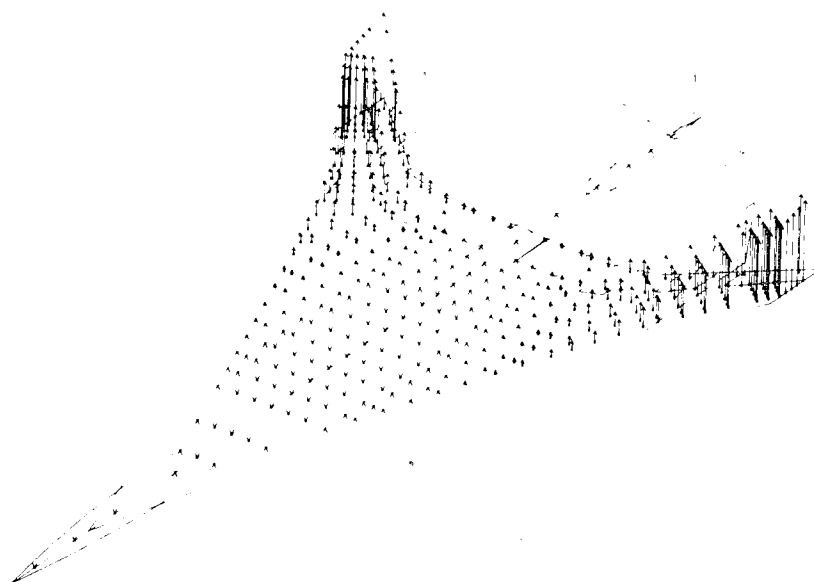


Figure 37.- Static aeroelasticity.

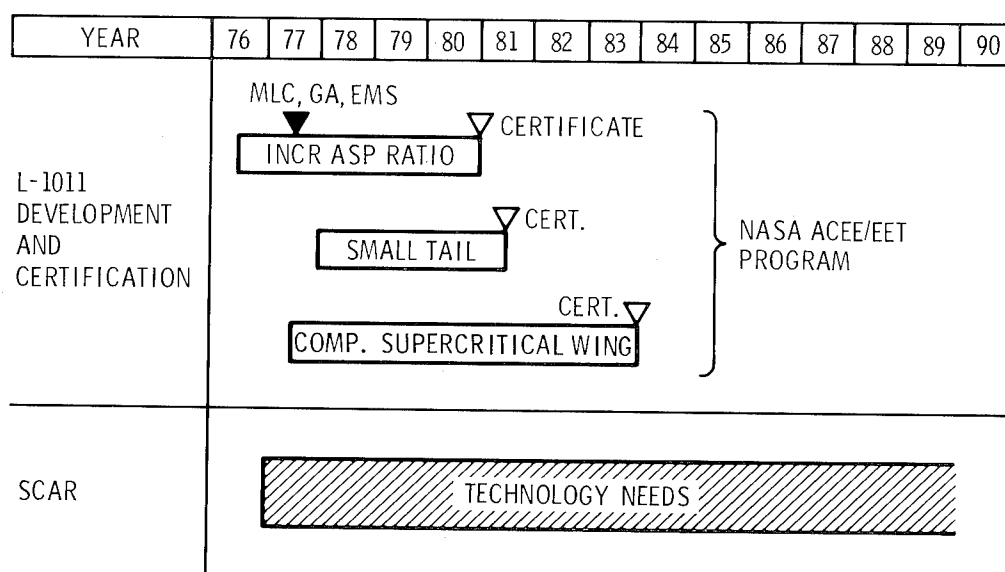


Figure 38.- Advanced controls technology development schedule.

NOISE RELIEF

- THROTTLE MANAGEMENT
- FLAP PROGRAMMING
- RELAXED STABILITY

MASS SAVINGS

- MANEUVER LOAD CONTROL
- GUST ALLEVIATION
- ELASTIC MODE SUPPRESSION
- RELAXED STABILITY

SAFETY

- FLIGHT STATION RIDE QUALITY
- ENVELOPE LIMITING

PERFORMANCE

- RELAXED STABILITY
- FUEL MANAGEMENT
- INLET CONTROLS

Figure 39.- Active controls benefits.

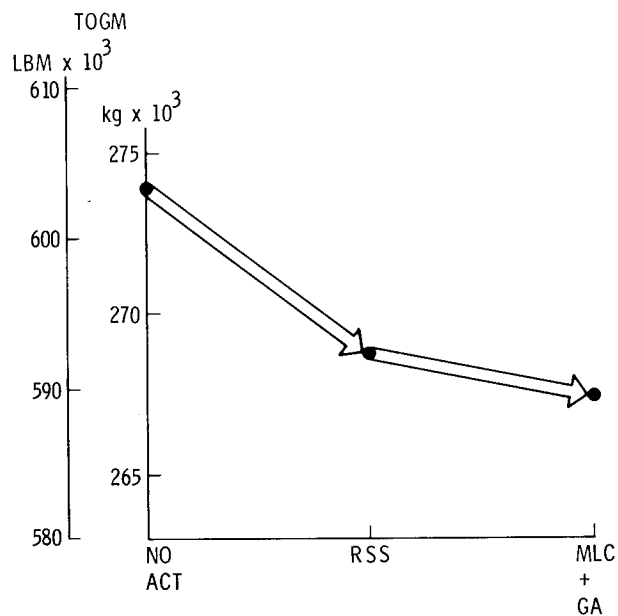


Figure 40.- Impact of active controls.

PROPULSION

- ADVANCED TURBOFAN ENGINE
- OVER-UNDER ENGINE ARRANGEMENT
- ADVANCED COMBUSTOR DESIGN
- TAILORED EXHAUST PROFILE
- SMALL ENGINE SIZE

AERODYNAMICS

- MODIFIED ARROW-WING PLANFORM
- SMALL WING AREA
- HIGH LIFT SYSTEM (FLAPS + AFT TAIL)
- RELAXED STATIC STABILITY

STRUCTURES

- POLYIMIDE TYPE COMPOSITES
- ADVANCED MANUFACTURING APPLICATIONS
- ACTIVE CONTROLS

Figure 41.- Features.

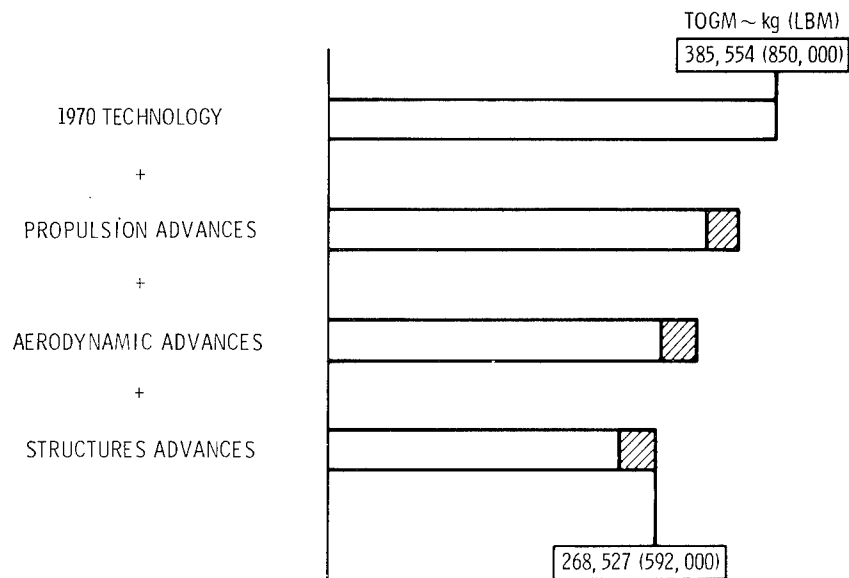


Figure 42.- Technology impact.

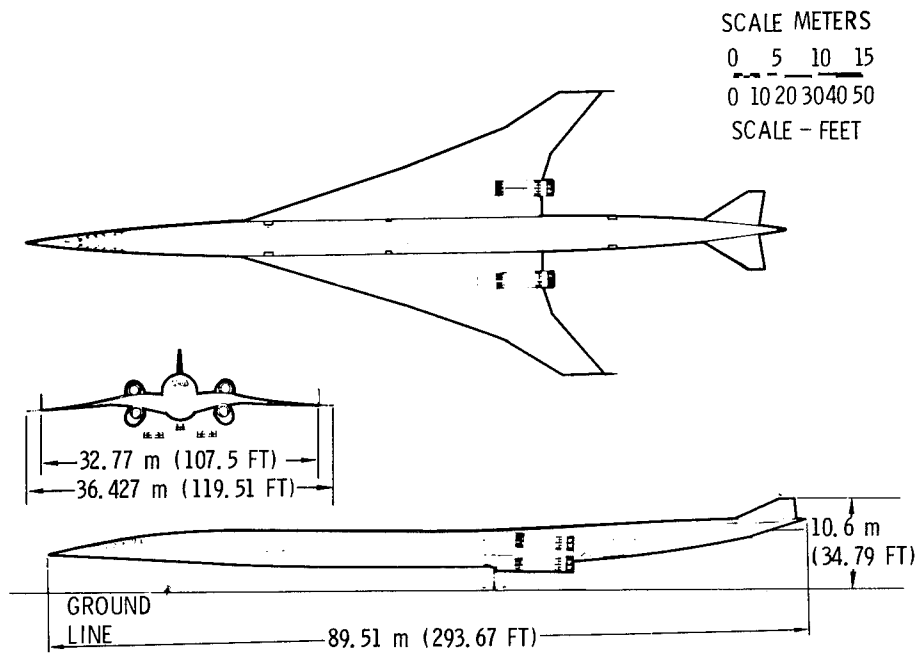


Figure 43.- SCV concept.

TOGM	268 527 kg	PAYLOAD	26 308 kg
OEM	106 594 kg	RANGE	7 593 km
CRUISE M	2.55	TOFL	3 353 m
ENGINE AIRFLOW	272.2 kg/s	APPROACH SPEED	81.3 m/s
WING AREA	624.3 m ²	NOISE	FAR 36 TO 36-3

Figure 44.- Characteristics summary.

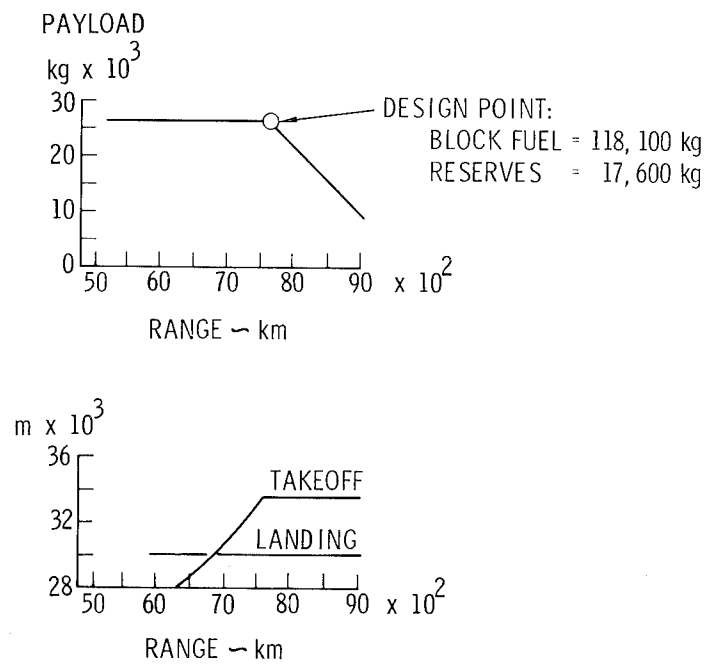


Figure 45.- Payload-range characteristics.

	L-2000-11 ADVANCED SCV	L-2000-1	L-2000-11 ADVANCED SCV	L-2000-1
RANGE	4100 N MI	3400 N MI	7593 km	6297 km
PASSENGERS	290	258		
CRUISE SPEED (MACH)	2.55	2.70		
WING AREA	6720 SQ FT	8486 SQ FT	624.3 m ²	788.4 m ²
LENGTH	294 FT	273 FT	89.6 m	83.2 m
TOGM	592,000 LBM	590,000 LBM	268,527 kg	267,619 kg
OEM	235,000 LBM	235,500 LBM	106,594 kg	106,821 kg
SONIC BOOM	1.7 PSF	1.7 PSF	81.4 N/m ²	81.4 N/m ²

Figure 46.- Characteristics comparison.

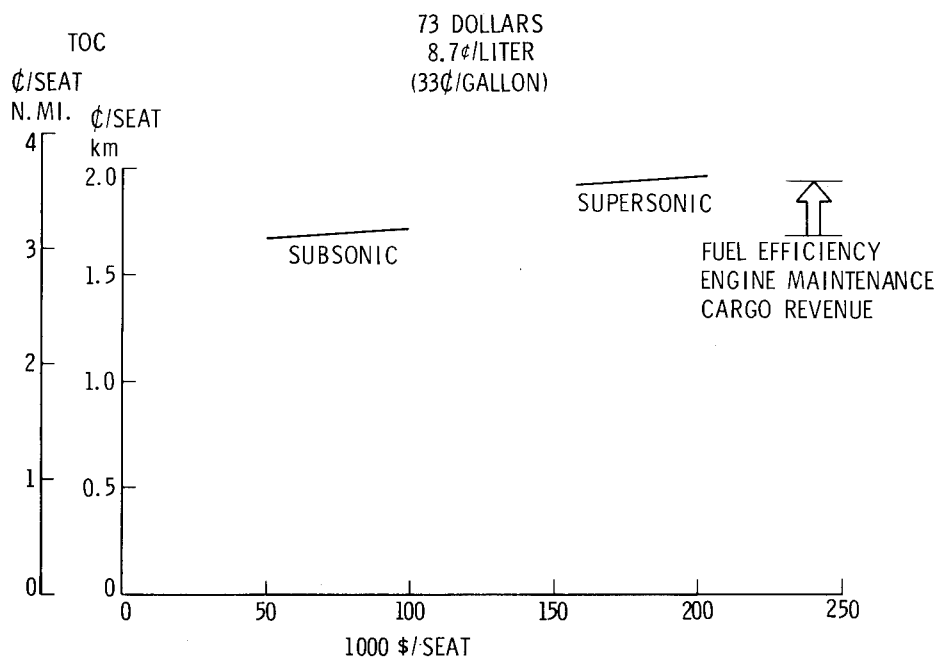


Figure 47.- Economics.

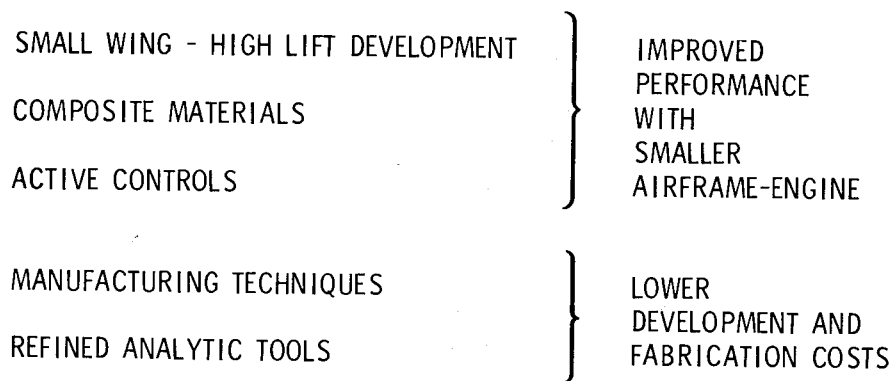


Figure 48.- SCAR technology accomplishments - economics.

NOISE

ENGINE CYCLE DEVELOPMENT	}	LIGHT WEIGHT, REDUCED EXHAUST VELOCITY, TURBOFAN
COANNULAR NOISE RELIEF		
JET SHIELDING	}	OVER-UNDER ENGINE CONCEPT
STRUCTURAL SHIELDING		

EMISSIONS

COMBUSTOR DESIGN

Figure 49.- SCAR technology accomplishments - ecology.

PROPULSION

- SCALED ENGINE DEMONSTRATOR
- INFLIGHT NOISE RELIEF TESTS
- INLET RESEARCH

AERODYNAMICS

- CONTINUED HIGH LIFT DEVELOPMENT
- ADVANCED CONTROL DEVELOPMENT
- VEHICLE SIMULATION

STRUCTURES

- ACCELERATED DEVELOPMENT OF MATERIALS
AND MANUFACTURING TECHNIQUES
- LARGE SCALE HARDWARE PROGRAMS

Figure 50.- Technology development priorities.

MARKET TRENDS

Richard D. FitzSimmons
McDonnell Douglas Corporation

SUMMARY

The public, by its reception and patronage of the widening Concorde supersonic service, will dictate whether a need exists for a second-generation supersonic transport. As of this writing, this need has not been demonstrated unequivocally; however, preliminary results are favorable . . . the public is willing to patronize supersonic service, even at premium fares, with marginal schedule frequency, and in less than spacious accommodations.

Without question, a second generation supersonic transport must meet society's needs, and at the same time be profitable for the operators and manufacturers, or such a program should not be initiated. Studies indicate that a design meeting the requirements can be described; however, unlike major civil aircraft developments of the past, an advanced supersonic transport cannot be conceived that would be economically competitive for all airline long haul passenger markets. The supersonic airplane direct operating costs (DOC) seem inherently higher than subsonic designs, both as envisioned today and for the foreseeable future. Accordingly, no case can be made for an AST to compete for the excursion traveler, who is economy minded and sees no economic value to increased speed.

A very large segment of the over water, long haul passenger market, 31% of the passengers who provide 42% of the passenger revenue, offers a significant market for an advanced supersonic transport. This is for both the first class and full-fare economy passenger markets. The supersonic transport may be more competitive here in spite of lower costs of subsonic transports, as passenger preference is a more powerful variable than DOC. This latter fact was amply demonstrated in the late fifties when the jets completely replaced the reciprocating engine transports on most world routes, in spite of slightly higher fares.

The civil aircraft market, through the year 2000, could reach 250 to 300 supersonic aircraft, given the timely availability of the necessary resources to undertake such a venture. Every indication to date is that a multi-nation, multi-government program may offer the only way such a program will come to fruition.

BACKGROUND

The North Atlantic air market, historically, has dominated world airline passenger markets, and a great deal can be learned from studying its operation. The market share split by mode started in 1959 with the initial offering of

less-than-first-class fares. The response was overwhelmingly favorable and a large increase in passenger travel occurred. International air travel became the largest sustained growth segment in the airline industry (fig. 1).

The impact on the first class market is a fact well known to all airplane designers, as the bulkhead between the first class section and the lower fare passengers was moved forward in the airplane. This seemed to occur almost every time new data was available on the latest split between first class and economy. 1975 data shows first class is about 5.8% of the North Atlantic scheduled passenger traffic (fig. 2). Finally, some stability to the market split seems to have been reached.

A look at the fares (fig. 3) shows how extensive these reduced fares have become. The cheapest, the excursion fares, are only 30% of the first class ticket, whereas there was but one fare 25 years ago. Another interesting comparison can be made using the growth of the consumer price index (CPI). Here, the excursion fare is but 20% of what inflation alone, as reflected by the CPI, would have driven the fare to, and the first class fare is also low, being 30% below the CPI trend line. These are facts little recognized by some regulators or critics of the airline industry. Airline travel remains one of the best buys in the recently inflated economies of the world.

Unfortunately, good historical data are not available on the full-fare economy passenger market, but there are data for the first class passenger market (fig. 4). In spite of the surge in tourist and economy traffic, the first class market has continued to be a growing market. Since 1963, for 12 years, it has grown at almost 9% per year, a surprisingly healthy figure. One would expect that the full-fare economy class would have grown even faster than the 9% growth of first class.

High fare business will always be attractive (fig. 5). An analysis of the PAA and TWA data shows that these airlines in 1975 realized about the same revenue from first class than from their more heavily publicized charter business. And to realize this they handled only 1/4 as many passengers.

ANALYSIS

Initially, in the market analysis conducted in 1973 (fig. 6) in the NASA contract effort, McDonnell Douglas examined more than 500 city-pairs throughout the world for supersonic service for the period 1985-1994 considering 12 world market groups such as North Atlantic, Europe-Mid-East, and North and Central Pacific. The initial city-pairs met the following qualifications: overwater routes (some tag-end city-pairs were included for joining traffic), minimum city-pair distance of 1667 km (900 miles) and all city-pairs capable of generating sufficient passenger traffic during the period 1985-2000 to support scheduled supersonic service. An iterative process of computer-aided market analysis was undertaken for these combined world market groups in which market growth rates were projected from the base year 1975 to the year 2000. The supersonic revenue passenger-kilometers (passenger-miles) are estimated to grow from 87 billion (47 billion) in 1980 to 261 billion (141 billion) by the year 2000. This is a 5.7 percent average annual growth rate over the forecast period.

The resulting revenue passenger-mile distribution by range is shown. The importance of being able to design a 8334-kilometer (4500-nautical-mile) range airplane to do 80 percent of the business as compared to 6112 kilometers (3300 nautical miles) or 40 percent of that business is most significant. Both the Concorde and the last U.S. SST were designed for the shorter range. The advanced technology capabilities identified during the past 4 years in the cooperative NASA/McDonnell Douglas design studies show that a 8334-kilometer (4500-nautical-mile) range can be realized. As civil aircraft manufacturers know well, airlines like long range. The value of range cannot be underestimated in international service.

A comparison is shown of the payload range capabilities of the various important supersonic transport programs as compared to typical city-pair distances (fig. 7). The Concorde and the former U.S. SST both show limited range as compared to what can be predicted for an advanced supersonic transport as a result of the cooperative NASA-Industry SCAR efforts of the past four years.

The payload range shows a 8519-kilometer (4600-nautical-mile) capability for a near term airplane, for a go-ahead in 1980 which would use a low risk engine cycle. Also shown is what could be done with an advanced engine (possibly a variable cycle engine) plus a moderate use of composites both for secondary structures and for reinforcing the primary structure for this otherwise metal airplane. A range of 10,556 kilometers (5700 nautical miles) is possible, which approaches the maximum ranges flown today by subsonic aircraft, which seemingly would satisfy future range requirements for a supersonic transport. Opening up the Pacific can become a reality and supersonic travel there can be especially appealing. Also shown is a 225-passenger design somewhat smaller than the DC-10-30 size used for the McDonnell Douglas baseline supersonic transport at 273 passengers. This seems to be a better size to match the passenger demand as a result of recently completed market trend studies. This subject of passenger size is discussed later in this paper.

Direct operating costs (fig. 8) in 1976 dollars have been recalculated since published 1973 results to include recent inflation both in manufacturing costs and in fuel costs. The results show a deterioration in direct operating costs of a 273 passenger supersonic aircraft as compared to a DC-10-30; however, the loss is not as great as many predict. Today, the supersonic aircraft direct operating cost is predicted to be 55% higher than for a DC-10-30 in similar seating configurations. In this comparison, in the prices used, there is a profit included in the supersonic aircraft airplane price as well as the cost of the money, whereas the DC-10-30 price has yet to reflect a profit. Direct operating cost of the Concorde is also shown for reference. A number of sensitivity studies have been made regarding increased jet fuel prices. Fuel cost accounts for a major fraction of the operating cost. The effect on the supersonic airplane of an increase in fuel cost from 12 to 35 cents per gallon, an increase of almost 200 percent in the cost of fuel, has been included in these cost comparisons. This impact is not as dramatic as one might expect. Looking to the future, we predict that increased labor expenses will have a greater impact on operating costs, for both subsonic and supersonic airplanes, than fuel expenses.

The total operating costs (fig. 9) show a better picture for the 273 passenger MDC supersonic transport, being only 28% higher than the DC-10-30. Again, the Concorde is shown for reference.

Today, the Concorde is providing the passenger with a tangible benefit for increased fare (fig. 10). This is the saving of travel time with the increase in usefulness that shorter travel time affords. Subsonic aircraft offer amenities, deluxe service and extra spaciousness, as the only inducements for higher fares. To the average business executive this is not sufficient except in unique instances as the economy section is quite good enough and both sections arrive together at the destination. The Concorde has changed this.

It is very possible that the supersonic airplane of the 1980's will follow this lead and afford special value to the traveler, whether first class or full-fare economy. The discounted fares require low operating cost airplanes and, accordingly, the subsonic DC-10 type transports will continue to carry this type of passenger. Additionally, increased capacity subsonic transports are now on the drawing boards that offer even lower seat mile costs making the supersonic transport economics even less attractive for purely economy minded passengers.

In analyzing the 1974 North Atlantic yield per passenger nautical mile (fig. 11), it is readily apparent that the first class yield of over 3.1 cents/seat kilometer (15 cents/seat mile) far exceeds the yield of the other segments of the market. It is 75% higher than full-fare economy class and over 2-1/2 times as high as the 22-45 day excursion yield. It is also significant that the yield of full-fare economy class is 50% higher than for the 22-45 day excursion.

To put yield in perspective, the total operating costs shown earlier (fig. 9) were 1.9 cents/seat kilometer (3.5 cents/seat mile) for the DC-10-30 and 2.4 cents/seat kilometer (4.4 cents/seat mile) for the MDC-AST in 1976 dollars. Also, the Concorde was shown at about 4.3 cents/seat kilometer (8 cents/seat mile) or about twice the DC-10-30. These total operating costs are well under the yield of first class and, in the case of the MDC-AST and DC-10-30, well under the full-fare economy; however, the DC-10-30 alone of the three looks attractive for the discounted fare low yield passenger market.

The North Atlantic market share that seems to be important for a supersonic airplane (fig. 12) can be roughly estimated to be 19% of the passengers who provide 27% of the revenue. The remaining 81% of the passengers would continue to be served by subsonic transports. Not all of the full-fare economy passengers can be expected to patronize supersonic service due to schedule problems, lack of traffic density, or other reasons.

In the McDonnell Douglas in-house studies, various market penetrations for supersonic travel have been investigated (fig. 13). Each city-pair seems to require a different penetration assumption, dictated by the historical market split between business and pleasure travel. Typical assumptions for market penetration range from a low of 17% from the recreation dominated Honolulu to Los Angeles market, to heavily business dominated routes like New York to Rio de Janeiro at 40%.

There are market penetration variations by service and by fare for supersonic service (fig. 14). One Concorde manufacturer varies market penetration with the ratio of total operating cost relative to competitive subsonic designs. To that basic curve can be added the values being used by McDonnell Douglas on some in-house studies. These values for the supersonic airplane are 90% penetration for the first class market, 50% for the full-fare economy market and zero

penetration for the discount market. It can be seen that on this basis the Concorde penetration will be small relative to what can be offered in a more economical second-generation supersonic transport, with low total operating costs.

One route was examined in detail, the North Atlantic (fig. 15). For this example, two cases were postulated. Case one assumed the DC-10-30 carried all the passenger traffic and realized the revenue just as it existed by class for the 1974 scheduled services offered. 1975 operating cost assumptions were used. The system resulted in a breakeven load factor of 43 percent for an all DC-10 fleet.

The second case assumed the traffic to split as described earlier. Initially, the airplane seating capacities did not match the traffic demand and the passenger split of both aircraft had to be tailored to match the markets. The 10% first class penetration for the DC-10-30 resulted in only one first class passenger per flight in the subsonic airplane so a high density 328 seat DC-10-30 was selected. The supersonic airplane on the other hand could not accommodate all the first class passengers of the market and accordingly a 35% first class, 65% full-fare economy split had to be obtained. The 273 seat MDC supersonic design fuselage became a 251 seat design to match the split in the market between first class and 50% of the full-fare economy.

The load factors that resulted, assuming no change to the 1974 fares levels, showed that the supersonic design at 35% load factor not only was competitive but was even slightly better than the all subsonic case. This is extremely important as it shows that a supersonic airplane can be a profitable investment for an airline and does not need fare increases to support it. Also, a 251 passenger airplane may actually be too large, 225 passengers may be better.

While there is every reason to believe that a fleet of supersonic airplanes can be operated by the airlines with no increase in fares (fig. 16) for first class or full-fare economy, indications are that a small increase in fares for all services can be tolerated without a loss in market share. This would increase the profitability of the entire airline system.

As of now, our market trend studies indicate that a 225 passenger supersonic airplane may better match the anticipated passenger demands through the year 2000. A typical interior arrangement is shown (fig. 17), which has 77 passengers in first class and 148 passengers in full-fare economy, almost all arranged in spacious 4 abreast accommodations.

McDonnell Douglas/NASA 1973 studies, more conservative than either Boeing or Lockheed, showed a large potential market for an advanced supersonic airplane from the mid-1980's to the end of the century. Present estimates (fig. 18) are that 250 to 300 aircraft would still be needed through the year 2000, even making allowances for high fuel costs and higher operating costs. Assuming a purchase price of approximately \$110 million per airplane, this represents a \$33 billion market. This is almost equivalent to the total free-world value - \$42 billion - of all the civil aircraft sales in history up through 1976. This is an important market and the U.S. should try to capture a major part of it.

The future requirement for subsonic aircraft for these same over water long range routes is close to 700 DC-10-30's (or equivalent) to put the supersonic transport market in perspective.

A look at the history of one U.S. civil aircraft program (fig. 19) seems to portray how the second-generation supersonic airplane program could develop. Both represent non-competitive major airplane programs designed to serve the long haul passenger on the prime routes of the world. Only time will tell if history will once again repeat itself.

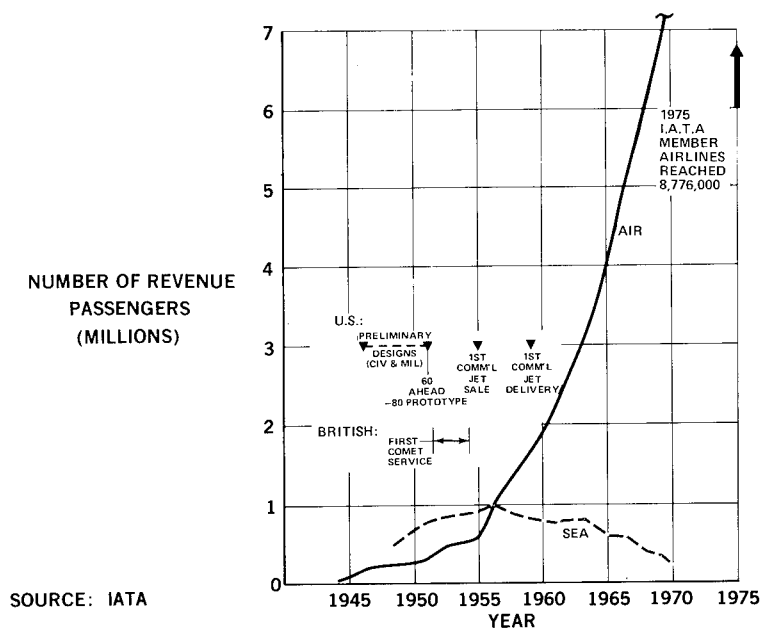


Figure 1.- North Atlantic traffic.

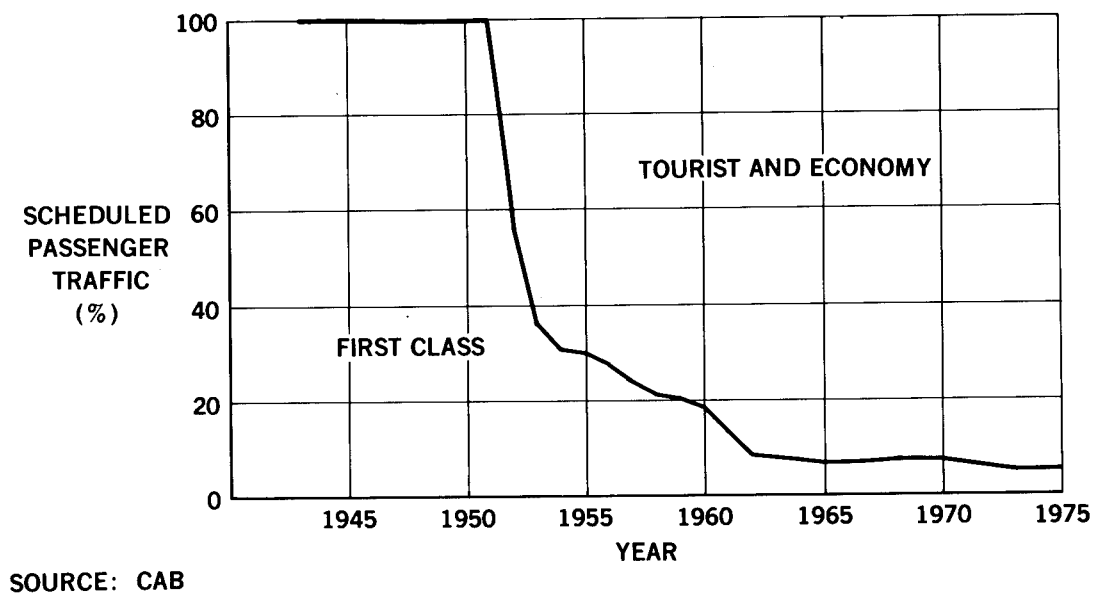


Figure 2.- Market share by mode - North Atlantic.

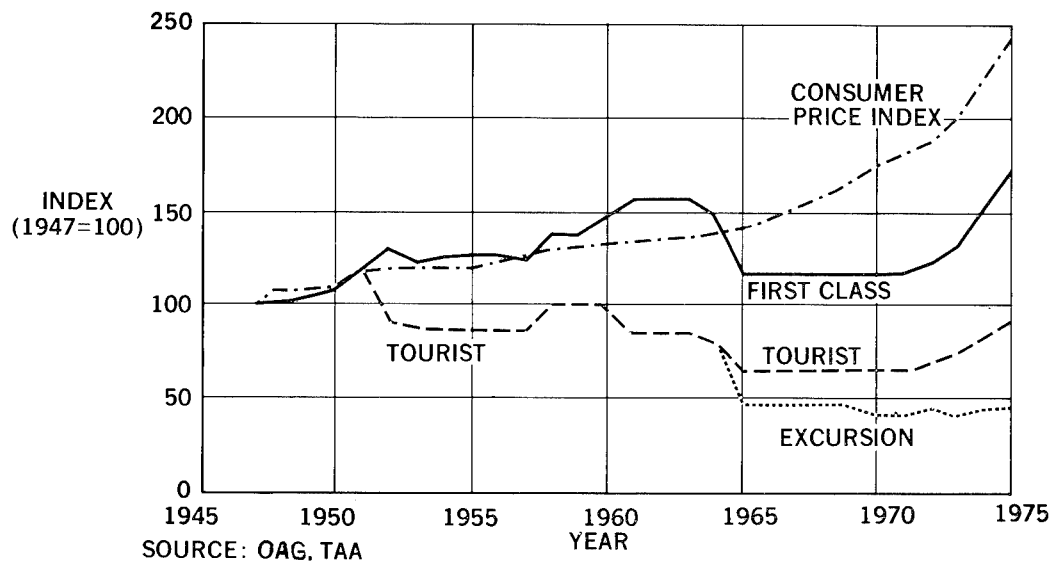


Figure 3.- North Atlantic fare trends versus consumer prices.

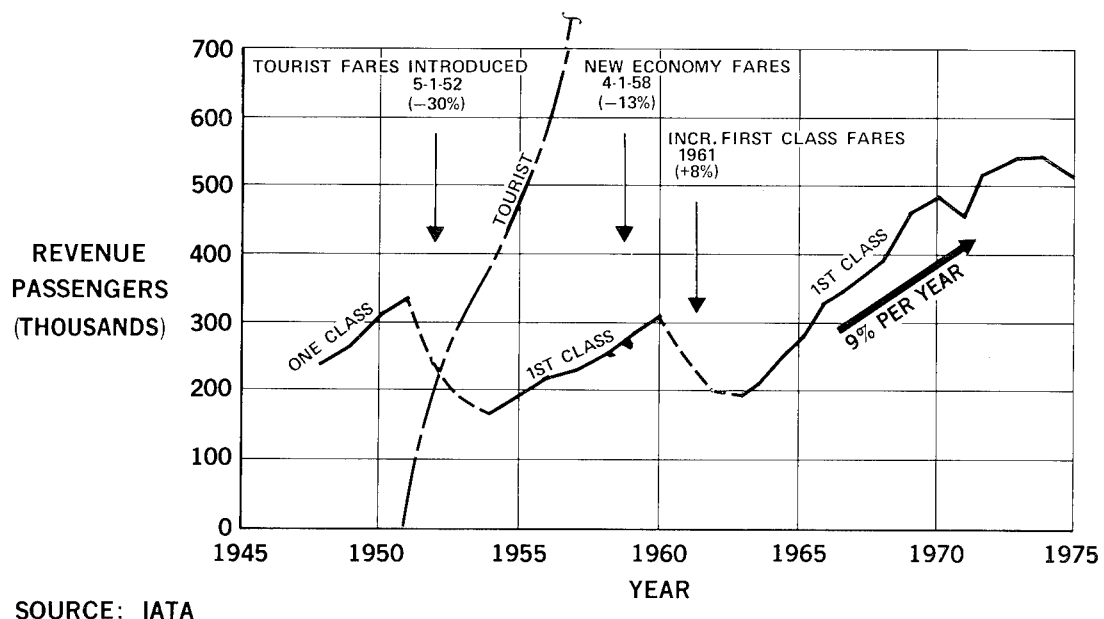


Figure 4.- History - 1st class market - North Atlantic.

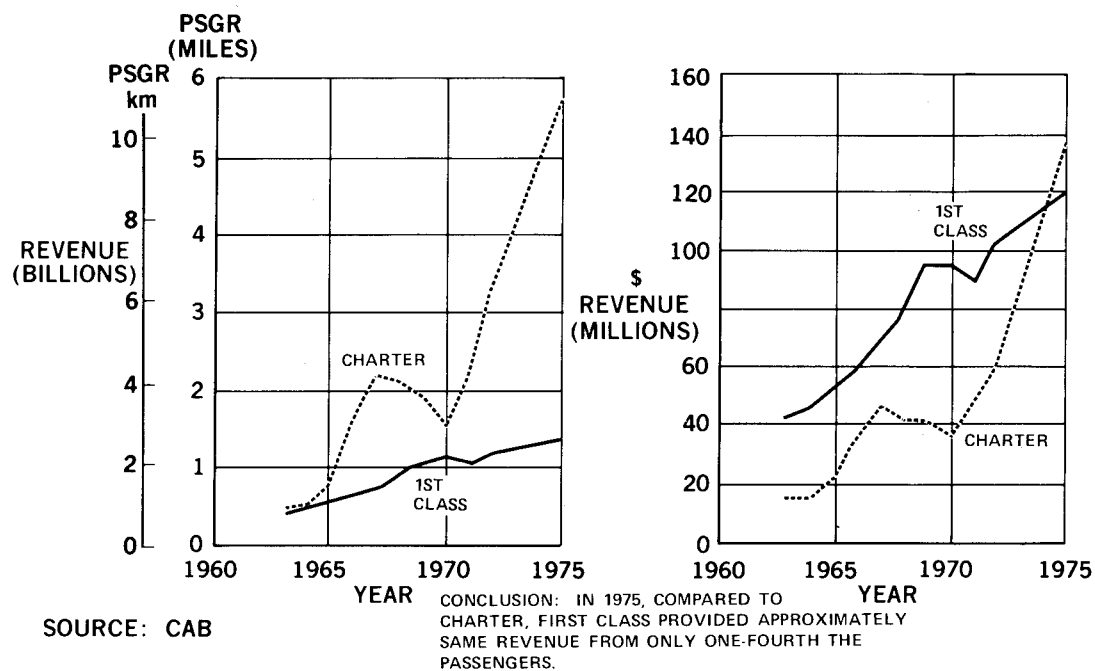


Figure 5.- 1st class market comparison with charter - TWA and PAA, North Atlantic.

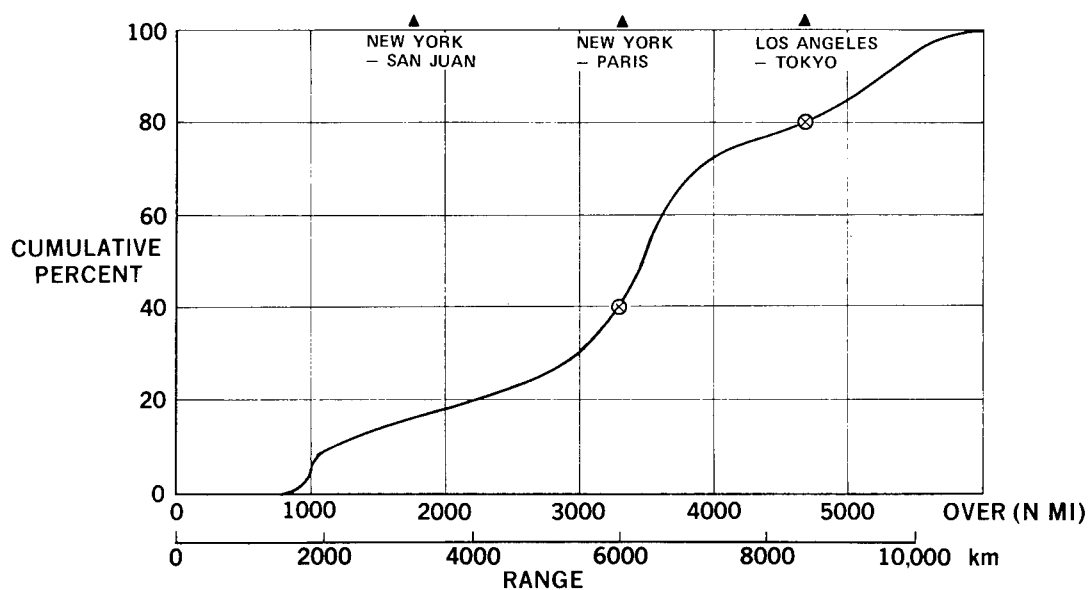


Figure 6.- AST revenue passenger-miles distribution by range.

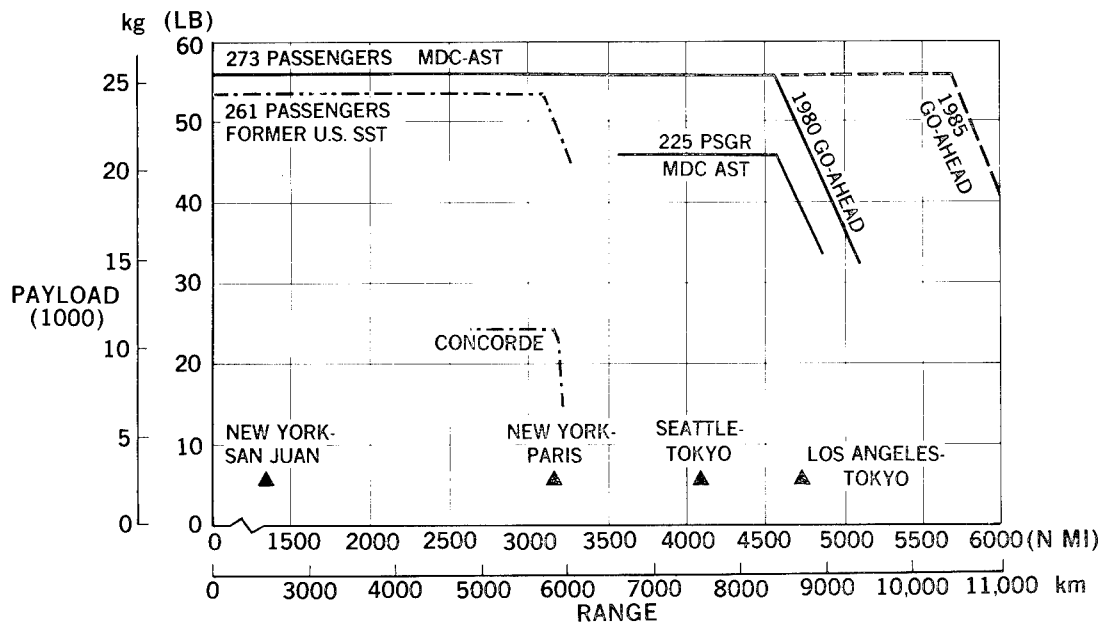


Figure 7.- Payload - range.

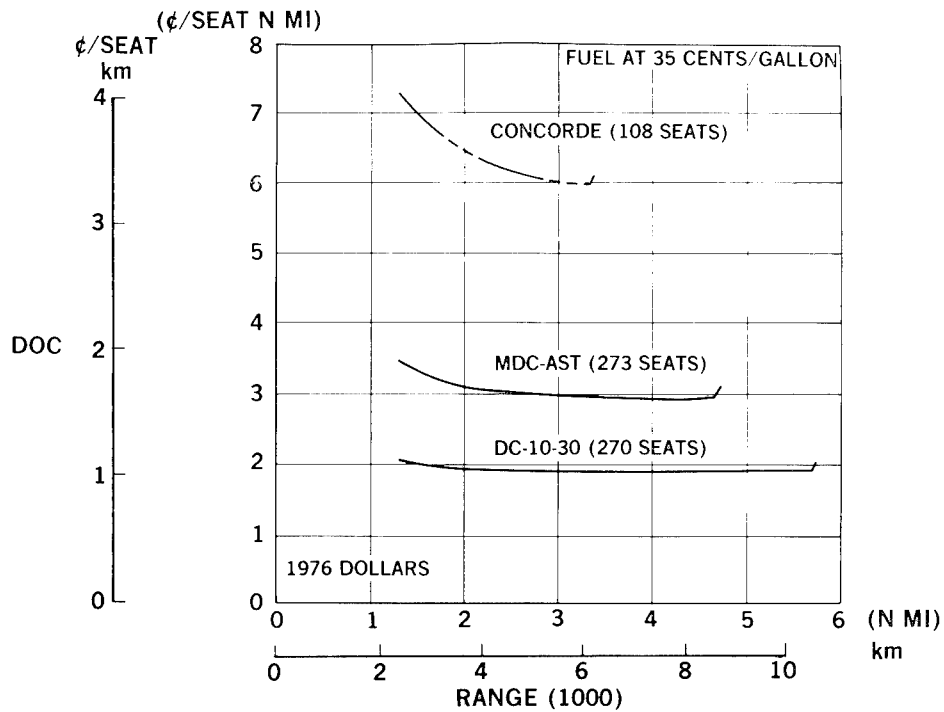


Figure 8.- Comparative direct operating costs.

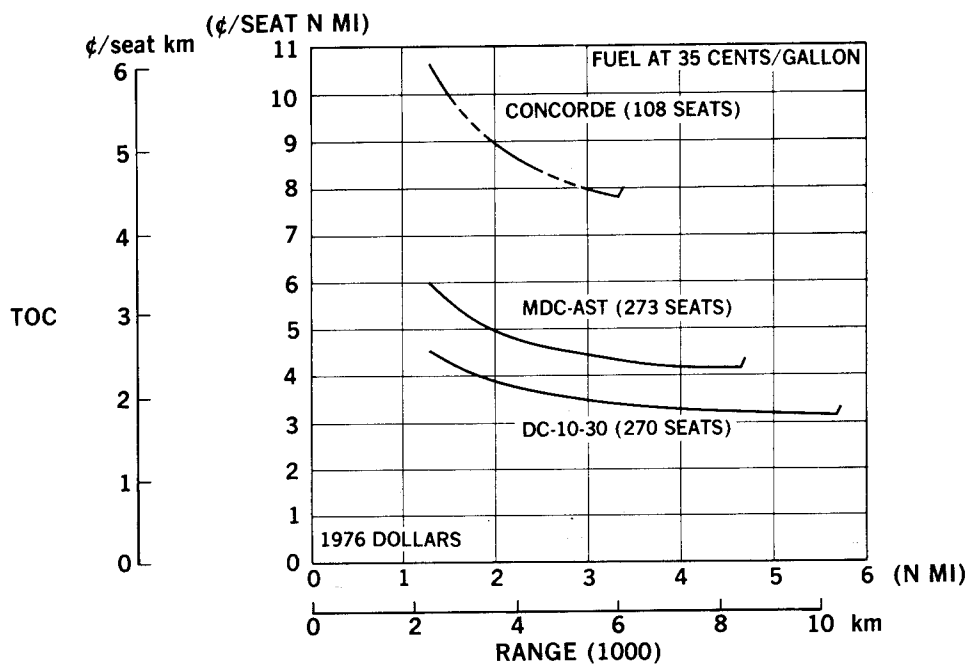


Figure 9.- Comparative total operating costs.

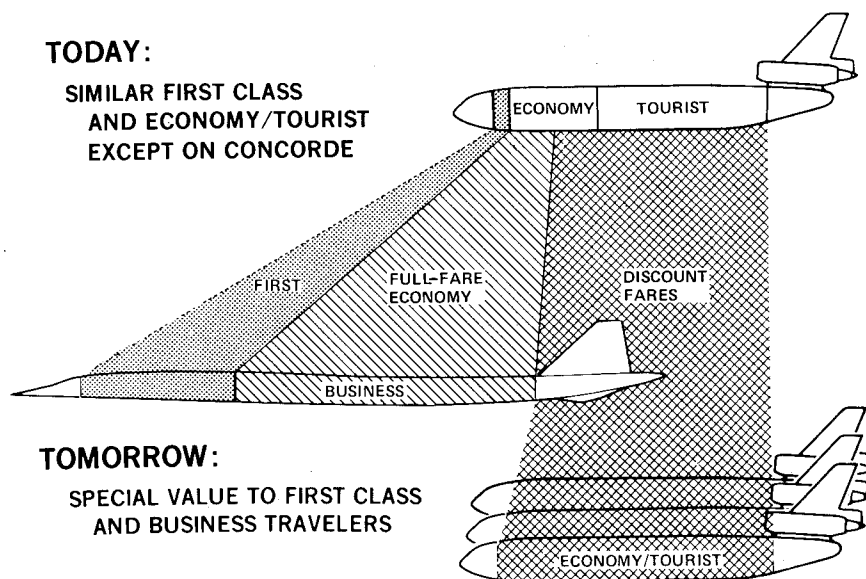


Figure 10.- Market separation by speed and fare.

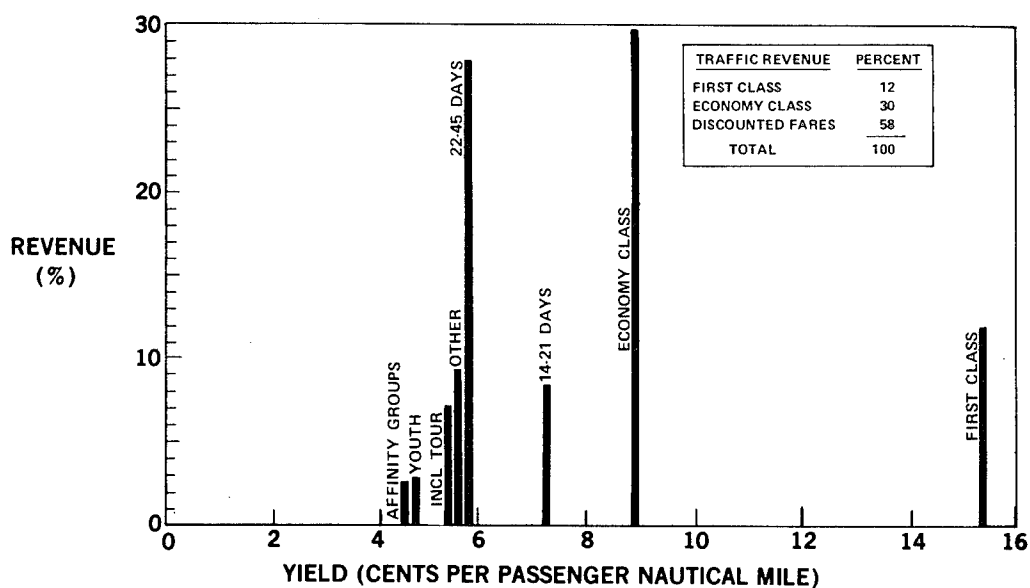


Figure 11.- Revenue distribution - 1974 North Atlantic scheduled passenger service.

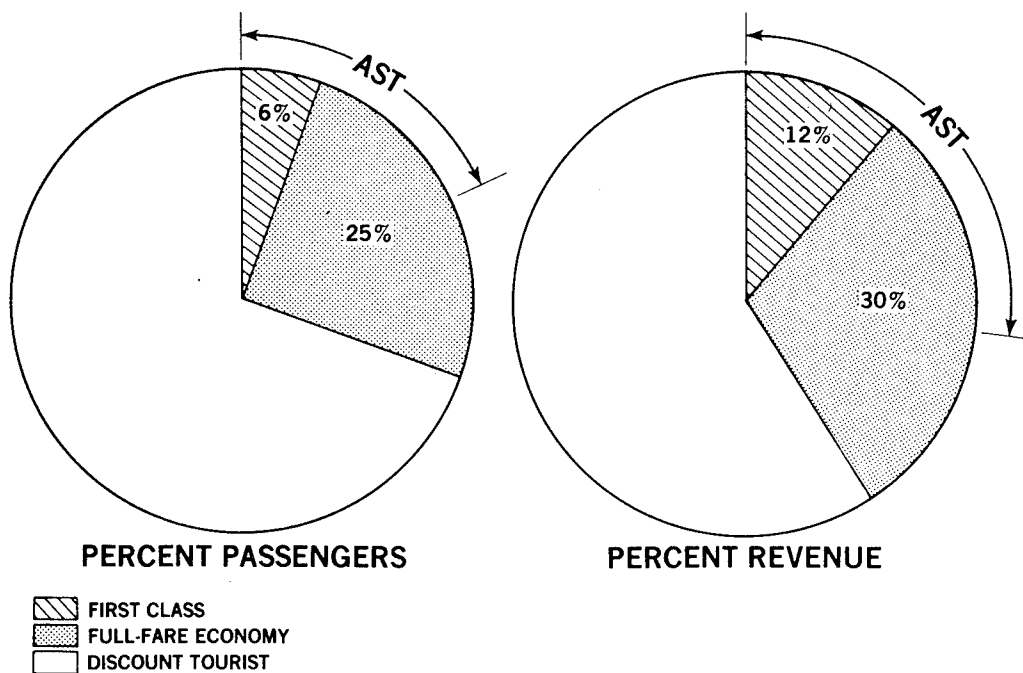


Figure 12.- Market shares - North Atlantic.

<u>CITY-PAIR</u>	<u>PERCENT PENETRATION</u>
HONOLULU-LOS ANGELES	17
HONOLULU-SEATTLE	20
HONOLULU-TOKYO	14
HONOLULU-SYDNEY	30
NEW YORK-LONDON	18
NEW YORK-FRANKFURT	17
NEW YORK-SAN JUAN	16
NEW YORK-MIAMI	12
NEW YORK-RIO	40
ETC.	

BASED ON 90-100% FIRST CLASS
50% FULL-FARE ECONOMY

Figure 13.- Typical market penetrations.

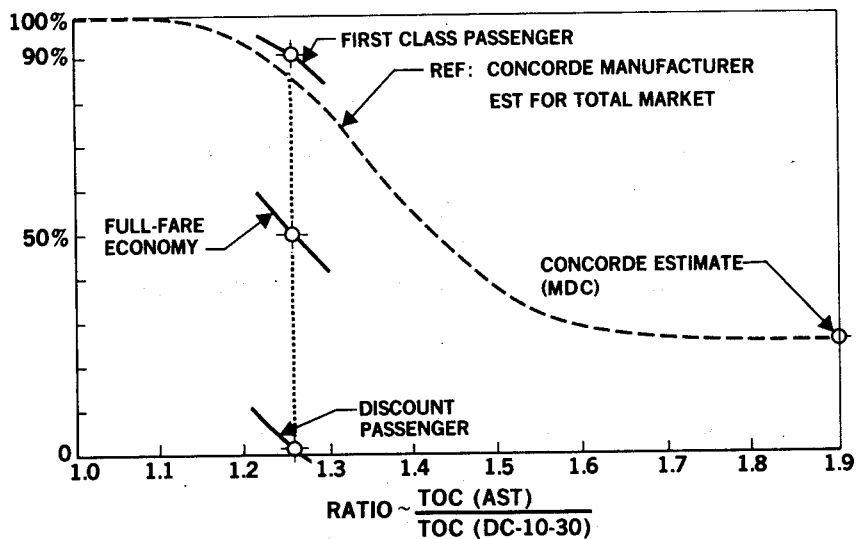



Figure 14.- Market penetration versus total operating cost.

NORTH ATLANTIC PASSENGER TRAFFIC — 1974 SCHEDULED SERVICE — RELATED FARES

TODAY

(IF DC-10 CARRIES ALL TRAFFIC)	DC-10-30 (270 SEATS)	AST (273 SEATS)
	57%	—

TOMORROW


(IF TRAFFIC SPLITS)	(328 SEATS) 10% FIRST CLASS 50% ECONOMY CLASS ALL DISCOUNTED TRAFFIC	(251 SEATS) 90% FIRST CLASS 50% ECON CLASS NO DISCOUNTED TRAFFIC
	53%	48%

Figure 15.- Relative breakeven load factors.

CASE 1

FIRST CLASS — SAME AS TODAY

FULL-FARE ECONOMY — SAME AS TODAY

DISCOUNTED ECONOMY — SAME AS TODAY

**BUT: THIS PROVIDES AIRLINES WITH LESS PROFIT
THAN TODAY'S SUBSONIC OPERATIONS**

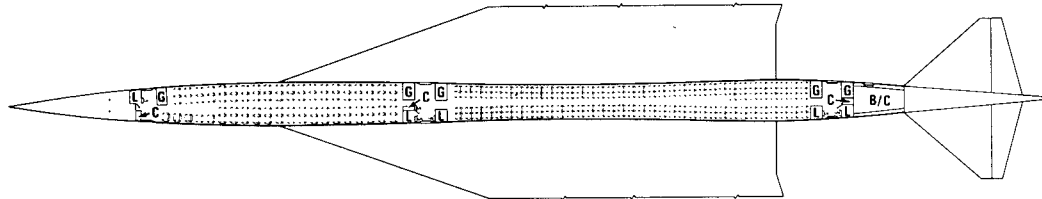
CASE 2

**FOR SAME AIRLINE PROFITS AS TODAY, INCREASE
ALL FARES BY 10%,
WHICH SEEMS DEFENSIBLE!**

Figure 16.- Airline fare options for North Atlantic case.

35% FIRST CLASS

65% FULL FARE ECONOMY



INTERIOR ARRANGEMENT

77 FIRST CLASS 148 ECONOMY

B/C = BAGGAGE/CARGO
C = COAT SPACE
C/A = CABIN ATTENDANT
G = GALLEY
L = LAVATORY

TAKEOFF WEIGHT 320,455 kg (705,000 LB)

Figure 17.- 225 passenger AST.

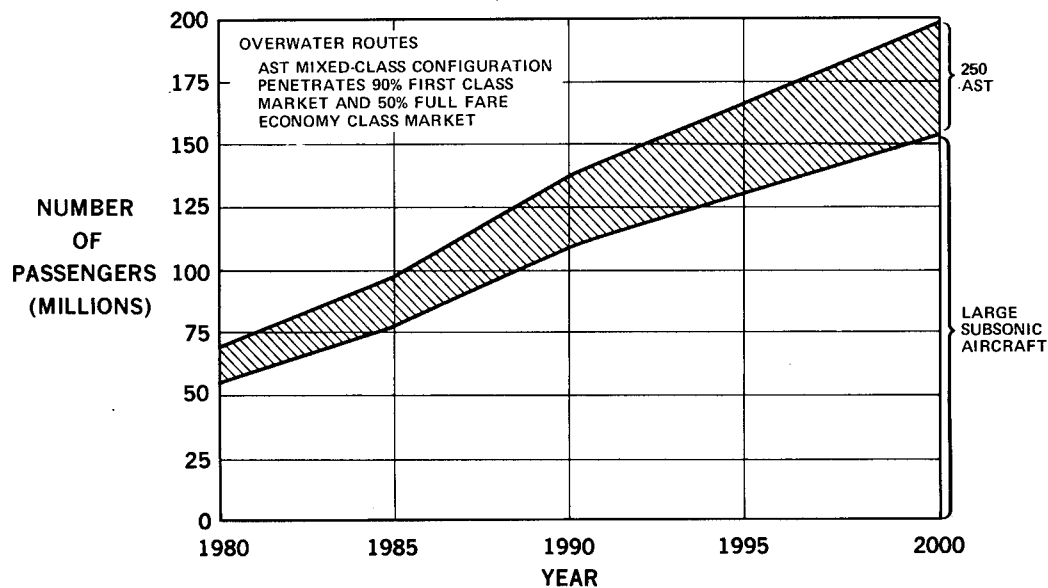


Figure 18.- Passengers by aircraft type, 1980-2000.

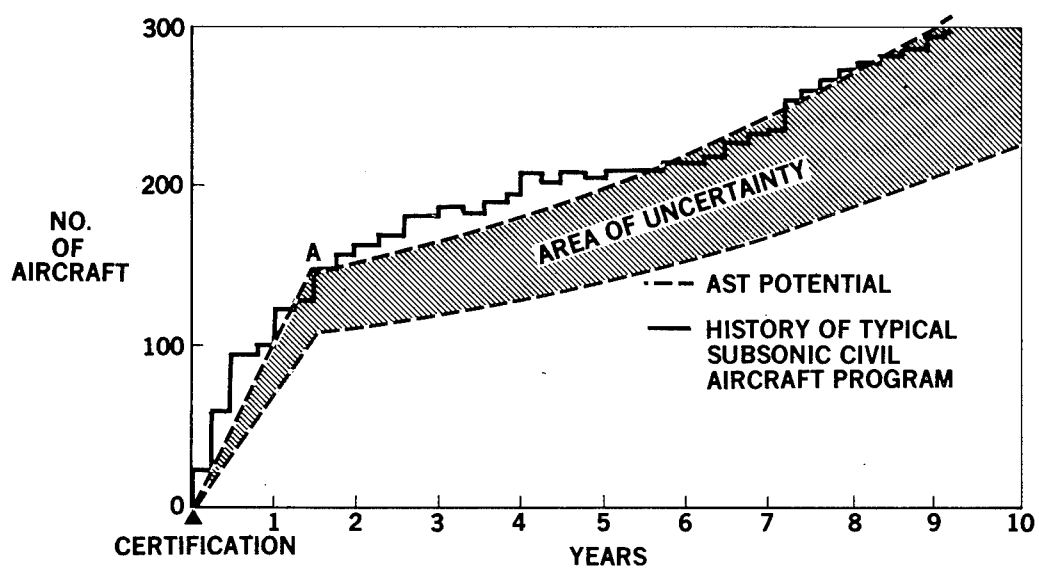


Figure 19.- AST market buildup.

SCAR CONFERENCE ATTENDEES

National Aeronautics & Space Administration Washington, DC

W. S. Aiken, Jr.	J. J. Kramer
A. K. Amos	N. F. Rekos
G. Banerian	R. H. Smith
P. D. Hauler	J. A. Suddreth
H. W. Johnson	A. O. Tischler (Retired)

National Aeronautics & Space Administration Ames Research Center Moffett Field, CA

R. L. Carmichael	W. E. McNeill
L. L. Erickson	R. W. Rosser

National Aeronautics & Space Administration Dryden Flight Research Center Edwards, CA

J. A. Albers	B. M. Kock
D. T. Berry	P. J. Reukauf

National Aeronautics & Space Administration Langley Research Center Hampton, VA

H. M. Adelman	J. W. Cheely	D. P. Hearsh
W. J. Alford, Jr.	P. L. Coe, Jr.	A. R. Heath, Jr.
E. L. Anglin	D. W. Conner	R. R. Heldenfels
T. T. Bales	C. T. D'Aiutolo	W. P. Henderson
H. T. Baber, Jr.	C. M. Darden	H. H. Heyson
R. L. Barger	S. C. Dixon	E. L. Hoffman
L. K. Barker	R. D. Doggett, Jr.	S. Hoffman
R. M. Baucom	S. M. Dollyhigh	H. H. Hubbard
R. M. Bennett	C. Driver	W. Illg
B. L. Berrier	J. E. Duberg	L. A. Imig
S. R. Bland	C. P. Eichelberger	C. M. Jackson
P. J. Bobbitt	D. E. Fetterman	J. L. Johnson, Jr.
S. M. Bobonick	W. E. Foss, Jr.	N. J. Johnston
H. L. Bohon	C. Fulton	W. B. Kemp, Jr.
R. W. Boswinkle	R. E. Fulton	P. J. Klich
R. E. Bower	G. L. Giles	R. E. Kuhn
E. Boxer	B. B. Gloss	A. C. Kyser
R. F. Brissenden	R. C. Goetz	E. J. Landrum
P. Brockman	W. D. Grantham	D. L. Lansing
W. A. Brooks, Jr.	H. A. Hamer	L. K. Loftin, Jr.
H. D. Carden	A. D. Hammond	D. L. Loving
H. W. Carlson	H. F. Hardrath	H. E. Lowder
G. T. Carson, Jr.	R. V. Harris, Jr.	I. O. MacConochie
J. R. Chambers	L. E. Hasel	R. J. Mack

Langley Research Center (Continued)

D. V. Maddalon	O. W. Nicks	J. L. Shideler
J. C. Manning	M. J. Norman	B. L. Shrout
R. J. Margason	S. P. Pao	J. Sobieszczanski
J. A. Martin	E. L. Peele	J. C. South, Jr.
V. R. Mascitti	B. Perry III	M. L. Spearman
E. E. Mathauser	W. Pfenninger	B. A. Stein
H. G. McComb, Jr.	E. C. Polhamus	D. G. Stone (Retired)
J. R. McGehee	R. A. Pride	O. O. Storaasli
M. O. McKinney	M. J. Queijo	R. T. Taylor
F. E. McLean	J. P. Raney	R. G. Thomson
C. H. McLellan (Retired)	W. H. Reed III	T. A. Toll (Retired, DRA)
H. C. McLemore	R. H. Rhyne	J. C. Townsend
R. R. McWithey	A. W. Robins	R. L. Trimpi
C. E. Mercer	J. C. Robinson	J. R. Tulinus
D. S. Miller	D. M. Royster	R. T. Whitcomb
H. G. Morgan	D. R. Rummler	A. H. Whitehead, Jr.
S. J. Morris	J. F. Runckel	C. M. Willis
M. T. Moul	J. W. Sawyer	E. J. Wolff
H. N. Murrow	O. E. Schrader	E. C. Yates, Jr.
A. L. Nagel	A. A. Schy	H. A. Yetter
M. J. Neubauer		

National Aeronautics & Space Administration
Lewis Research Center
Cleveland, OH

D. M. Bowditch	G. M. Reck
O. A. Gutierrez	R. A. Signorelli
K. W. Hiller	W. L. Stewart
A. G. Powers	R. D. Weber

National Aeronautics & Space Administration
Wallops Flight Center
Wallops Island, VA

D. C. Young

AEROSPACE COMPANIES

Boeing Commercial Airplane Company
Seattle, WA

C. H. Berman	W. D. Middleton	A. Sigalla
C. W. Clay	R. E. Miller	C. D. Simcox
J. M. Hoy	F. D. Neumann	R. W. Sudderth
F. T. Johnson	J. V. O'Keefe	M. J. Turner
M. R. Johnson	B. R. Perkin	J. D. Vachal
M. E. Manro	I. H. Rettie	C. F. Watson

The Boeing Company
Hampton, VA

B. H. Florsheim

British Aircraft Corporation

C. Leyman

Calspan Corporation
Arlington, VA

R. L. Davies

Douglas Aircraft Company
Long Beach, CA

R. E. Bates
J. B. Feather
J. E. Fischler
R. D. FitzSimmons
R. L. Roensch
W. T. Rowe

E. I. DuPont
Wilmington, DE

J. E. Goode, Jr.
W. E. McCabe

General Dynamics Corporation
Convair Division
Fort Worth, TX

R. G. Bradley G. M. Kaler
E. K. Hensley D. R. Kent

General Electric Company
Cincinnati, OH

R. D. Allan
R. Lee
L. C. Wright

General Electric Company
Lynn, MA

W. C. Gist
J. N. Krebs

Boeing Military Airplane Development
Seattle, WA

A. D. Welliver

Calspan Corporation
Buffalo, NY

J. P. Andes
P. A. Reynolds
E. G. Rynaski

McDonnell Douglas Corporation
Hampton, VA

H. B. Favre
J. R. Temple

McDonnell Douglas Corporation
St. Louis, MO

P. Czysz
T. L. Watson

General Dynamics Corporation
Convair Division
San Diego, CA

J. R. Kerr
J. F. Haskins

General Electric Company
Cleveland, OH

M. C. Toth

General Electric Company
Newport News, VA

J. F. Falta

General Electric Co.
Utica, NY

W. Y. O'Connor

Grumman Aerospace Corporation
Bethpage, NY

H. H. Forshe
C. A. Hoelzer
R. Meyer

Lockheed-California Company
Burbank, CA

R. L. Foss
W. J. Fox
W. A. Guinn
M. N. Osborn

L. Payne
I. F. Sakata
T. A. Sedgwick
W. A. Stauffer

D. M. Urie
B. R. Wright
R. E. Zalesky

Lockheed Aircraft Corporation
Hampton, VA

W. E. Farrar

Northrop Corporation
Hawthorne, CA

P. T. Wooler

Pratt & Whitney Aircraft
East Hartford, CT

R. W. Hines
V. R. Holcombe
R. A. Howlett

H. Kozlowski
R. E. Owens
W. H. Sens

Pratt & Whitney Aircraft
North Palm Beach, FL

J. Sabatella

Pratt & Whitney Aircraft
Grumman Aerospace Corporation
Bethpage, NY

N. S. Oleson

Pratt & Whitney Aircraft
Cleveland, OH

J. C. Chew
G. C. Falkenstein

Pratt & Whitney Aircraft
Hampton, VA

J. O. Wagner

Rockwell International Corporation
Los Angeles, CA

L. Ascani
G. Fair
R. A. Hibma

W. E. Palmer
J. K. Pulley

Rockwell International Corporation
Hampton, VA

J. G. Allen

Vought Corporation/Hampton Technical Center
Hampton, VA

J. P. Bailey
S. O. Beskenis
R. R. Combs, Jr.
R. A. Dacosta
J. DeYoung
B. F. Downie
G. J. Espil
W. L. Kurtze

R. W. LeMessurier
W. A. Lovell
G. L. Martin
L. A. McCullers
J. R. Newsom
C. W. Pearce
J. E. Price
L. C. Rash

R. H. Ricketts
J. W. Russell
N. J. Santoro
P. M. Smith
E. E. Swanson
A. L. Taylor
K. B. Walkley

Vought Corporation
Dallas, TX

H. Dahlke
E. A. Minter

Wyle Laboratories
Hampton, VA

A. Grayston

AIRLINES

Piedmont Airlines
Winston-Salem, NC

W. M. Magruder

GOVERNMENT

Department of Transportation
Office of Noise Abatement
Washington, DC

J. E. Wesler

DOT/Federal Aviation Administration
Washington, DC

J. Gwiazdowski
N. P. Krull

U.S. Government
Washington, DC

J. F. Alexander
J. W. Bittner

National Academy of Engineering
Aeronautics & Space Engineering Board
Washington, DC

J. P. Taylor
L. L. Teel

USAF

Ent Air Force Base, CO
Col. R. B. Coburn

AFSC Liaison Office
Langley Air Force Base, VA

Lt. Col. T. L. Griswold
N. G. Vretakis

Norton Air Force Base, CA
Lt. Col. A. S. Cooper

Scott Air Force Base, IL
Col. J. E. White

Wright-Patterson Air Force Base, OH

Capt. E. T. Bannink
H. M. Burte
E. M. Chase
V. Dahlem
Lt. Col. J. S. Ford III

J. M. Frederick
S. Inouye
R. D. Joblove
W. R. Kerr
R. D. Maddox
W. M. O'Connor
Capt. R. Rhode
Col. B. D. Ward

UNIVERSITIES

Auburn University
Auburn, AL
W. A. Foster

George Washington University
Washington, DC

M. Davis
P. Donely
A. B. Graham
J. L. Whitesides

Harvard Business School
Boston, MA

G. R. White

University of Tennessee
Knoxville, TN

C. Blackburn

New York University
New York, NY

M. I. Hoffert

Virginia Polytechnic Institute &
State University
Blacksburg, VA

O. Kandil
D. T. Mook